

CMS U1TDR

2011/01/14

2011/01/14

Head Id: 16688

Archive Id: 0:31369M

Archive Date: 2010/08/31

Archive Tag: trunk

TECHNICAL PROPOSAL FOR THE UPGRADE OF THE CMS DETECTOR THROUGH 2020

The Large Hadron Collider at CERN has begun operations at 7 TeV center of mass energy. CERN plans to run at this energy until the end of 2011 with the goal of providing an integrated luminosity of 1 fb^{-1} to the CMS and ATLAS experiments. The LHC will then shut down for 1 to 1.5 years to make the revisions necessary to run at $\sim 14 \text{ TeV}$. Operation resumes in 2013. In 2016, there will be another long shutdown to prepare the LHC to operate at and eventually above the design luminosity of $10^{34} \text{ cm}^{-2} \text{ s}^{-1}$. Operation will then resume with the luminosity rising gradually during this period to $2 \times 10^{34} \text{ cm}^{-2} \text{ s}^{-1}$. The two long shutdowns provide CMS an opportunity to carry out improvements to make the experiment more efficient, to repair problems that have been uncovered during early operations, and to upgrade the detector to cope with the ultimate luminosity that will be achieved during this period. The detector work involves the hadron calorimeters, the muon detectors, the pixel detector, the beam radiation monitoring and luminosity measurement system, the trigger, the data acquisition system, and the CMS infrastructure and facilities. The purpose of this report is to explain the need for these improvements, repairs and upgrades and the plans for carrying them out and installing them in the two shutdowns foreseen in 2012 and 2016.

DRAFT

10 **Contents**

11	1 Introduction	1
12	1.1 A brief introduction to CMS	3
13	1.2 The CERN “10 Year Technical Plan” for operation of the LHC	5
14	1.3 Challenges Addressed by the Phase 1 Upgrade Plan	7
15	1.3.1 Issues related to collisions	7
16	1.3.2 Issues related to non-collisional background	9
17	1.3.3 Other issues	9
18	1.4 Issues arising from the design of the CMS detector and its actual and projected 19 performance	10
20	1.5 Practical considerations for upgrading an operating detector	11
21	1.5.1 Radiation Safety	11
22	1.5.2 Constraints to the Design of the Upgrades	12
23	1.5.3 Physics Issues	12
24	1.5.4 Implications for the Upgrades	13
25	1.6 Summary of the proposed detector upgrades and improvements	13
26	1.7 Other Projects under Development in this Period	17
27	1.8 The Challenge Ahead	18
28	2 Physics Justification for the CMS Upgrade	19
29	2.1 Simulation Setup	20
30	2.2 Muon System Completion Simulation Summary	20
31	2.3 Hadron Calorimeter Simulation Summary	21
32	2.4 Pixel Upgrade Simulation Summary	23
33	2.5 Trigger Upgrade Simulation Summary	23
34	2.6 HLT and Physics Simulations	25
35	3 The CMS Muon System Upgrades	27
36	3.1 Introduction	27
37	3.2 CSC Muon Detector Upgrades and Repairs	29
38	3.2.1 Performance Limitations	31
39	3.2.2 Description of the Muon Detector Upgrade Plan	35
40	3.2.3 R&D needed in preparation for the Phase 1 TDR	38
41	3.2.4 Alignment with a possible Phase 2 upgrade	39
42	3.2.5 Schedule	39
43	3.3 DT Muon Detector	40
44	3.3.1 Introduction	40
45	3.3.2 Theta Trigger Board replacement	42
46	3.3.3 Sector Collector Upgrade	45
47	3.4 RPC Muon Detector	51
48	3.4.1 Introduction	51
49	3.4.2 Physics motivation for the forward up-scope	51
50	3.4.3 Detector design and layout	52

51	3.4.4	Electronics	55
52	3.4.5	Services	57
53	3.4.6	Production facilities	60
54	3.4.7	Project organization	64
55	3.5	Production and Installation Plans for the CMS Endcap Muon Upgrades	67
56	3.5.1	Introduction	67
57	3.5.2	CSC and RPC Production in Building 904	68
58	3.5.3	Installation	72
59	4	Central and Endcap Hadron Calorimeter Repairs, Improvements, and Upgrades	77
60	4.1	Outer Hadron Calorimeter (HO)	82
61	4.2	Barrel and Endcap Calorimeters (HB/HE)	87
62	4.2.1	Introduction	87
63	4.2.2	Problems Motivating the Improvement and Upgrade Program	89
64	4.2.3	Simulation Studies	97
65	4.2.4	Proposed Improvements and Upgrade Plan	99
66	4.2.5	R&D for Phase 1	112
67	4.2.6	Implementation and Infrastructure Issues	113
68	4.2.7	Alignment with possible Phase 2	113
69	4.2.8	Schedule	113
70	4.2.9	Conclusion	114
71	5	Forward Rapidity Calorimeter Systems	117
72	5.1	Forward Hadron Calorimeter (HF)	117
73	5.1.1	Large Energy Events in HF PMTs	119
74	5.1.2	HF PMT System Upgrade	119
75	5.1.3	Other Sources of Anomalous Signals in HF	121
76	5.2	CASTOR	122
77	5.2.1	Detailed description of tasks	123
78	5.2.2	Work details and schedule	126
79	6	Pixel Detector Improvements and Upgrades	129
80	6.1	Performance of Current Detector	132
81	6.1.1	Electronics and Readout	132
82	6.1.2	Sensor Radiation Hardness	132
83	6.1.3	Material In the Tracking Region	134
84	6.2	Description of the Pixel Detector Upgrade	136
85	6.2.1	Geometrical Layout	137
86	6.2.2	New Beam Pipe	138
87	6.2.3	Mechanical Support for BPIX	139
88	6.2.4	Mechanical Support for FPIX	139
89	6.2.5	CO ₂ Cooling	142
90	6.2.6	DC-DC Conversion	143
91	6.2.7	Front End Electronics	144

92	6.2.8	Sensor Module	146
93	6.2.9	Bump bonding	146
94	6.2.10	Pixel Module Assembly and Testing	147
95	6.2.11	Final integration and commissioning	147
96	6.3	Performance Studies	147
97	6.3.1	Studies of the Effects of Material in the Tracking Volume	148
98	6.3.2	Pattern Recognition and Efficiency Studies	148
99	6.3.3	Track Parameter Studies	150
100	6.3.4	Vertex Resolution Studies	151
101	6.3.5	<i>b</i> -tagging Studies	152
102	6.4	Further development for the innermost region	153
103	6.4.1	Frontend electronics and sensors	153
104	6.4.2	Performance studies	154
105	6.5	Schedule	155
106	6.6	Conclusions	155
107	7	Trigger System Improvements and Upgrades	159
108	7.1	Introduction	159
109	7.2	Calorimeter Trigger	160
110	7.2.1	Introduction	160
111	7.2.2	Present Calorimeter Trigger System Overview	161
112	7.2.3	Calorimeter Trigger Upgrade Algorithms	161
113	7.2.4	Calorimeter Trigger Upgrade Hardware Strategy	163
114	7.2.5	Calorimeter Trigger Upgrade Hardware Design	165
115	7.2.6	Calorimeter Trigger Upgrade Hardware Demonstrators	167
116	7.3	Muon Trigger	168
117	7.3.1	Introduction	168
118	7.3.2	Present Muon Trigger System Overview	168
119	7.3.3	DT Trigger Issues and Upgrade	172
120	7.3.4	RPC Trigger Issues and Upgrade	175
121	7.3.5	CSC Trigger Issues and Upgrade	176
122	7.3.6	Global Muon Trigger	179
123	7.4	Global Trigger and Central Trigger Control	179
124	7.4.1	Global Trigger	179
125	7.4.2	Central Trigger Control	180
126	7.5	Trigger Software	181
127	7.6	Schedule	182
128	7.6.1	Calorimeter Trigger	182
129	7.6.2	Global Trigger	182
130	7.6.3	Muon Trigger	183
131	8	Data Acquisition System Improvements and Upgrades	185
132	8.1	Introduction	185
133	8.1.1	Performance and limitations of the current system	187

134	8.1.2	Purchase and installation of the current system	187
135	8.2	Upgrade of the DAQ system	189
136	8.3	Implications of LHC running scenarios and subsystem upgrades on the require-	
137		ments for the DAQ system	189
138	8.3.1	Possible running scenarios of LHC for Phase 1	190
139	8.4	Discussion of the DAQ components	190
140	8.4.1	Hardware Control	191
141	8.4.2	Readout links	191
142	8.4.3	Fed-Builder	191
143	8.4.4	RU-Builder and HLT farm	191
144	8.4.5	Storage Manager	193
145	8.4.6	Online Database	194
146	9	Beam Instrumentation and Luminosity Monitoring Improvements and Upgrades	195
147	9.1	Present Beam and Radiation Monitoring Instrumentation	195
148	9.1.1	Protection Systems	197
149	9.1.2	Monitoring Systems	198
150	9.2	Motivation for Beam Instrumentation Improvements	200
151	9.3	Scheduled Plan 2012 and 2016 Shutdowns	202
152	9.4	Beam Conditions Monitors	202
153	9.4.1	2012: Preventative Maintenance	203
154	9.4.2	2016: Preventative Maintenance and BCM2 Rebuild	203
155	9.5	Interlocks	204
156	9.6	Fast Beam Condition Monitors Replacement	205
157	9.6.1	Improvements to the BCM1F in the technical stop 2011/12	205
158	9.6.2	The 2011/12 Shutdown	205
159	9.6.3	The 2016 Shutdown	205
160	9.6.4	Pad Detectors using GaAs Sensors	205
161	9.7	Beam Scintillator Counters Replacement	206
162	9.7.1	Functionality of the Current BSC System	207
163	9.7.2	Environmental Conditions	209
164	9.7.3	Performance of the BSC Minimum Bias Triggers	212
165	9.7.4	Available Locations	214
166	9.7.5	Read-Out System	215
167	9.7.6	Proposed Prototype System	216
168	9.7.7	Summary and Milestones for Beam Scintillator Counters Upgrade	218
169	9.8	Pixel Luminosity Telescope	219
170	9.8.1	Diamond Pixel Sensors	219
171	9.8.2	Readout	221
172	9.8.3	Performance	223
173	9.8.4	Test Beam Results	223
174	9.8.5	Status	223
175	9.8.6	Installation Plan	224

176	9.9	Beam Position Timing for the Experiments	224
177	9.10	Validating and Updating the CMS Cavern Simulation: LHC RADMON, Medipix,	
178		Neutron Detectors, Passives and Activation Measurements	225
179	9.10.1	Data from currently installed neutron monitors	225
180	9.10.2	Proposed Improvements to Slow Monitoring	225
181	9.10.3	Passives	226
182	9.11	Required Resources: Manpower Requirements, Schedule, and Expression of In-	
183		terest By Institutes	226
184	9.11.1	Manpower requirements	226
185	9.11.2	Proposed Schedule	227
186	9.11.3	Expression of Interest by institutes	227
187	10	CMS Common Systems, Infrastructure and Facilities	229
188	10.1	Introduction	229
189	10.1.1	Overview of the CMS Common Systems	229
190	10.1.2	Funding	230
191	10.2	Safety Systems	231
192	10.2.1	General safety	231
193	10.2.2	Detector Safety System (DSS)	231
194	10.2.3	Sensor systems	231
195	10.2.4	Nitrogen, dry air and compressed air	232
196	10.2.5	Fire prevention: detection, and extinguishing	232
197	10.2.6	Radioprotection precautions, measuring devices and equipment trace-	
198		ability	232
199	10.2.7	Access control	233
200	10.2.8	Safety training	233
201	10.3	Magnet Consolidation and Upgrade	234
202	10.3.1	Introduction	234
203	10.3.2	Power systems	234
204	10.3.3	Vacuum pumping systems	234
205	10.3.4	Safety and control systems (MSS, MCS)	234
206	10.3.5	Cryogenic systems	235
207	10.3.6	Miscellaneous	235
208	10.3.7	Field measurement and mapping	236
209	10.4	Yoke, Shielding, and Moving Systems	236
210	10.4.1	YE4 Disks	237
211	10.4.2	Radiation shielding	238
212	10.4.3	Forward Region	239
213	10.5	Experimental Beampipe	240
214	10.6	Logistics and Integration	243
215	10.6.1	Cranes and rigging equipment	243
216	10.6.2	Tooling and Working platforms	243
217	10.6.3	Logistics support teams	244
218	10.6.4	Engineering Integration	245

219	10.6.5	Electronic and Electrical Integration	246
220	10.7	Experiment Service Infrastructure	247
221	10.7.1	Responsibilities	247
222	10.7.2	Consolidation and Upgrade	247
223	10.7.3	Cooling Systems	247
224	10.7.4	Electrical Distribution	249
225	10.7.5	Heating, Ventilation and Air Conditioning (HVAC)	250
226	10.8	Beam, radiation, cosmic ray or environmental test facilities	250
227	10.8.1	Introduction	250
228	10.8.2	Better understanding of the existing detector	251
229	10.8.3	R&D for Consolidation and Upgrade	251
230	10.9	Surface assembly buildings, workshops, laboratories, and storage space	254
231	10.9.1	Introduction	254
232	10.9.2	Operation Support Centre (OSC) at Point 5	255
233	10.9.3	Building 904, Preveessin	258
234	10.9.4	Other facilities	261
235	10.10	Planning and Coordination	261
236	10.10.1	Organization	261
237	10.10.2	LHC planning 2010-2016	262
238	10.10.3	General constraints on planning	263
239	10.10.4	Shutdown 2012-13	265
240	10.10.5	Technical stops 2013-14 (if applicable) and 2014-15	266
241	10.10.6	Shutdown 2016	266
242	11	Cost, Schedule, and Management	269
243	11.1	Cost	269
244	11.2	Schedule	269
245	11.3	Management Structure	272
246	11.3.1	Organizational Principle	273
247	11.3.2	Phase 1 Upgrade Construction Project Manager	273
248	11.3.3	Phase 1 Upgrade Construction Project Deputy Program Managers	274
249	11.3.4	Phase 1 Upgrade Construction Technical Coordinator	274
250	11.3.5	Interaction among the CMS Spokesperson, CMS Technical Coordinator, and Upgrade PM	275
251			
252	11.3.6	Upgrade Subsystem Project managers	275
253	11.3.7	Cross Subsystem Coordinators	277
254	11.3.8	CMS Phase 1 Upgrade Construction Project Office	277
255	References		281
256	A	Phase 2 R&D	285
257	A.1	The Phase 2 Tracker Upgrade	285
258	A.1.1	Introduction	285
259	A.1.2	Sensor development	286

260	A.1.3	ASIC development	288
261	A.1.4	Data links	290
262	A.1.5	Power distribution	292
263	A.1.6	CO ₂ cooling	293
264	A.1.7	Modules with trigger functionality	293
265	A.1.8	Detector concepts	297
266	A.1.9	Outlook	298
267	A.2	Calorimetry in the High Luminosity LHC Era	299
268	A.2.1	Introduction	299
269	A.2.2	Barrel Electromagnetic Calorimeter in the HL-LHC Era	300
270	A.2.3	Forward Calorimetry in the HL-LHC Era	302
271	A.3	Muon System Phase 2 Upgrades	306
272	A.3.1	R&D Issues for the Muon Drift Tubes in Phase 2	306
273	A.3.2	RPC Phase 2 Upgrades	309
274	A.3.3	CSC Phase 2 Upgrades	310
275	A.4	Trigger R&D for Phase 2	310
276	A.4.1	Introduction	310
277	A.4.2	Upgrade Phase 2 Trigger Strategy	310
278	A.4.3	Upgrade Phase 2 Track Trigger R&D	311

DRAFT

DRAFT

279 Chapter 1

280 Introduction

281 The CERN Large Hadron Collider (LHC) is designed to reach a luminosity of $10^{34} \text{ cm}^{-2} \text{ s}^{-1}$
282 at a center of mass energy of 14 TeV. It is already the world's highest energy particle collider
283 and opening a new frontier in particle physics. When it achieves its design performance, ex-
284 periments will be able to fully probe the TeV energy scale relevant to electroweak symmetry
285 breaking and the Higgs phenomenon and increase significantly the discovery reach for super-
286 symmetry, extra dimensions of space and time, and other "Beyond the Standard Model (BSM)"
287 physics. This is expected to lead to an unparalleled opportunity for discovery and a revolution
288 in our understanding of particle physics.

289 The LHC began operation in late 2009 and is now producing collisions at 7 TeV center of mass
290 energy until the end of 2011. In July of 2010, CERN released a technical plan for LHC operations
291 describing the expected luminosity growth over the next two decades. This twenty year period
292 divides roughly into two equal parts:

293 **Phase 1** In this period, which started in March of 2010 and extends until 2020, the LHC will
294 achieve its design energy and luminosity. Towards the end of this period, the luminosity
295 should increase beyond the original design value to over $2 \times 10^{34} \text{ cm}^{-2} \text{ s}^{-1}$. Two major
296 shutdowns of longer than a year each will be needed to accomplish these objectives. Im-
297 provements and upgrades to some CMS sub-detectors will be necessary to fully exploit
298 the luminosity, especially towards the end of this phase. The two long LHC shutdowns
299 provide the access to the CMS collision hall needed to make improvements. The pixel de-
300 tector will be replaced and the trigger upgraded in 2016 but CMS will utilize the present
301 outer microstrip tracker throughout the Phase 1 period.

302 **Phase 2:** After 2020, there will be a major machine upgrade with an extended shutdown to
303 achieve considerably higher annual integrated luminosity, perhaps by a factor of 5, over
304 that achieved in the last part of Phase 1. At the same time as the accelerator is upgraded,
305 the experiment will also undergo major transformations to handle the higher luminosity.
306 In particular, CMS will completely replace the tracking detector and will make many
307 other changes to sub-detectors and the trigger and data acquisition systems.

308 It is the goal of CMS always to have a detector capable of profiting fully from the LHC perfor-
309 mance. Each shutdown for machine upgrades provides an opportunity to carry out improve-
310 ments to make the experiment more efficient, to repair problems uncovered during operations,
311 and to upgrade the detector to cope with the luminosity that will be achieved during the sub-
312 sequent running period.

313 This Technical Proposal presents the improvements, replacements, and upgrades to the detec-
314 tor to optimize CMS performance during Phase 1 of LHC operations and thereby maximize

315 its physics output. The work foreseen involves muon detectors, hadron calorimeters, the pixel
316 detector, the trigger and data acquisition, and the beam radiation monitoring and luminosity
317 measurement system. A series of improvements to CMS infrastructure will ensure efficient
318 implementation of the upgrades and maintenance of the upgraded detectors.

319 This proposal is based on the following key inputs:

- 320 1. the CERN “10 Year Technical Plan” for LHC operations presented in July of 2010, which
321 specifies shutdown periods allowing changes to the detector;
- 322 2. the challenges that arise from higher luminosities and the practical issues of maintaining
323 the detector for a decade or more;
- 324 3. the design of the CMS detector, its actual performance so far, and its projected perfor-
325 mance as the instantaneous luminosity rises above the design value and as the integrated
326 luminosity increases; and
- 327 4. practical considerations of how to modify an operating detector, which could be par-
328 ticipating in a “discovery in progress”. Example issues are the inability to make major
329 changes to the on-detector infrastructure, problems of working in an irradiated environ-
330 ment; the beam time sacrificed to commission a new detector, which must be compared
331 with the gains from superior performance of the replacement; and the risk of causing
332 damage while making modifications.

333 The outline of this Technical Proposal is as follows: First a brief description of CMS detector is
334 given, emphasizing features relevant to this proposal. In the remaining sections of this intro-
335 ductory chapter, the items enumerated above are discussed. There follows a brief summary of
336 each of the subdetector upgrade programs. In chapter 2, the physics motivation for the Phase
337 1 upgrade is outlined and selected sub-detector performance plots presented to demonstrate
338 benefits gained from the upgrades; this chapter should be viewed as a work in progress, as will
339 be explained. Chapter 3 presents the proposal for the upgrade for the CMS muon detection
340 subsystems. Chapter 4 presents the upgrades to the hadron calorimeters at low pseudorapidity
341 (less than 3). Chapter 5 discusses improvements to the calorimeters in the high pseudorapidity
342 regions. Chapter 6 presents the upgrade of the pixel detector, the only part of the CMS Tracker
343 that can be modified during Phase 1. Chapters 7 and 8 explain the changes required by the Trig-
344 ger and Data Acquisition systems to handle higher instantaneous rates and larger event sizes
345 arising from increased event pileup and larger channel counts that will be present towards
346 the end of Phase 1. Chapter 9 describes improvements to the beam monitoring system, which
347 protects the detector from beam-related accidents, provides inputs to the zero and minimum
348 bias triggers, measures the luminosity, and produces many measurements of beam quality and
349 beam-related backgrounds that are fed back to the accelerator teams. Chapter 10 discusses in-
350 frastructure improvements and facilities necessary for sustained operation and commissioning
351 of upgraded detectors before installation into CMS. Finally, chapter 11 provides a preliminary
352 schedule and a provisional estimate of the total cost.

353 To complete the picture, an appendix explains the R&D required for the Phase 2 upgrade,
354 which must proceed in parallel with Phase 1 developments in order to have upgraded detectors
355 ready for installation soon after 2020. The Phase 2 upgrades represent a serious challenge as
356 requirements are in many ways more difficult than those of Phase 1.

1.1 A brief introduction to CMS

An exploded view of CMS is shown in Fig. 1.1. CMS was assembled on the surface in sections that were lowered 100m through a large shaft into the collision hall. At the heart of the experiment is a 13m long, 6m diameter, 4T superconducting solenoid providing large bending power (12 T-m) for tracking measurements and whose return field is large enough to saturate the 1.5 m iron plates in the return yoke, used for muon track reconstruction. The gaps between the plates provide slots for the four muon tracking stations, each of which consists of several layers of aluminum drift tubes (DT) in the barrel region and cathode strip chambers (CSCs) in the endcap region. Each system is complemented by resistive plate chambers (RPCs).

The bore of the magnet is large enough to accommodate the inner tracker and the calorimetry systems. The tracking volume is contained in a cylinder of 5.8m length and 2.6 m diameter. CMS employs ten layers of silicon microstrip detectors, which provide the required granularity and precision to reconstruct efficiently high multiplicity events. The silicon microstrip tracker with its long bending path, combined with the strong solenoidal field, provides excellent momentum resolution. In addition three layers of silicon pixel detectors in the barrel region, complemented by two forward disks at each end, seed the track reconstruction and improve the measurement of the impact parameter measurements, as well as providing points to reconstruct secondary vertices.

The electromagnetic calorimeter (ECAL) provides coverage up to $|\eta| = 3$ and uses lead tungstate (PbWO_4) crystals whose scintillation light is detected by silicon avalanche photodiodes (APDs) in the barrel and vacuum phototriodes (VPTs) in the endcaps. A preshower system is installed in front of the endcap ECAL for π^0 rejection.

The ECAL is surrounded by a brass/scintillator sampling hadron calorimeter (HCAL) with coverage up to $|\eta| < 3$. The light is converted by wavelength shifting (WLS) fibres embedded in the scintillator tiles and channeled via clear fibres to hybrid photodiodes (HPDs) that provide some gain and can operate in high axial magnetic fields. This central calorimetry is complemented by a “tail-catcher” (HO) in the barrel region insuring that hadronic showers are sampled with nearly eleven interaction lengths. Coverage up to $\eta = 5$ is provided by an iron/quartz-fibre calorimeter (HF). The Cherenkov light emitted in the quartz fibres is detected by photomultipliers. The HF ensures full geometric coevidence for measurement of the transverse energy in the event. Two additional calorimeters, not shown in Fig. 1.1, provide coverage at even higher rapidities than the HF.

The modular construction of CMS is the key element for maintenance and provision of access for detector upgrades. The solenoid and the central yoke block, called YB0, are the only fixed structures in CMS. The other large slices through the experiment, either “rings” or “disks”, all move to permit access to the interior. The endcap disks can be pulled back and separated for access to the CSCs and endcap RPCs. The rings of the solenoid return yoke can be separated to provide access to the muon DTs. With the disk pulled back, it is possible to access the endcap HCAL, ECAL, and preshower, all of which are mounted on the disk closest to the Interaction Point. Also, with all disks retracted, there is access to the vacuum tank region. It is possible to remove the pixel detector, which is inserted in two halves around the beam pipe. This was a requirement because of the need to bake out the beam pipe. The pixel detector can be removed or reinstalled in a few days.

While the ECAL, HCAL and Silicon Strip tracker slide on rails, they cannot easily be extracted because it would require removal of a very large number of power and control cables, optical fibers and cooling pipes. However, the front end electronics of the HCAL is accessible when the

403 vacuum tank is opened. The front end electronics of the HO is accessible when the return yoke
 404 rings are separated. The HF can be lowered and moved to a special garage for maintenance.
 405 Finally, CASTOR and the Zero Degree Calorimeter (ZDC) can be removed from the beam line
 406 by cranes.

407 CMS is triggered by dedicated custom electronics located in an underground control room
 408 USC55, which forms various partial triggers using trigger primitives from the front ends of
 409 the calorimeters and muon detectors. These are then sent to the Global Level 1 trigger, which
 410 processes up to 40 million beam crossings per second and can accept up to 100,000 of them
 411 for further processing. The latency of the Level 1 trigger is $3.6 \mu\text{s}$ and data must be stored on
 412 the detectors during this time. When a Level 1 Accept occurs, data fragments from individual
 413 detectors are sent to the High Level Trigger (HLT), operating on a large computer cluster to
 414 build complete events. The HLT performs a lean version of the offline reconstruction using full
 415 event data and uses the result to decide if the event should be written, together with trigger
 416 information, to mass storage for subsequent analysis. CMS writes out up to 300 events/second.

417 A detailed description of the CMS detector is given elsewhere [1].

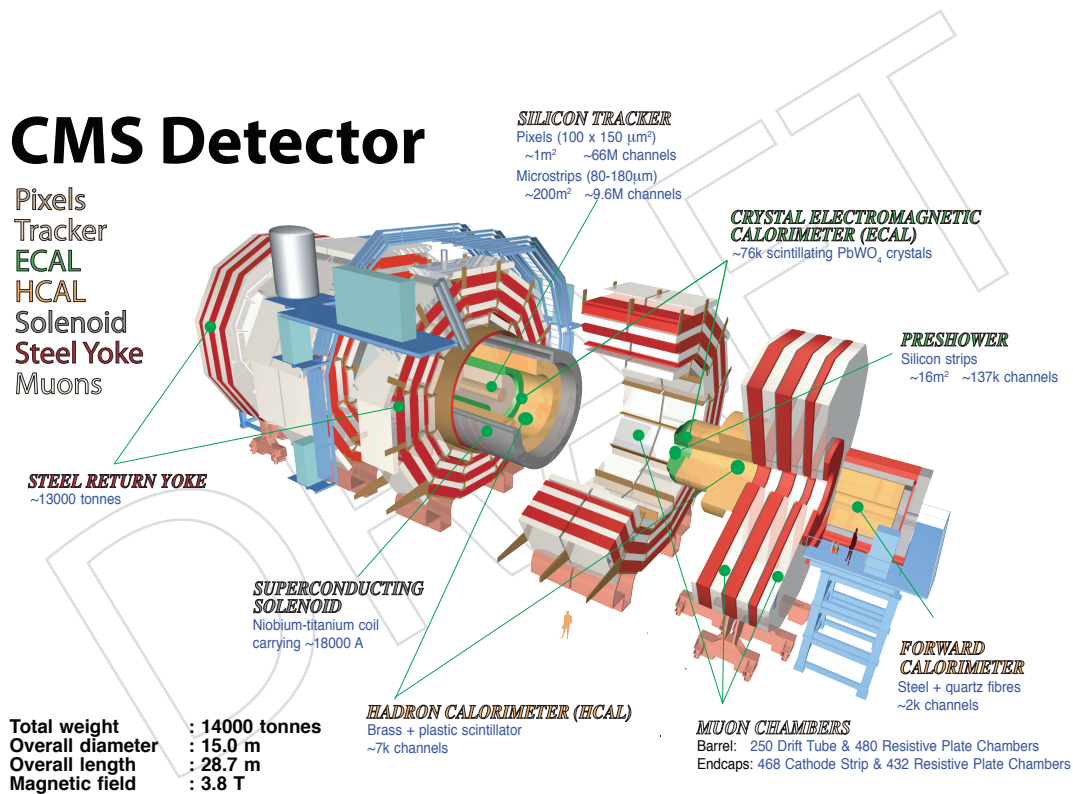


Figure 1.1: A schematic representation of the CMS Detector, with its various sections in retracted positions. The central yoke block is called YB0. The next yoke block 1 (YB+1, with a corresponding YB-1 on the other side of YB0), is shown partially moved away from YB0. The yoke block 2 (YB+2, with a corresponding YB-2 on the other side) is shown fully moved past the vacuum tank of the solenoid. The endcap calorimeters are shown attached to endcap disk YE+1, then the endcap CSCs and RPCs, then YE+2, more muon chambers, and YE+3, with additional muon chambers on the front and back. Eventually, another disk, YE+4 will be added at the end to provide shielding from beam-related backgrounds. This configuration is repeated on the other end, with designations now changed to YE-1, YE-2, YE-3, and eventually YE-4. In operation, the detector is closed by moving all the pieces together.

418 **1.2 The CERN “10 Year Technical Plan” for operation of the LHC**

419 The CERN 10 Year Technical Plan is shown schematically in Fig. 1.2. It has long periods of
 420 collider operation interleaved with shutdowns of a little more than a year each in 2012 and
 421 2016. The major intervals are:

422 **2010-2011: 7 TeV operation** to commission the LHC and the experiments and make early mea-
 423 surements of physics at this energy;

424 **2012: shutdown** to repair magnet splices to allow the LHC to operate safely at 14 TeV and to
 425 improve collimation to permit operation at high luminosity;

426 **2013-2015: 14 TeV run** to explore Terascale physics at moderate luminosity within the capabil-
 427 ity of existing detectors;

428 **2016: shutdown** to improve collimation in the LHC to enable operation at highest Phase 1 lu-
 429 minosities; to prepare the LHC for the addition of Crab Cavities and RF cryo-systems
 430 needed for Phase 2; to connect Linac4 into the injector complex; and to upgrade the en-
 431 ergy of the PS Booster to reduce the beam emittance; and

432 **2017- 2020: 14 TeV high luminosity run** to more thoroughly explore Terascale physics and to
 433 study in more detail new phenomena observed in the preceding runs using the upgraded
 434 detectors.

The 10 year technical Plan

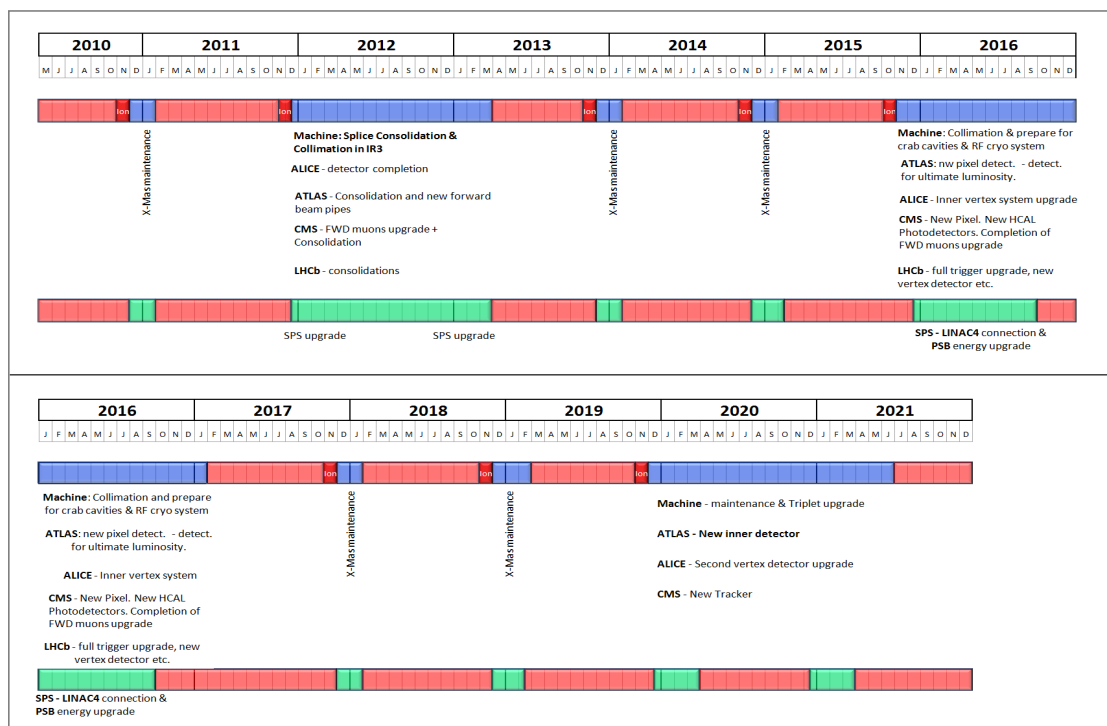


Figure 1.2: CERN technical plan for operations over the next decade announced in July 2010.

435 The LHC goal for peak instantaneous luminosity defines the number of interactions per beam
 436 crossing that the experiments must handle; and the goal for integrated luminosity determines

437 how radiation-resistant the detectors must be. The expected luminosity of the LHC is shown in
 438 Figs 1.3 and 1.4. Towards the end of Phase 1 the LHC will run at or above the original LHC
 439 design luminosity of $1 \times 10^{34} \text{ cm}^{-2} \text{ s}^{-1}$; about 80% of the total Phase 1 integrated luminosity will
 440 be delivered in the three year run starting in 2017. About half of the total will be delivered in
 441 annual periods with a peak luminosity **above** what the detectors were designed to handle. The
 442 two long shutdowns provide CMS with the opportunity to make improvements to cope with
 443 the evolution of the machine performance.

Year	TeV	OEF	β^*	Nb	lb	ltot	MJ	Peak luminosity	Pile up	pb-1/day	Physics Days	Integrated (fb-1/year)	Total Int (fb-1)
2010	3.50	0.20	2.00	796	8.0E+10	6.4E+13	36.0	1.886E+32	1.2643	3.3	20.0	0.1	0.07
2011	3.50	0.25	2.00	796	8.0E+10	6.4E+13	36.0	1.886E+32	1.2643	4.1	240.0	0.98	1.04
2012												0.0	1.0
2013	6.50	0.20	0.55	796	1.15E+11	9.2E+13	96.1	2.632E+33	17.6429	45.5	180.0	8.2	9.2
2014	7.00	0.20	0.55	1404	1.15E+11	1.6E+14	182.5	5.000E+33	19.0000	86.4	240.0	20.7	30.0
2015	7.00	0.20	0.55	2808	1.15E+11	3.2E+14	365.0	1.000E+34	19.0000	172.8	210.0	36.3	66.3
2016											0.0	0.0	66.3
2017	7.00	0.25	0.55	2808	1.15E+11	3.2E+14	365.0	1.000E+34	19.0000	216.0	240.0	51.8	118.1
2018	7.00	0.28	0.55	2808	1.50E+11	4.2E+14	476.1	1.701E+34	32.3251	411.6	240.0	98.8	216.9
2019	7.00	0.30	0.55	2808	1.70E+11	4.8E+14	539.6	2.185E+34	41.5198	566.4	210.0	118.9	335.8
2020											0.0	0.0	335.8
2021	7.00	0.20	0.30	2808	1.70E+11	4.8E+14	539.6	4.006E+34	76.1197	692.3	150.0	103.8	439.7
2022	7.00	0.27	0.25	2808	1.80E+11	5.1E+14	571.3	5.390E+34	102.4060	1257.3	220.0	276.6	716.3
2023	7.00	0.27	0.25	2808	1.80E+11	5.1E+14	571.3	5.390E+34	102.4060	1257.3	220.0	276.6	992.9
2024	7.00	0.29	0.25	2808	1.80E+11	5.1E+14	571.3	5.390E+34	102.4060	1350.5	220.0	297.1	1290.0
2025	7.00	0.29	0.25	2808	1.80E+11	5.1E+14	571.3	5.390E+34	102.4060	1350.5	220.0	297.1	1587.1
2026	7.00	0.29	0.25	2808	1.80E+11	5.1E+14	571.3	5.390E+34	102.4060	1350.5	220.0	297.1	1884.2
2027	7.00	0.29	0.25	2808	1.80E+11	5.1E+14	571.3	5.390E+34	102.4060	1350.5	220.0	297.1	2181.3
2028	7.00	0.29	0.25	2808	1.80E+11	5.1E+14	571.3	5.390E+34	102.4060	1350.5	220.0	297.1	2478.4
2029	7.00	0.29	0.25	2808	1.80E+11	5.1E+14	571.3	5.390E+34	102.4060	1350.5	220.0	297.1	2775.5
2030	7.00	0.29	0.25	2808	1.80E+11	5.1E+14	571.3	5.390E+34	102.4060	1350.5	220.0	297.1	3072.6

13

Figure 1.3: The expected luminosity for each year of LHC operations between 2010 and 2020. Shown are the energy per beam in TeV ; the operational efficiency fraction (OEF); the β^* at the CMS/ATLAS IRs in meters; the number of colliding bunches (Nb) in each beam; the number of protons (lb) in each bunch; the total number of protons in each beam (ltot); the energy in each beam (MJ); the peak luminosity in $\text{cm}^{-2}\text{s}^{-1}$; the pile up, that is the average number of interactions per crossing at the peak luminosity; the luminosity/day in pb^{-1} ; the number of days of running for physics; and the integrated luminosity/year in fb^{-1} . The last column shows the integrated luminosity from the beginning of the LHC program in 2010 in fb^{-1} .

444 Following the 10 year Phase 1 period, there will be a long shutdown for further improvements
 445 to the LHC to enable it to produce up to 300 fb^{-1} per year. This will be a new era characterized
 446 by ultra-high luminosity. The detectors, including the main tracking systems, must be rebuilt
 447 to deal with the extreme radiation levels and large numbers of interactions per beam crossing.
 448 There follows another ten years of operation at this new higher luminosity. During "Phase 2"
 449 of LHC Operation the experiments would integrate up to 3000 fb^{-1} , allowing them to complete
 450 their exploration and study of physics at the Terascale. The construction of detectors that can
 451 operate in Phase 2 is beyond the scope of this document except for the appendix on upgrade
 452 R&D noted above.

Preliminary Long Term Predictions

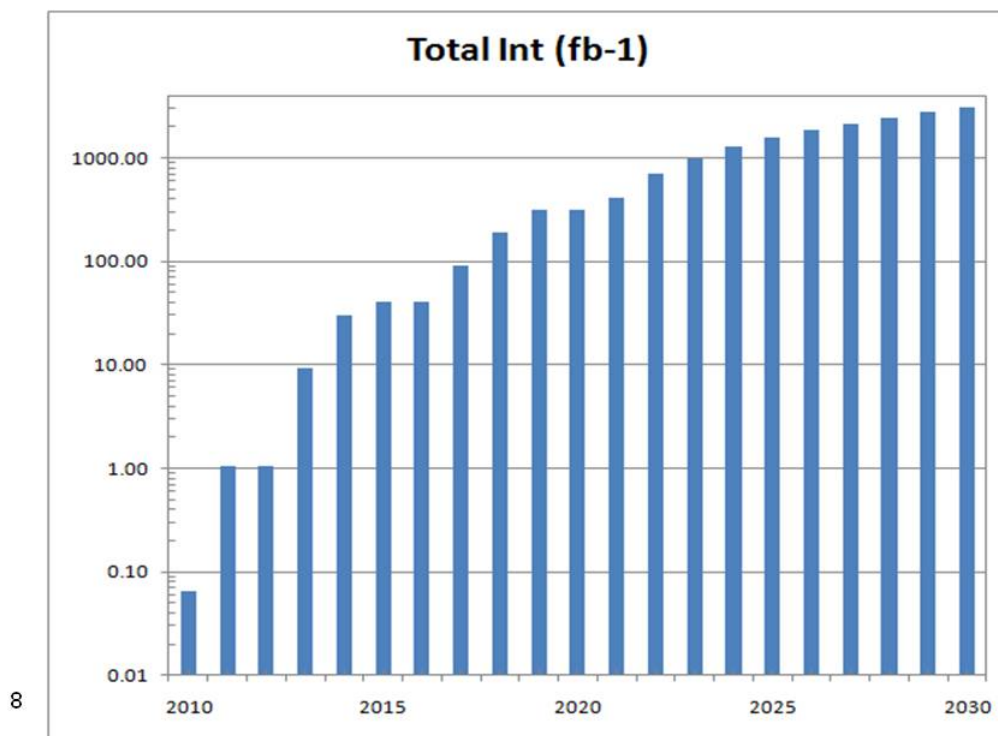


Figure 1.4: Log plot of the integrated luminosity as a function of year from 2010 to 2030

1.3 Challenges Addressed by the Phase 1 Upgrade Plan

At the end of the Phase 1 period, the peak luminosity is expected to exceed what CMS was designed for by a factor of two. Here follows a brief summary of the problems that must be addressed to operate successfully throughout Phase 1. Chapters 3-9 provide the details of the sub-detector challenges to be addressed, many of which are related to operating at high luminosity.

1.3.1 Issues related to collisions

1.3.1.1 Issues related to instantaneous luminosity

Bunches of approximately 1.15×10^{11} protons collide in the LHC every 25ns. About 20 interactions take place each crossing when the luminosity is $10^{34} \text{ cm}^{-2} \text{ s}^{-1}$, for which 2808 bunches are required, and 40 interactions/crossing towards the end of Phase 1, using an increased number of protons. The occurrence of many interactions in a crossing is called "pileup".

Most of the interactions are "soft" or "peripheral" interactions which do not make high mass states or contribute to the study of Electroweak or BSM physics. Very rarely a "hard collision" capable of making a high mass state and therefore of interest occurs. The CMS trigger recognizes such events (actually the crossing containing the event) and preserves it for subsequent analysis. For successful analysis, the detector must discriminate well between hard and soft collisions, which is more difficult in the presence of pileup. Dealing with pileup as the peak luminosity increases above the original design value is the motivation for several of the upgrades.

473 High instantaneous luminosity can confuse the CMS Level 1 trigger. To keep up with the
474 40MHz rate, it uses partial data from events in each beam crossing and dedicated, custom
475 hardware. With 20-40 interactions superimposed, and with only some of the information avail-
476 able, trigger performance will degrade at very high luminosity. Upgrades to the muon system
477 and the hadron calorimeters aim to preserve the Level 1 trigger capability by providing it with
478 more and higher quality inputs.

479 The CMS Higher Level Trigger that follows Level 1 has access to the full event data and is
480 performed on a large computer cluster so it is better able to cope with the confusion caused by
481 high pileup.

482 Pileup can also confuse the analysis. Interactions are distributed along the collision region over
483 several cm in z (direction parallel to the beams). CMS tracking has z -resolution better than a
484 1 mm and should usually associate charged tracks correctly to individual separated vertices,
485 although efficiency will worsen in extreme conditions. However, calorimeters lack precise di-
486 rectional capability and hence cannot associate neutral particles, which appear as deposits of
487 energy, with vertices. Hence some confusion and overlap between various interactions in the
488 crossing is inevitable.

489 Fortunately, most soft interactions deposit very little energy in the CMS calorimeters and many
490 of the events of real physics interest deposit large amounts. Discrimination using transverse
491 energy thresholds requires clear separation of high energy deposits in the calorimeters from
492 lower energies in surrounding regions, referred to as "isolation". Energy sums are constructed
493 using data from considerable areas of ECAL, especially for jets, and the ability to separate
494 energy clusters inevitably worsens in the presence of pileup owing to the presence of more
495 neutral pions. Some improvements can, nevertheless, be made to the calorimeters to improve
496 trigger performance.

497 The pileup discussed previously is from interactions in the same crossing as the interesting,
498 triggered event, referred to as "in-time-pileup." "Out-of-time pileup" refers to the case when
499 signals from a preceeding or following crossing contaminate the triggered crossing. This can
500 happen because the intrinsic response of the sensor, or electronics is longer than the 25 ns bunch
501 crossing interval. If the occupancy of a given channel is small, there is unlikely to be another
502 particle available to contaminate the triggered bunch. Increasing the segmentation of a detector
503 is one way to combat out-of-time pileup. Another method is to carry out more sophisticated
504 time analysis to try to unravel signals overlapping in time. Each of these tactics is employed in
505 the proposed upgrades.

506 Other sources of out-of-time pileup also exist. These include signals from very slow particles,
507 mainly neutrons, that have scattered multiple times in the detector and may eventually deposit
508 energy in an active element.

509 1.3.1.2 Integrated luminosity

510 Ionizing radiation in CMS also damages the detectors, so that over time the signals may decline
511 and the noise levels may rise, compromising the performance by degrading the resolution or
512 efficiency. Detectors may become less effective at detecting real signals and more vulnerable to
513 creating fake ones with obvious consequences for the overall physics capability of CMS.

514 The understanding of radiation damage mechanisms in particle detectors and the development
515 of radiation hard or radiation tolerant sensors and electronics was a major R&D effort for the
516 LHC experiments. Most CMS detectors can sustain the integrated luminosity of Phase 1 with
517 at most slight degradation.

518 There are two cases where radiation damage is sufficiently severe that it might be necessary to
519 replace damaged detectors before Phase 2: one is at the inner radius of the Forward Hadron
520 Calorimeter (HF) which receives very large doses that will reduce the transmission of the win-
521 dows of the Photomultiplier Tubes (PMTs); the other is the inner layer of the barrel pixel de-
522 tector which is only 4 cm from the colliding beams. The strategy to deal with these detectors is
523 discussed in chapters 5 and 6, respectively.

524 1.3.2 Issues related to non-collisional background

525 There are backgrounds from sources other than proton collisions at the interaction point, such
526 as

- 527 • **beam halo:** particles that migrate out of the beam and strike material such as a beam
528 pipe or collimator and eventually produce muons that leave the LHC beam pipe and
529 spread out. These particles are especially troublesome to large area systems such as
530 the muon detectors.
- 531 • **beam-gas interactions:** protons in one of the beams can hit a residual gas molecule
532 inside the vacuum pipe. The collision products may reach the detector on a direct
533 path or may strike other material producing more secondaries that eventually reach
534 the detector.
- 535 • **cosmic rays:** cosmic rays are always passing through the detector. Occasionally, they
536 will occur in time with a trigger and may be recorded as part of the crossing data.
537 Some may pass through the pixel detector and mimic genuine tracks.
- 538 • **residual radiation:** the particles passing through CMS can activate the elements
539 of the detector producing various radionuclides. Their decay products may cause
540 signals in some detectors.

541 Most of these backgrounds can be rejected by topological or timing cuts and both. However,
542 sometimes especially in the case of cosmics, the background will mimic a real track and can
543 cause confusion to the analysis.

544 1.3.3 Other issues

545 1.3.3.1 Minimizing downtime

546 Downtime refers to periods when the LHC is producing collisions but CMS is not in a condition
547 to record them. Examples are problems with the trigger or data acquisition system or malfunc-
548 tioning interlocks that prevent the beam from being injected into the LHC. What counts for the
549 physics productivity is the integrated luminosity recorded with a physics capable detector. If
550 there is a failure, CMS should be able to recover from it quickly. In some cases, this means hav-
551 ing a good supply of working spares and being able to install them quickly. Improvements to
552 the detector and the experiment infrastructure to prevent failures that would cause downtime
553 or help recover from failures more quickly all contribute to a successful CMS physics program.
554 The relocation of electronics for the Drift Tube Muon trigger (Sector Collectors) from a high
555 radiation to a low radiation area is an example of an upgrade to eliminate a potential source of
556 failure. Many of the infrastructure improvements discussed in chapter 10 are aimed at reduc-
557 ing downtime. CMS has a requirement to reduce downtime below 10% and eventually as an
558 advanced goal below 5%.

1.3.3.2 Coping with Obsolescence

CMS construction started in the late 1990's. The technology in CMS dates back, in many cases, more than 15 years. Maintenance of the detector sometimes depends on the availability of spare components that have become obsolete and may be in short supply in coming years, which puts the operation of CMS and its physics program at risk. Possible problems must be identified and replacement electronics based on more modern and available technology must be designed and built or otherwise obtained.

1.3.3.3 Schedule uncertainty

The current schedule of shutdowns is tied directly to necessary and well-understood upgrades needed by the LHC with the biggest uncertainty probably at the transition between Phase 1 and Phase 2. One possible consequence could be that there is an indication of a physics discovery that might become conclusive with another factor of two in data, which would take about 2-3 years. If the detector or machine upgrades were behind schedule, not impossible given their complexity, it might make sense to continue to run. If that were to happen radiation damage would be an issue for the pixel detector and perhaps some other detectors. This makes it highly desirable that there be contingency in the expected lifetime of the detectors to deal with schedule variations, especially at the end of Phase 1.

1.3.3.3.1 Flexibility and agility of CMS Because of its modular design, CMS has some detectors that can be repaired or replaced in relatively short shutdowns of three to four months. The pixel detector was designed for fast installation, extraction, repair and re-installation; this has been demonstrated. The upgraded detector will be designed to facilitate rapid replacement of the first and even the second layers. If the pixel detector inner barrel layer needed to be replaced once more, it should be possible to do it with only a modest change to the LHC operating schedule. The endcap muon systems can be worked on also in short shutdown and the last disk, on which new detectors will be installed, can be worked on without opening the detector. Thus if the work to install the last endcap disk was not completed in the 2012 shutdown as planned, it could be completed during the short technical stops that occur in operations after the startup in 2013.

1.3.3.3.2 Preparing for the unexpected As experience is gained in operating the experiment, it is likely that experts will continue to identify improvements in performance that could be gained by making changes not foreseen in the original design, most of which was carried out far in the past. Recent examples are the small fraction of beam gas events whose secondaries are highly visible in the pixel detector, and the knock on recoil atoms in the ECAL APDs, whose impact on operation was larger than expected. They will now be taken into account in future ASIC or FPGA firmware developments. Another potential development concerns the accelerator where operation with 50 ns bunch spacing has been discussed as an effective means of reaching the highest luminosity. Such a change has serious impact on pileup and the performance of CMS should be carefully studied, as well as being taken into account in new ASIC designs, for e.g., the pixel system.

1.4 Issues arising from the design of the CMS detector and its actual and projected performance

By early November 2010, CMS had recorded $>40 \text{ pb}^{-1}$ of data. The peak luminosity was rising quickly and had reached over $10^{32} \text{ cm}^{-2} \text{ s}^{-1}$. Even at this low luminosity, CMS was able to

602 observe the whole known family of Standard Model particles and to begin serious physics
603 studies at 7 TeV. For some final states, it was able to look for physics beyond the Standard Model
604 with unprecedented sensitivity. Sub-detectors performed according to expectations in almost
605 all respects. Collision data agree very well with Monte Carlo simulations and the detector
606 behaves as expected. In particular, the pattern of photon conversions and nuclear interactions
607 in the data is well reproduced by the material distribution in the simulation.

608 With the luminosity acquired so far, radiation damage is not seen. However, because of the
609 way the LHC operated in this period, the detectors began to see “in time” pileup. The LHC col-
610 lides low-emittance bunches with 1.15×10^{11} protons every 25 ns. There will eventually be 2808
611 bunches colliding. The LHC quickly reached the design protons/bunch but did not squeeze
612 them to the final density at the interaction point. It was colliding only a little more than 300
613 bunches in CMS. Even so in this configuration, the collisions of pairs of bunches had a lumi-
614 nosity similar to what one would experience at $10^{33} \text{ cm}^{-2} \text{ s}^{-1}$. The average number of interac-
615 tions per crossing is now about 2; in the data collected so far we already have many crossings
616 containing 10 or more interactions. Hence, it is possible already to study the behavior of the
617 detector with “in-time” pileup.

618 Since the luminosity will grow in steps, many projections, justifications for the upgrades, and
619 design optimizations will continue to rely on the simulation studies and, in the case of radia-
620 tion damage, on exposure studies in low energy accelerators with intense beams. Validating
621 the simulations with collision data is presently underway so a set of runs to finalize the de-
622 tails of upgrade designs can be undertaken. Meanwhile, the current simulation is adequate to
623 demonstrate the value of the proposed upgrades.

624 1.5 Practical considerations for upgrading an operating detector

625 CMS adopted the strategy of assembling the major infrastructure components of the detector
626 - the solenoid and the iron return yoke, and the detectors - on the surface near the experiment
627 site, and to commission and operate them above ground first and then later to lower them
628 into the Collision Hall. This approach also guaranteed that CMS could be easily opened for
629 maintenance and upgrades.

630 The installation of the upgraded detector components (discussed later in this report) presents
631 a serious challenge that is discussed in chapter 10. However, the ability to open the detector
632 quickly at the beginning of a shutdown and the accessibility of many components once the
633 detector is opened provides CMS with the flexibility to incrementally upgrade the detector in a
634 series of shutdowns. Some detectors, however, are not readily accessible and upgrading them
635 within the planned shutdowns is not possible.

636 Considerations of accessibility shape the approach to the upgrades planned for CMS and pre-
637 sented in this document. Several other issues that shape the upgrade are discussed next.

638 1.5.1 Radiation Safety

639 The Point 5 area is now a radiation zone and there are access controls, restrictions on the re-
640 moval and storage of equipment, and requirements to track and document any such move-
641 ments. In addition, there is the potential for exposure to ionizing radiation and contamination
642 of the workers maintaining the detector, removing old equipment and installing new equip-
643 ment.

644 Even though activation levels are expected to be fairly low, CERN has rather stringent lim-

its on the exposure permitted to its staff and experimenters, very similar to those in effect at other accelerator laboratories and are well below the limits established for general radiation workers. This will limit the amount of time individuals can work on removal and installation activities. This problem will increase as the integrated and instantaneous luminosity rise for each run. Early installation of the upgrades is therefore highly desirable. Possible exposures must be considered in the planning process using the guiding principle of ALARA (“as low as reasonably achievable”) that requires that personnel exposures must be carefully monitored and minimized. Resources for the implementation of the ALARA principle and for safe decommissioning of equipment that is replaced must be accounted for either in this upgrade project or in the ongoing maintenance and operation of CMS.

1.5.2 Constraints to the Design of the Upgrades

The key constraints on the individual detector upgrades are

1. each must be capable of being installed in one of the two long shutdowns planned in 2012 and 2016 or in one of the short annual technical stops of 3 to 4 months that will occur between the major shutdowns and after 2016. CMS must be in a physics-ready state at the end of each shutdown;
2. the risk of physical damage to the detector due to upgrade activity must be minimized;
3. the risk to the physics program through excess startup time for physics or compromised performance must be minimized; and
4. radiation exposure and accident risk must be minimized.

One practical aspect of these requirements is that the upgraded detectors must use the existing services. These include cables for power and high voltage, cables and fibres for signals, controls and monitoring, gas lines, and piping for cooling fluids. All the cable trays and tubes that carry these utilities are essentially full. The cables, pipes and cable trays will also become activated. The extraction of long cables running through YB0 would be incompatible with constraints (1) and (4) and possibly (3). Electrical ratings for existing power cables must be respected or, in a few cases, derogations obtained.

Another practical constraint is that some detectors cannot be removed and replaced. The pixel detector was designed to be extracted during a short shutdown for beam pipe bake-out. However, the other detectors inside the solenoid - the silicon strip tracker, the ECAL and the HCAL - cannot be removed. What can be replaced in the case of the HCAL is the front end electronics which is accessible when the detector is opened. The muon detector is outside the solenoid and is accessible, especially the endcaps, which are part of this upgrade. The back end electronics are in the underground control room, USC55. The main issue there is to integrate new electronics without incurring down time or creating a discontinuity in the data quality and consistency.

1.5.3 Physics Issues

When the upgrades are ready to be installed, CMS will be a physics experiment in progress. Many important topics require large integrated luminosity. Since the data from many years will need to be combined in a consistent way, changes have to be introduced very carefully. The new detectors or electronics will be replacing well-understood devices that, even if they are beginning to degrade, may be participating in a discovery in progress. Under that circumstance, the new detector, in order to be inserted, must demonstrate

- 688 • that it is physics-ready and will take quality data quickly without a long period of
689 commissioning, alignment and calibration with collisions that would result in lost
690 data; and
- 691 • that the data from it can be combined with data taken before it is installed

692 Even then, if the experimenters feel a discovery is imminent and that data from the next run
693 are likely to confirm it, the collaboration might well be reluctant to change parts of the detec-
694 tor or the electronics, especially those used in the trigger. In order to avoid conflict over the
695 value of replacements, each upgrade detector must demonstrate significant benefits compared
696 to running with the detector it is replacing, each detector must be ready for physics with very
697 little loss of beam time, and the software for its integration into the analysis must be available
698 and tested when it is installed.

699 1.5.4 Implications for the Upgrades

700 This discussion above highlights the problems of making changes to an experiment in progress.
701 They can be addressed by adequate testing before insertion into CMS, by developing tested
702 and efficient installation procedures, quick and reliable alignment and calibration techniques,
703 and accurate cross calibration with the devices that are being replaced. Achieving these goals
704 requires good design and in many cases special test stands and procedures. Test beam se-
705 tups with substantial detector modules may be needed to cross calibrate replacement detectors
706 against existing ones. The costs of equipment, facilities, and activities needed to accomplish
707 this must be included in the project costs and planning.

708 In the case of the off-detector trigger electronics, new devices can be installed alongside the
709 ones they are replacing. By sending the new devices a copy of the input signals, the new
710 and the old system trigger decisions can be compared for identical results. Only when it is
711 established that the new components perform as well or better than the original ones can the
712 new devices be used in the experiment and the old devices removed. For all electronics, test
713 and burn-in facilities will be needed.

714 CMS addresses these issues by requiring early delivery of detectors to CERN, assembly, com-
715 missioning and operation above ground, including demonstrations using cosmic rays if possi-
716 ble. For off-detector trigger and data acquisition components, CMS requires detailed emulation
717 and a means of parallel operation of existing and upgrade components (using split signals or
718 copies of information packets). CMS also requires the provision of complete calibration and
719 alignment procedures available in advance, complete detector simulation packages, and com-
720 plete reconstruction programs. The procedure for installing the detector should be complete
721 and designed to minimize risks. Trial insertions in mock ups are performed if possible. Some
722 improvements to the infrastructure for carrying out installation activities in Point 5 will be un-
723 dertaken as part of the upgrade program and are described in Chapter 10. When all these
724 conditions, which are very demanding, are met, there should be consensus to install the new
725 detector.

726 1.6 Summary of the proposed detector upgrades and improve- 727 ments

728 The specific changes that the CMS Collaboration proposes to carry out between now and 2016
729 to optimize data taking during the Phase 1 operating period of the LHC are;

- 730 1. Muon System:

By 2015, the luminosity will reach $10^{34} \text{ cm}^{-2} \text{ s}^{-1}$. The in-time pileup will be right at the edge of the CMS design envelope and will present special challenges for the Muon System to trigger on muons with high transverse momenta, which represent one of the key indicators of interesting electroweak interactions.

(a) Cathode Strip Chambers (CSCs): The CSC upgrade is driven by considerations of the impact of peak instantaneous luminosity on the muon trigger.

i. Addition of a fourth layer of chambers (ME4/2) and associated readout and triggering electronics and services to reduce the accidental trigger rate and to preserve a low P_T threshold for the Level 1 Muon Trigger at high instantaneous luminosity;

ii. Upgrade of the layer 1 (ME1/1) electronics with a new CSC “Digital” Front End Board (DCFEB) so every strip can be read out separately (they are now ganged into groups of three). This will allow ME1/1 to continue to contribute effectively to the muon trigger at high instantaneous luminosity so CMS can retain four-plane coverage from $2.1 < |\eta| < 2.5$; and

iii. Deployment of new muon trigger primitive electronics to deliver the additional muon track segments, which will be produced at high luminosity and by the additional planes, to the upgraded CSC Trigger Track-Finder.

(b) Barrel Muon Drift Tubes (DTs): The work on the DTs is driven by maintenance considerations over the life of the experiment.

i. Generation of a supply of BTIM chips (DT front end trigger primitive chip) which are in short supply due to unexpectedly high mortality. This is achieved by replacing the Theta Trigger Boards by an FPGA-based board (or new ASIC) and recovering the BTIM chips from them; and

ii. Relocation of the Sector Collector boards from the periphery of the detector where they are exposed to radiation and high magnetic fields, and where the cooling is marginal to the Underground Control Room where the environment is more congenial.

(c) Endcap Resistive Plate Chambers (RPCs) The RPC upgrade is driven by considerations of peak instantaneous luminosity on the muon trigger.

i. Addition of a fourth layer of RPCs to extend coverage to $\eta = 1.6$ to preserve a low P_T threshold for the Level 1 Muon Trigger at high instantaneous luminosity

ii. R&D to develop detectors that can extend coverage to the region $1.6 < |\eta| < 2.1$ or even higher. Possible technologies include RPCs optimized to handle the high rate or Multi-Pattern Gas Detectors.

2. Hadron calorimeters:

This upgrade is directed at handling instantaneous luminosity, integrated luminosity, overall robustness and efficiency and providing opportunities to make improvements to the trigger at all luminosities.

(a) Calorimeters inside the CMS Solenoid (HB/HE/HO)

i. Replacement of the HPDs in all three detectors with an improved photodetector, the Silicon Photomultiplier (SiPM). SiPMs have better quantum efficiency, higher gain, and better immunity to magnetic fields than HPDs. Since SiPMs operate at relatively low voltages, they do not produce large pulses from high

775 voltage breakdown that mimic energetic showers like HPDs do. These features
776 of the SiPMS together with their low cost and compact size compared to HPDs
777 enable several major changes to the HCAL.

- 778 ii. Implementation of depth segmentation which has advantages in coping with
779 higher luminosities and compensating for radiation damage to the scintillators.
780 This is made possible by the use of SiPMS;
- 781 iii. Use of timing to clean up backgrounds, made possible by the extra gain and
782 better signal-to-noise of the SiPMS
- 783 iv. New backend electronics designed to provide enhanced information to the up-
784 graded Regional Calorimeter Trigger (RCT).

785 (b) Forward calorimeters

- 786 i. Replacement of the photomultipliers of the Forward Hadron Calorimeter with
787 new photomultipliers that have thinner glass windows and metal envelopes to
788 reduce the amount of Cherenkov light generated by charged particles passing
789 through the glass. The Cherenkov light from the glass creates large pulse heights
790 that look like energetic particles to the trigger and analysis. The new PMTS also
791 have 4-way segmented anodes that provide additional rejection of these spuri-
792 ous signals. These PMTs also have higher quantum efficiency so the resolution
793 of the HF will improve, and HF will last longer under irradiation. Timing elec-
794 tronics may eventually be installed to further reject backgrounds.
- 795 ii. Replacement of the PMTs of the CASTOR detector with more radiation tolerant
796 PMTs and improvement of the calibration and monitoring systems. In addition,
797 improvements will be made to CASTOR's mechanical support system so it will
798 not move when the CMS Solenoid is energized. This motion currently brings it
799 very close to the fragile LHC vacuum pipe.

800 3. Pixel System

801 The goal of the Phase 1 upgrade is to replace the present pixel detector with one that can
802 maintain a high tracking efficiency at luminosities up to $2 \times 10^{34} \text{ cm}^{-2}\text{s}^{-1}$. The present
803 pixel system was designed for operation with a maximum luminosity of $1 \times 10^{34} \text{ cm}^{-2}\text{s}^{-1}$.
804 Due to severe data losses in the read out chip (ROC), the present system will not sus-
805 tain the extreme operating conditions expected in Phase 1 after 2016. The replacement
806 is therefore planned in the long shutdown of 2016, which is the best and perhaps only
807 opportunity before the luminosity exceeds $1 \times 10^{34} \text{ cm}^{-2}\text{s}^{-1}$. The main features of the
808 upgraded detector are:

- 809 (a) Replacement of the current 3-layer barrel (BPIX), 2-disk endcap (FPIX) system with
810 a 4-layer barrel, 3-disk endcap system for four hit coverage.
- 811 (b) Ultra-lightweight support with CO₂ cooling and displacement of the electronic boards
812 and connections out of the tracking volume for material reduction.
- 813 (c) Development of a new readout chip with reduced data loss at higher collision rates
814 expected in Phase 1.
- 815 (d) Development of high bandwidth readout electronics and links as well as DC-DC
816 power converters, which allow reuse of the existing fibers and cables.

817 The addition of the fourth barrel layer at a radius of 16 cm and the third forward disks
818 will maintain the present level of tracking performance even in the high occupancy en-
819 vironment of the upgraded LHC. In addition, it provides a safety margin in case the

820 first silicon strip layer of the Tracker Inner Barrel degrades more rapidly than expected.
821 The upgraded pixel system will have a reduced mass, a reduced innermost radius and
822 increased lever arm, altogether resulting in a significant improvement over the present
823 system in terms of tracking, vertexing and b jet identification.

824 4. Trigger

825 The trigger system will migrate to a new technology which is more maintainable and
826 more flexible with respect to data interconnection than the current VME system. The
827 candidate is μ -TCA, which has become important in many commercial areas, including
828 telecommunications and other applications requiring high speed and bandwidth, and has
829 been used in the current version of the Global Calorimeter Trigger. The trigger upgrade
830 includes:

- 831 (a) Rebuilding the Regional Calorimeter Trigger (RCT) using advanced technologies,
832 such as μ -TCA to take advantage of the full granularity of the data available from the
833 calorimeter front end and to implement more sophisticated clustering and isolation
834 algorithms. This will permit the trigger to handle higher rates and more complex
835 events;
- 836 (b) rebuilding the CSC Trigger Track-Finder to accommodate the additional information
837 from ME4/2 and ME1/1, to use more input segments and to combine a greater vari-
838 ety of tracks to enhance performance amidst greater occupancy and backgrounds;
- 839 (c) Rebuilding the RPC track finder to accommodate the additional plane of RPCs;
- 840 (d) Modification of the DT track finder to accommodate the move of the Sector Collectors
841 and convert to the new trigger technology; and
- 842 (e) Eventual implementation of a new Timing and Trigger Control system based on
843 more modern technology.

844 5. Data Acquisition System

845 It will be necessary to increase the bandwidth of the DAQ by a factor of 2 to 5 to handle
846 the larger data volume produced at $2 \times 10^{34} \text{ cm}^{-2} \text{ s}^{-1}$ and the larger number of detector
847 channels. It will be achieved as a result of several major technological improvements.

- 848 (a) Several systems will have to be upgraded since the commercial components they
849 use will become obsolete and unobtainable;
- 850 (b) The complete Event Builder will have to be replaced in 2016 using more modern
851 technologies capable of handling the data volumes and rates that will be encoun-
852 tered after the shutdown; and
- 853 (c) The processors of the High Level Trigger must be replaced with faster processors to
854 handle the increasingly complex calculations that will be needed to select events.

855 6. Beam monitoring

- 856 (a) Construction of the Pixel Luminosity Telescope (PLT), a dedicated luminosity mon-
857 itor consisting of two sets, one on each side at ± 1.8 m from the interaction point, of
858 3 rings of 8 diamond pixel detectors. The detectors, which are at radius of 5 cm rela-
859 tive to the beams, are organized into 8 towers each giving a three-fold coincidences
860 when a particle from a collision traverses it. The detector is read out every beam
861 crossing. The number of three-fold coincidences is proportional to the luminosity.
862 The PLT also provides information about beam backgrounds and beam quality.

- 863 (b) Replacement of the Beam Scintillation Counters (BSC), which have been used to
864 provide minimum bias triggers and measurements of the beam background. The
865 current BSCs will suffer radiation damage and are not optimally designed for the
866 important role they are currently playing in CMS, which was not originally foreseen.
867 Several options are being considered.
- 868 (c) Replacement of BC1F, a diamond detector also near the location where the PLT will
869 go, that provides single bunch readout to identify pathological beam conditions,
870 such as serious beam losses. It will suffer radiation damage and will need to be
871 replaced in 2016. More radiation hard devices are being evaluated.

872 7. Common Systems, Infrastructure Upgrades and Facilities

873 There are now more than two years of experience in operating the CMS detector and
874 maintaining it. This operational experience has revealed a number of vulnerabilities that
875 can cause downtime that can result in data loss. There are also well-understood ways to
876 reduce the risk of opening the detector to do maintenance work or to install upgrades.
877 The activities to strengthen the infrastructure at Point 5 both above and below ground
878 and to develop the facilities needed to execute the upgrades, including assembly areas,
879 test beam setups, and commissioning and “burn-in” areas, are an important part of this
880 proposal.

881 CMS Common Systems include:

- 882 (a) safety systems for protection of personnel and equipment;
883 (b) the CMS solenoid and associated systems;
884 (c) yoke, shielding, and moving systems;
885 (d) the section of beampipe through the experiment;
886 (e) beam and radiation monitoring systems;
887 (f) equipment for support of logistics and integration;
888 (g) experiment services infrastructure – power, cooling, supply systems for various
889 gases, cabling, piping, networking, the various control rooms, and test facilities; and
890 (h) surface assembly buildings, workshops and laboratories.

891 Each of these is described and the need and plans for related upgrades and improve-
892 ments is explained. Organizations that provide resources crucial to the support of CMS
893 and the upgrade, including an “Engineering Integration Centre (ENIC)” and an “Elec-
894 trical systems Integration Centre (ELIC)” are discussed. Development of facilities at the
895 CMS surface assembly building, SX5, at Point 5, and a detector assembly and electronics
896 integration facility in Building 904 on the CERN/Preveessin campus are described.

897 1.7 Other Projects under Development in this Period

898 The CMS collaboration is composed of a large number of energetic, creative and knowledgeable
899 people. While the plans presented in this document form the core of the upgrade, there are
900 many additional ideas on how to improve the CMS detector or give it features that will enable
901 it to address new physics topics. These ideas are not as far along as the ones presented in this
902 Technical Proposal. In some cases, the CMS collaboration has not yet endorsed the physics
903 goals. In other cases, the R&D is at an early stage and technical feasibility has not yet been
904 established. The current set of projects under development but not yet approved parts of the

905 upgrade is summarized in a document that is available from CMS Upgrade management[2].
906 It is expected that some of these projects will become part of the Phase 1 upgrade; others may
907 fall by the wayside for technical, scientific, or financial (priority) reasons and still others may
908 be deferred until Phase 2. In addition, we expect still other projects to emerge and to follow a
909 similar path. This is all part of the life of a healthy scientific enterprise.

910 **1.8 The Challenge Ahead**

911 The remainder of this document presents in detail the proposed CMS Upgrade Technical Plan
912 for Phase 1 of LHC operations. It will be a challenge for the CMS collaboration to operate the
913 experiment and analyze the data while completing R&D and designs, and then constructing
914 and installing these upgrades. At the same time, work must continue on the R&D for the Phase
915 2 upgrade. However, the CMS detector has demonstrated in its early operation at the LHC that
916 it is a remarkable scientific device. The prospects of doing physics with hundreds and even-
917 tually thousands of inverse femtobarns of data taken with the upgraded CMS is wonderfully
918 exciting and will be well worth the effort!

DRAFT

920 **Physics Justification for the CMS Upgrade**

921 **Note:** *Work is still in progress to quantify the physics benefits of the CMS upgrade. As such this chapter*
922 *is not ready for review. Rather it presents physics object level summary for each of the proposed upgrades,*
923 *extracted from the subsequent chapters, in one place for convenience. The CMS simulation software*
924 *program is now being configured with the upgraded detector choices presented in this document. It will*
925 *be used for simulation studies in the coming months to fully prepare the physics case for the proposed*
926 *upgrades.*

927 CMS would have seen few tens of fb^{-1} luminosity at nominal center of mass energy by 2015.
928 It is quite likely that signatures of the Standard Model like Higgs and new physics at TeV
929 scale are already discovered. In that case, the physics program beyond 2016 will be primarily
930 for thorough exploration of Higgs sector and any new physics phenomena discovered earlier.
931 Whether CMS has discovered something or not, the program continues with searches for rarer
932 processes with higher mass objects, which requires higher luminosities.

933 The CMS detector is built for operations integrating several hundred fb^{-1} luminosity at instan-
934 taneous luminosities up to $1 \times 10^{34} \text{cm}^{-2} \text{s}^{-1}$ with 25 ns bunch spacing. . It was not designed to
935 operate at $2 \times 10^{34} \text{cm}^{-2} \text{s}^{-1}$ with 25 ns bunch spacing or at $1 \times 10^{34} \text{cm}^{-2} \text{s}^{-1}$ with 50 ns bunch
936 spacing. The completion of the muon system by completing the fourth station of chambers
937 restores the original muon trigger rate and efficiency goals under these more demanding con-
938 ditions. An upgrade of the calorimeter photo-detectors and electronics is needed to mitigate its
939 noise problems. An upgrade of the pixel system is needed to avoid serious data losses for 50
940 ns operation at design luminosity or at twice design luminosity with 25 ns bunch spacing. The
941 50-ns operation or potentially twice the instantaneous luminosity will require an additional
942 factor of two reduction in trigger rate to keep the thresholds at the same level as planned for
943 nominal operations, requiring a rebuilding of the trigger electronics. Besides meeting these
944 necessary goals, we intend to further enhance the CMS physics capability by benefiting from
945 the evolution in technologies since the time we originally built these parts of CMS.

946 The forward muons upgrades will provide additional muon hit measurements to provide
947 higher efficiency and resolution for muons in certain pseudo-rapidity regions, providing the
948 necessary control on the trigger rates in those regions, in addition to significant additional ac-
949 ceptance for muons at the trigger level. The upgraded hadron calorimeter has potential to
950 provide more robustness in handling pileup by the use of appropriate weights for its different
951 longitudinal depths in the upgraded system, improving the jet energy resolution, and pro-
952 viding better isolation of leptons. This will restore or even enhance the original targets for
953 performance of CMS. The upgraded pixel system will provide improved b -tagging, pixel track
954 seeding and stand-alone tracking capabilities, which will enhance CMS physics reach in ex-
955 ploring the Higgs, where b -jets and τ -leptons are often produced in association with the Higgs
956 boson or in its decays, and the SUSY sector where third generation sparticle masses are ex-

957 pected to be lighter resulting in enhanced production of b-jets and τ -leptons. The enhanced
 958 trigger system will provide necessary factor of two reduction in rate allowing CMS to operate
 959 at low enough lepton, especially τ -lepton, trigger thresholds to enable the study of the Higgs
 960 boson properties in both Standard Model and MSSM scenarios, and to better explore SUSY
 961 states. Somewhat improved signal efficiencies is an added bonus.

962 2.1 Simulation Setup

963 In order to establish the physics justification for the proposed CMS upgrades we have begun
 964 a simulation exercise. A detailed simulation program ?? with updated geometries, detector
 965 materials and detector response to particles is used to make choices amongst several possible
 966 upgrade scenarios, whereas a parameterized fast simulation program is used to make trig-
 967 ger/physics studies because the full simulation is too time consuming. The standard CMS fast
 968 simulation ?? is used for trigger/physics studies with modifications to the parameterizations
 969 of performance of upgraded systems. In both cases the options are built as part of current CMS
 970 software, so that bulk of the detector description which remains as is, and the analysis infras-
 971 tructure is reused. Pileup of multiple events in a bunch crossing at the level expected during
 972 high luminosity operation beyond 2016, i.e., ~ 50 inelastic interactions per crossing, is simulated.
 973 While the detailed studies include both in-time and out-of-time pileup for 50ns operation, the
 974 fast simulation considers only the in-time pileup for simplicity. A summary of detailed detec-
 975 tor studies made is presented here, and further elaborations are provided in the sub-detector
 976 chapters. The fast simulation results of expected physics benefits from L1 trigger studies are
 977 presented below.

978 2.2 Muon System Completion Simulation Summary

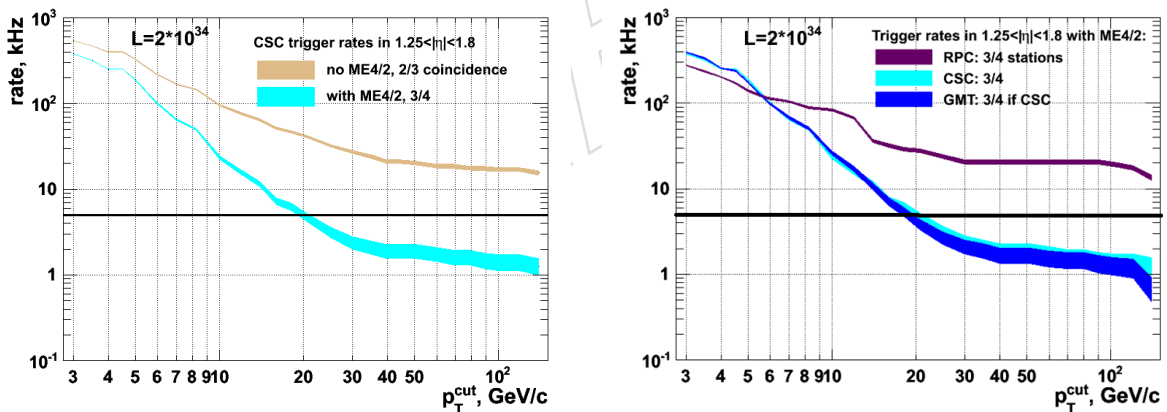


Figure 2.1: (a): Simulation predictions for the contribution to the CSC inclusive muon trigger rate from the region $1.25 < |\eta| < 1.8$ as a function of trigger p_T threshold. The curves demonstrate that the CSC trigger performance critically depends on the ME4/2. The target single-muon trigger rate of 5 kHz is indicated by the horizontal line; (b) Trigger rate of the upgraded standalone RPC and CSC systems (including the proposed RE4 and ME4/2 upgrades) as well as the Global Muon Trigger (GMT) rate. The RPC curve shown corresponds to the configuration optimized for high efficiency and not for rate rejection. In this configuration, the GMT trigger rate nearly entirely relies on the ME4/2 upgrade, making it critical from the standpoint of maintaining acceptable trigger performance.

979 The physics case for restoration of muon chambers which were descoped due to cost cutting

measures in the construction phase of CMS is also straight forward. The CSC system has reduced muon acceptance at trigger level in the region $1.6 < |\eta| < 1.8$ because of descopeed CSC muon stations. Restoration of these chambers enables efficient 3 out of 4 logic at the level-1 trigger restoring loss of trigger efficiency in this region. The installation of RPC chambers in the region $1.2 < |\eta| < 1.6$ provide the finer timing and redundancy for the corresponding CSC system, improving the quality of muons reconstructed in this region. Upgrade of ME1/1 chamber electronics improves the muon trigger in the $2.1 < |\eta| < 2.4$, especially in the high luminosity regime where the present ganging of some channels in these chambers results in an unacceptable number of spurious tracks. The improvements to the muon trigger are quantified by detailed simulations and are discussed in Section 3. The main benefit from the CSC upgrade is significantly lower rate with the use of ME4/2 and also ability to control the muon trigger background rate at the expected thresholds of about 30 GeV as shown in the Figure 2.1. The upgraded CMS configuration shows a decrease in rate as the threshold is increased compared to the expectations for the existing CMS muon system. Without such control we would be forced to prescale and randomly throw out good events. While the CSC upgrade provides bulk of the improvement the RPC upgrade provides the redundancy that we seek in the high background environment expected at high luminosities.

2.3 Hadron Calorimeter Simulation Summary

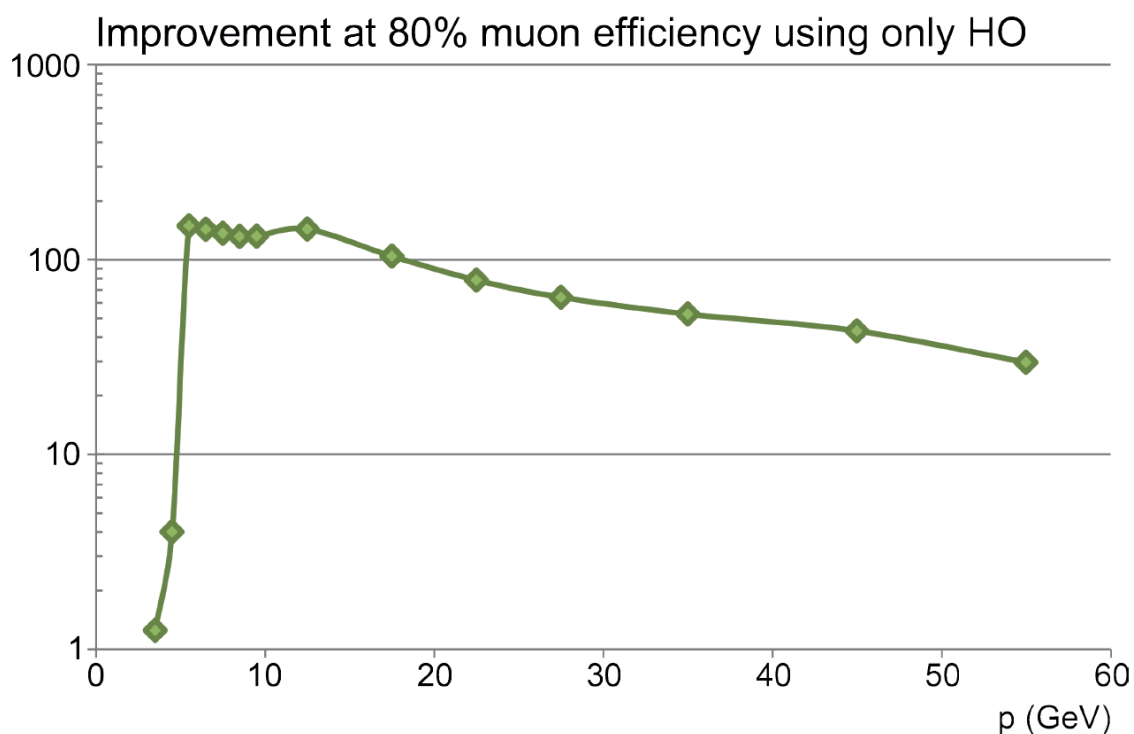


Figure 2.2: Improvement in π/μ rejection for a fixed muon efficiency of 80% due to replacement of HO photo-detectors.

The physics case for the outer hadron calorimeter (HO) is already justified in original HCAL TDR [?]. The addition of energy leaked into the HO for the high p_T jets is especially important in the case where new physics masses are very high. Similarly, the physics case for endcap (HE) and forward (HF) hadron calorimeters is also justified in the original CMS TDRs [? ?].

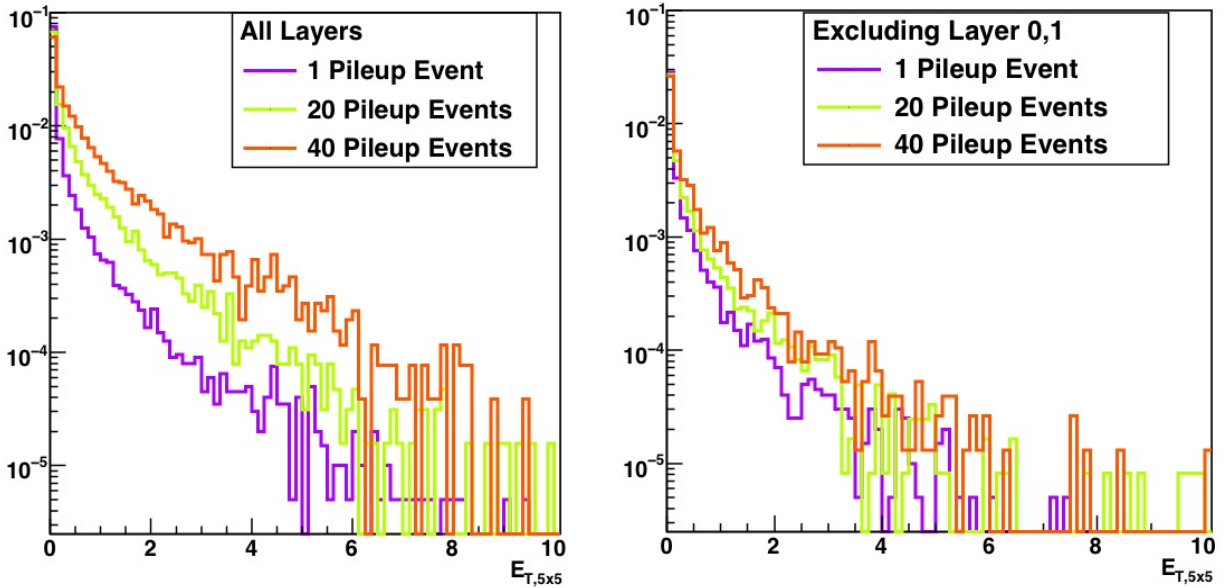


Figure 2.3: Energy distribution in the HB as a function of pileup when considering all layers (left) and when excluding the first two layers (right).

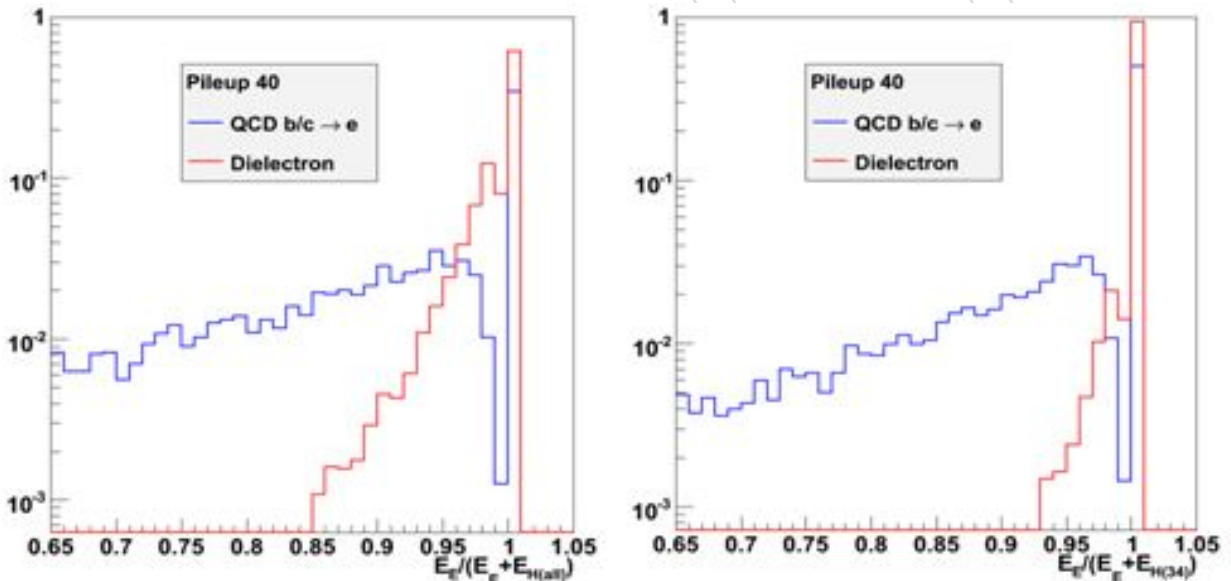


Figure 2.4: HCAL isolation variable computed using all layers (left) and ignoring the first layer (right).

1002 For instance the jets used to tag the vector-boson fusion process that results in production of a
 1003 central Higgs accompanied by fairly soft ($p_T \approx 30$ GeV) jets in the $2 < |\eta| < 5$, requires good
 1004 quality jet reconstruction. The existing detector suffers from a non-working HPDs in HO, oc-
 1005 casional coherent noise in multichannel HB/HE HPDs, and large spurious energy deposits in
 1006 HF because of Cherenkov light produced in the glass windows and walls of its photomultipli-
 1007 ers. The software algorithms designed to identify the spurious energy deposits by examining
 1008 the pattern of energy deposits and their signal time profiles is likely to suffer as the pileup in-

1009 creases at high luminosity. Therefore, mitigation of these problems in the hadron calorimeter
1010 by replacement of the HO/HB/HE HPDs with higher quality SiPMs and phototubes in HF
1011 with thinner window phototubes is necessary to restore the original performance.

1012 Simulations of upgraded HCAL indicate significant improvements in the detector response.
1013 For instance, the HO upgrade provides a better minimum ionizing particle response, thereby
1014 improving π/μ rejection as shown in Figure 2.2. In HB and HE there is degradation due pileup
1015 energy deposits, which can be mitigated by examining the longitudinal shower profile as it
1016 develops in the detector. Ignoring the first layers of the HCAL improves the detector response
1017 as shown in Figure 2.3. For electron/photon identification one can use only the latter layers of
1018 the HCAL to restore the discrimination capability as shown in Figure 2.4.

1019 2.4 Pixel Upgrade Simulation Summary

1020 The upgraded pixel system with four layers provides improved b-tagging capability and stand-
1021 alone tracking capability with higher efficiency. The mass reduction in the upgraded tracker
1022 reduces the photon conversion and electron bremsstrahlung probability enhancing the electron
1023 tracking and pixel based isolation of leptons. Full simulation results of the improvement in
1024 b-tagging are presented in chapter 6. The expected improvement in b-tagging is shown in the
1025 Figure 2.5. At operating point with fixed light jet fake efficiency, the b-jet tagging efficiency im-
1026 proves as much as 20%, which is quite substantial. Pixel-only tracking and b-tagging capability
1027 in the high level trigger are yet to be explored.

1028 2.5 Trigger Upgrade Simulation Summary

1029 The main benefit of the trigger upgrade is the improved performance for isolated electron,
1030 muon and τ triggers. Details of algorithms and their performance is given in chapter 7. Here
1031 we present simulation results. For these studies, we used fast simulation with pileup of $\tilde{25}$
1032 inelastic interactions per crossing. We defined two configurations of software, the existing
1033 CMS calorimeter trigger system and the upgraded calorimeter trigger.

1034 The efficiency turn-on and the integrated trigger rate versus the chosen threshold is shown for
1035 electrons and taus in Figure 2.6. The expected rate from the endcap muon system is shown in
1036 Figure 2.1.

1037 Sample Level-1 (HLT) trigger tables with thresholds and rates corresponding to 100 kHz (300
1038 Hz) total rate dominated by QCD (EWK) are shown in Table 2.1 for the case of instantaneous
1039 luminosity of $10^{34} \text{ cm}^{-2} \text{ s}^{-1}$ where an average of 25 pileup events are seen. [Currently only
1040 the L1 calorimeter trigger data is available. Muon and HLT simulation results are still under
1041 preparation.] The thresholds values represent energies where there is 80% (75%) efficiency for
1042 the electron/photon (tau) object. The rates corresponding to these thresholds for existing and
1043 upgraded calorimeter trigger system are shown. The total rate reduction is better than a factor
1044 of four. Note that the upgraded trigger system has more parameters that can be tuned to keep
1045 the rate at an acceptable level. Efficiencies corresponding to this reduced trigger table for a
1046 representative set of physics channels is shown in Table 2.2. Because we want to show the
1047 efficiency for triggerable events only we show the efficiency for each trigger for those events
1048 which have generated objects above the thresholds shown in Table 2.1, within the fiducial vol-
1049 ume of the detector. Absolute efficiencies for some of the triggers is rather low, e.g., the double
1050 τ thresholds is quite high (45 GeV), and therefore only significantly boosted Z bosons would
1051 have generated τ -leptons above that cut.

Table 2.1: A sample trigger table showing 80% (75% for τ) thresholds and rates which add up to 100 kHz (300 Hz) at Level-1 (HLT) for existing and upgraded CMS trigger systems.

Trigger Object	Threshold		Rate			
	Level-1 (GeV)	HLT (GeV)	Existing CMS		Upgraded CMS	
			Level-1 (kHz)	HLT (Hz)	Level-1 (kHz)	HLT (Hz)
Single Photon	37		28		8	
Double Photon	20		12		2	
Single Electron	37		28		8	
Double Electron	20		12		2	
Single Muon						
Double Muon						
Single Tau	85		29		23	
Double Tau	45		29		5	
Electron + Tau	20, 45					
Muon + Tau						
H_T (with b-jet)						

Table 2.2: L1 trigger efficiencies for a sample set of physics channels corresponding to the thresholds chosen with 80% efficiency for electron and 75% efficiency for taus for existing and upgraded CMS trigger systems. Note that the efficiency is calculated for those events that have generated object(s) above the selected thresholds in Table 2.1 within the fiducial volume of the detector.

Physics Process	Trigger Efficiency (%)					
	Existing CMS			Upgraded CMS		
	Single	Double	Cross	Single	Double	Cross
$W \rightarrow e\nu$	79.6	-	-	80.0	-	-
$Z \rightarrow ee$	83.7	68.8	-	88.9	71.4	-
$Z \rightarrow \tau_h \tau_h$	63.8	53.4	-	82.3	58.6	-
$Z \rightarrow \tau_e \tau_h$	69.9	62.9	46.7	82.3	64.4	48.6
$H(130) \rightarrow \gamma\gamma$	92.1	73.1	-	92.8	71.2	-
$H(135) \rightarrow \tau_h \tau_e$	69.1	44.1	39.0	79.5	49.4	40.2
$H(135) \rightarrow \tau_h \tau_h$	72.3	44.8	-	82.2	52.9	-
$tbH^+(200) \rightarrow \tau_h X$	62.6	-	-	88.0	-	-

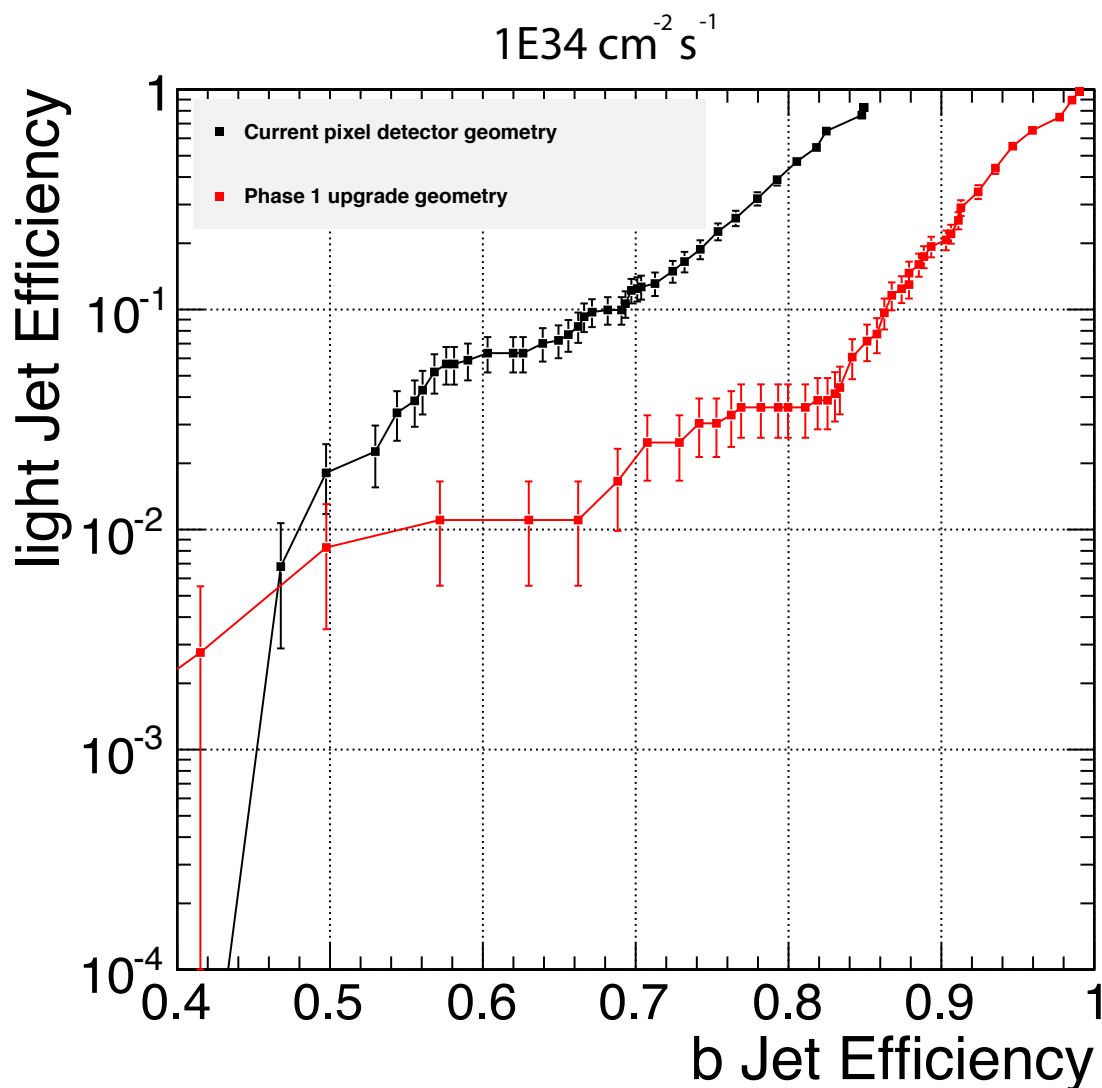


Figure 2.5: The efficiency for b-tagging using secondary vertex tag for true b-jets is plotted fake light quark jets efficiency in $t\bar{t}$ -events with the expected pileup of 25 events per crossing is shown for nominal and upgraded CMS configurations.

1052 We conclude that the calorimeter trigger upgrade will meet the required factor of two better
 1053 rate performance while slightly improving the physics yield for several physics processes.

1054 2.6 HLT and Physics Simulations

1055 The higher level trigger development and offline physics analysis studies with upgraded de-
 1056 tector are beginning, now that the upgrade plans are more firm and sub-detector level software
 1057 is becoming available.

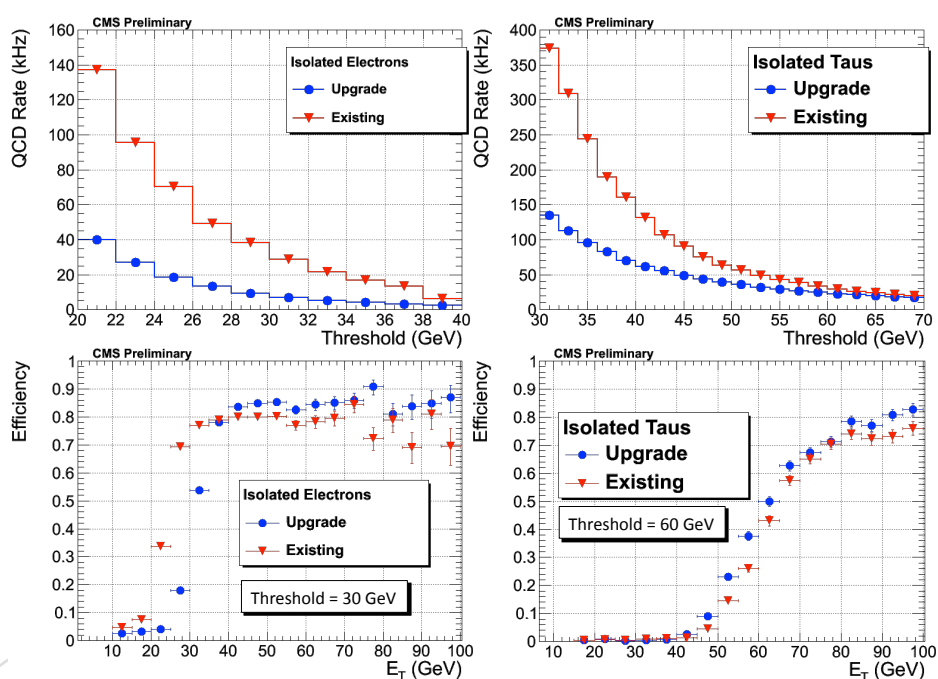


Figure 2.6: Integrated QCD rate (kHz) for electron (top-left) and tau (top-right) triggers is plotted versus trigger E_T cut for current LHC and upgraded algorithms with improved clustering. Corresponding efficiencies for isolated electrons (bottom-left) and hadronically decaying taus (bottom-right) are also plotted.

1059 The CMS Muon System Upgrades

1060 3.1 Introduction

1061 Muon detection is a powerful tool for recognizing signatures of interesting processes over the
 1062 very high background rate expected at the LHC. This is particularly true as the luminosity
 1063 increases. The CMS muon system has three functions: muon identification, momentum and
 1064 charge measurement, and triggering. Good muon momentum resolution and triggering are
 1065 enabled by the high-field solenoidal magnet and the flux-return yoke. This flux-return yoke
 1066 also serves as a hadron absorber, which enables the identification of the muons.

1067 The CMS muon system (Fig. 3.1) is designed to reconstruct the momentum and charge of
 1068 muons over the entire kinematic range of the LHC. CMS uses 3 types of gaseous particle de-
 1069 tectors for muon identification arranged as a cylindrical barrel region and planar endcaps. Be-
 1070 cause of the large area to be covered and the inaccessibility of the detector, it is important that
 1071 the muon detectors be cost-effective, reliable, and robust.

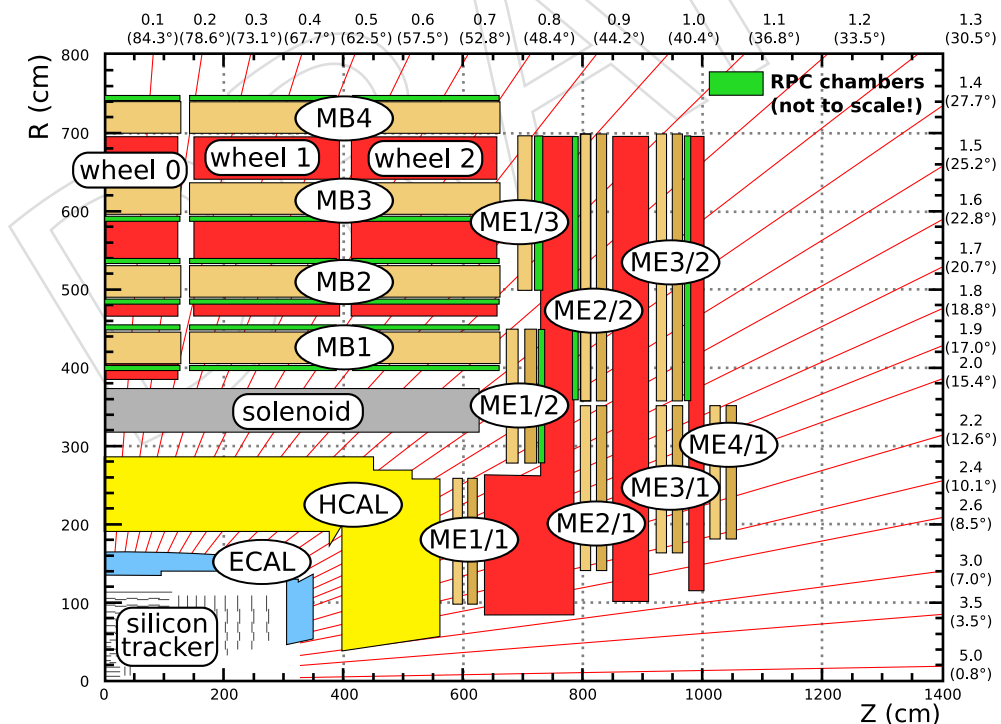


Figure 3.1: An r-z cross-section of one quadrant of the CMS detector with the axis parallel to the beam (z) running horizontally and radius (r) increasing upward. The interaction region is at the lower left. Shown are the locations of the various muon stations and the steel disks.

1072 In the barrel region, where the muon rate is low, the neutron background is relatively small, and
1073 the magnetic field is mostly uniform, drift chambers with rectangular cells are employed. The
1074 barrel drift tube (DT) chambers cover the pseudorapidity region $|\eta| < 1.2$. They are organized
1075 into 4 stations at different radii and mounted parallel to the beam between the flux return plates
1076 of the solenoid.

1077 In the two endcap regions of CMS, where the muon rates and background levels are high and
1078 the magnetic field is high and non-uniform, CMS uses cathode strip chambers (CSC). These
1079 chambers have a fast response time, fine segmentation, and relative immunity to the non-
1080 uniform field. The CSCs cover the region of $0.9 < |\eta| < 2.4$. Each endcap has 4 stations of
1081 chambers mounted on the faces of the endcap disks, and perpendicular to the beam. The cath-
1082 ode strips run radially outward and provide a precision measurement in the $r - \phi$ bending
1083 plane. The wires are roughly perpendicular to the strips.

1084 In addition to these muon detectors, CMS has added a complementary, dedicated triggering
1085 detector with excellent time resolution to measure the correct beam-crossing time at the highest
1086 LHC luminosities. The resistive plate chambers (RPC) are located in both the barrel and endcap
1087 regions, and they provide a fast, independent trigger over a large portion of the rapidity range
1088 ($|\eta| < 1.6$). The RPCs are double-gap chambers, operated in avalanche mode to ensure good
1089 performance at high rates.

1090 These muon detector elements cover the full pseudorapidity interval $|\eta| < 2.4$ with no accep-
1091 tance gaps, ensuring good muon identification over an angular range of $10^\circ < \theta < 170^\circ$, where
1092 θ is the polar angle between the beam and the muon track. Offline reconstruction efficiency
1093 for the muons with p_T greater than 3 GeV/c is typically 96-99% except in gaps between the DT
1094 station elements ($|\eta| = 0.25$ and 0.8) and the transition region between the DTs and the CSCs
1095 ($|\eta| \sim 0.9$). Due to the large amount of material before the first muon station, punchthrough is
1096 negligible. A crucial characteristic of the DT and CSC systems is that they can trigger on muons
1097 with good efficiency and high background rejection. DT and CSC triggers are combined in the
1098 overlap region ($0.9 < |\eta| < 1.2$).

1099 Thus, in CMS the triggering scheme for muons relies on independent and complementary trig-
1100 gering technologies: cathode strip chambers (CSC) in the endcaps plus drift tubes (DT) in the
1101 barrel, and resistive plate chambers (RPC) in both endcaps and barrel. The CSC and DT systems
1102 provide good momentum resolution and reasonable timing, while the RPC system provides
1103 excellent timing with somewhat worse momentum resolution. To be effective, the muon trig-
1104 ger must achieve good enough resolution to identify high- p_T tracks. Three stations are essential
1105 for the fast, accurate, and robust measurement of the muon momentum. With a primary-vertex
1106 constraint, two stations are sufficient to measure momentum in principle. However, the third
1107 station is highly desirable to provide for gaps in coverage, missing or dead chambers, muon
1108 bremsstrahlung, and multiple scattering. In the proposed system with 4 stations, any gaps in
1109 coverage within individual stations are complemented by good coverage in other stations, so
1110 that, in general, at least three stations will be hit by any muon.

1111 The original plans for the CMS endcaps included four stations for each of the CSC and RPC
1112 systems. However, only part (ME4/1) of the 4th CSC station was constructed, so we are now
1113 proposing to complete the 4th station with 72 ME4/2 chambers (36 on each endcap). We also
1114 propose to construct a new 4th station for the RPCs. In addition to these systems, which are
1115 now operating very effectively, CMS is considering adding a new system, the Micropattern Gas
1116 Detectors (MPGD) in the region $1.6 < |\eta| < 2.4$ (described elsewhere) not covered by the RPC
1117 system.

Without a 4th station, the CSC system does not have the necessary redundancy to control the trigger rate at the increased luminosity while preserving high trigger efficiency. With the trigger requiring segments in two out of three stations (requiring three will lead to a large efficiency loss due to inefficiencies and gaps in the coverage), the problem stems from momentum mis-measurements of low p_T muons contributing to the trigger rate. With the much higher flux of low-momentum muons at increased luminosity, these poorly measured muons dominate the trigger rate making it unacceptably high. The same effect occurs in the RPC system without the 4th station. Without a proper measurement, these low p_T muons cannot be eliminated with p_T cuts, so the muon trigger rate increases. With an additional station we will have four potential measurements. Since we only need three out of the four stations to get a good momentum measurement, we can be both correct and efficient in identifying high- p_T muons in the trigger.

The chamber construction for the 4th stations of both CSC and RPC will be done at CERN. A large fraction of the CERN building B904 has been allocated as a production facility for the CSC and RPC. The chambers will be assembled and tested in this building before being installed in CMS. At this time, the building is being refurbished and is expected to be ready for occupancy in early 2011.

The space available for the 4th station is very tight and we will need to plan the integration of this area carefully. The CSCs will be mounted on the back of the YE3 disk, and the RPCs will be mounted just behind the CSCs. As a consequence, the installation sequence requires the CSCs be installed first, then the RPCs. Once these chambers are installed and commissioned, a YE4 shielding wall will be mounted behind the 4th station and will protect the muon chambers from the spray of neutrons caused by losses in the LHC elements in the upstream beam lines.

An important consequence for the planning is that the installation of the CSCs must occur before the RPCs. The conservative schedule for the CSC construction requires roughly two years for the production of one endcap station (36 chambers), then an additional year for the next 36 chambers of the remaining endcap. The next long-term LHC stop is scheduled for 2012, so it is unlikely that the CSCs will be ready for installation at that time. Moreover, the funding for the CSCs is not yet in place. In contrast, the proposed 4th station of RPCs will be built by a large collaboration from many countries and much of the required funding has been pledged. Work has already begun on ordering materials. The RPC system expects to be ready for installation in a few years, possibly by 2012. This mismatch and possible resolutions are discussed in section 3.5.

In addition to the proposal for constructing additional CSC and RPC chambers, we propose replacing the ME1/1 front-end cathode electronics with new digital boards and upgrading the associated readout boards to increase the rate capability. The Drift Tube (DT) system electronics will also undergo some important changes, namely the replacement of some electronic components and the relocation of others, to make the system more reliable and robust and to resolve some problems with availability of spare components.

When these improvements and upgrades, described in detail in the following sections, are made to the three muon systems, CMS will be able to trigger on, identify, and reconstruct high- p_T muons with high efficiency and purity throughout the period until 2020.

3.2 CSC Muon Detector Upgrades and Repairs

The endcap Cathode Strip Chamber (CSC) muon system has been designed to provide robust triggering and muon identification over a wide rapidity range of $0.9 < |\eta| < 2.4$, and to

1162 improve the momentum measurement for ultrahigh energy muons with momenta of several
 1163 hundred GeV/c or greater. The current CSC detector consists of 468 large 6-layer chambers
 1164 arranged in Muon Endcap (ME) stations, as shown in Fig. 3.2(a) (note that the drawing also
 1165 includes station ME-4/2 proposed in this document, which is not part of the current system).
 1166 The full system contains more than 2 million wires and nearly half a million readout channels,
 1167 which are processed by a multi-layer readout and trigger electronics systems. The six layers
 1168 of each chamber provide a track segment that gives an excellent measurement of the azimuthal
 1169 angle, ϕ , of the muon track impact point in the plane of the station. The difference of the az-
 1170 imuthal angle between stations provides a measurement of the transverse momentum. The
 1171 layout of the CSC electronics system is shown in Figure 3.2(b). On-detector boards digitize the
 1172 data and send it to a system of 60 nearby VME crates, which form trigger primitives, store the
 1173 data blocks, and send them to the underground service cavern over optical fibers.

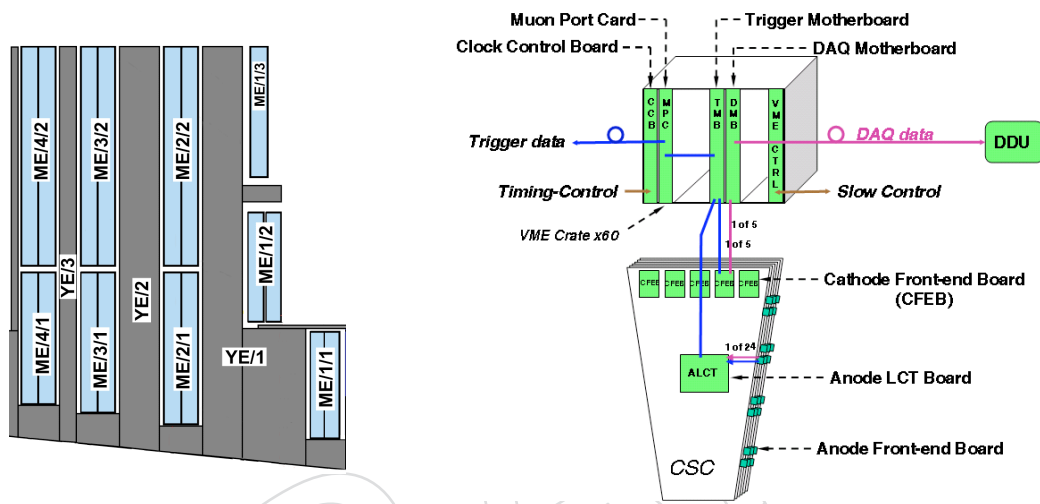


Figure 3.2: (a) An r-z cross-section of one endcap of the CSC muon system showing the new station ME4/2 (upper left) proposed in this document. In the drawing, the axis parallel to the beam (z) runs horizontally and radius (r) increasing upward, the interaction region is on the right, off the page. Shown are the locations of the various muon stations in blue and the steel disks between them in gray. Both station ME4/2 and ME1/1 (lower right) are specifically mentioned in the text; (b) A block diagram of the CSC electronics system.

1174 The CSC system is one of the principal systems for triggering the CMS experiment on muon
 1175 particles that pass through the endcap region. The task of the Level-1 CSC trigger is to effi-
 1176 ciently select events with muons of a high enough transverse momentum, p_T , while reducing
 1177 the rate of incoming events by about four orders of magnitude by rejecting background events.
 1178 For the trigger to measure p_T , the CSC trigger electronics reconstructs muon tracklets (stubs)
 1179 in CSC chambers and passes this information to the CSC Track Finder (CSC TF). The CSC TF
 1180 electronics (further discussed in the Trigger/DAQ section of this proposal) measures the dif-
 1181 ferences between ϕ values in the various CSC muon stations (i.e., ME1, ME2, ME3, and ME4)
 1182 and translates that information into muon candidate p_T .

1183 While the CSC chambers themselves are expected to survive the increased radiation levels from
 1184 the LHC luminosity upgrades, the current system will not be able to sustain its performance in
 1185 the face of increasing luminosity. Apart from a smaller scale electronics replacement needed to
 1186 maintain the system performance at current luminosities (the TMB daughtercard replacement
 1187 will take advantage of newly available technologies), continued robust performance of the CSC

1188 system at the SLHC luminosities will require increasing the redundancy of the system. The key
 1189 elements are building a new station ME4/2 and upgrading station ME1/1. While meeting these
 1190 goals requires replacing several electronics components for station ME1/1, such replacement
 1191 is also necessary on its own merits in order to maintain the CSC trigger and reconstruction
 1192 efficiencies. Replacement electronics will meet all the requirements of operating the upgraded
 1193 CSC system.

1194 From a physics perspective, not upgrading the current CSC system will cause a dramatic de-
 1195 crease in the CMS acceptance in the range of $0.9 < |\eta| < 2.1$ for physics signatures with muons
 1196 due to inefficiencies at increased luminosity and a complete shutdown of triggering capabili-
 1197 ties in the region of $2.1 < |\eta| < 2.4$. Because muons are critical for most signatures of Higgs or
 1198 new physics including Supersymmetry, the CMS physics reach in those areas will be severely
 1199 diminished. Shutdown of the very forward region ($2.1 < |\eta| < 2.4$) will have a substantial
 1200 reduction in acceptance for signatures with one triggerable muon (e.g. SUSY, or $h \rightarrow \tau\tau$ in
 1201 the “golden” muon plus hadronic tau channel) and diminished acceptance for two-muon sig-
 1202 natures. The very forward region is also critical for the measurement of $\sin^2 \theta_{eff}$ and Parton
 1203 Distribution Functions using forward-backward asymmetry A_{FB} in $Z \rightarrow \mu\mu$ events. Accurate
 1204 knowledge of PDFs plays a key role in predicting Standard Model backgrounds in searches for
 1205 new physics. Today’s technologies allow us to remove these deficiencies and provide robust
 1206 muon triggering and reconstruction up to $|\eta| = 2.4$.

1207 3.2.1 Performance Limitations

1208 At higher instantaneous luminosities, the much increased hit occupancies lead to both an un-
 1209 acceptable increase in the CSC trigger rates as well as a significant decrease of muon trigger
 1210 efficiencies. Without an upgrade, preserving the muon trigger rate within the allowed range
 1211 would require unacceptably high muon Level-1 trigger thresholds, which will severely dimi-
 1212 nish CMS physics reach. The root cause of the rate problem is the lack of redundancy of the
 1213 system, which prevents us from tightening trigger purity without unacceptable sacrifices in ef-
 1214 ficiency. Construction of the new station ME4/2 and unganging of channels in station ME1/1
 1215 will alleviate these shortcomings.

1216 Apart from the trigger rate problems, the particularly high rate and occupancy of hits in the
 1217 CSC chambers in station ME1/1 will cause a significant decrease in trigger reconstruction ef-
 1218 ficiency in the forward half of the CSC region due to the limitations of the existing electronics
 1219 system. The CSC electronics was not designed for instantaneous luminosity beyond the nom-
 1220 inal LHC range and was limited by the technology available at the time of the original system
 1221 design. A specific example of technology limitations is a less than powerful TMB daughtercard
 1222 FPGA. If the TMB FPGA is not replaced, the muon trigger will have to be shut down in the
 1223 region of $2.1 < |\eta| < 2.4$ at already nominal LHC luminosities.

1224 3.2.1.1 Lack of Redundancy in the Region $1.2 < |\eta| < 1.8$

1225 With the current CSC detector, the CSC Track Finder selects muons using a two-out-of-three-
 1226 station triggering configuration. Two stations supply a single difference in ϕ positions; this
 1227 is the minimal coincidence that measures muon momentum, leaving no redundancy for mul-
 1228 tiple scattering or mis-measurement. At high luminosity simulations show that the two-out-
 1229 of-three-station triggering configuration needed for high efficiency suffers from a high rate of
 1230 background from mis-measured low- p_T muon tracks, as shown in Fig. 3.3. A three-out-of-
 1231 three-station triggering configuration cannot be used because of large and uncertain losses due
 1232 to requiring perfect muon information from every muon station, because it suffers the third
 1233 power of the per-station efficiency, which comes from many factors:

- 1234 • chamber geometry gaps.
- 1235 • high-voltage isolation gaps within chambers where the gas gain is lower.
- 1236 • position determination errors due to muon bremsstrahlung, which increases dra-
- 1237 matically at high momentum.
- 1238 • electronics dead-time at higher luminosity and timing errors due in part to early
- 1239 background hits including those from neutrons.
- 1240 • “real-world” losses due to individual chamber problems such as high-voltage break-
- 1241 down and electronics malfunctions.

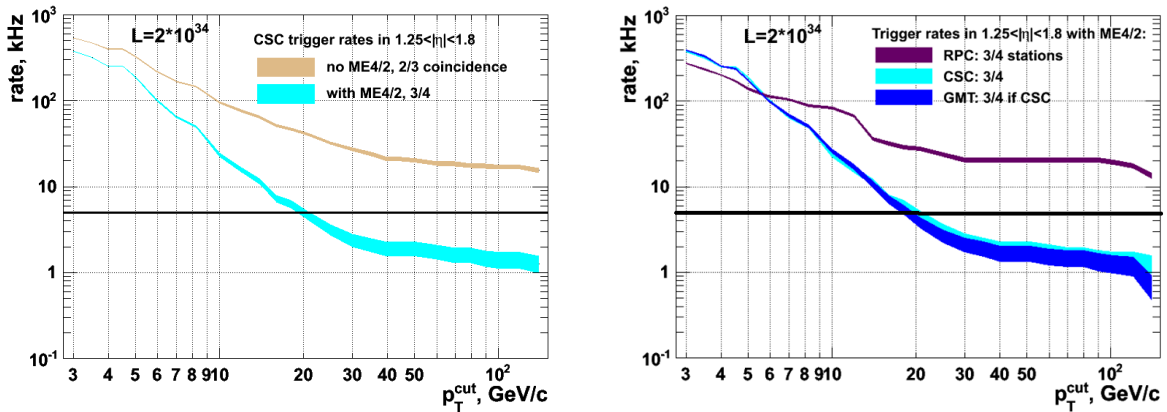


Figure 3.3: (a): Simulation predictions for the contribution to the CSC inclusive muon trigger rate from the region $1.25 < |\eta| < 1.8$ as a function of trigger p_T threshold. The curves demonstrate that the CSC trigger performance critically depends on the ME4/2. The target single-muon trigger rate of 5 kHz is indicated by the horizontal line; (b) Trigger rate of the upgraded RPC and CSC systems (including the proposed RE4 and ME4/2 upgrades) as well as the Global Muon Trigger (GMT) rate. The RPC curve shown corresponds to the configuration optimized for high efficiency and not for rate rejection. In this configuration, the GMT trigger rate nearly entirely relies on the ME4/2 upgrade, making it critical from the standpoint of maintaining acceptable trigger performance.

1242 With an upgrade to build the ME4/2 CSC chamber station covering the rapidity range 1.2 to
 1243 1.8, the CSC Track Finder will be able to select muons using a highly efficient three-out-of-four-
 1244 station triggering configuration. Figure 3.3(a) shows the expected rate curves from simulation
 1245 with and without the ME4/2 station at SLHC Phase-1 luminosity, with the target rate of 5
 1246 kHz for the Level-1 muon trigger rate as indicated. Without the upgrade, the increase and
 1247 flattening of the trigger rates leads to an effective loss of triggering in that region. With the
 1248 upgraded ME4/2, the trigger p_T threshold can be maintained at 20 GeV/c, allowing for efficient
 1249 triggering on W, Z, and top quark muonic decays. The W, Z, and top particles in turn are some
 1250 of the best signals for Higgs, Supersymmetric, and other sought-after particles.

1251 Figure 3.3(b) shows the performance of the GMT with both upgraded RPCs and CSCs. The
 1252 presented RPC trigger rate curve is based on the 3/4 layer coincidence that will be possible
 1253 only after the RPC upgrade and, in accord with current practice, was optimised for efficiency
 1254 rather than rate rejection. With a different optimization, the RPCs could contribute more to
 1255 the over all trigger rate reduction at a loss of efficiency. However the pseudorapidity interval
 1256 $1.24 < |\eta| < 1.6$ presents special difficulty for the RPCs. Moreover, all the rate curves shown are
 1257 very optimistic, as they take into account only the real muon (primary or secondary) spectrum.
 1258 It is known that background rates in the endcap region from neutrons, albedo particles, and
 1259 beam-halo muons have caused serious problems for other collider detectors lacking sufficient

1260 redundancy in the past. Figure 3.3(b) indicates that the ME4/2 upgrade remains critical even
 1261 with the RPC RE4 upgrade, since the performance of the CSC muon trigger has such a strong
 1262 impact on the CMS Global Muon Trigger (GMT) rate.

1263 3.2.1.2 Loss of Performance in the Region $1.6 < |\eta| < 2.4$

1264 The ME1/1 muon station shown in the lower right portion of Fig. 3.2(a) covers the forward
 1265 half of the CSC rapidity range. Because of its proximity to the interaction point (least multiple
 1266 scattering compared to other stations) and its location in the region before the magnetic field
 1267 changes direction, ME1/1 is the most important station for standalone momentum resolution
 1268 for muons with $|\eta| = 1.6 - 2.4$. The standalone muon momentum resolution is, in turn, crucial
 1269 to the Level-1 and Level-2 trigger event selection, and is also used offline for muon identifica-
 1270 tion. This makes it imperative to maintain high local track reconstruction efficiency in ME1/1
 1271 chambers. Because of the proximity to the beam line, the ME1/1 chambers receive the highest
 1272 particle rates of any of the CMS muon chambers. In addition to the prompt muons, ME1/1 is
 1273 exposed to high long-lived neutron and beam backgrounds that are particularly significant in
 1274 the very forward region. As an illustration, Fig. 3.4(a) shows the density of hits sharply peaking
 1275 in station ME1/1 as observed in early LHC beam-halo events. At higher luminosity, the high
 1276 background rates cause significant losses in efficiency due to shortcomings of station ME1/1
 1277 electronics.

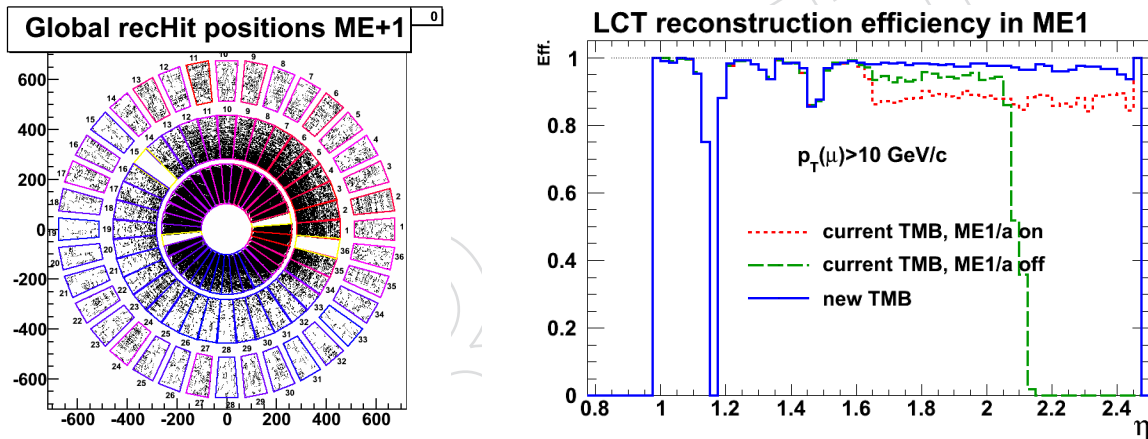


Figure 3.4: (a): The distribution of beam-halo muon hits in station ME1 using actual LHC data shows the rate is highly peaked in station ME1/1, which is closest to the beam; (b) Simulation prediction for the efficiency of finding a local muon track in station ME1 as a function of muon pseudorapidity for muons with $p_T > 10 \text{ GeV}/c$. The decrease in efficiency is due to backgrounds from pile-up (note that this calculation includes prompt contributions only, i.e. no beam or neutron backgrounds). Because of the features of the TMB board, the efficiency over the entire range of $|\eta| = 1.6 - 2.4$ is sensitive to the background rate in the region of $|\eta| = 2.1 - 2.4$. Upgrade of the TMB board allows recovering robust muon triggering in the entire range of $1.6 < |\eta| < 2.4$.

1278 Furthermore, technology constraints at the time the system was originally designed led to a
 1279 decision to divide all ME1 chambers into two halves covering regions $1.6 < |\eta| < 2.1$ and
 1280 $2.1 < |\eta| < 2.4$ and to implement a 3:1 ganging of cathode strips in the high- η part of the
 1281 chambers. The ganging is done at intervals of 16 strips so that, for example, strips 1, 17, and 33
 1282 are directly connected to electronics channel 1; strip 2, 18, and 34 are connected to electronics
 1283 channel 2, etc. At higher luminosity, such grouping leads to a rapid increase in the trigger

rate, which cannot be controlled by tightening trigger requirements due to an effective loss in system redundancy caused by ganging.

3.2.1.2.1 Sub-optimal Trigger Segment Reconstruction Performance An important issue was identified with the muon trigger that is relevant for the region $|\eta| = 2.1 - 2.4$ already at nominal LHC luminosities. One of the key elements of the muon trigger sequence is the reconstruction of local muon tracks in chambers, which is handled by the Trigger MotherBoard (TMB). Because of a feature of the board (driven by the limitations in FPGA technology at the time of the board design), the board becomes blind to any new muons for several bunch-crossings after reconstructing a local track anywhere in the chamber. Since both the high- and low- η regions of the ME1/1 chambers are handled by a single TMB board, the efficiency of muon triggering in the entire region of $|\eta| = 1.6 - 2.4$ becomes highly sensitive to the rate of backgrounds in the region of $|\eta| = 2.1 - 2.4$. Even though the current simulation lacks critical contributions from neutron and beam-induced backgrounds, the effect is apparent, as demonstrated in Fig. 3.4(b) showing a large decrease in muon trigger efficiency in the entire region of $|\eta| = 1.6 - 2.4$. While it is possible to improve performance in the lower η region by turning off triggering in the region of $|\eta| = 2.1 - 2.4$, this option fails due to physics reach considerations. Apart from a lower efficiency, the strong susceptibility of trigger performance to the precise level of backgrounds in the region with highest and most difficult-to-predict backgrounds diminishes the robustness of the trigger.

Resolving this problem requires an upgrade of the current TMB boards used in station ME1/1 to utilize a new generation of FPGA chips and deploy a new nearly deadtime-less algorithm with additionally developed background suppression options. While the new TMB algorithm will recover efficiency, one still needs to address the high contribution to the trigger rate coming from the region of $|\eta| = 2.1 - 2.4$ as shown in Fig. 3.5(a). To control the rate, the CSC Track Finder (CSCTF) will be configured to require 3-out-of-4 station coincidence for candidate tracks with $|\eta| > 2.1$. Because of the much increased robustness of reconstruction in station ME1/1, this will present a safe and efficient solution (solid line in Fig. 3.5(a)).

3.2.1.2.2 Front-End Readout Dead Time with Increasing Luminosity An important element of the CSC front-end readout is the Switched Capacitor Array (SCA) cells that form the analog charge storage pipeline. They hold the data until they can be digitized and read out. At higher luminosities, the SCA cells can become fully occupied by data before they are digitized, so effectively the board is dead for a time. Also, the pedestal for each time sample can be disturbed by the presence of earlier hits, so that the accuracy of the position determination is degraded. Alleviating the high-data-rate readout problems in ME1/1 requires replacing the existing cathode front-end boards (CFEBs). We propose that the current “analog” CFEBs that use the SCA and 16:1 multiplexing digitizers (ADCs) be replaced by “digital” DCFEB boards that flash-digitize data from every channel simultaneously and store the results in a digital pipeline.

3.2.1.2.3 Rapid Trigger Rate Growth in $2.1 < |\eta| < 2.4$ with Increasing Luminosity While an upgraded TMB restores robust triggering for the near term, at Phase 1 luminosities the 3:1 ganging of ME1/1 channels presents a fundamental problem as it leads to a large increase in muon trigger rate as well as complicating the reconstruction due to combinatorics. The CSC trigger depends on the measured ϕ difference between muon stations and the desirable high- p_T muons have very small ϕ differences. Because of the ganging, there is a high rate of low- p_T muons that will be seen as nearly straight (infinite momentum) if their bending in the magnetic field takes them roughly 16 or even 32 strips away. Fig. 3.5(b) shows the large

1330 enhancement in the number of muon trigger candidates at $|\eta| > 2.1$ even with the three out of
 1331 four station coincidence requirement for the current system. This problem also exists in offline
 1332 muon identification, where muon stubs are matched in position with inner-detector tracks. At
 1333 Phase 1 luminosities, the trigger rate from that region will become unacceptable.

1334 Maintaining muon trigger performance in the region $2.1 < |\eta| < 2.4$ will require the removal
 1335 of channel ganging and mounting additional DCFEB boards on each ME1/1 chamber so that
 1336 every strip can be read out separately. The TMB and DMB boards, which receive trigger and
 1337 data readout information from the CFEs in ME1/1, will concurrently need to be modified
 1338 to handle the additional DCFEBs. A backward/forward compatible design of the new TMB
 1339 daughtercard discussed in Section 3.2.2.2.1 will allow upgrading the system without replacing
 1340 the TMB boards themselves. Instead, the TMB boards will undergo only minor modifications
 1341 to route optical links directly to the new TMB daughtercard and will be ready to operate with
 1342 the new DCFEB boards using a new version of the firmware.

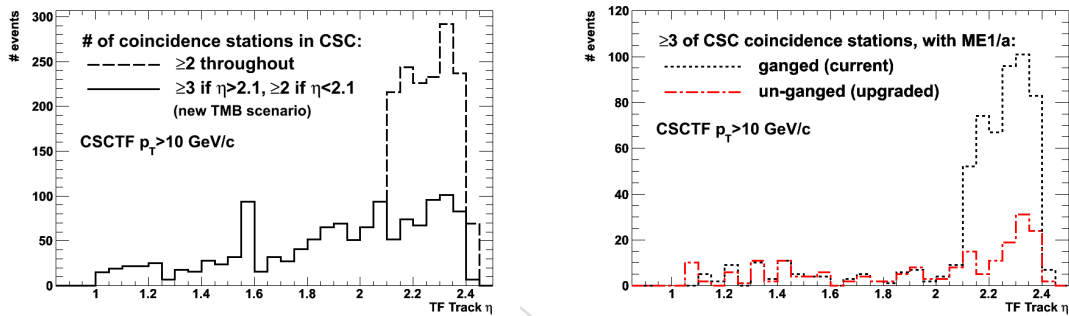


Figure 3.5: (a) Simulation predictions for the pseudorapidity distribution for background events passing the current L1 trigger (dashed line). The enhancement in the region $|\eta| > 2.1$ is due to the strip ganging in ME1/1a. For LHC luminosities, the requirement of a three-out-of-four station coincidence and an improved TMB algorithm (solid line) help decrease the rate to an acceptable level. (b) For the highest Phase 1 luminosities, the trigger purity will have to be substantially improved again. Addition of station ME4/2 and requiring a three station match in the entire CSC detector (dotted line) will bring the rate in the lower $|\eta|$ range to acceptable level. Suppressing the large remaining contribution to the trigger rate from $|\eta| > 2.1$ requires unganging the strips in ME1/1a chambers (dash-dotted line), which in turn necessitates the DCFEB upgrade.

1343 3.2.2 Description of the Muon Detector Upgrade Plan

1344 The proposed upgrade of the CSC detector consists of three specific activities, which have
 1345 important interdependencies:

- 1346 • The construction and installation of a new CSC station ME4/2 to provide the badly
 1347 needed redundancy in the region of $1.2 < |\eta| < 1.8$. New chambers will require
 1348 either new electronics or the recovered electronics from station ME1/1 (after ME1/1
 1349 electronics replacement).
- 1350 • The design and installation of new digital front-end boards (DCFEBs) for station
 1351 ME1/1 and unganging of cathode strip channels in the high- η half of the chambers.
 1352 This will also require a replacement of the readout and trigger electronics for ME1/1
 1353 chambers (i.e. TMB and DMB boards) with more powerful chips to implement im-
 1354 provements to the reconstruction algorithm. This will provide a long-term solution
 1355 for triggering in the region of $1.6 < |\eta| < 2.4$.

- The replacement of the TMB boards responsible for the formation of trigger primitives for station ME1/1 will recover triggering in the region of $2.1 < |\eta| < 2.4$ at nominal LHC luminosity without a degradation of efficiency in the region of $1.6 < |\eta| < 2.1$.

3.2.2.1 Construction of ME4/2 Chambers

For the ME4/2 chambers, detailed engineering designs already exist, as these chambers are identical to the existing ME2/2 and ME3/2 chambers that were built at Fermilab and assembled and tested at UCLA and University of Florida. Space for the ME4/2 chambers on the YE3 iron disks already exists. Therefore, these chambers should be straightforward to build and deploy. Each ME4/2 chamber subtends 10 degrees in ϕ , and the full system with two endcaps contains 72 CSC chambers. Two spare chambers will also be built.

In 2008 it was found that the previous vendor no longer produces the large 5'x12' flat FR4 panels. After much difficulty, a replacement vendor was found, and these panels and other parts were procured to build a new ME4/2 prototype chamber. Most of the necessary chamber-building tooling was restored from the previous production of ME2/2 and ME3/2 chambers, and during FY09 this prototype was assembled, tested at Fermilab, and then shipped to CERN, where it was installed on the back side of the YE+3 disk. Thus, we have demonstrated that the tooling and expertise currently exists for production of the chambers and that suitable parts can still be acquired.

It is anticipated that Fermilab and Wisconsin will handle the bulk of chamber parts procurement and the modest amount of engineering associated with reviving the tooling and the drawings. Panel production (including precision milling of cathode strips patterns) will take place at FNAL. Assembly of the ME4/2 chambers will be done at a factory that will be set up in Building 904 at CERN, which will be available for first occupancy in early 2011. This offers some advantages, such as the possibility of strong contributions of manpower from foreign collaborators and CERN, the presence of substantial U.S.-funded manpower resident at CERN, and the ability for hands-on training of CMS graduate students with a substantial detector-building and testing project.

A management plan for the ME4/2 construction project is being developed. An overall ME4/2 upgrade manager will coordinate activities at the FNAL and CERN sites. There will be site managers at FNAL and CERN who supervise appropriate personnel (site-specific project engineer, floor manager, QA/QC technicians, etc.), as well as a Final ASsembly and Test (FAST) facility. Discussions have already taken place regarding specific personnel, including CERN and non-U.S. collaborators such as Russia (PNPI, Dubna) and China (IHEP).

Associated with the new ME4/2 chambers are a variety of electronics boards and other infrastructure associated with each CSC. The electronics board acronyms are: Anode Front End Board (AFEB), Cathode Front End Board (CFEB), DAQ Motherboard (DMB), Anode Local Charged Track Board (ALCT), Trigger Motherboard (TMB), Low Voltage Distribution Board (LVDB), and Low Voltage Monitoring Board (LVMB). Unoccupied slots for these boards are available in existing electronics crates for all associated readout and trigger electronics. Besides electronics boards, there are cables, cooling plates, HV, LV, cooling, and gas infrastructure items.

While the expertise and capabilities to build additional quantities of these boards are both available, one money-saving element of the muon upgrade plan as a whole is that as ME1/1 chambers are pulled out to install the new DCFEBs, the current CFEBs will be removed from ME1/1 and then subsequently installed on the new ME4/2 chambers. Other electronics boards

1401 freed up as a part of the ME1/1 electronics replacement plan (old DMB, TMB, LVDB, LVMB)
1402 will also be moved to station ME4/2 as they become available.

1403 **3.2.2.2 Improving Trigger Performance in the Region $|\eta| = 1.6 - 2.4$**

1404 There are several specific improvements needed to address suboptimal trigger performance in
1405 the higher $|\eta|$ half of the ME1/1 region. These improvements focus on improving efficiency
1406 and robustness of the trigger as well as preserving trigger rates within the acceptable range,
1407 which is particularly difficult in the forward region.

1408 **3.2.2.2.1 Replacement of the TMB Board Daughter Cards** The first part of the upgrade
1409 of the TMB board is the replacement of the mezzanine card holding the FPGA chip to allow for
1410 a more complex algorithm required to restore reliable triggering in the region of $|\eta| > 2.1$. With
1411 the deployment of the new DCFEB boards (described next), the TMB board itself will undergo
1412 some minor modifications to accommodate new optical fibers bringing data from the front-end
1413 boards. No changes to the mezzanine cards holding FPGAs will be required at that time. The
1414 total number of mezzanine cards needed is 72 plus 20% spares, all of which will rely on XILINX
1415 Virtex-6 FPGA chips. Neither procedure (the first one being essentially a repair) requires a long
1416 shutdown or any significant LHC down-time, since the new TMB cards can be installed during
1417 one of the many LHC short technical stops.

1418 With the new algorithm, the efficiency of reconstructing stubs will be assured for the entire
1419 station ME1/1 and pseudorapidity up to $|\eta| = 2.4$, as shown in Fig. 3.4(b). For luminosities
1420 approaching $\simeq 10^{34} \text{ cm}^{-2}\text{s}^{-1}$ (still prior to Phase I LHC upgrade), the acceptable trigger rate
1421 can be achieved by improved background rejection in the TMB algorithm and a requirement
1422 of three (out of four) stubs for muon tracks in the CSC Track Finder (CSCTF) (see Fig. 3.5(a)).
1423 For Phase-1 luminosities, removal of cathode strip ganging will provide another powerful tool
1424 in reducing the trigger rate by removing the ambiguity in selecting muon stubs, and will also
1425 further improve the efficiency by reducing the effective TMB dead-time in the high- η portion
1426 of the chamber.

1427 **3.2.2.2.2 DCFEB Boards and Removal of Channel Ganging in ME1/1 Chambers** The
1428 “digital” Cathode Front-End Boards (DCFEBs) for ME1/1 that flash-digitize every channel si-
1429 multaneously have a very simple architecture: low-noise amplifiers are connected directly to
1430 flash ADCs, whose output is fed in parallel into memories in a programmable gate array for
1431 storage until readout. The current CFEB boards can handle a steady input rate of 2 kHz, while
1432 the new boards will be able to handle 50 kHz (the rate of the local muon trigger in coincidence
1433 with the Level-1 trigger) with no deadtime.

1434 The ganging of cathode strips in the inner portion of the ME1/1 chambers was done using
1435 a small passive printed circuit board. The outer portion of ME1/1 chambers covers $|\eta| =$
1436 $1.5 - 2.1$ and contains 64 cathode strips per layer, while the inner portion contains 48 strips
1437 per layer. The outer portion can be read out by four CFEB boards, while the 3:1 ganging of the
1438 inner section allowed it to be read out by a single CFEB board. With the removal of the ganging
1439 of strips in ME1/1, three DCFEB boards will replace one CFEB on each ME1/1 chamber for
1440 readout of the inner portion, making a total of seven DCFEB boards per ME1/1 chamber, or a
1441 total of 504 DCFEB boards to be built for the 72 ME1/1 chambers, plus 20% spares.

1442 It is anticipated that the outputs of the CFEB boards, currently two SCSI-50 connectors, will
1443 be retained on the DCFEB boards for “legacy” purposes, but supplemented in parallel by two
1444 high-speed optical connectors. The optical links from the DCFEB will allow easier cable instal-
1445 lation in CMS, as well as more reliable data transmission. Using the legacy connections and

up to five boards per chamber, the DCFEBs could be connected to the current DMB and TMB boards. However, with seven boards per ME1/1 chamber and with optical links, the DMB and TMB boards must be revised. The CFEB, TMB, and DMB cards currently operating on ME1/1 chambers will be recycled by moving them to the new ME4/2 chambers.

3.2.2.2.3 DCFEB Compatible Electronics for Station ME1/1 Deployment of the new DCFEB boards with new optical links for station ME1/1 will necessitate replacement of certain electronics components, most notably the TMB and DMB boards. The previously described repairs to the TMB board will make the new TMB board compatible with the new links after some minor modifications to the board. This will require 72 new modified DMB boards to operate with the new DCFEB and optical links. In addition, 72 updated LVMB and LVDB boards will have to be built, which will likely require only small design changes to enable the handling of seven (instead of five) front-end boards per chamber. For each board type, 20% spare boards will be produced to allow stable operations of the system in the long term.

3.2.3 R&D needed in preparation for the Phase 1 TDR

The ME4/2 chambers use an existing design, and therefore the R&D needs related to chamber construction are modest. One area we are working on is evaluation of vendors and currently available technologies related to building the panels for new chambers as the original vendor is no longer available. In FY09, a new fully operational ME4/2 prototype chamber was built using panels from a new vendor. Since then, another potential vendor has been identified and the studies aimed at evaluating long term reliability and physical aging of the panels have started. In order to build additional electronics boards, cables, etc. that are needed for use on ME4/2, we anticipate a modest amount of engineering R&D related to re-evaluating parts availability, vendors, PC boards and assembly houses. For example, the requirement to transition from leaded to non-leaded ICs happened since the original boards were built.

The DCFEB board is a new design and work has begun on evaluating this device. It has been found that the outputs of the existing low-noise amplifiers need to be buffered before serving as inputs to the new flash-ADC devices. We anticipate production of a DCFEB prototype board for evaluation in 2011. Work on improving the performance of the TMB boards in station ME1/1 has also begun and the first prototype of the replacement mezzanine board is expected in 2010. Engineering effort will be needed to finalize the design of the daughter card, implement the new algorithm in firmware, and to work out modifications of the main TMB board that allow it to receive data over optical links and communications with the trigger electronics downstream from TMB. Similarly, in order to build a revised DMB board for the ME1/1 electronics replacement, engineering effort will be needed to address issues related to optical link technology, board redesign, and FPGA evaluation. For all board types, engineering will be needed for prototype design, production, production supervision, deployment, and commissioning of the new system.

In addition to electronics engineering work specific to the CSC system, certain generic R&D studies related to the deployment of new generation of electronics components will be necessary. A number of radiation tolerance and hardness studies need to be planned and performed to ensure that both the new FPGA chips (Virtex-6 family) as well as optical-link components will be able to operate reliably throughout the lifetime of the experiment.

A high priority is the simulation studies of the high-rate conditions for the CSC detector. Those studies are ongoing and have already been critical in identifying the shortcomings of the current system, developing solutions and evaluating robustness of the proposed solutions. Moreover, extensive studies of muon system backgrounds, such as neutrons, albedo particles, and

1492 beam-halo are also ongoing. Apart from improving simulations to include these effects, the
1493 measured LHC data on these backgrounds needs to be fed back into the high-rate simulation
1494 software. Neutron-induced hits in particular, while not penetrating like muons, produce large
1495 numbers of hits everywhere in the muon system. Present uncertainty of a factor of three in the
1496 rates of these hits is obtained from comparing existing simulation parameterizations, and re-
1497 ducing this uncertainty using the real data is important for Phase 1 upgrades and will become
1498 a dominant concern for proper planning of further Phase 2 upgrades.

1499 **3.2.4 Alignment with a possible Phase 2 upgrade**

1500 Based on previous irradiation studies, we expect the CSC muon chambers to perform as de-
1501 signed and not to degrade intrinsically to any significant degree even at SLHC Phase 2 lumi-
1502 nosities. However, the current trigger and readout schemes were not designed for such high
1503 luminosities, and we may anticipate that other electronics upgrades than those instituted for
1504 Phase 1 will be necessary. The Phase 1 upgrades will, in any case, be critical for Phase 2. The
1505 additional ME4/2 station will help reject low-momentum muons and other backgrounds, and
1506 the engineering put into building DCFEBs, upgraded TMBs, and upgraded DMBs will prove
1507 very useful, since additional boards of these types may need to be built for CSC stations other
1508 than ME1/1 as the background rates increase.

1509 An additional board, the Muon Port Card (MPC) may become a CSC muon trigger bottleneck
1510 and, if so, will have to be replaced in order to use dramatically faster optical links. The MPCs
1511 must be upgraded at the same time as the Trigger system's CSC Track Finder cards to which
1512 they link.

1513 Additionally, it is possible that on-chamber anode trigger and readout boards (ALCT) will need
1514 replacement due to degraded performance. If these on-chamber CFEB and/or ALCT boards
1515 need to be replaced, it will require a large program of removing chambers to obtain the neces-
1516 sary access.

1517 The numbers of CSC muon electronics boards involved in a full program of electronics replace-
1518 ment for Phase 2 include: 2196 DCFEBs; 468 each of TMBs, DMBs, and ALCTs; 60 MPCs, and a
1519 large number of optical fibers.

1520 If a Level-1 track trigger is implemented for Phase 2, it will probably allow a somewhat de-
1521 graded performance of muon-only triggering. On the other hand, some of the backgrounds,
1522 such as from neutron overlaps with muons, may scale as a power of the luminosity and be-
1523 come surprisingly large. These factors will need to be carefully evaluated with simulations and
1524 background-rate determinations from LHC collisions.

1525 **3.2.5 Schedule**

1526 The schedule of the two tasks related to production of chambers for the new station ME4/2
1527 and electronics replacements for station ME1/1 are presented in this section. While the two
1528 activities are mostly independent, the installation and commissioning of the ME4/2 chambers
1529 on both endcaps requires the production of additional electronics boards (CFEB, TMB, DMB,
1530 LVMB and LVDB) to equip the new chambers. To reduce the overall costs, our plan calls for
1531 recycling the existing electronics, which will be freed-up as a result of the ME1/1 electronics re-
1532 placement, on station ME4/2. This creates a dependency of the schedules of the two upgrades
1533 and emphasizes importance of planning as discussed in what follows.

1534 3.2.5.1 ME4/2 Chamber Production

1535 The schedule is well-understood: the process of producing ME4/2 chambers requires first pro-
1536 curement of parts, then the production of panels and chamber assembly can proceed. This
1537 will be a pipelined process in which the early chambers are being equipped with electronics
1538 and tested, while later chambers are being built. Installation of the chambers in CMS is rela-
1539 tively rapid and can be accomplished in a few weeks. Access to CMS, on the other hand, is
1540 expected to be quite difficult, especially in the 2016 shutdown, because of the major improve-
1541 ments scheduled by the Technical Coordinator.

1542 From the start of Project funding, it will take approximately one year for production of the first
1543 chamber, and it will then be 2 additional years until production is complete. Additional time
1544 will, of course, be needed to install the chambers in CMS, and to connect the cables and other
1545 services needed for full operation. Time will also be needed for testing and commissioning.
1546 Some of the details of this schedule are shown in Section 3.5.

1547 The muon upgrade plan couples the schedule for DCFEB production for ME1/1 to that of
1548 the ME4/2 chambers, due to the recycling of ME1/1 CFEB boards on the ME4/2 chambers.
1549 Because of difficult access to the ME1/1 region and the production schedule for the new DCFEB
1550 boards, the replacement of the ME1/1 CFEB boards can occur only in the 2016 shutdown.
1551 While the first endcap of ME4/2 chambers can be populated with spare electronics, the second
1552 endcap cannot be installed until the recovery of the CFEB boards from ME1/1. Specifically,
1553 the first endcap of ME1/1 chambers must undergo CFEB to DCFEB replacement before the
1554 installation of ME4/2 chambers for the second endcap. In order to remove this dependency of
1555 the second ME4/2 station, we would need to produce additional CFEB boards of the old style.

1556 3.2.5.2 ME1/1 Electronics Repairs and Improvements

1557 The ME1/1 system will need 504 new DCFEB boards (7 boards per each of the 72 chambers),
1558 72 redesigned TMB boards, and 72 new DMB boards. In addition, the LVDB and LVMB boards
1559 will require modest modifications to account for the increase in the number of front-end boards
1560 per chamber.

1561 The installation of the new ME1/1 electronics will be accomplished during the 2016 shutdown.
1562 The requirement of a shutdown is mainly driven by the necessity to access the ME1/1 chambers
1563 to install the new DCFEB boards. While it is more convenient to perform all replacements
1564 simultaneously from the logistics stand point, some of the ME1/1 repairs do not require a
1565 shutdown and can be installed during LHC technical stops. One such example is the TMB
1566 replacement, which will allow us to alleviate chamber level trigger efficiency concerns and
1567 which can be done even before the DCFEBs are replaced.

1568 3.3 DT Muon Detector

1569 3.3.1 Introduction

1570 The barrel muon system forms the central, outer part of CMS. It is composed of 5 roughly
1571 identical wheels centered on the beam pipe. Each wheel contains 4 layers of drift chambers
1572 (DT) interspersed with the iron of the return yoke and 50 drift chambers, so the barrel system
1573 has 250 chambers.

1574 The Drift Tube (DT) Muon system is a wide area detector with distributed on-detector readout
1575 and trigger electronics accessible only when the detector is open. See Figure 3.6 for a schematic
1576 view of the readout and trigger electronics. All the devices located on the Minicrate, as defined

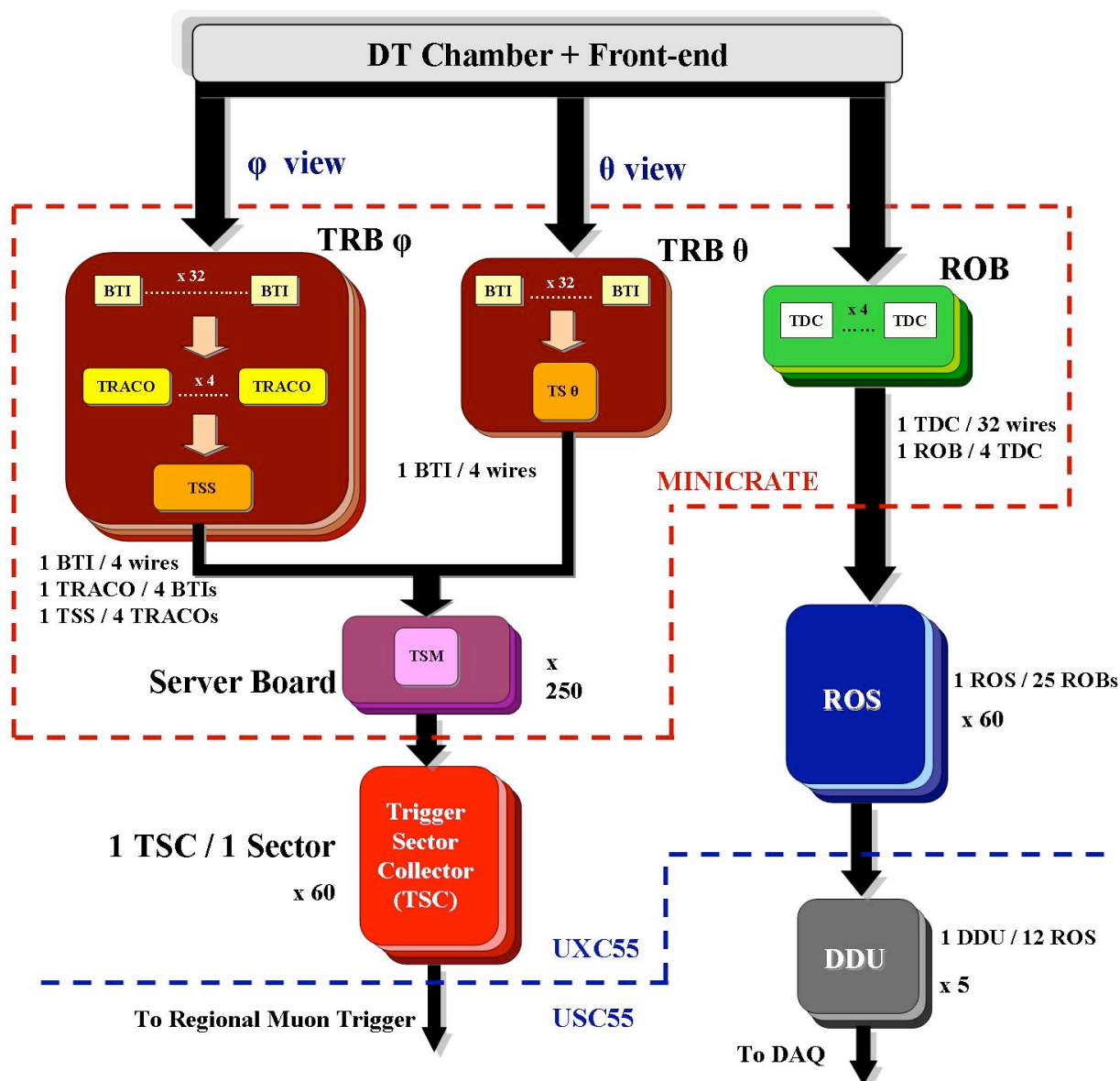


Figure 3.6: A schematic view of the readout and trigger electronics of the DT system.

1577 by the dashed shape in Figure 3.6, are not accessible without opening the detector. Any foreseen
 1578 upgrade should therefore cope with the limited access time and should aim to interventions
 1579 that have limited impact on the single detector. This means that unless a really critical problem
 1580 is found, the chamber itself and the on-detector electronics should not be touched.

1581 A long cosmic ray data acquisition campaign and the first data registered from pp collisions
 1582 provided information about system performance and permitted the evaluation of the weak-
 1583 nesses of the detector.

1584 The study did not reveal any relevant weakness in the overall detector performance (resolu-
 1585 tions, tracking capabilities, efficiencies), but spotted a few problems for the electronics. They
 1586 were found in three devices:

- 1587 • Trigger Boards
- 1588 • Sector Collector

- Drift Tubes Track Finder

1589

1590 While the Sector Collector and the Track Finder boards are always accessible during any shut-
1591 down, the Trigger Boards are instead placed close to the detector. The difficult access to them
1592 requires a careful plan to allow an intervention. Details of the problems found in Trigger
1593 Boards and Sector Collector, together with proposed solutions are reported in the following
1594 paragraphs, while the Drift Tubes Track Finder ones are described in the Trigger section of the
1595 proposal.

1596 3.3.2 Theta Trigger Board replacement

1597 3.3.2.1 Motivation

1598 The weakest point of the DT electronics is the BTIM hybrid circuit, a device carrying four
1599 Silicone-topped BTI ASICs (the front end barrel muon trigger device) bonded on a ceramic
1600 support (Figure 3.7).

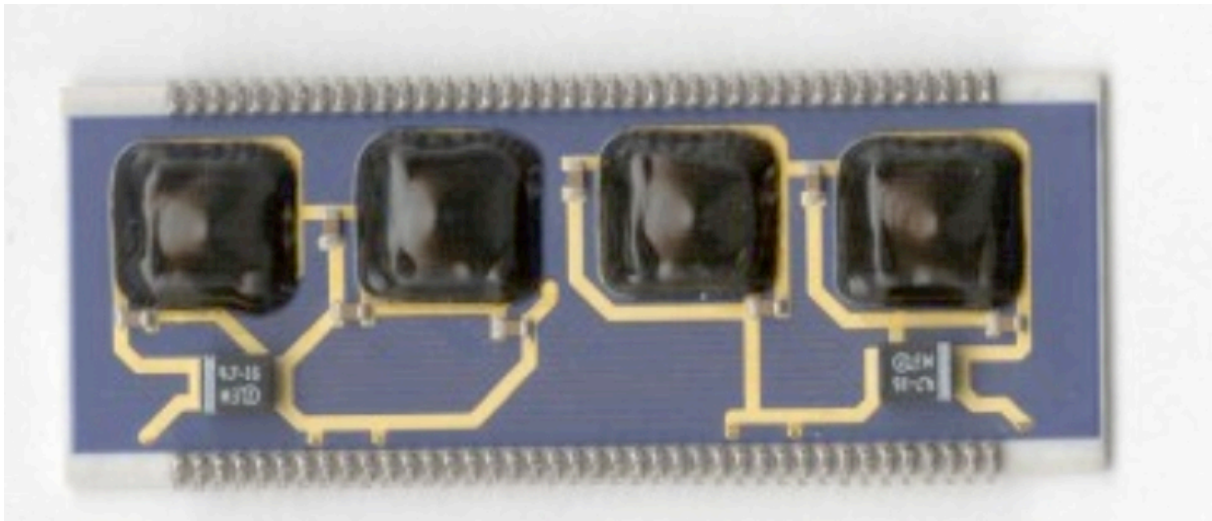


Figure 3.7: Picture of the BTIM hybrid module.

1601 Eight BTIMs are placed on each Trigger Board (TRB). After detector installation TRBs were
1602 replaced at a rate of approximately 1%/year (19 boards were replaced during the detector
1603 commissioning phase and 24 in the setup period). Failures are probably related to thermal
1604 stresses of the BTI ASIC bonds caused by the continuous power cycling of the electronics dur-
1605 ing the commissioning and detector setup phases. Although we produced a large number of
1606 BTI spares (25%), the BTIM mortality was very high already during BTIM production tests
1607 and currently we are left with about 3% spare devices (Table 3.1) obtained, with high yield, by
1608 recovering good parts from faulty boards.

1609 With the measured failure rate we will be running out of spares in about three years. But
1610 some caution must be taken since the unusual detector operation of the past years may have
1611 reduced the device lifetime and therefore the failure rate needs to be understood during steady
1612 operation. However, the two long shutdowns in 2012 and 2016, followed by startups, may
1613 subject the detector to conditions similar to those experienced in 2007-2009 with similar results.

1614 3.3.2.2 Proposed solution

1615 The BTI was fabricated in the ATMEL 0.5μ technology, which is now obsolete. Thus there
1616 is no chance for new production. Hence the only possibility left to solve this spares crisis is

Table 3.1: Available spares of boards carrying BTIM devices. The number of spares is estimated assuming a 80% yield on BTIM recovery from discarded boards and includes those mounted on good spare boards.

Board type	TRBPFI128	TRBPFI32	TRBTHETA	BTIM
Total installed	1080	60	360	10640
Spares	12	6	4	370

Table 3.2: Results of the radiation test of FPGA candidates with 60 MeV protons at PSI.

FPGA type	test fluence (p/cm ²)	MTBF (LHC years)	Comments
XILINX Virtex 5 LX 110 with SEU Controller Macro	6x10 ⁸	0.1	Current increase detected
XILINX Virtex 5 LX 110 with Blind Scrubbing	2.7x10 ⁹	0.5 - 0.8	Current increase detected
ACTEL A3PE1500 std com	2.6x10 ¹¹	150	Stopped working at 360 Gy
ACTEL A3PE3000L-1 com low power	1x10 ¹¹	85	Still working after 130 Gy

1617 a migration to a more recent ASIC technology or to an FPGA device. We have investigated
 1618 the second choice, since migrating to an FPGA optimizes the production timescale and leaves
 1619 space for possible modifications that may be needed for the future high luminosity operation.
 1620 Once the migration to an FPGA is completed, its conversion to an ASIC can be reasonably fast.

1621 The TRBs are installed close to the detector in an environment that is not hostile in terms of
 1622 radiation dose ($\sim 0.4\text{Gy}$ in 10 years of LHC operation), but subject to a substantial probability
 1623 of Single Event Effects (expected fluence 5×10^{10} p/cm² in 10 years of LHC operation). Hence,
 1624 after the BTI algorithm was migrated to a few possible FPGAs and its performance was veri-
 1625 fied using the old ASIC test vectors, the prototype boards were irradiated at PSI with 60 MeV
 1626 protons.

1627 Each FPGA under test was running two BTI cores at nominal frequency (80/40 MHz) and was
 1628 fed by a monitor board with the same test vectors. Error counting was done comparing the
 1629 trigger parameters on output of both BTIs to the expected benchmark results. The test results
 1630 are reported in Table 3.2. The Xilinx FPGA is not suitable as a BTI replacement, while both
 1631 ACTEL devices showed very good performance and are indeed fit also for operation in the
 1632 SLHC environment.

1633 Now that we have an appropriate FPGA device, a long term replacement strategy should be de-
 1634 veloped. Indeed the new boards production plan must consider detector survival and possible
 1635 trigger algorithm improvements for future high luminosity scenarios. The best-suited action is
 1636 the replacement of all currently installed THETA TRBs with the newly produced FPGA-based
 1637 ones. The removed boards could be used as a source of spare BTIMs to be used to repair the
 1638 failing PHI TRBs. If we follow this option, 2300 spare devices would be available allowing
 1639 survival of PHI TRBs to the Phase 2 luminosity era. However, this replacement is an expen-
 1640 sive option and is probably not worth it if the new BTI is performing exactly like the old one.
 1641 Hence an alternative option could be the replacement of only a part of the boards: changing

1642 for instance one full station layer (e.g. MB1) we could recover 780 BTIM so that even assum-
 1643 ing a steady failure rate, there would be enough to cover the detector needs until the Phase 2
 1644 luminosity upgrade.

1645 In the meantime it will be possible to understand if the theta trigger projection logic needs
 1646 modifications for SLHC, as discussed later. The new algorithm could be uploaded to the al-
 1647 ready installed FPGAs, while choosing a less expensive ASIC option for the production of the
 1648 remaining boards, which could be installed during the long LHC shutdown in 2020 preceding
 1649 the beginning of the high luminosity run.

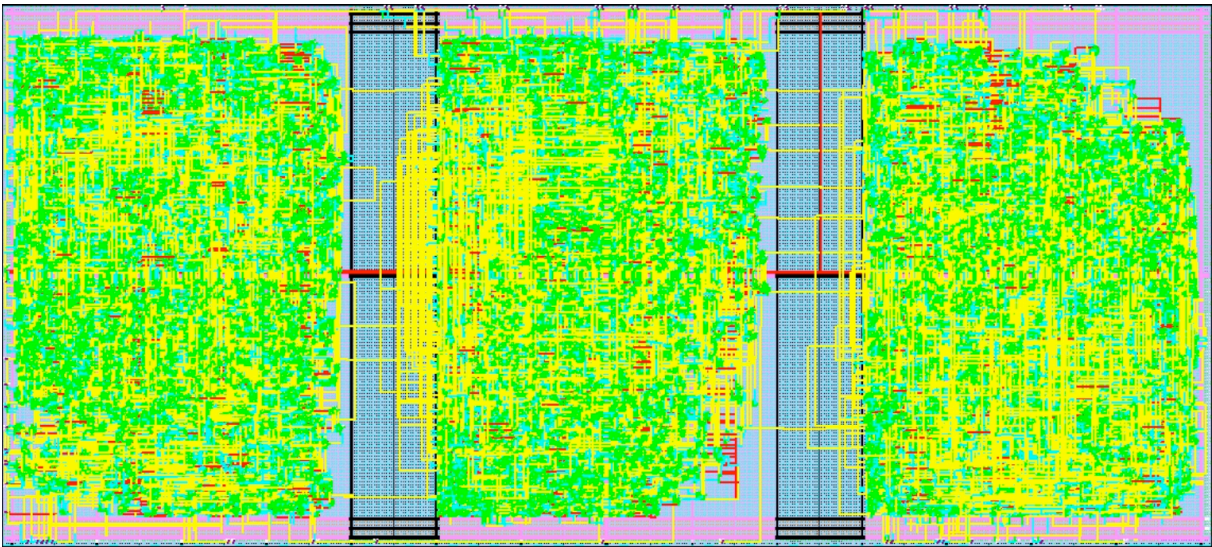


Figure 3.8: Layout of 3 BTIs included in an ACTEL A3PE3000L FPGA.

1650 The cost of the replacement will depend on the number of FPGAs needed which in turn de-
 1651 pends on the number of BTIs that can be programmed inside each of them. An ACTEL A3PE3000L
 1652 can easily contain 2 BTIs while it is far more difficult to include 3 or even 4 of them. Currently
 1653 3 BTIs have been included in one chip (Figure 3.8) although the timing is not yet correct (76
 1654 MHz against 80 MHz), while inclusion of 4 of them is really at the limit since $\sim 90\%$ of the
 1655 FPGA resources are used. The number of FPGAs needed for each TRB is 16 if two BTIs/FPGA
 1656 are included, while it is 11 if three BTIs/FPGA are included. Although rather problematic the
 1657 inclusion of 4 BTIs/FPGA is still an option being pursued. A prototype board is being devel-
 1658 oped in order to understand if there is any critical aspect in the project and eventually solve it.
 1659 Main problems currently being addressed are power supply schemes, power dissipation and
 1660 network configuration of the board.

1661 There is, in fact, only one major improvement that can be made in a new THETA TRB. Cur-
 1662 rently the triggers in this projection are OR-ed in groups of 8 BTIs, leading to a local z-position
 1663 resolution of 16 cm, while the intrinsic resolution of the chamber is ~ 1.2 mm. The new board
 1664 could then be programmed to transmit a more accurate value allowing a better resolution. The
 1665 polar angle resolution for a few different cases, assuming a beam spot with 5 cm z-spread, is
 1666 shown in Figure 3.9. There is room to halve the current polar angle resolution. Incorporating
 1667 this improved resolution will require changes to the DT Track Finder.

1668 3.3.2.3 Schedule

1669 The actual implementation program will largely depend on the final decision about access
 1670 to the Minicrates. The main bottleneck is access to the minicrates since the detector must be

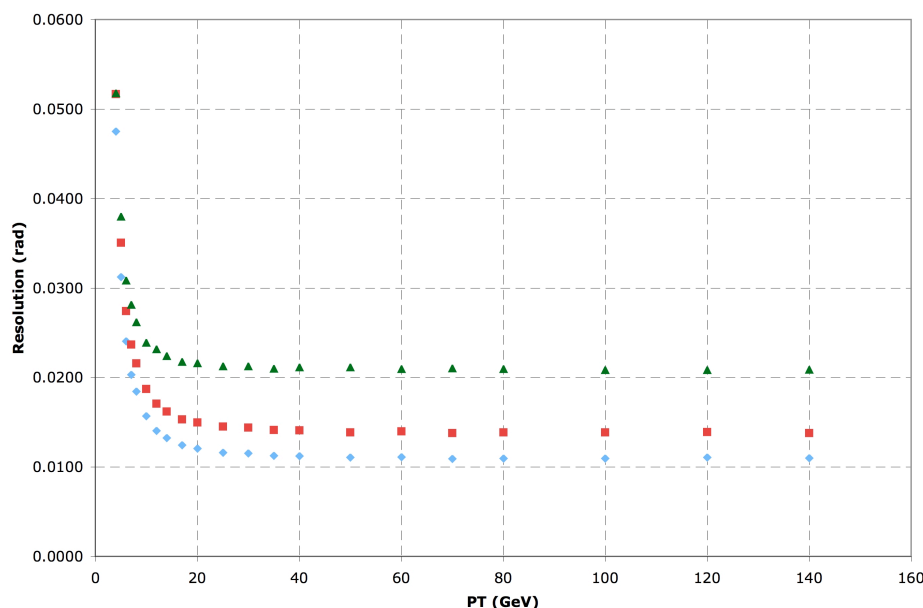


Figure 3.9: Expected resolution of the polar angle θ as a function of the muon momentum for current resolution (green), only BTI number transmitted (red), full resolution (blue). The primary vertex z - position is smeared with a Gaussian of $\sigma = 5$ cm.

Table 3.3: Upgrade schedule

2010	production of 2 prototype boards
2011	bench tests and decision on replacement strategy
2012-2013	mass production and test
2014-2015	installation
2015	decision about strategy in high luminosity operation

1671 opened to allow board replacements. The interventions should be easier on external wheels,
 1672 but on average we expect to be able replace and test two minicrates/week. From the detector
 1673 performance point of view the best solution is the replacement by stations in such a way that
 1674 the detector preserves a uniform response. This choice optimizes the access time, since the
 1675 replacement on any wheel can be done in parallel with the interventions on other detectors,
 1676 thus adapting the work to the general CMS maintenance schedule. Taking into account all the
 1677 constraints the total access time needed to replace all boards of one station is about 6 months.
 1678 We propose to replace all the boards in one full station (e.g. MB1) with the FPGA version by
 1679 2015. The replacement in the other stations will be decided only if needed and when it will be
 1680 clear which one will be the best option to pursue. We propose the schedule shown in Table 3.3.

1681 3.3.3 Sector Collector Upgrade

1682 3.3.3.1 Overview of present Sector Collector system

1683 The Sector Collector (SC), second level of DT trigger and read-out electronics, is sitting in the
 1684 tower racks on one side of the CMS wheels. It is made of 10 VME crates that host 60 ROS
 1685 (Read-Out Server) boards, 60 TSC (Trigger Sector Collector) boards and 10 TIM (TTC Interface
 1686 Module) boards.

1687 Each ROS board is in charge of data merging and data quality monitoring, reducing data over-

1688 head to build a synchronized event fragment of one sector. They collect the information from
1689 25 ROBs (Read-Out Boards), which are located inside the Minicrates. Each ROB sends its read-
1690 out information to the ROS through an LVDS copper link, up to 40 meters long, at 240 Mbps.
1691 Merged data is sent from each ROS through a 60 meters optical link at 800 Mbps to the DDU
1692 (Device Dependent Units), located in the Underground Service Cavern (USC55) at the S1 floor.

1693 Local trigger data of each chamber are output using serial LVDS running at 480 Mbps on two
1694 FTP cables, up to 40 m long. The TSC boards collect and synchronize the trigger information
1695 from one sector (4 or 5 chambers). They send the encoded information of position, transverse
1696 momentum and track quality through 1.6 Gbps optical links (about 60 m long path) to the
1697 counting room, where optical receiver boards (Opto-RX) fan out the trigger data to the Drift
1698 Tube Track Finder (DTTF).

1699 3.3.3.2 Motivations for Sector Collector upgrade

1700 The proposed upgrade of the Sector Collector is not motivated by the physics performance of
1701 the sub-detector as of today, but by the fact that aging and other risks may jeopardize detector
1702 operation and contribute to an accelerated degradation.

1703 The Sector Collector is a complex electronic system located in an environment with significant
1704 magnetic fields and radiation doses up to 0.2 Gy per year of LHC run (charged particle fluxes
1705 of $20 \text{ cm}^{-2} \text{ s}^{-1}$) that intrinsically becomes a weak point in terms of maintenance of the detector.
1706 A failure in one ROS or TSC board may handicap a large fraction of the detector (one sector
1707 out of 60) and a failure in one TIM board turns into half a wheel lost both in the trigger and
1708 read-out chains. A fast reaction time is needed in order to minimize the impact of such fail-
1709 ures. However, limited access to the CMS cavern, which is subject to technical stops in LHC
1710 operation and radiation protection issues, increases dramatically the impact of a failure in the
1711 system, and renders a significant fraction of the DT system useless in the meantime.

1712 Another point of concern is the power consumption due to the limited cooling capacity of
1713 the tangential turbines capable of operating under such magnetic fields. Aging of the present
1714 turbines, will lead to operation of SC electronics at higher temperature, and thus, accelerated
1715 aging and increased failures. The power dissipation of the present Sector Collector electronics
1716 is already marginal for the CMS cooling system, so any increase in performance cannot be
1717 accompanied by an increase of power consumption if these electronics remain in their present
1718 location.

1719 Furthermore substitution of the present electronics with higher performance designs that may
1720 improve functionality is subject to the constraints of being able to operate in the radiation en-
1721 vironment. This requires identification of proper devices through radiation campaigns, which
1722 increase significantly the design timescale and price. Moreover, in some cases, increased per-
1723 formance may be limited itself by the radiation tolerance of the devices. On top of previous
1724 arguments, the accumulated experience points to several aspects related to the Sector Collector
1725 electronics that leave room for performance improvement.

1726 **3.3.3.2.1 ROS boards** The read-out electronics was designed to work beyond the ex-
1727 pected data rates at LHC. However, during the last years we have observed the presence of
1728 bursts of noise affecting large areas of the detector (more than one sector) that have an impact
1729 on buffer occupancies throughout the read-out chain. In fact, the maximum number of hits per
1730 HPTDC (High Performance TDC chip produced by CERN) in the ROB boards has been lim-
1731 ited at present to be able to cope with the present noise without flooding the data acquisition
1732 system.

Table 3.4: Number of links between Minicrates and Sector Collector electronics.

	Per Sector	Per Wheel	Totals
ROB to ROS	25	300	1500
SB to TSC	32/40	400	2000
Total	57/65	700	3500

1733 ROS design includes some parallelism in channel processing, but each group of 6 input chan-
 1734 nels is processed sequentially since input FIFOs are external to the FPGA controller. The pro-
 1735 grammable logic devices market has evolved to allow embedded deserializers and placement
 1736 of large memories inside each device. Profiting from these higher performance devices, ROS
 1737 functionality could be improved significantly by increasing its parallelization and thus, reduc-
 1738 ing its processing time. The benefit could be twofold; not only will the effect of noise be reduced
 1739 at this level by means of larger buffer capabilities, but also, higher performance FPGAs could
 1740 allow suppression mechanisms that filter out noise events avoiding saturation of higher level
 1741 buffers. However these new devices cannot survive in the cavern radiation environment.

1742 **3.3.3.2.2 TSC boards** The Opto-RX boards that collect TSC information turned out to be
 1743 very sensitive to the clock frequency shifts intrinsic to LHC energy ramps, which by unlocking
 1744 the links create high rate input noise that propagates through all the trigger chain resulting
 1745 in an unsustainable trigger rate. Unfortunately slow control of these Opto-RX boards through
 1746 a JTAG interface is also unstable and allows very limited programmability in the devices. It
 1747 is also worth noting that DT trigger latency is one of the largest in the CMS trigger system
 1748 and reducing the serialization/deserialization stages may allow a faster triggering mechanism.
 1749 This may be achieved by the integration of TSC and Opto-RX devices in one single module.

1750 3.3.3.3 Description of the proposed upgrade

1751 The proposed solution to Sector Collector electronics problems consists of its relocation to the
 1752 USC counting room, freeing it from the hazardous environment in the cavern and minimizing
 1753 the downtime in case of failure. Since SC inputs are based on copper links whose length cannot
 1754 be increased without compromising its reliability, a simple copper to optical fiber conversion
 1755 should be placed in the cavern. As a first approach, a suitable place to allocate this optical
 1756 converter is in the present SC tower racks. The total number of copper-pair differential links
 1757 reaching the SC crates is 3500, distributed as shown in Table 3.4.

1758 Several options for this optical conversion are under study. The preferred one at present is a
 1759 direct 1-to-1 copper to optical fiber conversion. This implies 3500 optical fibers to be routed
 1760 from the cavern to the counting room. Taking as a reference the DT optical links currently
 1761 installed between SC and USC, consisting of 10 multi-ribbon cables 48 fibers each, the minimal
 1762 number of cables to route is 73 (plus spares). Each of these cables is 10 mm diameter, so the
 1763 total cross section required would be in the order of 100 cm².

1764 Present SC crates space would be replaced by an array of 3500 electrical to optical converters,
 1765 by means of a very simple (and, therefore, robust) electronics system based on a line equalizer,
 1766 laser driver and laser diode. The actual implementation of this solution is still under study,
 1767 but the main components are already identified and some of them are already in operation in
 1768 the current system, so no further characterization may be required. It is also possible that the
 1769 solutions under study in the CERN Versatile Link project may fit our requirements.

1770 Accordingly, present SC electronics would be moved to USC, where it would be necessary to

1771 implement a conversion back from optical to electrical signals. The input stages of the present
 1772 TSC and ROS boards are implemented in mezzanine boards, so they can be replaced to receive
 1773 the appropriate optical links instead of the present copper ones with minor modifications of
 1774 the SC boards and thus reduced cost. Moreover, the interface with present DDU and DDTF
 1775 would remain unchanged, avoiding dependencies with upgrading different parts of the system
 1776 simultaneously. The basic schematic of this proposal is shown in Figure 3.10 for an individual
 1777 DT sector. The reverse optical to copper conversion is represented as an independent module to
 1778 emphasize that ROS and TSC main functionality does not necessarily need to be fully redone.

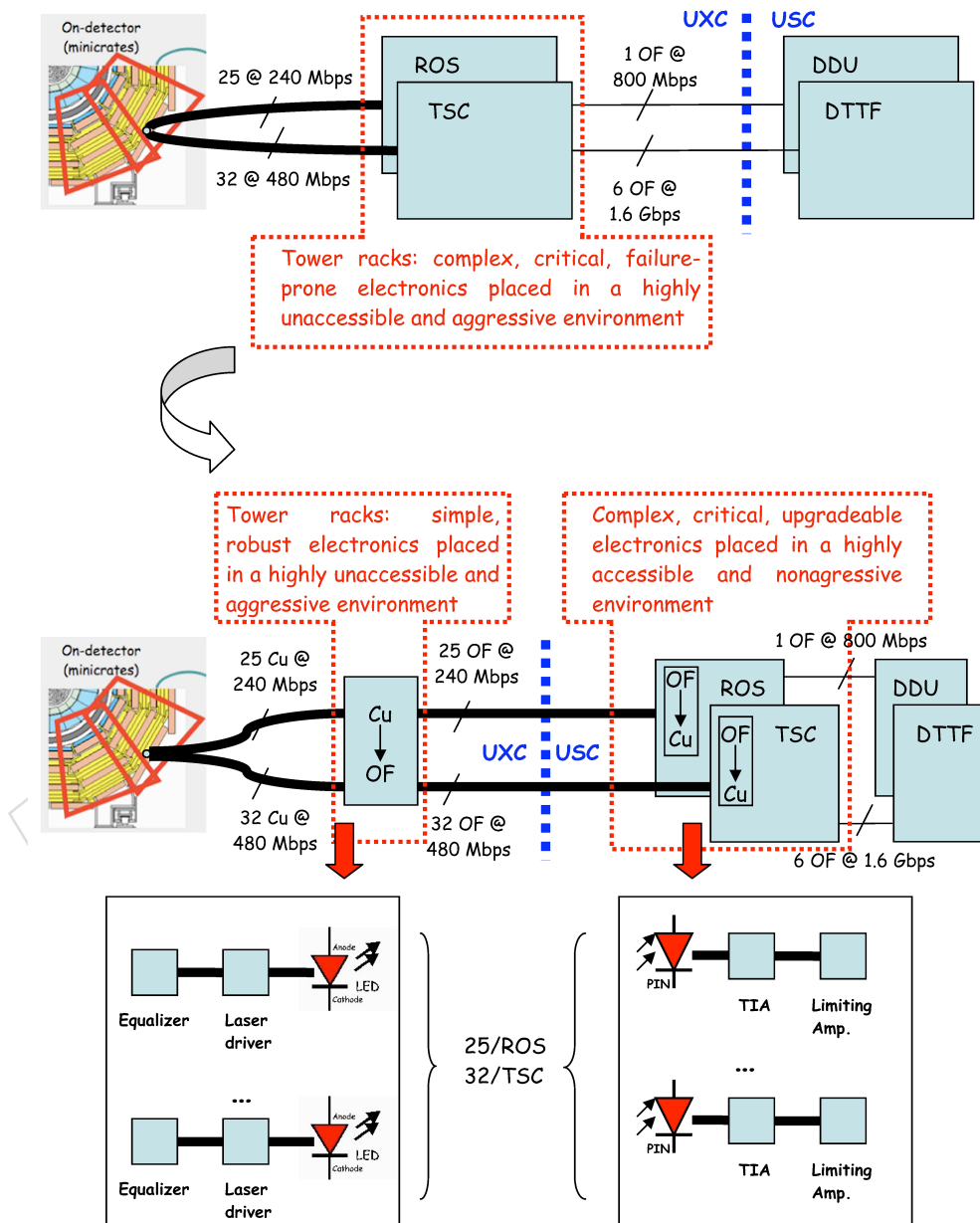


Figure 3.10: Schematic view of the proposed upgrade for Sector Collector electronics. The top part of the figure shows the current situation, while the bottom part sketches the situation after the proposed upgrade.

3.3.3.4 Examination of the upgrade and alternatives

There are many advantages of this proposal:

1. The complex SC electronics is located in a less hostile environment where the possibility of failure is reduced.
2. Access on demand in case of failure can easily take place, thus, minimizing downtime.
3. Copper to optical conversion in tower racks is much simpler and more robust than present SC electronics, with much smaller power consumption, so the probability of failure is minimized.
4. The solution allows a gradual, controlled replacement plan for current SC electronics in order to implement future upgrades.
5. The relocation of SC electronics in USC provides great benefits in view of future upgrades to improve the physics performance of the system by allowing the use of commercial off-the-shelf devices without radiation tolerance requirements. New designs will profit from a reduced price at a higher performance.

The main disadvantage of the proposal is the increased number of fibers and optical transmitters that need to be installed. Solutions allowing the minimization of the number of optical links by means of multiplexing are under study. Direct multiplexing the 240 or 480 Mbps serial links may not be feasible due to timing constraints: the high speed and phase difference of the various independent inputs does not allow a proper sampling of the links guaranteeing signal integrity.

An alternative could be multiplexing the input links once deserialized by means of a large data-width high-speed serializer. Accordingly, the number of optical fiber links to be routed can be reduced by a factor N , where N can be at most 3 to 4 for devices available on the market (even GBTx). It has to be also noted that the added complexity in the copper to optical fiber conversion system will compromise the advantage of this design compared to present SC electronics. On top of that, it is unclear if the reduction in the number of optical components entails a cost reduction. What is clear is that cost will not be reduced by a factor N , due to several factors: the higher number of components that will be required to perform the copper to optical multiplexed conversion; their increased performance requirements; the higher speed of the new link which is directly associated with its grade requirements. Moreover, the demultiplexing will have to be done within the new SC electronics, also increasing accordingly the complexity and cost of the new design. Furthermore, additional multiplexing and demultiplexing stages will increase trigger latency as compared with a direct copper to optical conversion. The impact of a latency increase is critical in our case, since DT trigger latency is already the largest one in CMS and will have a non negligible impact in other CMS subdetectors. Finally, this approach is much less compatible with a possible future upgrade that would allocate the copper to optical conversion nearby or within Minicrates.

3.3.3.5 Implementation and infrastructure issues

The feasibility of the relocation of the Sector Collector from UXC is subject to various constraints from the infrastructure point of view. The most relevant ones are the routing of a large amount of fibers between the cavern and the counting room and the availability of the space required to allocate present Sector Collector electronics in USC.

1821 **3.3.3.5.1 Routing of new fibers** As previously mentioned, the number of links if TSC
1822 and ROS were to be moved to the counting room can be up to 3500 fibers. By using multi-
1823 ribbon fibers the required cross section could be minimized down to 100 cm². Enough space
1824 should be made available not only in the tunnels that exit the cavern, but also in the cable
1825 chains of the external wheels and in the Patch Panel frames below the tower racks. Preliminary
1826 inspections indicate that space is available for the cables, but more detailed studies should
1827 be done about connector fanouts and proper integration. Furthermore, the available space to
1828 recover extra cable lengths below the S1 floor in USC55 needs to be verified.

1829 One important point to be taken into account is that trigger fibers must follow the shortest
1830 possible path to avoid increasing trigger latency. Therefore, at least trigger fibers should be
1831 routed through the fast channels that provide a short path of less than 60 meters. We are also
1832 investigating the possibility to install all those fibers with the “blowing technique” by means of
1833 a specialized CERN group.

1834 **3.3.3.5.2 Relocation of crates in USC55** The Relocation of Sector Collector electronics
1835 is a complex operation that should be planned carefully to be fully compatible with the present
1836 system throughout all of the upgrade steps. A gradual approach would be much more con-
1837 venient in some cases, minimizing system failure risks and allowing proper testing of the new
1838 solution before full installation. In order to decouple copper to optical conversion and redesign
1839 of new Sector Collector electronics, a feasible proposal is to reuse at a first stage present SC
1840 boards in USC with modified mezzanines that host the receivers for the Minicrate data with
1841 optical receivers. In either case, the required space to allocate Sector Collector electronics in
1842 USC remains constant. Accordingly, at least the same amount of space presently used in UXC
1843 should be made available in USC: 10 VME 9U crates, i.e., 120 U, would be needed. Roughly,
1844 that would imply using 3.5 racks. At present, about half of that space could be available among
1845 racks S1D10, S1D08 and S1D03, presently assigned to the DT system. Again, it is important to
1846 take into account that to minimize trigger latency, at least, TSC boards should be placed near
1847 the DTF rack. The previously mentioned racks accomplish this.

1848 **3.3.3.5.3 Interferences and dependencies** The installation of new fibers is a major task
1849 that requires a long shutdown and could not be accomplished before 2012. However, fiber
1850 installation and Sector Collector relocation are two tasks that can be decoupled in time. In
1851 fact, relocation of Sector Collector in USC could be split into several tasks that are independent
1852 from the opening of CMS wheels, and thus, from LHC long shutdowns. Accordingly, this op-
1853 eration can be performed during the short end-of-year technical stops. The minimal advisable
1854 granularity is half a wheel, i.e., one Sector Collector crate.

1855 In a first scenario, the plan would be to reuse the present SC boards in USC but modify the
1856 mezzanines that host the receivers for the Minicrate data. In this way, a complete redesign of
1857 the system, if desired, does not need to be tied to the schedule in the present proposal. The
1858 tower rack space, presently used for Sector Collector electronics, will accommodate the copper to
1859 optical fiber conversion modules, which would be simple and robust. The number of compo-
1860 nents to be used is minimal and therefore, less prone to failures. Power consumption will also
1861 be strongly reduced, ensuring longer term operation.

1862 **3.3.3.6 Proposed schedule**

1863 There are 5 major tasks that must be done:

- 1864 1. Installation of fibers between UXC and USC (up to 3500 links distributed in 73 multi-

1865 ribbon cables). This can be divided into three stages:

- 1866 • 30 cables through YB+ tunnel
- 1867 • 15 cables through YB0 tunnel
- 1868 • 30 cables through YB- tunnel

- 1869 2. Relocation of TSC and ROS in USC according to the space made available.
- 1870 3. Modification of TSC and ROS input mezzanines to support optical link reception.
- 1871 4. Redesign of ROS electronics with a new slow control interface and higher performance.
- 1872 5. Redesign of TSC and Opto-RX electronics integrated in a single unit compatible with the
- 1873 new DTTF design.

1874 The optical fibers installation requires opening the cable chains. Such an intervention is quite
1875 time-consuming and can be done only by an experienced team. The cost of installation is also
1876 largely dependent on the technique used. If we were to redesign completely ROS and TSC an
1877 extra cost of 600 kEuros should be added assuming the costs are similar to those of the currently
1878 installed boards.

1879 3.4 RPC Muon Detector

1880 3.4.1 Introduction

1881 3.4.1.1 The CMS muon trigger system

1882 At the LHC, the bunch crossing frequency is 40 MHz, which, at the nominal luminosity of
1883 $10^{34} \text{ cm}^{-2}\text{s}^{-1}$, leads to about 800 million proton-proton collisions per second. CMS has put
1884 emphasis on the detection and identification of muons. Every 25 ns some 1000 particles emerge
1885 from the interaction point into the CMS spectrometer. In less than 3 μs a first level trigger
1886 has to reduce this rate to 100 kHz without losing potentially interesting collisions requiring
1887 further analysis. The CMS muon system described in the CMS Muon Technical Design Report
1888 [CERN/LHCC 97-32] contains two complementary technologies:

- 1889 • Wire chambers that track the muons with precision through the iron yoke and return
1890 field: Drift Tubes (DT) in the barrel part; Cathode Strip Chambers (CSC) in the end
1891 caps. In both cases, there are four layers of chambers and they provide a reasonable
1892 estimate of the trigger timing.
- 1893 • Resistive Plate Chambers (RPC) that determine precisely the time of passage of the
1894 muons as well as an estimate of their transverse momentum.

1895 3.4.2 Physics motivation for the forward up-scope

1896 The first level trigger based on the RPCs provides CMS with the most precise timing in both the
1897 barrel and endcap region. Six concentric layers of chambers are used in the barrel part, while
1898 four layers have been foreseen in total for the end caps to cover a rapidity up to $|\eta| = 2.1$. A
1899 Memorandum Of Understanding (MOU) commitment for the production of the forward RPC
1900 system was signed with university groups in Islamabad (Pakistan), Peking (China) and Seoul
1901 (Korea). Due to insufficient funding availability, only 3 layers were built in the endcap which
1902 provided a limited rapidity coverage up to $|\eta| = 1.6$ as shown in Figure 3.11. It was expected
1903 that the fourth layer chambers could be constructed later so that coverage of the full rapidity

1904 range of the original design could be achieved. The key element of this proposal is to construct
 1905 the 4th layer of RPCs in the endcap.

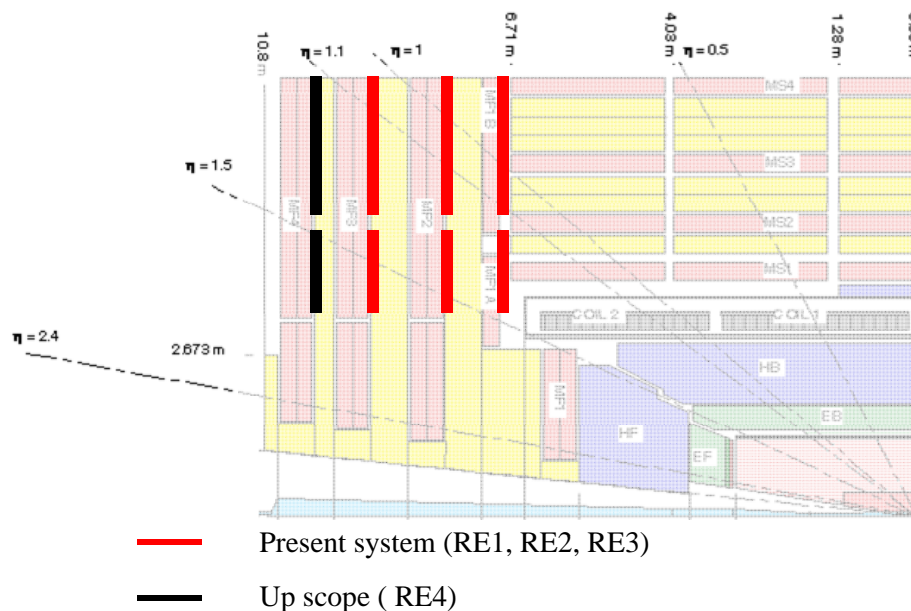


Figure 3.11: Profile of the CMS endcap region showing the existing RPC stations (RE1, RE2, and RE3) and the proposed upgrade station RE4.

1906 In Figure 3.12 the simulated trigger efficiency as a function of η is shown in case of the present 3
 1907 layers and compared to the result for a 4-layer system. The advantage in extending the detector
 1908 to include the fourth station is clearly evident.

1909 The completion of the forward RPC system to 4 layers per end cap is therefore a priority. CMS
 1910 has decided to split the up-scope project into two distinct phases:

- 1911 • Phase 1: completion of the low $|\eta|$ part ($|\eta| < 1.6$).
- 1912 • Phase 2: completion of the high $|\eta|$ part ($1.6 < |\eta| < 2.1$).

1913 This section will be focused on the restoration of a full low η system which will provide an
 1914 efficient and robust trigger operation at the LHC design luminosity. The groups from Pak-
 1915 istan, China and Korea have already committed themselves to this completion. In addition,
 1916 groups from Belgium, India, and Egypt have confirmed their involvement in the project while
 1917 negotiations with Italy are under way to provide the off-detector electronics. Other countries
 1918 (Finland, Poland) have expressed an interest in joining the project, although they have not yet
 1919 committed to any financial contribution. Nonetheless, their participation and expertise is an
 1920 important aspect of the project. Recently interest has been expressed from Iran and Colombia
 1921 and negotiations have started to define possible contributions and areas of involvement.

1922 3.4.3 Detector design and layout

1923 3.4.3.1 Description of the detector geometry

1924 The forward stations are wedge-shaped detectors with a double gap RPC. A schematic layout
 1925 is shown in Figure 3.13a. The actual system consists of 432 chambers mounted in a staggered
 1926 way in two concentric rings on the endcap disks to cover its surface ($\sim 150 \text{ m}^2$ per disk) as
 1927 illustrated in Figure 3.13b. A photograph of the RPC third layer on the +z endcap is shown

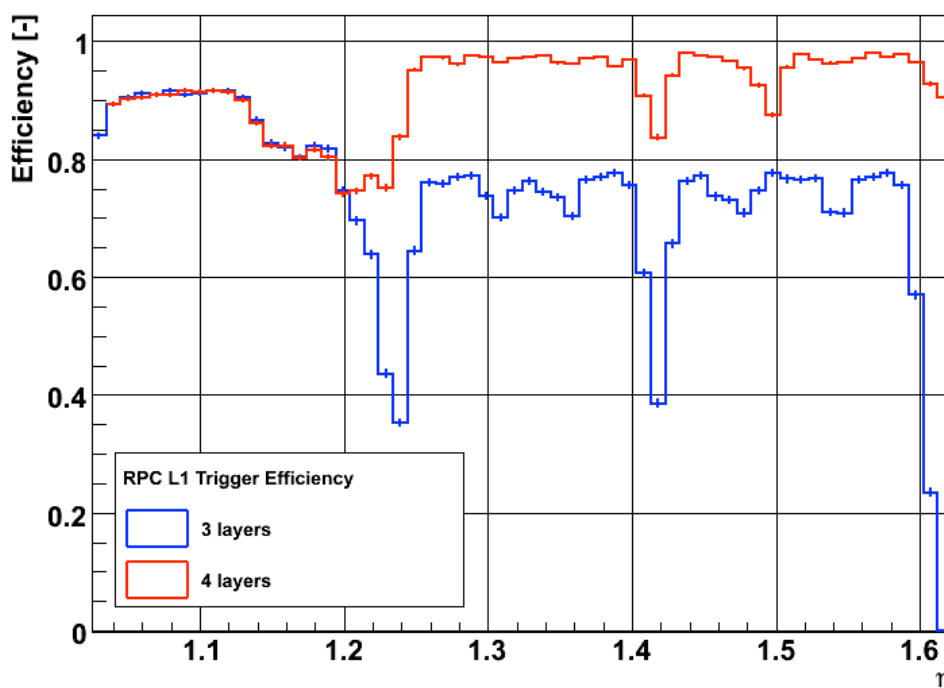


Figure 3.12: Simulated trigger efficiency as a function of the number of layers of RPCs.

1928 Figure 3.14. The completion of the forward RPC system for $|\eta| < 1.6$ region will require an
 1929 additional layer, (RE4), composed of 144 new chambers. These new RE4 chambers will be
 1930 composed of two concentric rings (RE4/2 and RE4/3) of RPC chambers. Each ring is therefore
 1931 composed of 36 chambers. These new RPC chambers will be of the standard CMS forward
 1932 design.

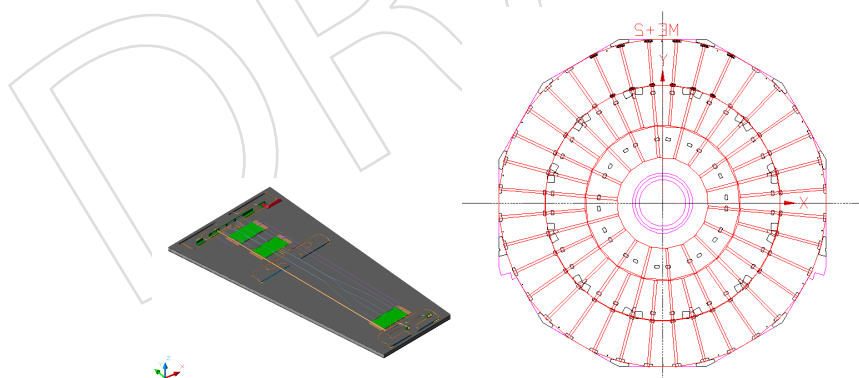


Figure 3.13: a) Schematic layout of a forward double gap chamber; b) Layout of an RPC station on the endcap yoke disk.

1933 3.4.3.2 Integration of station RE4

1934 The new RE4 station will be installed on the back of the YE3 yoke, mounted independently
 1935 of the CSC chambers. The RE4 detectors will be mounted on an aluminum interface frame,
 1936 supported on the existing threaded M16 holes at the extension of the CSC mounting posts, as
 1937 illustrated in Figure 3.15. This solution decouples the installation of RE4 from the existence of

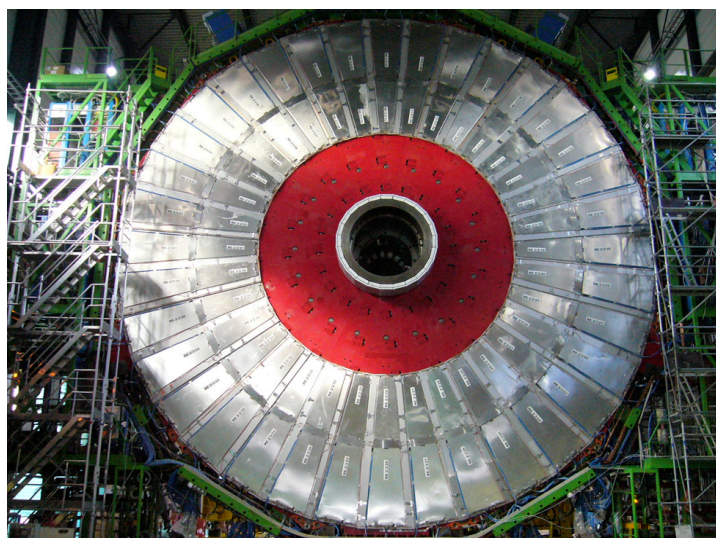


Figure 3.14: The third station of RPC chambers on the +z endcap disk.

1938 the YE4 shielding wall. The nominal clearance to the shielding wall will be 9 mm provided the
 1939 interface frames have a thickness of 8 mm.

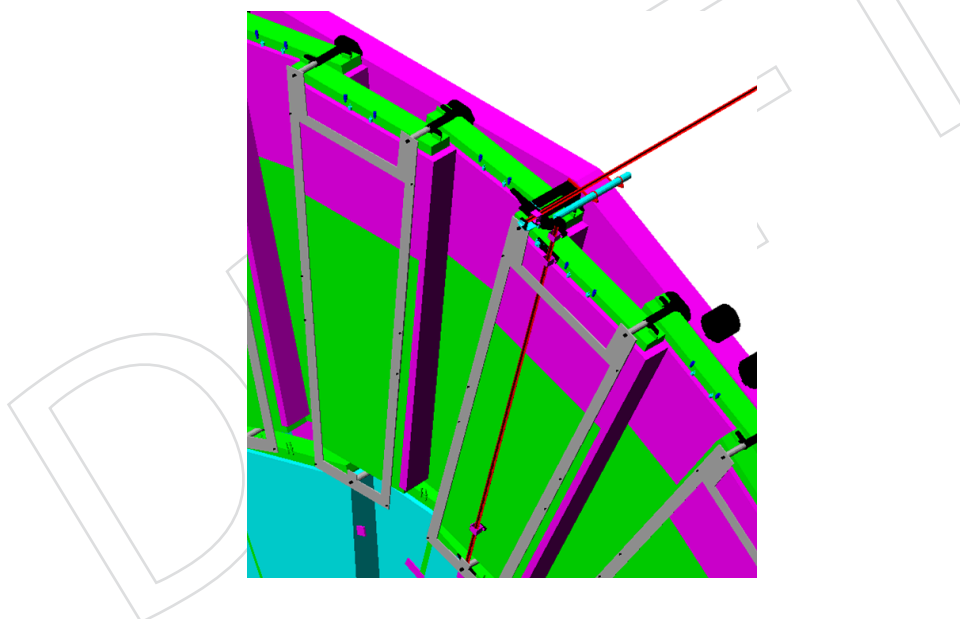


Figure 3.15: Mounting of the RE4 chambers on the back side of the YE3 disk with the interface frame attached to the disks.

1940 The services to RE4 will be housed on the YE3 towers where the infrastructure will need to be
 1941 completed. No services to RE4 have been installed since they were part of the staging scenario
 1942 that originally involved mounting the RE4 chambers on the YE4 shielding wall. The infrastruc-
 1943 ture services that now must be added to YE3 are:

- 1944 • A gas distribution rack with 72 channels and the necessary pipe work to the local
 1945 bulkheads.
- 1946 • The manifold and pipe work for the proper distribution of the cooling fluid.
- 1947 • The low voltage (LV) system, including crates and cabling to the power supply sys-

1948 tem in the YE3 towers.

- 1949 • The HV cabling to the YE1 Patch Panel (requires insertion in the minicable chain)
- 1950 and to USC (requires insertion in the main cable chain).
- 1951 • The necessary Link Board Boxes and the related cables and optical fibers.

1952 As a consequence the endcap main cable chains will have to be opened to install the missing
 1953 HV umbilical links to the SX5 cavern (this will be a major intervention that requires an expert
 1954 team). It will be possible only when the main cable chain will be accessible, which will require
 1955 the complete opening of YE1s. Adequate space for these cables has been reserved in the main-
 1956 and mini- cable chains in the original construction of CMS.

1957 3.4.4 Electronics

1958 The layout of the RPC electronics is shown in Figure 3.16. The chamber readout data are ini-
 1959 tially analyzed at the Front-End electronics Boards (FEB), which forms LVDS digital signals
 1960 and sends them to the Link Boxes, which are located on the balconies at the yoke periphery.
 1961 Here synchronization and data reduction is performed before transmitting the information via
 1962 optical fiber to the trigger electronics in the control room.

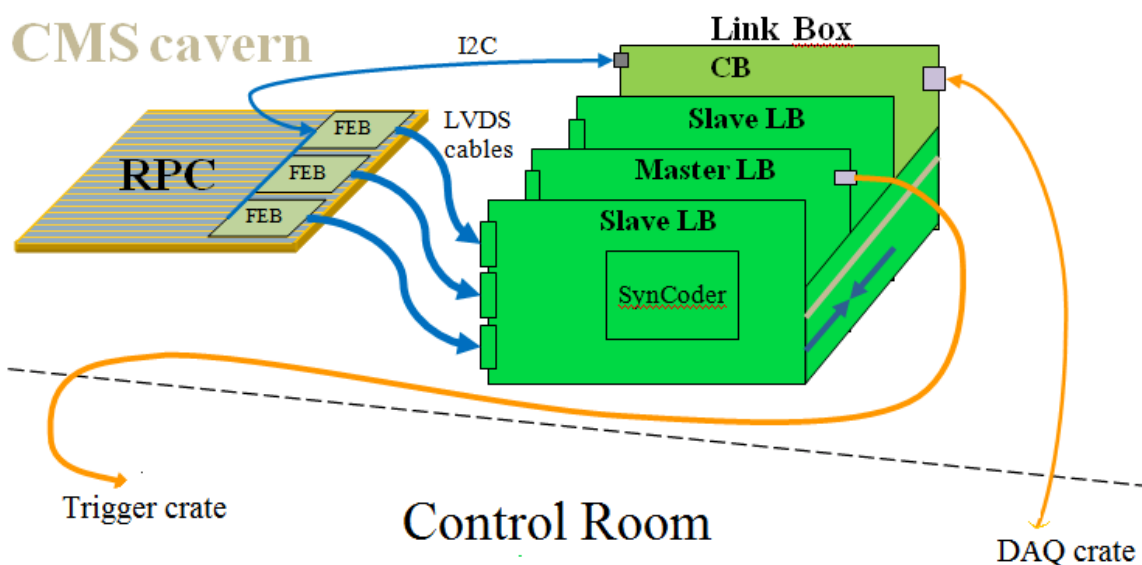


Figure 3.16: Layout of the RPC electronics.

1963 3.4.4.1 Front-end boards

1964 The same RPC Front-End Board (FEB) that was developed in the past and mounted on the
 1965 current chambers will be employed. The front end has four 8-channel ASIC Front-End Chips
 1966 (FEC) each consisting of an amplifier, discriminator, monostable and differential LVDS line
 1967 driver. The connection between the RPC strips and the FEB is made with 50-Ohm coaxial
 1968 cables, that are soldered on small adapter boards such that they are easily pluggable to the
 1969 FEBs. FECs are available from the past production. However, new boards will be necessary to
 1970 instrument the new RE4 layer and production is scheduled to be done in Pakistan. Figure 3.17
 1971 shows a picture of one 32-channel FEB.

1972 Pakistan will be responsible for FEB mass production in Pakistan. Plans call for 50 FEBs to be
 1973 produced by the end of October 2010. After a complete validation of FEBs, mass production

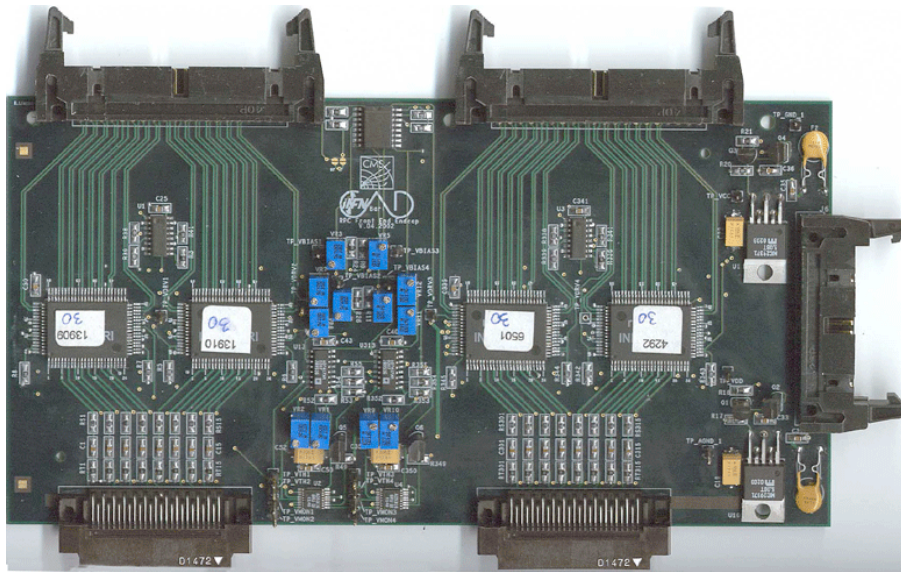


Figure 3.17: Front-end board.

1974 will be started at the beginning of 2011. We require 600 FEBs, which includes 10% contin-
 1975 gency. The required production time is approximately three months, which includes the time
 1976 of procuring of components, developing of PCBs, mounting the components, and testing of
 1977 final FEBs. Before shipment to CERN, validation tests, such as voltage threshold setting (VTH),
 1978 voltage biasing setting (VBIAS), voltage monitoring (VMON) and I2C for quality assurance,
 1979 will be performed in Pakistan.

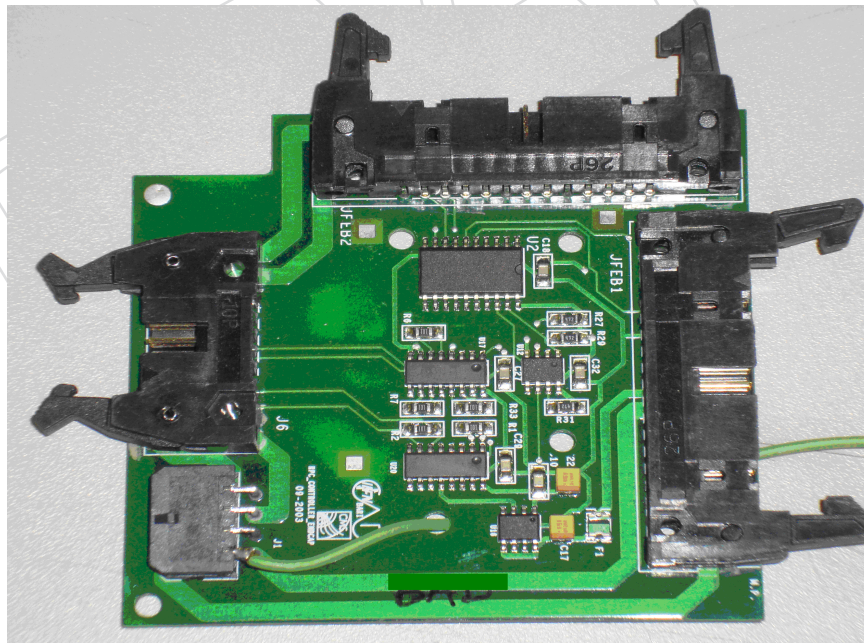


Figure 3.18: Distribution board.

1980 Each chamber also contains one Distribution Board (Figure 3.18) that receives power and slow
 1981 control communication through power cables and I2C bus and distributes them to the FEBs

Table 3.5: List of Link Board system components needed for RE4.

	RE4/2,RE4/3 on YE3		
	needed	spare	total
LB mechanics	12	2	14
LB Back Plane	12	2	14
MLB	48	10	58
SLB	96	10	106
CB	24	6	30
FP	24	6	30

1982 using flat cables. 200 additional Distribution boards will be required.

1983 3.4.4.2 Off-detector electronics

1984 The output of the FEBs is sent to the Link Board system (LB) where the synchronization with
 1985 the LHC clock, the optical conversion and the transmission to the Trigger Electronics are per-
 1986 formed. The new layer, RE4, has to be equipped with a complete new set of LBs. Table 3.5
 1987 gives the number of additional components needed to complete the LB system on the detector
 1988 side. The new electronics will include minor design improvements to overcome a few prob-
 1989 lems observed during operation. However, it will be fully compatible with the present system.
 1990 A special role is played by the Control Board (CB) which drives each LB crate, provides inter-
 1991 crate communication and hosts the main software for the connection to the readout and the
 1992 trigger systems. While only minor improvement will be considered for the additional CBs to
 1993 be procured in the present upslope project, a major redesign is planned for the 2016 upgrade.
 1994 INFN is willing to take responsibility for the production and to gain expertise in the operation
 1995 of the new system. The tests and the installation of the new boards should be done under Ital-
 1996 ian responsibility. Poland is expected to provide expertise to allow the transfer of knowledge
 1997 and to take the responsibility for the integration of the trigger system of the new electronics.

1998 3.4.5 Services

1999 3.4.5.1 Gas system

2000 At present no work has been done for the fourth station besides the necessary piping for the
 2001 control of the intended gas rack. The supply and return piping to RE3 chambers has been
 2002 designed to allow RE4 chambers to be connected to it. It will be necessary to find the space for
 2003 an additional gas rack. Space is available next to the RE3 gas rack, while space above is slightly
 2004 obstructed by the existing RE3 piping.

2005 3.4.5.2 Cooling

2006 Cooling has been a difficulty in the past. Our experience indicates that most of the heating is
 2007 due to external sources, not to the heating of the gaps themselves. Now we are confident that
 2008 the present cooling setup is adequate to compensate for the heat produced by RPC electron-
 2009 ics, which is only 12 watts, but we know that RPC gaps are still suffering from temperature
 2010 increase. We are requesting a cooling connection every 10 degrees on the manifold so we do
 2011 not have 3 chambers on a cooling circuit. Moreover we will have 2 pipes on each side of a
 2012 copper plate. As stated before there are no spigots at present available on YE3 for RE4. Signifi-
 2013 cant reworking of the manifold must be considered. In addition, we are considering mounting
 2014 thermal insulation between the CSC and RPC chambers. We know that RPC operation is quite

2015 temperature sensitive. Best thermal working conditions for RPC are with chambers at 18°C.
2016 23°C is the maximum temperature where we must switch off the chambers. Given the present
2017 performance, the current cooling system in CMS endcap demands significant revision to insure
2018 the best working conditions for RPC. Hence quality assurance procedures in the cooling system
2019 will be particularly important.

2020 3.4.5.3 Signal read out

2021 The data readout and transmission to the trigger crate will need some additional cables that
2022 have to be procured, connectorised, labelled, tested and installed:

- 2023 ● 864 signal cables and 72 DCS (I2C) cables between the RE4 chambers and the Link
2024 Board boxes.
- 2025 ● 48 fibers from LB boxes to RE3 tower patch panels in UXC.
- 2026 ● 24 single-mode TTC fibers from the Link Board boxes to the TTCOC.
- 2027 ● 84 DCS Ethernet (class 7) cables between the Link Board.
- 2028 ● 96 multimode fibers between the Splitter boards and Trigger Boards in USC.

2029 3.4.5.4 High voltage

2030 For the 144 RE4 chambers, a total of 288 HV channels are needed (each gas gap is supplied
2031 separately). However, the number of channels can be reduced by using distribution boxes.
2032 This allows cost reduction while still maintaining the ability to handle problems in case of
2033 a single gap failure. Each distributor (Figure 3.19) will transform 10 input channels into 40
2034 output channels. A total of 8 HV distribution boxes will be needed.



Figure 3.19: HV Distribution board.

2035 A total of 12 HV CAEN A3512 boards (72 channel in total) will be necessary to complete the
2036 system. The existing HV EASY Crates have enough free slots to allow installation of these new
2037 boards. New HV cables need to be pulled from the RE4 chambers to HV patch panel (PP)
2038 at the base of the YE1 disk through mini-cable chains, while additional umbilical cables need
2039 to be installed from PP to reach the USC HV racks. The HV cables from chambers to the PP
2040 will be connectorized and tested before installation, whereas umbilical cables from PP to USC
2041 will be connectorized and tested after installation. Extensive quality tests on the cables will be
2042 performed prior the installation following the same protocols already developed.

2043 3.4.5.5 Low voltage

2044 The Low Voltage (LV) system supplies power to Link Board Boxes (LBBs) as well as Front End
2045 Boards (FEBs). In the case of LBB supply, 8 new A3016 boards will be installed in the existing

2046 EASY Crate (Figure 3.20). The FEB supply would need 12 additional A3009s. In this case, 4
2047 new EASY Crates (3000S) will be installed in each near and far side tower at suitable levels.
2048 The choice of level depends on available space in racks and cable length. New cables from the
2049 CAEN A3009 power supplies to the RE4 chambers will have to be procured, connectorised,
2050 tested and routed in mini-cable chains. The FEB's LV Crates will take the 48V from the existing
2051 RE3 MAO by using a special type of splitter at the PP75 connector. Two new branch controllers
2052 are required, each one controlling near and far side LV-FEB EASY Crates of the same yoke.



Figure 3.20: Available slots for the RE4 LBB boards.

2053 3.4.5.6 Temperature and Humidity sensors

2054 Temperature and relative humidity are parameters that affect the response of RPC detectors.
2055 Several studies on dark current monitoring carried out during CMS commissioning in 2008
2056 and 2009 have shown that the thermal stabilisation of RPCs in the 21-23°C range is essential
2057 for the operation and that the working point depends strongly on temperature. The depen-
2058 dence on humidity is less crucial. However, the stabilization is much more critical due to the
2059 dimensions of SGX5 and the cavern humidity variation range. Presently temperature and hu-
2060 midity monitoring is performed with six conventional electrical sensors in each of the existing
2061 RE stations, while each Barrel chamber has one temperature and humidity sensor. The typical
2062 desired precision is $\pm 0.2^\circ\text{C}$ for temperature monitoring and 2% for humidity monitoring.

2063 The development of optical sensors based on the Fiber Bragg Grating (FBG) technique for tem-
2064 perature measurement has provided a better solution than the electrical sensors with respect
2065 to radiation hardness, insensitivity to magnetic field, lack of electrical noise, ease of installa-
2066 tion, minimal cabling, and precision ($\pm 0.2^\circ\text{C}$). Two Italian groups, Frascati and Naples, have
2067 extensive experience in the development and deployment of FBG sensors for a variety of mea-
2068 surements. Each RE4 chamber will be equipped with one optical sensor for temperature mea-
2069 surement. The sensors will be purchased bare and enclosed in a heat conducting housing.

2070 The sensors will be tested in Frascati for radiation hardness, and installed at CERN on the
2071 RE4 chambers. The design of housings will allow ease of disassembly from chambers prior to
2072 chamber removal from disks for maintenance and repair. Optical fibers will be routed to the
2073 existing CERN system for readout and integrated into the CMS sensors slow-control frame-
2074 work. Humidity monitoring will be performed via conventional electrical sensors, identical to
2075 those employed in the existing RE disks (4 sensors/disk).

2076 Finally, an R&D programme has started in early 2010 for the development of optical sensors
2077 for hydrofluoric acid detection in the RPC gas mixture. Options will be considered in case
2078 of positive results to install a few sensors in the USC gas distribution racks, upstream and
2079 downstream of the RPC detectors in the closed loop recirculation gas system.

2080 **3.4.6 Production facilities**

2081 In the following, the main aspects relevant to the chamber production will be briefly reviewed.
2082 All the numbers quoted below refer to the production of 200 new chambers, out of which
2083 144 will be needed for the RE4 station and the remaining 56 will be kept as spares for the
2084 RE2/RE3/RE4 forward system.

2085 **3.4.6.1 High Pressure Laminate production**

2086 Production of High Pressure Laminate (HPL) will follow the same procedure already estab-
2087 lished in the past. The main steps are:

- 2088 • Production of the HPL foils.
- 2089 • Quality check for resistivity measurement and surface quality.
- 2090 • Cutting the foils to the required size and finally surface cleaning of the obtained
2091 components.

2092 Raw material production will take place at the Puricelli industry near Milan. This company
2093 has the necessary expertise and experience to produce low resistivity ($1-6 \times 10^{10} \Omega \text{ cm}$) HPL as
2094 required (they have hired some expert personnel from PamPla firm, a previous supplier of HPL
2095 for the particle physics community). Recently a small production with the same CMS specifi-
2096 cations has been successfully achieved at the Puricelli site, ensuring that the proper production
2097 set parameters can be reproduced. About six hundred $1620 \times 3200 \text{ mm}^2$ foils for a total of 3110
2098 m^2 are necessary. A preliminary planning draft discussed with the producer shows that about
2099 2 months are required for the production assuming a 3 week cycle for the production and qual-
2100 ity control of batches of 200 foils. A quality check will be performed at the Pavia INFN site.
2101 Here the resistivity measurement table already used in the past will be re-commissioned and
2102 made available for operation. The Pavia group will provide supervision for the operation of
2103 the device, while measurement operations will be under RPC community responsibility. Suc-
2104 cessive cutting and surface cleaning procedures will follow according to the scheme already
2105 established in the past respectively at RIVA (Milano) and General Tecnica (Frosinone).

2106 **3.4.6.2 Gap production**

2107 The gas gaps for the forward upgrade RPC chambers will be produced by KODEL at Korea
2108 University. KODEL will use the same technology as developed for the production of the initial
2109 432 forward RPC chambers. A total of about 660 gaps are needed for the proposed new RE4
2110 station production (including spares). The general production procedures can be divided into
2111 several sequential steps:

- 2112 • Initially HPLs will be inspected for defects in color, scratches on the surface and
2113 any mechanical damage on the edges and corners. The surfaces of all selected HPLs
2114 will be properly cleaned before the graphite coating. The next step is to insulate
2115 the graphite surface with PET film. PET film is glued to the graphite surface by the
2116 machine shown in Figure 3.21a. The gaps are then assembled and placed under a
2117 pressing machine (Figure 3.21b) for 24 hours for glue hardening.
- 2118 • All assembled gas gaps are treated with linseed oil mixed with heptane. The rate
2119 of linseed oil administration into the gas gap placed in its vertical position is 100
2120 cm^3/hour . After the completion of the linseed oil administration, a small compres-
2121 sor is used to immediately remove the remaining oil in the gas gap. Then, dry air at
2122 40°C is circulated over the oiled surfaces of the gaps. The flow rate of air is from 60
2123 to 100 liters/hour. The period of the air circulation is from 48 to 72 hours.
- 2124 • A check of the mechanical and electrical quality of the gas gap is finally performed.
2125 The criteria for accepting the gas gap are very strict. For the mechanical test, no
2126 pop-up spacer should be found when the gas gap is pressurized with +20 hPa for 10
2127 minutes. In addition, the rate of leakage of the gas gap should be less than 0.2 hPa for
2128 10 minutes. For the electrical test of the gas gaps, high voltage is applied to the gas
2129 gap and the amount of current drawn is recorded. First a voltage of 8.5 kV is applied
2130 for 12 hours, then a voltage 9.4 kV is applied for 96 hours. The current limit for
2131 accepting large gaps is $3.0\ \mu\text{A}$. For the gas gaps which pass the tests, transportation
2132 is arranged. Wooden boxes are specially designed for safe transportation. The gaps
2133 inside the wooden box are stored vertically and are clamped by using partially pre-
2134 stressed bars.



Figure 3.21: a) Electrode insulation machine; b) Gas assembly machine.

2135 Korea expects to have the preproduction gaps delivered to CERN for evaluation in October
2136 2010. Mass production will then take place from January to December 2011.

2137 3.4.6.3 Chamber mechanics

2138 The chamber mechanical system is composed of several parts:

- 2139 • honeycomb box
2140 • auxiliary parts
2141 • cooling circuit, FEB support and screen box
2142 • readout strips plane

Table 3.6: Chamber assembly responsibilities.

Type of chamber	numb. chambers	Assembly site
RE4/2	40	Mumbai, Chandigarh
RE4/2	60	CERN - B904
RE4/3	40	Gent
RE4/3	60	CERN - B904

2168 the mechanics within three months after signing the contract. Considering the time needed for
 2169 the transportation, ordering the mechanics six months before the chamber assembly is recom-
 2170 mended.

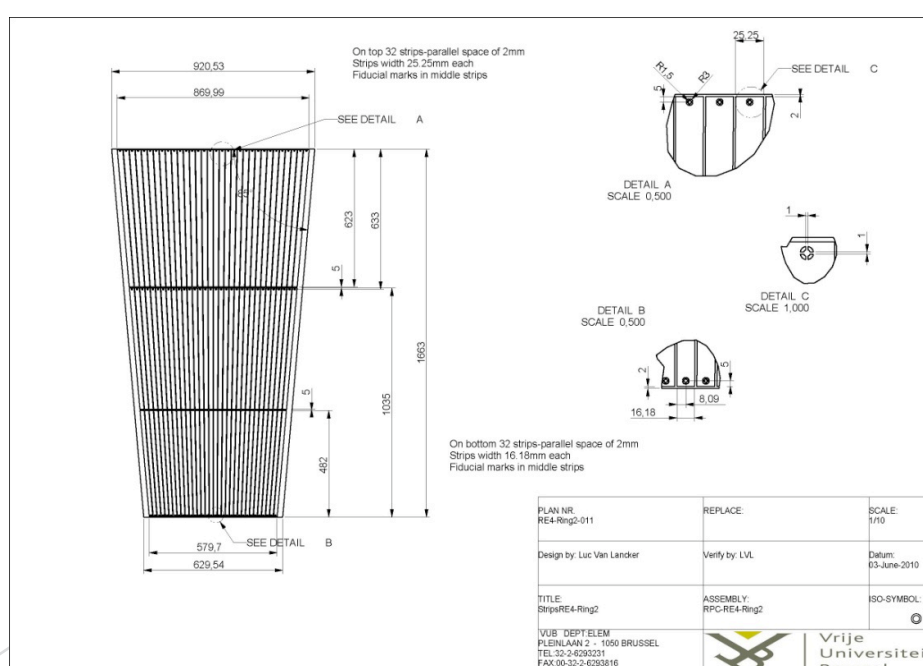


Figure 3.23: Layout of the RE chamber strip patterns.

2171 3.4.6.4 Chamber assembly and test sites

2172 The 200 new RE2 chambers will be assembled and tested at different sites according to Table 3.6.

2173 **3.4.6.4.1 CERN Building 904 site** On the 904 premises at CERN, an assembly and test
 2174 laboratory will be set up for the production of the RPC chambers. This facility will include
 2175 the assembly tables and tooling facilities for the gas gap QC/QA for leak tightness, popped
 2176 spacers, and HV behaviour. A cosmic hodoscope will also be available to test up to 10 detectors
 2177 at once and determine all physical working chamber parameters. The manpower to run this
 2178 facility will be provided by the respective institutes when their detectors are being tested. The
 2179 Pakistan group, which has experience in chamber assembly, will provide qualified manpower
 2180 for the assembly and test. A more detailed description of the 904 infrastructure will be given
 2181 in a dedicated section of the CMS upgrade technical proposal document.

2182 **3.4.6.4.2 Belgium site** The chamber construction will be the main effort of the University
 2183 of Gent. At this institute a chamber assembly and test facility is presently being set up. It is

2184 foreseen that in Gent 40 new RE4/3 chambers will be assembled to instrument an entire new
2185 RE4 outer ring station. The manpower to perform the assembly will be provided by both
2186 the University of Gent and the Vrije Universiteit Brussel. The fabrication of assembly tools,
2187 small mechanical detector pieces, signal readout cables, storage racks, etc. will be handled by
2188 the mechanical workshop in Brussels and Gent. All commercially available components, e.g.
2189 cooling lines, gas tubes, connectors, foils etc. that are required for the chamber assembly will
2190 be purchased in common orders with other sites to ensure a uniform chamber construction.
2191 The gas gaps will undergo a basic quality control before the assembly. The test procedures will
2192 be similar to those performed in the previous construction phase at the CERN ISR test facility.
2193 All gas gaps will be tested for unglued spacers and gas tightness using Argon. High voltage
2194 behaviour will also be tested with a gas mixture of Freon and Iso-butane (no SF6). Once the
2195 chambers are assembled, a complete test with a cosmic hodoscope will be performed before
2196 the transportation to CERN.

2197 **3.4.6.4.3 India sites** Under India-CMS-RPC collaboration, RPC assembly and testing would
2198 be done at two sites: Nuclear Physics Division-Bhabha Atomic Research Centre (NPD-BARC)
2199 at Mumbai; and Panjab University at Chandigarh. The RPC Lab at NPD-BARC, Mumbai is
2200 fully operational and basic quality control procedures have been set up for assembly and test-
2201 ing. Recently ten RPCs which have been assembled and tested there, in collaboration with
2202 Panjab University and Delhi University, are at CERN. The lab has an associated storage area
2203 and is backed by a robust workshop for handling all the relevant mechanical jobs. The HV,
2204 LV, 4 channel gas mixing unit, 8 channel gas flow system and gas recovery unit are fully op-
2205 erational. The cosmic ray stand can handle eight RPCs of RE4/2 type at a time. Scintillators
2206 of the relevant sizes are under fabrication at BARC, Centre for Design and Manufacture and
2207 accordingly the cosmic hodoscope would be set up to study the chamber performance. Efforts
2208 are underway to have an independent air conditioning system for controlling the relative hu-
2209 midity at 45-50% level round the clock. Electronics and DAQ have to be upgraded to handle
2210 more chambers simultaneously. Expertise from CERN would be required for setting up the
2211 cosmic hodoscope to test up to 8 detectors together and determine all RPCs physical working
2212 parameters. The Panjab University RPC lab is also equipped with a 4-channel gas-mixing unit,
2213 DAQ for the Cosmic Ray test, scintillator hodoscopes, mechanical and electrical workshops,
2214 etc.

2215 **3.4.7 Project organization**

2216 **3.4.7.1 Responsibility assignments**

2217 Restoration of the low η RPC forward system will involve a large community of physicists
2218 around the world. Besides the major responsibilities already discussed in this document for the
2219 chamber production, other relevant responsibilities related to important detector components
2220 or to infrastructure services should be acknowledged. Table 3.7 gives a complete overview of
2221 the responsibilities for all the items related to the RE re-scope.

2222 As already mentioned some of these responsibilities will be related to deliverables and appro-
2223 priate funding commitment of the funding agencies. In other cases they refer to the coordina-
2224 tion of some relevant parts of the projects based on existing expertise and competence already
2225 available from the group involved in the design and construction of the initial system.

2226 **3.4.7.1.1 HPL production and certification** CERN will coordinate the logistics for the
2227 HPL production and quality assurance. In this context INFN Pavia will make available the
2228 proper tooling for the QA and some expertise will be available for its maintenance during

Table 3.7: Overview of the responsibilities of each of the institutes (legend: BL=Belgium, CH=CERN, CN=China, IN=India, IT=Italy, KL=Korea, FI=Finland, PK=Pakistan, PL=Poland).

Item	BL	CH	CN	IN	IT	KL	FI	PK	PL
HPL production/QA		x			x				
Gap production						x			
Cham. mechanics	x		x						
Chamber assembly	x	x		x					
Front-end production								x	
HV/LV system	x			x					
LB design					x				
LB production & testing					x				x
T/RH sensors		x			x				
Infrastructure		x							

2229 2010.

2230 **3.4.7.1.2 Gap production** KODEL has the primary responsibility for gap production,
2231 certification and delivery to the chamber assembly sites.

2232 **3.4.7.1.3 Front-end board** Pakistan has the primary responsibility for FEBs production,
2233 certification and delivery to the chamber assembly sites. Fifty FEBs will be produced at the
2234 end of October. After complete validation of FEBs , mass production will be started at the
2235 beginning of 2011. We require 600 FEBs including a 10% contingency. Required time is approx-
2236 imately three months which include the time of procuring of components, developing of PCBs,
2237 mounting of components and testing of final FEBs. Before shipment to CERN, validation tests
2238 will be performed in Pakistan, such as voltage threshold setting (VTH), voltage biasing setting
2239 (VBIAS), voltage monitoring (VMON) and I2C for quality assurance. Pakistan will also take
2240 charge of preparing on-chamber signal cables and FEB adapter for signal transmission to the
2241 off-detector electronics.

2242 **3.4.7.1.4 Off detector electronics** Italy will take major responsibility in the re-design,
2243 production and pre-test of the Link Boards and Control Boards. The final validation will take
2244 place at the CERN 904 CMS electronic lab with the initial help of Poland.

2245 **3.4.7.1.5 HV/LV system** The power system is an obvious extension of the one already
2246 installed in CMS, produced by CAEN (Italy). The procurement responsibility will be shared
2247 among all institutions contributing to the chamber delivery. CERN may play a role by centrally
2248 coordinating the procurement procedures.

2249 **3.4.7.1.6 Infrastructure** CERN will have a major role in the infrastructure definition and
2250 assessment such as cooling, signal cabling, HV/LV cabling. It will also have the responsibility
2251 of the 904 test site running and maintenance.

2252 **3.4.7.2 Schedule**

2253 The overall schedule for the RE up-scope project should foresee as final achievement the cham-
2254 bers installation during the 2011-2012 winter break. The schedule is shown in Figure 3.24.

2255 The major milestones are:

Activity	2010		2011				2012			
	Jul 2010	Oct 2010	Jan 2011	Apr 2011	Jul 2011	Oct 2011	Jan 2012	Apr 2012	Jul 2012	Oct 2012
HPL pre-production	←→									
Mechanical components pre-prod.	←→									
First chamber prototype&test		←→								
HPL production		←→	←→							
Mechanical components prod.		←→	←→							
Fron end bord production		←→	←→							
Gas gap production			←→	←→	←→	←→				
Chamber assembly&test - India			←→	←→	←→	←→				
Chamber assembly&test - Belgium			←→	←→	←→	←→				
Chamber assembly at 904				←→	←→	←→	←→	←→		
Chamber QA at 904					←→	←→	←→	←→	←→	
Chamber installation								←→	←→	←→

Figure 3.24: Schedule for RE4 production and installation during the 2012 LHC shutdown.

- 2256 • Start up of the HPL production – September-November 2010
- 2257 • Start up of the gap production – January 2011
- 2258 • Start up of the FEB preproduction – October 2010
- 2259 • Preparation of the assembly sites – end of 2010

2260 3.4.7.3 Organization chart

2261 A draft organization chart of the project is shown in Figure 3.25. An overall upscope manager
 2262 will coordinate the project. A production manager will supervise the production at different
 2263 sites with the help of local site managers who will train appropriate crews for assembly, QA
 2264 and logistics. General procurement of components will be coordinated by the production man-
 2265 ager, the technical coordinator and the electronic coordinator through appropriate responsible
 2266 person designed for each given task. This organization will be fully integrated into the present
 2267 RPC project to allow synergies between operation and upscope teams to be exploited.

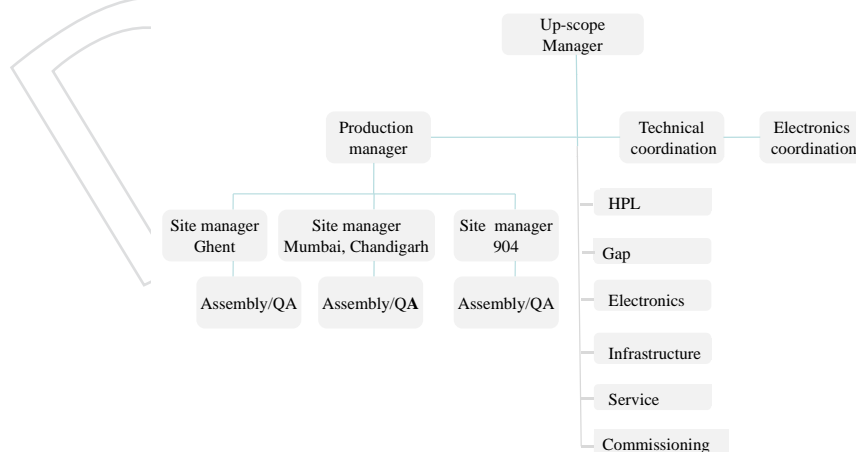


Figure 3.25: Organization chart of the RPC Upgrade Project.

3.5 Production and Installation Plans for the CMS Endcap Muon Upgrades

3.5.1 Introduction

As described in the preceding sections, the amount of upgrade work in the endcap region is quite large. As expected this will present challenges to the installation plans, which are already complicated by other subsystems such as HCAL and pixel. The DT upgrade occurs in the barrel region and is relatively independent of the endcap installations (except for crane usage of course). The basic endcap installation plan is that the ME4/2 chambers (CSC) must be installed prior to the RE4 chambers (RPC). After these are installed and commissioned, the YE4 wall is installed. However, this basic plan has a variety of complications:

- The full funding for the CSCs is not yet in place. At this time it appears possible to get some partial funding from CERN/CMS that would make it possible to complete one endcap by the end of 2012. A nominal schedule (typical of previous production) shows roughly two years from the start of funding to a point where one endcap is ready for installation. The other endcap will take roughly another year. Assuming the ME4/2 funding appears, it should be possible to get most of the chambers needed for one endcap ready for installation in 2012. Then the corresponding endcap of the RE4 chambers could be installed on top of the ME4/2.
- The LHC schedule foresees a shutdown for 16 months during 2011-2012 which would be a good opportunity to install the 2 muon systems. However, due to the lack of funding for CSCs, it is not realistic to expect that all the CSCs could be ready in time for this stop. This may block the installation of some of the RE4 chambers. If the proposed funding appears, it should be possible to install one of the CSC endcaps (and corresponding RE4 chambers) during the 2012 shutdown. The next foreseen LHC technical stop occurs during 2016, which would be a more reasonable match for the muon upgrade schedule. However, CMS is planning to replace the pixel detector and upgrade the HCAL during the 2016 shutdown so this would be a difficult addition. This makes it important that we install the first endcap of the CSCs (and subsequently the RE4 endcap) during the 2012 shutdown if at all possible.
- The first ME4/2 endcap can be fitted with the spare electronics that presently exist. However, the remaining endcap must derive its electronics from the boards removed from the ME1/1 replacements. Hence the installation of the digital CFEB boards on ME1/1 becomes linked to the completion of the second ME4/2 endcap. The ME4/2 chambers cannot be installed without the on-board electronics. Thus the second ME4 station cannot be installed until after recovering the electronics from the first ME1/1 station.
- The digital CFEB boards for ME1/1 are in design at the moment, but are not expected to be available for the 2012 shutdown. Hence, they must be installed during the next opportunity to open CMS: the 2016 shutdown. We estimate the refitting, testing, and installation of the new DCFEB boards will take roughly 12 weeks per endcap. This adds additional work to the already heavy installation schedule during this 2016 shutdown.
- After one (or both) CSC endcaps are installed, cabled, and commissioned, the overlying RE4 chambers must also be installed, cabled, and commissioned. We expect that one RE4 station could be installed after the ME4/2 installation during the 2012 shutdown (or possibly during the 2013 Xmas stop since installation times are short

2314 and opening CMS is not required). The remaining RPC station would be installed
2315 following the installation of the second ME4 station in the 2016 shutdown.

2316 • Finally, the YE4 wall must be installed. The heavy sections of the YE4 wall must be
2317 pieced together after all chambers (CSC and RPC) have been installed. The design of
2318 the YE4 wall allows it to be removed intact and “stored” on the end wall of the UXC
2319 cavern to allow for maintenance of the CSC and RPC chambers. If possible, one YE4
2320 wall should be installed after the one endcap of ME4/2 and RE4 chambers during
2321 the 2012 shutdown. If the YE4 wall cannot be installed during the 2012 shutdown
2322 it makes good sense to perform a trial construction of the YE4 wall in SX5 (upstairs
2323 assembly hall at point 5) to understand and fix any problems so the actual instal-
2324 lation in UXC will be faster and easier. Clearly, delays in installing these chambers
2325 will increase the work necessary during the 2016 shutdown.

2326 Of course, it is likely that the LHC schedule will change as we ramp up to the desired lumi-
2327 nosity, and we must plan to be prepared for whatever occurs. Nonetheless, the amount of
2328 work required in the 2015-2016 shutdown is huge, and it will require a very detailed design
2329 plan for installation. The most important need at this time is to get the funding situation for
2330 the ME4/2 upgrade clarified. Any process that would allow us to speed up the procurement
2331 and production of the ME4/2 chambers could alleviate the foreseen logjam during the 2016
2332 shutdown.

2333 A large advantage we have is that the work required for the installation of the muon systems
2334 is essentially the same as for previous muon stations. To a large extent, the infrastructure is
2335 either in place or very similar to previous stations. Hence, the solutions are known and should
2336 be relatively straightforward to put in place. The actual installation of chambers will proceed
2337 quickly (roughly 2 weeks per endcap) and the cabling should also be fairly quick (3 weeks per
2338 endcap). Nonetheless, accessibility will be poor so the commissioning is an important step and
2339 may take more than a month per endcap. We can, of course, work multiple shifts to order to
2340 comply with the CMS schedules for the short stops in 2013 and 2014, and the long (16 month)
2341 shutdown in 2016.

2342 **3.5.2 CSC and RPC Production in Building 904**

2343 **3.5.2.1 Introduction**

2344 CERN has agreed to provide assembly areas for both the CSC and RPC upgrades in Building
2345 904. The area allocated for the CSCs is roughly 1100 m² of open, well-lighted space; the area
2346 for the RPCs is slightly less. This building was previously used for LHC production and is
2347 well-suited for chamber assembly and testing. Nonetheless, the building does require some
2348 renovation before it can be used for chamber assembly. In the latter part of 2010, repairs will be
2349 made to the roof and walls. The floor will be cleaned and repainted. Infrastructure for services
2350 (gas, water, air, network, etc.) will be updated to the levels required for chamber assembly
2351 and the entire area will be air-conditioned. CERN will cover the majority of these costs. The
2352 subsystems (CSC and RPC) are requested to pay only for the new gas mixers (roughly 25 KCHF
2353 each). We expect that the infrastructure repairs and upgrading will be completed by the end of
2354 2010, and that CMS will have beneficial occupancy beginning in January 2011.

2355 However, the space available in B904 will not be adequate to store all the finished chambers.
2356 So additional space must be found at CERN. At this time CERN is considering a tent structure
2357 adjacent to Building 904.

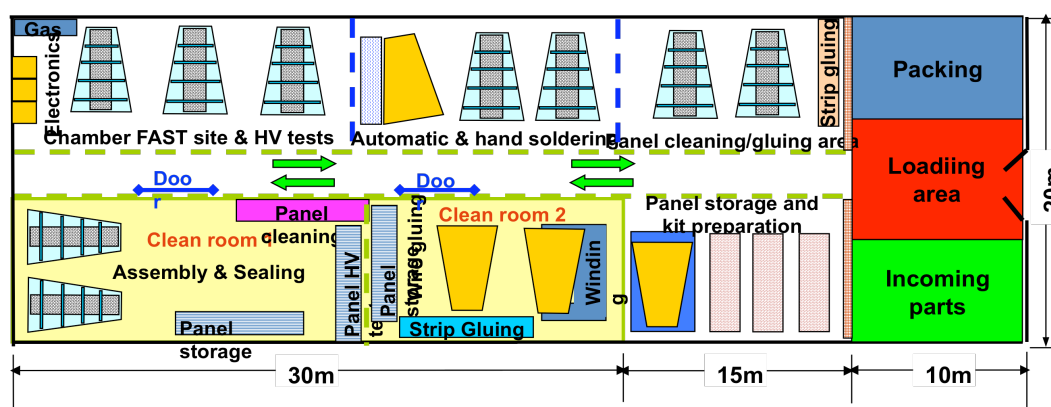


Figure 3.26: Layout for the CSC factory in Building 904.

3.5.2.2 CSC Production

2358

2359 We propose to assemble 75 ME4/2 chambers in Building 904 and expect to produce 4 chambers
 2360 per month once the factory is operating at the rates achieved during the original production.
 2361 Figure 3.26 shows a floor plan for the CSC factory. Each CSC chamber requires us to assemble
 2362 7 large honeycomb panels, 3 of which have wires wound with a spacing of 3.2 mm, with the
 2363 correct spacers to produce a sandwich with 6 active wire planes. The panels will be manufac-
 2364 tured commercially and machined at Fermilab. At CERN the first step is cleaning the panels,
 2365 then winding wires and soldering. The wire work is done with a wire-winding machine and an
 2366 automatic soldering machine, both of which were used for the original production of the CSC
 2367 chambers. Once the HV and readout circuitry is added, a frame is attached. Then the chamber
 2368 is tested for gas tightness and HV current. These chambers are identical to the 150 chambers
 2369 built at Fermilab for the prior production.

Table 3.8: ME4/2 chamber production schedule.

t_0	Funding Approval
$t_0 + 3$ months	orders sent out for all parts
$t_0 + 6$ months	tooling assembled in B904
$t_0 + 9$ months	chamber parts delivered/ shipped to CERN
$t_0 + 12$ months	production begins at B904 2 CSC/month
$t_0 + 15$ months	production ramps to 4 CSC/month
$t_0 + 18$ months	FAST assembly/testing begins
$t_0 + 24$ months	42 CSCs finished and tested, install 1st endcap
$t_0 + 33$ months	all CSC production finished
$t_0 + 36$ months	all FAST assembly, testing finished

2370 Then the chamber moves to the FAST (Final ASsembly & Test) area where the front-end elec-
 2371 tronics are added and the chamber is tested using cosmic rays. After passing the tests, it is
 2372 crated and stored for installation. Table 3.8 shows the estimated production schedule, which is
 2373 based on the experience of the original production at Fermilab.

3.5.2.3 RPC Production

2374

2375 The RPC upgrade requires 72 additional double-gap chambers per endcap, so the plan is to
 2376 produce a total of 200 chambers (including spares). These chambers are identical to the cham-

2377 bers already produced and currently collecting data. The new RE4 chambers will be assembled
 2378 according to Table 3.9. Regardless of where the chambers are assembled, all chambers will be
 2379 brought to B904 at CERN for a quality-assurance test at the cosmic ray telescope site before the
 2380 installation.

Table 3.9: RE4/2 assembly plan.

Chamber Type	Number of Chambers	Assembly Site
RE4/2	40	Mumbai, Chandigarh
RE4/2	60	CERN – B904
RE4/3	40	Gent
RE4/3	60	CERN – B904

2381 Major components for the assembly will be delivered to B904 from different sites: gaps from
 2382 Korea, mechanical parts and strips from China, front end electronics and signal cables from
 2383 Pakistan. Additional minor components, such as gas and cooling circuits will be prepared in
 2384 situ.

2385 The B904 facility will include tooling for the gas gaps quality-control (QC) and quality-assurance
 2386 (QA) (such as leak tightness, popped spacers, and HV behaviour) and proper tables for the
 2387 chamber assembly. A cosmic hodoscope will also be available to test up to 10 detectors at once
 2388 and thus determine all physical working chamber parameters. The manpower to run this facil-
 2389 ity will be provided by all institutes involved in the production. In addition, Pakistan, which
 2390 has experience in chamber assembly, will provide qualified manpower for the assembly and
 2391 testing.

2392 The plan for the RE4 assembly station in B904 is being developed and is shown in Fig 3.27.
 2393 Trucks can deliver materials through the large doors. The storage of raw materials (panels,
 2394 aluminum cases, copper strips, Bakelite gaps, Mylar sheets, etc.) may be done on the shelving
 2395 located close to the door. Scissor tables will be used to transport fragile or heavy materials from
 2396 one part of the assembly line to the other. The assembly line comprises a granite table, and few
 2397 other tables, on which the RPC is assembled by filling the aluminum case like a sandwich from
 2398 the bottom up, starting with a Mylar sheet for insulation, copper sheet for ground, sensitive
 2399 gaps, and readout strips, which are then connected to the electronics. All these activities take
 2400 place on tables specifically designed for the activity. Plastic and copper tubing for gas and
 2401 cooling inside the detectors are formed and then fitted.

2402 Once all the predefined tasks like cable preparation, honeycomb panel milling for HV connec-
 2403 tions and services, gas tube forming etc. are done, the chamber assembly can start. According
 2404 to the general schedule for the RPC upslope, we should be able to start the production in April
 2405 2011. We expect a production rate of 4 chamber/week once the operation reaches steady state.

2406 After assembly, the chambers undergo rigorous cosmic tests at the test stand, also located in
 2407 Building 904. The cosmic stand has the capacity to certify 8/10 chambers simultaneously. The
 2408 duty cycle for a complete test is roughly 2 weeks. We therefore expect to be able to test about 15
 2409 chambers/month. The QC and QA procedures also involve long term tests. Chambers, once
 2410 past the cosmic test, must undergo long term current measurement under nominal operational
 2411 voltage. A special area in B904 separated from the cosmic telescope will be instrumented for
 2412 this purpose. Table 3.10 shows the expected production and test schedule starting from the t₀
 2413 date, which is assumed to be April 2011.

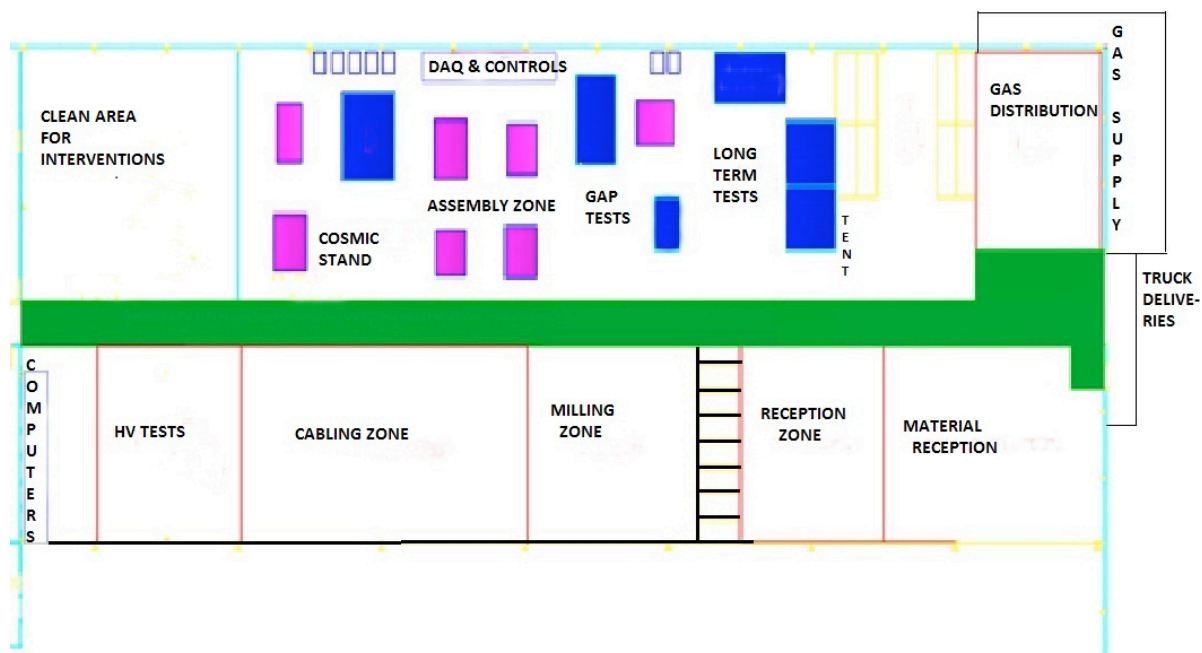


Figure 3.27: Layout of the RPC assembly area in Building 904.

Table 3.10: RE4/2 and RE4/3 production schedule.

Date	RE4 Production in B904		Test Production in B904	
	number/month	total accumulated	number/month	total accumulated
April 2011	2			
May 2011	4		2	
June 2011	8		4	
July 2011	8	22	8	14
August 2011	8		8	
September 2011	12		12	
October 2011	12	54	12	46
November 2011	12		12	
December 2011	12		12	
January 2012	12	90	12	82
February 2012	12		12	
March 2012	12		16	
April 2012	6	120	18	128
May 2012			18	
June 2012			18	
July 2012			18	
August 2012			18	200

2414 3.5.3 Installation

2415 3.5.3.1 CSC chambers

2416 Last year a new ME4/2 prototype chamber and four previously built spare chambers were
 2417 mounted with associated electronics, cables, etc. on the ME4/2 station of the plus z endcap of
 2418 CMS (Figure 3.28). No particular problems were encountered, and the installation serves as an
 2419 existence proof that the ME4/2 infrastructure in CMS (mounting holes and posts, HV, LV, gas,
 2420 cooling services, cabling, etc.) is ready. These 5 chambers are currently operational and reading
 2421 out data, along with the other CSC chambers.



Figure 3.28: 5 ME4/2 chambers installed on the back side of the YE+3 disk.

Table 3.11: Installation times for ME4/2 chambers per endcap

Mount back chambers (6/day+ contingency)	4 days
Cable back chambers (3/day)	6 days
Mount front chambers (6/day+contingency)	4 days
Cable front chambers (3/day)	6 days
Attach cooling, gas, HV, LV, test	10 days
total	30 days

2422 Based on the experience of installing the first 473 chambers, we have made a conservative
 2423 estimate of the time it will take to install the ME4/2 chambers on each endcap. The contingency

2424 is because the crane is not always available. The mounting posts are now being manufactured
 2425 and they will be mounted during the 2012 shutdown. Table 3.11 shows the estimated times for
 2426 installing one endcap with ME4/2 chambers.

2427 We have also estimated the time it will take to replace the DCFEB boards (and LVDBs) on
 2428 the ME1/1 chambers. This is a much more difficult task and is likely to be a critical path
 2429 item for the entire sequence of operations during the 2016 shutdown. The ME1/1 chambers
 2430 are not easily accessible since they are located in a slot in the nose. Each chamber must be
 2431 removed completely to a location where the electronics can be replaced and tested. Then the
 2432 chamber must be replaced in the slot where it can no longer be accessed for debugging, etc.
 2433 At this time we are considering whether to remove all 36 chambers on one endcap at one
 2434 time (minimizing the crane time) or to do the chamber replacement one at a time (minimizing
 2435 the space needed for replacement). The correct approach is not clear at this time. Table 3.12
 2436 shows the estimated time for replacing DCFEBs on one endcap. Once one endcap of ME1/1
 2437 electronics has been replaced, the freed-up electronics is sufficient to equip and test the second
 2438 ME4/2 station. Depending on the CMS schedule, the installation of the second ME4/2 station
 2439 can then proceed.

Table 3.12: Time for installing the DCFEB boards on one endcap.

Remove chambers (3/day)	12 days
Mount new DCFEB & test (4/day)	9 days
Install cables	9 days
Replace chambers (3/day)	12 days
Attach cooling, gas, HV, LV, test	10 days
total	52 days

2440 During the 2016 shutdown the major tasks are the installation of a new pixel detector and the
 2441 replacement of HCAL sensors. These tasks require the endcap disks to be located against the
 2442 far walls of the UXC cavern, so only the nose on YE1 is accessible. Hence, it looks possible that
 2443 the replacement of the DCFEB boards can be done concurrently with the other prime tasks. It
 2444 is important to configure the 2016 shutdown to ensure that all tasks can be completed in the
 2445 available time.

2446 3.5.3.2 RPC chambers

2447 The new RE4 station will be installed on the back of the YE3 yoke but mounted independently
 2448 of the CSC detector. The RE4 chambers will be mounted on an aluminum interface frame,
 2449 which is supported on the existing threaded M24 holes on the CSC mounting posts. This solu-
 2450 tion decouples the installation of RE4 from the existence of the YE4 shielding wall. The nominal
 2451 clearance to the shielding wall will be 12 mm provided the interface frames have a thickness
 2452 of 8 mm. 2 RPC chambers will be preassembled on each Al interface frame. Thus a total of 36
 2453 such packages will constitute one RE4 station.

2454 From our previous installation experience, we can mechanically mount 12 such 10° packages
 2455 per working day, which results in a total installation period of 6 working days for the two end-
 2456 caps. Initial connection of the detectors to their services (HV, LV, signal cables and fibers, gas
 2457 and cooling) on the YE3 yoke, is estimated to require 3 weeks per end-cap. Additional services
 2458 to be routed through the YE1 main cable chains will have to be studied with an experienced
 2459 team. Once these services have been installed and tested, removal and reinstallation of an entire

2460 RE4 station can be done in two working weeks per end-cap allowing for CSC installation with
2461 only 2 weeks overhead due to the RPC station.

2462 **3.5.3.3 Proposed Installation Plans**

2463 **3.5.3.3.1 2012 shutdown** Based on the funding situation, it seems possible that one end-
2464 cap of ME4/2 CSC chambers will be available for this shutdown. Of course, we will install as
2465 many as possible since it eases the work in subsequent stops. However, there is a substantial
2466 amount of infrastructure work required which must be done during the 2012 shutdown.

2467 The cooling manifold is properly sized for the new stations, but there are not sufficient lateral
2468 connections. Hence, the manifolds (supply and return) must be removed from both YE3 disks,
2469 new holes drilled and half-couplings welded into place. Then the manifolds need to be rein-
2470 stalled and commissioned. This is a more difficult task now with all the cabling and piping in
2471 place than when the manifold was originally installed on a bare disk.

2472 The gas system for the RE4 station must be built and installed. This includes the standard gas
2473 rack and all the associated manifolds. In addition, LV and HV cables for the RE4 chambers
2474 must be installed in the cablechains.

2475 As mentioned before, the remaining 134 mounting posts for installing all the CSC and RPC
2476 chambers can be installed during the 2012 shutdown. Both the CSCs and RPCs use the same
2477 posts. These posts have been funded and will be available.

2478 We anticipate an opportunity to perform maintenance on the existing CSC chambers. For ex-
2479 ample, we have some dead CFEB boards which are under overlapped chambers. We expect to
2480 have time during the 2012 shutdown to remove the overlapped chambers, replace the faulty
2481 boards, and then replace the chambers.

2482 Assuming one endcap of ME4/2 chambers is successfully installed during 2012, the RE4 cham-
2483 bers could be installed above this station of ME4/2 chambers. Once both ME4/2 and RE4
2484 chambers are in place, the YE4 wall could be installed if time permits.

2485 **3.5.3.3.2 2013 and 2014 stops** These are short stops at the end of each year and include
2486 parts of December and January. As a backup option is possible to install the ME4/2 chambers
2487 not installed during the 2012 shutdown since CMS does not need to be opened (and won't be
2488 over a short stop). It does require that the HF subsystem must be lowered to provide access
2489 to the back face of YE3. Installation during these Xmas stops provides an option to complete
2490 work not accomplished during the 2012 shutdown. Our schedule for installation is such that
2491 we should be able to fit into the available time window (see Table 3.11). RE4 installation also
2492 requires a short window so completion of one endcap before the 2016 shutdown is likely. Any
2493 installation, such as the YE4 wall, that we can complete during these short stops will be less
2494 work for the 2016 shutdown.

2495 **3.5.3.3.3 2016 shutdown** At this time, the 2016 shutdown is scheduled to last for 16
2496 months. We plan to replace all the ME1/1 electronics during this shutdown, as well as in-
2497 stalling the ME4/2 and RE4 chambers not already installed. Since we expect that additional
2498 work (replacing the pixel detector and the HCAL sensors) will have priority and will consume
2499 considerable time, we must be flexible and develop clear, efficient plans to make use of what-
2500 ever time becomes available. It is essential that we end the 2016 shutdown with an operational
2501 4th station for both ME4/2s and RE4s. At the end of the 2016 shutdown, we must add the
2502 remaining YE4 wall(s) to the back of the YE3 disk.

2503 **3.5.3.3.4 installation summary** Coordination of all the conflicting requirements for in-
2504 stallation will be very challenging. It would be best if the ME4/2 chambers were available first,
2505 then the RE4 chambers, and finally the YE4 wall. This is not likely to be the situation, and we
2506 must develop a set of options that work for each subsystem. At this time, the best option is
2507 to install one endcap of ME4/2 and RE4 chambers during the 2012 shutdown assuming the
2508 necessary funding becomes available. The final plans, of course, will depend on the delivery
2509 of items. We have been successful in past installations and it gives us confidence that we will
2510 accomplish this also.

DRAFT

DRAFT

2511 Chapter 4

2512 Central and Endcap Hadron Calorimeter 2513 Repairs, Improvements, and Upgrades

2514 Introduction

2515 In CMS, for central rapidities, the hadron calorimeters, along with the electromagnetic calorimeters, silicon tracking and muon systems, provide combined measurements of jet energies and Missing E_T . At higher rapidities beyond the coverage of the tracking systems, the calorimeters continue to provide rapidity coverage for energetic forward jets. Since the radiation hardness requirements vary significantly versus rapidity, a transition occurs in the detector technologies used for sampling hadronic calorimetry at a rapidity of $|\eta| = 3$ between the use of plastic scintillating tiles and quartz fibers/tiles as a source of scintillation and Cherenkov light, respectively. The high energies in the forward calorimeter make the use of Cherenkov light feasible, despite the relatively low light yield of the Cherenkov process. Table 4.1 describes these devices. At higher luminosities than originally foreseen at the LHC, the endcap regions near $|\eta| = 3$ of the plastic scintillator technology and the $|\eta| = 4.5 - 5.0$ regions of the quartz fiber with plastic cladding technology begin to degrade below the design performance.

2527 The goal of measuring Missing E_T (MET) places strict performance requirements on the hadron calorimeters since any source of noise or inefficiency can become a false indicator of missing E_T and therefore a source of background to key searches, such as the search for collider-produced dark matter candidates. Similarly, the hadron calorimeters in the outer, barrel, and endcap regions provide critical isolation criteria to separate hadronic showers from leptons and photons measured in complementary detectors, electrons and photons in ECAL and muons in the central tracker and muon spectrometer. In addition, the calorimeters are one of the two main sources for selecting events through firmware-level trigger primitive generation in the hardware and through the full fine-granularity readout in the software level trigger. The primary trigger objects from the calorimeters are presented in chapter 2. The performance of the hadron calorimeter directly impacts the trigger capabilities of the experiment through measurements of jets, missing E_T , H_T , MH_T , τ leptons and isolation parameters for electrons, photons, and muons. Degradation of the calorimeter performance can lead to trigger inefficiencies or to high rates of false triggers impacting a wide range of physics analyses.

2541 In the remainder of this section we discuss some of the issues that are common to more than one of these calorimeters. Then there follow sections describing the modifications planned through 2016 for the barrel, endcap, and outer hadron calorimeters. The plans for the Hadron Forward Calorimeter (HF), CASTOR, and the ZDC systems are presented in Chapter 5.

Table 4.1: Some Properties of CMS Hadron Calorimeters.

device	η range	absorber	active material	photo-detector
Barrel Hadron Calorimeter (HB)	$0 < \eta < 1.3$	brass	scintillator	HPD
Outer Hadron Calorimeter (HO)	$0 < \eta < 1.3$	brass+ cryostat	scintillator	HPD
Endcap Hadron Calorimeter (HE)	$1.3 < \eta < 3.0$	brass	scintillator	HPD
Forward Hadron Calorimeter (HF)	$3 < \eta < 5$	steel	quartz fiber	PMT
CASTOR	$-6.6 < \eta < -5.2$	tungsten	quartz plate	PMT
Zero Degree Calorimeter (ZDC)	$ \eta > 8.3$	tungsten	quartz fiber	PMT

Improved Photon Detection with Silicon Photomultipliers

2545

2546 The Barrel Hadron Calorimeter (HB), the Endcap Hadron Calorimeter (HE), and the Outer
 2547 Hadron Calorimeter (HO) all use Hybrid PhotoDiodes (HPDs) as their photodetector. At the
 2548 time when it was necessary to commit to a photodetector for the construction of CMS, the HPD
 2549 was the only technology that met all requirements, including the ability to run in a high (4T)
 2550 magnetic field, radiation hardness, compactness, and cost. The performance of the HPDs has
 2551 not been as good as expected forcing the devices to be operated at lower HV and, in some
 2552 cases, the gain of the devices has fallen short of the original requirements. The low signal-
 2553 to-noise in the outer hadron calorimeter prevents its use for muon identification, and similar
 2554 performance reductions affect low energy measurements for lepton isolation in the barrel and
 2555 endcap regions.

2556 A new photodetector technology, the Silicon PhotoMultiplier (SiPM), has recently become avail-
 2557 able. SiPMs are a rapidly emerging technology that are replacing photomultipliers and other
 2558 photodetectors for many applications, becoming common in commercial products such as PET
 2559 scanners. SiPMs are pixel arrays of Avalanche Photodiodes operating in Geiger mode. Each
 2560 pixel that is struck by a photon makes a single pulse of charge with uniform amplitude. The
 2561 outputs of all the pixels are added together inside the chip to give a single output that is a mea-
 2562 surement of the number of photons striking the SiPM, providing that more than one photon
 2563 does not often strike the same pixel and that all pixels are active at the time of detection.

2564 SiPMs have significant advantages relative to HPDs. SiPMs have quantum efficiencies that are
 2565 a factor of two higher than HPDs and the gain of a SiPM is similar to that of photomultipliers,
 2566 ($\sim 10^5 - 10^6$ depending on the pixel size), a factor of 50–500 more than the HPDs. Compared
 2567 to HPDs and their corresponding readout electronics, the SiPMs with an optimized readout
 2568 electronics have a factor of 8 increase in signal-to-noise ratio. SiPMs are compact and relatively
 2569 inexpensive. Pixel sizes as small as $10\mu\text{m}$ have been achieved while maintaining high pho-
 2570 todetection efficiency. The SiPMs have lower operating voltages, of order 100V, compared to
 2571 HPDs, which are vacuum tubes that run at $\sim 10\text{KV}$. Low voltages have operational advantages,
 2572 i.e. no high voltage breakdown as observed in the current HPDs. High voltages present safety
 2573 hazards and can cause breakdowns that lower tube lifetime.

2574 SiPMs are not affected by magnetic fields of up to 4T. The HPDs operate well at zero field and
 2575 in strong fields of 3.5-4T. However, at lower fields of order 0.2-3.0T approximately 10% of the
 2576 devices experience rapid breakdown. While the HPDs in the HB/HE are in high fields of 3.8T,
 2577 the HO ring-1 and ring-2 are located in the problematic 0.2-0.3T range. The magnetic field
 2578 value restrictions of the HCAL HPDs could potentially constrain CMS data-taking operations
 2579 in situations where the solenoid field needs to be reduced. In addition, the performance of the

2580 HPDs is also affected by the alignment of the E-field in the tube with the external magnetic
2581 field. It is difficult to control this alignment in the return flux and fringe fields outside of the
2582 CMS solenoid, especially for the HO.

2583 For the HO, which is in a low rate environment and sees only a small fraction of the energy of
2584 a hadronic shower, there are already commercially-available SiPMs that meet the requirements
2585 of a replacement for the HPDs. The number of pixels, the time for a pixel to recover from
2586 its Geiger discharge, and radiation hardness are issues that must be addressed before one can
2587 confidently use SiPMs to replace HPDs in the HB and HE. No currently available SiPM meets
2588 all the requirements for the HB and HE.

2589 The key issues for the SiPM R&D that must be addressed before they can be used as replace-
2590 ments for the HPDs in the HB and HE are:

- 2591 • When a pixel fires, it is paralyzed for an interval of time until it can be recharged.
2592 The reset time must be reduced enough so that response to a subsequent signal is
2593 not affected.
- 2594 • Pixel density is an important consideration. Each photon should hit a separate and
2595 active pixel or the linearity of the SiPM output will be affected. The number of pixels
2596 determines the dynamic range obtainable with the SiPM. The number of pixels must
2597 be significantly larger than the expected number of photons.
- 2598 • SiPMs are sensitive to temperature and operating voltage, with the gain depending
2599 linearly on the voltage above the breakdown point, called the “overvoltage”. Typ-
2600 ical overvoltage values are 1-3V. These operating parameters must be adequately
2601 controlled for the gain to be stable and to minimize cell-to-cell variation.
- 2602 • The rate of single-pixel self-firing must be kept low because a pixel becomes disabled
2603 briefly each time it emits a pulse.
- 2604 • Crosstalk is possible when light or charged particles emerging from the Geiger break-
2605 down fall on an adjacent pixel. This causes both extra deadtime and an error in the
2606 photon count. The crosstalk of the SiPM device will be minimized as part of the
2607 R&D program.
- 2608 • Radiation tolerance. The amount of radiation that the SiPM must handle varies from
2609 relatively small in the HO, to moderate in the HB and HE. Long-term radiation ex-
2610 posure will increase the leakage currents and begin to degrade the signal-to-noise
2611 performance.

2612 All these issues are being addressed by a systematic R&D program. Nearly every requirement
2613 for the HB and HE has been met by an available SiPM but no single device has been identified
2614 that satisfies all of the requirements. The R&D program is described below including the
2615 presentation of promising initial results on available devices.

2616 Longitudinal Segmentation

2617 An important attribute of the CMS HB and HE (and the HO) are that they are “tile-fiber”
2618 calorimeters. Tiles of scintillator are interleaved with absorbers (brass) to form calorimeter
2619 towers. Each tile has a wave length shifting (WLS) fiber embedded in it that absorbs a frac-
2620 tion of the light emitted by the tile and re-emits the light shifted to a longer wavelength. The
2621 wavelength of the emitted light is well-matched to the spectral response of an HPD (or SiPM)
2622 and the optical numerical aperture of the fiber, allowing it to be propagated over long dis-
2623 tances through internal reflection in the fiber. The light from the WLS fiber is transmitted to the
2624 photodetector via an optically-spliced clear fiber with a long attenuation length.

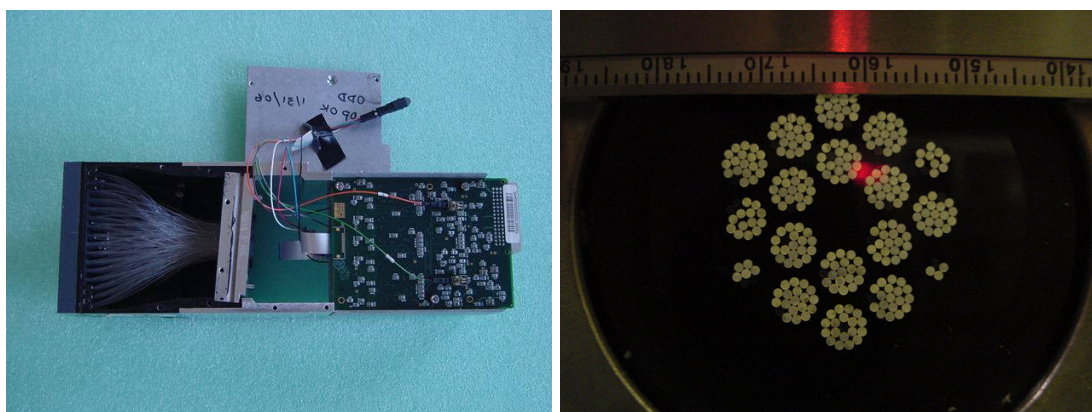


Figure 4.1: Each individual tile-fiber from the calorimeter is optically mapped to an element on the photodetector. The current optical decoding unit (ODU) is shown on the left, indicating how all of the 18-fiber ribbon cables from a barrel wedge are routed to the Hybrid PhotoDiode (HPD) photocathode surface. An end view of the ODU, on the right, shows how the depth segmentation was hardwired into the construction of the ODU with some depths having a small number of tiles (plus light calibration signals) and others having all 17 scintillators optically added into one readout channel and thereby limiting the barrel to one depth segmentation.

2625 In the current HB and HE calorimeters, there are over an order of magnitude fewer photode-
 2626 tector elements than tile-fiber channels in the detector. This reduction is achieved by piping
 2627 the light from groups of fibers to a single photodetector element, thereby optically summing
 2628 the tile-fiber signals before the photodetector. For most of the HB and HE towers, all the light
 2629 from the 17 tile-fibers of the tower are summed together resulting in a complete loss of infor-
 2630 mation about the longitudinal development of the hadronic shower in the readout. This choice
 2631 was made in the original calorimeter design due mainly to the low gain of the HPDs and cor-
 2632 responding low signal-to-noise of the readout and because finer segmentation was physically
 2633 prohibitive due to the large mechanical size of the HPD.

2634 Because SiPMs are compact, high gain and relatively inexpensive, it is possible to implement
 2635 longitudinal segmentation of the fiber readout to obtain a calorimeter readout that provides
 2636 more information than can be obtained from the HPDs. The optical grouping of channels in
 2637 the HPD system is shown in Fig. 4.1 where the number of groups and number of fibers per
 2638 group are constrained by the HPD geometry. Few geometric constraints are present in the
 2639 SiPM upgrade and this opens up the possibility of increasing the number of longitudinal seg-
 2640 ments by either grouping a smaller number of fibers to illuminate a given SiPM device or by
 2641 introducing separate SiPM devices for each optical fiber and electrically adding the outputs.
 2642 The advantages of longitudinal segmentation are described in the section on the HB/HE. The
 2643 compactness is crucial because the total space for the photodetectors and associated front-end
 2644 electronics is fixed and cannot grow to accommodate the extra photodetectors needed to im-
 2645 plement the additional segmentation.

2646 Timing

2647 Because of the nature of hadronic showers, the calorimetry does not have to be highly seg-
 2648 mented for jet energy and angular measurements (except in particle flow based measurements,
 2649 where finer transverse segmentation would have improved neutral hadron identification). In
 2650 fact, the hadron calorimetry has by far the fewest channels of any of the CMS detectors. Con-
 2651 sequently, its channels have the highest average occupancy.

2652 When the LHC runs at or near design luminosity, there are multiple interactions in every bunch
2653 crossing. When the trigger selects a crossing of interest, it is possible for tile-fiber light emis-
2654 sion from previous and subsequent crossings to pollute the “in-time” signal, where each signal
2655 in the HB/HE/HO has a duration of approximately 100ns affecting up to 4 bunch crossings.
2656 Similarly, the timing of a signal relies on there being no significant contribution from the neigh-
2657 boring bunch crossings, where overlapping pulses mean that more data must be collected and
2658 disentangled to separate out the data from each individual bunch crossing. The current ver-
2659 sion of the CMS calorimeter output provides timing information based on peak detection al-
2660 gorithms in the hardware trigger, and software fits that assume isolated signal pulses. The
2661 inherent capability of the calorimeter to provide fine-grained timing available in the analog
2662 pulse information is therefore not being utilized. It is a major theme of the hadron calorimeter
2663 upgrade to provide better timing resolution so as to maintain and improve the capabilities of
2664 the existing detector in a high instantaneous luminosity environment.

2665 In addition to the problem discussed above there are other backgrounds such as beam halo and
2666 cosmic rays that produce signals in the calorimeters that come at random times with respect to
2667 the proton-proton collision. Timing information is also a crucial tool for rejecting these back-
2668 grounds. Non-collision backgrounds are especially pernicious in the search for very rare events
2669 signifying new physics. Many rare processes are detected using the calorimeters and in some
2670 cases only a few events per year are expected. For such investigations, cosmic rays and beam
2671 halo superimposed on collision data can mimic a rare event. This is discussed below in the
2672 section on the HB/HE calorimeters. Timing is a powerful tool for rejecting such backgrounds.

4.1 Outer Hadron Calorimeter (HO)

2673

2674 The HO, is situated in the barrel return yokes (YB) by the first layer of muon chambers. The YBs
2675 consist of 5 rings (or wheels) of return iron: YB0, YB \pm 1, and YB \pm 2. Rings R0, \pm 1 (R \pm 1), and
2676 \pm 2 (R \pm 2) of the HO system are located in YB0, YB \pm 1, and YB \pm 2, respectively. The purpose of
2677 the HO is to measure any energy from showers due to particles hitting the HB that leaks out of
2678 the back end of the HB. Detectors that perform this function are often called “tail-catchers”.

2679 The HO uses HPDs for photo-detection. They are mounted on the rings of the muon detector
2680 and so are immersed in the stray return field of the solenoid coming from gaps in the iron return
2681 yoke. The HPDs have been found to produce large noise pulses when operated in the magnetic
2682 field environment of the outer rings (\pm 1 and \pm 2). The magnetic field at the HPDs in this region
2683 is in the range of 0.2-0.3T at the 3.8T operating field of the CMS magnet. Under these conditions
2684 a large fraction (10% or more) of the HPDs produce large discharges leading to permanent
2685 damage. The noise pulses are larger and more frequent if the E-field of the HPD is not well-
2686 aligned with the local B-Field. As a permanent solution to this problem, we are going to replace
2687 the HPDs in \pm R1 and \pm R2 with SiPMs, devices that do not have these problems. While the
2688 HPDs in R0 experience fewer breakdowns, they are actually the most important detectors in
2689 the HO since they are located at 90° to the beam line, where the HCal and ECal present the
2690 least material. Consequently, we are also developing a plan to replace the R0 HPDs due to the
2691 significant performance improvements on reducing leakage tails in the energy measurement
2692 for high energy jets in the central barrel.

2693 Because of operational problems with the HO in the fringe field regions, it has been necessary
2694 to run the HPDs at less than optimal HV. The lower HV results in lower gain and worsens the
2695 HO performance. Because of the low gain, electronics noise is more important and the HO is
2696 not as useful for jet and muon physics. The higher noise levels limit the utility of the HO for
2697 tagging shower leakage, the original goal of the detector. Replacing the HPDs with SiPMs re-
2698 establishes the baseline performance of the detector. An additional benefit of the replacement is
2699 that the much quieter detector provides for excellent muon identification, improving the CMS
2700 capabilities for low momentum central muons.

2701 Figure 4.2 shows the distributions of signals for minimum ionizing particles (MIP) and pedestal
2702 values for SiPMs (above) and HPDs (below). The MIP signal is extremely clear in the SiPMs.
2703 This points to a marked improvement in MIP identification using the SiPMs. The higher gain
2704 of the SiPM relatively suppresses the electrical noise (pedestal) and makes the HO better suited
2705 for any energy measurement.

2706 Figure 4.3 shows the improvement in π/μ rejection for SiPMs compared to HPDs. In this
2707 algorithm the HO alone is used for pion rejection. The rationale for this is that muons are
2708 deeply penetrating while pions shower and are absorbed in the calorimeter. Hence a MIP signal
2709 in HO is indicative of muons and absence of a MIP signal indicative of pions. Replacing HPDs
2710 with SiPMs vastly improves the MIP/pedestal separation and consequently improves the π/μ
2711 rejection. From this figure we see that the improvement is up to 150 times, depending on the
2712 momentum. This improved π/μ rejection will play an important role in low momentum muon
2713 identification, where the muon does not penetrate far enough into the steel yoke to record hits
2714 in the Drift Tube muon system chambers. In addition, a muon identification algorithm that
2715 does not require the use of the muon chambers provides for an independent measurement of
2716 their efficiencies.

2717 The plan for the HPD replacement is to remove the HPDs from the Readout Modules (RMs)
2718 and have “drop-in” SiPM packages that have the same pixel locations as the existing HPDs.

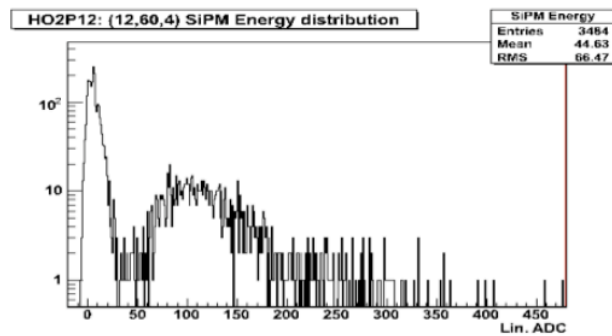


Figure 10a: Individual energy distribution, mwgr18, for a single HO channel, HO($\eta=12$, $\phi=60$). Here energy E_s is not corrected for muon angle of incidence.

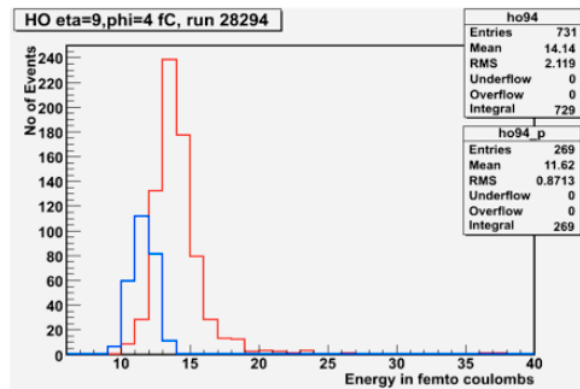


Figure 10b: For comparison, individual energy distribution, single HO channel read out with HPD, TB2007 data. Blue line: pedestal events, red line: muon signal.

Figure 4.2: Comparison of muon response in HO for SiPM and HPD. The top plot is the SiPM performance where the pedestal is in the lower peak and the muon signal is well separated from the pedestal. The bottom plot is for the HPD and due to the lack of separation, the pedestal triggers are plotted separately in the left distribution and the muon signal is plotted on the right indicating the HPD MIP is barely separated from the pedestal.

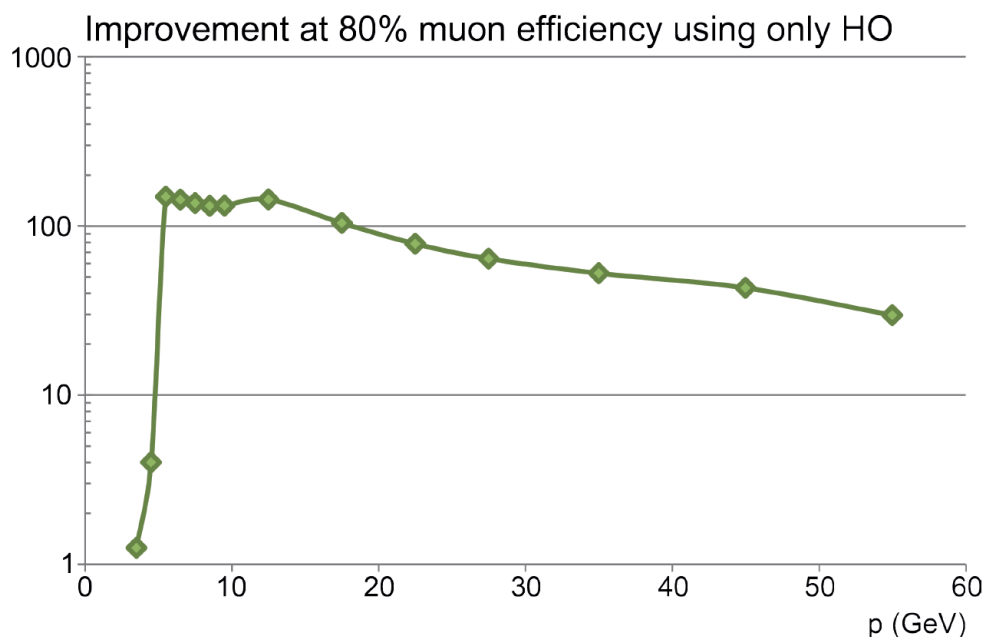


Figure 4.3: Improved π/μ rejection for a fixed muon efficiency of 80%. For low momentum the improvement is about 150 times. As the momentum increases pions become more likely to have shower leakage into the HO, and hence the rejection worsens.

2719 The HPD in the RM is replaced with a 2-card “sandwich”. One of the cards, the Mounting
 2720 Card, contains the array of 18 SiPMs corresponding to the 18 pixels of the existing HPD, shown
 2721 in Figure 4.4, and Peltier coolers for SiPM temperature control.

2722 The second card, the Control Card, supplies needed voltages, control and monitoring functions.
 2723 The control board is shown in Figure 4.5. It receives the analog signals from the SiPMs, shapes
 2724 them, and then transmits them to the QIE (Charge Integrating and Encoding) cards. Bias volt-
 2725 ages for the SiPMs are generated there, as well as the Peltier temperature control. SiPM leakage
 2726 currents are also monitored here. Most parts of the RM (the ODU, structure, QIE card packs)
 2727 remain unchanged and only the 2 card “sandwich” replaces the HPD.

2728 HPDs in two HO Readout Box (RBXs) consisting of 8 RMs have been replaced with SiPMs and
 2729 are currently installed in the CMS detector. In total they consist of 144 SiPMs out of which 36
 2730 channels are from the company Zecotek [3] and 108 channels from Hamamatsu [4]. They were
 2731 installed in April 2009 and have been operated most of the time since then.

2732 The SiPM replacement project is on schedule to replace the HO HPDs in all 5 rings during the
 2733 next LHC shutdown, starting in the late fall of 2011 and extending through 2012 into early
 2734 2013. The RMs will be removed from the HO detector, taken to the surface hall at Point 5
 2735 where a small factory will be established. The RMs will have the HPDs replaced with the
 2736 SiPM sandwich cards, and will be tested and burned in. Then the modified RMs will be taken
 2737 back to the HO detector in SX5, re-installed and verified. Depending on detector access the
 2738 replacement can be made in a few months. The schedule for delivery of the HO electronics is
 2739 show in Table 4.2.

2740 The replacement activity for Rings ± 1 and ± 2 is planned as a joint effort between TIFR Mumbai
 2741 and several U.S. CMS institutes. The team has developed a list of tasks and assigned them,
 2742 shown in Table 4.3.

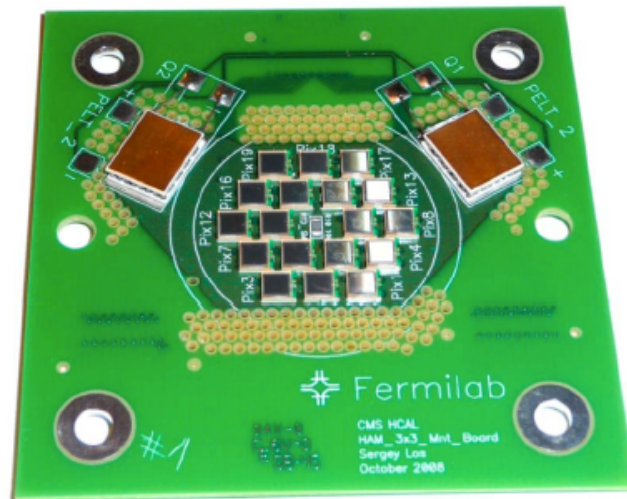


Figure 4.4: SiPM Mounting card. The larger rectangles are the 2 Peltier coolers. Also seen is a grid of 18 SiPMs with the same placement as the HPD pixels.



Figure 4.5: The Control Board. This board generates the SiPM bias voltages, measures the leakage currents, controls the Peltier cooler, and monitors voltages and temperatures.

Table 4.2: HO Schedule.

30-Aug-10	2000 Hamamatsu SiPMs ordered.
30-Aug-10	Design of final electronics cards complete.
30-Sep-10	Evaluations (radiation, reliability, noise) of final electronics cards complete.
31-Sep-10	Launch of fabrication of electronics.
30-Oct-10	Evaluation of first batch of assembled cards.
30-Nov-10	QC testing of SiPMs begins.
14-Nov-10	Electronics Production started.
30-Dec-10	All SiPMs delivered.
15-Jan-11	Electronics Production complete.
14-Mar-11	Start of fabrication of completed electronics and SiPMs (and burn-in).
14-May-11	Start of delivery of completed electronics and SiPMs to CERN.
17-Sep-11	Finish of fabrication of completed electronics and SiPMs.
14-Oct-11	Finish of Delivery of completed electronics/SiPMs to CERN.
15-Oct-11	Start development of Point 5 factory.
14-Nov-11	Ready for installation work.

Table 4.3: HO Project Task Assignments.

Lay out boards and test preproduction boards at FNAL
Specification of SiPMs (CERN/FNAL/TIFR)
Place SiPM order (FNAL/TIFR) (SiPMs to be delivered to CERN)
Receive and test initial batch of SiPMs (CERN/Boston/FNAL/TIFR)
Send SiPM samples to TIFR (CERN SiPM Team)
Production SiPM testing at Ooty (TIFR)
Make trial run of boards (BEL/Ooty,TIFR)
Hand-load SiPMs on pre-production boards (Ooty, TIFR)
Initial tests of trial run (TIFR/Boston/FNAL, Boards sent to CERN and FNAL)
Production run (Ooty, TIFR)
Production tests (TIFR)
Production tests random verification done at CERN/FNAL
Inventorying at CERN
Setup of factory at Point 5 (CERN/FNAL/TIFR)
Supply techs from TIFR and FNAL (2 techs from each institution)

4.2 Barrel and Endcap Calorimeters (HB/HE)

4.2.1 Introduction

The barrel (HB) ($0 \leq |\eta| \leq 1.3$) and endcap (HE) ($1.3 \leq |\eta| \leq 3$) hadron calorimeters are made of alternating plates of brass absorber and scintillator with wave-length shifting (WLS) optical readout. As shown in Figure 4.6, there are 17-layers of scintillator with individual WLS fibers coming from nearly 72,000 individual tiles. Due to the intrinsic signal-to-noise limitations of the detected WLS light using hybrid photodiode (HPD) detectors and the corresponding front-end noise from the readout electronics, the analog calorimeter signals are digitized with a minimum number of individual electronics channels. The bulk of the η - ϕ barrel segmentation is read out with a single depth segmentation. Limited depth segmentation is present in the endcap, but is not optimally configured for radiation damage compensation foreseen in high luminosity SLHC operation. Since the development of the original calorimeter design, several physics analyses with initial LHC collision data have identified areas where an improvements in the hadron calorimeter will directly impact the physics productivity of the CMS experiment. The major performance limitations are all addressed in varying degrees by the upgrades and can be summarized as follows:

- 1) Need for calorimeter clean-up algorithms to reduce non-collision signals coming from numerous sources,
- 2) Limited discriminating power of the HCAL/ECAL energy ratio for separating pions from electrons,
- 3) Degradation of the electron isolation quantities with increasing instantaneous luminosity,
- 4) Limited efficiency for muon isolation and identification using the HCAL barrel and endcap,
- 5) Large calibration biases using isolated hadrons below 5 GeV due to showering in dead material between ECAL and HCAL,
- 6) Inefficient bunch-crossing identification for low-energy signal impacting large area summations used for hardware trigger-level lepton isolation, jet energy and global energy sums,
- 7) Strong η -dependent radiation damage in the endcap scintillators at high luminosity introducing non-uniform light loss and constant term energy resolution degradation, and
- 8) Limited number of discriminating quantities to reject beam-related backgrounds not originating from the interaction region.

The degree to which the upgrades improve each of the performance issues listed above is described in more detail in the simulation section. The upgrade tackles these limitations by making the following physical changes in the on-detector instrumentation and front-end electronics:

- a) Replacement of photodetector to eliminate the sources of anomalous signals and to improve the front-end signal-to-noise by an order of magnitude,
- b) Four-fold increase in longitudinal segmentation to reduce pile-up/high-occupancy performance degradation coming from the first layer of scintillator, to improve clustering and geometric discrimination against non-collision backgrounds and to increase channel redundancy, and

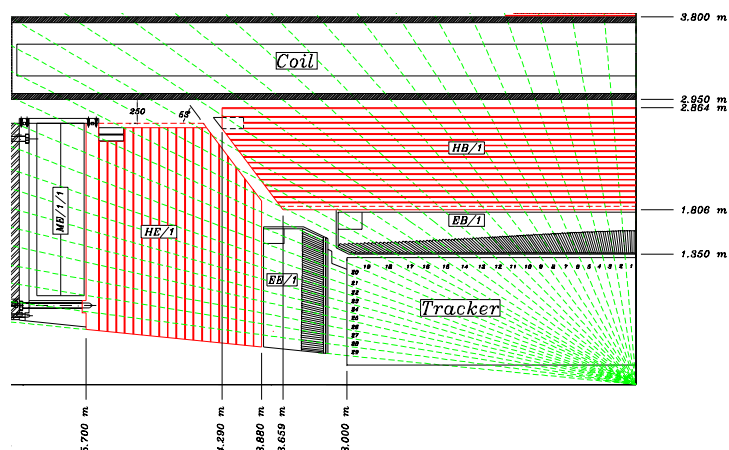


Figure 4.6: Quarter view of the barrel and endcap hadron calorimeters, showing the intrinsic longitudinal segmentation capabilities. The front-end readout electronics, the readout boxes or “RBX”, are located directly behind tower 15 in the barrel and directly behind tower 18 in the endcap.

- 2787 c) Scintillator time (TDC) measurements per bunch crossing with nanosecond timing
 2788 resolution down to MIP energies to provide independent rejection for beam halo,
 2789 cosmic ray, and other non-collision backgrounds.

2790 To accommodate the front-end electronics upgrades and to fully benefit from the increased front-
 2791 end capabilities, a complement of upgrades is proposed for the back-end trigger and readout
 2792 electronics. The back-end electronics upgrades address the following new capabilities:

- 2793 1) Front-end to back-end data bandwidth increases from increased longitudinal seg-
 2794 mentation and TDC information in the readout of the HB and HE;
- 2795 2) Data volume management and integration with the central DAQ;
- 2796 3) Increased trigger processing needs to provide total energy sums, separate lepton
 2797 isolation quantities and to apply the new front-end timing information;
- 2798 4) Increased bandwidth to the trigger system to provide finer granularity information,
 2799 including full granularity in the HF region, additional fine-grain information, and
 2800 separate total energy and lepton isolation sums.

2801 The goal of the HCAL upgrade plan for Phase 1 of the SLHC is to maintain and improve oper-
 2802 ation of the HCAL for physics. Our plan maximizes the inherent capability of the HB/HE for
 2803 physics, especially for both high- p_T physics and luminosity increases beyond the LHC design
 2804 luminosity of $10^{34}/\text{cm}^2/\text{s}$, where pileup becomes increasingly difficult. The proposal for Phase
 2805 1 consists of modifications to the front-end electronics (FE) and trigger/readout receiver back-
 2806 end electronics (BE) for the barrel and endcap detectors. The front-end and back-end electronics
 2807 are accessible and can be replaced without any modifications to the physical components of the
 2808 barrel and endcap sampling calorimeters. For Phase 2, with a luminosity of $5 \times 10^{34}/\text{cm}^2/\text{s}$, we
 2809 anticipate that the large integrated radiation doses might be sufficient to make high η regions of
 2810 the endcap (HE) unusable. The Phase 1 upgrade components, photodetectors and on-detector
 2811 electronics, will be specified and qualified to maintain performance standards through the en-
 2812 tire Phase 2 period. For the physical components of the endcap calorimeter, ECAL and HCAL,
 2813 R&D is needed to answer the questions of performance limitations from radiation damage.
 2814 Overall, our Phase 1 upgrade plan is constructed to be able to meet the physics goals of the

2815 LHC program and high instantaneous luminosity extensions to the program with the lowest
2816 possible cost.

2817 **4.2.2 Problems Motivating the Improvement and Upgrade Program**

2818 **4.2.2.1 The Effects from Increasing Luminosity**

2819 CERN's plan for increasing the LHC's luminosity to the design value and beyond between now
2820 and 2020 is described above. When the luminosity increases, one has to consider the effects of
2821 an increased instantaneous luminosity and an increase in the overall integrated luminosity. For
2822 the former the effects are almost entirely due to an increase in the pileup, both in-time and out-
2823 of-time. Such pileup has the potential to severely compromise the detector performance and
2824 physics capability of CMS. For the latter (integrated luminosity increase), the main effect will
2825 be radiation damage to the detectors and front-end electronics.

2826 In the CMS Upgrade, the upgraded detector must be able to handle up to $300\text{-}500\text{ fb}^{-1}$, which
2827 will be accumulated through the end of Phase 1. This estimate takes into account the fraction
2828 of the year that the machine will be run for physics, peak luminosity vs integrated luminosity,
2829 live times, duty cycles, etc., and is sanctioned by the LHC machine group. Using the above
2830 schedule, we estimate that we will receive roughly 300 fb^{-1} for Phase 1, and roughly 3000 fb^{-1}
2831 for Phase 2. These numbers are important to the discussion of radiation damage.

2832 Peak and integrated luminosities are obviously related, and as they increase CMS will become
2833 more sensitive to higher mass states, and smaller cross sections. As a result, it will be more
2834 important to have ways to reduce those backgrounds that are not from the beam crossing at
2835 the center of CMS, e.g. cosmic rays, beam gas and halo, neutron albedo, acute detector prob-
2836 lems, etc. As will be explained shortly, the HCAL upgrade will take into account all of these
2837 backgrounds.

2838 **4.2.2.1.1 Effects Due to an Increase in Instantaneous Luminosity**

2839
2840 At LHC design luminosities of 10^{34} , the average multiple interaction rate is approximately
2841 20 per crossing. Note that for HB and HE, the HCAL towers are approximately 0.087 in η
2842 and exactly $1/72$ in ϕ . As the instantaneous luminosity increases, the tower occupancy will
2843 increase, and the occupancy as a function of a fixed threshold cut will increase faster than lin-
2844 early as more particles are included in the tower and the energy increases. Also for HCAL,
2845 as explained below, a larger DC level from the huge occupancies from multiple interactions
2846 will make it extremely difficult to use the current scheme for timing the arrival of showers,
2847 especially at lower transverse energies. These two effects, occupancy and timing, are detailed
2848 below, and dealing with them forms the basis of the HCAL upgrade.

2849 **Occupancy**

2850
2851 At the original LHC design luminosity of 1×10^{34} , Monte Carlo simulations tell us that for
2852 HCAL, with a reasonably small zero suppression threshold the average tower occupancy can
2853 be limited to around 15% in the readout, dominated by the underlying event, and includes both
2854 in-time and out-of-time pileup. SLHC Phase 1 will have the same time structure (40MHz cross-
2855 ings) and so the multiple interaction rate will scale linearly with luminosity, rising to an average
2856 of ~ 40 at 2×10^{34} . We can estimate the effect this will have on the trigger and DAQ by using the
2857 same threshold and calculating the occupancy rate as approximately by $1 - (1 - 0.15)^3 = 39\%$,
2858 or just under a factor of 3 more particles (and more energy) per tower. Note, that for Phase 2,
2859 with a 50ns beam crossing and luminosity of 10 times the LHC design luminosity of 10^{34} , there

2860 will be 20x more multiple interactions per event, increasing the in-time pileup. However, there
 2861 will be no out-of-time pileup since most of the HCAL energy is contained within 2 of the 25ns
 2862 buckets. This model results in a total occupancy of $1 - (1 - 0.15)^{20} = 96\%$, clearly suggesting
 2863 that a higher threshold will need to be applied. Note also that this model is only valid when
 2864 the occupancy is small. For a larger occupancy, where the pileup adds to the total amount of
 2865 energy in a tower, one therefore has to apply a single threshold not to each particle individu-
 2866 ally but to the sum of all the particles, and this will make the occupancy rise more than linearly
 2867 with luminosity. The CMS DAQ readout limits the data rate from any Front-End Driver (FED),
 2868 which transmits the data from the readout VME crates to the DAQ). As we detail below, the
 2869 amount of data for HCAL will increase by almost a factor of 4. With the same zero suppression
 2870 threshold as for the 10^{34} running, the HCAL will be sending 4x more channels. The important
 2871 point here is that the pileup will have a big impact on both the Level 1 trigger and the DAQ
 2872 bandwidth requirement.

2873 Timing

2874

2875 The current HCAL electronics is based on a linear current splitter for range determina-
 2876 tion, charge integration, and analog-to-digital conversion. Overall, the electronics needs ap-
 2877 proximately 3 beam crossings (75 ns) to deliver all the charge from real energy deposition in
 2878 the HB and HE, as shown in Figure 4.7. By setting the phase of the integration clock relative
 2879 to the LHC beam crossing, one can choose what fraction of the total charge is integrated in
 2880 what beam crossing. For colliding beam running, the current plan is to tune to approximately
 2881 75%/20%/5% in the 3 successive beam crossings. Knowing these fractions allow one to fit the
 2882 arrival time of the signal (which should be the same for all signals in any given tower) with a
 2883 precision of approximately 2ns. However, as the amount of tower energy from the underlying
 2884 event increases, the ability to do timing in this way diminishes for lower signal energies. This
 2885 can be seen clearly in Figure 4.8, where the pileup begins to be comparable to the energy of
 2886 particles from the hard scattering. At lower energies, the pileup completely dominates and
 2887 and it is no longer possible to determine the timing from the shape.

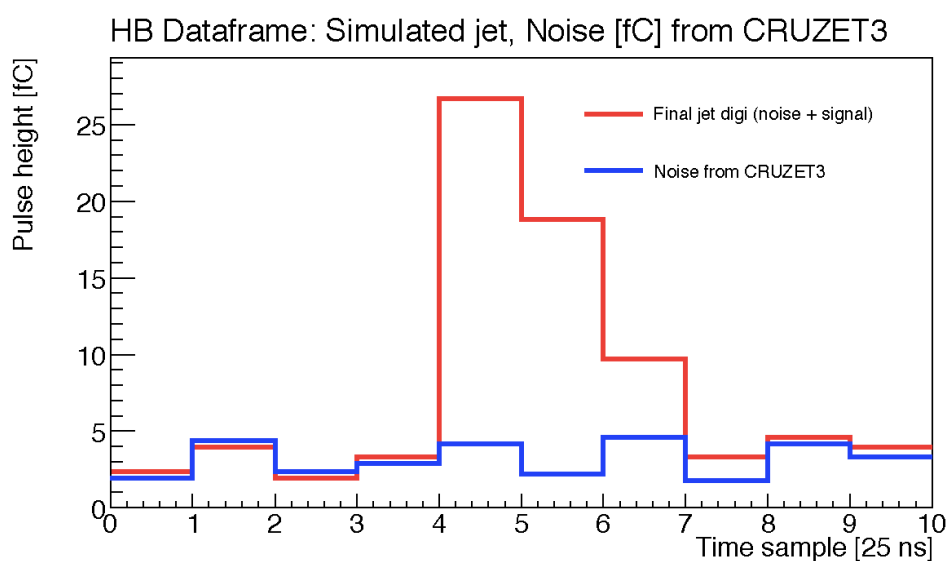


Figure 4.7: Energy in an HCAL tower needs 3 beam crossing times to fully integrate.

2888 The use of HPDs made it impossible to have a separate TDC readout, as the devices have very

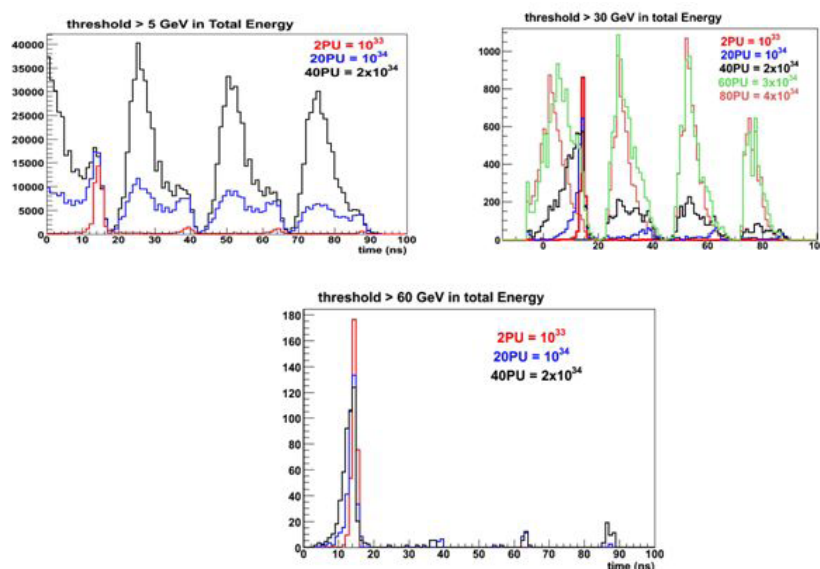


Figure 4.8: Determination of shower timing using 3-bucket fits for a 5 GeV, 30 GeV, and 60 GeV energy deposition. For all 3 plots, the time of the shower is in the first bucket, as seen in the 60 GeV deposition plot. Note that for the lower 2 energies, significant pileup causes the time to be incorrectly estimated to be in subsequent buckets, making such a technique ineffective

2889 low gain (2000) and splitting the signal would have introduced unacceptably large electronic
 2890 noise per channel. In order to achieve low front-end noise (about 4000 electrons at 40 MHz),
 2891 compromises were made in the front-end ADC ASIC, called the QIE (Charge Integrating and
 2892 Encoding). The QIE was designed to have a dynamic input impedance that depends on the
 2893 amplitude of input pulse. This generates an apparent time slew in the output pulse sent to the
 2894 flash ADC. Figure 4.9 shows the time slew vs input energy pulse. We see that at lower energies
 2895 there is an increased time slew. This sets limits on our ability to localize in time the input
 2896 event energy. For isolated large energy events this is not a problem as all the tower energies
 2897 can be associated with the high-energy depositions of the event. As luminosity increases and
 2898 the occupancy from the multiple interactions grows, our ability to correctly assign energies
 2899 to the correct event will diminish. It will be extremely challenging to apply sensitive cuts as
 2900 illustrated above.

2901 Note that in the very forward (HF) region ($3 \leq |\eta| \leq 5$), PMT readout occurs on a time scale
 2902 that is smaller than the 25ns between buckets, making any timing measurement impossible
 2903 with the current electronics. We plan to introduce the same electronics into HF that we will
 2904 introduce into HB and HE in order to have a similar timing measurement. Since we will not
 2905 necessarily be increasing the number of channels in HF, it will constitute an increase in the
 2906 timing electronics purchases of order 20% over the entire HCAL detector.

2907 4.2.2.1.2 Radiation Damage Effects Due to an Increase in Integrated Luminosity

2908
 2909 Although radiation map simulations indicate that the barrel (HB) and very forward (HF)
 2910 calorimeters will be able to withstand Phase 1 radiation levels, this is most likely not the case
 2911 for the endcap (HE) detector, which sits in the forward region $1.3 \leq |\eta| \leq 3$. We anticipate that
 2912 damage from ionizing radiation will cause a reduction in the light from the inner HE layers.
 2913 Introducing sufficient longitudinal segmentation in the HE will allow this effect to be mitigated
 2914 by applying different weighting to the segments in the energy sum.

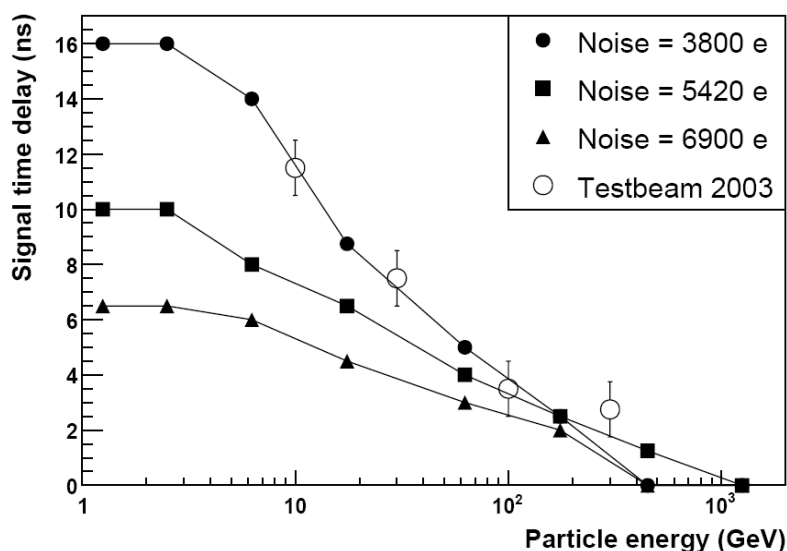


Figure 4.9: Time slew versus energy for the HCAL front end ASIC

2915 Radiation damage considerations for Phase 1 require an understanding of the integrated ion-
 2916 ization radiation in the scintillator for HE causing a reduction in number of photons per GeV,
 2917 and radiation at the front-end readout boxes. For the former, an understanding of both the
 2918 ionization and neutron fluence is required to be sure that the electronics will be able to last in
 2919 that environment. Requirements for radiation tolerance for the HE scintillator will be set by the
 2920 Phase 1 luminosity, however the radiation tolerance for the electronics for all of HCAL will be
 2921 set by the Phase 2 luminosity, which is nominally 10 years at $5 \times 10^{34} \text{ cm}^{-2}\text{s}^{-1}$. Similar stud-
 2922 ies for the ECAL endcap are also essential to understand the overall performance degradation
 2923 with radiation dose for the combined calorimeter performance.

2924 Figure 4.10 shows the radiation contours for 10 years of LHC running ($500fb^{-1}$) for the HB
 2925 and HE, with the contour units in Grays (100 rad = 1 Gray). From these maps we see that the
 2926 ionization radiation levels of order one hundred Rad in the RBX region, and of order 10 kRad in
 2927 the HB, all for integrated doses which are consistent with LHC and Phase 1 running. However
 2928 in the lower part of HE, the radiation levels will approach 1 MRad, a significant amount. To
 2929 understand the impact of these doses, we see in Figure 4.11 the effect of various ionization
 2930 doses to the scintillator, and that for doses in excess of \sim few MRad the scintillator light output
 2931 will be reduced by a non-trivial amount, to be checked with LHC running. This motivates the
 2932 longitudinal separation of layers in order to apply re-weighting to adjust for the degradation.
 2933 It is also clear that for Phase 2, where the radiation levels will be 10x higher for a long period
 2934 of time, the light output from the HE scintillators will drop below a few percent, of their pre-
 2935 radiation levels and the HE will no longer be viable. This motivates a completely new R&D
 2936 effort for Phase 2, which is discussed in the appendix.

2937 4.2.2.2 Problems with Backgrounds and Overall Sensitivity to Small Cross-sections

2938 Effects from non-beam-crossing related signals (e.g. beam gas and halo, high energy muons
 2939 from downstream scraping, cosmic rays, electronics problems, etc.) will become more critical
 2940 as the focus turns to ever rarer physics processes with increased luminosity and data samples.
 2941 Indeed at the Tevatron these effects are the highest contribution to the raw MET rate in the
 2942 trigger and the offline. These upgrades will allow reweighting for radiation damage (from

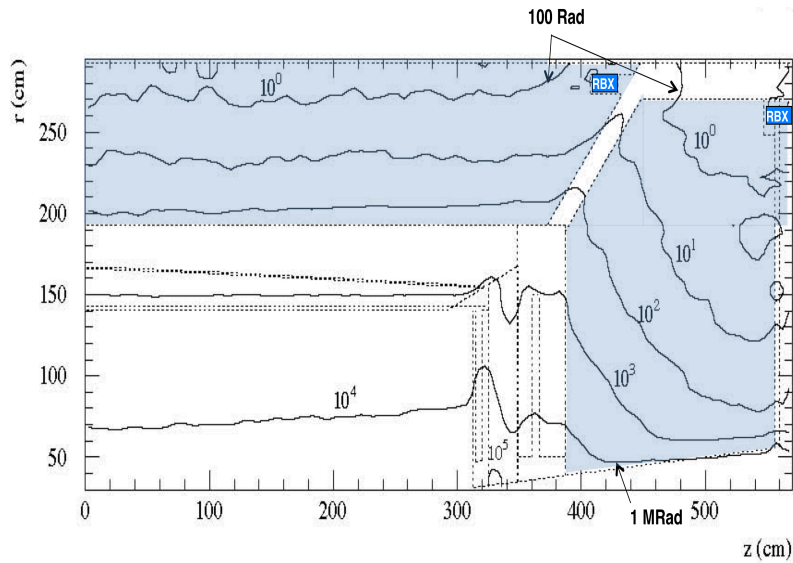


Figure 4.10: Radiation contours for CMS from FLUKA calculations, units of Grays, after $500fb^{-1}$ (10 years at LHC design luminosity). HB and HE begins at $r > 180cm$ and $z > \sim 400cm$ respectively.

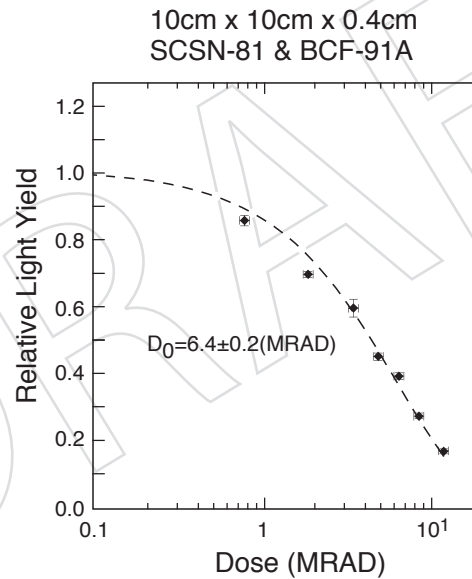


Figure 4.11: Scintillator degradation as a function of ionization radiation.

2943 segmentation, mostly in HE), add redundancy and shower shape information (segmentation,
 2944 in HB and HE), and timing (HB, HE, and HF) to help reduce non beam-crossing-related signals
 2945 and out-of-time pileup. This proposal will increase the discovery potential of CMS, for example
 2946 for long-lived heavy NLSPs such as gluinos from “Split SUSY” that decay asynchronously with
 2947 the beam crossing.

2948 Missing ET (MET) and missing HT (the vector sum over clustered energies and muons, MHT)
 2949 is a very important signature for new physics such as SUSY and dark matter searches, and are
 2950 extremely sensitive to contaminations from non-beam-related signals, the most important of
 2951 which are cosmic rays, beam halo, and detector malfunctioning. Good timing information in

2952 the calorimeters to reject out-of-time events and redundancy in the detector measurement to
 2953 check for consistency in several readout channels are the classic handles for dealing with these
 2954 contaminants. Since some of these very rare backgrounds are extremely difficult to simulate
 2955 realistically, we can profit from the CDF and D0 experience at the Tevatron. Figure 4.12 illus-
 2956 trates the gain that CDF realizes by imposing timing (and jet) cuts in the MET distribution.
 2957 One can clearly see the importance of removing these contaminations as the highest MET rate
 2958 is reduced by about 2 orders of magnitude.

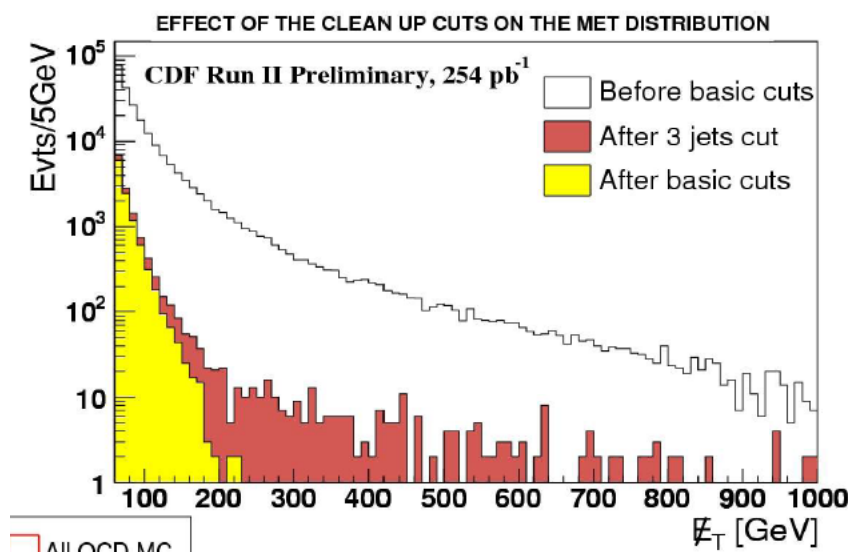


Figure 4.12: CDF MET distribution.

2959 As the integrated luminosity of LHC increases, CMS will be sensitive to physics processes
 2960 of lower and lower cross section. Hence flat or constant cross section backgrounds will be-
 2961 come more and more important. In particular, the highest energy cosmic rays will start to be a
 2962 problem for missing ET signals. Figure 4.13 from CDF shows signal + background for gamma-
 2963 gamma + MET. Note that the non-collision background due to halo and cosmic ray events is
 2964 roughly flat in MET out to 100 GeV/c and contribute a sizeable fraction of the total rate at
 2965 higher MET.

2966 In a recent CDF analysis [5], the highest E_T dijet event recorded (about 800 GeV per jet) was
 2967 determined to be a cosmic ray event with a double bremsstrahlung. This event is shown in
 2968 Figure 4.14. It was estimated that CDF would record only a few such events per year.

2969 It is interesting to compare expected cosmic rates for CDF and CMS. CDF is sensitive to cosmic
 2970 roughly 10ns out of each 396ns (bunch spacing). Correspondingly, CMS will be sensitive to 10ns
 2971 out of each 25 ns or about a factor of 20 more than CDF. CMS sits under 100 meters of earth
 2972 while CDF is under about 5 meters, however for energies greater than about 40 GeV, cosmic
 2973 muons can easily penetrate the CMS overburden. Therefore we expect that CMS will have
 2974 substantially more background due to cosmic rays in the multi-hundred GeV region. These
 2975 events are rare and will not affect larger cross section measurements that will be done early in
 2976 the CMS experiment lifetime. However as integrated luminosity increases, the effect of these
 2977 rare events will become more important and techniques for detection and removal will have to
 2978 be implemented.

2979 Out-of-time events (due to cosmic rays and beam halo) are an important source of background
 2980 in SUSY searches in D0 and CDF. An important upgrade for CDF was the addition of timing

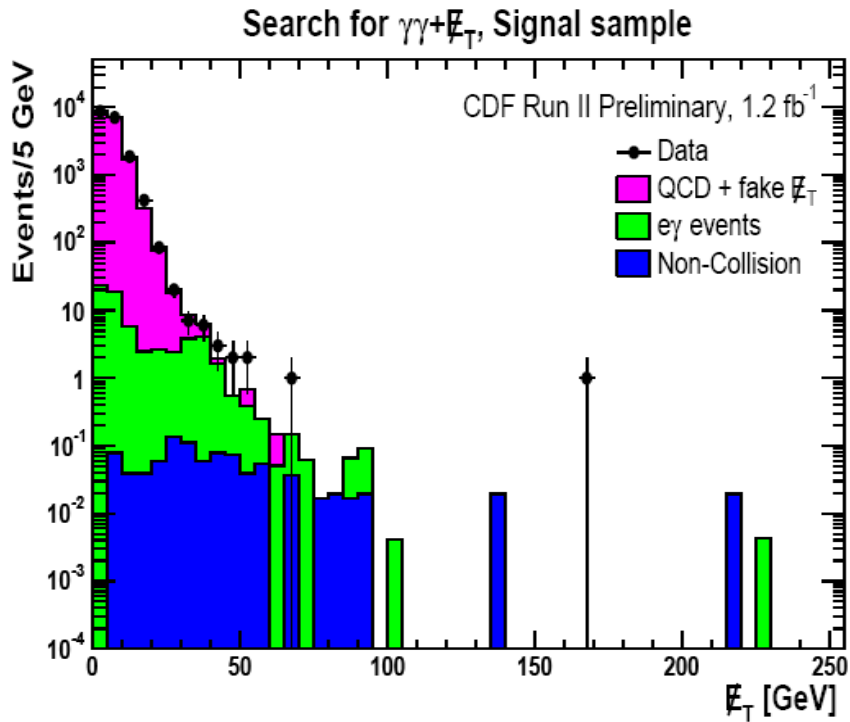


Figure 4.13: CDF MET distribution for $\gamma\gamma + \text{MET}$ analysis showing irreducible backgrounds.

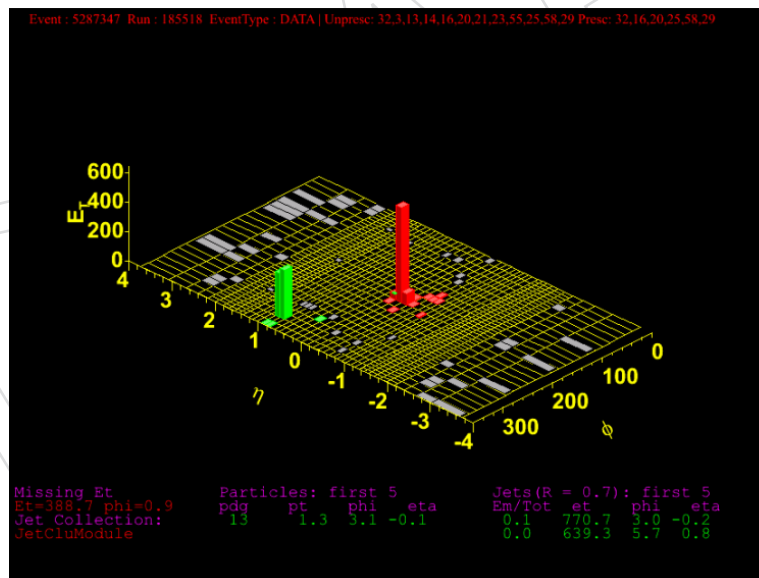


Figure 4.14: Highest ET dijet event seen by CDF determined to be from a cosmic ray.

2981 information in the calorimetry. Figure 4.15 on the left shows a CDF MET distribution for Monte
 2982 Carlo and data (before cleanup cuts). Figure 4.15 on the right shows the same data after a
 2983 requirement that less than 5 GeV was measured out of time with respect to the main event.
 2984 There is a very significant reduction in the tail. The rate of events with MET > 100 GeV has
 2985 been reduced by more than a factor of 10.

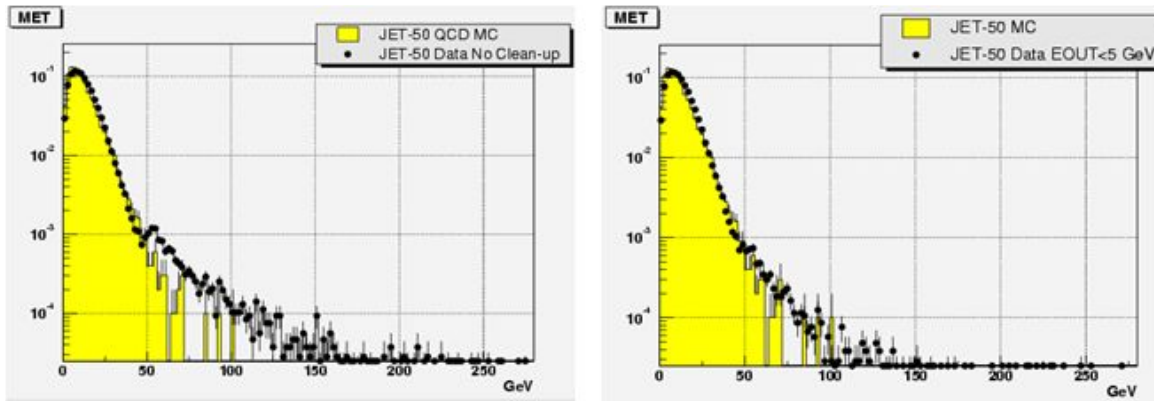


Figure 4.15: CDF missing ET distribution and effect of timing cut.

2986 One of the largest backgrounds to isolated high E_T electrons will be from jet fluctuations. We
 2987 studied this in the HE where the effect will be pronounced. By exploiting depth segmentation
 2988 a much greater rejection factor can be achieved. For the plots in Figure 4.16, the HCAL was
 2989 divided into 2 segments: a thin inner layer, and the rest in an outer layer, as in the HCAL TDR.
 2990 The hadron energy used for the isolation and had/em cuts was in the outer layer, effectively
 2991 throwing away the inner layer and using it as an absorber. From the plots in Figure 4.16, we
 2992 can see the effect of depth segmentation on the isolation and electromagnetic energy fraction
 2993 had/em efficiencies for this background rejection, and this strongly suggests that this technique
 2994 will be even more important at luminosities of 1 or $2 \times 10^{34} \text{ cm}^{-2} \text{ s}^{-1}$ or higher where the in-
 2995 time pileup is large.

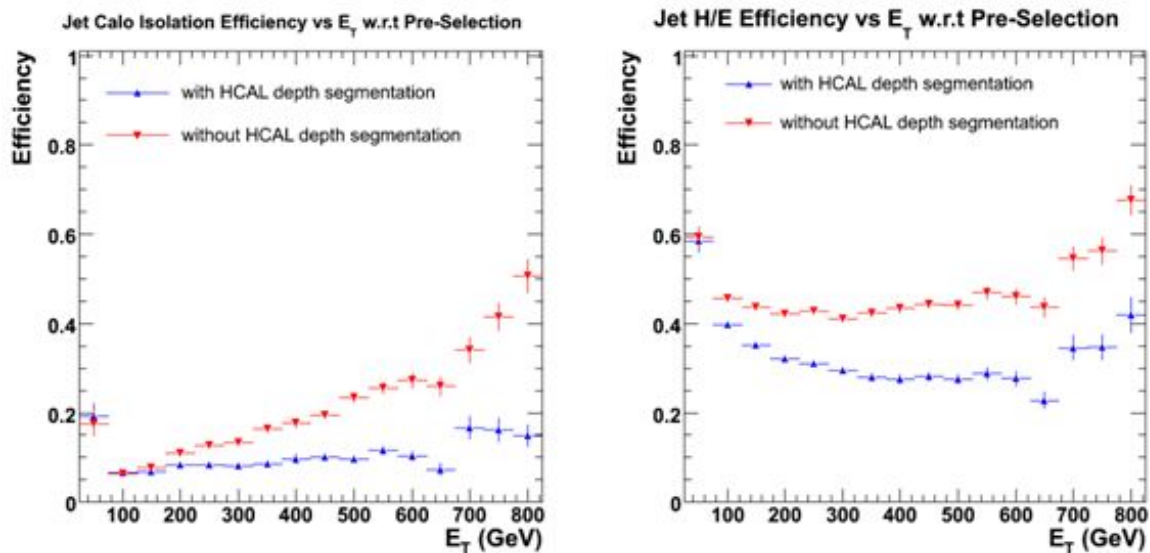


Figure 4.16: Effects from nominal depth segmentation in HCAL on backgrounds to isolated electrons

2996 All of these issues (pileup, degradation of timing capability, sensitivity to smaller cross-sec-
 2997 tions, radiation damage, etc) can be mitigated by an upgrade that focuses on changes to the
 2998 front-end (FE) electronics by adding longitudinal segmentation and front-end electronics tim-
 2999 ing capability. This is detailed below.

4.2.3 Simulation Studies

Studies of physics processes are fundamental to optimize the design of the HCAL upgrade in the context of the combined measurement capabilities of the calorimeters, ECAL and HCAL, and tracking systems for doing physics at high luminosity. We are performing detailed studies to understand the expected improvements in triggering, isolation, energy resolution, and background rejection due to the increased longitudinal segmentation and TDC timing. These studies will provide input as to how to reestablish the current low-luminosity physics capabilities in the high luminosity era, and allow us to have a more powerful detector for triggering and offline analysis as the luminosity approaches several times 10^{34} , expected at the SLHC in Phase 2. Some of the analyses will need to be re-evaluated after CMS completes extensive data analysis from low-luminosity running. The upgrade path is designed with this flexibility in mind. For instance, the choice of longitudinal segmentation is not a constraint that impacts the fabrication of the front-end electronics and can be configured at a late stage in the upgrade timeline. The goals of the front-end simulation studies are to define the physics benchmarks to be used to form a straw-man definition of the required SiPM specifications, the front-end signal optimization, response time, digitization dynamic range and coding granularity, the choice of longitudinal segmentation and the performance optimization of front-end TDC measurements.

An initial setup for the simulation studies has been implemented in CMS software environment (CMSSW_2_2_13) and will be ported to a more recent version once the upgrade framework is supported in the standard software release. The HCAL upgrade software consists of layer-by-layer hit information to provide maximum flexibility in the study of possible configurations of the longitudinal segmentation and digitization parameters. The hit information is used to generate a calorimeter hit (PCaloHit) collection and is capable of feeding a new expanded set of channels (CaloDataFrames) incorporating multiple depths, improved signal-to-noise, SiPM pulse shapes, SiPM response time and TDC information. These CaloDataFrames are used to compute an expanded set of trigger primitives that will be able to feed the existing L1 trigger emulation software. Incremental improvements to the trigger primitives from replacing peak finding methods with TDC-based bunch-crossing identification can be studied directly. New quantities, such as lepton isolation cones, will be formed as part of SLHC L1 trigger primitive object and used to supplement the information of the existing L1 decision tree.

There are several possible schemes for longitudinal segmentation; Figure 4.17 illustrates two. The scheme on the left has finer segmentation where the energy density is greatest, and therefore optimizes the resolution, shown here for four depths of readout with the first depth consisting of layer-0, the second of layers 1-4, the third of layers 5-8 and the fourth of layers 9-16. This multi-depth configuration is referred to the 1-4-4-8 configuration. The scheme on right side of figure 4.17 optimizes redundancy and robustness by interleaving the rear two depths. The standard CMS simulation package does not record the energies deposited in the copper absorber plates and therefore the energy weighting studies have been performed with a separate standalone version of GEANT looking at different configurations for the purpose of improving jet resolution.

Simulation studies will focus on the SiPM device parameter requirements, the increased longitudinal segmentation and the ability to time the pulse to 1-2 ns within the 25ns window. This latter requirement stems from the fact that at high luminosity, out-of-time pileup (with average number of interactions per crossing increasing into the 100s) will preclude any pulse timing measurement with any accuracy below 10 GeV using the energy detected in 25ns buckets.

The largest performance improvement comes from the intrinsic signal-to-noise improvements from an SiPM photodetector and optimized readout electronics. Table 4.4 shows a preliminary

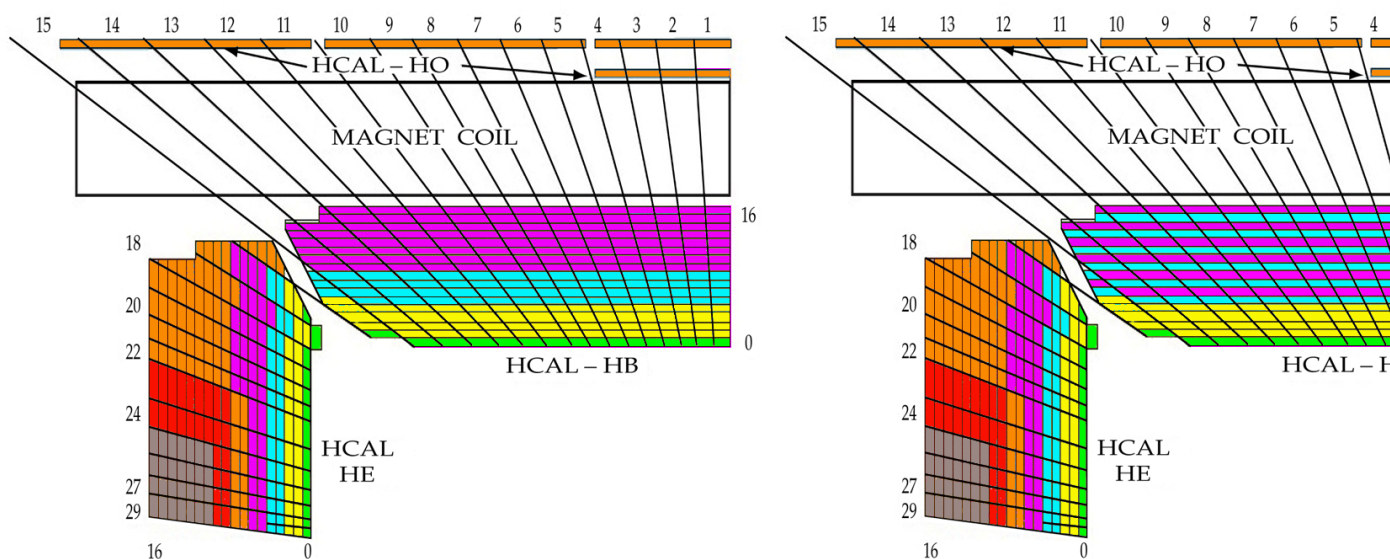


Figure 4.17: Two differing longitudinal segmentation schemes with each color code representing the layers that are grouped into separate readout channels. The one on the left maximizes resolution by concentrating separate readout channels to groups of layers where the energy density is highest. The one on the right maximizes redundancy and robustness of the calorimeter by providing two rear readout channels with interleaving sampling of the hadronic showers.

3047 comparison of the pedestal widths in GeV for the existing HPD and readout electronics for
 3048 array of towers used for different purposes physics analysis and triggering: 1×1 for muon
 3049 energies, 3×3 through 5×5 for isolation variables for electrons, muons and τ s, and 12×12 and
 3050 larger for jets, transverse missing energy and global energy sums. The reduction in noise levels
 3051 shown in Table 4.4 corresponds to improvements of signal-to-noise from a factor of 3 summed
 3052 over all longitudinal depths to a factor of 14 for the signal in Depth-1, consisting of layer-0 of
 3053 scintillator. In the upgrades, the layer-0 neutral density filter would be removed in the upgrade
 3054 yielding a factor of 2.4 more light for a given reference energy deposition in the scintillators.
 3055 The purpose of the filter in the original design of the calorimeter was to reduce the signal in
 3056 layer-0 at the hardware level to allow the signal to be added to subsequent layers optically
 3057 without degrading the linearity of the energy response. With a separate readout, the full signal
 3058 of layer-0 can provide a powerful tagging mechanism for non-interacting pions entering the
 3059 HCAL barrel and for the detection of shower leakage from the ECAL for a more sensitive H/E
 3060 discriminating variable. All layers will see a photoelectron light yield improvement currently
 3061 approximated to be twice that of the current HPDs. In addition, the photoelectron equivalent
 3062 of the pedestal noise will reduce from the current level of 3 photoelectrons to something closer
 3063 to $1/3$ of a photoelectron. For Depth-4, the 10% larger thickness of the rear absorbers can be
 3064 separately applied and yields a corresponding 10% shift in energy scale to further improve
 3065 response linearity of the calorimeter.

3066 One of the most critical uses of the HCAL energy in the trigger is for the longitudinal isolation
 3067 of electron and photon showers. This cut is traditionally placed between 2% and 5% of
 3068 the total ECAL+HCAL energy. Some preliminary simulation studies on how to make use of
 3069 longitudinal segmentation look promising. For instance, Figure 4.18 shows the effect of pileup
 3070 on the ability to trigger on isolated leptons. At 2×10^{34} , with 40 multiple interactions per cross-
 3071 ing on average, the pileup is large enough that there is a high probability for a particle to get

Table 4.4: Pedestal widths (GeV) for HPD readout and SiPM readout with 4 depth segmentations in the 1-4-4-8 configuration.

	1×1	3×3	5×5	12×12
HPD	0.260	0.780	1.300	3.12
SiPM Depth 1	0.018	0.038	0.092	0.15
SiPM Depth 2	0.044	0.131	0.220	0.53
SiPM Depth 3	0.044	0.131	0.220	0.53
SiPM Depth 4	0.048	0.144	0.240	0.58
SiPM All Depths Summed	0.081	0.242	0.403	0.967

3072 through the ECAL into the first layer of the HCAL, compromising the EM fraction for an iso-
 3073 lated electron. By eliminating the first HCAL layer from the trigger, we can recover an effective
 3074 isolated electron capability. This is made possible by introducing longitudinal segmentation in
 3075 the readout. This will become important towards the end of Phase 1 and even more so in Phase
 3076 2 where the number of multiple interactions is 5x that in Fig. 4.18.

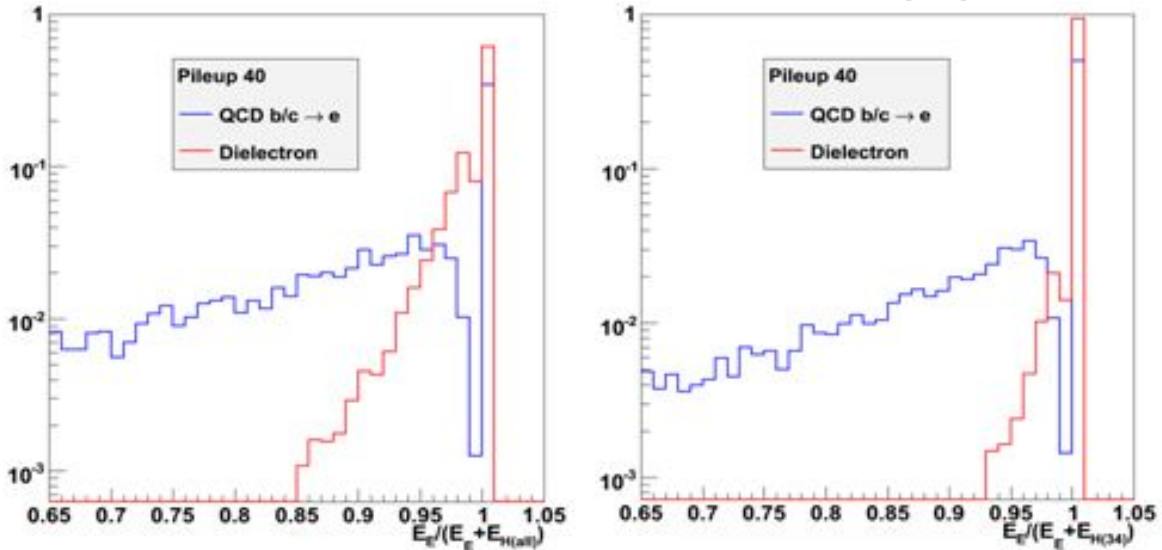


Figure 4.18: Pileup at 2×10^{34} can reduce the capability to trigger on isolated leptons. The left side of the figure shows the impact of using all HCAL layers in the determination of isolation; the right hand side shows how this improves when the first layer of the HCAL is not used.

3077 Another way of seeing this effect is by looking at the shape of the single tower distribution
 3078 for HCAL towers as a function of pileup. The results in Figure 4.19 clearly indicate that the
 3079 electron/photon trigger path will suffer from luminosity-dependent inefficiency if it uses the
 3080 full HCAL energy for isolation. It is better to exclude the first few layers. However, the jet and
 3081 MET paths will likely be more stable with the inclusion of this energy. This motivates separate
 3082 hadronic energy measurements for the jet and electron paths of the calorimeter trigger.

3083 4.2.4 Proposed Improvements and Upgrade Plan

3084 4.2.4.1 Photodetector and front end electronics

3085 The key element of the upgrade of the HB/HE is the replacement of the HPDs by SiPMs. A
 3086 picture of a SiPM is shown in Figure 4.20. The devices have a high gain (up to 10^6 compared to

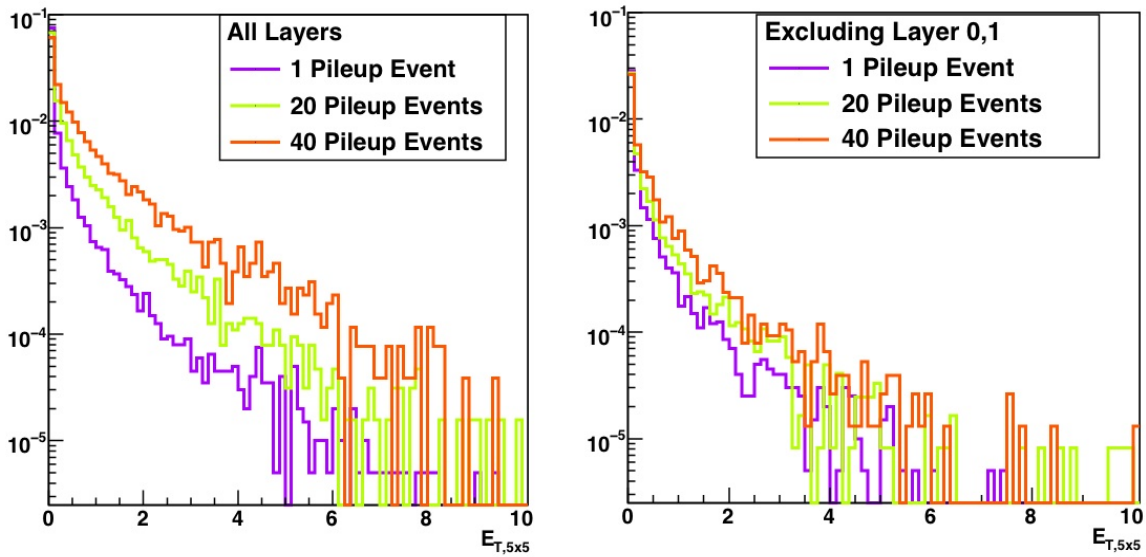


Figure 4.19: Energy distribution in the HB as a function of pileup when considering all layers (left) and when excluding the first two layers (right). The distributions are normalized to match the integral of the two leftmost bins, allowing a shape comparison.

3087 1500 for the HPD), a high QE (~ 2 over the HPD), and operate at much lower voltages (~ 50 V)
 3088 compared to the HPD (~ 7 kV). The higher gain of the SiPM will reduce the electronic noise levels
 3089 in the calorimeter, improving the sensitivity for low energy showers. The lower operating
 3090 voltage should largely eliminate breakdowns, there is no vacuum hence no ion feedback, and
 3091 the device is insensitive to magnetic fields, in contrast to the HPDs. SiPMs are linear up to the
 3092 point where the probability for more than one photon per pixel gets large; however, this effect
 3093 is mitigated by increasing the number of pixels (see Figure 4.21).

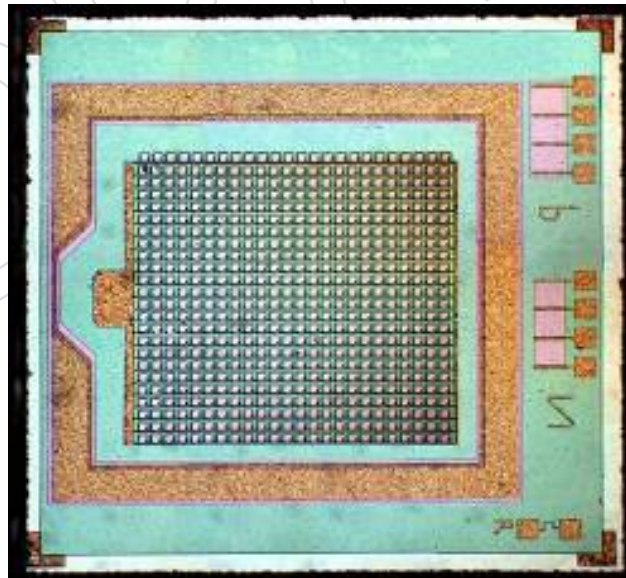


Figure 4.20: SiPM candidate chip from Hamamatsu

3094 Our R&D plan is designed to identify candidate SiPMs that meet our requirements and that
 3095 will be available commercially on the timescale needed at an affordable cost.

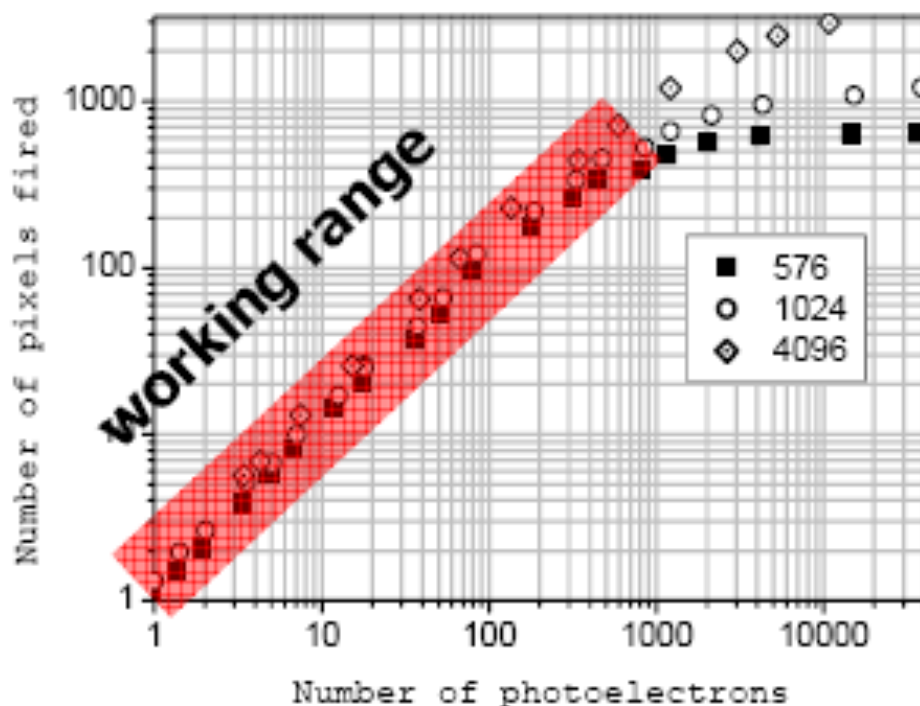


Figure 4.21: SiPM linear range as a function of the number of pixels per square mm.

3096 In setting the characteristics and performance requirements for the SiPMs to be used in CMS,
 3097 some of the more important factors we identified are: 1) active area; 2) signal-to-noise; 3) pho-
 3098 ton detection efficiency; 4) insensitivity to magnetic field; 5) radiation tolerance; 6) linearity
 3099 of response for single pulse; 7) rate capability; 8) lifetime; 9) temperature sensitivity; and 10)
 3100 variation in operating voltage at constant gain for an ensemble of parts. We are currently for-
 3101 malizing the requirements document to present to the CMS electronics steering committee.

3102 A very important part of the R&D will be to procure SiPM samples from various vendors
 3103 for evaluation. Known vendors include Hamamatsu (Japan), FBK (Italy), CPTA (Russia), and
 3104 Zecotek (Singapore). We plan to purchase sufficiently large samples of existing SiPMs and
 3105 evaluate their performance. We will purchase larger quantities of promising devices and are
 3106 prepared to work with the vendors to tailor them to our needs. In total, approximately 800 cm²
 3107 of SiPM photodetection area is required for the barrel and endcap upgrade. Uniformity of the
 3108 SiPM devices will be important for calibration and would therefore point to having at most
 3109 one vendor for the entire barrel but with the possibility of potentially a separate vendor for the
 3110 endcaps.

3111 The integrated dose of neutrons with $E > 100$ keV during the lifetime of the SLHC is ex-
 3112 pected to be in the range $1 - 3 \times 10^{12}$ for HB/HE readout box regions. Neutrons in this energy
 3113 range are particularly important as they have been shown to induce leakage current in silicon
 3114 devices. The SiPM and ADC must survive these doses with limited degradation. We have
 3115 started exploring radiation damage to various SiPMs. Figure 4.22 shows relative loss in ap-
 3116 parent QE/gain (ratio of peak of LED response) as a function of the dose, using protons with
 3117 $E = 212$ MeV. We see that the candidate Zecotek devices (MAPD) look very promising.

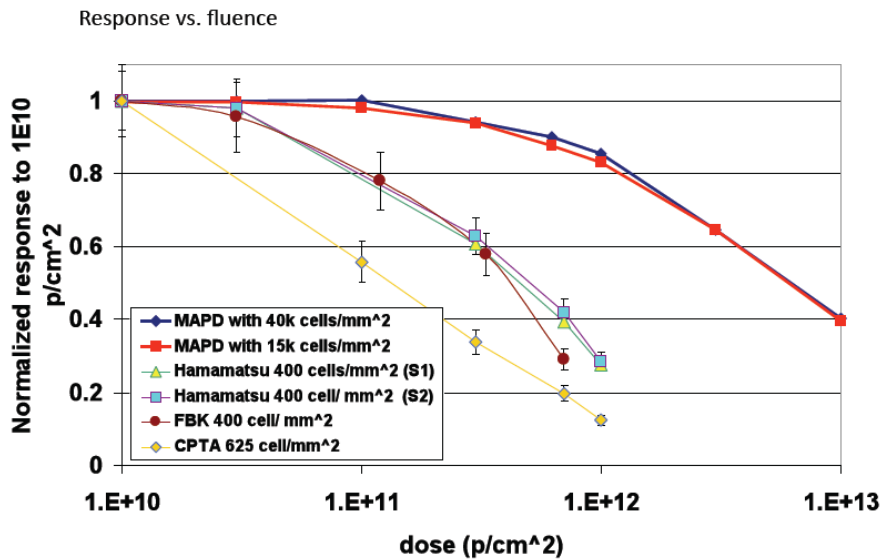


Figure 4.22: Change in LED peak value as a function of proton dose.

4.2.4.1.1 Longitudinal Depth Segmentation, Options for Optical and Electrical Decoder Units

To incorporate multiple depth segmentation in the calorimeter we will replace the ODU (Optical Decoder Unit) that receives the calorimeter analog optical signals from the scintillators and optically sums it into towers. We are investigating a new approach that allows us to read out each fiber with a SiPM and then make an analog sum of the output signals of the set of SiPMs (tiles) that would comprise the depth segment of the calorimeter. We believe that this will be both easy to build into the existing system, and would give us maximum flexibility in how we combine longitudinally. We call this new development the Electrical Decoder Unit (EDU). To build the EDU we need to create a design for the packaging that will allow the optical signals from the calorimeter to reach the SiPM and be formed into a readout segment. We will design the EDU to mate to the existing CMS HCAL fiber connectors, which consist of 18 individual 0.9 mm fibers.

Figure 4.23 shows the general concept of the EDU. Optical cables from the calorimeter are plugged into a mating array of SiPMs (linear array). These arrays are mounted on a PC board. Connectors couple the electrical signals from the SiPMs to electronics cards located below the readout electronics. The perpendicular arrangement of the readout card relative to the linear array allows for easy summation of fibers (tiles) into tower segments.

Figure 4.24 shows a detail of one of the SiPM linear arrays. In this implementation we would construct the linear array from individual packaged SiPMs bonded to a substrate. We plan on working with vendors to develop monolithic arrays of SiPMs. The first version would be 18 1mm diameter SiPMs in a linear array on a single piece of silicon. Having the integrated linear array rather than single parts will make handling easier, guarantee alignment, and reduce packaging costs. Figure 4.25 shows the details of the SiPM strip array packaging.

An important part of our R&D is to work with vendors to develop strip array SiPMs that would suitably mate to the analog optical cables from the calorimeter.

Options for optical addition are also being explored. The advantage of optical addition is that

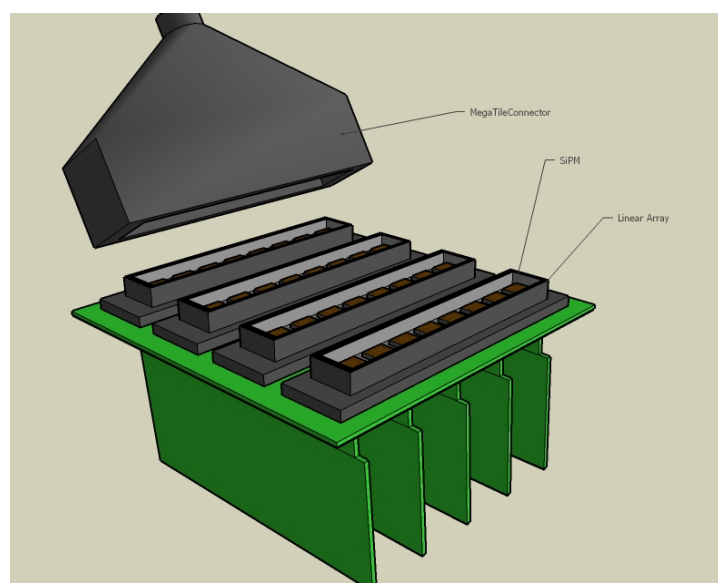


Figure 4.23: Electrical Decoding Unit (EDU)

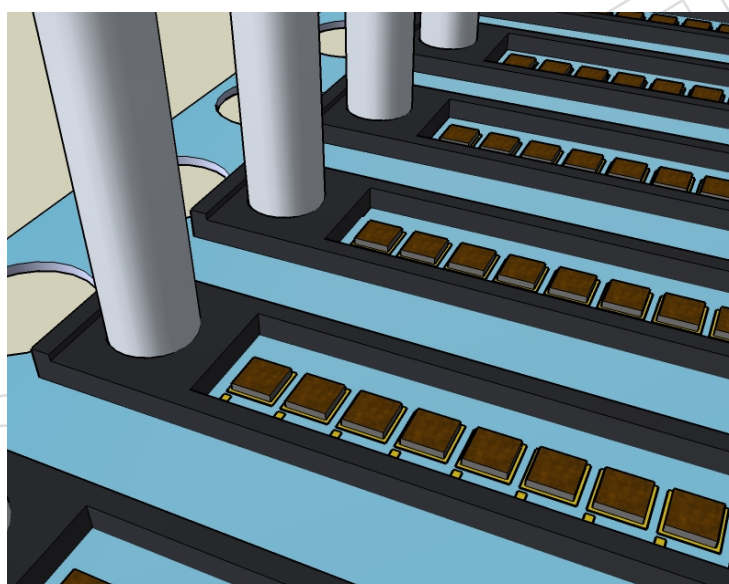


Figure 4.24: EDU detail showing linear arrays of SiPMs

3146 any given fiber can be used to illuminate an incrementally larger photodetection surface with
3147 a correspondingly larger number of SiPM pixels. The total number of SiPM pixels sets the
3148 available dynamic range of the SiPM photodetector. This option is particularly important for
3149 devices where the feature size limits the pixel density to ~ 5000 pixels/mm².

3150 4.2.4.1.2 Timing

3151

3152 We foresee the new front-end readout will incorporate TDCs on at least some of the chan-
3153 nels. As stated above, we can learn from the experience of experiments at the Tevatron, where
3154 CDF has found that TDCs on the calorimeter readout are very useful in various background
3155 rejections. Additionally they open the door to new physics, for instance slow heavy stable par-

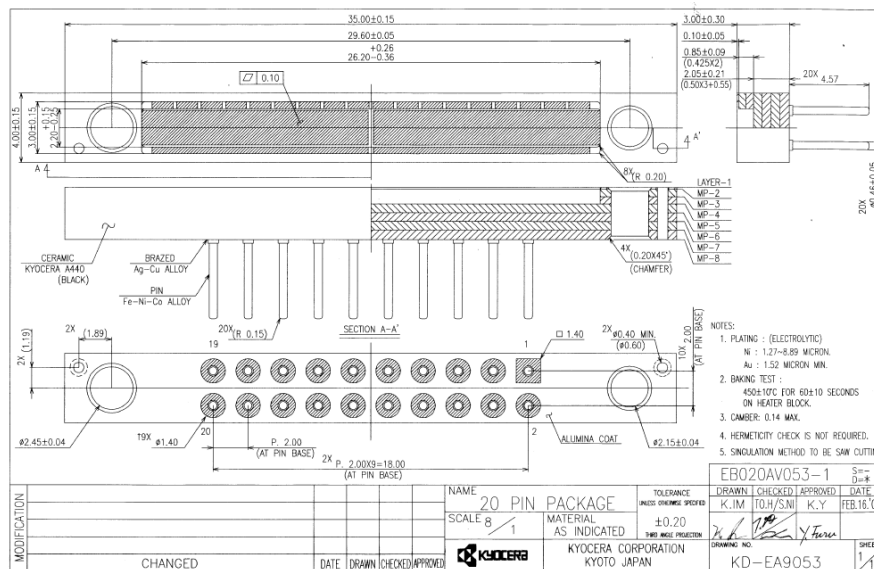


Figure 4.25: Kyocera strip SiPM package

3156 title detection. The TDC information has the potential to improve the bunch crossing identification accuracy over the current peak detection methods used for trigger primitive generation, especially for low energy quantities such as lepton isolation energies. We envision implementing a timing measurement in the FE electronics by first producing a fast discriminated pulse out of the QIE (see below), and then timing that pulse with a fast clock relative to the bunch crossing (BX) time, perhaps inside a radiation hard programmable logic chip. If the clock were to run at 320 MHz, or $8\times$ faster than the BX clock, and use the leading and rising edge of the discriminator pulse, we could get a timing measurement to around 1-2 ns. We will be focusing part of our R&D effort in this area.

3165 4.2.4.1.3 Readout

3166 The current HCAL readout is via a charge integrating and encoding chip, called the QIE, developed at Fermilab. It has a large dynamic range, approximately $10^4:1$, accomplished via input current splitting and comparison on 4 ranges, and digitizing the selected voltage representing the integrated charge with an FADC, and compressing by eliminating needless codes. Since the HCAL towers are large, the shaping is necessarily limited to short times to minimize out-of-time pileup. The sample-and-hold capacitors are necessarily very small in order to have a gain of approximately 1 fC/bin on the most precise scale. In order to make as linear a device as possible, a BiCMOS process was used for the current HCAL QIE (version 8, or QIE8), and at the time the QIE8 was developed the best process had a 0.8μ feature size.

3176 For the upgrade we are exploring two possible ADC schemes for the readout: (a) an enhanced (and radiation hardened) QIE charge integration directly from the SiPM, and (b) a voltage following integrator similar to the ECAL scheme (called the MGPA/ADC). For the QIE, we will propose an upgrade that will use a finer feature size (0.35μ), slightly greater functionality (e.g. some phase adjustments and fast discriminated pulse built-in), greater dynamic range ($\times 10$) and greater precision (6 instead of 5 bits on the FADC mantissa of the encoded output). For the MGPA/ADC option we will explore both the ECAL solution and commercial solutions. We note however that the ECAL solution was built for a detector that had 25x smaller tower sizes, and thus much less occupancy, which allowed stretching out the pulse to over 10 bunch cross-

ings in order to make a precision measurement. Extending the length of the front-end pulse is not optimal for the HCAL; however, we want to consider all possible solutions that minimize the risk and cost. For either solution we will continue to compress the ADC output to save data bandwidth out of the calorimeter.

Both readout schemes are multi-range systems, but the dynamic range of the SiPM and its non-linear behavior at the high-end need dedicated studies to determine how best to match the SiPM with these different ADC systems. The channel density is also a major concern as the power and cooling of the existing services (the Readout Box, or RBX) are significant constraints. Our initial evaluation is that the QIE is most suitable for the SiPM HCAL upgrade. The QIE will therefore be our major focus for development in the short term. We will continue to study the MGPA as a possible solution. A test stand using ECAL VFE cards has been set up.

The performance of the SiPM system is closely tied to the ADC digitization for reasons of dynamic range and sensitivity. A new generation of the QIE is needed to match the SiPM gain ($\sim 5 \times 10^4 \rightarrow 10^6$ compared with $1 \rightarrow 2 \times 10^3$ for the HPD). As stated above, we plan on having the new QIE create a discriminated output pulse for use in an external TDC circuit.

The current HCAL QIE has an associated control chip, the CCA (Clocking Control ASIC). In the current implementation this is an ASIC. We plan to replace the CCA functionality with an FPGA that will implement some of the QIE control functions. It will also provide a digitized output for the TDC signal sent from the QIE. Additionally it will do error checking on the QIE. The FPGA will handle all QIEs in the readout module ($18 \times 4 = 72$ channels) and format the data for the digital link. The options for the digital link are being explored in the context of the Cern Gigabit Transceiver (GBT) development group. For testing purposes, we are operating commercial off-the-shelf high-speed data links using FPGAs to serialize. We note that the exact format of the data stream feeding the front-end optical drivers can be defined relatively late in the upgrade plan in response to the needs and experiences with the first LHC collision data. In order to keep the high power electrical components in better contact with the readout box (RBX) cooling, we will build a separate board for the FPGA and optical drivers. Figure 4.26 shows a drawing of the layout of the new electronics cards in the Readout Module, showing 4 QIE cards plugged into a single FPGA card.

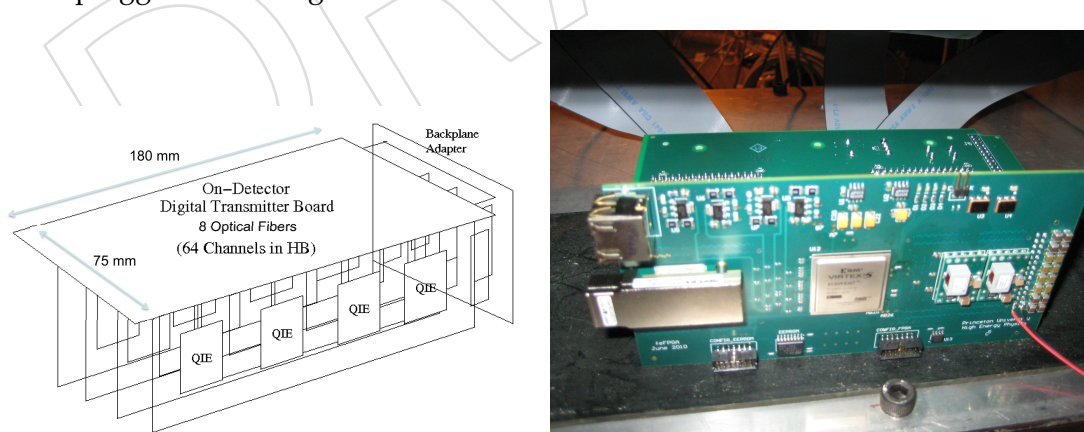


Figure 4.26: Layout of Readout Module boards, where the placement of the optical links and FPGA are optimal for the existing RBX cooling circuits. A functional schematic is on the left and a photograph of a prototype from the 2010 test beam is on the right.

The SiPM needs stable bias voltage and temperature for optimal performance. We are developing a Cockroft-Walton circuit to generate the bias voltages. The circuit will also provide

leakage current readback. The SiPMs in the EDU will be thermally isolated and solid-state (Peltier) coolers will lower and stabilize the temperature.

4.2.4.1.4 Front-end crate mechanics and cooling

The mechanical design of the FE package has several components. The optical decoding units must be redesigned to handle up to 4 readout depths that map to individual SiPM devices. The cooling pack for the ADC/TDC electronics needs to be expanded to handle the front-end channel increase. The outer mechanical case of the RM must accommodate the SiPM support and Peltier cooling and meet the outer dimensional requirements of the existing RBXs.

The cooling capacity in the RBX is limited by the cooling plant and existing pipework. The layout of the readout cards should be optimized to ensure that additional heat load in the new front-end does not cause an increase in the chip temperatures, currently at about 25–30°C.

We are studying a design modification to allow the highest power parts (GOLs/GBTs, FPGA, voltage regulators) to be very close to the heat exchange. Figure 4.26 above shows the proposed new layout. The heat exchange plates of the RBX are on top and bottom. Note the placement of the GOLs and FPGA close to this plate.

4.2.4.1.5 Front-end controls

The current front-end controls cannot accommodate an upgraded project using SiPMs, and it is envisioned that the TTC (Trigger Timing and Control) will evolve to something more powerful using the Cern Gigabit Transceiver (GBT) chips. Extensive R&D will be needed to design the controls upgrade. This includes accommodating the GBT on the front-end cards, interfacing the GBT controls signal to the rest of the front-end electronics in the RBX crate, and integrating the slow controls with the CMS runtime system.

4.2.4.2 HCAL Back-End (BE) Trigger/Receiver Upgrade

The calorimeter backend electronics are built to receive the data from the front-ends, ensure time alignment across the links, pass the necessary information to the trigger path, and collect the data in response to Level 1 Accepts. As outlined above, the HCAL Phase 1 upgrade makes major revisions to the front-end electronics that will result in more data (longitudinal segmentation and timing) transmitted to the back-end (BE). As the current HCAL Trigger Receiver boards (HTRs) cannot be modified to receive data at a higher rate, and as the upgrade to the front-end (FE) electronics will require transmitting more data on the same number of fibers, a new backend is required.

The BE upgrade will take advantage of progress in commercial technology since the HTRs were designed in 2002, specifically in programmable logic (FPGAs), increased integration (e.g. deserializers built into the FPGAs decrease the IO burden), and newer and more powerful infrastructure for crate data sharing and handling. At the same time this will allow a more powerful physics trigger. The system we envision should be optimal for HCAL, and scalable in ways that the current system is not. We will keep in close touch with the evolution of ECAL and the CMS Level 1 trigger so as to be in a position to share technology and take advantage of economies of scale.

Given the higher luminosity and multiple interaction rate, we want to allow for increases in the BE capabilities that will allow CMS to do a better job of identifying jets. For instance, in the barrel and endcap region, the trigger primitives with a transverse granularity of 0.087×0.087

3260 in $d\eta \times d\phi$ are sent to the Regional Calorimeter Trigger (RCT) which subsequently reduces the
3261 granularity into larger $4 \times 4 \eta - \phi$ regions for physics considerations in the trigger. However,
3262 for the HF, the regions are constructed inside the HCAL HTR boards for historical reasons.
3263 Implementing a jet-finding trigger that will use a finer granularity than our current trigger
3264 will require hardware changes to both the HCAL BE and the RCT, both envisioned as part of
3265 Phase 1. We point out that by increasing the granularity in this region, we will be increasing
3266 the capability to trigger on jets right in the region where the jet cross-section from W-boson-
3267 fusion Higgs production diagrams is largest (see Figure 5.1): at the HE/HF boundary ($|\eta| \sim 3$).
3268 This particular production channel constitutes the highest cross-section for associated Higgs
3269 production.

3270 As a result of an increase in the number of multiple interactions, in-time and out-of-time pileup,
3271 and the effect on the trigger, the proposed structure of an upgraded HCAL backend must sup-
3272 port an increased bandwidth between the HCAL front-end data and the electromagnetic and
3273 Jet/MET portions of the calorimeter trigger. Such an upgrade could be achieved in two ways.
3274 The straightforward option is an increase in the data volume from HCAL to the trigger system
3275 by 160% to accommodate electromagnetic object isolation variables. The second option is to
3276 combine HCAL data with ECAL trigger primitive data at an earlier stage, allowing the def-
3277 inition of electromagnetic energy and isolation bits to be made separately from the jet/MET
3278 energy definition. For the existing ECAL front-ends, this integration could be made relatively
3279 cheaply as the slow data links from the ECAL trigger front-ends can be received with conven-
3280 tional FPGA inputs, leaving optical receivers as the only hardware cost. If the ECAL front-ends
3281 are upgraded, a different design may be more reasonable. These issues are under investigation.
3282 Note that the baseline HCAL upgrade is to move forward with a new back-end that will ac-
3283 commodate a higher input bandwidth and a higher trigger (and DAQ) bandwidth as required,
3284 working in conjunction with the evolution of the calorimeter trigger and potential changes and
3285 upgrades to the ECAL back-end readout.

3286 4.2.4.2.1 Electronics System Structure

3287
3288 To receive the data from the front-ends, the back-end electronics must accept the signals
3289 from the high-speed optical links. For the HCAL, these links will run over the current 850 nm
3290 multi-mode fibers, currently running at a speed of 1.6 Gbps (1.28 Gbps data rate). Since we will
3291 be increasing segmentation and sending more data, we will need to increase the data trans-
3292 mission rate, and we calculated that we will need a speed of 3.25 Gbps or higher. We will also
3293 utilize unused fibers in the existing fiber ribbons to increase the data throughput. The baseline
3294 proposal for the front-end upgrade includes the usage of the products of the GBT project at
3295 CERN. These components transfer data at a raw rate of 4.8 Gbps with a user data payload (af-
3296 ter error correction and scrambling) of 3.28 Gbps. There is a possibility to increase the user data
3297 payload beyond 3.28 Gbps by using the 8B/10B transfer protocol. These products are expected
3298 to be radiation tolerant and to have adequate latency performance. The data link of the GBT
3299 will be received directly into a field programmable gate array (FPGA) using the high-speed
3300 deserializers built into these chips.

3301 Time alignment, connection to the trigger, and the data acquisition system all require that the
3302 back-end hardware be integrated into an architecture that allows for clock and fast control dis-
3303 tribution as well as the local concentration of data before transmission to the DAQ system. In
3304 the original CMS electronics, the most common infrastructure solution was VME64, particu-
3305 larly the 9U-400 mm card format. VME is a parallel bus standard that has been used for years
3306 in high energy physics, but which is a poor match with the recent trends towards high speed
3307 serial data transmission for most interconnects. A commercial standard, the Micro Telecom-

3308 munications Architecture (μ TCA) is being considered, and this standard appears to match the
3309 requirements more closely. The μ TCA standard specifies moderate-size cards (similar in size to
3310 3U or 6U VME cards) that can communicate at high rates using up to twenty-one bidirectional
3311 high speed serial ports on each card. The interconnection of these ports is specified by the back-
3312 plane, either by the construction of the backplane or by an active device such as a crosspoint
3313 switch. The active element is generally housed in a special hub slot of the backplane (called an
3314 MCH), but it can be integrated directly into the backplane as well.

3315 The μ TCA standard provides for the necessary high-bandwidth communication required for
3316 global data acquisition as well as a powerful local control and data acquisition path through
3317 gigabit Ethernet connections to each card. The standard is generic in many ways, however, and
3318 significant engineering effort is needed to resolve key issues such as the distribution and man-
3319 agement of clocks (including the LHC clock) and the handling of fast controls. In particular,
3320 the HCAL backend electronics will likely be deployed before any upgrade of the TTC system
3321 is complete. Thus, the system architecture must be designed to allow for operation with the
3322 legacy TTC system until a new TTC system is available, then allow an upgrade if needed. This
3323 may be particularly relevant for next-generation DAQ designs.

3324 The installation of upgrades in the running CMS detector will demand a serious attention to
3325 the physics risks of any change to the detector. At the point when the SLHC-related upgrades
3326 would begin, the detector would be acquiring high quality and high value physics data. One
3327 strength of the CMS HCAL design is the ability to access and upgrade it in a short shutdown.
3328 However, it would be very risky to replace the full front-end, back-end, and trigger electronics
3329 in a single short shutdown. Instead, the electronics must be capable of interfacing with older
3330 trigger electronics and the legacy front-ends, which allows flexible upgrade scenarios. In par-
3331 ticular, the readout portion of the new system should be capable of running parasitically (using
3332 optical splitters to obtain a copy of the data sent to the existing electronics) to gain operational
3333 experience. These considerations add significant pressure to the back-end schedule. Rather
3334 than being a task to be attacked after the front-end is completely settled, as was basically the
3335 case for the original CMS electronics, the back-end production must be completed earlier than
3336 the front-ends.

3337 The proposed structure for the upgraded HCAL backend electronics requires two separate
3338 classes of functionality, hosted on separate cards. These two cards may be physically identical
3339 depending on the requirements imposed by the backplane and external portions of the data
3340 acquisition and trigger system. One card has the role of receiving the front-end data, construct-
3341 ing and transmitting trigger primitives to the Level 1 calorimeter trigger system, and holding
3342 the pipeline of front-end data for data subpacket creation in the case of a Level 1 Accept. In
3343 analogy with the existing HCAL Trigger/Readout card (HTR), which has a similar function,
3344 the card will be called the UberHTR (uHTR) in this document. The second card has a dual role
3345 of collecting the subfragments from the UberHTR cards and building event fragments that are
3346 distributed to the DAQ and also of receiving the fast control and clock signals and distributing
3347 them to all the cards in the crate. This dual role is expressed in the term used for this card in
3348 this document: the DAQ and Timing Card (DTC).

3349 As shown in Figure 4.27, each crate of the upgraded system would consist of twelve UberHTRs
3350 and a single DTC card. As a baseline, we consider the use of commercial crates that provide
3351 inter-slot connectivity through the backplane and through special “hub slots” that have en-
3352 hanced connectivity to all slots. In particular, the baseline proposal specifies a crate with two
3353 MCH slots and twelve standard μ TCA card slots. One MCH slot would be used for a commer-
3354 cial card providing the standard μ TCA shelf management functionality, and a gigabit Ethernet

3355 connection to each site for use in configuration and control. The second site would be used by
 3356 the DTC and would necessarily have three high-speed ports distributed to all μ TCA cards (one
 3357 for DAQ data, one for the legacy TTC, and the third for future fast controls). Additionally, the
 3358 DTC will distribute a copy of the LHC clock to all cards over the backplane.

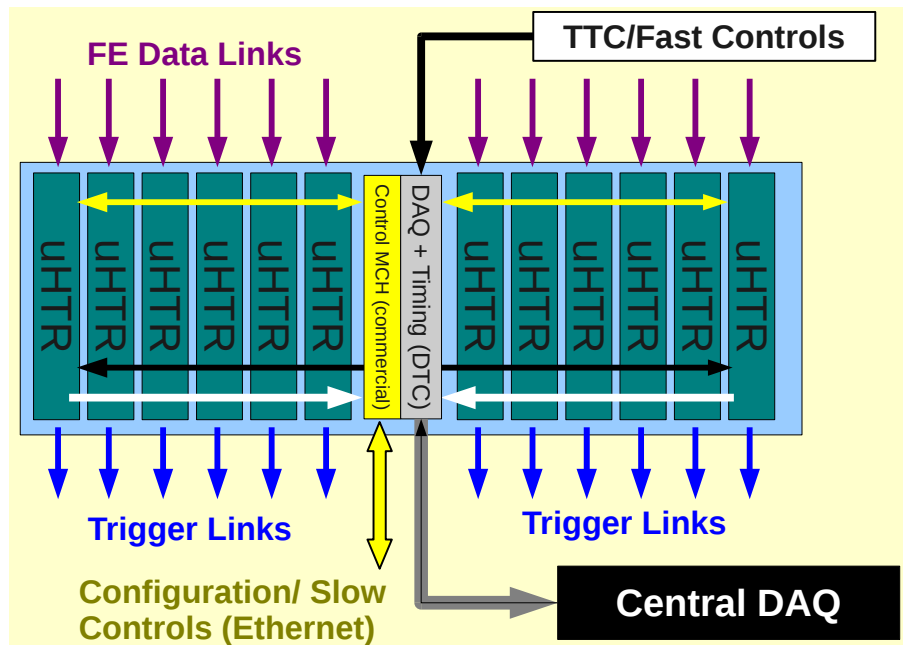


Figure 4.27: Conceptual design of μ TCA crate with “UberHTRs” (receiver, trigger, pipeline buffer) boards combined with a DCC and trigger/timing card (DTC).

3359 4.2.4.2.2 UberHTR Design Considerations

3360

3361 Much of the functionality of the UberHTR is set by the technological requirements of its
 3362 inputs and outputs. The GBT links will be received using the high-speed built-in FPGA deseri-
 3363 alizers and decoded using firmware provided by the CERN microelectronics group. Sufficient
 3364 memory will be available on the board to hold the data for the entire Level 1 decision time
 3365 (which is expected to increase by a factor of 2 in Phase 2). The data must be formatted and
 3366 transmitted to the DTC for inclusion in the full event fragment. There are two significant is-
 3367 sues to be considered which require careful design work and new implementation effort. The
 3368 first is the construction and distribution of the trigger primitives to the Level 1 calorimeter
 3369 system. The second is the inclusion of regional zero suppression (sometimes called selective
 3370 readout), which could have significant requirements for additional buffering and computation
 3371 and is discussed later. The most challenging requirement for the HCAL backend electronics
 3372 is the production of the trigger primitive information to be used in both electron/photon and
 3373 jet/MET paths of the Level 1 trigger. These are custom-hardware systems operating under a
 3374 strict latency budget. In particular, the Phase 1 upgrades do not envision replacement of the
 3375 Tracker pipelines, so the present Level 1 latency must be maintained even when the luminosity
 3376 is increased.

3377 UberHTR Detailed Prototype Design

3378

3379 While the final design for the UberHTR will depend on the results of ongoing research

3380 and development, a baseline proposal, shown in Figure 4.28, is useful to demonstrate the fea-
 3381 sibility of the design and the applicability of the proposed technologies.

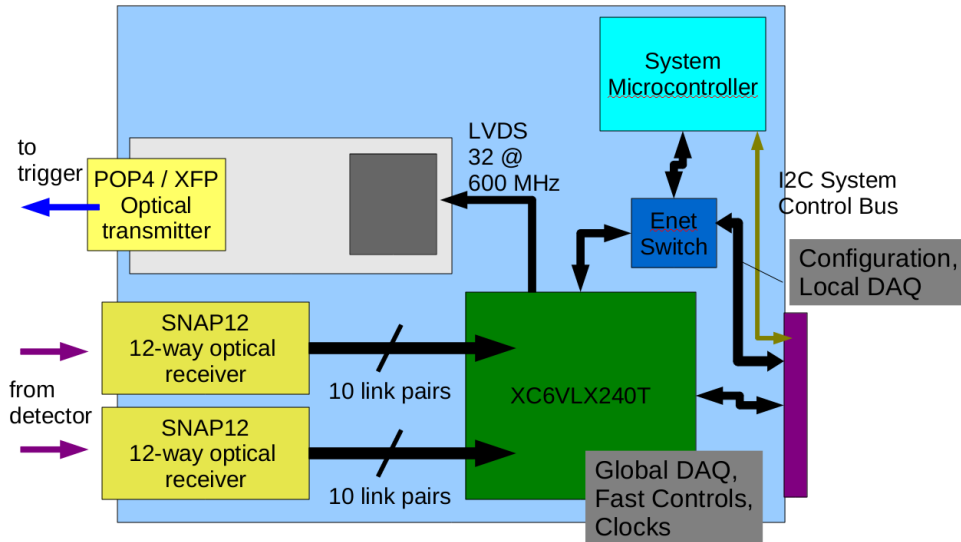


Figure 4.28: UberHTR conceptual design.

3382 The UberHTR will receive eighteen front-end links using two SNAP-12 format parallel optical
 3383 receivers. Nine links are necessary for a single HCAL wedge (18 towers in pseudo-rapidity),
 3384 including the overlapping region between the barrel and endcap hadron calorimeters. This
 3385 coverage also maps directly to the ECAL barrel coverage. The hadronic endcap will require
 3386 fewer links as the number of towers is smaller, due to the change in ϕ -granularity from 5° to 10°
 3387 which occurs at $|\eta| = 1.83$. If the UberHTR is to be built as a general-purpose card (appropriate
 3388 for several uses within CMS), it would be appropriate to connect all 24 optical receivers to
 3389 high-speed transceivers on an FPGA. However, there are a limited number of FPGAs that have
 3390 sufficient resources to accommodate this number of links as well as the three additional links
 3391 required by the system (Gigabit Ethernet control, data acquisition, and future fast controls).
 3392 The baseline proposal, therefore, is the use of a 24 transceiver FPGA to receive up to 20 front-
 3393 end links with four links for fast controls and data acquisition.

3394 The link between the UberHTR and the trigger will be housed on a mezzanine card. This struc-
 3395 ture will allow the trigger link to be upgraded/adjusted as necessary as there are changes in
 3396 the CMS trigger system. In particular, direct transmission at 10 Gbps is not supported by cur-
 3397 rent FPGAs, but future trigger upgrades may take advantage of newer technology and require
 3398 faster data links from the detectors. As a baseline proposal, the necessary trigger bandwidth
 3399 could be provided by four fibers per mezzanine (e.g. POP4 connector). The mezzanine is pro-
 3400 posed to use the same connector technology as the SNAP12 transceiver, which is robust and
 3401 capable of very high data rates. The communication between the UberHTR main FPGA and
 3402 the mezzanine would occur over a DDR LVDS bus, a solution that should be reliable and very
 3403 low-latency.

3404 The integration of the UberHTR into the μ TCA crate will be supported by a microcontroller
 3405 that will serve as the slow-control interface point for the system-management I2C bus. The
 3406 microcontroller will be responsible for implementing the relatively complex “enumeration”
 3407 process of the μ TCA bus and for providing an emergency path for reprogramming the FPGA’s
 3408 flash memory chip. An I2C connection is necessarily only an emergency path given its low

3409 speed. Ideally, the microcontroller could use the Ethernet bus to provide faster programming
3410 (and become the primary solution), but most currently available microcontrollers do not sup-
3411 port gigabit Ethernet or the μ TCA standard. However, if a microcontroller with reasonable cost
3412 and complexity can be identified which supports gigabit ethernet, it might be most effective to
3413 pass the gigabit fast control stream through the microcontroller, which could save a high-speed
3414 transceiver on the FPGA.

3415 4.2.4.2.3 DAQ and Timing Card (DTC) Design Considerations

3416
3417 As stated above, there will be a single DTC per crate to handle all DAQ and timing and
3418 clock signals, described below. At this time, an upgraded DAQ hardware interface has not yet
3419 been specified, therefore for prototyping we will provide 10 gigabit/sec class optical outputs
3420 with bandwidth 8-10 times the current FRL bandwidth. The existing S-LINK hardware is not
3421 readily compatible mechanically with μ TCA, so we propose to develop a separate interface
3422 module for legacy DAQ operation. An S-LINK converter module would then be designed so
3423 that it could be housed in a separate chassis (perhaps surplus 9U VME crates). The DAQ output
3424 link would require a modest-bandwidth return path for backpressure. The legacy TTS outputs
3425 would also be mounted on the external modules that house the S-LINK source cards.

3426 4.2.4.2.4 Selective Readout

3427
3428 The combination of the SLHC luminosity and the HCAL upgrade will significantly in-
3429 crease the HCAL data size. Considering simply the data volume, we expect to increase the
3430 data by a factor of more than four. This factor arises from the increase in channel count along
3431 with the additional TDC information that will be provided as well. On the other hand, the
3432 increase in luminosity at SLHC will significantly increase the average occupancy. The net re-
3433 sult of these effects will be a requirement to significantly increase the amount of data sent from
3434 HCAL to the central DAQ (either more FEDs or faster SLINKs) and/or perhaps very stringent
3435 zero suppression requirements.

3436 The ECAL experience has indicated that a balance between data volume and physics object
3437 quality can be achieved by a seeded readout scheme. Large energy deposits cause the cells
3438 around them to be read with reduced zero-suppression thresholds, a technique called "Selec-
3439 tive Readout". Such a scheme would be ideal for SLHC, particularly if ECAL and HCAL were
3440 capable of cross-seeding. It is important to read out the HCAL energy directly behind elec-
3441 tromagnetic candidates and it is also important to read out the ECAL with high precision in
3442 τ -lepton and some other classes of jet events.

3443 The upgraded HCAL electronics should allow the DTC to participate in the selective readout
3444 process, at least to the level of accepting the selective readout bits from the ECAL selective
3445 readout processor (SRP). Depending on the behavior of the ECAL SRP at high pileup for taus
3446 and similar events of high interest, a bidirectional flow of selection information may be nec-
3447 essary. The integration of SRP will necessarily add latency to the DAQ-side of the processing
3448 (which is not considered a significant issue) and will increase the requirement for event data
3449 storage while the selective readout calculations are proceeding. This storage may be either on
3450 the UberHTRs or the DTC.

3451 The UberHTR is proposed to maintain the same modularity as the current HTR (48 front-end
3452 channels), or possibly double the modularity (96 front-end channels). The front-end data vol-
3453 ume is assumed to increase by about 4X as discussed above. For purposes of this document we
3454 assume that the double-density UberHTR option is taken, so the data volume increases by 8X.

3455 It is realistic to send all non-zero-suppressed data from the UberHTR to the DTC. The current
3456 data volume from HTR to DCC is about 50 MByte/sec per HTR. Applying our 8X factor from
3457 above gives 400 MByte/sec, which is reasonable for a single μ TCA fast backplane port.

3458 **4.2.4.2.5 Trigger, Timing and Fast Controls**

3459
3460 The other major function of the DTC is to distribute triggers (L1A) and other time-critical
3461 control signals to the UberHTRs. Like the DAQ path, a well-defined legacy system (TTC) and
3462 the new (as yet to be finalized) replacement system (GBT timing features) must be supported.
3463 The most conservative approach is to distribute the encoded TTC stream on a dedicated back-
3464 plane pair for legacy operation, and use a separate port to support a future fast controls path.
3465 The GBT provides a control path between the UberHTR and the front-ends, but the details of
3466 the fast control path are not well defined at this time.

3467 In addition, one or more low-jitter clocks will be distributed by the DTC on the dedicated clock
3468 pairs allocated on the μ TCA backplane.

3469 **4.2.4.2.6 Management Interfaces**

3470
3471 The DTC will support both the I2C management interface and gigabit Ethernet. The de-
3472 tails are similar to those discussed above for the UberHTR. Some additional work is needed
3473 in order to specify the details of Ethernet communication, high speed data input (e.g. config-
3474 uration, look-up-tables, etc) and output (local data acquisition and monitoring) on the typical
3475 commercial backplanes. This R&D is underway.

3476 **4.2.4.2.7 Packaging**

3477
3478 It is assumed that the DTC will be a double-width, full-height MCH-type μ TCA module.
3479 There are two variations possible, depending on the type of backplane which can be obtained:

- 3480 • DTC in MCH slot 1; commercial MCH in slot 2
- 3481 • DTC in MCH slot 1 (performs essential MCH functions)

3482 It is difficult to combine a commercial MCH and a custom DTC in the same MCH site, since no
3483 power supply connections are available on MCH connectors 2-4.

3484 **4.2.5 R&D for Phase 1**

3485 The following list summarizes the R&D needed for Phase 1:

- 3486 1. Electrical and/or optical decoding unit (prototyping, production, assembly)
- 3487 2. SiPM characterization and vendor determination
- 3488 3. RBX mechanics (cooling, prototyping, production, assembly)
- 3489 4. GBT validation and FPGA simulation
- 3490 5. μ TCA prototyping and production
- 3491 6. QIE radiation characterization, redesign, prototyping and production
- 3492 7. Front-end controls (CCM, slow controls, and TTC evolution)

3493 4.2.6 Implementation and Infrastructure Issues

3494 As discussed above, it is important that the back-end plan be staged in such a way that proto-
3495 types can be commissioned quasi-statically and run parasitically during the first phase of CMS
3496 running at the LHC. The key component in such a requirement will be the digital data on the
3497 current fibers, and the data rate that HCAL currently uses (1.6 Gbps 8B/10B encoding). To
3498 make the UberHTRs backwards compatible means that the prototype boards must be able to
3499 receive data at the current 1.6 Gbps rate and encoding scheme, and also at the higher rate using
3500 the CERN GBT rate of approximately 4 Gbps with an as yet unfinalized protocol (unfinalized
3501 but not expected to be the usual and current gigabit Ethernet physical protocol “8B/10B”). This
3502 requirement can, however, be implemented in one of the more current Xilinx or Altera FPGAs,
3503 which support differential high speed signals to be decoded by a built-in deserializer. The as-
3504 yet-to-be-finalized protocol for the GBT project will be handled with a logic core that will be
3505 supplied by the CERN GBT group, as is their commitment to CMS and HCAL. The new back-
3506 end will be designed so that it is capable of running with an existing HCAL front-end for a year
3507 to gain full confidence in the system.

3508 The current electronics testing and commissioning facility in Building 904 will play an impor-
3509 tant role for the HCAL upgrade. Running prototype back-end systems will be brought up in
3510 904 before moving to Point 5, and prototype front-end systems can be integrated and tested
3511 with the new back-end electronics. HCAL will therefore need a presence in 904 for the foresee-
3512 able future.

3513 4.2.7 Alignment with possible Phase 2

3514 The electronics upgrade for Phase 1, both front-end and back-end, will be constructed such
3515 that it will be able to be used for any possible Phase 2 upgrade. This requirement is fairly
3516 straightforward with respect to the electronics capability (bandwidth, etc), however it places a
3517 greater specification for radiation tolerance. HCAL will necessarily require that all front-end
3518 electronics meet with the radiation specification for 10 years of operation at $5 \times 10^{34} \text{ cm}^{-2}\text{s}^{-1}$
3519 luminosity. We will update the projected radiation contour maps for this condition, and test
3520 all electronics to the appropriate levels for both total dose and instantaneous rate single-event
3521 effects.

3522 4.2.8 Schedule

3523 The Phase 1 HCAL upgrade is focused on producing new electronics on both the front-end
3524 and back-end. The front-end electronics will have new analog-to-digital conversion, new re-
3525 quirements for services in the existing front-end readout boxes, and new transmitters using
3526 the current fibers. R&D towards production will necessarily require extensive testing in test
3527 beams. The test beam schedule at CERN, typically with a run each summer, constrains some
3528 of the important milestone dates in the HCAL upgrade schedule. The following are plans for
3529 the next 3 slice tests that will result in a project that can be commissioned in 2015:

- 3530 1. Summer 2009. Validate half density EDU with SiPM devices.
- 3531 2. Summer 2010. Test TDC circuits, prototype FPGA card and front-end to back-end high
3532 bandwidth communication with prototype μ TCA readout.
- 3533 3. Summer 2011. Extensive comparisons between possible SiPM devices and possible ODU/EDU
3534 readout configurations. Test prototype cooling system for ADC and FPGA cards. Take
3535 data with first μ TCA preproduction prototype crate and cards.

- 3536 4. Summer 2012. Test new QIE cards with pre-production front-end electronics cards, using
3537 μ TCA prototypes. Test final candidates for SiPMs and ODU/EDU and finalize the analog
3538 section of the FE electronics. Evaluate GBT performance.
- 3539 5. Summer 2013. Pre-production prototype with final SiPM and final FE analog and digital
3540 electronics. Validate pre-production FE/BE electronics including all needed RBX services
3541 and integration issues.

3542 We indicate below those aspects most critical to the upgrade timeline.

- 3543 • RM assembly. Assembly of all boards into the RMs must begin by 2015 to be ready
3544 for extensive burn-in at the building 904 electronics integration center and the sub-
3545 sequent Phase 1 shutdown, when installation and commissioning begins.
- 3546 • Front-end boards. FE boards (FPGA + GBT + laser) must be ready for production by
3547 the end of 2013 so that RM assembly can begin in 2015.
- 3548 • GBT and front-end boards. The GBT project calls for production to begin in 2012,
3549 which means that the HCAL front-end boards have to be designed and ready for
3550 GBT inclusion in 2013.
- 3551 • Front-end controls. All FE control R&D must be completed by 2013 in time for inte-
3552 gration tests in the 2013 testbeam.
- 3553 • QIE. New QIE chips (QIE10) development began in 2009 and will finish in 2012
3554 for the analog section and in 2013 for the digital section, followed by 6 months of
3555 production, ending in early 2014.
- 3556 • QIE card. QIE card production, QC, and calibration begins in 2014, completing by
3557 late 2014 in time to meet the RM assembly, with contingency.
- 3558 • EDU/ODU. R&D, preproduction, and prototyping began in 2009, takes several test-
3559 beams to go through the development cycle, finishing in the summer of 2012, fol-
3560 lowed by 1.5 years of production and assembly and QC, finishing at the beginning
3561 of 2014 in time for RM integration.
- 3562 • SiPM. General R&D began in 2008. Vendor selection, procurement and delivery will
3563 begin in 2011 and last until January 2012. QC and assembly will begin in mid 2012
3564 and last until the beginning of 2014, in time for RM integration.
- 3565 • μ TCA. R&D and preproduction is already in progress, with increasing complexity
3566 tested during the 2009, 2010, and 2011 testbeams. Production and QC will begin in
3567 the fall of 2011, lasting until mid 2012 and take at least 1 year but will be in time
3568 for final installation and commissioning in advance of the 904 burn-in and Phase 1
3569 shutdown. Note that pre-production crates and electronics will be installed at Point
3570 5 to be used parasitically with real HCAL data following the 2012 shutdown.
- 3571 • Fiber optics. HCAL plans to keep the current fiber optics infrastructure, but we
3572 envision that a patch panel will be needed for the redistribution of the fibers. Plans
3573 call for the fiber patch panel R&D to begin in mid 2011 and take 1 year, to be ready
3574 for installation at point 5.

3575 4.2.9 Conclusion

3576 Recently CERN has defined the schedule for operations and shutdowns over the next two
3577 decades and has stated the goals for delivering luminosity during this period. The first phase
3578 of this plan will already require upgrades to the hadron calorimeters to deal with radiation

3579 damage and increased occupancy that would otherwise degrade the performance of these de-
3580 tectors, which play a key role in many CMS physics investigations. The key element in the
3581 upgrade is the replacement of HPDs with SiPMs, a new photodetector technology that has re-
3582 cently become available. The low cost, high gain, and compactness of the SiPMs permit the
3583 introduction of more longitudinal segmentation and the provision of detailed timing informa-
3584 tion. The SiPMs that are required for the HO are currently available. More R&D is required to
3585 obtain SiPMs that will satisfy the more demanding requirements for the upgrade of the HB and
3586 HE. The use of SiPMs to improve the CMS calorimeters result in more data to be read out and
3587 provides better information to the trigger. This in turn requires changes to all the front end and
3588 back end electronics. CMS has developed a strong plan to make these changes over the next 5
3589 years. This plan will guarantee good performance from the hadron calorimeters through the
3590 Phase 1 period and will provide a solid foundation for an upgrade to handle the even higher
3591 luminosity of Phase 2.

DRAFT

DRAFT

3592 Chapter 5

3593 Forward Rapidity Calorimeter Systems

3594 Introduction

3595 The forward rapidity calorimeters make use of quartz radiators to produce Cherenkov light.
3596 The choice of quartz is driven by radiation hardness requirements. The rapid time response
3597 of Cherenkov radiation is also a benefit in the high occupancy environments of the forward
3598 calorimeters. As the Cherenkov process produces less light, the number of photoelectrons per
3599 GeV of energy deposited in the calorimeter is two orders of magnitude smaller than the plastic
3600 scintillating tile with WLS readout of the HB, HE, and HO calorimeters.

3601 The forward calorimeter readout uses high gain photomultiplier tubes (PMT) and must con-
3602 tend with fringe fields from the CMS solenoid. The PMT window material and UV transmis-
3603 sion sensitivity of the fibers and light guides are also affected by the high radiation environment
3604 of the forward rapidity regions. Due to the low yield of photoelectrons (due to the low number
3605 of photons) per deposited energy, currently 0.25 photoelectron per GeV in the HF, any inter-
3606 actions with the fibers outside of the calorimeter or with the photodetector window material
3607 can generate signals that are as large as those made by 1 TeV of energy deposited in the cal-
3608 orimeter. In fact, the 11m long decay path between the collision point and the HF detectors,
3609 allows in-flight decay from hadrons from minimum bias events to produce muons that pass
3610 directly through the photodetector window material with similar (though not identical) timing
3611 and signal-correlated properties as normal events. Other sources of anomalous signals in the
3612 forward calorimeters are also present. These non-calorimetric sources of Cherenkov light in
3613 the readout system place additional constraints on the forward calorimeters that are further
3614 complicated by high instantaneous luminosity operation.

3615 The following sections describe the current problems seen in the forward calorimeter systems
3616 and the plans for repairs, improvements, and upgrades to these systems through 2016. There
3617 are separate sections describing the forward hadron calorimeter (HF) and CASTOR. The 2012
3618 shutdown work for the zero-degree calorimeter (ZDC) involves the installation of lifting equip-
3619 ment already foreseen in early running.

3620 5.1 Forward Hadron Calorimeter (HF)

3621 The Hadron Forward (HF) Calorimeters consist of two modules, located symmetrically at
3622 about 11 m from either side of the interaction point (IP), covering a pseudorapidity range of
3623 $3 \leq |\eta| \leq 5$. By extending the reach of the central calorimetry, the HF plays an important role
3624 in identifying tagging jets, determining missing E_T , and measuring the luminosity.

3625 By providing forward jet tagging capability, the HF calorimeters enhance the CMS physics
3626 program. Of the major modes of Higgs production at the LHC, Vector Boson Fusion (VBF) is

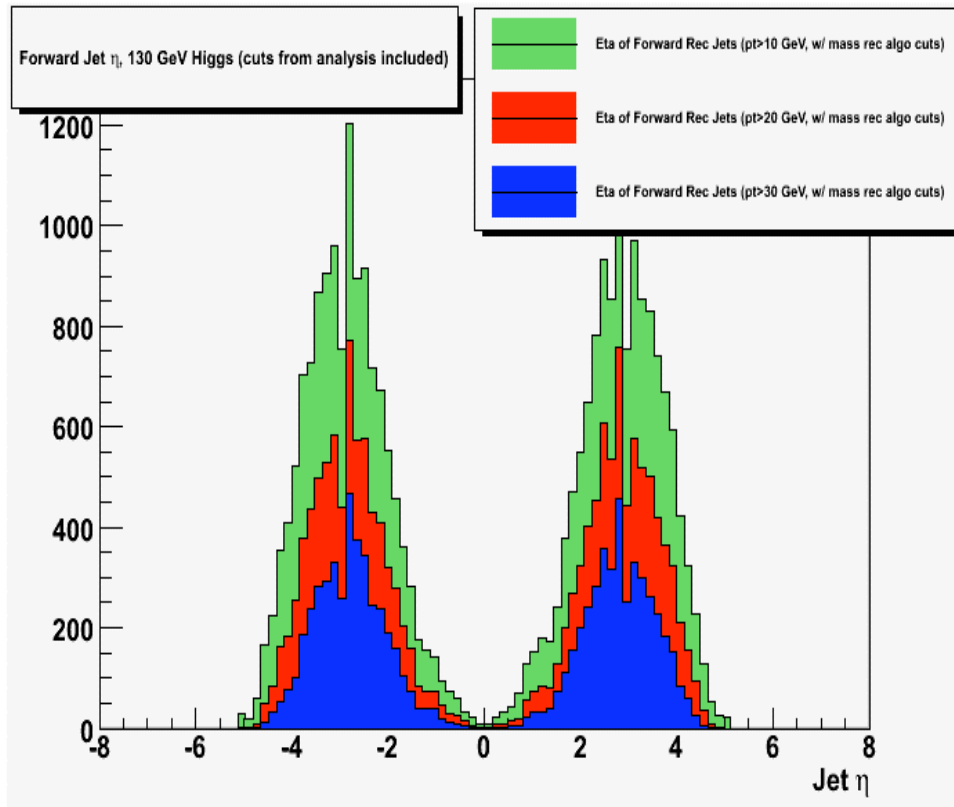


Figure 5.1: Forward jet η distribution for 130 GeV Higgs mass in the qqH channel. The analysis selection is applied, and the three different histograms indicate levels of the p_T threshold on the forward jets: $p_T > 10$, $p_T > 20$, and $p_T > 30$ GeV/c.

3627 the second most dominant mechanism for Higgs production. Forward jets (especially in VBF)
 3628 extend Higgs boson coupling measurements and complement the measurement of the light
 3629 Higgs boson width. Also, HF extends the $|\eta|$ coverage to 5 and thus provides better coverage
 3630 for missing E_T measurements (important for many BSM searches). Figure 5.1 shows the η
 3631 distribution of the forward jets after appropriate analysis cuts are applied to select the qqH
 3632 final state. With a 10 GeV/c transverse momentum requirement on the jets, about 77% of the
 3633 total events have at least one jet in the HF region. If the forward jet p_T cut is tightened to 30
 3634 GeV/cm, the fraction remains above 70%. This suggests that a precise forward jet measurement
 3635 with HF is necessary e.g. for this particular Higgs discovery channel.

3636 Each HF calorimeter consists of 36 steel wedges forming an approximately annular ring of
 3637 absorber, extending from a radius of 12.5 to 120 cm, from the beam line in the forward direction,
 3638 11m from the interaction point. The length along the beam is 1.65 m or $10\lambda_{abs}$. Quartz fibers
 3639 (QF), the active component of the calorimeter, are embedded throughout the steel absorber
 3640 in evenly spaced grooves that run parallel to the beam axis. Half of the fibers in alternating
 3641 grooves run the full length of the absorber; the other half, read out separately, start 22 cm
 3642 back from the absorber front face. The fibers are bundled to divide the calorimeter into 13
 3643 segments in rapidity, and 72 segments in ϕ for a granularity of $d\eta \times d\phi = 0.175 \times 0.175$, with
 3644 the exception of the two innermost rings, which have half the ϕ segmentation. The fibers are
 3645 read out with photomultiplier tubes. The segmentation of the HF gives a total of 864 readout
 3646 channels per module for a total of 1728 channels.

3647 The QF in HF are plastic-clad fibers (QPF), and the high $|\eta|$ ring (ring 10-13, $\eta = 4.5$ -5.0) may

3648 have 50% losses after 10 years at $\mathcal{L} = 10^{34} \text{ cm}^{-2} \text{ s}^{-1}$ which is about 1 Grad. These predictions
3649 do not take into account recovery of the fibers between exposures. We expect the fibers to
3650 recover at least 20% at each shutdown. There are fluorine-doped silica cladding fibers (QQF),
3651 which can stand ~ 20 Grads, with $\leq 10\%$ light loss, but the choice of QPF was driven by the
3652 cost (QQF fibers cost ~ 5 times more than QPF fibers).

3653 The photo-detectors in HF are PMTs manufactured by Hamamatsu (R7525HA), and they are
3654 well shielded. They have 8 stages of dynodes, a 25 mm diameter bialkali photocathode, a
3655 borosilicate glass window of average thickness 0.6 cm, and a maximum quantum efficiency
3656 (QE) at 450 nm of 22%. The PMTs would receive a radiation dose of about 8-10 krad/ 10 years
3657 at $\mathcal{L} = 10^{34} \text{ cm}^{-2} \text{ s}^{-1}$ ($\sim 10^{12} n/cm^2/10$ years at 10^{34}). The PMT windows (borosilicate glass)
3658 have significant damage (induced absorption with more than 20-30% loss of transmission at
3659 420 nm) after ~ 120 krad (gamma-irradiation); for neutrons, the effects are smaller except for
3660 fluences above $2.5 \times 10^{14} n/cm^2$.

3661 5.1.1 Large Energy Events in HF PMTs

3662 Although the HF detectors are hermetically shielded (by ~ 40 cm of concrete, and 5 cm of
3663 polyethylene) from stray particles, a small fraction of the muons produced by the proton-
3664 proton collisions or by the cosmic rays are likely to reach the readout region and register signals
3665 that mimic very high energy events (referred to as PMT events). The PMT events occur when
3666 a muon or other energetic charged particle traverses the PMT window glass, producing a large
3667 number of Cherenkov photons. The PMT events can also be produced by charged particles
3668 from late showering hadrons in HF. These events can be tagged and rejected in off-line analysis
3669 with, on average, $\sim 80\%$ efficiency (which is too low for sensitive searches for new particles).
3670 The PMT events can cause problems in trigger rates by producing fake missing transverse en-
3671 ergy. Also, luminosity monitoring and minimum bias event triggering can be affected by PMT
3672 events. The real impact on physics is being investigated using detailed Monte Carlo simula-
3673 tions.

3674 The HF PMT events were observed in the 2004 HF test beam data. The average signal recorded
3675 by a single calorimeter readout channel from an x - y position scan of muons passing through
3676 the entire system of iron absorbers, quartz fiber bundles, and the PMT window is shown in
3677 Figure 5.2. The figure clearly shows signal enhancement regions corresponding to interactions
3678 in the fiber bundle and a hot region corresponding to the PMT window. For 150 GeV muons
3679 traversing the PMT glass, the generated signals are equivalent to 120 GeV (Figure 5.3) pions
3680 impacting the HF absorber. This is equivalent to ~ 30 photoelectrons. There is a long tail as-
3681 sociated with these events that extends out to nearly a TeV. Such events have already been
3682 observed in the early running at the LHC.

3683 HF is a stand-alone device. There is no tracker or electromagnetic calorimeter in front, no
3684 muon system behind, and only two quite non-independent segmentations. Furthermore, the
3685 DAQ system does not even remotely make use of most of the raw performance characteristics
3686 or most of the information produced by the PMT - fake events are easily identified using an
3687 oscilloscope. Reducing the fake events is therefore both crucial and possible.

3688 5.1.2 HF PMT System Upgrade

3689 We propose as an upgrade replacing the present R7525 with a new PMT having the following
3690 properties:

- 3691 • a thin (< 1 mm) front window that reduces the amount of Cherenkov light;

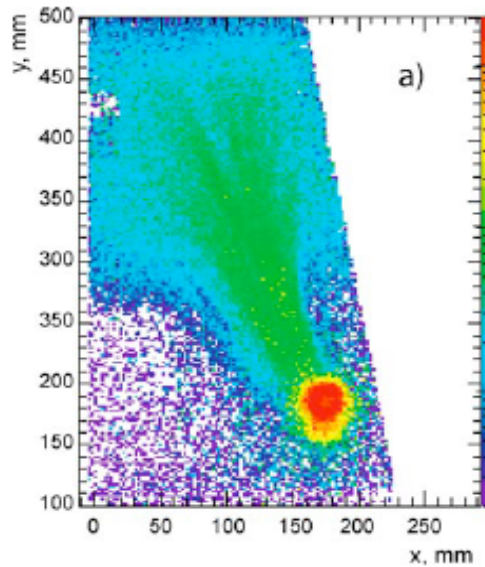


Figure 5.2: The average signal from muons passing through the entire system of HF iron absorbers, quartz fiber bundles and the PMT window, recorded as an x - y position scan with $2 \times 2 \text{ mm}^2$ resolution and using a single calorimeter readout channel. Signal enhancement regions from particles passing through the PMT window (red circle) and the quartz-fiber light guide bundle (green fan-shaped wedge extending from the PMT window upward and to the left) are clearly visible.

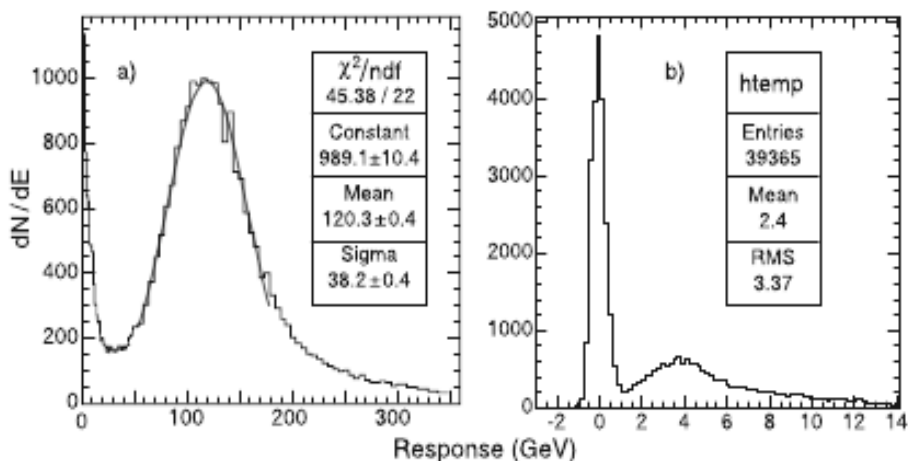


Figure 5.3: High energy muons impacting the PMT glass generate spuriously large energies (a). The response distribution clearly shows the single photoelectron peak at 4 GeV, as expected (b).

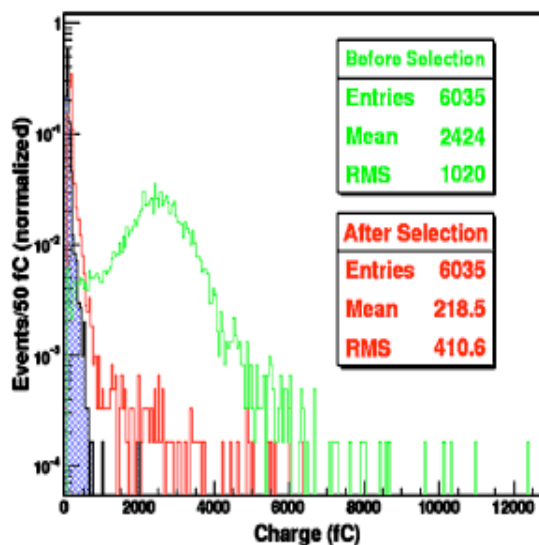


Figure 5.4: PMT window event selection and signal recovery for the four anode PMT with front incidence of muons. No pedestal subtraction was applied to the data. The blue, crossed area is the pedestal.

- 3692 • a metal envelope that further eliminates Cherenkov light made by particles travers-
- 3693 ing the side of the PMT;
- 3694 • 45% peak QE; and
- 3695 • four-way segmented anodes that allow further rejection of PMT events by using
- 3696 the pattern of light distribution among the anodes, which is different than signals
- 3697 coming from energy deposited in the HF absorber.

3698 We developed and tested a simple tagging and signal recovery algorithm for the four anode
 3699 PMT. Figure 5.4 demonstrates the application of this algorithm to the front incidence data with
 3700 a 150 GeV/c muon beam in the CERN H2 beamline. The algorithm proves to be more than
 3701 96% efficient. The initial proposal is to use the planned HCAL electronics upgrade to provide
 3702 two readout channels per PMT, each channel being the sum of two anodes. A future upgrade
 3703 allowing all four channels to be read out separately is not precluded.

3704 5.1.3 Other Sources of Anomalous Signals in HF

3705 While Cherenkov light from the PMT windows is the dominant source of anomalous signals in
 3706 HF, there is a secondary contribution from broad scintillation signals tens of nanoseconds after
 3707 the pp interaction due to albedo background at P5. The primary source of this scintillation is a
 3708 short section of mirror material used in the connection between the light-guides and the PMTs.
 3709 Possible other scintillation sources, such as the epoxy used in the fiber bundles, are believed to
 3710 contribute much less to high energy anomalous signals.

3711 The connection between the light guides and the PMTs will be replaced along with the PMTs.
 3712 The new design will match the cross-section of the original light-guides to the new PMTs, and
 3713 will utilize non-scintillating material.

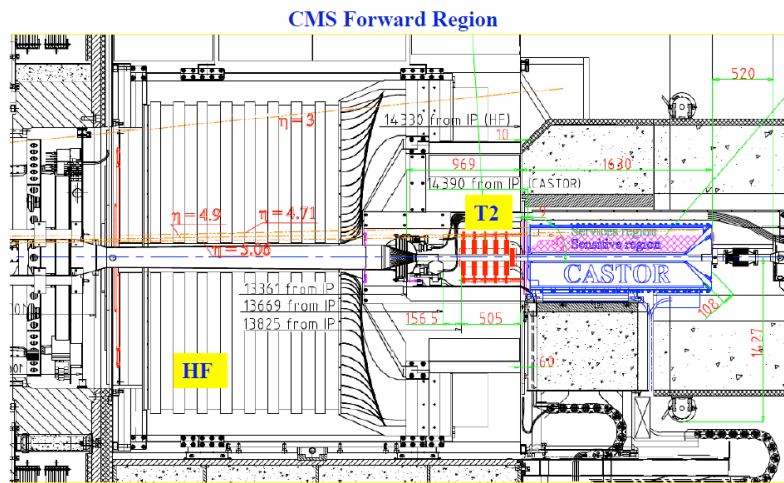


Figure 5.5: Location of CASTOR in the CMS forward region.



Figure 5.6: CASTOR calorimeter and support.

5.2 CASTOR

3714

3715 The CASTOR detector is a quartz-tungsten sampling calorimeter, installed at 14.38 m from the
 3716 interaction point, covering the pseudorapidity range $-6.6 < \eta < -5.2$. The detector is de-
 3717 signed for the very forward rapidity region in heavy ion and proton-proton collisions in CMS.
 3718 The detector is built in two halves that surround the beam pipe when closed. The clam shell
 3719 design allows the detector to be removed without disturbing the beam pipe or breaking the
 3720 vacuum. It was proposed originally to have a CASTOR module on each side of the interaction
 3721 region. For financial reasons, only one module has been built, and is installed on the negative
 3722 rapidity side of CMS.

3723 Figure 5.5 shows the location of CASTOR relative to other components of the CMS detector.
 3724 The support system with CASTOR in the closed and open position is shown in Figure 5.6.

3725 CASTOR is a Cherenkov-based calorimeter constructed from layers of tungsten plates as ab-
 3726 sorber interleaved with quartz plates as the active medium. It has two sections: an electro-
 3727 magnetic section (EM) with ten sets of 5.0 mm tungsten plates and 2.0 mm quartz plates; and
 3728 a hadronic section (HD) with sixty 10.0 mm W plates and 4.0 mm quartz plates. The plates are
 3729 inclined at 45° to maximize the collection of the Cherenkov light. The Cherenkov light from the

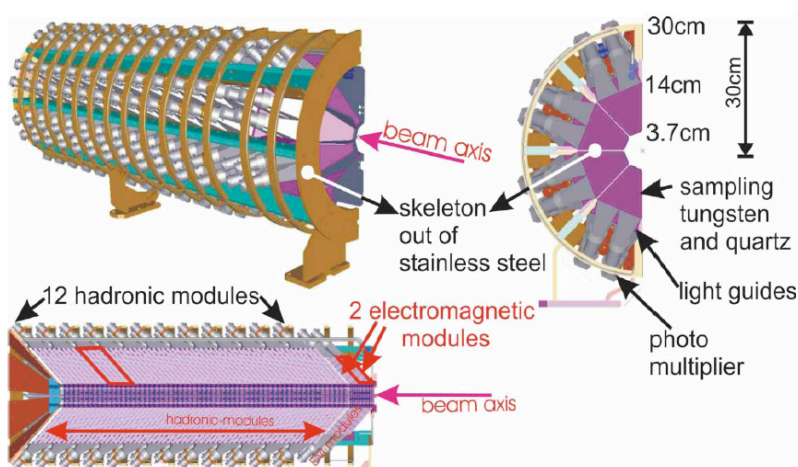


Figure 5.7: Details of the components and geometry of the CASTOR calorimeter

3730 quartz is collected and focused by air light guides onto Hamamatsu R5505 phototubes. Each
 3731 light guide collects the light from 5 quartz plates. Figure 5.7 shows the detailed layout of the
 3732 detector.

3733 CASTOR is installed in CMS and is operating for the 2010-2011 run. However, the fringe field
 3734 in this region was found to be significantly higher than expected (see the discussion below). As
 3735 a result, a different phototube model had to be chosen than the one originally planned, and the
 3736 phototubes must be operated with high voltage settings and gains which are non-uniform.

3737 The present phototubes must be replaced with more radiation hard phototubes for long term
 3738 operation, and modifications to the magnetic shielding are highly desirable to achieve a more
 3739 uniform detector response. Additionally, improvements are needed to establish good calibration
 3740 and monitoring. The planned improvements are described below.

3741 In order to carry out these improvements, CASTOR must be removed from the CMS collision
 3742 hall and brought to the surface. Some of the work involves improving the mechanical stability
 3743 of various support structures, improving the shielding from the fringe field of the CMS
 3744 solenoid, and monitoring the position of the beam pipe, which is very close to CASTOR. These
 3745 tasks are undertaken by CMS Technical Coordination in consultation with the CASTOR team.

3746 5.2.1 Detailed description of tasks

3747 5.2.1.1 Consolidation work on CASTOR

3748 CASTOR was constructed and instrumented during the first 6 months of 2009. Under time
 3749 pressure to complete the installation ahead of the final CMS closing and LHC startup, some
 3750 of the work was not done at the design level. Although the calorimeter worked well during
 3751 the 2009 and 2010 LHC run, some improvements are still pending. This work is enumerated
 3752 below:

- 3753 1. Exchange some of the EM and HAD light guides, which were slightly damaged during
 3754 installation.
- 3755 2. Exchange the damaged fibers and increase the number of the LED fibers that go to the
 3756 light guides, as well as the fibers connecting the LED source to the patch panel.

- 3757 3. Construct a new LED pulser with more outputs and independent firing, for a more effi-
3758 cient operation.
- 3759 4. Construct a new patch panel using a PCB, for easier connection, possibility of changes
3760 and maintenance in situ.
- 3761 5. Develop and execute procedures for gain/signal equalization of the new PMTs (see be-
3762 low), using the new LED system.
- 3763 6. Repair the far side of the outer circuit of the cooling system, which developed a small
3764 leak after an accidental hit during the closing of the collar shielding.

3765 5.2.1.2 Exchange R5505 PMTs with the equivalent radiation hard model R7494

3766 The original information on the strength of the stray magnetic field in the CASTOR region pre-
3767 dicted a field of the order of 10 Gauss. Based on this, the CASTOR team purchased the R7378A
3768 standard dynode, radiation hard PMT from Hamamatsu. However, it was discovered in 2008
3769 that the B-field in the forward region was higher by a factor of more than 20. This necessitated
3770 the use of fine-mesh PMTs, capable of running in a high field environment. Due to the very
3771 short time and lack of money, DESY donated 250 units of the R5505 fine-mesh PMTs from the
3772 H1 SPACAL calorimeter. These PMTs have a borosilicate window and are not radiation hard.
3773 They are being used in the 2010-2011 LHC run, when the integrated luminosity is expected to
3774 be 1 fb^{-1} and the received dose within tolerable levels. The radiation environment near CAS-
3775 TOR and its PMTs is shown in Fig. 5.8. Irradiation results for the R5505 PMTs are shown in
3776 Fig. 5.9.

3777 For the high luminosity pp and the subsequent heavy ion running beyond 2012, a radiation
3778 hard version, R7494, of the fine mesh R5505 is required. These PMTs, with synthetic silica
3779 window, will withstand the dose collected for more than 20 fb^{-1} of integrated luminosity.
3780 Irradiation tests on the similar window R7378A PMTs gave excellent performance up to 20
3781 Mrad tested, as shown in Fig. 5.10.

3782 The installation of the new PMTs will be followed by gain studies with LEDs and possibly with
3783 a radioactive sourcing system.

3784 The funds for the purchase of these PMTs (cost $\sim 550 \text{ kCHF}$) are being collected. At present
3785 the amount of 310 kCHF has been secured from Brazil (210 kCHF) and Adana (100 kCHF). The
3786 remainder is expected to be pledged soon. The purchase order should be placed by the end of
3787 2010 for full delivery and testing (at Adana) by end of 2011.

3788 5.2.1.3 CASTOR Gain/Signal Equalization Issues

3789 The adverse effects of the strong magnetic field still remain for $\sim 2-3$ sections at the center of
3790 CASTOR (in the gap between the Collar and Rotating shielding), where the direction of the
3791 field is almost perpendicular to the axis of the PMT. To partially compensate for this, the HV to
3792 these PMTs was increased to close to the limit and the HV values of other PMTs were changed
3793 for signal equalization. These changes of the HV settings negate any gain/signal equalization,
3794 obtained in the absence of magnetic field (beam test, calibration with sources).

3795 CASTOR faces a very difficult gain/signal equalization task, due to the strong variation of the
3796 response along the length of the calorimeter due to the fringe field of the CMS solenoid magnet.
3797 Therefore, any calibration should take place in situ with the solenoid magnet at 3.8T. The possi-
3798 ble use of halo muons, with a specific muon trigger, is being investigated for such a study. The

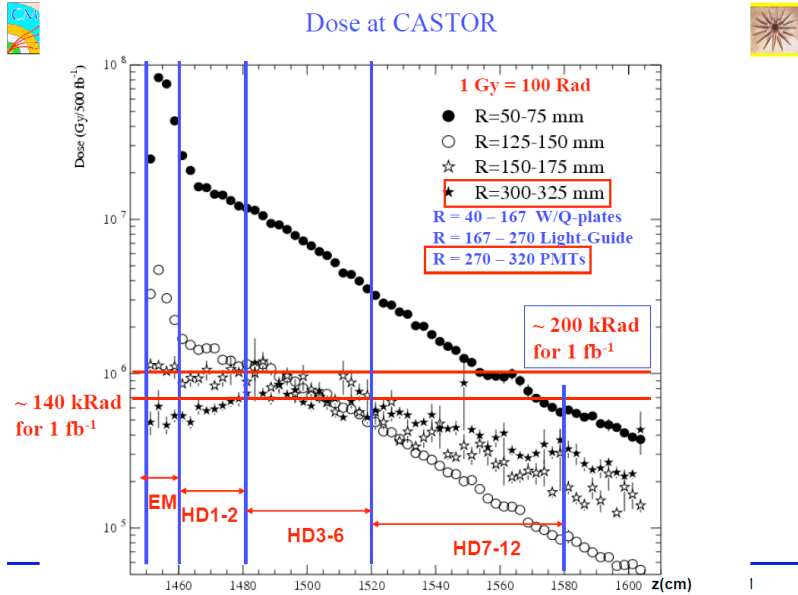


Figure 5.8: Radiation environment of CASTOR and its PMTs.

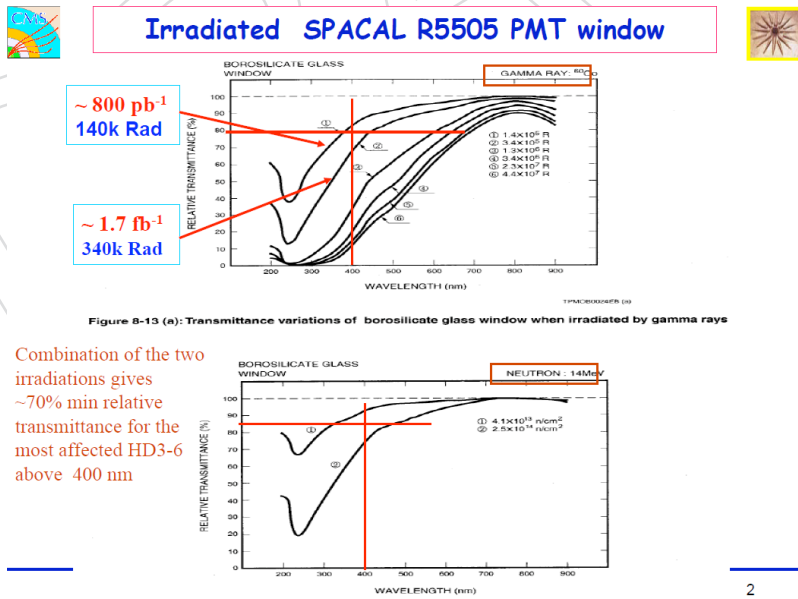


Figure 5.9: Irradiation results for R5505 PMTs.

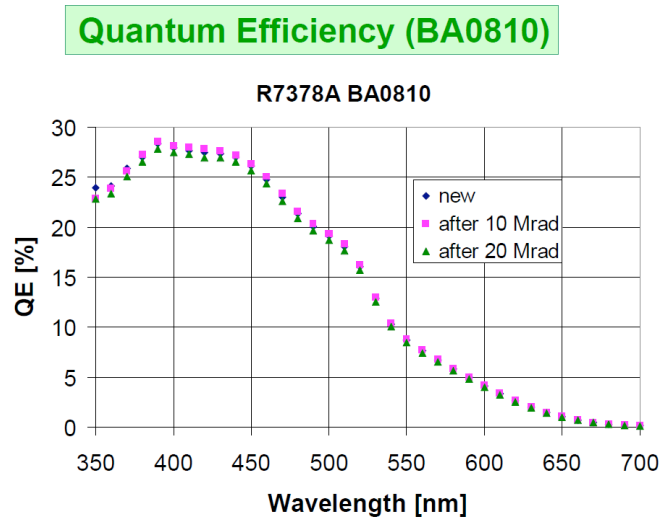


Figure 5.10: Gamma irradiation results for a R7378A PMT with synthetic silica window (same as in a R7494 PMT).

3799 feasibility of a radioactive source system similar to the system used for HF is also being dis-
 3800 cussed. This source calibration would be accomplished during the 2012 shutdown. The most
 3801 efficient solution, however, will be to minimize the stray field and this is being investigated.
 3802 The idea is to fill this gap with thin iron sheets, a task that will be done during the 2012 winter
 3803 shut down.

3804 5.2.2 Work details and schedule

3805 5.2.2.1 Work in 2012 with Castor moved to the surface lab

3806 The various tasks and the institutional responsibility for them is listed:

- 3807 1. Exchange light guides (DESY, Athens, Adana)
- 3808 2. Exchange R5505 PMTs with the radiation hard version R7494 (Antwerp, DESY, Brazil)
- 3809 3. Exchange LED fibers (Athens, Adana, Brazil)
- 3810 4. New LED pulser (Antwerp, ITEP)
- 3811 5. Exchange Patch Panels and check mappings (Antwerp, DESY, Brazil)
- 3812 6. Signal/gain equalization with LED (DESY, Antwerp, Adana)
- 3813 7. Repair water leak in half cooling system (CMS Technical Coordination)
- 3814 8. Sourcing of full calorimeter (DUBNA, Athens, Adana)

3815 Estimated time for this work is 5-6 months from the time when CASTOR arrives in the above-
 3816 ground workspace.

3817 5.2.2.2 Work coordinated with CMS Technical Coordination

3818 In addition to the work described above, CMS Technical Coordination will make various im-
3819 provements in the infrastructure supporting CASTOR. Some key elements of this work are:

- 3820 1. Radiation-shielding box for calorimeter - This shielding box is not needed for the initial
3821 removal of CASTOR in 2012, but will be part of the installation and removal procedure
3822 thereafter. It must be ready before CMS closes again in 2012.
3823
- 3824 2. Improvement of the magnetic field situation in the CASTOR region. This will require
3825 new magnetic shield pieces to be installed in 2012.
3826
- 3827 3. Installation of monitoring for the beampipe temperature, local deformations, humidity,
3828 and possibly magnetic field.
3829

3830 Additional details may be found in chapter 10.

DRAFT

DRAFT

Chapter 6

Pixel Detector Improvements and Upgrades

At the heart of CMS is the silicon pixel detector [6]. It aims to provide three high-precision space point measurements to reconstruct charged particle trajectories. These three points are sufficient to produce good track information for the High Level Trigger (HLT) and for the efficient seeding of the reconstruction of longer tracks in the full tracker volume. The close proximity of the first detector layer to the interaction point (4.4 cm) minimizes multiple scattering effects and extrapolation uncertainties making the pixel information crucial for the reconstruction of the initial position and direction of the charged tracks. The pixel detector therefore plays a key role in the identification of primary vertices, secondary vertices, and secondary tracks. These elements are essential for the efficient identification of long lived particles, such as b quarks, and for the search for new physics at the LHC.

The present CMS pixel detector was conceived over 10 years ago and designed for a maximum luminosity of $1 \times 10^{34} \text{ cm}^{-2}\text{s}^{-1}$. Following the Phase 1 upgrade of the LHC, the peak luminosity is foreseen to reach $2 \times 10^{34} \text{ cm}^{-2}\text{s}^{-1}$ before the next long shutdown. The present pixel system will not be able to sustain such extreme operating conditions due to large data losses in the read out chip (ROC) and must be replaced in the long shutdown of 2016. This is the best, and perhaps only, opportunity to install and commission a new system before the luminosity will exceed $1 \times 10^{34} \text{ cm}^{-2}\text{s}^{-1}$. The modular design of CMS allows good access to the pixel system, which can be extracted relatively easily, independently of the beam pipe or the strip tracker.

The baseline plan presented here is to replace the current system with an ultra-light pixel detector, with improved ROCs, having four barrel layers and three end-cap disks. The conceptual layout for the Phase 1 pixel detector is shown in Figure 6.1. The addition of the fourth barrel layer at a radius of 16 cm and the third forward disks will maintain the present level of tracking performance even in the high occupancy environment of the upgraded LHC. In addition, it provides a safety margin in case the first silicon strip layer of the Tracker Inner Barrel (TIB) degrades more rapidly than expected.

This upgrade of the pixel system will address all of the following shortcomings of the current detector:

- The most severe limitation is the ROC, which is just adequate at the LHC design luminosity of $1 \times 10^{34} \text{ cm}^{-2}\text{s}^{-1}$. At this luminosity, buffer size and readout speed limitations are estimated to produce a dynamic inefficiency of 4% ($> 16\%$) if the bunch spacing time is 25 ns (50 ns). The dynamic inefficiency increases exponentially with increasing luminosity. At $2 \times 10^{34} \text{ cm}^{-2}\text{s}^{-1}$ and 25 ns bunch spacing the ROCs in the inner region will suffer an inefficiency of 15%, leading to a major degradation of the overall level of tracking performance.
- The three-hit coverage of the detector is not completely hermetic, leading to 10-

3868 15% inefficiencies at $|\eta| < 1.5$ and larger track seeding inefficiencies in the region
 3869 $1.5 < |\eta| < 2.5$. This limits the efficiency of HLT tracking triggers and slows the full
 3870 tracking algorithm. The situation will degrade even further at higher luminosities.

- 3871 • The radiation hardness of the detector is not sufficient for operation up to the end
 3872 of Phase 1, when the integrated luminosity will be around 350 fb^{-1} . Although the
 3873 detector was constructed using the most radiation resistant technology known at the
 3874 time of its fabrication, radiation damage will degrade its performance and necessi-
 3875 tate replacement of the inner regions.
- 3876 • The detector contains significant passive material that degrades tracking and calorim-
 3877 tric measurements due to multiple scattering, photon conversions and nuclear
 3878 interactions.

3879 The goal of the Phase 1 upgrade is to provide a pixel detector that can maintain a high efficiency
 3880 at a luminosity of $2 \times 10^{34} \text{ cm}^{-2} \text{ s}^{-1}$, with less material, and will provide 4 hits over pseudora-
 3881 pidities up to 2.5. In the years since the design of the current detector, innovations in cooling,
 3882 power distribution, mechanical support, CMOS electronics, and sensor materials enable the
 3883 construction of a significantly more performant detector.

3884 Radiation damage is still expected to significantly degrade the performance of the innermost
 3885 regions during the three year Phase-1 run beginning in 2017. The position resolution of the
 3886 detector will worsen by roughly a factor two after a fluence of $10^{15} \text{ n}_{\text{eq}} \text{ cm}^{-2}$. The dynamic inef-
 3887 ficiency is expected to be greater during the second half of this run as the luminosity increases.
 3888 We are therefore considering the development of replacement parts based on smaller pixels, a
 3889 more radiation-resistant sensor technology, and an improved readout chip based on a denser
 3890 CMOS technology. The replacement would occur near the middle of the run and would ensure
 3891 that detector performance increases rather than decreases during the period when the largest
 3892 data samples are being acquired.

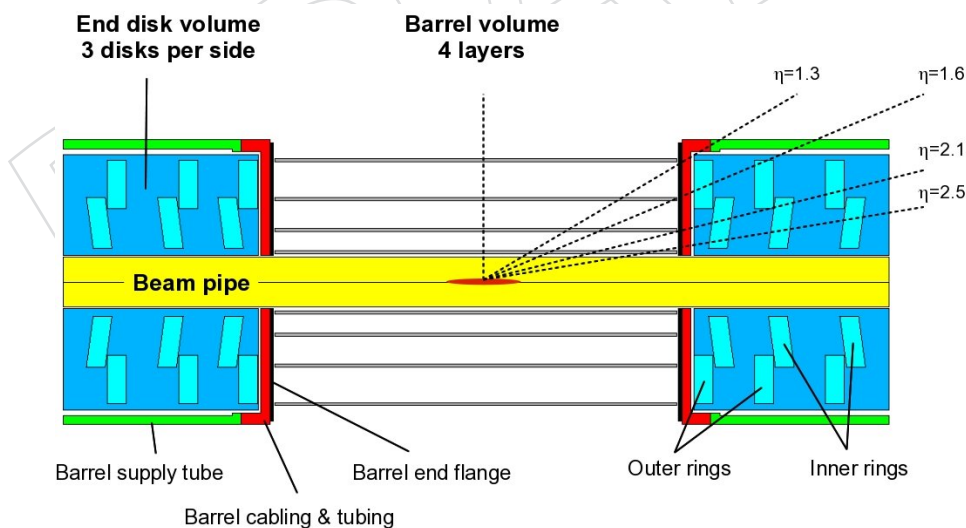


Figure 6.1: Schematic view of the Upgrade Layout. It consists of four barrel layers and three endcap disks on each side, with each disk separated into an inner and outer ring. The disks are placed in locations so as to maximize the 4-hit η coverage.

3893 The implementation of the Phase 1 pixel detector would largely improve all aspects of CMS
 3894 tracking:

- 3895 • The addition of the extra layers will dramatically improve the efficiency and resolu-

tion of pixel-only tracks. Pixel tracks are a crucial part of the HLT and they are also used to seed the full tracking, leading to an increase of the efficiency and a decrease of the fake rate for full tracks.

- The decrease in the amount of material and the increase in the number of measurement points improve the resolution of all track parameters. In particular, the resolution of longitudinal and transverse impact parameters are significantly improved.
- The efficiency and resolution enhancements lead to much improved primary and secondary vertexing. Vertexing is essential to associate the final state particles with the correct primary vertex in the high pile-up LHC environment. Secondary vertexing plays a key role in b -tagging and the search for various long-lived exotic states.
- The improvements in tracking efficiency, fake rate, parameter resolution, and vertexing all contribute to significant improvements in the b -tagging performance of the tracker. The b -tagging performance for the present and upgraded detectors is shown in Fig. 6.2 for operation at an instantaneous luminosity of $1 \times 10^{34} \text{ cm}^{-2} \text{ s}^{-1}$ with 25 ns bunch spacing. The upgraded detector would reduce the light quark background of the Combined Secondary Vertex Tag by a factor of 6 for a b -efficiency of 60%, or conversely, it would increase the b -quark efficiency by approximately 50% at the fixed light-quark efficiency of 5×10^{-2} .

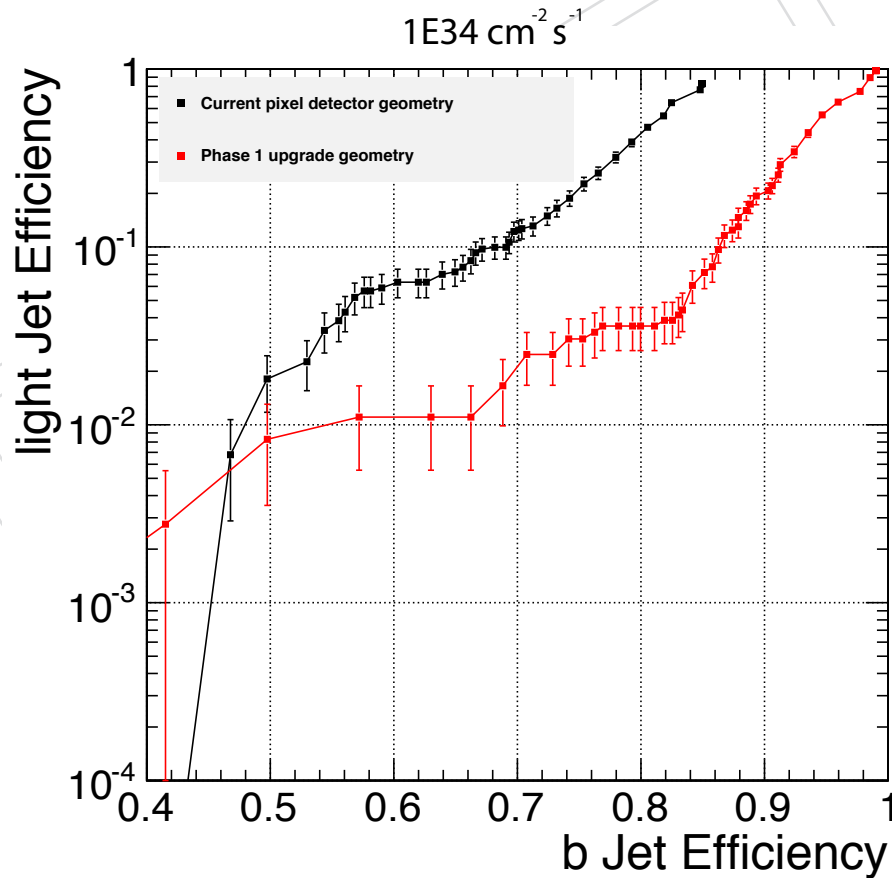


Figure 6.2: The light quark and b quark efficiencies of the Combined Secondary Vertex b -tagging algorithm are shown for the present and upgraded detector (with inner radius of 3.9 cm, $285 \mu\text{m}$ thick sensors and $100 \times 150 \mu\text{m}^2$ pixels) at an instantaneous luminosity of $1 \times 10^{34} \text{ cm}^{-2} \text{ s}^{-1}$ with 25 ns bunch spacing.

3914 In this chapter we outline the basic performance characteristics of the current pixel detector.
 3915 We also point out some of the factors that limit its performance, and describe the proposed
 3916 improvements to the mechanics, layout and electronics which would significantly enhance our
 3917 physics capabilities during the first stages of the major upgrades to the LHC. This upgrade
 3918 to the pixel detector significantly improves charged particle tracking for CMS and greatly en-
 3919 hances the experiment's physics reach during the crucial Phase 1 upgrade to the LHC when a
 3920 large fraction of the luminosity will be delivered.

3921 6.1 Performance of Current Detector

3922 In this section, we discuss in more detail the performance of the current pixel detector and
 3923 enhancements that the proposed detector upgrade will provide.

3924 6.1.1 Electronics and Readout

3925 The current pixel readout electronics were designed and optimized for the data rates and pixel
 3926 occupancies expected up to the LHC design luminosity of $1 \times 10^{34} \text{ cm}^{-2} \text{ s}^{-1}$. There will be a
 3927 dynamic inefficiency of about 4% from the current readout chip, PSI46v2, at this luminosity in
 3928 the innermost layer. These losses are shown in Figure 6.3 as a function of the level-1 trigger
 3929 accept (L1A) rate as measured in test beam runs with particle fluxes as expected for LHC de-
 3930 sign luminosity [7]. At the nominal L1A accept rate of 100 kHz, the data loss will increase to
 3931 16% in the innermost layer as the luminosity goes up by a factor of two (for 25 ns bunch cross-
 3932 ing) to $1 \times 10^{34} \text{ cm}^{-2} \text{ s}^{-1}$. These losses are understood by simulations and characterizations of
 3933 the PSI46v2 readout chip to be coming from two sources: the column drain dead time (0.8%)
 3934 and readout-related losses (3.0%). Hit pixels are transferred using column drain readout to the
 3935 chip periphery where the hits are stored in buffers during the L1 trigger latency (3.2 μs). If in-
 3936 stead the LHC runs with 50 ns bunch spacing at $2 \times 10^{34} \text{ cm}^{-2} \text{ s}^{-1}$, then the data losses continue
 3937 to increase almost exponentially, with losses on the order of 50% for the innermost layer for
 3938 example.

3939 Figure 6.4 illustrates the impact on performance of charged particle tracking from these data
 3940 losses. In these simulated $t\bar{t}$ events at instantaneous luminosities of $2 \times 10^{34} \text{ cm}^{-2} \text{ s}^{-1}$ with 25 ns
 3941 bunch spacing, we see substantial decreases in the tracking efficiency. These high luminosities
 3942 also lead to a large fake rate even without the previously mentioned data losses. The degrada-
 3943 tion with 50 ns bunch spacing would be substantially worse. The conclusion is that the current
 3944 readout chip is not able to cope with these rates in the innermost layers of the pixel detector.

3945 In the present operation of the pixel detector events are observed with much higher pixel hit
 3946 counts than expected from minimum bias event simulations. They are attributed to beam-gas
 3947 collisions with charged tracks going almost horizontally through the barrel layers. These events
 3948 can cause problems at the system level including the loss of event synchronization. By now,
 3949 beam-gas events can largely be suppressed in the readout by excluding certain background
 3950 triggers. However, the rate of these events scales with beam intensity and hence it could be-
 3951 come more problematic in the future when we have to deal with high numbers of multiple
 3952 collisions. Changes to the readout chip and downstream electronics would be one course of
 3953 action to alleviate these problems.

3954 6.1.2 Sensor Radiation Hardness

3955 At the design luminosity of $\mathcal{L} = 10^{34} \text{ cm}^{-2} \text{ s}^{-1}$ the pixel system will be exposed to particle
 3956 fluences of 3×10^{14} , 1.2×10^{14} , and $0.6 \times 10^{14} \text{ n}_{eq}/\text{cm}^2/\text{yr}$, at the first, second, and third layer,

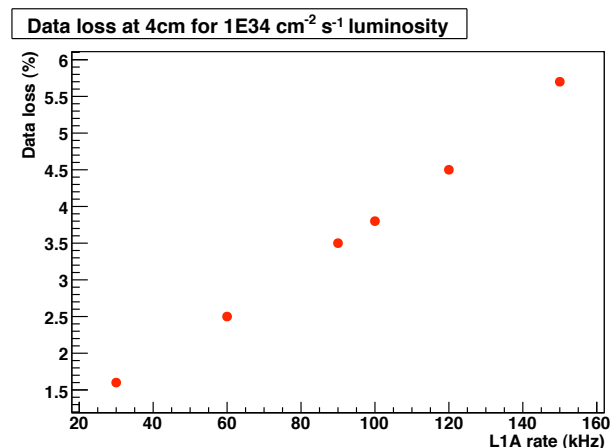


Figure 6.3: Left: Data losses as a function of the L1 accept rate of the innermost layer of the current pixel detector [7]. The instantaneous luminosity is $10^{34} \text{ cm}^{-2} \text{ s}^{-1}$ and the bunch spacing is 25 ns. CMS has been designed for maximum average L1 trigger rates of 100 kHz. The data points beyond this rate in the plot simply illustrate the linear nature of this data loss at this particular instantaneous luminosity with the PSI46v2 readout chip.

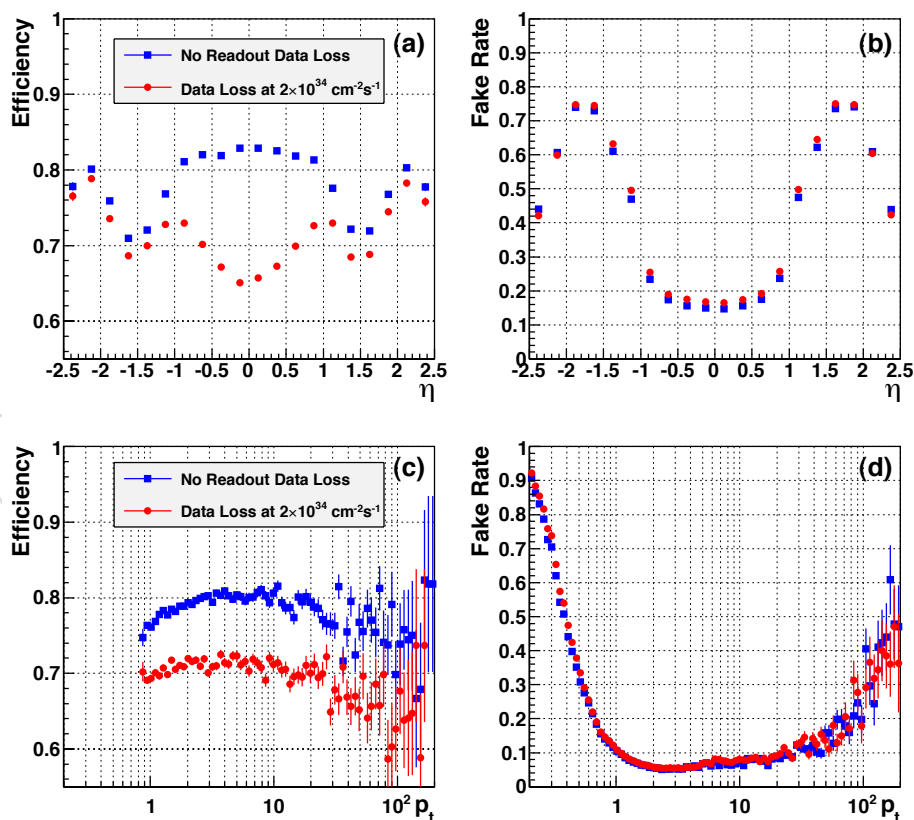


Figure 6.4: Performance of the current pixel detector in $t\bar{t}$ events at $2 \times 10^{34} \text{ cm}^{-2} \text{ s}^{-1}$ with no data loss (blue) and with the estimated data loss from buffer overflows mentioned in the text (red): (a) tracking efficiency vs pseudorapidity; (b) fake rate vs pseudorapidity; (c) efficiency vs p_T ; (d) fake rate vs p_T .

3957 respectively. Fluences for the endcaps are comparable at the same radii. All components of the
 3958 current system are specified to operate up to a total particle fluence of at least $6 \times 10^{14} \text{ n}_{eq}/\text{cm}^2$.
 3959 The sensors for BPIX and FPIX have been developed to operate efficiently up to this dose. They
 3960 are n^+ -on- n (n^+ implants on n bulk silicon) devices [8]. Electron collection has the advantage
 3961 that after radiation-induced space charge sign inversion, the highest electric field is located
 3962 close to the collecting electrodes, so even when the detector is not fully depleted after radiation
 3963 damage, the depletion zone is near the side that is read out. Moreover, since electrons have
 3964 larger mobility and consequently a lower trapping probability than holes, electron collection
 3965 leads to a higher charge collection efficiency (CCE) after irradiation.

3966 Studies of the radiation damage effects on the performance of both the BPIX and the FPIX
 3967 sensors have been performed. The barrel-type pixel sensors with their readout chips have been
 3968 exposed to radiation fluences up to $5 \times 10^{15} \text{ n}_{eq}/\text{cm}^2$ [9–11]. Charge collection of signals have
 3969 been measured as shown in Figure 6.5. After a fluence of $1.1 \times 10^{15} \text{ n}_{eq}/\text{cm}^2$ only about 50% of
 the charge is collected for $V_{bias} > 400 \text{ V}$.

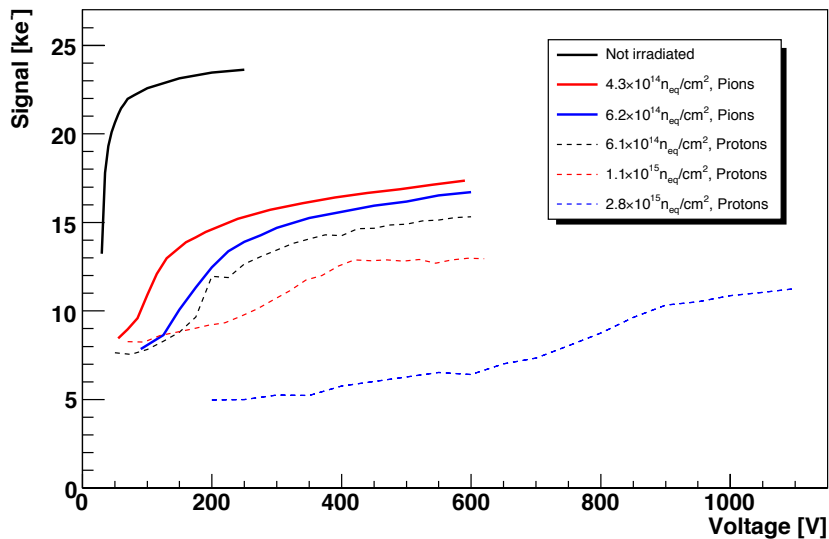


Figure 6.5: Most probably value of signal charge collected from single clusters as a function of the sensor bias for various irradiation fluences of barrel pixel sensors [9]. (It should be noted that biasing the sensor to 1000 V is not considered feasible with the actual detector and power supplies.)

3970

3971 Hit detection efficiency and resolution is expected to deteriorate with irradiation. For a ra-
 3972 diation fluence above $10^{15} \text{ n}_{eq}/\text{cm}^2$ the hit efficiency measured in beam tests is below 97%.
 3973 Figure 6.6 shows the simulated hit resolution as function of the track pseudorapidity before
 3974 and after irradiation. The fluence $1.2 \times 10^{15} \text{ n}_{eq}/\text{cm}^2$ is expected to be exceeded during Phase
 3975 1. After this exposure, the detector's hit resolution deteriorates by roughly a factor of two in
 3976 the transverse plane and would require a replacement of the innermost layer. The Phase 1 up-
 3977 grade pixel detectors must be designed to facilitate this partial replacement. This presents an
 3978 opportunity to adopt more radiation hard sensors, if they can be developed in time.

3979 6.1.3 Material In the Tracking Region

3980 The services (including cables, cooling lines, printed circuit boards) and mechanical support
 3981 structure (e.g. end flanges) for the current pixel detector introduce a non-negligible amount

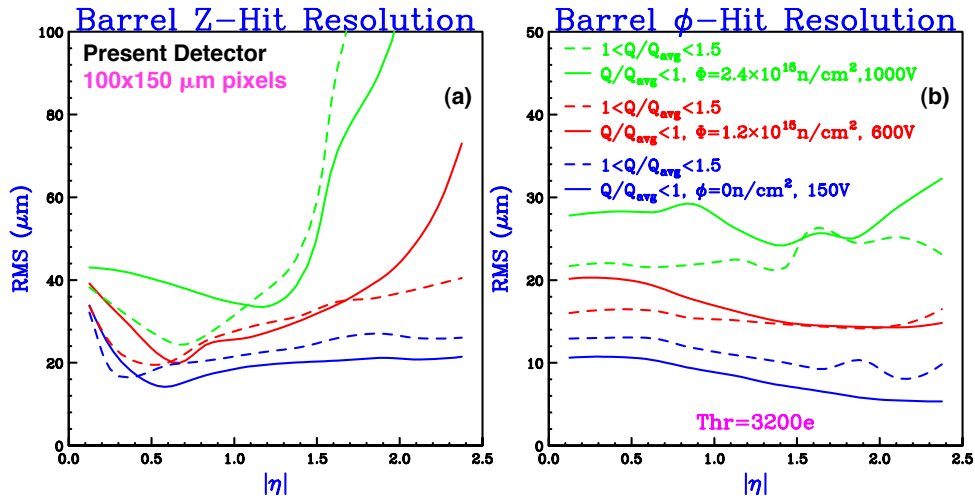


Figure 6.6: Hit position resolution (RMS) as function of the track pseudorapidity for an unirradiated (blue lines) and irradiated detectors (red and green lines). Longitudinal (a) and transverse hit resolution (b) are show separately. The solid lines correspond to hits with total charge Q below the average charge. Dashed lines correspond to hits with total charge $1 < Q/Q_{avg} < 1.5$.

3982 of material in the tracking volume. This reduces the track reconstruction efficiency and de-
 3983 grades the impact parameter resolution. The material distribution of the current pixel detector
 3984 is shown in Figure 6.7 in terms of radiation lengths and nuclear interaction lengths as function
 of η .

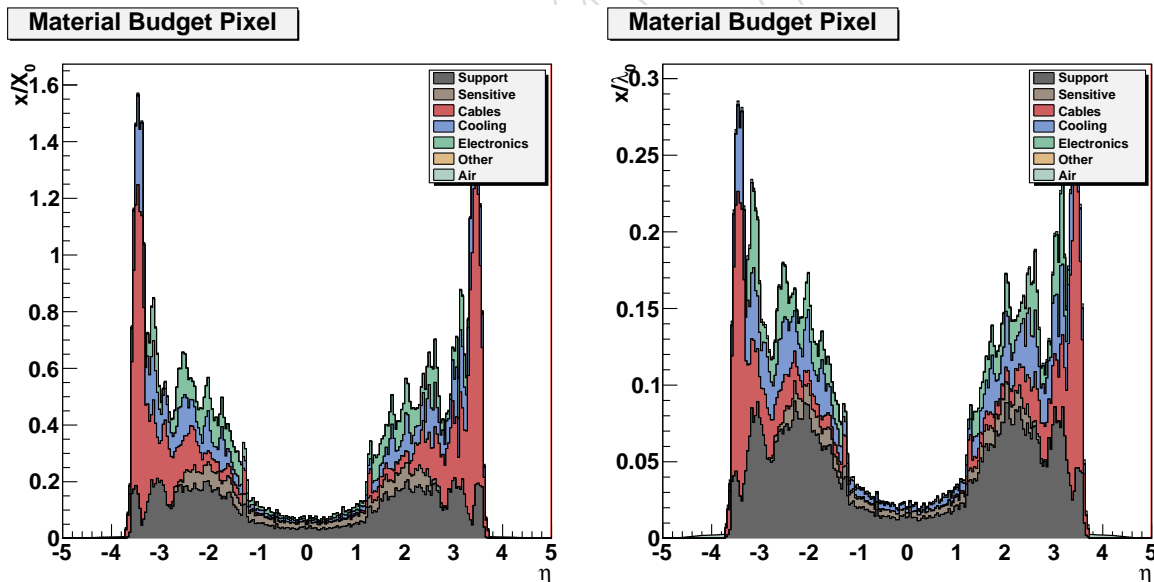


Figure 6.7: Radiation length (left) and nuclear interaction length (right) of current pixel detector.

3985

3986 Figure 6.8 shows the location of various parts and components for the current pixel detector
 3987 along the z-direction. For BPIX, all the power and signal cables are routed to two end-flanges,
 3988 behind both ends of the barrel region, and then directed to an optical link system that converts
 3989 the electrical signals into optical. The signal is then sent over a 2 m long optical fiber to the patch
 3990 panel on the tracker bulkhead. In the central region ($|\eta| < 1.2$), the main contribution to the

3991 total amount of material comes from the silicon sensors, the chips, the mechanical structure,
 3992 cooling pipes, and Kapton flex cables. For $|\eta| > 1.2$, before getting to the FPIX, the main
 3993 contributions are due to the cooling manifolds, the PCB end-flange print with more than 800
 3994 plugs and the Kapton cables. In addition, the cooling manifolds and the PCB end-flange are
 3995 directly in front of the first forward disk of the FPIX system. Most of the material between
 3996 $1.2 < |\eta| < 2.4$ is in the FPIX disks (brazed aluminum cooling loops) and electronics (ZIF
 3997 connectors and adapter boards), and between $2.4 < |\eta| < 3.6$ in cables and cooling.

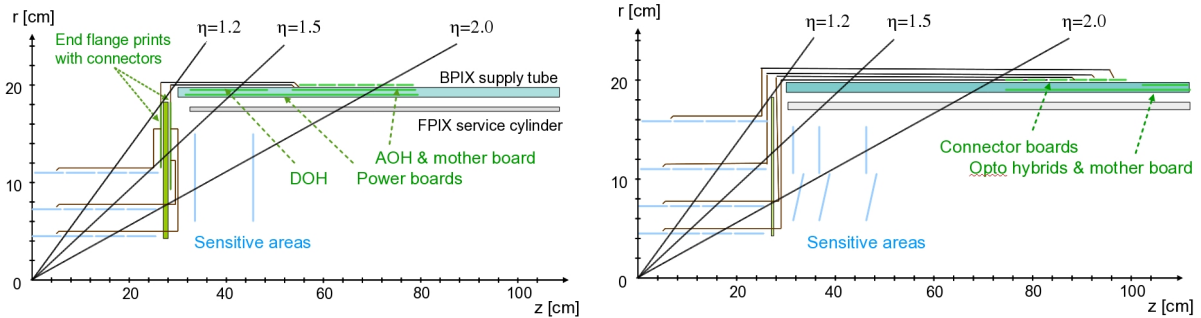


Figure 6.8: Location of components as a function of z and η for the current pixel detector (left), and for the proposed upgraded detector (right). In the current detector, there are a substantial number of connectors and electronics boards in the tracking volume, in particular at the end flange between the BPIX and FPIX. These have all been moved further downstream in z in the new design.

3998 The passive material plays a visible role for tracks with low and intermediate momenta, as
 3999 illustrated in Figures 6.9 and 6.10, which show the impact parameter resolutions as measured
 4000 in recent collision data, compared to simulation, versus track η and ϕ [12]. At low momenta
 4001 the transverse impact parameter resolution worsens at higher η due to the material traversed
 4002 by the track. The impact of the 18 cooling pipes is clearly visible for lower momentum tracks
 4003 versus ϕ .

4004 6.2 Description of the Pixel Detector Upgrade

4005 The design of the pixel detector must satisfy the following requirements and constraints:

- 4006 • Minimize data loss due to latencies and limited buffering in high luminosity run-
 4007 ning;
- 4008 • Minimize degradation due to radiation damage;
- 4009 • Optimize detector layout for 4-pixel-hit coverage over the η range with minimal
 4010 innermost layer radius;
- 4011 • To reduce material, adopt two-phase CO_2 cooling and light-weight mechanical sup-
 4012 port, moving the electronic boards and connections out of the tracking volume;
- 4013 • To reuse the current patch panel and off-detector services (cooling pipes, cables and
 4014 fibers), adopt DC-DC power converters and higher bandwidth electronics;
- 4015 • Reduce number of module types and interfaces;

4016 The objective is to have the system installed and commissioned during the 2016 shutdown.
 4017 In this section we describe our progress, as well as some of the R&D needed for the Phase 1
 4018 upgrade and how it relates to future upgrades.

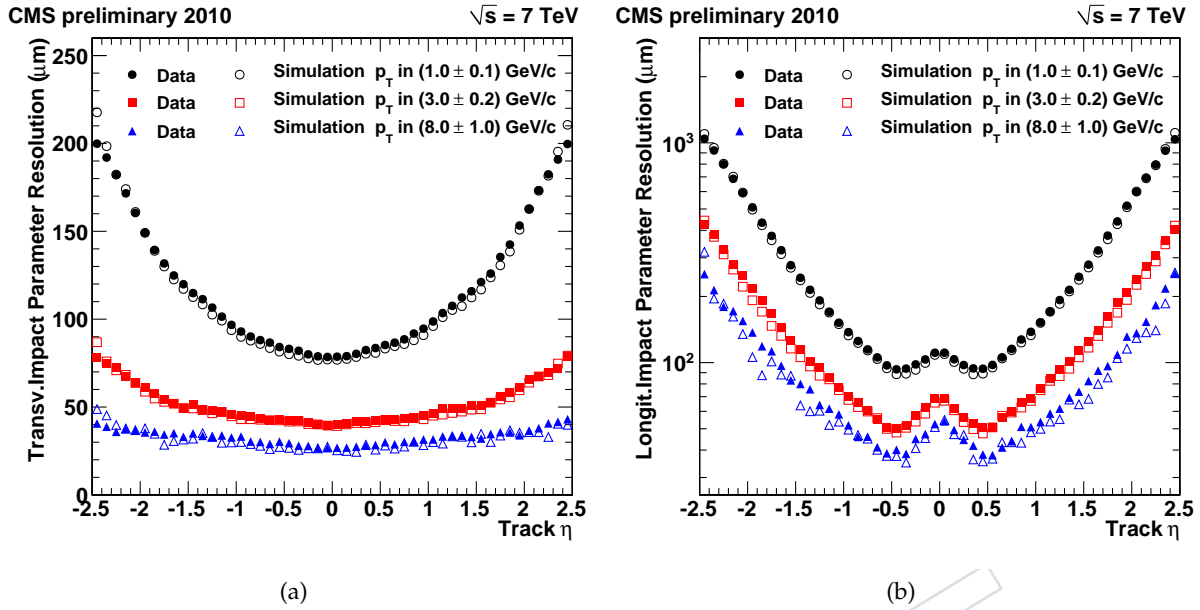


Figure 6.9: Measured resolution of the track transverse (a) and longitudinal (b) impact parameter as a function of the track η for transverse momenta in 1.0 ± 0.1 GeV/c (circles), in 3.0 ± 0.2 GeV/c (squares) and in 8.0 ± 1.0 GeV/c (triangles). Filled and open symbols correspond to results from data and simulation, respectively [12].

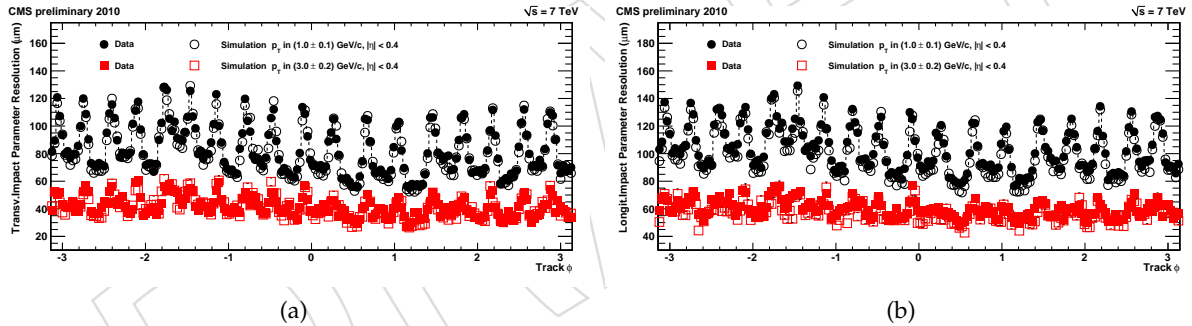


Figure 6.10: Measured resolution of the track transverse (a) and longitudinal (b) impact parameter as a function of the track ϕ for transverse momenta in 1.0 ± 0.1 GeV/c (circles) and in 3.0 ± 0.2 GeV/c (squares). Filled and open symbols correspond to results from data and simulation, respectively [12]. The 18 peaks correspond to the 18 cooling structures in the BPIX as described in the text.

4019 6.2.1 Geometrical Layout

4020 For the Phase 1 upgrade of the CMS detector, we propose a pixel detector with 4 barrel layers
 4021 and 3 disks in each endcap. The 4 barrel layers are of equal length and are placed at radii of
 4022 3.9, 6.8, 10.9, and 16.0 cm. The three end-cap disks are placed on each side of the central barrel
 4023 detector, with a radial coverage ranging from 4.5 to 16.1 cm. The location of the first disk along
 4024 the beam line is at 29.1 cm from the interaction point, the second and third disks are located at
 4025 39.6 cm and 51.6 cm from the interaction point.

4026 In the new design, there will be only one type of module with 16 readout chips in a 2×8 ar-
 4027 rangement. They will be mounted on ultra-lightweight support structures integrated with the

4028 cooling distribution system. Two-phase CO₂ cooling will replace the current single phase C₆F₁₄
4029 resulting in significant material reduction. We plan to use thin-walled stainless steel pipes with
4030 a diameter of about 1.6 mm and wall thickness of 0.1 mm which will provide enough cooling
4031 power for each pixel sub-assembly based on a continuous loop. Further material reduction will
4032 be achieved by using longer twisted pair or light-weight flex-cables to carry the signals to the
4033 optical hybrid boards; these boards, as well as the port cards and cooling manifolds, will be
4034 moved out of tracking region.

4035 The outer and inner parts of the detector will be designed such that they would allow the inner
4036 layers and rings to be easily replaced after radiation damage. For FPIX, this requires each half-
4037 disk be divided into an inner and outer ring. Figure 6.1 shows a cross-sectional view of the new
4038 pixel system and its sections. Similar to the current detector, the blades in the forward disks
4039 are rotated by 20° in a turbine like geometry to induce charge sharing. The separation of each
4040 half disk into an inner and outer assembly allows us to optimize the orientation and tilting to
4041 obtain the best position resolution in both radial and ϕ directions. Our baseline is to tilt the
4042 inner assemblies into an inverted cone at 12° towards the interaction point.

4043 The upgraded pixel detector is constrained by the existing insertion volume and services. The
4044 cabling of the current CMS tracker detector, which includes the 200 m² silicon strip detector,
4045 was facilitated by the installation of two patch panels, denoted as PP1 and PP0, outside the
4046 tracker volume. This infrastructure will not be changed during the Phase 1 upgrade except for
4047 the cooling pipes between PP0 and PP1. Therefore, the upgraded pixel detector must use the
4048 existing power cables, fibers, and cooling lines from the cooling plant to PP1. Cables, fibers, and
4049 other required utilities are already installed up to PP0 for 3 forward disks; however, space for
4050 making changes to utilities between PP1 and PP0 is severely limited. The existing rail system
4051 for insertion and extraction will be used.

4052 6.2.2 New Beam Pipe

4053 To improve the physics performance of a pixel detector in terms of impact parameter resolution
4054 and vertex resolution the first active layer should be as close as possible to the beam, requiring
4055 a beam pipe of minimum possible radius. This requirement has to be balanced against the safe
4056 and efficient operation of the accelerator with minimum background in the experiment. For the
4057 safety of the detector, the last machine element in the interaction region should always be the
4058 point of smallest aperture. In addition, the minimum diameter is constrained by mechanical
4059 stability under vacuum. The CMS beam pipe spans over ± 18 m from the interaction point to
4060 both ends of the experimental cavern. It is segmented into a central section and 4 sections on
4061 each end. The central section is 6.2 m long and consists of a cylindrical part of 1.8 m length and
4062 conical ends. The cylindrical piece is made out of 0.8 mm thick beryllium; the conical parts are
4063 of 0.8-1.2 mm thick stainless steel. The inner diameter at the interaction point is 58 mm.

4064 The LHC machine group has studied the beam aperture for the LHC upgrade scenario. It was
4065 concluded that changing the minimum diameter of the central part of the CMS beam pipe from
4066 58 mm to 50 mm will not cause any aperture problems in the CMS interaction region, provided
4067 all tolerances can be controlled to 11 mm. Therefore, it is proposed to install a new central beam
4068 pipe with an inner diameter of 50 mm together with the new pixel detector. The smaller beam
4069 pipe diameter allows the reduction of the first barrel layer radius from 4.4 cm to about 3.9 cm.
4070 A further reduction to 3.4 cm is under study. The opening angle of the conical part of the beam
4071 pipe will be preserved. The cylindrical part will be shorter by about 28 cm on each end. There
4072 are two options for building the pipe. Either the conical part is again made out of stainless
4073 steel, leading to a shorter beryllium section, or we maintain the length of the cylindrical part

4074 of the beryllium section and connect the stainless steel section onto the conical beryllium ends.
 4075 Detailed background studies have to be performed to judge the possible effect of a shorter
 4076 beryllium section. The other solution, though in principle possible, is much more complicated
 4077 from the production point of view. For both solutions detailed calculations using FEM have to
 4078 be done to estimate the mechanical strength and the deflection. Also, the vacuum performance
 4079 and the beam impedance have to be re-evaluated for the smaller radius.

4080 6.2.3 Mechanical Support for BPIX

4081 A comparison of the current 3-layer barrel and the new 4-layer system is shown in Figure 6.11.
 4082 The addition of the fourth layer reduces significantly the gap between the pixel detector and
 4083 the TIB. The BPIX mechanical support structure consists of 200 μm thick carbon fiber ladders,
 4084 with cut-outs to reduce mass, glued onto the stainless steel cooling tubes. Each ladder is glued
 4085 to two tubes. The end flange is made also of carbon fiber glued onto 4 mm thick Airex foam
 4086 profiles. The bends of the tubes are made from 1.8 mm diameter 100 μm thick stainless steel
 4087 soldered to the straight section. Figure 6.12 shows the prototype of the layer 1 mechanical
 4088 structure.

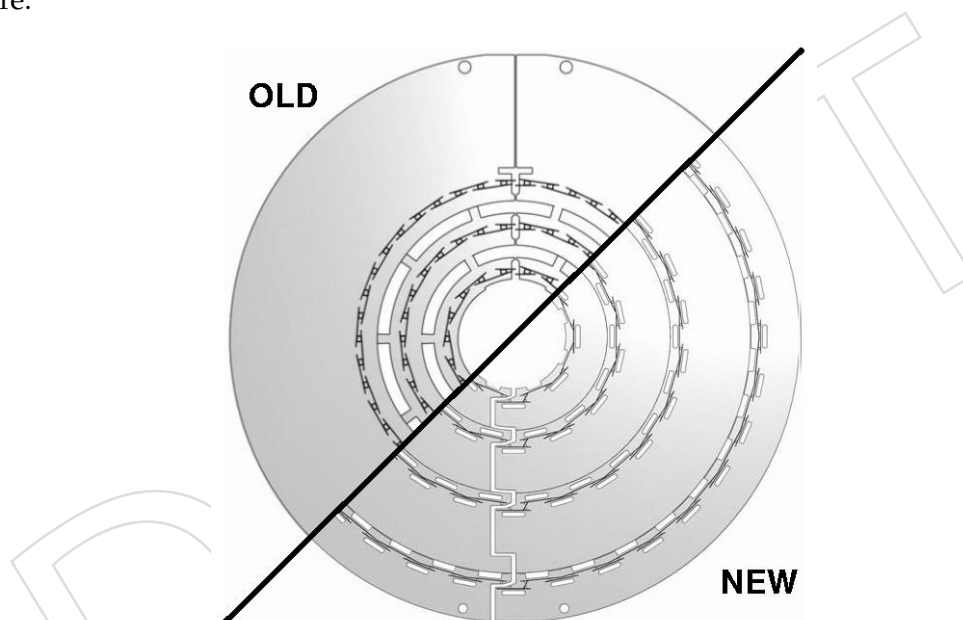


Figure 6.11: Cross sectional view of the old 3 layer barrel (top) and the new 4 layer system (bottom).

4089 The electronic components of the services are moved to the forward direction, away from the
 4090 active tracking region. The PCBs on the supply tubes are moved to $|\eta| > 2$ and those on
 4091 the end flange have been removed entirely (see Figure 6.8). This has been made possible by
 4092 the development of the low mass micro-twisted pair cables described later. Modules are now
 4093 connected directly to the readout optical hybrids (ROH) which are about 1 m away. A new
 4094 supply tube has been designed (see Fig. 6.13) to provide optimal η coverage between BPIX and
 4095 FPIX. A prototype has been built, made out of carbon fiber ribs, panels, and tubes as well as
 4096 Airex foam. The total weight of the supply tube is 2900 g.

4097 6.2.4 Mechanical Support for FPIX

4098 The current FPIX detector has 7 module types on beryllium panels placed between $r = 59.7$ mm
 4099 to 144.6 mm (there are a total 84 modules per half disk, or 540 ROCs per half disk). The upgrade



Figure 6.12: Prototype of the mechanical structure for the innermost layer. To illustrate its light-weight, a carbon fiber ladder is laid upon the half-barrel. The mechanical stability of the ladder is given by the cooling tubes.

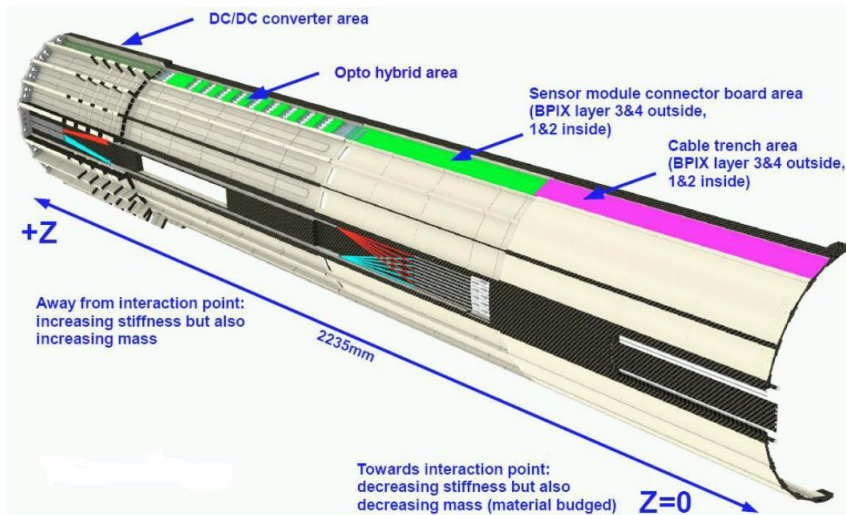


Figure 6.13: Schematic drawing of the new BPIX supply tube.

4100 layout uses only one module type (2x8 ROCs) arranged radially on panels placed between
 4101 $r = 45$ mm to 161 mm (there are a total 56 modules per half disk, or 896 ROCs per half disk).
 4102 Half-disks are divided into an outer ring with 34 modules and inner ring with 22 modules. The
 4103 inner assembly is supported off the outer assembly by some rods and the two assemblies can
 4104 be easily separated. The pixel modules are attached by a module holder to the substrate and
 4105 are removable and replaceable without disassembling half-disks.

4106 All the outer radius sensors are located to minimize the gap in 4-hit coverage between the
 4107 end of the 4th-barrel layer and the innermost disk. The design maximizes the 4-hit coverage
 4108 between the end of 4th barrel layer up to $|\eta| = 2.5$, for particles originating at the IP ± 5 cm,
 4109 using a minimum number of modules.

4110 Each blade will have one module placed on opposite sides of the same substrate (see Fig. 6.14).
 4111 The radial orientation of the rotated turbine aligns the $150 \mu\text{m}$ dimension of each pixel in the
 4112 radial direction and the $100 \mu\text{m}$ dimension in the ϕ direction, with more overlap between neigh-
 4113 boring sensors than in the current design. This will ease the spatial alignment for track recon-
 4114 struction. We plan to use thermal pyrolytic graphite (TPG) for the substrates. TPG is a material
 4115 with excellent in-plane thermal conductivity. The stainless steel cooling tubes for CO_2 cooling
 4116 are embedded in the outer and inner assembly rings made out of light-weight carbon-carbon

(C-C) material as shown in Figure 6.15.

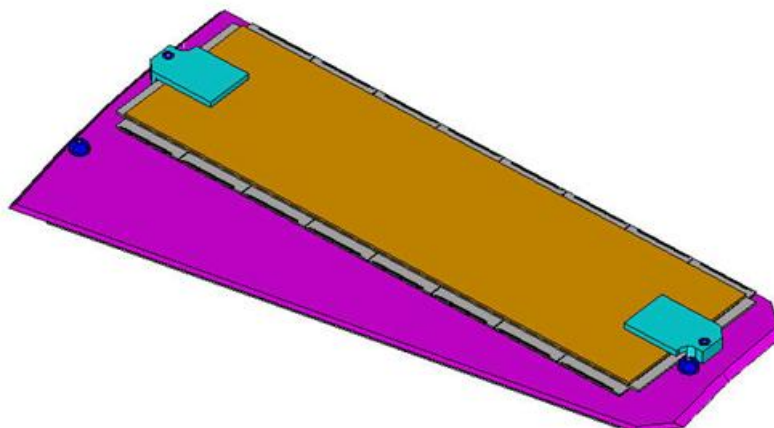


Figure 6.14: FPIX Upgrade Blade - identical blades are used in the inner and outer assemblies of all half disks.

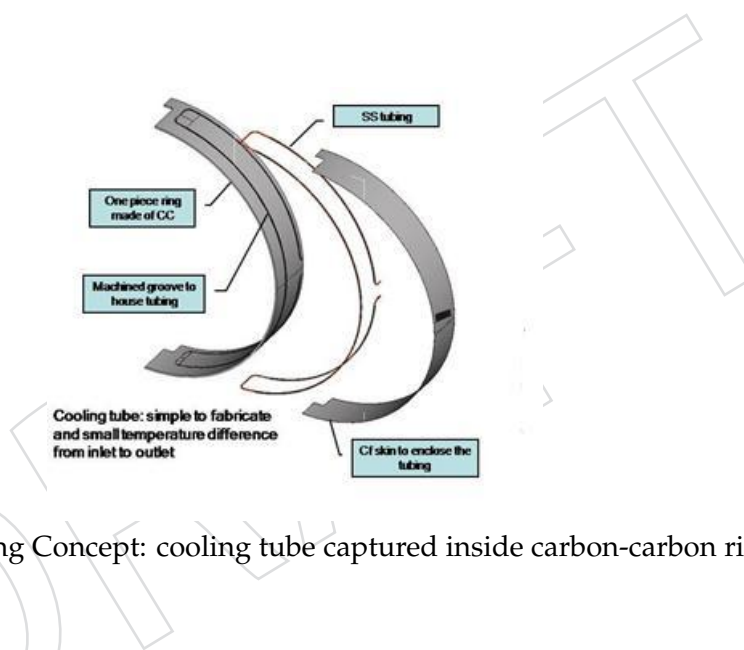


Figure 6.15: Edge Cooling Concept: cooling tube captured inside carbon-carbon ring with carbon fiber skins.

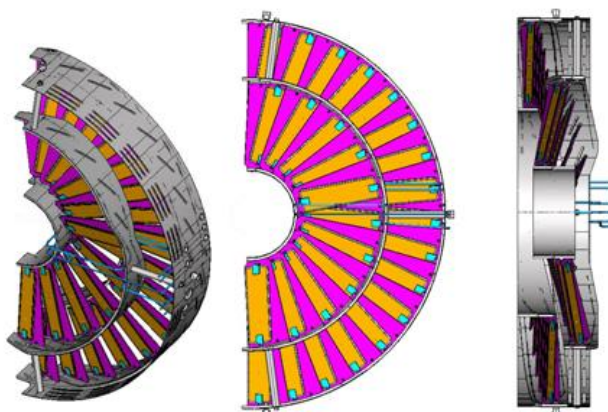


Figure 6.16: FPIX Upgrade half-disk design: Inner Blade assembly supported by Outer Blade assembly, with all blades attached permanently to the C-C assembly rings.

4117

4118 The design of the FPIX Upgrade blade is shown in Figure 6.14. It features:

- 4119 • Solid TPG (0.68 mm thick) encapsulated with carbon-fiber facings (0.06 mm thick).
- 4120 • All blades are identical with one 2×8 ROCs module mounted on each side.
- 4121 • Each module has a pair of module holders made out of G9 glued at each end for
- 4122 attachment to the precision holes on the substrate.
- 4123 • Cooling is provided at the end(s) of the blade by contact with the actively CO_2 -
- 4124 cooled ring(s).
- 4125 • Each substrate is glued permanently to the rings so that the whole ring and sub-
- 4126 strate assembly with embedded cooling tubes could be constructed as a complete
- 4127 structure.

4128 Figure 6.16 shows the complete half disk, with the inner assembly ring supported by the outer
4129 assembly ring.

4130 6.2.5 CO_2 Cooling

4131 In the present pixel detector, cooling pipes, manifolds, heat exchanger contacts and the C_6F_{14}
4132 coolant itself represent a major contribution to the overall detector material in the Tracker ac-
4133 ceptance. CO_2 two-phase cooling has been identified as the most promising option to improve
4134 upon the present mono-phase fluorocarbon system, in order to achieve enhanced cooling per-
4135 formance with a lightweight system. CO_2 -based cooling has been successfully adopted in other
4136 detectors, notably the LHCb VELO.

4137 In general, CO_2 offers significant advantages compared to mono-phase fluorocarbon:

- 4138 • Excellent thermodynamic properties for small channels: low mass, less viscosity,
- 4139 low liquid/vapor density ratio, low dT/dP , high heat transfer coefficient, and high
- 4140 latent heat;
- 4141 • A factor of ~ 2 lower density, in liquid phase;
- 4142 • At ~ 1 CHF/kg, it is substantially cheaper than C_6F_{14} (~ 100 CHF/kg).

4143 The high heat transfer coefficient allows smaller heat-exchanger contacts. The high latent heat
4144 allows more heat load per channel, possibly reducing needs for manifolding and the size of the
4145 manifolds, as well as the size of the individual pipes. CO_2 also offers the required radiation
4146 hardness.

4147 The development of the CO_2 cooling system for the pixel detector requires a substantial R&D
4148 program, covering the three main areas discussed below.

- 4149 **1. Characterization of heat transfer.** The pixel detector cooling uses miniature pipes involv-
4150 ing a domain of CO_2 heat transfer and two-phase flow for which very little experimental
4151 measurements exist, and available theoretical models do not give reliable predictions.
4152 A fundamental research line consists in performing laboratory measurements to charac-
4153 terize the process in the relevant domain, and improve the existing theoretical models
4154 accordingly.
- 4155 **2. Optimization of the on-detector cooling.** The optimization of the on-detector part of the
4156 cooling system is the key to reduce the detector material, and hence achieve the required
4157 improvement on its performance. The heat transfer from the silicon sensors to the struc-
4158 ture, through the pipe walls into the coolant has to be maximized, while minimizing the

4159 amount of material and at the same time ensure reliable thermal joints with reproducible
4160 performance. The crucial aspects are the choice of the pipe material and size, pipe fittings
4161 and connection techniques, design of thermal joints and choice of thermally conductive
4162 materials.

4163 **3. System design and integration in CMS.** Many aspects have to be addressed, including:
4164 (i) design of the cooling station, choice of the active components and of the accumulator;
4165 (ii) design of the control and monitoring system, choice of the instrumentation (especially
4166 of the active parts that will have to be installed in the experimental cavern), interface to
4167 the detector monitoring system; (iii) design of the cooling channels between PP0 and PP1
4168 and choice of dielectric fittings in PP1; (iv) connection to existing cooling pipes from PP1
4169 to the cooling station, and re-qualification of the pipes; (v) interface with surroundings in
4170 the UX cavern and with the main chiller in the US cavern; (vi) optimization and validation
4171 of system operation, including startup at warm temperature, study of safety issues and
4172 failure modes.

4173 The first area of research is already well advanced, with several labs performing measurements
4174 in parallel on different setups. A large amount of data have been collected, analyzed and
4175 carefully compared, providing evidence that a suitable phase-space of working parameters is
4176 available, compatible with performance requirements and system constraints.

4177 The optimization of the on-detector cooling is also advancing well; prototypes of mechani-
4178 cal structures of both BPIX and FPIX have already been tested with CO₂ cooling in realistic
4179 conditions, and extensive thermal modelling studies are underway. Although substantial opti-
4180 mization work is still to be done, the results collected so far indicate that suitable performance
4181 can be achieved with miniature pipes and lightweight contacts.

4182 System design and integration studies will be a main focus for the coming 1-2 years. A full-
4183 scale system has been built in the CERN CryoLab, and will be used as test setup to qualify
4184 components for the cooling plant as well as the control and monitoring system; it will be also
4185 used to study system aspects with long pipe runs mimicking the geometry of the CMS service
4186 channels. Preliminary safety studies indicate that the installed pipes are compatible with the
4187 required operating pressure. Excellent progress has been made in updating as-built models of
4188 the existing cooling system and of the cavern infrastructure, which are the basis of the studies
4189 for the integration of the system in CMS.

4190 **6.2.6 DC-DC Conversion**

4191 The routing and installation of the current pixel detector's services (power cables, fibers, cool-
4192 ing lines) was a major technical challenge. Due to the space constraints of the conduits and
4193 other sub-detectors, it would be quite difficult to route additional power cables. The pixel up-
4194 grade will increase by about a factor of two the number of ROCs. Therefore, more power will
4195 be needed than in the current detector, supplied at a higher current. To limit resistive losses
4196 in the ~ 50 m long power cables, a novel powering scheme based on the DC-DC conversion
4197 technique is proposed. The idea is to bring the power into the detector at a higher voltage but
4198 at a lower current (thereby significantly reducing the power losses in the cable) and to use a
4199 DC-DC buck converter close to the detector to convert the input voltages to the operation volt-
4200 ages needed by the pixel modules with high efficiency ($\sim 80\%$). A separate converter is used
4201 for the digital and analog voltages. These converters need to be tolerant of both the radiation
4202 and magnetic field inside the tracker volume. Since commercial converters could not satisfy
4203 these requirements, a dedicated ASIC development is needed. A prototype is currently being

4204 developed. The DC-DC conversion chip and other components will be assembled on a small
 4205 printed circuit board which will be placed on the support half cylinder, close to the pixel mod-
 4206 ules. Prototypes of these converter PCBs have been fabricated and tested for electromagnetic
 4207 noise emissions in a set-up with silicon strip modules. The results of these tests are promising
 4208 and indicate that the application of DC-DC converters in the pixel system should be feasible.

4209 Tests are ongoing to study the performance of pixel modules powered by the same CAEN
 4210 power supply modules currently in use and with the long power cables needed by the exper-
 4211 iment with and without DC-DC conversion. As space is rather tight, it is also important to
 4212 minimize the dimensions of the converters. Furthermore, since all the power to the detector
 4213 will go through these converters which are closely packed, we have to understand the effect of
 4214 temperature and provide a means of cooling to these devices.

4215 Even with DC-DC conversion, there is concern that the current needed will exceed the ratings
 4216 of the current power supply modules made by CAEN S.A (Italy). We have contacted the man-
 4217 ufacturer to look into ways of modifying the low voltage supply power modules to have a
 4218 higher rating that can meet our needs. An alternative that we are investigating is to use a two
 4219 step conversion process. This involves a step-up conversion using commercial parts close to
 4220 the power supply modules and then a step-down conversion close to the detector.

4221 6.2.7 Front End Electronics

4222 The pixel readout chip used in the current detector (PSI46v2) is well understood, tested. It
 4223 is also sufficiently radiation hard to survive the Phase 1 integrated luminosity. However, as
 4224 noted earlier, it will incur rate dependent inefficiencies in the inner regions when the peak
 4225 instantaneous luminosity exceeds $10^{34} \text{ cm}^{-2}\text{s}^{-1}$. Although modifications are needed to allow
 4226 for the luminosity that we will have for Phase 1 and possible operation with a 50 ns bunch
 4227 spacing, we would like to keep its core unchanged as much as possible. Changes to the ROC
 4228 are needed for two reasons:

- 4229 • **Single hit efficiency:** To cope with the increased luminosity for Phase 1, the size of
 4230 the internal data buffers must be increased. An additional internal buffer stage on
 4231 the ROC will be needed which holds the level 1 trigger verified hits until a readout
 4232 token arrives. Doubling the buffers in the $0.25 \mu\text{m}$ process will increase the size of the
 4233 chip periphery by 0.6 mm which can be accommodated in the module design. There
 4234 is also good progress on designing an improved chip architecture with an additional
 4235 buffering stage in the column periphery to reduce or eliminate the readout-induced
 4236 dead time, which limits the efficiency of the innermost layer. This reduces dead time
 4237 related to readout latency and allows for a more efficient use of the output band-
 4238 width. Simulation shows that for the innermost layer at 3.9 cm, the peak inefficiency
 4239 of this upgraded ROC at a luminosity of $2 \times 10^{34} \text{ cm}^{-2}\text{s}^{-1}$ is about 4.7% with an
 4240 average over the whole LHC fill of 2.1%, assuming a fill lifetime of 10 hours, and a
 4241 collision rate of 40 MHz (25 ns bunch crossing).
- 4242 • **Fast readout:** Since we will have more modules than the current detector and the
 4243 number of optical fibers is limited, we need to have a faster readout. The present
 4244 readout uses 40 MHz analog links, with the pixel addresses encoded using six analog
 4245 levels (2.5 bits), for an effective bandwidth of 100 Mbps. Increasing the clock rate on
 4246 the analog links to 80 MHz presents a significant risk due to the limited rise time
 4247 of the ROC and Token Bit Manager (TBM) signals. Instead, we are developing a
 4248 digital readout (with an on-chip ADC) from ROC to TBM at 160 MHz (160 Mbps).
 4249 In addition, a multiplexing TBM combines two token rings into a 320 Mbps digital

4250 link, giving three times the throughput of the existing analog links on the same fiber
4251 plant. Besides increased bandwidth, advantages of the digital output from the ROC
4252 and TBM are lower power and less material in the cables.

4253 The core of the ROC, including the pixel front end amplifier, threshold comparator with trim-
4254 ming and the column drain architecture remain unchanged. A phase-lock circuit (PLL) capable
4255 of up-converting the 40 MHz LHC clock to 80/160/320 MHz has been successfully tested. A
4256 successive approximation 8-bit ADC has also been tested; revised designs for both PLL and
4257 ADC have already been submitted and tested in 2009; further improvements to the ADC for
4258 higher clock rates are underway. With these functional blocks designed, laid out and tested,
4259 the redesign of the 0.25 μm ROC is on sound footing. The full layout for the upgrade ROC is
4260 expected to be ready in Summer 2011, with first test submission following shortly.

4261 In case of a 50 ns bunch crossing scenario of the LHC, the data losses described above would
4262 increase by roughly a factor of two. A further reduction of these losses would require modifi-
4263 cations to the complex circuit block in the ROC that manages the double column data buffers.
4264 Indeed, we intend to pursue such improvements to address readout-related data losses in a
4265 follow up submission of the ROC.

4266 Changes are also required to the TBM to accept and produce digital signals. The TBM chip is
4267 needed to control a module. The core of this chip will remain largely unchanged. However,
4268 modifications will be needed to deal with the new fast up-link protocol. Only modest changes
4269 to the input and output stages are required, again using functional blocks already developed
4270 for new low-power electrical micro-twisted pair links between the module and downstream
4271 electronics. The TBM must also multiplex signals from two token rings run at 160 MHz into
4272 a single 320 MHz output to an optical link. The modifications that will be needed include
4273 replacing the analog switch drivers by digital multiplexers, a PLL for clock generation, and
4274 digital receivers and line drivers.

4275 Digital signals would travel from the TBM on a new set of extremely low mass, flexible cables
4276 to an optical hybrid board, and then along optical fibers to the off-detector data acquisition
4277 electronics. Micro-twisted pair cable of copper-clad aluminum wires with 125 μm diameter
4278 have been developed. On these cables, signals are sufficiently robust over 1 m lengths, to allow
4279 the electrical to optical link boards for the barrel to be placed outside the fiducial volume.
4280 For FPIX, we are currently evaluating the use of a flat flex-cable made out of Al. Simulation
4281 shows good performance when operated digitally at 320 MHz. Prototypes of this cable will be
4282 available sometime in early Fall 2010. We are also investigating robust connectors for the both
4283 the Al cable and the micro-twisted pair cable.

4284 The current Analog opto-hybrid (AOH) will be replaced with a new readout optical hybrid
4285 (ROH) to transmit the data through long fibers to the Front End Driver (FED). The current
4286 baseline is to build link boards similar to the existing analog optical hybrids, using 1310 nm
4287 lasers qualified for radiation hardness by the CERN Versatile Link project, intended for raw
4288 data rates of 5 Gbps, which is well beyond the required 320 Mbps for Phase 1. Several lasers in
4289 commercial TOSA packaging and attached fiber pigtailed will be mounted on a common readout
4290 link PCB designed to fit in the service cylinders. Prototype lasers and link boards are expected
4291 to be available for testing in late 2010. Linear Laser Driver (LLD) chips from the CERN opto-
4292 electronics group were used in the original analog links and have been radiation qualified and
4293 tested at 320 Mbps. The baseline option is to use the LLD to operate these links at 320 Mbps over
4294 approximately 100 m to the FEDs in the Underground Service Cavern, USC55, at CMS where
4295 most of the back end electronics is located. A suitable optical receiver has been identified and
4296 tested at 320 Mbps.

4297 At the FED, the flash ADC and analog data packet decoder will be replaced by a deserializer,
4298 since the incoming signals will be fully digital. The existing FED design has a 9U VME mother-
4299 board with daughter cards hosting ADCs or FPGAs for data decoding and event building. One
4300 option is to replace the ADC daughter cards with a deserializer FPGA, leaving the architecture
4301 of the motherboard intact, where in fact changes are not likely to be necessary. If required,
4302 FPGA daughter cards can be replaced with faster FPGAs from the current generation of de-
4303 vices from Altera. A preliminary design for the replacement cards includes an extension for
4304 mounting the new optical receivers, leaving the old analog receivers intact. This may prove
4305 useful for prototyping and conversion of existing FEDs for digital readout. To accommodate
4306 the increased data rates at the FED output, the existing S-Link64 interface cards on the VME
4307 mezzanine boards would be replaced with new daughter boards implementing a new interface
4308 to the CMS DAQ system.

4309 The downlink protocol for control and configuration of the detector is unchanged, both electri-
4310 cally and logically. New parts have to be procured for the digital control links and Front End
4311 Controller (FEC).

4312 6.2.8 Sensor Module

4313 A 4-layer barrel detector would comprise about 1200 full modules compared to the presently
4314 installed 770 full and half-modules. The number of pixels grows by a factor 1.7 from 48M
4315 to 80M. There are 672 modules in the upgraded 2×3 -disk forward pixel detector, the same
4316 number as the current FPIX detector. However, since the size of each module will be larger, the
4317 number of pixels will grow from 18M to just under 45M.

4318 The proposed upgraded pixel detector has only one type of sensor module with two rows of
4319 8 ROCs each. This will simplify considerably the sensor production, module assembly, and
4320 testing. The active area of the module is $16.2 \times 64.8 \text{ mm}^2$. The pixel size will remain the same
4321 as before, $100 \times 150 \text{ }\mu\text{m}^2$. For the sensors our baseline is to use the same n^+ -on- n technology
4322 as for the current detector. Nevertheless, there is some ongoing R&D activity to evaluate other
4323 radiation tolerant sensor technology. The sensor is bump-bonded to 16 ROCs which for Layers
4324 1 and 2 for BPIX, will be thinned down to $75 \text{ }\mu\text{m}$. For the rest of the layers and the end-cap
4325 disks, the ROCs will be thinned down to about $200 \text{ }\mu\text{m}$. A high density interconnect (HDI)
4326 is glued on top of the sensor with wire bond pads to connect to the corresponding pads on
4327 the ROCs. Electrical signals will be sent from/to the ROCs through the HDI and then to the
4328 downstream electronics. The TBM chip will be mounted on the HDI as well. A small clip is
4329 glued to the ends of the module to allow the assembly of the module to its support structure.

4330 For future replacements of the the detector innermost layers and rings we are considering other
4331 possibilities as outlined in Section 6.4.

4332 6.2.9 Bump bonding

4333 Bump bonding was a cost and schedule driver for the current pixel detector [13]. Since the
4334 number of pixels of the upgraded pixel system will increase by about 90%, some development
4335 work will be needed to increase the throughput as well as reduce the cost. For the current
4336 BPIX detector, bump bonding was done by PSI whereas for FPIX by two industrial companies.
4337 Industry is progressing steadily on bump bonding and lower cost processes for micro-bumps
4338 at $30 \text{ }\mu\text{m}$ diameter and $100 \text{ }\mu\text{m}$ pitch are becoming available. For example, at PacTech [14], pre-
4339 fabricated solder balls are individually placed through a capillary and fused by laser-melting
4340 at a speed of 5–10 per second on a step-motor controlled machine. A special under-bump metal
4341 is still required, but the processing steps for the deposition and forming of Indium balls can be

4342 omitted. Any new vendor and process will have to be qualified to make sure that they meet
4343 our needs. In addition, the production yield and throughput must be evaluated in a sequence
4344 of prototype runs.

4345 **6.2.10 Pixel Module Assembly and Testing**

4346 Starting from the bump-bonded pixel module, a high density interconnect will be glued onto
4347 the back of the sensor and wire bonded to the readout chips (about 700 bonds per module).
4348 Production of the necessary gluing and placement tools, based on assemblies used to build
4349 the current detector, has started. These assembly stations will include both manual and auto-
4350 matic procedures. The design and testing of fixtures, adhesive dispensing machines, and the
4351 necessary software are being commissioned.

4352 Once assembled, the full modules then have to be fully tested and characterized at room tem-
4353 perature and at the foreseen operation temperature around -20°C . The tests include trimming
4354 the analog thresholds of all of the pixels to achieve uniform efficiency. The pixel detector
4355 achieves a point resolution of about $10\ \mu\text{m}$ with $100\ \mu\text{m}$ pitch by using the charge sharing in-
4356 duced by the Lorentz effect. The amplification is non-linear for small pulses and needs to be
4357 calibrated for each pixel using X-ray sources between 10 and 30 keV to reach the design reso-
4358 lution. The modules should also be tested at high rate, which can be done using an X-ray test
4359 stand.

4360 In BPIX the final modules of one layer have to be mounted on a carbon-fiber frame which
4361 also includes the cooling pipes. A rotating fixture is needed, as adjacent ladders are mounted
4362 alternating from the inside and outside.

4363 A system test of the fully assembled layer would require a CO_2 cooling plant of about 1kW, HV
4364 and LV supplies, optical links, control and readout boards, and a cosmics trigger.

4365 **6.2.11 Final integration and commissioning**

4366 Our plan is to do the final integration followed by system commissioning in the Tracker In-
4367 tegration Facility (TIF) at CERN. For BPIX, fully assembled layers will be transported from
4368 the various assembly sites to CERN. For FPIX, completed half disks and half cylinders will
4369 be shipped separately to CERN. At TIF, we will re-mount the half-disks to the half cylinders
4370 and carry out a commissioning of each half cylinder. Finally, extensive system tests of both
4371 BPIX and FPIX together will be performed at TIF prior to installation in CMS. 9 months are
4372 scheduled for this phase to minimize further commissioning in CMS for physics operations

4373 A program of high rate tests will be performed to uncover issues with the interoperability
4374 of the readout chain. This system test will allow us to exercise all firmware and software in
4375 the system. Cooling system tests will be performed to assure smooth, leak-free operation. In
4376 preparation for these tests, we will equip TIF with all the necessary electronics, power supply
4377 modules, as well as a CO_2 cooling system. The full readout and data acquisition chain will be
4378 present. We will also have a full control and safety system (DCS/DSS) installed and tested.

4379 **6.3 Performance Studies**

4380 The Phase I pixel detector has significantly reduced mass and significantly increased three-hit
4381 coverage. The net effect of these improvements on the amount of material, pattern recognition,
4382 track parameter resolution, vertexing, and b -tagging performance of the Tracker is summarized
4383 in the following sections.

6.3.1 Studies of the Effects of Material in the Tracking Volume

The upgraded detector will roughly double the number of pixels in the system. Despite this, we aim to reduce the amount of material in the tracking region by at least a factor 2 with respect to the current system.

The amount of material from the barrel pixel detector can be significantly reduced both in the active regions and even more in the service regions located in front of the pixel disks and the silicon strip tracker [15]. The use of serial CO₂ cooling with reduced density and pipe wall thickness is one important ingredient. This will reduce multiple scattering, photon conversions, and nuclear interactions. Within the region $|\eta| < 2.1$, the weight of the supply tube is 408 g and the total weight of the 4 barrel layers plus supply tube within this η region is estimated to be 7 kg, about a factor 2.4 less than the current BPIX detector with only 3 layers.

We estimate the overall mass of the FPIX detector can be reduced by $\sim 40\%$. The half disks contribute most to the FPIX material in the region $1.5 < |\eta| < 2.5$. It is feasible to remove 50% of the mass in the half disk by removing the very high density interconnect circuit (VHDI) and by using CO₂ cooling. The weight of the new half-disk is estimated to be 420 g, to be compared with the present 607 g. Within $|\eta| < 2.5$, the total weight of each half cylinder, including the three half-disks, cables, and cooling lines, is estimated to be 1.82 kg.

These reductions in material inside the pixel tracking volume are shown in Figure 6.17 and Figure 6.18 for BPIX and FPIX, respectively.

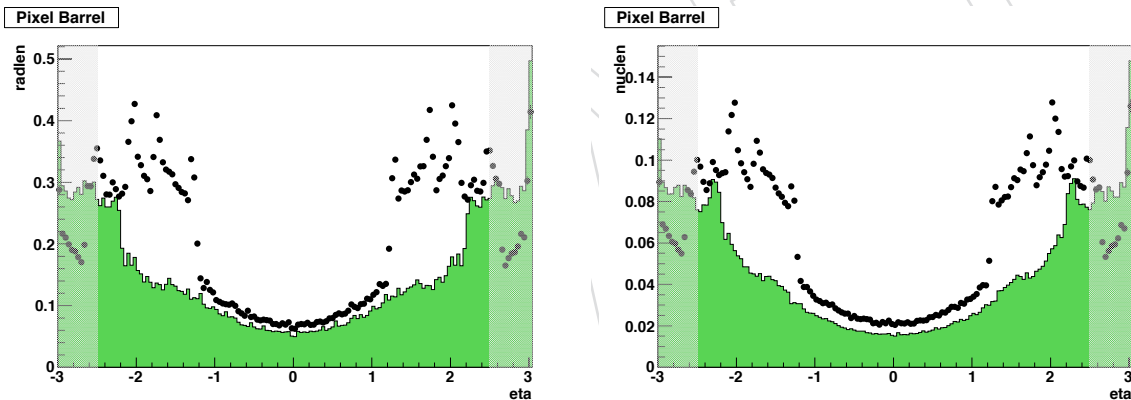


Figure 6.17: Radiation length (left) and nuclear interaction length (right) of current barrel pixel detector (dots) and proposed upgrade (histogram). The shaded region shows the material distribution outside the fiducial tracking volume.

Such reductions in the amount of passive material will have a large impact on charged particle tracking efficiency as well as electron and photon identification and resolution. For example, for a photon at $|\eta| = 1.5$, the probability that it would convert into an electron-positron pair inside the pixel volume (where the presence of pixel hits is crucial for distinguishing photons from electrons) is 22% with the current detector, but would be 11% with the proposed upgraded detector. Such improvements would have a positive impact on final state signatures involving photons, such as $H \rightarrow \gamma\gamma$.

6.3.2 Pattern Recognition and Efficiency Studies

The number of overlapping events during Phase 1 operation will be two to four times larger than during previous LHC operation. The interesting physics to be pursued during Phase 1 is likely to involve the reconstruction of tracks in high- p_T jets. These realities will emphasize

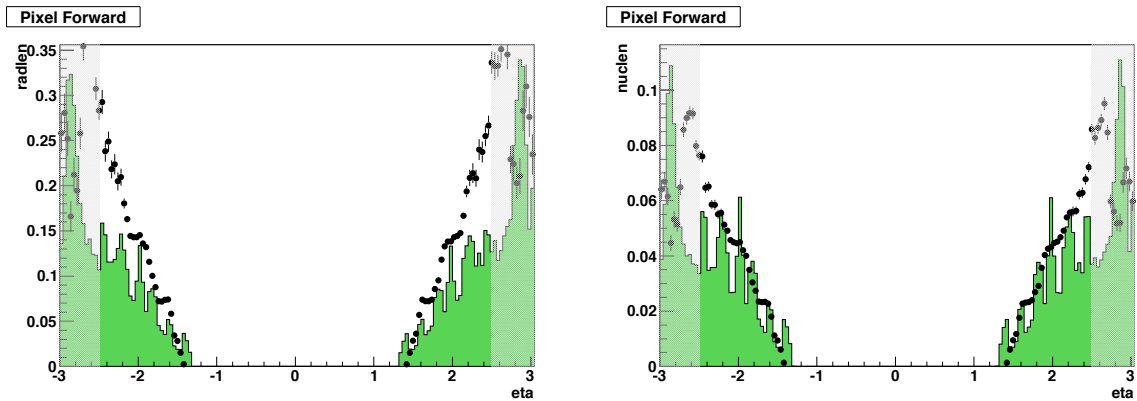


Figure 6.18: Radiation length (left) and nuclear interaction length (right) of current forward pixel detector (dots) and proposed upgrade (histogram). The shaded region shows the material distribution outside the fiducial tracking volume.

4414 the importance of reliable tracking in environments with high local hit densities. The challenge
 4415 of maintaining high tracking efficiency and low track fake rate in dense hit environments has
 4416 been studied as part of the CMS heavy ion program. It was found that seeding with three-hit
 4417 combinations in the pixel detectors results in more precise initial estimates of the track param-
 4418 eters, which produces more reliable identification of the associated silicon strip hits and lower
 4419 fake rates. Unfortunately, due to module boundary gaps in the current pixel detector with three
 4420 barrel layers and two disks, this requirement leads to losses in efficiency. The new design with
 4421 four barrel layers and three disks alleviates this problem by providing substantial redundancy
 4422 for three hit seeds. The fourth layer also guarantees at least reasonable track seeding after high
 4423 integrated luminosity. With four layers, even if the inner layer performance starts to degrade,
 4424 the fourth layer will still provide three layer seeds.

4425 In order to quantify the physics benefit that can be expected from the upgraded pixel detector,
 4426 samples of jet events and $t\bar{t}$ events were generated for both geometries using the standard CMS
 4427 simulation software and assuming an instantaneous luminosity of $2 \times 10^{34} \text{ cm}^{-2}\text{s}^{-1}$. CMS
 4428 has adopted an iterative tracking algorithm consisting of multiple steps. In the first step, hit
 4429 triplets from the pixel detector or the innermost strip layer are used as seeds for the subsequent
 4430 track finding and fitting. With the upgraded detector, in addition to triplets, quadruplets of
 4431 pixel hits can also be used which cleans up the subsequent pattern recognition and reduces
 4432 the fake rate. The left-hand plots of Fig. 6.19 show the track finding efficiency for the two
 4433 geometries as a function of pseudorapidity and p_T . The track selection criteria are the same
 4434 ones used in the recently released tracking performance studies [12] and represent the typical
 4435 requirements used in recent physics analyses. The redundancy provided by the additional pixel
 4436 layer in the Phase 1 geometry results in an increase of track seeding efficiency and a much lower
 4437 fake rate. Losses due to nuclear interactions in the tracker material, which presently increases
 4438 from about $0.4 X_0$ in the central region to $1.8 X_0$ at $|\eta| = 1.5$ (see Figure 6.7), and which is
 4439 dominated by dead material of the strip detector, lead to a significant drop of efficiency towards
 4440 the acceptance limits of the barrel pixel detector. The comparison of the tracking efficiency in
 4441 the two configurations demonstrates however that the gain in track seeding efficiency can be
 4442 retained also for physics analyses.

4443 The plots on the right-hand side of Fig. 6.19 show the corresponding fake track rate as a func-
 4444 tion of pseudorapidity for the current and Phase 1 detectors. Fake tracks are caused by the
 4445 incorrect association of hits and are much more likely in regions with more passive material.
 4446 They cause significant problems for b-tagging and are much reduced in the upgraded detector.

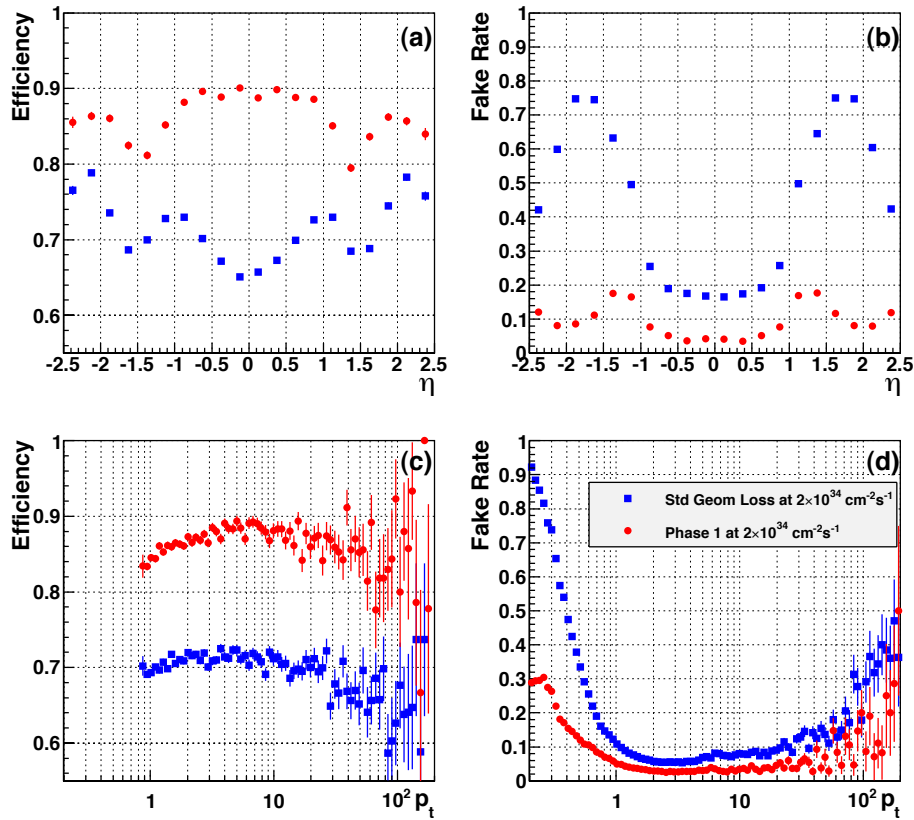


Figure 6.19: Comparison of tracking efficiency and fake rate for the current (blue) and upgraded (red) detectors in $t\bar{t}$ events at $2 \times 10^{34} \text{ cm}^{-2} \text{ s}^{-1}$ with 25 ns bunch spacing. The tracking algorithm with the current detector uses pixel triplets to seed pattern recognition, and pixel quadruplets and triplets with the upgraded detector. Shown are: (a) tracking efficiency vs pseudorapidity; (b) fake rate vs pseudorapidity; (c) efficiency vs p_T ; (d) fake rate vs p_T .

6.3.3 Track Parameter Studies

The primary purpose of the pixel detector is to make precise measurements of the track direction and position before that information is degraded by multiple scattering. The increased sampling and reduced mass of the Phase 1 pixel detector also improve the track parameter resolution. The full-track impact parameter resolutions for the current detector and for the Phase 1 upgrade are shown as functions of pseudorapidity and momentum in Figures 6.20-6.21. Substantial improvement to the impact parameter resolution is a result of four main factors:

1. Reduced material in the tracking volume which reduces multiple scattering;
2. Moving the innermost layer closer to the interaction region;
3. Adding a fourth layer to the BPIX and a third disk to the FPIX which improves the track "lever arm" in the pixel region;
4. Improving the transverse impact parameter resolution in the forward regions by orienting the pixel sensors so that the $100 \mu\text{m}$ pitch (as opposed to the $150 \mu\text{m}$ pitch) contributes to the FPIX cluster resolution in the transverse plane.

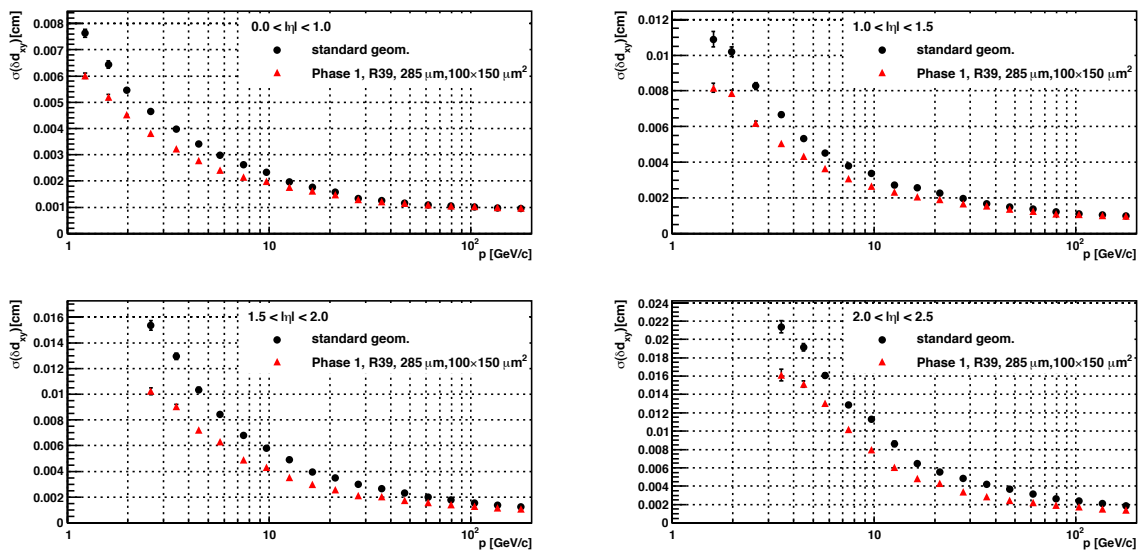


Figure 6.20: The transverse impact parameter resolution for the present and upgraded versions of the pixel detector as functions of track momentum in different pseudorapidity regions.

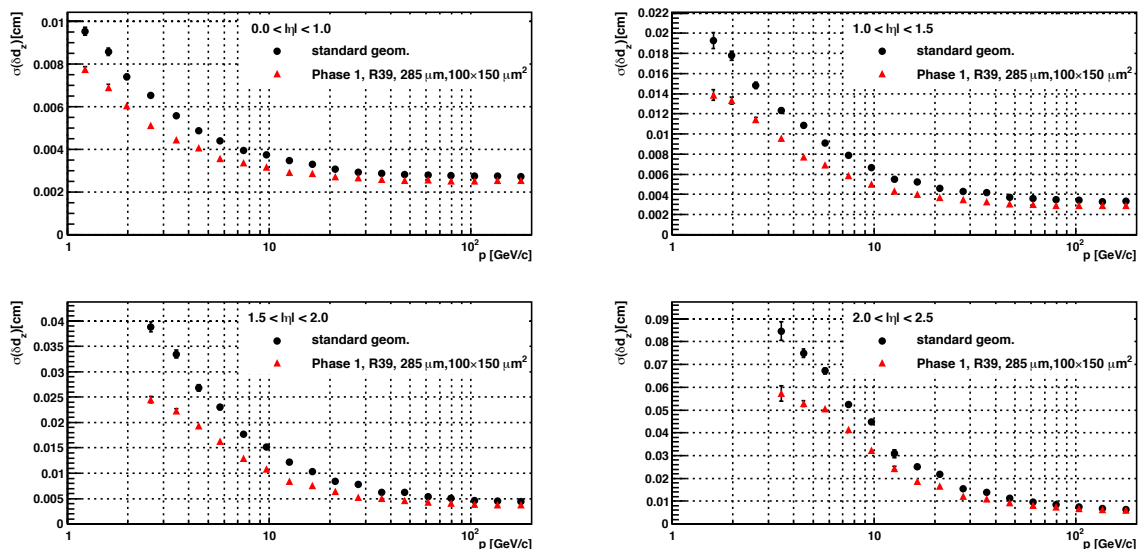


Figure 6.21: The longitudinal impact parameter resolution for the present and upgraded versions of the pixel detector as functions of track momentum in different pseudorapidity regions.

4461 As a consequence, vertex resolution and b-tagging performance also improve, as described in
4462 the following sections.

4463 The addition of a fourth barrel pixel layer increases the measured radial track length by a factor
4464 two, thus improving the momentum resolution for stand-alone pixel tracks by a factor four.
4465 This improves both the seeding and the extrapolation into the first layer of the strip tracker,
4466 and provides more powerful information to the HLT.

4467 6.3.4 Vertex Resolution Studies

4468 One of the primary functions of the CMS Tracker is to reconstruct primary and secondary ver-
4469 tices. It is expected that the Phase 1 detector will operate in an environment with a mean of

4470 20-40 pp interactions per bunch crossing. Efficient and precise vertexing and the efficient asso-
 4471 ciation of individual tracks to vertices are essential to untangle the accidental coincidences of
 4472 less interesting event topologies that could otherwise appear to signal important discoveries.
 4473 The efficient and precise reconstruction of secondary vertices is a crucial element in b -tagging
 4474 and in the search for possible long-lived exotic states. The longitudinal and transverse res-
 4475 olutions of simulated primary vertices are shown in Fig. 6.22 as functions of the number of
 4476 tracks for the present detector and for the upgraded detector. Overall, the upgrade gives an
 improvement in the resolution of about 20%.

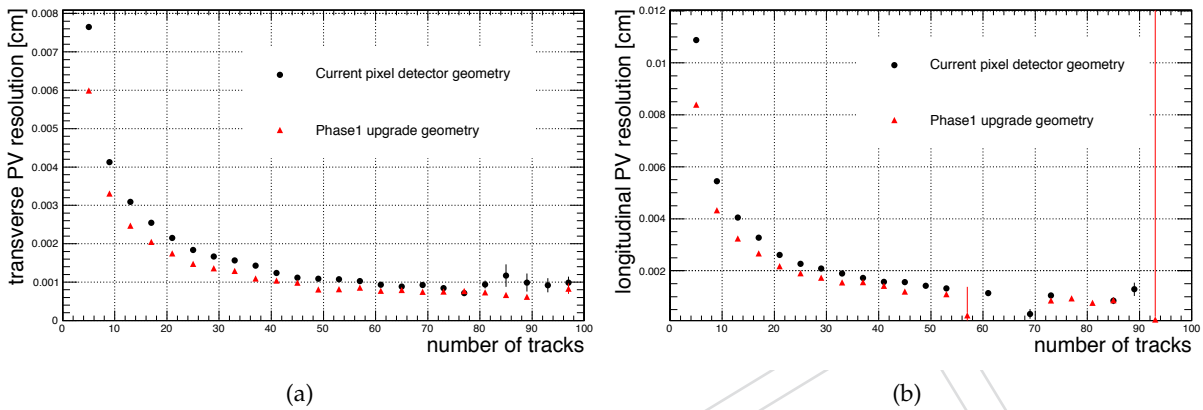


Figure 6.22: The (a) transverse and (b) longitudinal primary vertex resolutions for the present and upgraded versions of the CMS pixel detector as functions of number of tracks in simulated $t\bar{t}$ events at $10^{34}\text{cm}^{-2}\text{s}^{-1}$.

4477

4478 6.3.5 b -tagging Studies

4479 A number of interesting physics channels such as top quarks, Higgs bosons, and supersymmet-
 4480 ric particles produce b jets in the final state. For example, a low mass Standard Model Higgs
 4481 boson dominantly decays into a pair of b quarks, while the top quark decays almost exclusively
 4482 into a W boson and a b quark. Various supersymmetric scenarios can produce final states with
 4483 four or more b quarks. The efficient and pure identification of b jets is therefore a major element
 4484 in the CMS physics program. The identification of b jets relies upon the relatively distinct prop-
 4485 erties of b hadrons such as large proper lifetime ($\tau \approx 1.5$ ps, $c\tau \approx 450$ μm), large mass, decays
 4486 to final states with high charged track multiplicities, relatively large semileptonic branching
 4487 ratios, and a hard fragmentation function. Efficient track reconstruction, and in particular pre-
 4488 cise spatial reconstruction close to the interaction point, are thus key ingredients for almost all
 4489 b -tagging algorithms. The performance improvements provided by the Phase 1 upgrade also
 4490 enhance the b -tagging performance as shown in Fig. 6.23 for a sample of simulated $t\bar{t}$ events.
 4491 Fig. 6.23a shows the detector performance for low instantaneous luminosity and Fig. 6.23b
 4492 shows the performance for operation at an instantaneous luminosity of $10^{34}\text{cm}^{-2}\text{s}^{-1}$ with 25 ns
 4493 bunch spacing. The b -tagging performance of the present detector is seriously degraded by the
 4494 large number (~ 20) of overlapping interactions in each bunch crossing. The upgraded detector
 4495 would reduce the light quark background of the Combined Secondary Vertex Tag by more than
 4496 a factor of 6 for a b -efficiency of 60% or conversely, it would increase the b -efficiency by 50%
 4497 at the fixed light-quark efficiency of 5×10^{-2} . The search for new physics frequently involves the
 4498 identification of multi- b -quark final states. These searches would benefit by a factor of $(1.5)^n$
 4499 where n is the number of final state b quarks.

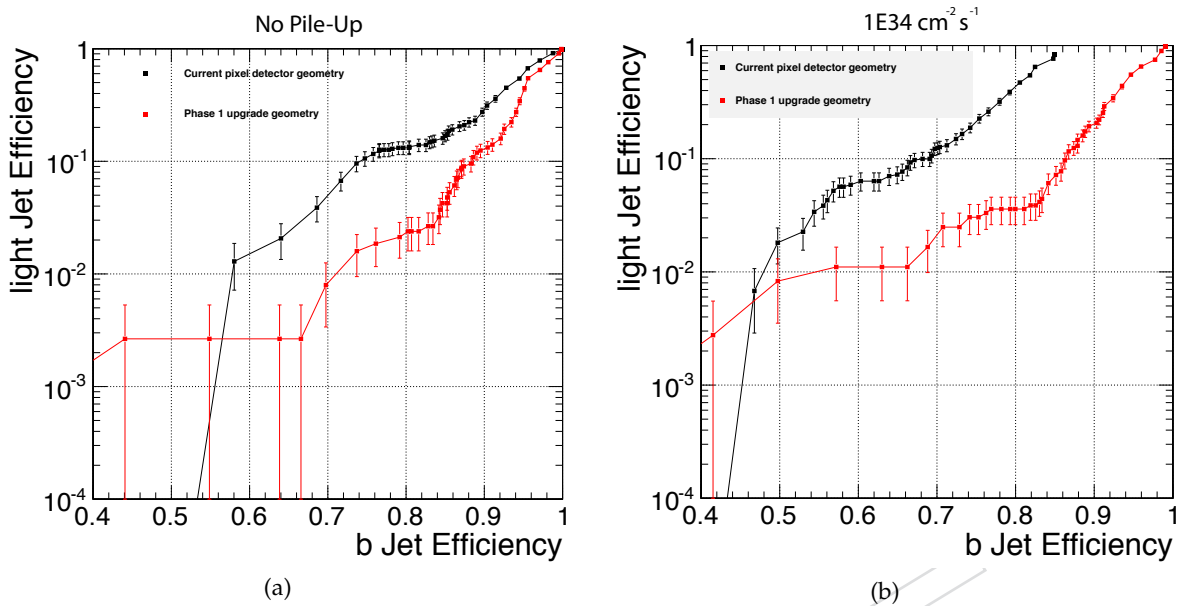


Figure 6.23: The b quark efficiency of the Combined Secondary Vertex Tag is plotted versus the light quark (and gluon) efficiency for a sample of $t\bar{t}$ events in two different luminosity scenarios. The black points represent the performance of the current tracker and the red points represent the performance of the Phase 1 upgrade. (a) The instantaneous luminosity is assumed to be low enough that there are no multiple collisions. (b) The instantaneous luminosity is assumed to be $10^{34} \text{ cm}^{-2} \text{ s}^{-1}$ with 25 ns bunch spacing.

6.4 Further development for the innermost region

The innermost region of the pixel detector is expected to suffer degradation when the LHC reaches its high luminosity running in the later stages of Phase 1. The inner layers and rings have been designed, as described above, to be independently replaceable. An R&D line should continue for new detector modules with smaller pixel size and other enhanced features. The most important improvements target the module efficiency, radiation-hardness, and spatial resolution, aiming not only at better performance, but also more headroom relative to LHC conditions, or radiation backgrounds, which could exceed our expectations. The new modules must remain fully compatible with the rest of the Phase 1 mechanics, cooling and electrical systems.

6.4.1 Frontend electronics and sensors

Development of a new ROC is under consideration using CMOS technology of 130 nm or smaller. This will enable the engineering of a module with a smaller pixel size and lower read-out thresholds. This will result in better spatial resolution and better ability to resolve tracks inside high momentum jets, where the present pixel size leads to overlapping hits in jets of energy above 100 GeV. The new ROC should also be able to operate with high efficiency with LHC operating conditions up to $2 \times 10^{34} \text{ cm}^{-2} \text{ s}^{-1}$ and 50 ns bunch separation.

The replacement of the innermost layers and rings also constitutes an opportunity to adopt sensors with greater radiation hardness. Recent measurements shown in Figure 6.24 show that sensors processed on mCz silicon collect the same signal at a lower bias voltage than those processed on FZ material. We are currently evaluating n-on-n and n-on-p single-chip pixel detectors processed on FZ, DOFZ and mCz material from different producers. A small number

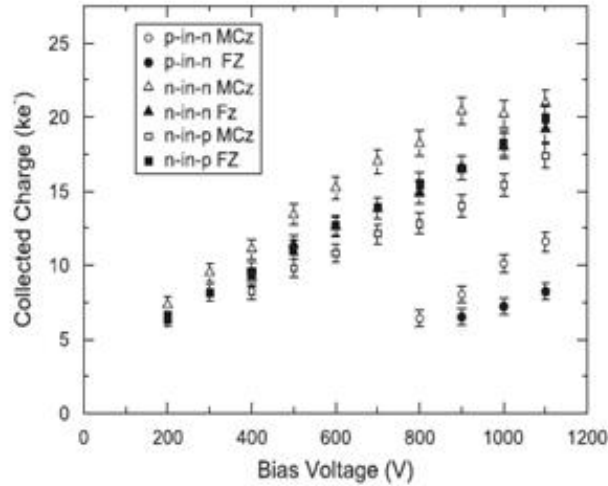


Figure 6.24: Collected charge as a function of bias voltage for six types of sensors irradiated with neutrons to $10^{15}n_{eq}/cm^2$ [16]

4522 of n-on-p samples of FZ and mCz are available from Micron, IRST and CiS. A larger quantity of
 4523 samples produced on different wafer types (FZ, mCz, epi) of different thickness and technology
 4524 (n-in-n and n-in-p with p-stop and p-spray isolation) has been delivered recently by HPK and
 4525 Sintef. Other options under consideration include the development of non-planar (so called
 4526 3-D) and diamond sensors.

4527 6.4.2 Performance studies

4528 The development of a readout chip with higher granularity and lower readout thresholds
 4529 would offer the opportunity for further improving the detector later in Phase 1 in several key
 4530 aspects:

- 4531 • Enhanced hit resolution and detection efficiency after irradiation;
- 4532 • Improved track parameter resolution;
- 4533 • Improved jet reconstruction and b jet identification.

4534 The pixel hit resolution is determined by the cell size, the charge sharing due to the combined
 4535 effect of electric and magnetic fields, and by the readout threshold. The resolution can be
 4536 improved by adopting pixel cells with smaller dimensions and front end electronics with lower
 4537 readout thresholds. Figure 6.25 shows the hit resolution after irradiation for a hypothetical
 4538 scenario with a smaller pixel cell size, thinner sensors ($220\ \mu m$) and lower readout thresholds
 4539 (2000 electrons). We are considering further R&D on CMOS frontend electronics and sensors
 4540 in these directions.

4541 At large momenta, the resolution on the track impact parameters and angles are largely de-
 4542 termined by the hit resolution and radius of the innermost layer, and precision of the spatial
 4543 alignment. For instance, with a hypothetical pixel cell of $75 \times 100\ \mu m^2$ in the 39 mm radius
 4544 innermost layer, the longitudinal impact parameter resolution could be improved by 25%, as
 4545 shown in Figure 6.26. Additional small improvements can be expected by further reducing
 4546 the radius of the innermost layer. However, any reduction with respect to the baseline radius
 4547 would require a careful assessment of the risks associated to the clearances during installation.

4548

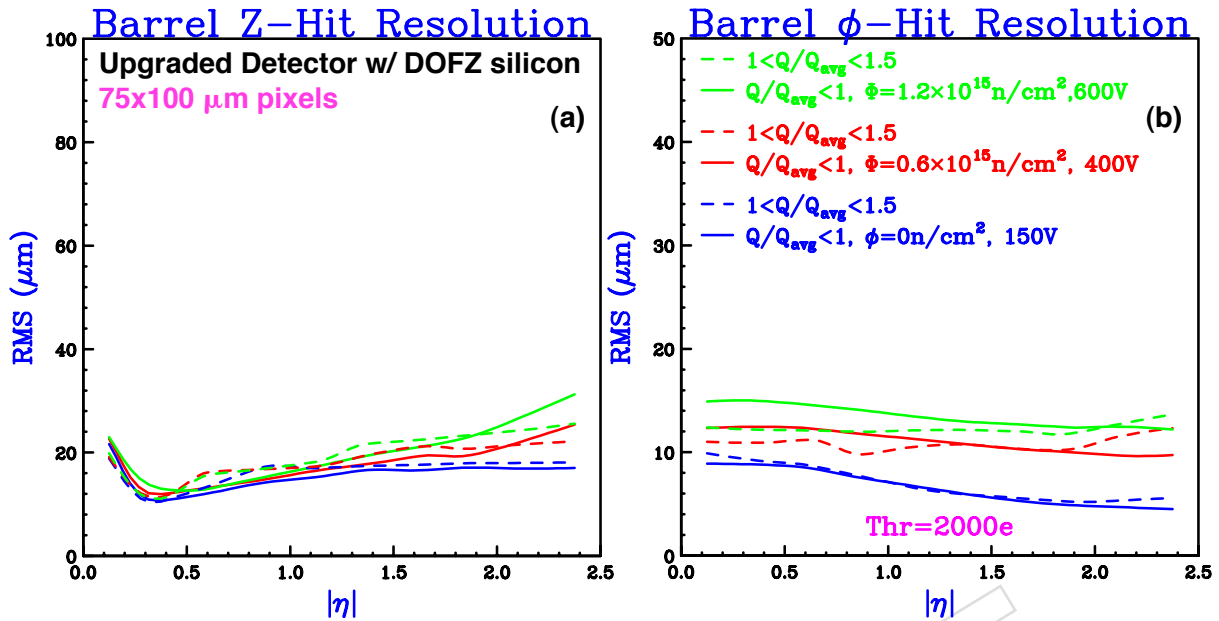


Figure 6.25: Hit position resolution (RMS) as function of the track pseudorapidity for an unirradiated (blue lines) and irradiated detectors (red and green lines). The pixel cell size is set to $75 \times 100 \mu\text{m}^2$ and the sensor thickness to $220 \mu\text{m}$. (a) Longitudinal and (b) transverse hit resolution are shown separately. The solid lines correspond to hits with total charge Q below the average charge. Dashed lines correspond to hits with total charge $1 < Q/Q_{avg} < 1.5$.

4549 Primary and secondary vertex resolution is largely determined by the number of tracks associ-
 4550 ated to the vertex and resolution of track parameters. However, the hadronization of b quarks
 4551 with large transverse momentum produces collimated jets which result in overlapping hits in
 4552 the innermost pixel layer. In the current detector, for a 200 GeV b jet about 20% of the tracks
 4553 have merged hits in the first layer. The effect produces a sizable deterioration of the b jet identi-
 4554 fication for jets with transverse momenta above 200 GeV. Future replacements of the innermost
 4555 layer with sensors featuring smaller cell sizes, therefore, represent an opportunity to improve
 4556 b jet identification in this upper kinematic range.

4557 6.5 Schedule

4558 Figure 6.27 shows a tentative schedule for the Phase 1 pixel upgrade.

4559 6.6 Conclusions

4560 The Phase 1 upgrade of the LHC, starting with the long shutdown in 2016, presents CMS with
 4561 both the requirement and the opportunity to upgrade the present pixel detector. The peak
 4562 LHC luminosity after the Phase 1 upgrade is expected to reach up to $2 \times 10^{34} \text{ cm}^{-2}\text{s}^{-1}$ with a
 4563 possibility of 25 ns or 50 ns bunch spacing. Such conditions are a factor two to four more intense
 4564 than the nominal LHC conditions for which the present pixel detector was designed. The
 4565 present system with its three-hit layout would suffer greatly in terms of performance in these
 4566 conditions, severely compromising the ability of CMS to fully exploit the delivered luminosity
 4567 from the upgraded LHC.

4568 A thorough revision of the design of the ROC has been made, aiming to reduce the dynamic
 4569 inefficiency to an acceptable level, while leaving the underlying architecture unchanged. So far,

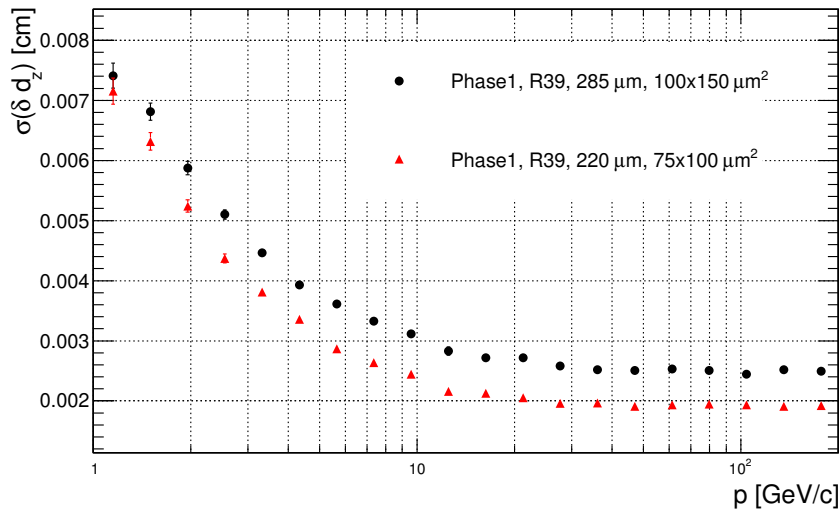


Figure 6.26: Longitudinal impact parameter resolution for the baseline upgrade scenario (black dots) and with a hypothetical replacement of the innermost layer adopting a reduced pixel cell size (red triangles).

Preliminary Pixel Upgrade Schedule	2010				2011				2012				2013				2014				2015				2016				2017			
	Q1	Q2	Q3	Q4																												
Technical Design Report																																
Sensors procurement and qualification																																
ROCdig new layout																																
ROCdig testing and pre-serie																																
ROCdig procurement and qualification																																
System, TBM Development and pre-serie																																
TBM Procurement and qualification																																
HDI Development and preseries																																
HDI procurement and qualification																																
Module pre-production qualification																																
Module production																																
Detector Mechanics and Supply tube																																
FED development and construction																																
Optical Link Development																																
Optical Link Construction																																
Power System Development																																
Power System Construction																																
Cooling System Development																																
Cooling System Construction and test																																
System Integration																																
System long term test at TIF																																
Installation at P5																																
Commissioning																																
Ready for Physics																																

Figure 6.27: Tentative schedule for the Phase 1 upgrade pixel detector.

4570 a large reduction of inefficiency has been achieved with the new design, and effort will continue
 4571 towards further reducing the data loss. The bandwidth of the readout has been doubled in the
 4572 new design allowing the much larger system to be read out with the same number of fibers.

4573 The addition of extra barrel and endcap layers will preserve our present excellent level of track-
 4574 ing performance even at the higher luminosity expected in Phase 1. Recent advances in CO₂
 4575 cooling, DC-DC powering, and readout links enable this ambitious proposal for the complete
 4576 replacement of the present three-hit pixel system with a much larger ultra-lightweight system
 4577 of four barrel layers and three endcap disks. The upgraded pixel system will have a reduced
 4578 mass, a reduced innermost radius and increased lever arm, altogether resulting in a significant
 4579 improvement over the present system in terms of tracking, vertexing and b jet identification.

4580 Radiation effects will be of growing importance as the luminosity increases. The innermost
 4581 detectors are expected to require replacement before the end of Phase 1 LHC operations. Such

4582 an intervention can be done during an LHC winter maintenance period. This replacement of
4583 the innermost layers presents a further opportunity to improve the detector performance at a
4584 later stage. Long term R&D is being done with the objective of having available sensors with
4585 greater radiation resistance. We are also considering designing a new readout chip in a more
4586 advanced CMOS technology, aiming to enhance the performance in terms of hit-efficiency and
4587 threshold, while also profiting from the potential to employ a smaller pixel size. There is a clear
4588 synergy here with R&D required for Phase 2 upgrade of the full Tracker system, which is also
4589 the case for the R&D on CO₂ cooling, power and readout systems.

4590 The new system has to be commissioned and ready to take good physics data very soon after
4591 installation. The proposed schedule is compatible with having the detector integrated well in
4592 advance of the installation date, allowing time for extensive system tests at CERN and com-
4593 missioning of large parts, if not the entire detector, prior to installation.

DRAFT

DRAFT

4595 **Trigger System Improvements and Upgrades**4596 **7.1 Introduction**

4597 The present CMS trigger will work well up to the LHC design luminosity of $\mathcal{L} = 10^{34} \text{cm}^{-2} \text{s}^{-1}$
4598 with the design bunch spacing of 25 ns, but will need significant modifications to operate above
4599 the LHC design luminosity. Due to the increased occupancy of at each crossing toward the end
4600 of Phase 1 of the LHC, when the luminosity will reach $2 \times 10^{34} \text{cm}^{-2} \text{s}^{-1}$, the Level-1 trigger
4601 systems will experience degraded performance of the algorithms presently planned to select
4602 100 kHz of crossings from the input rate of 40 MHz (25 ns bunch spacing). For example, this
4603 increase in occupancy would cause electron and τ isolation algorithms to have reduced rejection
4604 at fixed efficiency and the muon trigger to have increased background rates from random
4605 coincidences. The same degradation would also occur if the LHC operates at design luminosity
4606 with a 50 ns bunch spacing due to the factor of two increase in occupancy.

4607 While the modifications to the trigger systems described below will provide good trigger per-
4608 formance during the LHC Phase 1 operations or the LHC operating at design luminosity with
4609 a 50 ns bunch spacing, they also provide enhanced capabilities and improved performance at
4610 luminosities below the LHC design luminosity. Thus the modifications proposed provide the
4611 opportunity to increase the physics yield of the CMS detector by installing them before the
4612 LHC luminosity exceeds $\mathcal{L} = 10^{34} \text{cm}^{-2} \text{s}^{-1}$.

4613 The modifications proposed for the Level-1 Trigger systems for Phase 1 must deliver the Level-
4614 1 trigger accept signal within the same time period as the present Level-1 Trigger systems since
4615 there is no possibility to increase this time until the present CMS tracker is replaced as part of
4616 Phase 2. This overall processing time constraint is independent of whether the LHC runs with
4617 25 or 50 ns bunch spacing.

4618 In order to meet the challenges for the DAQ of the higher LHC luminosity our approach is to
4619 hold the overall Level-1 trigger rate at the LHC design value of 100 kHz while increasing the
4620 DAQ readout bandwidth. This approach avoids rebuilding front-end and readout electronics
4621 as much as possible. However, maintaining a 100 kHz L1 rate during Phase 1 operations will
4622 increase the burden on the DAQ, which will need to transport more than the LHC design
4623 luminosity data size of about 1 MB per event.

4624 The existing CMS Level-1 Trigger System shown in Figure 7.1 is organized into three major
4625 subsystems: the Level-1 calorimeter trigger, the Level-1 muon trigger, and the Level-1 global
4626 trigger. The calorimeter trigger combines information from the ECAL and HCAL, including
4627 the HF. The muon trigger is organized into subsystems that process the three different muon
4628 detector systems: the Drift Tube (DT) Trigger in the barrel, the Cathode Strip Chamber (CSC)
4629 trigger in the endcap and the Resistive Plate Chamber (RPC) trigger covering both barrel and
4630 endcap. The Level-1 muon trigger also has a global muon trigger that combines the trigger

4631 information from the DT, CSC and RPC trigger systems and sends this to the Level-1 Global
4632 Trigger (GT).

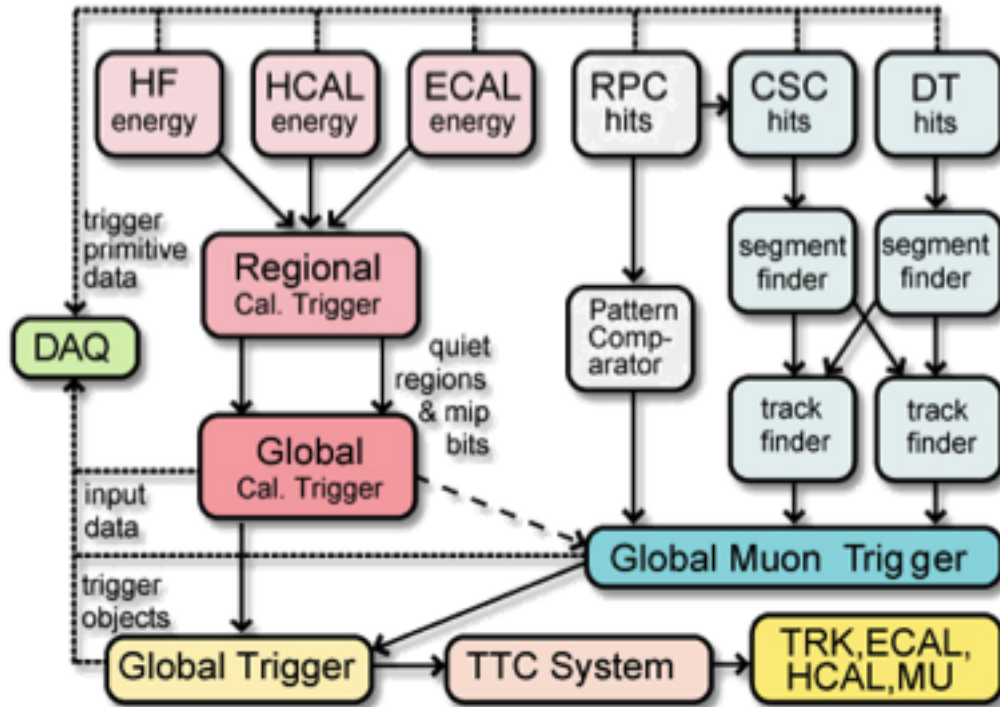


Figure 7.1: Overview of the present Level-1 Trigger System

4633 In the following, we present the plans for upgrading each major trigger subsystem to improve
4634 the ability to maintain the system, to operate it reliably, and to handle the highest luminosities
4635 that will be experienced through 2020 with high efficiency and adequate rejection.

4636 7.2 Calorimeter Trigger

4637 7.2.1 Introduction

4638 Increased luminosity results in several issues for the Calorimeter Trigger. First, the rate at
4639 which triggers fire goes up at least proportionately to the increase in luminosity. Second, the
4640 increased occupancy in the calorimeter renders some of the isolation cuts used in the calorime-
4641 ter trigger less effective. This results in a decrease in the trigger efficiency, which can only be
4642 compensated by weakening the isolation requirement, which in turn results in a higher trig-
4643 ger rate. Third, multi-object triggers can also be affected by spurious coincidences of trigger
4644 objects in different interactions within the large number of pileup events. The net effect is that
4645 the trigger thresholds need to be increased, which may result in an inability to capture physics
4646 of interest for electro-weak symmetry breaking studies, even though the very highest p_T new
4647 physics is not affected.

4648 To compensate for problems caused by high event occupancy the new calorimeter trigger up-
4649 grade design must significantly improve the efficiency and rejection ability of the Level-1 trig-
4650 ger algorithms. This is done by:

- 4651 • Increasing the granularity of the calorimeter trigger *internal* processing. Due to lim-
4652 itations in the bandwidth and processing technologies available at the time of its

construction, the calculations of the present calorimeter trigger do not completely exploit the full (0.087×0.087 in $\eta \times \phi$) granularity of the ECAL and HCAL trigger towers transmitted to its inputs. The design of the upgrade calorimeter trigger completely exploits the full granularity of the ECAL and HCAL trigger towers in its calculations which enables improved algorithms that assure good performance up to twice the design luminosity or occupancy.

- Using the greatly increased flexible processing power in the new generation of FPGAs to implement sophisticated cluster algorithms that exploit the full trigger tower granularity. The raw trigger data can then be pre-clustered and the clusters then form the input to all calorimeter trigger algorithms. This improves dramatically the transverse energy resolution of the trigger output objects (Electrons, Jets, Transverse Energy Sums) and therefore makes the trigger thresholds sharper. Furthermore it allows for improvements in the isolation calculations, which (as shown below) exploit the full tower granularity to produce about a factor of two reduction in the trigger rate for the same efficiency.
- Using state-of-the-art Telecom technology to support the increased bandwidth requirements imposed by the higher granularity of the trigger input data.
- Providing the option to further exploit the higher granularity for eventual matching with a Level-1 Tracking trigger in Phase 2. Since the found calorimeter objects are located with significantly higher spatial granularity (half-a-trigger-tower resolution), there is the opportunity to enable matching with the tracking system at the highest granularity possible to better control the rates.

7.2.2 Present Calorimeter Trigger System Overview

The upgrade Calorimeter Trigger will replace the existing Regional Calorimeter Trigger (RCT) and Global Calorimeter Trigger (GCT). As shown in Figure 7.2 the existing RCT receives Trigger Primitives (TPs) consisting of eight-bit energies and a data quality bit for each calorimeter tower ($0.087\eta \times 0.087\phi$) from the HCAL and ECAL Trigger Primitive Generators (TPGs). The TPGs of both ECAL and HCAL use the Synchronization and Link Board (SLB). The RCT uses the TPs to find e/γ candidates and calculate four-by-four tower regional calorimeter sums that are sent to the GCT for sorting, jet finding, and calculating global quantities such as missing E_T . The RCT hardware consists of one clock distribution crate and 18 double-sided crates containing custom boards, ASICs, and backplanes. The Global Calorimeter Trigger (GCT) consists of 6 Source Card crates which convert the data to optical and a main crate which performs the jet finding and sorting, e/γ candidate sorting and calculation of all transverse energy quantities.

7.2.3 Calorimeter Trigger Upgrade Algorithms

The Phase 1 upgrade Calorimeter Trigger algorithms are based on the existing input trigger-tower granularity of $0.087\eta \times 0.087\phi$. The upgrade calorimeter trigger algorithms start with a particle-level cluster finder that makes 2×2 tower cluster sums along with setting of $e\gamma$ -like or τ -like flags. The upgrade calorimeter trigger reduces the jet and missing energy trigger rates by clustering jets in multiples of 2×2 trigger towers: $6 \times 6, 8 \times 8, 10 \times 10$, with a sliding window that sums clusters of towers in one or two tower steps, and by the use of higher resolution scales with more precise geometry for missing energy.

The input information per tower consists of 8 bits of non-linear E_T information accompanied by a single feature bit determined from a fine grain analysis of the energy profile within the tower. For the ECAL, HCAL and HF, the feature bits indicate isolated electromagnetic energy,

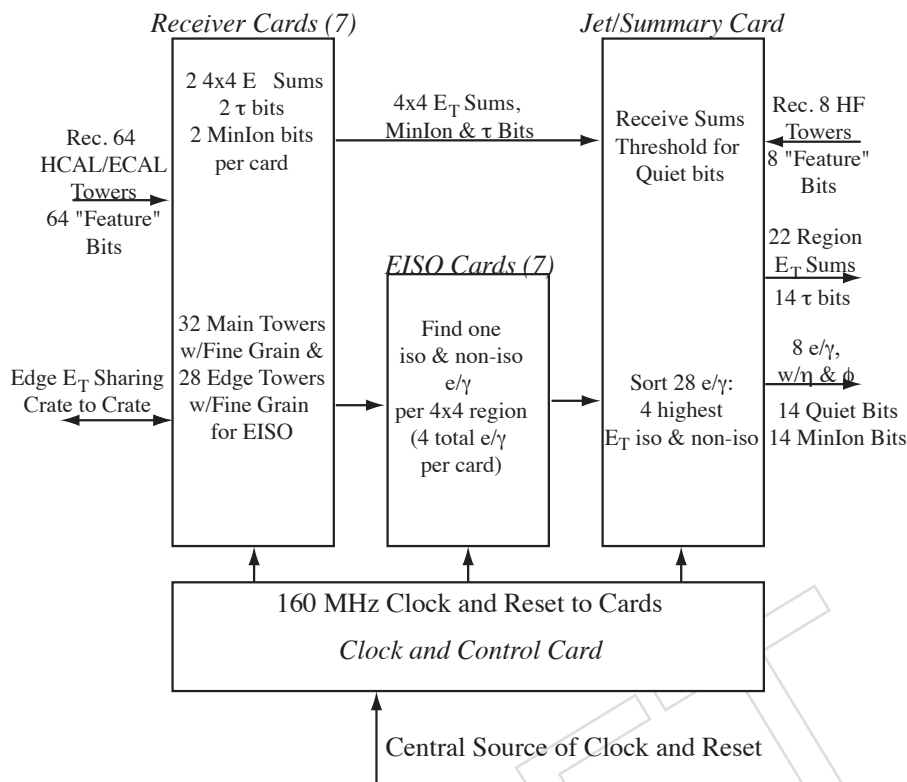


Figure 7.2: Schematic diagram of the present Regional Calorimeter Trigger data flow showing the trigger primitives entering from the calorimeters, the sharing of tower data between crates, processing for energy sums, jets, electrons and muons, followed by data transmission to the Global Calorimeter Trigger. Minlon refers to bits indicating the presence of a minimum ionizing particle; EISO refers to electron signals that are isolated from other nearby energy deposits; quiet means no energy present up to the threshold for minimum ionizing; Fine Grain refers to the bit set by the ECAL front end when the energy deposit in a 5×5 trigger tower of crystals is concentrated in one or two strips of 5 crystals; “Feature” refers to a single bit set in the HF indicating the energy in the trigger tower was concentrated in one or two HF cells.

4698 minimum ionizing energy, and energy concentrated in a single tower, respectively. The output
 4699 consists of the highest E_T objects in three categories: 4 electromagnetic objects, 4 τ objects
 4700 and 12 jet objects, ranked by E_T , plus a set of global event characteristics: missing transverse
 4701 energy (MET), total transverse energy (SumET), total jet transverse energy (HT) and missing
 4702 jet transverse energy (MHT).

4703 The algorithms create collections of isolated and non-isolated electromagnetic objects, isolated
 4704 and non-isolated τ objects and jet objects. The algorithms are organized in several steps with
 4705 progressive data reduction. These include a particle cluster finder that reconstructs overlap-
 4706 ping clusters of 2×2 calorimeter towers and applies electron identification, a cluster overlap
 4707 filter that removes overlaps between the clusters, locates local maxima and determines the
 4708 cluster position; a particle isolation determination, jet reconstruction, particle separation and
 4709 sorting that creates object collections sorted in E_T and passes on the highest E_T object in each
 4710 collection to next step in Level-1 trigger processing; and finally the calculation of MET, MHT,
 4711 and SumET from the cluster E_T values.

4712 An initial series of studies of the algorithm performance used fast simulation with pileup of

4713 25 inelastic interactions per crossing. We defined two configurations of software, the existing
 4714 CMS calorimeter trigger system and the upgraded calorimeter trigger. The initial simulation
 4715 results indicate a factor of four reduction in rate for improved efficiency, as shown in Figure
 4716 7.3. The output object location precision showing better than half-tower resolution is shown
 4717 in Figure 7.4. The improved performance of the calorimeter trigger stand-alone algorithms is
 4718 sufficient for Phase 1. This improved location precision will also be important for matching
 4719 with tracker trigger information in Phase 2.

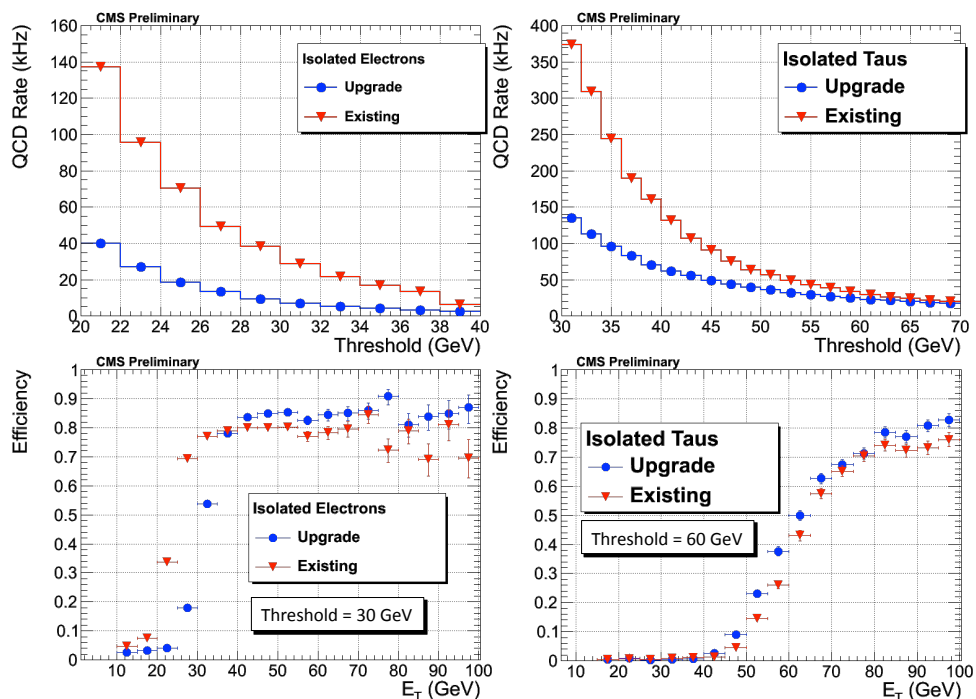


Figure 7.3: Integrated QCD trigger rate (kHz) for electron (top-left) and tau (top-right) triggers is plotted versus trigger E_T cut for the existing LHC and LHC Phase 1 Upgrade algorithms with improved clustering. Corresponding efficiencies for isolated electrons (bottom-left) and hadronically decaying taus (bottom-right) are also plotted for E_T thresholds of 30 and 60 GeV respectively.

4720 A sample Level-1 trigger table with thresholds and rates corresponding to 100 kHz total rate
 4721 dominated by QCD (EWK) are shown in Table 7.1 for the case of instantaneous luminosity of
 4722 $10^{34} \text{ cm}^{-2} \text{ s}^{-1}$ where an average of 25 pileup events are seen. The thresholds values represent
 4723 energies where there is 80% (75%) efficiency for the electron/photon (tau) object. The rates
 4724 corresponding to these thresholds for the existing and upgraded calorimeter trigger system are
 4725 shown. The total rate reduction is better than a factor of four. Note that the upgraded trigger
 4726 system has more parameters that can be tuned to keep the rate at an acceptable level.

4727 7.2.4 Calorimeter Trigger Upgrade Hardware Strategy

4728 The LHC Phase 1 Upgrade trigger hardware will be based on modern FPGAs instrumented
 4729 with fast Multi Gigabit Transceivers (MGTs) connected to optical links. The combination of
 4730 large and fast FPGAs with Multi-GB/s optical links represents a revolution in online comput-
 4731 ing and the signal processing industry. These state of the art devices combine very powerful
 4732 computing capabilities with a large number of fast links which concentrate and process data
 4733 very efficiently.

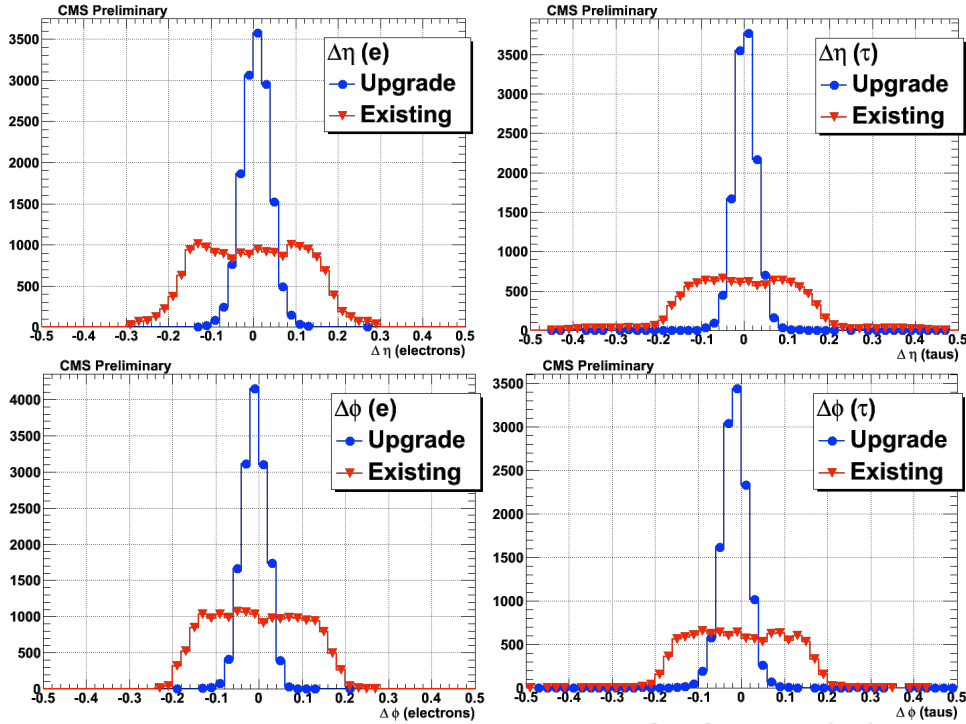


Figure 7.4: Position resolution of isolated electron, $\Delta\eta$, (top-left), $\Delta\phi$ (bottom-left) and hadronically decaying tau, $\Delta\eta$, (top-right), $\Delta\phi$ (bottom-right), for the existing LHC and LHC Phase 1 Upgrade algorithms with improved clustering, indicating better than half-tower resolution for the latter.

Trigger Object	Threshold (GeV)	Rate (kHz)	
		Existing CMS	Upgraded CMS
Single Photon	37	28	8
Double Photon	20	12	2
Single Electron	37	28	8
Double Electron	20	12	2
Single Tau	85	29	23
Double Tau	45	29	5

Table 7.1: A sample trigger table showing 80% (75% for τ) thresholds and rates which add up to 100 kHz at Level-1 for existing and upgraded CMS trigger systems.

4734 FPGA capabilities in speed and capacity almost double with each generation. The most powerful devices on the market at present are Virtex-5 devices which are instrumented with 32×6
 4735 GB/s MGTs. Devices operating at 10-12 GB/s should be available in the next two years. These
 4736 devices are ideal for all trigger algorithms and making the Level-1 Trigger (L1T) decision. Apart
 4737 from technological advantage, they address a chronic problem in trigger systems, namely lack
 4738 of standardisation. Speed requirements demand that L1T systems utilise custom electronics.
 4739 For this reason L1T systems have limited capabilities but focus on fast execution of specific
 4740 algorithms. They are adapted to the detector whose data they use and they are tuned for absolute
 4741 minimum requirements sufficient for the physics selection. Thus hardware developed for
 4742 muon triggers is not applicable for calorimeter triggers. The effect is that a trigger system consists
 4743 of many different designs and technologies, which makes development, maintenance and
 4744

4745 operation very slow and expensive. Many different pieces of hardware, software and firmware
4746 must be maintained by experts for the duration of the experimental programme, typically over
4747 ten years. The current CMS trigger system consists of at least one hundred different electronic
4748 cards, each requiring different maintenance, software and expertise.

4749 Due to technology advances this trend of specific hardware for specific tasks is no longer nec-
4750 essary. Large FPGA parts with vast computing resources are readily available at reasonable
4751 prices. Modern FPGAs can cater to very different detector and physics needs. The physics ap-
4752 plications are evident in the present CMS GCT where a complex system was designed quickly
4753 using essentially one processing board. This is capable, using suitable firmware, to execute all
4754 calorimeter trigger related algorithms, which range from electron sorting and missing trans-
4755 verse energy calculations to tau-jet finding. Thus, the use of different firmware on a single
4756 board type to service the various algorithm processing needs has already been demonstrated.
4757 While the opportunity to follow this strategy for the upgrade trigger does not justify the up-
4758 grade itself, its application to the upgrade will yield a more cost-efficient and easier to maintain
4759 system.

4760 **7.2.5 Calorimeter Trigger Upgrade Hardware Design**

4761 We propose to design the upgraded calorimeter trigger system based on FPGAs and Multi-
4762 GBit/sec links that adheres to the micro-TCA (μ TCA) crate Telecom standard. Details about
4763 this industry-standard platform can be found in [17]. It is compact, hot swappable, and has a
4764 high-speed serial backplane. The capability will be built in for an eventual Phase 2 combination
4765 of the calorimeter trigger with tracker trigger information to enable both track matching for
4766 electron and tau objects, and provide tracker based isolation for photons, electrons and τ s. The
4767 plan involves building the complete calorimeter trigger system based on high-speed optical
4768 interconnects and large FPGAs for data reception and processing.

4769 We envision the new calorimeter trigger system to comprise up to 10 crates with up to 12 cards
4770 each. The goal is that the trigger processing cards will be uploaded with different versions
4771 of firmware each performing different processing tasks in the system. We will develop a new
4772 optical transmission system, which will connect the present calorimeter to either a new optical
4773 link or the present copper cable connections to the ECAL and HCAL Trigger Primitive Genera-
4774 tion electronics and provide an additional output to connect to the upgrade calorimeter trigger
4775 so that both systems may be operated in parallel with physics data during a transition period.
4776 This can be done in a number of ways. As an example, a new optical Serial Link Board (oSLB)
4777 can replace the current SLBs on the HCAL and ECAL TPG electronics, and the current Receiver
4778 Mezzanine Card on the RCT Receiver Card.

4779 The proposed platform for the upgraded Calorimeter Trigger processing is an Advanced Mez-
4780 zanine Card (AMC)-style (μ TCA) module (148.8mm high by 181.5mm deep). We are evaluat-
4781 ing two possible architectures. One design uses three card types. The Input Cards will receive
4782 the TPGs and perform inter-region data sharing as needed. The Processing Cards will receive
4783 partial products from the Input Cards, perform second level sharing, complete the regional
4784 processing and deliver the output to the Summary Processing Cards that transmit their re-
4785 sults to the Global Trigger. The TTC/DAQ card interfaces the crate to the Trigger Timing and
4786 Control (TTC) and DAQ systems, including the Trigger Throttling System (TTS) that provides
4787 back-pressure from the DAQ.

4788 A block diagram of the above example of a new calorimeter trigger crate is shown in Figure
4789 7.5. A single crate encompasses the full η -width from -5 to +5, including the full Forward
4790 Calorimeter (HF) granularity. A custom backplane would contain a combination of passive

4791 and switched interconnections. The passive portion would be a good choice for the inter-crate
 4792 sharing in η and the switches allow for some routing between the Input and Processing Cards.

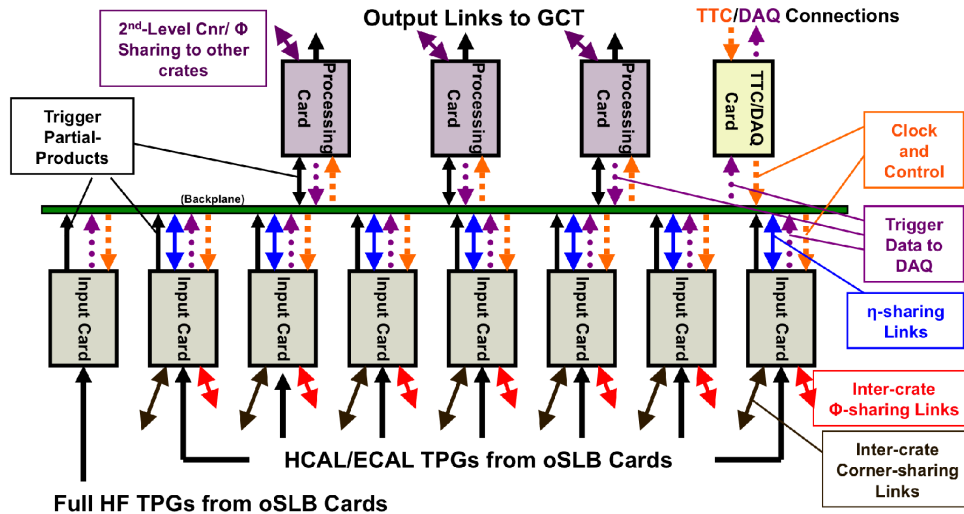


Figure 7.5: Block Diagram of an example of an upgrade RCT crate, showing cards and internal/external data flow. Eight Input cards will allow coverage in η from -5 to $+5$ and 30° in ϕ . Three Processing Cards would forward regional information to the GCT. A TTC/DAQ card would enable readout and handle Trigger Throttling System (TTS) interaction, receive the clock and control signals from the TTC system, and distribute these signals.

4793 In order to verify that the upgrade calorimeter algorithms are implementable, firmware is being
 4794 developed in Xilinx tools for these improved clustering and filtering algorithms with increased
 4795 position resolution. The initial indications are that about 8×16 trigger towers worth of information
 4796 can be processed in a single Virtex 5 FPGA using a good fraction of its 6.5 Gbps GTX
 4797 multi-gigabit transceivers and 50% of the available logic. The processing can be done at or
 4798 above 200 MHz with a latency of 185 ns, which would keep this processing well within the
 4799 latency envelope of the present RCT calculations.

4800 An alternative architecture, the Time Multiplexed Trigger (TMT), is also under evaluation. In
 4801 a TMT data from a single bunch crossing (bx) are concatenated and delivered to a process-
 4802 ing system over several bx. This approach requires several processing systems operating in a
 4803 round-robin scheduling manner (i.e. processing system 1, takes $bx = n$, processing system 2,
 4804 takes $bx = n+1$). The alternative architecture currently includes 10 of these processing systems.

4805 An example of the TMT architecture is shown in Figure 7.6. Main Processor (MP) nodes are
 4806 split across two cards (MP+ and MP- for $\pm\eta$). There are 10 of these MP nodes operating in
 4807 a round robin scheduling manner, each only receiving data for every tenth bunch crossing.
 4808 The two cards receive a single 9.6Gb/s link from each Pre Processor card in their respective
 4809 η half. They also receive 4 links from the 4 adjacent towers in the opposite η half so that they
 4810 have sufficient boundary information to build physics objects at the boundary between the two
 4811 processing nodes.

4812 The TMT Pre-Processor (PP) cards, that span the barrel and endcap, each receive ECAL and
 4813 HCAL data in a ring that is 1 tower wide in η and spans the full ϕ circumference. The lack of
 4814 ECAL data in the HF region enables these rings to be 2 towers wide in η . This requires 2×28
 4815 cards for the barrel and endcap and a further 2×28 for the HF and thus 72 PP cards and 92
 4816 cards in total. The total number of cards can be reduced to 56 if the calorimeter link speeds are

4817 increased from 2.4 Gb/s to 4.8 Gb/s.

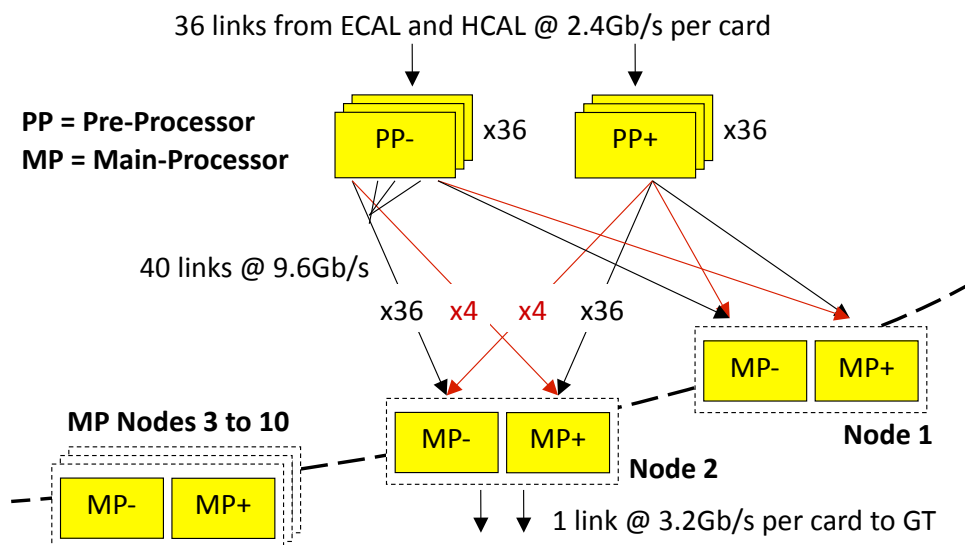


Figure 7.6: Time Multiplexed Trigger Architecture.

4818 The construction of the upgrade calorimeter also offers the opportunity, so far realized for only
 4819 the ECAL, to apply a global calorimeter selective readout of both ECAL and HCAL using in-
 4820 formation from both ECAL and HCAL. This feature would enable the full-granularity readout
 4821 of regions of the calorimeter with significant energy deposits and a more sparse readout of re-
 4822 gions with minimal activity. This can be incorporated into the calorimeter trigger logic where
 4823 energies from the ECAL and HCAL are summed and then processed by dedicated logic for
 4824 transmission to the readout logic of the HCAL and ECAL.

4825 7.2.6 Calorimeter Trigger Upgrade Hardware Demonstrators

4826 The first step towards building the upgrade calorimeter trigger is to connect a number of μ TCA
 4827 prototype boards utilizing their configurable links according to a given architecture and build
 4828 demonstrators for the Level-1 Triggers. The upgrade calorimeter trigger hardware technology
 4829 has been validated through a successful program of hardware demonstrators based on μ TCA
 4830 modules and Xilinx Virtex FPGAs. Researchers at Imperial College London have built and
 4831 tested a series of calorimeter trigger processing cards in order to evaluate the feasibility of the
 4832 TMT architecture, gain experience in the latest technologies (e.g. MicroTCA) and develop the
 4833 core firmware and software blocks that are common to both a TMT and conventional design.
 4834 A double width, full height AMC card, MINI-T5, was designed, manufactured, tested and a
 4835 TMT electron algorithm was implemented. The results show that the TMT design is consis-
 4836 tent with the latency budget and the logic resources of a pipelined algorithm are, as expected,
 4837 small. Researchers at University of Wisconsin Madison have built four trigger prototype cards
 4838 integrated in a backplane fabric to demonstrate the running and data exchange of calorimeter
 4839 trigger algorithms. Figure 7.7 shows photographs of these demonstrators.

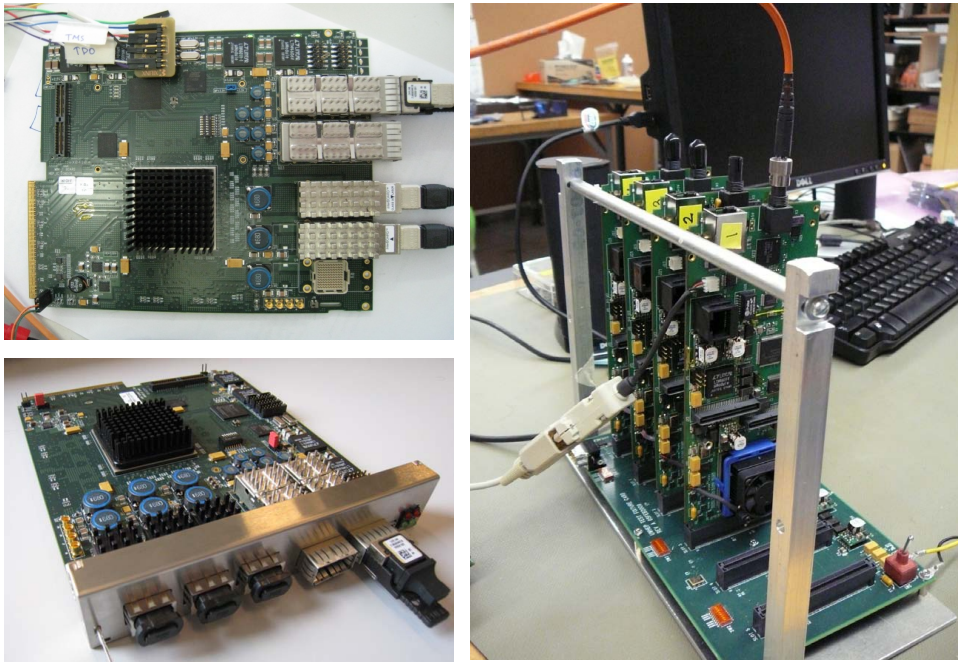


Figure 7.7: Photographs of modules built for the upgrade calorimeter trigger demonstrator program. Left: two of the Imperial College calorimeter trigger processing cards; Right: four of the University of Wisconsin calorimeter trigger algorithm test cards mounted on a test backplane fabric.

4840 7.3 Muon Trigger

4841 7.3.1 Introduction

4842 Increased luminosity also results in several issues for the Muon Trigger. The single muon trig-
 4843 ger rates as a function of the p_T threshold are shown in Figure 7.8 for LHC design luminosity
 4844 ($10^{34}\text{cm}^{-2}\text{s}^{-1}$). The rates are shown separately for Level-1 (L1 Trigger information only), Level-
 4845 2 (HLT reconstruction using full-resolution muon system data only, with isolation calculated
 4846 from full-resolution calorimeter data), and Level-3 (HLT track momentum and isolation calcu-
 4847 lated from silicon strip and pixel tracking data), with and without isolation applied at Levels 2
 4848 and 3. Also shown is the single muon rate predicted by the event generator. A threshold of 31
 4849 GeV/c reduces the single-muon Level-3 rate to 50 Hz with isolation (100 Hz without isolation).

4850 In Figure 7.8 the Level-2 rates have a reasonable reduction with increasing muon p_T cut up to 20
 4851 GeV/c, where the rate is 200 Hz. Above a p_T of 20 GeV/c, the reduction of rate with increasing
 4852 muon p_T cut is very slow, dropping only a factor of 2 with an increase in p_T cut up to 60 GeV/c.
 4853 Therefore if we bring the full power of the Level-2 algorithm performance (without tracking) to
 4854 bear in Level-1, above a p_T threshold of 20 GeV/c the only effective method to reduce the rate
 4855 with increasing threshold is to use Level-3 algorithms, which involve tracking. This motivates
 4856 examining the eventual use of tracking information in the LHC Phase 2 Upgrade L1 trigger.

4857 7.3.2 Present Muon Trigger System Overview

4858 7.3.2.1 DT Track Finder

4859 The Drift Tube Track Finder (DTTF) identifies muon candidates in the barrel muon detector
 4860 and determines their transverse momenta, position and quality. The candidates are then sorted

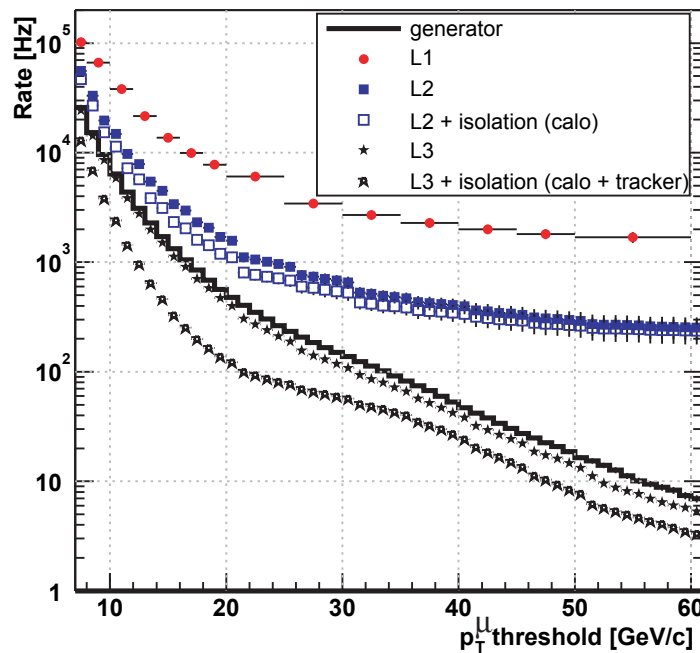


Figure 7.8: The HLT single-muon trigger rates as a function of the p_T threshold for a luminosity of $10^{34} \text{cm}^{-2} \text{s}^{-1}$. The rates are shown separately for Level-1, Level-2, and Level-3, with and without isolation applied at Levels 2 and 3. The rate generated in the simulation is also shown[18].

4861 by rank (based on p_T and number of hits) by dedicated cards and the highest four are sent to
 4862 the Global Muon Trigger. The track finding principle relies on extrapolation from a source track
 4863 segment in one muon station to a possible target segment in another station according to a pre-
 4864 calculated trajectory originating at the vertex. Target segments compatible with the expected
 4865 extrapolation position and bending are linked to the source segment. Compatible segments
 4866 form a track, to which a transverse momentum is assigned.

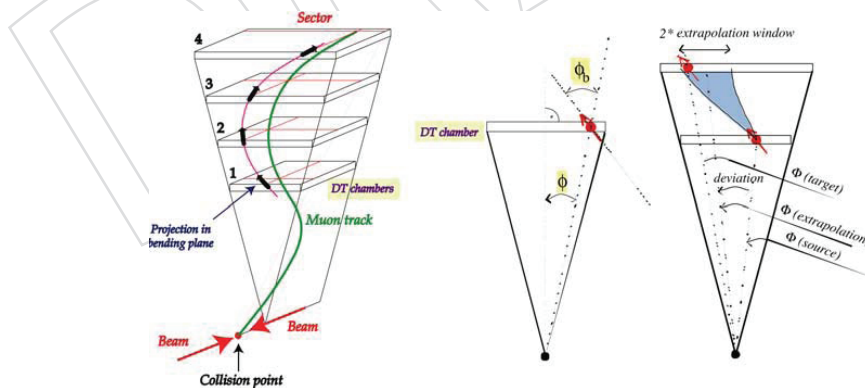


Figure 7.9: DTFE extrapolation scheme

4867 The extrapolation principle is shown in Figure 7.9. The DTFE operates in the $r - \phi$ -projection.
 4868 A coarse assignment of η is nevertheless possible by determining which chambers were crossed
 4869 by the track. The DTFE works on sectors and wedges. The DT system is divided into twelve
 4870 30° wedges in ϕ . Each wedge is divided into six sectors in z . The central wheel is split into
 4871 2×12 half-width sectors, while the four outer wheels are each subdivided into 12 full-width

sectors. Every sector contains four DT chambers. The track finding is performed by 72 sector processors. Each sector processor receives at most two track segments per chamber from the DT local trigger (the Sector Collector card) through optical links. Each segment is described by its position in the sector local frame (12 bits), bending angle (9 bits), quality code (3 bits) and θ information (16 bits). The sector processors attempt to join track segments to form complete tracks. The parameters of all compatible segments are pre-calculated. Extrapolation windows, which are adjustable, are stored in look-up tables. Muon tracks can cross sector boundaries, so data are exchanged between sector processors. A cancellation scheme is incorporated to avoid duplicated tracks.

7.3.2.2 RPC Trigger System

An overview of the present RPC trigger system is shown in Figure 7.10. The analog strip signals are discriminated and formed into 100 ns binary pulses at the 7200 Front End Boards (FEBs) placed on the chambers (Figure 7.10). The signals are sent from FEBs in the LVDS standard through copper cables to Link Boards (LB). The LBs (1232 boards) are located around the detector (in the CMS cavern). The LB electronics synchronizes the signals with the clock provided by the TTC and compresses the data (zero suppression). The data from two Slave LBs are transmitted to the Master LB. The Master LB multiplexes the data from Slave LBs and from itself and converts them into optical signals (1.6 GHz) transmitted through a fiber to the Trigger Boards (TB) located in the Counting Room. In total there are 444 fibers varying in length from 20 to 80m. Since the data from every optical link has to be delivered to two or four TBs, the links are split by Splitter Boards (SpB, 60 pieces).

Each of 84 Trigger Boards receives signals from up to 18 links. On the TB the data are distributed through the OPTO Receiver FPGAs (6 chips on each TB) to the PAC FPGAs (3 or 4 chips on each TB, placed on the mezzanines; each PAC receives data from all links). The PACs execute the trigger algorithm based on the Pattern Comparator (PAC) strategy: the chamber hits are compared with predefined patterns of muon tracks obtained from simulations, the coincidence of hits in the same BX in at least 3 layers of chambers is required. In total about 110K RPC strip signals are compared with more than 2 million patterns in every BX across the entire system.

The muon candidates found by PACs are transmitted to the GBSORT chip. Since the PAC algorithm is performed for segments of the detector that overlap, the same muon can be found by several segments. Therefore, in the GBSORT, the muon candidates from neighbouring segments are suppressed (ghost-buster algorithm). Then remaining candidates are sorted according to their quality. Since the amount of data that has to be transmitted on the TB is large (432 bits per BX from six OPTOs to every PAC, then 432 bits from four PACs to the GBSORT), to reduce number of paths on the board the data are transmitted with fast LVDS lines with frequency of 320 MHz (i.e. one line transmits 8 bits during one BX).

The muon candidates returned by the GBSORT are further processed at the next levels of the ghost-busters and sorters tree: on the custom backplane of the Trigger Crate (TC GBSORT) containing the TBs, and then on the Half Sorter Boards (HSB) and Final Sorter Board (FSB) located in the Sorter Crate (SC). From FSB, up to 8 highest momentum muon candidates are sent to the Global Muon Trigger (GMT) every BX.

7.3.2.3 CSC Track Finder

The task of the CSC Track-Finder (CSCTF) is to reconstruct muon tracks in the CSC endcap muon system and to measure the transverse momentum (p_T), the azimuthal angle (φ), and

4935 purpose of regional track finding. Thus, 12 SP identify the three best muons (if present) in each
 4936 60° azimuthal sector. Each processor is a 9U VME card housed in a crate in the underground
 4937 counting room of CMS. Each SP receives its data from MPCs resident in separate crates of the
 4938 periphery of the CMS endcaps. The MPCs collect track segments from up to nine CSCs.

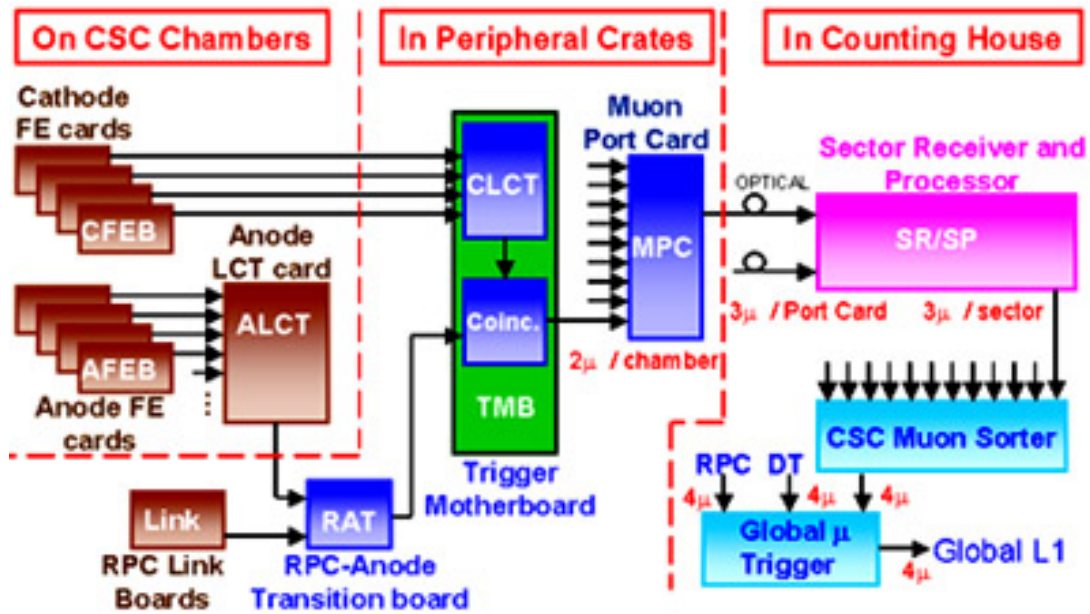


Figure 7.11: Schematic diagram of the CSCTF data flow.

4939 A maximum of six track segments are delivered to an SP from the first muon station (ME1) of a
 4940 sector. These track segments arrive from three MPCs, each delivering up to two track segments
 4941 in a 20° subsector. For the other muon stations (ME2-ME4), one MPC per station delivers three
 4942 track segments. In addition, up to four track segments from the barrel DT muon system are
 4943 propagated to a transition board in the back of the crate and delivered to each SP as well.
 4944 The output of the Track-Finder consists of the four best-identified muons together with their
 4945 kinematic and quality descriptions. These are sorted by the Muon Sorter and then transmitted
 4946 to the Global Muon Trigger (GMT). In the region near $\eta \sim 1$, the CSC and DT systems overlap
 4947 and their respective Track-Finders exchange information to make composite tracks.

4948 7.3.2.4 Global Muon Trigger System

4949 The Global Muon Trigger sorts the RPC, DT and CSC muon tracks, converts these tracks into
 4950 the same η , ϕ and p_T scale, and validates the muon sign. It then attempts to correlate the CSC
 4951 and DT tracks with the RPC tracks. The final ensemble of muons is sorted based on initial
 4952 quality (e.g. number of stations included in the track), correlation and p_T and then the 4 top
 4953 muons are sent to the Global Trigger.

4954 7.3.3 DT Trigger Issues and Upgrade

4955 The highest priority in the design of the current DT Track Finder system was minimizing trigger
 4956 latency. This required adopting specialized fast data transmission and processing techniques
 4957 in the design. The adopted techniques have been found disadvantageous for production and
 4958 maintenance, as experienced during trigger operation.

4959 One of the critical issues for maintenance and operations is the data exchange between sec-
 4960 tors. A DTTF basic unit processes data from one of the 72 available sectors of the CMS barrel

4961 muon detector. The DTF input data are transmitted serially through optical links from Sector
4962 Collector cards to the DTF system, where they are decoded and processed. The Sector Collec-
4963 tor cards are located on the CMS detector, and the DTF crate is located in the Underground
4964 Counting Room (USC). To minimize latency, once received, the input data are always treated
4965 as a bit-parallel data stream forwarded on wide data paths. In order to reconstruct muons
4966 crossing sector boundaries, connections need to be made not only to the neighboring units in
4967 φ , but also the neighboring unit in z . The z connections between DTF units are done through
4968 the backplane, but the φ connections are implemented with high density flat cables due to me-
4969chanical constraints on the backplane. This resulted in highly complex and error prone cabling.
4970 The complexity of the connections makes error detection and maintenance work very difficult.

4971 Data transfer requirements put further constraints on the flat cable. On one hand, the trans-
4972 mission has to be completed in 25 ns, which sets the upper limit on its length. On the other
4973 hand, the mechanical arrangement inside the DTF crate dictates its minimum length. The
4974 cable length has been designed to fulfill these constraints, but detector operations show seri-
4975 ous problems with this design. Tests demonstrated that the present data transmission timing
4976 works at the physical limits. In addition, the noisy environment makes it difficult to establish
4977 an optimal data transmission.

4978 7.3.3.1 Considerations for DTF Redesign

4979 The biggest motivation for a DTF Upgrade is to eliminate drawbacks of the present design.
4980 Staying within trigger latency requirements with the available technology turned out to be
4981 more limiting than originally estimated. Faster FPGAs developed in the recent years allow
4982 more flexibility in distributing tasks. The possibility to re-prioritize permits the development
4983 of a new DTF design that addresses most present problems.

4984 Several DTF upgrade approaches are considered. Each approach results in different system
4985 structures and requires different levels of changes. For all possible solutions, their technical
4986 feasibility and their impact on system performance will be investigated. The standard VME
4987 bus is subject to early obsolescence and there are CMS-wide efforts to find new standards. The
4988 μ TCA system is considered the standard for most future developments. This standard offers
4989 high speed interconnects between boards and a fast, centralized control scheme. These qualities
4990 coincide very well with the needs of the DTF system. Furthermore, we plan to investigate if
4991 fast interconnects or an extended JTAG structure for internal control and monitoring can be
4992 implemented more efficiently. The different upgrade schemes are depicted in Figure 7.12.

4993 On the Trigger Primitive side, the Sector Collector (SC) electronics will be moved off the detec-
4994 tor and into the underground counting room. This increases the flexibility of the new system.
4995 Moving the SC into the counting room provides more headroom in the latency budget, allow-
4996 ing a more generous design of the system-wide data flow. If the SC and the optical receiver are
4997 integrated, the double optical \rightarrow copper, copper \rightarrow optical transformation is omitted.

4998 The biggest problem in the present design is the complexity of the Trigger Object distribution
4999 among the Track Finder boards. There are several possible solutions available to achieve a more
5000 “streamlined” system. All these solutions have a common point: the connections must use fast
5001 serial data transfer instead of the wide parallel data connections. This will help increase the
5002 signal quality and reliability, while simplifying data verification, monitoring and maintenance.
5003 There is no feasible solution to change or extend the present DTF hardware design towards
5004 fast serial links because the entire electronics construction was designed around the required
5005 parallel connections.

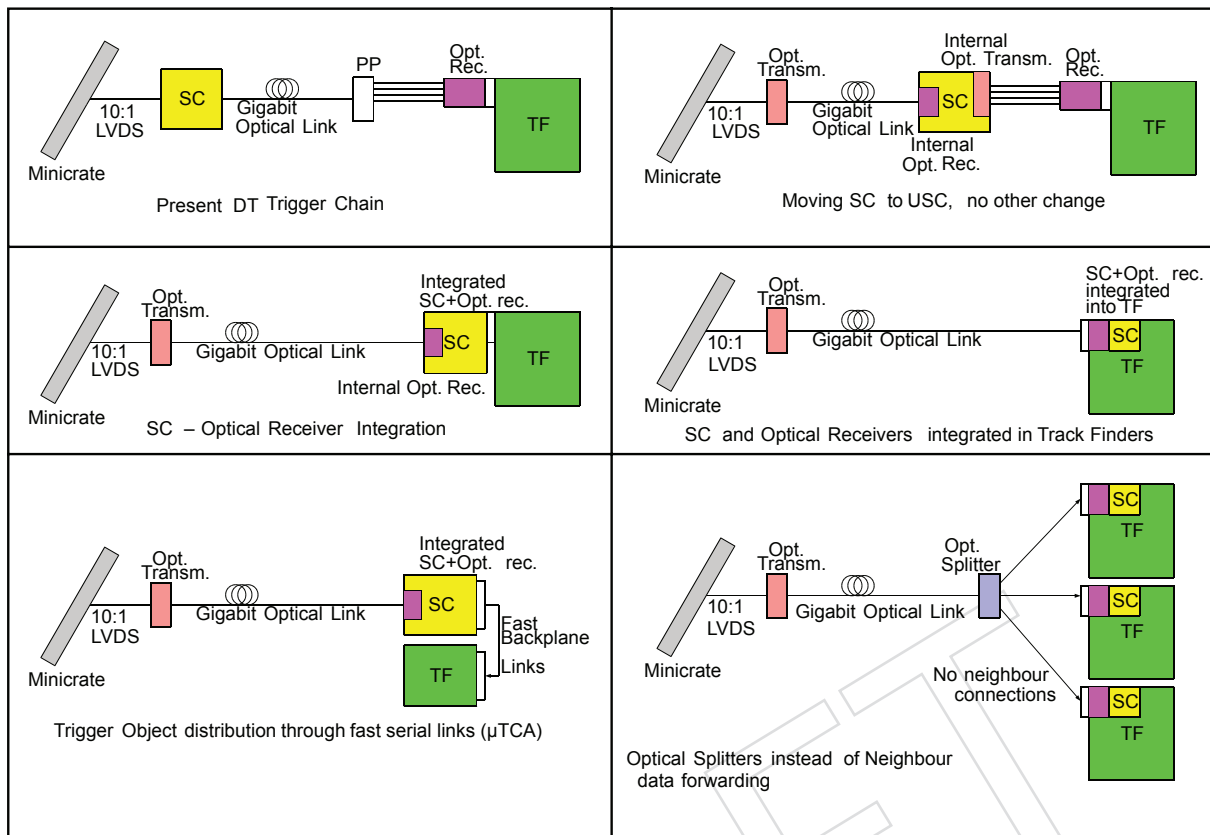


Figure 7.12: Possible layouts for the upgraded DT trigger scheme.

5006 Conceptually, the simplest upgrade strategy is to keep the same data flow design of the DTTF
 5007 system, but replace neighbour connections by fast optical links. This would require redesigning
 5008 and rebuilding the TF boards; the number of boards would not change. The resulting system
 5009 would have the same complexity and roughly the same cost as the present system. It would
 5010 also not address the problems of the obsolete VME standard.

5011 Another option being considered is an integration of DTTF and TSC functions. The upgraded
 5012 DTTF could include the Optical Receivers and the SC functions. This solution would allow
 5013 integration of TF processors for several sectors on a single board, decreasing the system size
 5014 (number of boards, number of crates). The neighbour data exchange can be achieved using
 5015 high speed optical links. This solution can not be implemented with the present backplane and
 5016 crate structure. The possible integration of the Track Finding functions of several sectors into
 5017 one board decreases the number of boards and thus crates.

5018 A third option is to eliminate neighbour connections, but distribute the input data using opti-
 5019 cal splitters. In this design, all TF parts receive all information they use directly from the DT
 5020 minicrate format. This also means the TSC functions would be multiplied for all inputs receiv-
 5021 ing optical links. The benefits and drawbacks of this solution must be clarified in a feasibility
 5022 study.

5023 7.3.3.2 System Layout

5024 The most straightforward upgrade solutions foresee merging the TF functions of several sectors
 5025 on one single electronics board. This merging task can be performed in several ways. Detailed
 5026 studies of different options will be performed in the context of a Feasibility Report that can be

5027 part of the future Upgrade TDR.

5028 7.3.3.3 Demonstrators

5029 In order to develop firmware for the upgrade, a demonstrator system must be built. Depend-
5030 ing on the choice of system layout, this can be constructed on the present DTF Prototypes or
5031 rather using a μ TCA system. Demonstrator tests will determine the capacity of the fast serial
5032 connections, speed and bandwidth margins within a real hardware environment. Parallel de-
5033 velopments should be avoided. Developments for the CMS Global Trigger and Calorimeter
5034 Trigger Upgrades should be taken into account; only hardware whose functionality cannot be
5035 achieved with the existing boards will be developed.

5036 7.3.4 RPC Trigger Issues and Upgrade

5037 The CMS RPC system is designed for highly efficient detection of muons with precise timing
5038 over the entire active area of the CMS detector. In order to save costs for the low luminosity
5039 detector, the CMS collaboration reduced the number of layers in the forward RPC system from
5040 4 to 3 and the coverage in η from 2.1 to 1.6. The restoration of this original scope forms the
5041 two upgrades of the RPC trigger system. The first upgrade is adding station 4 for $|\eta| < 1.6$.
5042 This upgrade is trivial from the trigger point of view. The system is ready to include station 4,
5043 as soon as chambers and missing parts of the link system are available. The second upgrade
5044 extends the RPC coverage to $|\eta| < 2.1$. This requires that additional chambers be added to the
5045 detector. For the trigger, the upgrade requires building additional copies of the existing trigger
5046 boards. Roughly 20% additional boards need to be added. The fourth endcap plane upgrade is
5047 proposed for 2012-2013, and the expansion to $|\eta| < 2.1$ for 2016.

5048 As the LHC approaches its design luminosity, the restoration to 4 layers of RPC in the forward
5049 direction will provide a substantial improvement in efficiency since CMS can require 3 planes
5050 out of 4 in coincidence instead of requiring 3 out of 3. The exact amount of rate improvement
5051 depends on the details of noise, neutron flux and charge particle flux. The increase in η cov-
5052 erage from 1.6 to 2.1 increases the discovery reach for new physics by increasing the available
5053 geometrical acceptance for muons by 31%. This η region also has the maximum muon bend-
5054 ing power in the CMS endcaps, providing additional measurement power beyond the gain in
5055 acceptance. The present RPC system is built so that the additional RPCs are able to be installed
5056 in a straightforward manner. There are well-understood plans to incorporate additional planes
5057 into the trigger logic. There are additional on-detector Link Boxes that would be placed in re-
5058 served locations which would then connect to additional boards in provided locations in the
5059 trigger logic crates. Two additional trigger boards would be required for each of the 12 RPC
5060 trigger crates for a total of 24 plus spares. One additional Data Concentrator Card (DCC) would
5061 be needed to complement the present three. Since the RPC system uses the ECAL DCC, this is
5062 straightforward.

5063 One possibility is the option of populating the forward region of η from 2.1 to 1.6 with more
5064 advanced gaseous detectors, which could be able to cope with high particle rates and hence
5065 provide CMS with enhanced physics performance at the highest luminosities. Micro-Pattern
5066 Gas Detectors (MPGDs) are being explored for the upgrade of the forward part of the muon
5067 system, as they can provide precision tracking and fast trigger information simultaneously,
5068 and they can be designed with sufficiently fine segmentation to cope with the high particle
5069 rates expected at LHC and its upgrades. If these detectors are used in place of the RPCs in
5070 this region, there would be further changes required in the RPC trigger system. In order to
5071 minimize these changes, the data produced by the MPGDs would be transmitted in a format
5072 identical to that of the RPC data. Nevertheless, due to the higher granularity and therefore

5073 greater volume of the MPGD data, two additional TBs would be required for each of the 12
5074 crates for a total of 48 instead of 24. In addition, the existing 12 TB crate backplanes would need
5075 to be extended to connect to the additional TBs. These 12 new backplanes plus spares would
5076 need to be manufactured and tested for the upgraded system if MicroPattern Gas Detectors
5077 (MPGDs) were selected. The Trigger Boards themselves as they presently exist should be able
5078 to handle the extra patterns since for the upgrade the focus is on high p_T muons whose straight
5079 tracks do not create as many additional patterns as low- p_T tracks.

5080 7.3.5 CSC Trigger Issues and Upgrade

5081 Detailed studies of the performance of the muon detector system upgrade are documented in
5082 Chapter 3. One of the key findings, shown again in Figure 7.13 is the importance of completing
5083 the coverage of the CSC detector to control trigger rates. The projected rate for a trigger thresh-
5084 old of 20 GeV/ c drops from 60 to 20 kHz. From the CSCTF point of view, the improvement
5085 is due to the better resolution of the muon momentum measurement. Due to excellent shield-
5086 ing, the CSC system seldom reconstructs fake muons. The rate is driven by resolution effects,
5087 namely promotion of soft muons to high momenta by mis-reconstruction. Since the magnetic
5088 field is weak between stations 3 and 4, the reasoning for adding station ME4/2 to improve
5089 resolution is not completely intuitive.

5090 Lacking ME4/2 coverage in the muon system, we cannot require LCTs in three muon stations
5091 without compromising efficiency. A two-LCT muon trajectory (CSC 2/3) uses three spatial
5092 measurements to fit the trajectory: the beam spot and the two LCT positions. This is not an
5093 over-constrained fit. Mis-matching a real muon LCT with a punchthrough LCT will cause
5094 the muon momentum to be randomly mis-measured. The trigger system, by construction,
5095 always keeps the highest momentum muon candidate. The highest momentum muon can be
5096 a mis-reconstructed combination of real muon and punch-through, thus promoting the event
5097 above trigger threshold. A three-LCT trajectory (CSC 3/4) is an over-constrained fit; wrong
5098 LCT combinations are rejected and therefore do not enter into the momentum fitting logic. So
5099 while the weaker field between stations 2,3 and 4 does not dramatically extend the fit lever
5100 arm, the third LCT “tags” the correct trajectory through the muon system. The significant rate
5101 increase from 20 to 60 kHz in Figure 7.13, shows that the loss of ME4/2 information cannot be
5102 compensated by the RPC trigger system.

5103 In the following, we discuss the expected impact of both the high luminosity environment and
5104 the CSC detector upgrades on the design of the upgraded CSC trigger.

5105 The occupancies of the Cathode Strip Chamber (CSC) system will increase with increasing lu-
5106 minosity. Detailed simulations of the occupancy of Local Charged Tracks (LCTs), which are
5107 the trigger primitives from the CSCs, indicate that due to prompt pile-up per Muon Port Card
5108 (MPC), approximately 0.05 LCTs per bunch crossing (BX) are expected for $2 \times 10^{34} \text{cm}^{-2} \text{s}^{-1}$,
5109 with large fluctuations at the level of 0.25. Therefore at 2σ , about 0.5 LCTs/BX must be accom-
5110 modated in bursts. Simulation results on the number of LCTs/BX from 400 prompt pile-up
5111 events ($10^{35} \text{cm}^{-2} \text{s}^{-1}$ with 50 ns bunch crossing) are shown in Figure 7.14.

5112 Additional LCT occupancy occurs from the neutron background, which is expected to grow
5113 faster than linearly with luminosity because of the limited penetration of the converted gamma
5114 rays (so that multiple random hits are needed to fire an LCT pattern). While highly uncer-
5115 tain until measured at the LHC, this background potentially can exceed the prompt pile-up
5116 background at the LHC Phase 1 Upgrade luminosities. Therefore, the MPC must be able to
5117 accommodate more than one background LCT per BX per sector, which exceeds the current
5118 CSC trigger design assuming that a dimuon signal must be captured at high efficiency in the

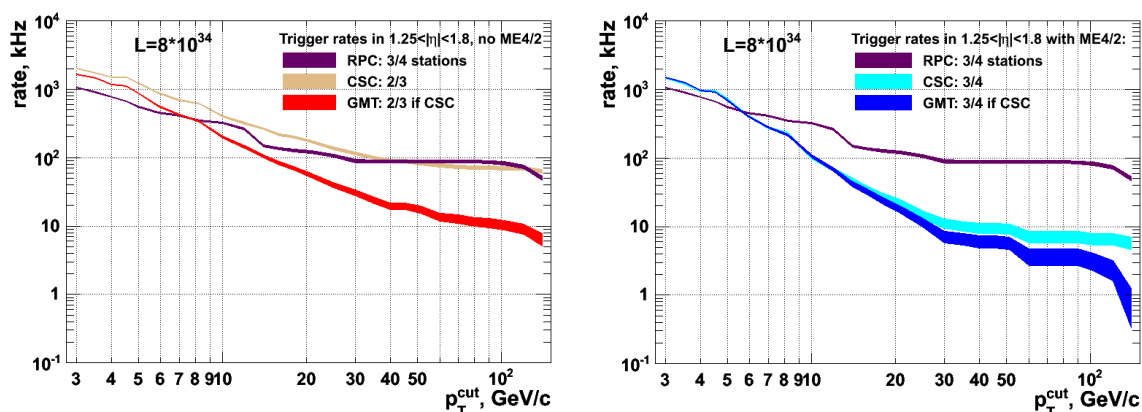


Figure 7.13: Simulated global muon trigger rates for $\mathcal{L} = 8 \times 10^{34} \text{cm}^{-2} \text{s}^{-1}$. The plot on the left (right) shows the trigger rates without (with) ME4/2 with the Global Muon Trigger requiring 2 out of 3 (3 out of 4) CSC planes on the track. The RPC curve shown corresponds to a configuration optimized for high efficiency and not for rate rejection. In this configuration, the CSC system with completed coverage drives the triggering rate. The muon trigger rates without full CSC coverage are significantly higher.

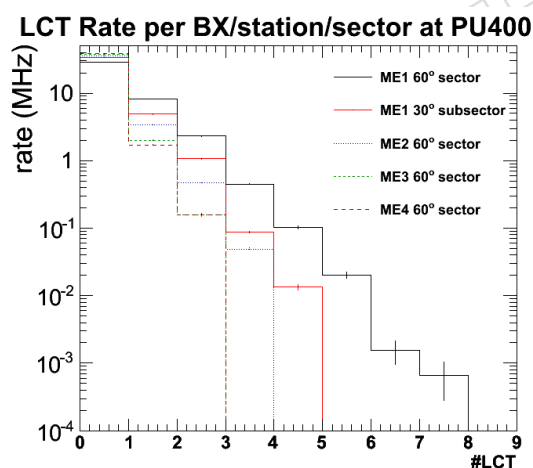


Figure 7.14: Number of LCTs per sector or relevant subsector expected for 400 prompt pile-up events, by station.

5119 sector covered by the MPC. Since we target a single upgrade capable also for handling Phase
 5120 2 occupancies, the MPC should be capable of delivering the full 18 LCTs/BX for each trigger
 5121 sector.

5122 Additionally, the CSC Trigger Motherboards connected to the ME1/1 chambers need to be re-
 5123 placed in order to expand triggering to include the region $\eta > 2.1$. This also will increase
 5124 the average number of LCTs sent to the MPC and transmitted to the Sector Processors. There-
 5125 fore, additional bandwidth is needed to transmit LCTs to the Track-Finder crate, and additional
 5126 processing logic will be required to identify and measure tracks in this higher occupancy envi-
 5127 ronment.

5128 The Muon Port Card (MPC) is a choke point in the CSC trigger path (designed that way to
 5129 reduce optical link costs for LHC). It sorts and filters up to 18 LCTs from 9 chambers in one

5130 60 degree sector for one station to a maximum of only 3 LCTs. Assuming 2 LCTs are from a
5131 dimuon signal, allowing 1 additional LCT for background is not enough for Phase 1 occupan-
5132 cies beyond $\mathcal{L} = 10^{34} \text{cm}^{-2}\text{s}^{-1}$. Moreover, triggering on ME1/1a (high η region) will add still
5133 additional LCTs for the MPCs residing in ME1 peripheral crates. Therefore, the MPC needs
5134 to be redesigned to allow more throughput with additional sorting logic in a larger FPGA to
5135 transmit more than three LCTs, and using upgraded optical links to minimize cabling and in-
5136 puts to the Sector Processors (already at a front-panel limit of 15 optical links). However, we
5137 must keep 3 optical links of the original type in addition to new links to maintain the existing
5138 CSCTF crate in parallel while commissioning the new one. This allows the new MPCs to act as
5139 an active splitter for the old and new Track-Finder crates. In total 60 Muon Port Cards must be
5140 replaced on the peripheral crates.

5141 The 12 Sector Processors in the CSC Track-Finder crate in the underground service cavern also
5142 must be upgraded to accept the higher number of LCTs per BX from each MPC for robust-
5143 ness against Phase 1 occupancy. The optical receivers must be upgraded to match the higher
5144 bandwidth MPC transmitters, and the logic space must be increased to handle the additional
5145 combinatorics in the track-finding algorithm. Moreover, a new scheme for applying the geom-
5146 etry conversion in the FPGA logic rather than in numerous external LUTs as presently must be
5147 developed given the higher occupancy (otherwise there are problems with board space occu-
5148 pied by the memory chips).

5149 The momentum resolution of the current CSCTF system is limited by the available onboard
5150 memory ($2 \text{ Mb} \times 16 \text{ bits}$). The purity of the CSC track finder muons is very high; rate control is
5151 mostly driven by the track finder resolution. In the last five years, faster, smaller and cheaper
5152 memory chips have become available, and it makes sense to revisit the momentum assignment
5153 algorithm. We plan to investigate what highest p_T resolution we can ultimately reach at Level
5154 1 by studying outputs of the offline standalone muon fit when using LCT coordinates as input.
5155 Should a significant improvement seem feasible, the next step is to understand what additional
5156 information or algorithm induces the strongest improvement to the momentum resolution.

5157 The upgrade to the CSC Track Finder crate ideally should only be done once, so it should meet
5158 the design requirements of Phase 2 even though it is deployed with Phase 1. In Phase 2, the key
5159 new component in the trigger chain is the matching of pixel and silicon strip tracking informa-
5160 tion to CSC tracks, allowing track confirmation, isolation, vertex-finding and improvement on
5161 momentum resolution. To accommodate this, refined position information from the CSC Track-
5162 Finder ($\eta \times \phi$) is needed to match to the pixel and/or strip hits. In the current LHC CSC trigger
5163 design, this information is only reported on a $(0.05 \times 2.5^\circ)$ granularity to the Global Muon Trig-
5164 ger for matching to calorimeter towers, although intrinsically the information is available on
5165 a much finer scale $(0.0125 \times 0.015^\circ)$. In order to use this fine scale resolution more bits will
5166 be needed to be transmitted from the Sector Processors to a new Muon Sorter for eventual
5167 combination with the silicon tracker $\eta \times \phi$ information.

5168 With finer information transmitted by the Sector Processors, the backplane and the Muon Sorter
5169 in the Track-Finder crate must be redesigned to accommodate the additional data transmission.
5170 Serialization of the data at frequencies higher than the current 80 MHz is necessary because the
5171 current Track Finder crate backplane design has utilized essentially already all available space
5172 for copper transmission lines. Therefore the Muon Sorter must be upgraded to handle the
5173 higher frequency transmission from the Sector Processors. It also needs the provision to send
5174 more than the current 4 CSC muons per BX to the Global Muon Trigger because of the higher
5175 occupancies which requires additional data lines in the output path.

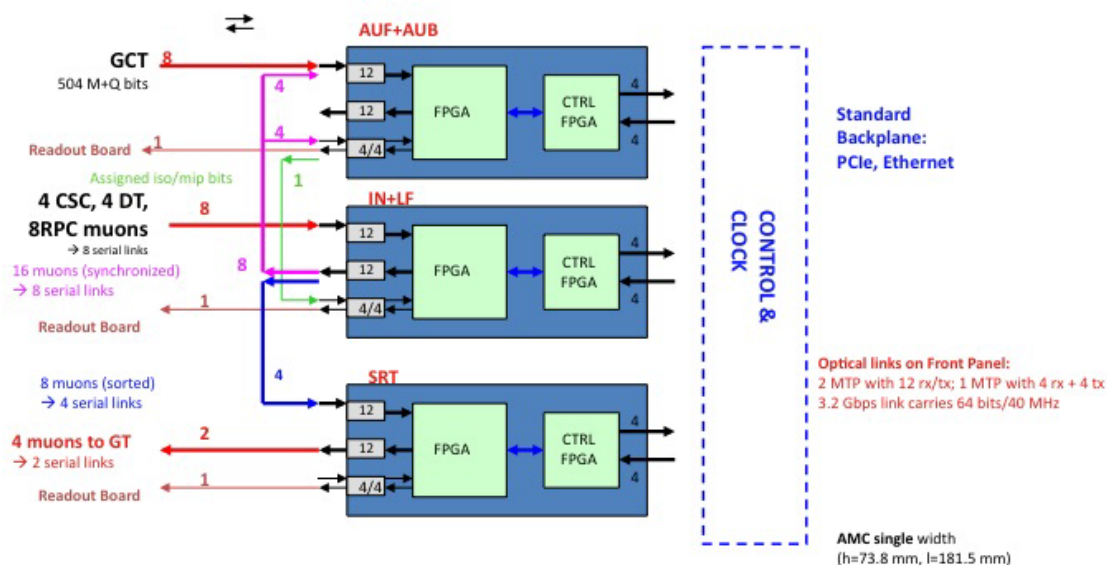


Figure 7.15: Global Muon Trigger.

7.3.6 Global Muon Trigger

5176

5177 As for the present GMT, the best muon candidates across the experiment must be determined.
 5178 For this purpose information from the three muon subsystems and the Global Calorimeter
 5179 Trigger is combined and analysed. The GMT combines the results of the muon subsystems
 5180 making use of the quality information associated with the tracks from the regional triggers.
 5181 The GMT generally forwards a candidate if it was seen by both RPC and DT/CSC system
 5182 regardless of quality. If the candidate was seen by only one system quality criteria are applied
 5183 to decide whether to forward it. Specific quality criteria can be applied depending on detector
 5184 types, detector regions and transverse momenta. The best candidates are sent to the Global
 5185 Trigger. The logic board will consist of a single width AMC module with a standard μ TCA
 5186 backplane (Figure 7.15).

7.4 Global Trigger and Central Trigger Control

5187

7.4.1 Global Trigger

5188

5189 The upgraded Global Trigger will be designed to have the same basic categories of functions
 5190 as the present GT, but will have more algorithms and more possibilities for combining trig-
 5191 ger objects and technical triggers (e.g. independent trigger signals from detectors that are not
 5192 combinable with other triggers):

- 5193 • Synchronizing all trigger objects to arrive at the same time at the logic chip;
- 5194 • Sending all trigger objects into one chip to make any correlation between them;
- 5195 • Using an FPGA to change trigger conditions as required by physics;
- 5196 • Calculating physics trigger algorithms in parallel (FPGA branch);
- 5197 • Performing a final OR mask for all algorithm bits;
- 5198 • Prescaler and Counter for each algorithm.

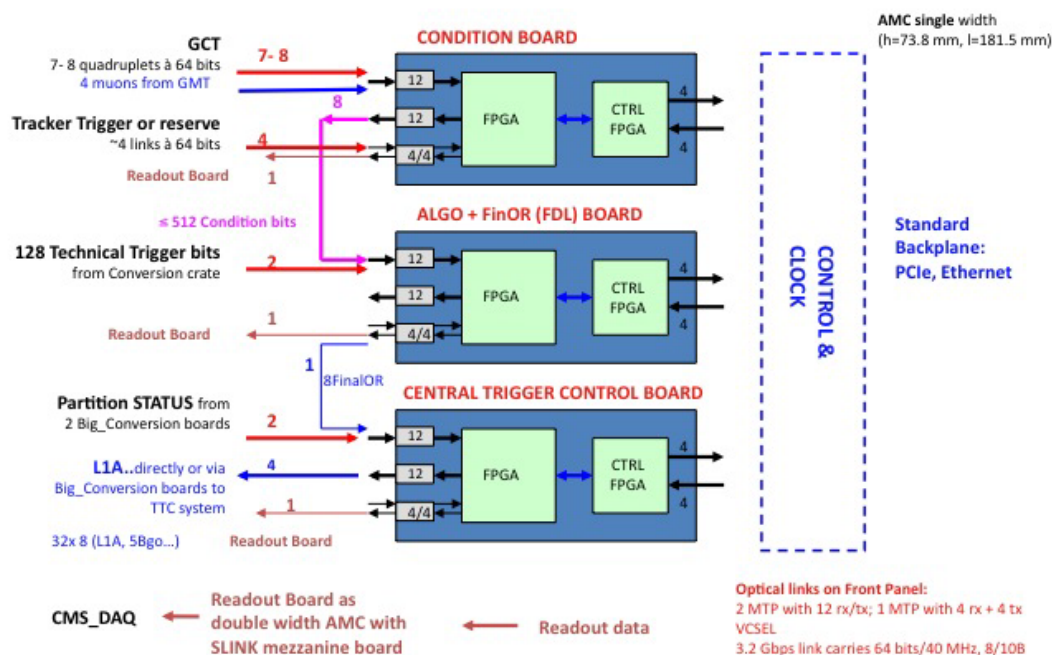


Figure 7.16: Upgrade Global Trigger Crate showing the inputs from the Global Calorimeter Trigger, provision for an eventual tracking trigger for Phase 2, and technical trigger bits from dedicated logic. Also shown are interfaces to the DAQ and TTC systems.

5199 The upgraded GT will be able to process at least double the present 128 algorithms and 64
 5200 technical triggers. It may use the DSP cores now available on the newer FPGAs for complex
 5201 triggers. These DSPs would enable firmware compilation of C++ code to produce triggers with
 5202 constant latency. Each trigger object of 64 bits at 40 MHz will be assigned one optical link. The
 5203 hardware will be realized in a single μ TCA crate with a standard backplane.

5204 The GT boards shown in Figure 7.16 will be single-width AMC modules. Apart from the con-
 5205 dition board and the combined algorithm/final OR board the central trigger control board (sec-
 5206 tion 7.4.2) is also housed in the GT crate. A second μ TCA crate contains all required conversion
 5207 boards connecting the Global Trigger and Central Trigger Control to the other trigger boards
 5208 and later to the final trigger electronics which sends or receives 40 MHz differential data.

5209 7.4.2 Central Trigger Control

5210 The Central Trigger Control system, as at present, will receive status information from the
 5211 Global Trigger processor, the detector partitions and the buffer emulators. It will transmit the
 5212 L1 accept signal to the partitions and provide other control signals. It will be housed in two
 5213 crates, the GT crate and a second crate called the Conversion Crate. The CTC module is located
 5214 in the GT crate. The Conversion Crate will contain six double width interface boards with the
 5215 functionality of the current GT Conversion Boards and L1AOUT modules that process the GT
 5216 signals. There will also be two boards receiving the technical triggers from other subdetectors.
 5217 It will have a standard backplane and carrier hub. Optical links provide the data transfer
 5218 between the two crates. Figure 7.17 shows the setup.

5219 For a gradual transition from the present VME-based trigger system we plan to mount a simple
 5220 9U interface board in the slot of the TCS board of the actual GT crate, which sends the current
 5221 eight final ORs, four GT status bits and the reset signal to the conversion crate. In the final
 5222 version an optical link will transfer them directly to the CTC board.

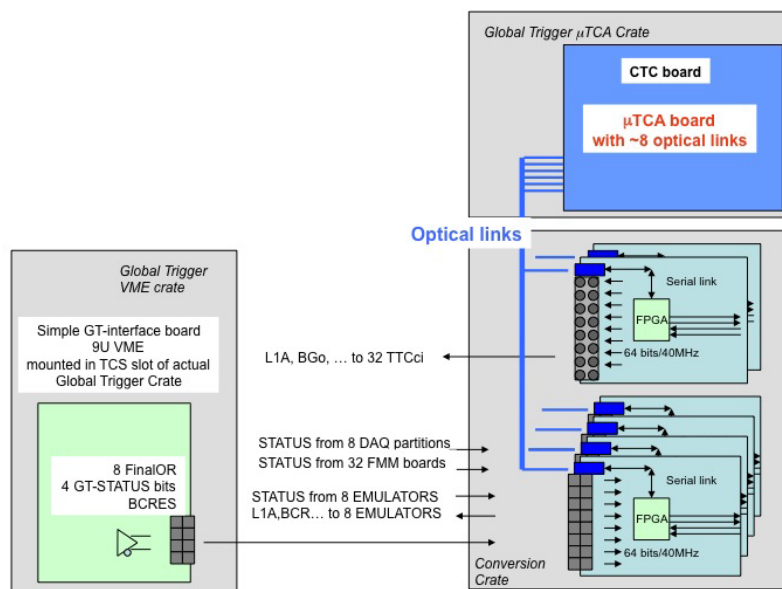


Figure 7.17: Central Trigger Control system with the interface to the current system.

7.5 Trigger Software

5223

5224 The current L1T system is supported by a large variety of software packages and components.
 5225 These include online software and drivers for the setup and monitoring of the trigger com-
 5226 ponents; diagnostic and monitoring packages for trigger tests; and offline software for trigger
 5227 hardware emulation and performance estimation. The overall software system is large and
 5228 complex, reflecting the nature of the hardware. Substantial effort is spent in maintaining and
 5229 adapting the trigger software. This effort is needed well beyond the end of hardware commis-
 5230 sioning, as it is essential for the maintenance and monitoring of trigger performance during
 5231 LHC running.

5232 As the trigger hardware moves towards the use of more similar hardware modules specialised
 5233 for different purposes, an upgraded software system is required to support this. An analogous
 5234 approach will be used, making use of a set of common software components specialised for
 5235 different functions. The key design goals for the new system are: maximum commonality
 5236 between the software supporting different hardware subsystems; maintainability through use
 5237 of common components and good software engineering practices; reduction of effort through
 5238 use of off-the-shelf libraries and drivers; and scalability, such that the same software approach
 5239 may be used for Phase 1 and subsequent upgrades.

5240 One key driver for the software upgrade is the adoption of ethernet-based control mechanisms
 5241 in the μ TCA hardware. This allows proprietary and/or custom hardware drivers to be re-
 5242 placed with standard network protocols using commodity hardware and standard OS drivers.
 5243 Examples of candidate network technologies for this control and/or local DAQ applications
 5244 are TCP/IP and Fibre Channel over Ethernet (FCoE).

5245 A candidate upgrade software architecture is under development. Central components of this
 5246 new architecture include:

- 5247 • Use of commodity GB/10GB ethernet switches and High Bandwidth Architectures
- 5248 (HBA) for high speed control and local DAQ.

- 5249 • Firmware and embedded CPU software for direct ethernet communication with FP-
5250 GAs, implementing a simple common protocol for memory-mapped access to hard-
5251 ware.
- 5252 • A control hub component that arbitrates access to hardware, provides a common
5253 software interface for both ethernet-based protocols and legacy hardware (e.g. VME
5254 bus adaptors) and performs simple hardware monitoring functions.
- 5255 • A higher-level C++ object model that allows trigger control / local DAQ applica-
5256 tions to be written without detailed knowledge of the communications protocol or
5257 medium, and provides library functions for control of common firmware compo-
5258 nents.

5259 Each of these layers will make maximum use of off-the-shelf components, e.g. software com-
5260 munications libraries and firmware cores for protocol decoding. In the critical areas (e.g. the
5261 control hub) proven components and software techniques from the telecommunications in-
5262 dustry will be used in order to guarantee robustness and scalability. The new software must
5263 interface seamlessly with the CMS run control system, and provide a clear upgrade path for
5264 future redevelopment of existing trigger software as hardware is replaced or extended.

5265 7.6 Schedule

5266 7.6.1 Calorimeter Trigger

5267 The Calorimeter Trigger schedule is based on installation of a prototype system that can run
5268 in parallel with the existing Calorimeter Trigger system during the 2012 shutdown and in-
5269 stallation and testing of the final systems during the 2016 shutdown. The development and
5270 production of this system, including the selective readout capability, requires 4 FTE engineers,
5271 4 FTE physicists, and 3 FTE technicians.

5272 The development, design, production, test, integration and commissioning schedule is planned
5273 as follows:

- 5274 • Technology demonstrator: July 2011;
- 5275 • Prototype cards: July 2012;
- 5276 • Preproduction and testing: Dec. 2013;
- 5277 • Construction and testing: Dec. 2015;
- 5278 • Installation and testing: Dec. 2016.

5279 7.6.2 Global Trigger

5280 The Global Trigger schedule presented below includes also the Global Muon Trigger and the
5281 Central Trigger Control. The development and production of this system requires 1 FTE engi-
5282 neer, 1 FTE physicist, and 2 FTE technicians.

5283 The development, design, production, test, integration and commissioning schedule is planned
5284 as follows:

- 5285 • Technology demonstrator: Dec. 2011;
- 5286 • Design, firmware, software, test environment Prototype: Dec. 2012;
- 5287 • Design, production, test environment, verification Production System: Dec. 2014;
- 5288 • Full system test: Dec. 2015;

- 5289 • Integration: July 2015;
- 5290 • Commissioning: 2016.

5291 **7.6.3 Muon Trigger**

5292 **7.6.3.1 DT Trigger**

5293 Taking in account the known LHC and CMS operation schedule the DTTF upgrade can only
5294 be planned for the 2016 shutdown. The development and production of this system requires 1
5295 FTE engineer, 1 FTE physicist, and 1 FTE technician.

5296 The development, design, production, commissioning and test schedule is planned as follows:

- 5297 • Feasibility Report: Dec. 2010;
- 5298 • Technology demonstrator: Dec. 2011;
- 5299 • Design, firmware, software, test environment Prototype: Dec. 2012;
- 5300 • Design, production, test environment, verification Production System: Dec. 2013;
- 5301 • Full system test: Dec. 2014;
- 5302 • Commissioning: 2016.

5303 **7.6.3.2 CSC Trigger**

5304 The CSC Trigger schedule is based on installation of a prototype system that can run in parallel
5305 with the existing CSC Trigger system during the 2012 shutdown and installation and testing of
5306 the final systems during the 2016 shutdown. The development and production of this system
5307 requires 1 FTE engineer, 1 FTE physicist, and 1 FTE technician.

5308 The development, design, production, test, integration and commissioning schedule is planned
5309 as follows:

- 5310 • Technology demonstrator: July 2011;
- 5311 • Prototype cards: July 2012;
- 5312 • Preproduction and testing: Dec. 2013;
- 5313 • Construction and testing: Dec. 2015;
- 5314 • Installation and testing: Dec. 2016.

5315 **7.6.3.3 RPC Trigger**

5316 The development, design, production, test, integration and commissioning schedule is planned
5317 as follows:

- 5318 • Construction and testing: Dec. 2011;
- 5319 • Installation and testing: Dec. 2012.

5320 **7.6.3.4 Overall Trigger Schedule**

5321 The schedule is designed for installation during the 2016 shutdown and commissioning and
5322 operation with first beam after that.

- 5323 • R&D and Prototype Phase: 2011-12;
- 5324 • Pre-production and testing: 2013;
- 5325 • Construction and testing: 2014-15;

Trigger Component	Engineers	Physicists	Technicians
Calorimeter Trigger	4	4	3
Muon Trigger	3	3	3
Global Trigger	1	1	2
Total	7	7	8

Table 7.2: Estimate of FTE support required for upgrade of the CMS trigger systems.

Country	Calorimeter	Muon	Global
Austria			X
France	X		
Greece	X		
Italy		X	
Poland		X	
Portugal	X		
UK	X		
USA	X	X	

Table 7.3: Country interest in trigger upgrades.

- 5326 • Installation and testing (incl. full system tests): 2016;
- 5327 • Commissioning and Operation: 2017.

5328 Table 7.2 shows the average estimated FTE support for the development, production and in-
 5329 stallation of the calorimeter, muon and global trigger systems. Table 7.3 presents the informal
 5330 interest of the countries involved in the trigger upgrade. Personnel in these countries have ex-
 5331 perience with the present CMS trigger system and these countries were responsible for building
 5332 most of it.

Chapter 8

Data Acquisition System Improvements and Upgrades

8.1 Introduction

The existing CMS DAQ system reads out data fragments from approximately 700 sub-detector specific Front End Drivers (FEDs), builds events from these data fragments using commercial network switch technologies, and provides these to the High Level Trigger computing farm where they are analyzed to generate a final trigger decision. Triggered events are temporarily stored before they are transferred to the Tier-0 Computing Center at CERN.

The system has been designed to work at a maximal first level trigger rate of 100kHz for an LHC accelerator operating at a peak luminosity of $10^{34} \text{ cm}^{-2}\text{s}^{-1}$ with 25 ns bunch spacing. In this configuration the average event size was expected to be around 1MB.

The DAQ system can be divided into five major components:

- The Readout system built from custom electronics components. It comprises the SLINK64, the Front-end Readout Link (FRL) cards and the synchronous trigger throttling system (sTTS) implemented by the Fast Merging Modules (FMMs).
- The first stage of the CMS Event-Builder called the Fed-Builder. It is implemented by a commercial Myrinet network. Together with the Readout system this system is also called “Data to Surface” (D2S) system.
- The second stage of the CMS Event-Builder called the RU-Builder. It is implemented by a commercial Gigabit Ethernet switching network.
- The High Level Trigger (HLT) farm which is implemented by a computer cluster.
- The Storage-Manager (SM) which is implemented by two PC racks attached to a Fiber Channel SAN.

Figure 8.1 shows a vertical section through the DAQ system, called the DAQ column, which contains all DAQ components and its logical interfaces to the trigger system. Also shown are the logical networks used to implement the various functionality. Details can be found in[18][19].

Figure 8.2 shows a more detailed diagram of the Event-Builder. On a Level-1 trigger, every Front End Driver (FED) is sending data fragments via the SLINK to the FRL. In the Fed-Builder these fragments are collected and grouped together to form larger superfragments which are then distributed to eight Readout-Builders according to a simple round-robin algorithm. Superfragments on average contain eight FRL data fragments. The resulting 72 superfragments are then concatenated in the second stage (the RU-Builder) to form entire event data structures

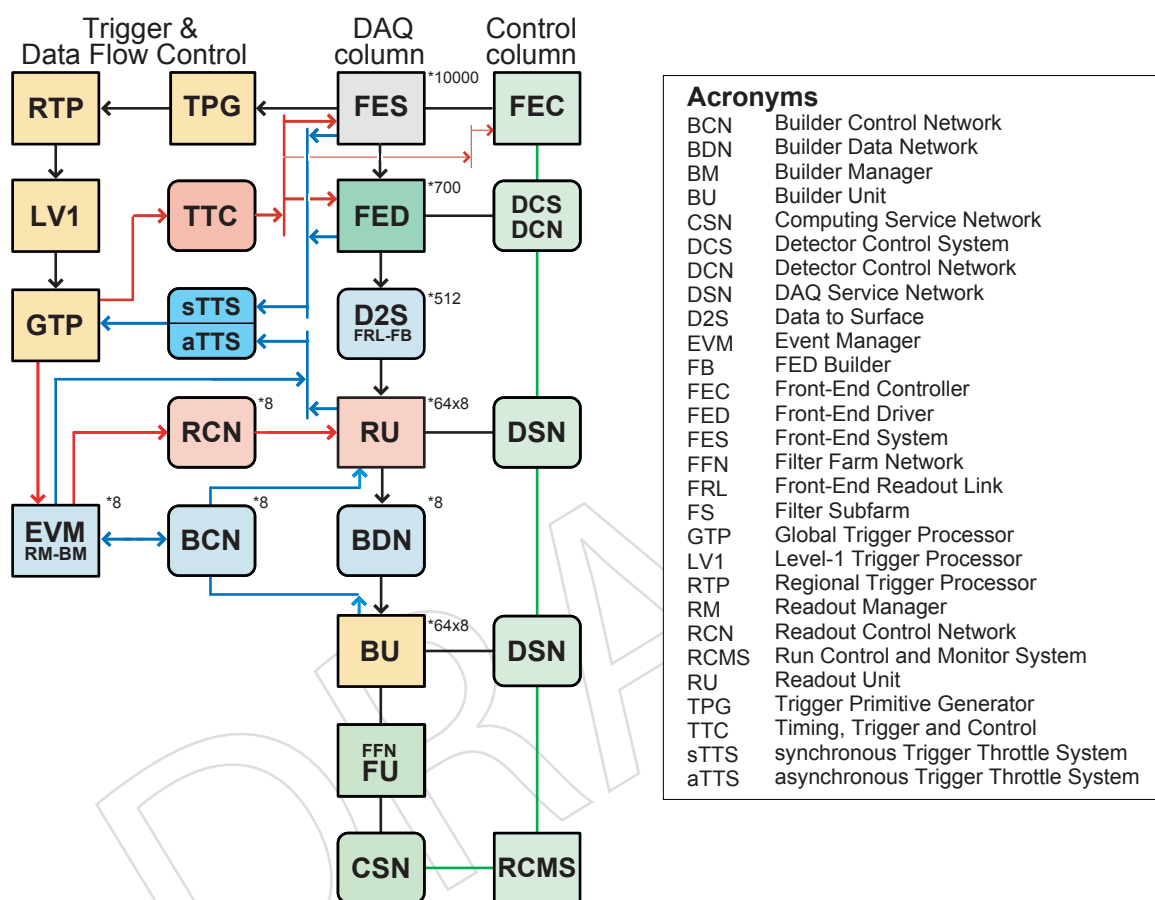


Figure 8.1: The Readout Column of the existing CMS DAQ system. A vertical slice of the DAQ system shows all logical components of the DAQ system and its interfaces to the trigger system. The small numbers next to the units indicate their multiplicity in the complete system. The event data flows vertically through the DAQ column. The data flow is shown up to the Filter Units.

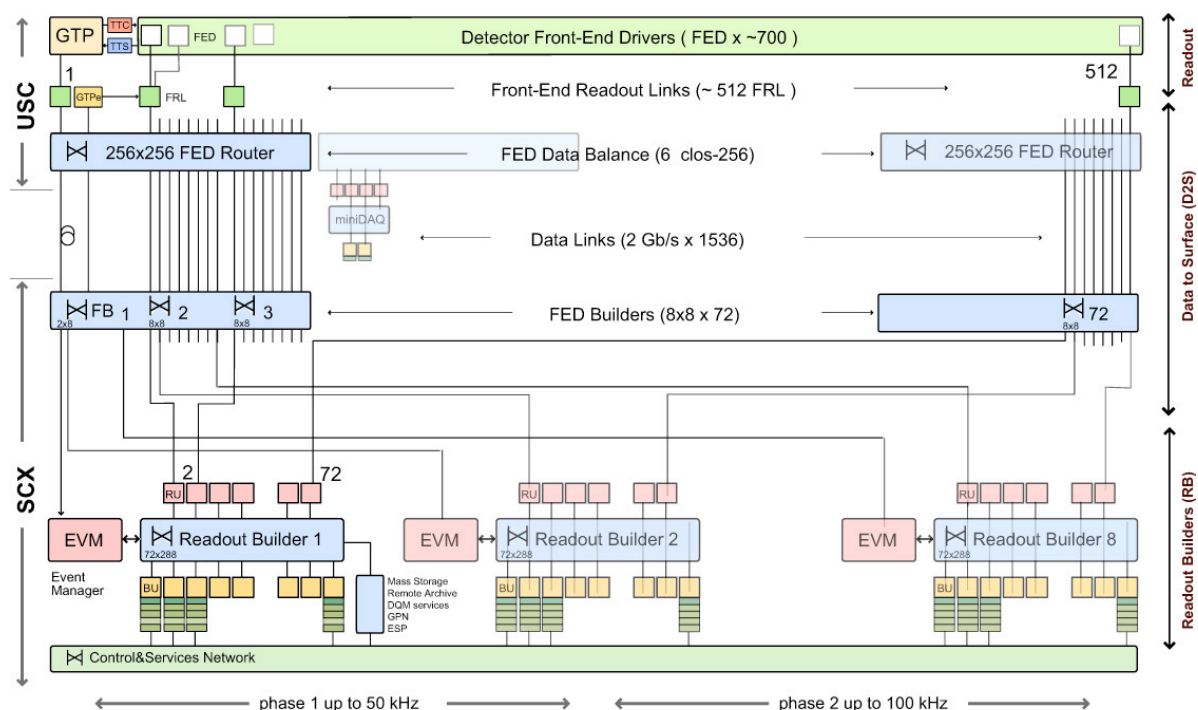


Figure 8.2: The two stages of the CMS Event-Builder.

5367 in the Builder Units (BUs). There the events are analyzed by Filter Unit (FU) processes in order
 5368 to find the High Level Trigger (HLT) trigger decision. Triggered events are then transferred to
 5369 the Storage Manager where they are temporarily stored until they are transferred to the Tier-0
 5370 center.

5371 8.1.1 Performance and limitations of the current system

5372 The design of DAQ system was driven by the requirements of the CMS experiment operating
 5373 at the design luminosity $10^{34} \text{ cm}^{-2} \text{ s}^{-1}$. The maximal first level trigger rate is 100 kHz. Table 8.1
 5374 summarizes the performance and the limitations of the various components of the current sys-
 5375 tem. The network of the Fed-Builder is implemented by a Myrinet network. It consists of two
 5376 switch fabrics operating in parallel. Every input port effectively runs at 240 MB/s. However
 5377 due to the particular pattern of the network traffic in the Event-Builder where many sources
 5378 transfer data to the same destination, in the worst case only half of this performance is available
 5379 for event building[18]. Therefore in the table a performance of 120 MB/s per port is given.

5380 8.1.2 Purchase and installation of the current system

5381 The components of the central DAQ system have been installed and commissioned succes-
 5382 sively since 2005. Table 8.2 summarizes the purchase and installation of the various compo-
 5383 nents which implement the current system.

5384 The HLT farm currently contains processing power to handle 50% of the maximal data volume
 5385 expected at $10^{34} \text{ cm}^{-2} \text{ s}^{-1}$.

Component	Quantity	Description	Performance
SLINK	≈ 700	Custom hardware read-out	400 MB/s.
FRL	≈ 500	Data formatting and interface to commercial hardware. Input stage of the Fed-Builder.	400 MB/s.
Fed-Builder Network	Two 774×774 switch fabrics operating in parallel. (≈ 500 of the 756 inputs currently used).	Data transfer from the underground area to the surface area. Data routing for the first stage of the Event-Builder.	120 MB/s for each input port. Every FRL is connected to 2 input ports (see text).
RU-Builder Network	8 slices with 72 RUs and 80 BUs and a multiple Gigabit network.	2nd stage event building.	360 MB/s via 3 Gigabit rails.
HLT farm	900 PCs with Intel Xeon-5430 Quad Cores CPUs (2.66 GHz) and 16 GB RAM	High Level Trigger algorithms.	See text.
Storage Manager	16 PCs and 2 hot spares with SAN	Temporary data storage.	220 TB storage. Performance Test: 2 GB/s writing and 1 GB/s reading concurrently.

Table 8.1: The performance of the various DAQ components currently installed in CMS.

Component	Purchase / Production	Installation	Remark
SLINK	2005	2006	custom hardware
FRL	2005	2006	custom hardware
FMM	2005	2006	custom hardware
Control PCs	2005	2006	Used to control custom electronics. No maintenance contract anymore.
RU PCs (PE2950)	2007	2007	Maintenance contract until 2012.
BUFU PCs (PE1950)	2008	2008	Maintenance contract until 2012. 50% of nominal Performance.
Myrinet Network equipment	2006	2007	
Gigabit Data-Network equipment	2006	2007	
Storage Manager hardware	rack1: 2007 rack2: 2008	rack1: 2007 rack2: 2008	Storage hardware on maintenance contract.

Table 8.2: Purchase and installation of the various components of the current CMS DAQ system.

8.2 Upgrade of the DAQ system

The upgrade of the DAQ system is different from the upgrade of other detector components for the following reasons:

1. The DAQ system is not involved in the process of generating data used for physics analysis but merely transports data produced by the sub-components of the experiment and provides the necessary CPU power in order to run the HLT algorithms. Therefore its upgrade is driven by the requirements in terms of data transportation and CPU power on one side, and the availability of affordable network and computing technology on the commercial market on the other side. The details of these requirements are unknown today. Neither do we have detailed designs for the sub-system upgrades, nor can we reliably estimate the expected data volumes produced by the subsystems. On the other hand data acquisition systems use commercial technologies which every year experience large performance improvements, since their development is driven by the requirements of growing markets like telecommunication. The upgrade of the DAQ system will profit from these improvements and once the requirements are well defined a suitable technology will be chosen to satisfy the needs at reasonable cost.
2. The DAQ system interfaces to all sub-detector systems and therefore needs to stay compatible with all of them i.e. with those being upgraded as well as with those not being upgraded. This excludes radical changes of its architecture.
3. To a large extent the DAQ system is built from commercial components. A large fraction of these are under maintenance contracts. The hardware needs to be replaced when it becomes obsolete in order to keep the reliability of the system high. Depending on the component being replaced this implies no or little work to be done on the system (e.g. when computers are being replaced by similar types) or major development work (e.g. when networking technologies have to be replaced).
4. The DAQ system continuously has to adapt to new running conditions. In particular throughout Phase 1 the luminosity is expected to gradually increase. This implies continuously changing operating conditions. In order to keep reliability of the system high, the DAQ software will undergo a smooth continuous upgrade which gradually improves the reliability of the system and deals with newly arising problems by improving fault tolerance and diagnostics.

8.3 Implications of LHC running scenarios and subsystem upgrades on the requirements for the DAQ system

The amount of data the DAQ system has to handle depends on the following factors:

- The rate of Level-1 triggers. This will stay 100 kHz in all upgrade scenarios.
- The data volume the DAQ system has to transfer for each event triggered by Level-1.
- The average processing power needed by the HLT to process an event.

The data volume of a single event has two contributions: A fixed term and a term proportional to the occupancy of the detector. The fixed term contribution can be determined by measuring the size of an empty event. These events contain contributions due to noise and a fixed overhead of the event structure.

5427 In CMS the detector with the largest contribution to the event size is the tracker system (strips
5428 and Pixel). The occupancy of these detectors is proportional to the number of underlying min-
5429 imum bias events. This in turn depends on the luminosity per bunch crossing. At 14 TeV and
5430 nominal luminosity of $10^{34} \text{ cm}^{-2}\text{s}^{-1}$ and a bunch spacing of 25 ns approximately 19 underly-
5431 ing minimum bias events are expected for each bunch crossing. The DAQ system had been
5432 designed under the assumption that under these conditions the event size would be $\approx 1 \text{ MB}$.
5433 It follows that the system is capable of building events at 100 GB/s ($1 \text{ MB} \times 100 \text{ kHz}$).

5434 8.3.1 Possible running scenarios of LHC for Phase 1

5435 Up to the first shutdown in the years 2012/2013 the center of mass energy of LHC will stay at 7
5436 TeV and the luminosity per bunch crossing will stay an order of magnitude below the nominal
5437 one. No significant pileup of minimum bias events is expected and therefore the DAQ system
5438 will be able to easily handle the data volume, even if triggering at 100 kHz.

5439 After the first shutdown, the energy of the beam will be increased from 7 to 14 TeV and the lu-
5440 minosity is expected to first increase to $5 \times 10^{33} \text{ cm}^{-2}\text{s}^{-1}$ with a bunch spacing of 50 ns and later
5441 to the nominal $10^{34} \text{ cm}^{-2}\text{s}^{-1}$ but with 25 ns bunch spacing. Both scenarios have the same lumi-
5442 nosity per bunch crossing and therefore in both cases 19 underlying minimum bias events are
5443 expected in each triggered event. The DAQ will operate at its originally foreseen performance.

5444 After the second shutdown foreseen around the years 2015/2016, LHC might be able to deliver
5445 up to $2 \times 10^{34} \text{ cm}^{-2}\text{s}^{-1}$ with 25 ns bunch spacing. In this case around 40 pile up events are
5446 expected and the occupancy of the detector will be proportionally higher. Moreover, additional
5447 readout channels will further increase the expected data volume to be handled. For example
5448 the data volume of the Pixel detector will increase by more than 50% due to the introduction of
5449 the fourth barrel layer and the third set of endcap disks. Similarly the data volume of the HCAL
5450 detector is expected to increase significantly from the introduction of longitudinally segmented
5451 readout. To continue to be able to trigger at 100 kHz the readout system, the Event-Builder and
5452 the HLT farm must be upgraded.

5453 The design choices for the DAQ upgrade foreseen in the year 2015/2106 will have to be made
5454 around the years 2012/2013, i.e. leaving 3 years for prototyping, production, installation-testing
5455 and commissioning. At that time it will be impossible to design a system that would also fulfill
5456 the requirements of the Phase 2 upgrade at a reasonable cost. In addition, many components
5457 chosen for the 2015/16 upgrade will be obsolete by 2020.

5458 8.4 Discussion of the DAQ components

5459 The CMS DAQ system is implemented to a large extent with commercial computing hardware
5460 (e.g. PCs and network equipment). These components are purchased with maintenance con-
5461 tracts which provide efficient repair in case of failures. Once a product is declared obsolete, it
5462 is no longer possible to renew its maintenance contracts. The operation of obsolete equipment
5463 becomes a risk for the experiment, since a sufficient number of spares cannot be guaranteed
5464 anymore. The time before a given model of server PC becomes obsolete is typically 3 years.
5465 For network switching equipment this time is slightly longer (6-7 years). This defines a natural
5466 cycle when all the commercial DAQ equipment from the Fed-Builder to the Storage Manager
5467 is to be replaced.

5468 A similar problem exists for custom hardware modules. After a given time components used
5469 in the modules cannot be purchased anymore. As soon as the number of functioning spare
5470 modules falls below a minimum, the operation of that hardware becomes a risk factor.

5471 Modifications in all components of the DAQ system will be necessary in order to cope with the
5472 expected data volume after the second shutdown.

5473 **8.4.1 Hardware Control**

5474 The PCs currently used to control the custom hardware were purchased in 2005 (approximately
5475 200 PCs). Their performance is sufficiently high but their maintenance contract terminates in
5476 2011. These computers are essential to configure the readout electronics at the beginning of
5477 each run. It is foreseen to replace them in the shutdown 2012/2013.

5478 The custom hardware in CMS is currently implemented in VME modules for the sub-detector
5479 specific electronics and in compact PCI modules for the FRL modules of the DAQ. The relevant
5480 crates are interfaced to the control PCs via commercial bridges (PCI to VME or PCI to PCI
5481 resp.). It is foreseen to replace these bridges together with the control PCs in the shutdown
5482 2012/2013 with bridges connecting to a PCIe bus on the side of the host computer.

5483 **8.4.2 Readout links**

5484 For the 2016 shutdown a new custom readout link will be designed employing state of the art
5485 electronics components. It is expected that this link will be able to transfer data at a rate of
5486 about 10 Gbit/sec. The link will replace the old obsolete hardware of the current SLINK and
5487 will meet the requirements of the new readout link for higher data throughput. The link must
5488 be designed in a way that it can be interfaced to legacy FEDs of sub-detectors which do not
5489 need to be upgraded, and to newly designed FEDs which will be able to transfer substantially
5490 higher data volumes to the DAQ. Currently it is clear that the HCAL system will replace their
5491 FEDs with μ TCA based FEDs in the second shutdown period. They are capable of delivering
5492 up to eight times more data than the current FEDs. In the trigger system, μ TCA FEDs will also
5493 be added. The new Pixel detector will deliver substantially more data. However, it has not
5494 been decided yet if the FEDs will be rebuilt.

5495 **8.4.3 Fed-Builder**

5496 The Fed-Builder will be replaced in the second shutdown with modern network technology
5497 which can be interfaced reasonably easily to the custom hardware of the readout link. Similarly,
5498 the RU-Builder will be replaced by a state of the art network switch, based on multi-gigabit
5499 links, in order to be able to cope with the higher data throughput.

5500 **8.4.4 RU-Builder and HLT farm**

5501 The present filter farm that runs the Higher Level Triggers contains 720 Dual Quad Core Intel
5502 Xeon 5430 PCs running at 2.66 GHz and with 16 GB of memory. This provides about 5,000
5503 instances of HLT processes running simultaneously. This is sufficient to process an input of 50
5504 (100) kHz of Level-1 triggered beam crossings with each crossing taking 100 (50) ms on average
5505 to process. Figure 8.3 shows the Monte Carlo distributions of the average processing times,
5506 including both unpacking and algorithmic portions, for the nominal trigger menu for a center
5507 of mass energy of 14 TeV and a luminosity of $10^{32}\text{cm}^{-2}\text{s}^{-1}$ (where the pileup is negligible) for
5508 minimum bias events[20]. The mean value is 42.7 ms. Figure 8.4 shows a timing study taken
5509 with 30K minimum bias data events at a center of mass energy of 7 TeV and a luminosity of $5 \times$
5510 $10^{29}\text{cm}^{-2}\text{s}^{-1}$ where the pileup averages about 1.2 events due to the small number of colliding
5511 bunches. The full HLT menu contains commissioning triggers that are being temporarily used
5512 to look at pixel tracks at the full Level-1 accept rate and has a mean time of 59 ms. When the
5513 commissioning triggers are removed, the mean time is 32 ms. Therefore we conclude that the

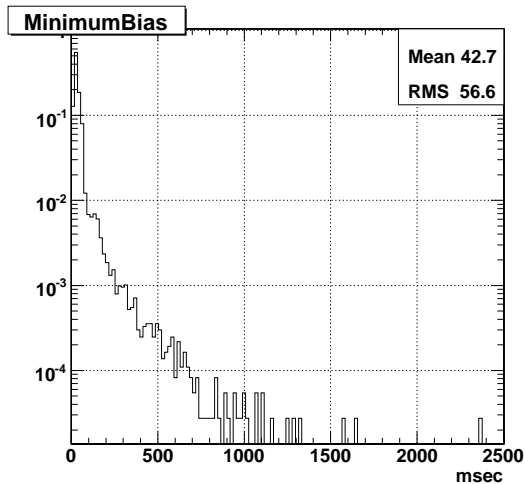


Figure 8.3: MC study of average processing-times (Core 2 5160 Xeon 3.0 GHz) for running the full HLT Menu including the data unpacking time. Measurements taken with L1-accepted un-binned minimum bias MC sample at a luminosity of $10^{32} \text{cm}^{-2} \text{s}^{-1}$ [20].

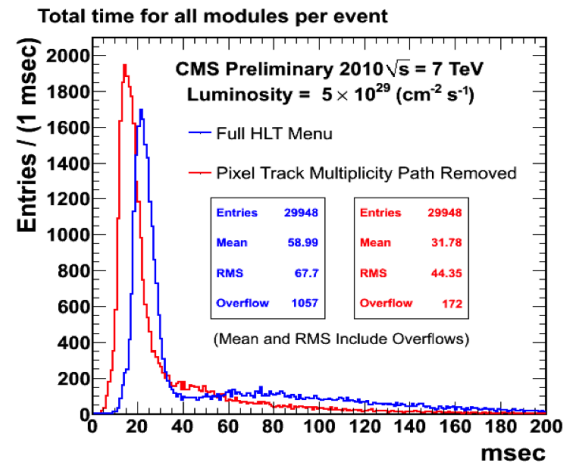


Figure 8.4: Average data processing-times (Core 2 5430 Xeon 2.66 GHz) for running the full HLT Menu including the data unpacking time. Measurements taken with 30K minima's data events from data at a luminosity of $5 \times 10^{29} \text{cm}^{-2} \text{s}^{-1}$.

5514 present HLT CPU time is reasonably well understood with data and MC for events with small
5515 or negligible pileup and that the figure of 50 ms per event is a reasonable figure on which to
5516 base extrapolations to higher luminosities.

5517 In order to do so, we use the present data with between 1 and 7 reconstructed vertices per
5518 event and interpreting each reconstructed vertex as a separate interaction as shown in Figures
5519 8.5 and 8.6. The event size on average starts at 0.5 MB and increases by 20 KB per additional
5520 interaction. For the running period after the 2013 shutdown we expect a maximal luminosity
5521 of $10^{34} \text{cm}^{-2} \text{s}^{-1}$. With a bunch crossing interval of 25 ns one would expect 19 minimum bias
5522 events per bunch crossing resulting in an event size of $\approx 900 \text{KB}$. From 2013 onwards LHC
5523 is expected to operate at the nominal energy, i.e. 14 TeV. Since the particle multiplicity scales
5524 approximately with the square root of the center of mass energy it is expected to increase by
5525 41%. Assuming that a large fraction of the event size with only one interaction (0.5 MB) is
5526 constant, and only scaling the contribution due to the minimum bias events, we obtain a final
5527 event size of 1.1 MB.

5528 Assuming that the required HLT processing power is proportional to the event size, the inves-
5529 tigations above show that an enhancement in processing power of a factor 2 is needed in order
5530 to cope with the expected data volume at 100 kHz. This estimation neglects that the processing
5531 time of many HLT algorithms might have a stronger dependence on the event size. Experience
5532 in other experiments indicates that this effect might be more or less important (D0 and CDF).
5533 Therefore we add some margin and intend to increase the processing power of the HLT farm
5534 in the shutdown period 2012/2013 by a factor of 3.

5535 The present computer rack infrastructure is only half populated with PCs since the PC's pur-
5536 chased had twice the CPU power used to specify the original infrastructure. Since the present
5537 PC's will be 5 years old at the 2012/13 shutdown, we will replace the existing PC's with new
5538 ones, rather than enlarging the existing farm. This will still leave still half of the infrastructure

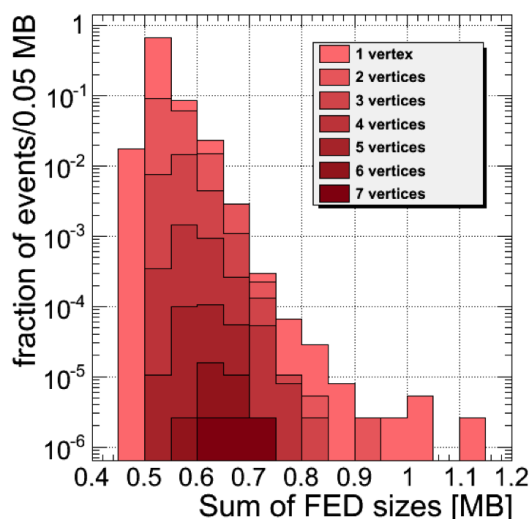


Figure 8.5: Event sizes for different numbers of reconstructed vertices from data at a luminosity of $5 \times 10^{29} \text{ cm}^{-2} \text{ s}^{-1}$.

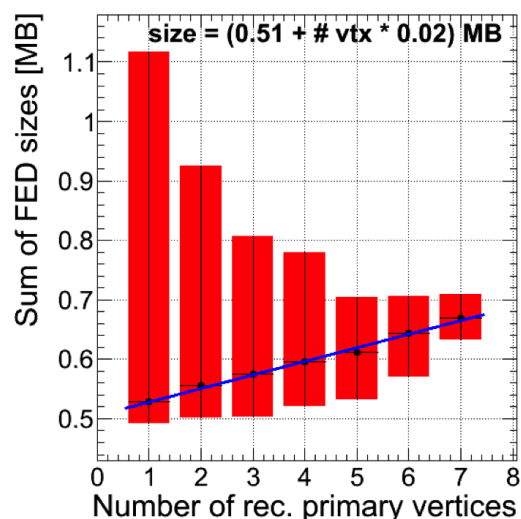


Figure 8.6: Event size dependence on number of reconstructed vertices from data at a luminosity of $5 \times 10^{29} \text{ cm}^{-2} \text{ s}^{-1}$.

5539 unpopulated providing contingency in case of an unexpected increase in HLT CPU needs. In
 5540 2013 the cooling power of the SCX computer room will be increased to 1 MW as originally
 5541 foreseen.

5542 The next increment in HLT farm CPU power will be required during the 2016 shutdown,
 5543 in order to provide the capability to operate at luminosities up to twice design luminosity
 5544 ($2 \times 10^{34} \text{ cm}^{-2} \text{ s}^{-1}$). Forty minimum bias events per crossing are expected in this scenario. We
 5545 estimate that this will require approximately 3 times the CPU power of the filter farm installed
 5546 in 2012. Therefore, the plan is to replace all existing filter farm CPUs and to fill all of the rack
 5547 infrastructure with PCs that are significantly more performing than those installed in 2012. In
 5548 addition, the increased data will require an upgrade to the network switch infrastructure.

5549 8.4.5 Storage Manager

5550 The Storage Manager stores selected events temporarily on a local disk array and concurrently
 5551 transfers the data to Tier-0. Once data has been verified at Tier-0 it is deleted from the Storage
 5552 Manager disks. The transfer to Tier-0 is implemented with two 10 Gbit/s links. In normal
 5553 operation only one link is used the other serving as a spare in case of failure of the first link.
 5554 The two links can also be trunked together and operated simultaneously in order to increase
 5555 the performance of the transfer system.

5556 Currently the limitation of the CMS recording performance is given by the Tier-0 processing
 5557 power that is limited to about 300 Hz event rate. Depending on the configuration of the tracker
 5558 readout, the event size varies from 350 kB to 500 kB in the ongoing 2010 run. The total data
 5559 volume written to disk depends on the configuration of the data output streams of the HLT.

5560 In preparation of the Heavy Ion run during 2010 a series of performance tests have been carried
 5561 out. During these the Storage Manager wrote 2 GB/s to disk and concurrently transferred 1
 5562 GB/s to Tier-0. This performance is estimated to be sufficient for the proton physics program
 5563 and also for the initial Heavy Ion program of Phase 1 up to 2015.

5564 It is necessary, however, to regularly replace the hardware of the Storage Manager to keep its

5565 reliability high.

5566 **8.4.6 Online Database**

5567 The online database of CMS is implemented by an Oracle database. The hardware components
5568 (PCs and storage) will be regularly replaced to keep the reliability of the system high. In par-
5569 ticular during the shutdown 2012/2013 it is foreseen to replace the hardware of the database.
5570 The required storage space will grow during the lifetime of the experiment. It is also expected
5571 that the total data rate written into, and read from the database will increase, since during
5572 the upgrade of the experiment the number of channels for various sub-detectors will increase.
5573 Therefore more parameters and conditions will be written to the database. During the lifetime
5574 of the experiment the performance of the database will need to increase in order to satisfy these
5575 requirements.

DRAFT

5576 Chapter 9

5577 Beam Instrumentation and Luminosity 5578 Monitoring Improvements and Upgrades

5579 Comprehensive and flexible beam instrumentation was invaluable during the LHC startup
5580 in understanding beam conditions with a view to reducing beam losses and optimising LHC
5581 efficiency and luminosity. Moreover, the provision of beam instrumentation which protects the
5582 CMS detector against catastrophic beam losses which could damage the detector is absolutely
5583 essential. This is done by initiating a “beam abort” in the event of such dangerous losses.

5584 The beam instrumentation installed for the startup proved flexible enough to fulfill all these
5585 roles as well as providing a stable and well-understood trigger to allow efficient data taking
5586 and resultant physics publications even during the initial period where all triggers were un-
5587 dergoing a thorough commissioning period. The CMS protection system similarly has worked
5588 seamlessly and invisibly, having been active and commissioned since the first LHC beams.

5589 In the coming years, the expected intensities and beam conditions will develop rapidly. Ad-
5590 ditionally, there will be significant changes to the CMS detector configuration. To be able to
5591 continue to successfully protect and optimise conditions for CMS, it is necessary to consolidate
5592 the currently installed array of beam instrumentation to adapt to the changing machine con-
5593 ditions and detector configuration. Building upon the experience with the system so far, the
5594 changes necessary to do this are presented in this chapter.

5595 In this chapter, first an overview of the present beam and radiation monitoring instrumentation
5596 is presented, followed by the motivation for improving the present system and a summary
5597 timeline for these improvements. Then each improvement is presented in some detail, starting
5598 with those which are most central to the primary aims of the beam instrumentation project.
5599 Finally, details are given as to the resources needed to undertake these upgrades in terms of
5600 manpower requirements, material costs and schedule.

5601 9.1 Present Beam and Radiation Monitoring Instrumentation

5602 The Beam and Radiation Monitoring systems (BRM) [19, 21, 22] perform both a monitoring and
5603 a protection function for CMS. To this end, multiple and redundant systems have been installed
5604 some of which can be used to initiate LHC beam aborts and/or CMS equipment control, others
5605 of which can be used for fast beam/detector optimisations. All systems will provide long term
5606 monitoring of the received radiation dose in various regions of the CMS detector.

5607 The CMS experiment sits in an unprecedentedly high radiation field for a HEP experiment
5608 and much effort has gone into the design and construction of systems with very high radiation
5609 tolerance. Nevertheless the LHC is designed to run with 362 MJ of stored energy in each beam
5610 and with proton intensities in excess of 10^{14} per beam. Even very small fractional losses of this

5611 beam risk causing serious damage to detector elements. Whilst the LHC itself has extensive
 5612 instrumentation designed for machine protection, CMS requirements dictate that CMS must
 5613 be able to detect beam-related problems as they develop and to assert beam aborts if required.
 5614 In addition, CMS must be able to log data and perform post-mortem analyses in the case of
 5615 accidents and understand the accumulated dosage and potential longer term damage to the
 5616 detector elements. To this end CMS has implemented the BRM systems.

5617 While radiation damage can lead to long term effects, the most likely damage scenarios involve
 5618 very fast bursts of radiation/energy-dissipation in detector elements. Thus the protection sys-
 5619 tems must be sensitive to very fast changes in beam conditions; the BRM systems can detect
 5620 changes at the 25 ns level, though the initially deployed protection systems will react in times
 5621 of order 3-40 μ s. Additionally the BRM systems provide monitoring and tuning data to permit
 5622 operator intervention to diagnose and improve beam conditions. In addition, all BRM systems
 5623 can be used to monitor integrated dose and detector component aging over the years of LHC
 5624 operation.

5625 CMS imposed several requirements on the design of the system:

- 5626 • the systems have to be live at any time when beam is in the LHC independent of the
 5627 state of CMS operations;
- 5628 • systems must have readout and post-mortem capabilities very similar to those of the
 5629 LHC machine protection systems; and
- 5630 • they must possess a high degree of redundancy and a wide dynamic range for pro-
 5631 tection and monitoring scenarios.

5632 Given these constraints, the system, which is summarised in Table 9.1, was implemented. The
 5633 nomenclature and locations of the BRM subsystems in CMS are represented in Figure 9.1.

Subsystem (Sensor type)	Location Distance to IP (m)	Sampling Time	Function	Interface LHC/CMS type	# Sensors
Passives (TLD+Alanine)	CMS and UXC	\sim months	Monitoring	N/A	>200
Medipix (Silicon pixel detector)	UXC and USC $z=15$ m, $x=12$ m	1 minute	Monitoring	CMS Standalone	3
RADMON (RadFets, PIN Diodes, SRAM)	CMS and UXC	1 s	Monitoring	Standard LHC	20
BCM2 (Polycrystalline Diamond)	TOTEM T2 $z=\pm 14.4$ m	40 μ s	Protection	Standard LHC	24
BCM1L (Polycrystalline Diamond)	Pixel Volume $z=\pm 1.8$ m	5 μ s	Protection	Standard LHC	8
BSC1 (Scintillator Tiles)	Front of HF $z=\pm 10.9$ m	\sim ns	Monitoring	CMS Standalone	32
BSC2 (Scintillator Tiles)	TOTEM T2 $z=\pm 14.4$ m	\sim ns	Monitoring	CMS Standalone	4
BCM1F (Single Crystal Diamond)	Pixel Volume $z=\pm 1.8$ m	\sim ns	Monitoring	CMS Standalone	8
BPTX (Button Beam Pickup)	Upstream of IP5 $z=\pm 175$ m	200 ps	Monitoring	CMS Standalone	2

Table 9.1: The subsystems deployed as part of the initial BRM. The table is ordered from top to bottom in increasing time resolution.

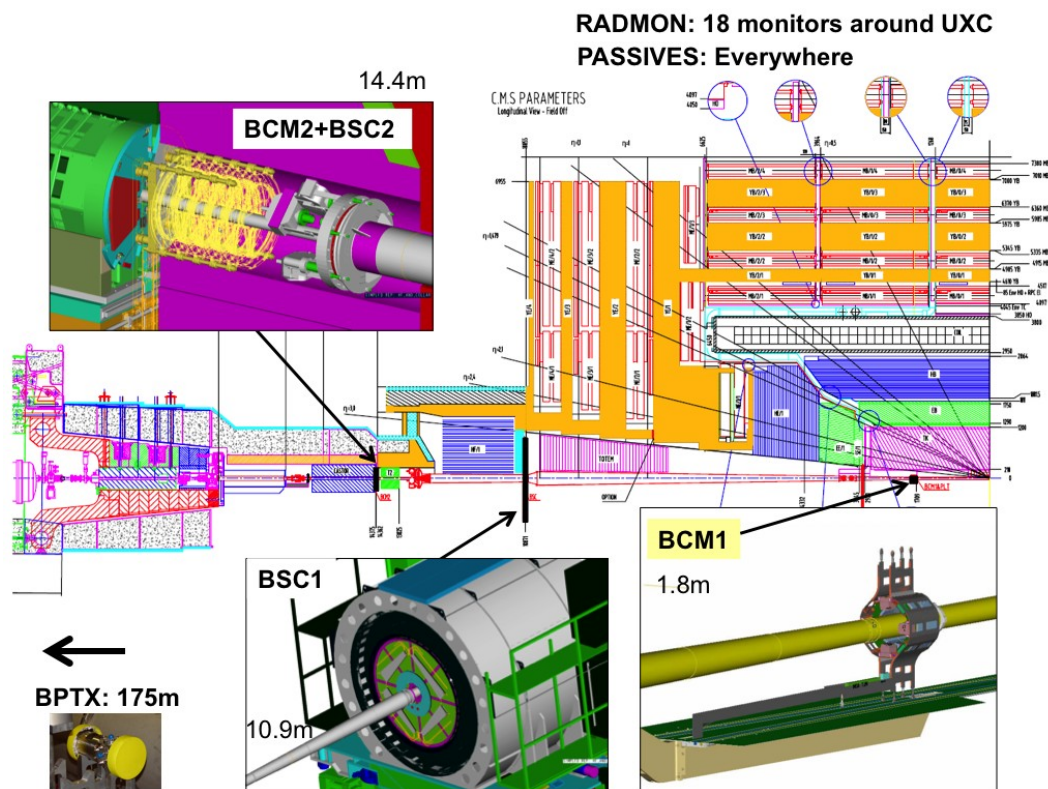


Figure 9.1: The layout of CMS BRM systems.

9.1.1 Protection Systems

5634

5635 The Protection systems are based on chemical vapour deposition diamond detectors [23, 24]
 5636 similar to those that have been widely used in recent collider experiments [25, 26] where they
 5637 have proven to be radiation hard [27], fast enough to match beam abort scenarios, and small
 5638 enough to be inserted into areas close to key detector components without adding substantial
 5639 material or services.

5640 In CMS there are two protection systems foreseen for initial LHC operation [28?]. The first is
 5641 the BCM1L which is four polycrystalline diamonds, each 10x10x0.4 mm, positioned on either
 5642 side of the IP at Z values of ± 1.8 m close to the beam pipe and the pixel detectors at a radius
 5643 of 4.5 cm. The second protection system is the BCM2. This is a set of twelve polycrystalline
 5644 diamonds, each 10x10x0.4 mm, on either side of the IP behind the TOTEM T2 detector at a z
 5645 position of ± 14.4 m. On each side of the IP, a set of eight sensors are deployed at an outer
 5646 radius of 29 cm and an additional four at an inner radius of 5 cm. Here BCM refers to Beam
 5647 Conditions Monitor, the index 1 or 2 refers to the two locations in z and the final character L
 5648 indicates that these detectors are used in a leakage current measurement mode as relative flux
 5649 monitors, typically integrating the leakage current over micro-second time scales. The BCM1L
 5650 diamonds are arranged on the x and y axes. The BCM2 comprise eight diamonds at 45 deg
 5651 intervals at large radius and four on the x,y axes at small radius.

5652 The diamonds used for BCM1L and BCM2 are essentially identical, but the two systems differ
 5653 in the readout methods adopted. The BCM2 uses a completely standard LHC Beam Loss Mon-
 5654 itor (BLM) electronics and data processing [29, 30] that is read out asynchronously with the
 5655 LHC orbit clock with a 40 μ s sampling period. The BCM1L readout uses the same LHC BLM
 5656 backend electronics, but uses an alternative mezzanine card to provide sub-orbit sampling. The

5657 readout is synchronised with the LHC orbit clock, allowing user-configurable sampling over
5658 the 89 μ s orbit so that the sampling can be matched to the bunch trains within the LHC orbit.

5659 Using a set of thresholds in the readout systems and a combinatorial logic to reduce sensitivity
5660 to individual noise events, a hardware beam abort signal can be generated and transmitted to
5661 the LHC machine via the beam interlock system [31, 32], leading to the controlled extraction of
5662 the beams within 3-5 turns. A lower threshold value can be used to send hardware signals to
5663 CMS sub-detector clients to initiate high and/or low voltage ramp-downs.

5664 In the event of a beam abort initiated by CMS, or any of the other LHC- or experiment- protec-
5665 tion systems, a full history of the BCM1L and BCM2 signals is produced and transmitted to the
5666 LHC control room.

5667 **9.1.2 Monitoring Systems**

5668 Several monitoring systems are listed in Table 9.1. The BCM1F is also based upon diamond sen-
5669 sors, but with readouts able to resolve the sub-bunch structure; the Beam Scintillator Counters
5670 (BSC) are a series of scintillator tiles designed to provide hit and coincidence rates; the BPTX
5671 is designed to provide precise information on the bunch structure and timing of the beam; and
5672 the RADMON, MEDIPIX and Passives systems give calibrated information on the radiation
5673 field within the CMS cavern.

5674 The BCM1F, BSC and BPTX are sensitive to time structure below the 25 ns level; as such they
5675 also provide several dedicated trigger inputs into the global Level-1 CMS trigger. In particular,
5676 the inputs from the BPTX and BSC will provide zero- and minimum- bias triggers respectively.
5677 Additionally, all three of these systems are sensitive to all machine intensities including the
5678 LHC pilot beam, where a single low intensity bunch is injected for studies or to confirm pa-
5679 rameter settings prior to full intensity injection.

5680 The BCM1F [?] consists of eight single crystal diamonds, each 5x5x0.5 mm, four positioned on
5681 either side of the IP at z values of ± 1.8 m at a radius of 4.5 cm, in close proximity to the BCM1L
5682 detectors. The purpose of the BCM1F is as a diagnostic tool to be able to flag problematic beam
5683 conditions resulting in “bursts” of beam loss over very short periods of time. Such beam losses
5684 are expected to be one of the principle damage scenarios for the CMS detector systems. The
5685 location for the BCM1F is close to the optimal position in terms of timing separation between
5686 ingoing and outgoing particles from the IP (i.e. 6.25ns from the IP). The gated rate information
5687 from the BCM1F therefore give a very good handle on the comparative rate of background from
5688 beam halo to that from luminosity products. The sensor is connected to the JK16 radiation hard
5689 amplifier [33], after which the signal is transmitted to the counting room over an analog optical
5690 link built from the tracker optical components [34].

5691 The detector and sensor is sensitive to one MIP and has a timing resolution for single hits
5692 of a few ns. The performance of the front end electronics is shown. Good separation can
5693 be seen between the signal and the noise. The pulse height was found to saturate at 100 V
5694 bias voltage across the sensor. The back end readout produces rate, multiplicity, timing and
5695 coincidence information independently of the CMS DAQ. However there is the possibility to
5696 feed information into the event stream via a standard CMS SLINK.

5697 Beam Scintillator Counters (BSC) [?] are a series of scintillator tiles designed to provide hit
5698 and coincidence rates, with a design similar to those used at previous experiments [35]. The
5699 scintillators and PMTs used for the BSC are recycled from OPAL [36]. The BSC1 is located
5700 on the front of the HF, at ± 10.9 m from the IP, and consists of two types of tiles. Next to
5701 the beampipe are the disks, segmented into 8 independent slices in ϕ with an inner radius of

5702 22 cm and an outer radius of 45 cm. The primary function of the disks is to provide the rate
5703 information corresponding to the beam conditions. In addition, there are four larger area tiles
5704 further out, at a radial distance of between ca. 55 cm and ca. 80 cm, which in addition to
5705 providing rate information, will also provide coincidence information which can be used to
5706 tag halo muons passing through the detector for calibration purposes. The area covered by the
5707 BSC perpendicular to the beamline is about 25% that of the tracker; therefore these tiles can be
5708 indicative of activity within A bunch crossing, and is used to provide a minimum-bias trigger
5709 for commissioning and systematic studies as required. The BSC2 is located behind TOTEM T2
5710 at ± 14.4 m from the IP. It consists of two tiles on each side of the IP, with an inner radius of
5711 between 5 cm and an outer radius of 29 cm. The primary function of the BSC2 is to distinguish
5712 between ingoing- and outgoing- particles along the beamline, as there is a 4 ns timing difference
5713 between them. The rates at this location can therefore be gated as to whether they are incoming
5714 (beam halo only) or outgoing (collision products and beam halo).

5715 The Beam-Pickup Timing for the eXperiments (BPTX) [?] is a beam pickup device specifically
5716 installed to provide the experiments with the timing structure of the LHC beam. This beam
5717 pickup is a standard button monitor used everywhere around the LHC ring for the beam po-
5718 sition monitors. Two are installed for CMS; 175 m left and right upstream of the IP. At this
5719 location, there are two beampipes, and so therefore the timing measurement is only of the in-
5720 coming beam. To optimise the timing measurement, the four buttons (left, right, up, down) of
5721 the pickup have been electrically connected together, so there is no position information but
5722 the signal strength is maximised and hence the resolution on the timing.

5723 An oscilloscope-based read out was chosen for the BPTX and developed in common with AT-
5724 LAS [37]. The BPTX provides accurate information on the timing and phase of each bunch and
5725 its intensity. The phases of all the experimental clocks can be compared to the measured phase
5726 of each bunch at a precision better than 200 ps - presently variations at the level of 60 ps can be
5727 understood. This will also allow a z position for the interaction point to be calculated from the
5728 relative phases of the BPTX measurements on opposite sides of the IP. The BPTX also detects
5729 problems with the bunch structure, as well as measurements on the proportion of beam which
5730 has drifted into the neighbouring RF buckets.

5731 In parallel to the oscilloscope based readout, the signals from the BPTX are discriminated, sim-
5732 ple logical combinations are derived from this and sent as inputs to the CMS global Level-1
5733 trigger. This will provide flags on each bunch crossing as to whether a bunch is present in each
5734 beam, either beam or both beams. The flag where bunches are present in both beams is indica-
5735 tive of whether collisions can occur in this bunch crossing, and therefore provides a zero-bias
5736 trigger for commissioning of the trigger system. This input is also essential to determine the
5737 relative timing between the LHC bunch clock and CMS experimental clock.

5738 At 20 locations around the CMS cavern, RADMON [38, 39] detectors are installed. The RAD-
5739 MON detectors each provide calibrated measurements at these locations of the dose and dose
5740 rate using RadFETs; the hadron flux with energies above 20 MeV and the single event upset rate
5741 using SRAM; the 1 MeV equivalent neutron fluence using PIN diodes. RADMON detectors are
5742 also installed all around the LHC ring, and in the experimental insertions. The RADMON de-
5743 tectors at CMS will be integrated into, and read-out via, the accelerator-wide LHC RADMON
5744 system.

5745 The integrated radiation dose throughout the CMS cavern will be measured during each run
5746 period with passive dosimetry. This will provide a map of the radiation field throughout the
5747 cavern and will be used to validate the simulations of the anticipated doses. This gives an
5748 absolute scale to the other measurements. The dosimeters chosen are TLDs and Alanine.

9.2 Motivation for Beam Instrumentation Improvements

5749

5750 The motivation for the improvements to the beam instrumentation proposed here is essen-
5751 tially to be able to provide a detailed monitoring capability as the expected beam intensities,
5752 luminosities and conditions evolve. In addition, there will be significant changes to the CMS
5753 detector configuration. As such, it is essential that the beam instrumentation adapts to the
5754 changing machine conditions and detector configuration.

5755 The two CMS beam conditions monitors are the primary devices for protection of the CMS
5756 detector against adverse beam conditions. Within the CMS cavern, a span of ± 20 m they are
5757 only devices connected to the LHC ABORT system. Since there are therefore various categories
5758 of losses where the LHC protection system does not offer effective protection for the CMS
5759 detector, it is vital to ensure that the CMS protection system is maintained and active at all
5760 times. A detailed understanding of the detectors and their response is required to do this.

5761 To ensure that the protection devices are always in optimal condition, during the LHC shut-
5762 downs, a preventative maintenance campaign is foreseen for both of the beam conditions mon-
5763 itors. Continued compatibility with the LHC Beam Loss Monitors is part of this strategy to en-
5764 sure a system that is well understood. Additionally, it will be necessary to have a rebuild of the
5765 Beam Conditions Monitor 2 system during the 2016 shutdown, due to the changed geometry
5766 of the CASTOR region, with a larger beampipe being installed. Minor consolidation changes
5767 are also foreseen for the interlocks provided from the beam monitoring systems.

5768 The beam monitoring system, scattered at various location in CMS, is invaluable in under-
5769 standing beam conditions, to be able to understand sub-optimal conditions. The present sys-
5770 tem (consisting of the BCM1F, BSC and BPTX) is independent of the CMS DAQ, and always
5771 active, providing data for immediate online use, and also for later detailed offline understand-
5772 ing of beam conditions. Excellent timing resolution is a key aspect of the present system, as
5773 this is unavailable elsewhere within the CMS detector. The ability to feed into the L1 trigger
5774 has proved to be a strength during the initial run periods, and will be similarly useful in the
5775 future.

5776 The improvements proposed here afford an improved monitoring capability throughout the
5777 LHC Phase 1 detector operations, based upon the strengths of the present system, and adapted
5778 for the increasing levels of luminosity, beam intensity and corresponding beam background.
5779 One notable improvement is through the provision of a trigger signal, which is designed to
5780 tag incoming beam background with a high purity and efficiency. Improvements in the instru-
5781 mentation are proposed for the BPTX, BCM1F and BSC. Additionally, as an additional option
5782 to the core improvements proposed, a set of forward scintillators is proposed, which would
5783 extend the beam monitoring capabilities into the LHC tunnel, close to IP5. This is potentially
5784 interesting as it would allow the possibility of locating the origin of beam-gas interactions close
5785 to IP5.

5786 The radiation environment in the CMS cavern is of particular concern for two reasons: first
5787 because high levels of radiation can damage sensitive electronics and second because the radi-
5788 ation will cause activation, particularly of materials close to the beam-pipe.

5789 Every effort was made during the design and construction of the CMS detector to ensure that all
5790 sub-detectors are sufficiently radiation-hard for the anticipated levels of irradiation. The antic-
5791 ipated radiation fluences and doses were simulated using the design geometry. As an ongoing
5792 effort it is necessary to validate these simulations against real data measured in the cavern, to
5793 ensure accuracy for the simulation results. Additionally, the simulations should be updated
5794 with the various upgrades and changes in configuration in the CMS detector. To be able to pro-

5795 vide confidence in the simulation results, and ensure that they can always be validated against
5796 measured doses and fluences a suite of detectors, based upon those already available, is pro-
5797 posed to ensure that this is possible. Lastly, the levels of activation are a matter of concern, in
5798 particular for planning shutdown work based upon the ALARA principles. As such, it should
5799 be foreseen that each extended technical stop and shutdown give an opportunity to determine
5800 that the levels of activation are as expected, and that suitable detectors are available to measure
5801 this activation map with great accuracy.

5802 The luminosity measurement is a key aspect of beam instrumentation that is used to monitor
5803 the LHCs performance in real time and to provide an overall normalization for physics analy-
5804 ses. The design goal for the real time measurement is to determine the average luminosity with
5805 a 1% statistical accuracy in 0.1 s. For offline analyses, the design goal is a systematic accuracy of
5806 5 to $10^{34} \text{ cm}^{-2} \text{ s}^{-1}$ and possibly beyond. In addition to providing average luminosity measure-
5807 ments in real time and integrated luminosity values for offline analyses, the luminosity system
5808 will produce bunch-by-bunch luminosities useful for accelerator diagnostics and potentially
5809 also for accurate modeling of underlying event backgrounds. Other important and desirable
5810 features of the luminosity system include a capability for Always ON, operation and a book-
5811 keeping system that is robust and easy to use. Always-ON operation means that luminosity
5812 information should be available for real-time monitoring of the LHC, whether or not the main
5813 CMS DAQ is operational.

5814 The pixel luminosity telescope is designed to address all of these design goals, in particular
5815 it excels as an online luminosity monitor as it is independent of the CMS DAQ. The Pixel Lu-
5816 minosity Telescopes (PLT) detector will be a dedicated luminosity monitor based on arrays of
5817 small angle tracking telescopes each consisting of three planes of diamond pixel sensors on
5818 each side of the IP. By providing a count of the number of three-fold coincidences seen in each
5819 bunch crossing, the pixel luminosity telescope will determine the relative luminosity of each of
5820 the 2835 bunch-on-bunch interactions occurring within the LHC to a statistical precision of 1%
5821 in a time period of $\tau = (0.55 \text{ s})(L/L_0)$ where L is the luminosity and $L_0 = 10^{34} \text{ cm}^{-2} \text{ s}^{-1}$.

5822 Additionally, the pixel luminosity telescope has considerable potential to vastly enhance the
5823 understanding of the beam dynamics, by being able to provide real-time online measurements
5824 of the luminous region, and of the relative rates and distribution of background within the pixel
5825 region. Having these parameters available online means that the LHC operators can potentially
5826 tune the parameters with feedback from data provided by the pixel luminosity telescope.

5827 The pixel luminosity telescope is complementary to the HF luminosity measurement [?], in the
5828 sense that the method is track-based rather than calorimetric-based method. At the Tevatron,
5829 both CDF and D0 found advantages in measuring relative luminosity using tracks rather than
5830 calorimetric quantities.

5831 Some of the upgrades proposed in this chapter also have a subsidiary role which improves the
5832 CMS physics reach for certain analyses. To a large extent, this is by improving the systematic
5833 understanding of the detector as a whole, in particular enabling absolute trigger efficiencies
5834 to be continuously measured with data, using the zero- and minimum- bias triggers provided
5835 by the BPTX and BSC respectively. Systematics can be further reduced by understanding the
5836 background conditions, as already motivated earlier in this section, with the beam background
5837 triggers provided by the BSC and Forward Scintillator Counters (FSC) and diagnostics pro-
5838 vided by the BCM1F. A small bandwidth dedicated to these triggers will allow high cross sec-
5839 tion analyses to be performed in the future. It is therefore vital to make sure that the BSC is
5840 upgraded to continue in its role as a well-understood minimum-bias trigger. In particular at
5841 every restart of the LHC after a shutdown, simple well-understood minimum-bias triggers are

5842 invaluable for an efficient recommissioning of CMS during the short low-luminosity phase that
5843 will occur during each LHC restart period.

5844 The BSC also has an important role to play in the triggering for the heavy ion running. As the
5845 aim during the heavy ion running is to trigger on every event, it will be one of the key triggers
5846 for the run providing one of the two core minimum bias triggers. Additionally, more exotic
5847 triggers will be incorporated to select on certain event topologies (high multiplicity, forward-
5848 backward asymmetries).

5849 The forward scintillator counters option will add to the CMS physics reach in the forward
5850 region during both pp and heavy ion running. The counters will cover $7 \lesssim |\eta| \lesssim 11$, where
5851 $\eta = -\ln \tan \frac{\theta}{2}$ is the pseudorapidity, depending on the particle type and p_T . They extend
5852 the total rapidity coverage of the CMS detector to nearly $\Delta\Omega = 4\pi$. They will help increase
5853 our understanding of all high cross section processes, which is important for understanding
5854 the “underlying event” backgrounds to most physics searches. Full details of the proposed
5855 physics programme from the forward scintillator counters is given in [?].

5856 9.3 Scheduled Plan 2012 and 2016 Shutdowns

5857 The improvements are listed here, divided into the improvements which will be done prior to
5858 the 2012 shutdown, and those foreseen for the 2012 and 2016 shutdown. The list prior to the
5859 2012 shutdown will be done either during the 2011 extended technical stop, or parasitically
5860 during luminosity running in 2011.

5861 Here is the list of improvements planned prior to the 2012 shutdown:

- 5862 • Interlocks
- 5863 • BPTX Trigger System
- 5864 • Forward Scintillator Counters

5865 Here is the list of improvements planned for the 2012 shutdown:

- 5866 • Beam Conditions Monitors: Preventative Maintenance
- 5867 • Beam Scintillator Counters Upgrade (Baseline)
- 5868 • Pixel Luminosity Telescope
- 5869 • Improvements to the instrumentation for validating the simulations (Passives, Medipix
5870 and Neutron Monitoring)

5871 Here is the list of improvements proposed for the 2016 shutdown:

- 5872 • Beam Conditions Monitor 2: Rebuild due to larger CT2 beampipe
- 5873 • Fast Beam Conditions Monitor: Replacement
- 5874 • Beam Scintillator Counters Upgrade (Possible Extensions)

5875 It should also be borne in mind that some R&D work will be needed for upgrades beyond the
5876 scope of this present proposal. This is presented in this note in an appendix to the main text.

5877 9.4 Beam Conditions Monitors

5878 Studies of the radiation hardness of the diamonds and associated equipment in the LHC cavern
5879 show that they should all be sufficiently radiation hard to survive to the end of Phase 1. This is

5880 demonstrated in Table 9.2, where the expected lifetime of the equipment is shown in nominal
 5881 LHC years. At all diamond detector locations, the expected lifetime exceeds that of the nominal
 5882 LHC machine.

	BCM2I	BCM2O	BCM1F	BCM1L
DPA per pp	1.46×10^{-23}	5.92×10^{-23}	2.31×10^{-24}	4.95×10^{-24}
Error	1.14×10^{-24}	2.32×10^{-24}	5.22×10^{-25}	7.5×10^{-25}
Error %	7.82	3.92	22.62	15.16
Hardness factor	0.00835	0.03384	0.00132	0.00283
Seconds at nominal luminosity to reach 50% efficiency	1.06×10^9	2.61×10^8	6.68×10^9	3.12×10^9
In CMS years ($1 \times 10^7 s/a$)	105.7	26.1	668.5	312.2

Table 9.2: Expected radiation damage for all beam condition monitor diamonds installed in CMS. Shown are displacements per atom (DPA), the hardness factor normalised to 24 GeV protons and the expected time in NOMINAL LHC Years to reduce the diamond detector efficiency to 50%.

5883 9.4.1 2012: Preventative Maintenance

5884 In 2012, while there will be access to both the BCM1L and BCM2 systems, it is not foreseen
 5885 that any major work will be required. However, given the critical nature of the systems to the
 5886 protection of CMS, it would be wise to foresee a campaign of work on a sub-selection of the
 5887 diamonds to qualify that they are still in good working order. It is also necessary to anticipate
 5888 problems that may occur between the present time and the 2012 shutdown. This work would
 5889 entail, on a couple of diamonds from each system, checking wirebonds, the metallisation of the
 5890 diamonds, the electrical connections, and the grounding of the system, as well as the state of
 5891 cables and connectorisation and finally recalibrating the system in-situ. Assuming that nothing
 5892 out of the ordinary was found, not further work would be done.

5893 Similarly, given the critical nature of the Beam Conditions Monitors, and in particular the grow-
 5894 ing importance of the BCM inside the tracker region, it should be expected that both the Patch
 5895 Panel boards in the service cavern and the BCM1L Readout boards should be replaced and
 5896 upgraded based upon what is learnt in the first 2 years of running. The patch panel boards,
 5897 as well as mapping the cables to the power supply, provide filtering and correct treatment of
 5898 the grounding. The BCM1L Readout boards are mezzanine cards with a sensitivity of $\sim nA$,
 5899 despite being 100m away from the sensor. While already highly optimised, these cards have
 5900 already been patched, and there is a great deal of recent understanding gained from analysis of
 5901 the data. As such, further improvements in sensitivity and immunity to exterior noise sources
 5902 can be expected if a new set of cards is produced.

5903 A contingency item is the option to install a local UPS in the BCM racks with the aim of isolating
 5904 the power supply from fluctuations on the mains grid. Experience over the first two years of
 5905 running will show whether this is necessary.

5906 9.4.2 2016: Preventative Maintenance and BCM2 Rebuild

5907 Similarly in 2016, preventative maintenance should be carried out on the Beam Conditions
 5908 Monitor systems, in a similar fashion to that done in 2012. However, in addition to this, three
 5909 major items should be foreseen:

- 5910 1. Rebuild of the mechanics of BCM2

5911 2. Possible replacement of the BCM2 “Tunnel card” Front End electronics.

5912 3. Replacement of the VME crate interface board PCs.

5913 The first of these items is required only if the CT2 beampipe diameter is increased subsequent
5914 to the removal of the CASTOR and TOTEM T2 sub-detectors at the end of the low luminosity
5915 phase of the experiment. This is likely to occur during the 2016 shutdown, but could take
5916 place as early as the 2012 shutdown. This would require a complete mechanical rebuild of the
5917 BCM2, as well as a replacement of the front end cabling for the BCM2, which would not survive
5918 such a rebuild intact. This was quite a delicate aspect of the original BCM2, requiring several
5919 attempts to produce a mechanically robust and radiation hard solution. Part of this work may
5920 be mitigated by the fact that it will be needed in some form for the work on replacing the
5921 BSC2 detectors. The rest of the cabling between the CASTOR table and the T2 rack on the HF
5922 platform is also likely to need some work due to the general overhaul of the HF platform. A
5923 simple replacement of this cabling should probably be foreseen.

5924 The second item depends upon the LHC BLM group. At present, they plan to develop a new
5925 version of the tunnel card electronics in the next year or so. It is a possibility that they may in-
5926 stall these in the LHC in the 2016 shutdown, and therefore a complete replacement of the tunnel
5927 cards should be reserved as a possibility for this shutdown, to remain compatible with the LHC
5928 Beam Loss Monitors. The change foreseen for the tunnel cards is from using a radiation-hard
5929 FPGA to an even more radiation-hard ASIC, based upon the present design of the tunnel card.
5930 This change will also remove the distinction between the dual ADC and CFC acquisition elec-
5931 tronics, mis-matches of which cause minor degradation of the monitoring data from the BCM2
5932 detector. Additionally, the upper-end of the dynamic range of the detector will be increased.
5933 The overall result will be a card with a single DAQ system with greater reliability for monitor-
5934 ing and simplicity in interpreting the data. Quite aside from the fact that this card should be
5935 changed for compatibility with the Beam Loss Monitor system, these simplifications will pay a
5936 dividend in understanding the beam from the monitoring. As the luminosity increases towards
5937 the nominal LHC luminosity, detailed understanding of beam background will be vital, as any
5938 deviations from the nominal expected background decrease directly the luminosity reach.

5939 The third item depends upon the LHC BLM and Controls groups. At present they are testing
5940 new board computers with Intel chips running LINUX as a replacement for the present RIO-3
5941 Power PC boards installed all around the LHC. If, as is presently planned, these are replaced
5942 all around the LHC ring in front-end crates, it would be unwise not to follow these changes. In
5943 addition, it will be imperative to test extensively these devices prior to installation in the BCM2
5944 system.

5945 **9.5 Interlocks**

5946 In addition to the beam permit (i.e. beam abort) functionality provided from the Beam Con-
5947 ditions Monitors, several other interlocks are provided to add to detector safety as well as an
5948 adaptable set of logic, to counter developing needs in improving detector safety and smooth
5949 running. These tasks belong to the core responsibility of the Beam Instrumentation, and as
5950 such should be optimised for simple operation and maintainance as well as reliability.

5951 Presently this adaptable logic is performed in a combination of two crates:

- 5952 • A dedicated PLC crate to handle the Emergency Crash Buttons located in the CMS
5953 SX5 Surface Control Room at Point 5. The crash buttons are for the Beam Permit (i.e.
5954 Beam ABort) and for the Injection Inhibit.

- 5955 • A dedicated VME crate, with standard CAEN logic cards to handle coincidence
5956 logic, and registering of safe hardware states sent by the machine, “Safe Beam Flags”,
5957 as well as input into the Injection Inhibit based upon these states and a disable signal
5958 to the Pixel and Tracker CAEN Voltage crates, in case of bad beam conditions.

5959 It is presently under review as to whether, during the 2010-11 extended technical stop, these
5960 crates should be combined into an expanded PLC crate, for the sake of simplicity and ease of
5961 maintainance. A PLC crate is expected to also give a higher level of reliability.

5962 **9.6 Fast Beam Condition Monitors Replacement**

5963 **9.6.1 Improvements to the BCM1F in the technical stop 2011/12**

5964 The DAQ and publishing software will be maintained and possibly upgraded, based on the
5965 experience acquired during running at higher luminosities. Also, the ring-buffer and post-
5966 mortem analysis tools will be implemented and further improved.

5967 Hardware supplements foreseen are coincidences gated with the BPTX signal to separate colli-
5968 sion products from beam halo and signals delayed with respect to the bunch-crossing time.

5969 **9.6.2 The 2011/12 Shutdown**

5970 Some limited damage is expected in the front-end readout of BCM1F. The form this will take
5971 is radiation damage of the FE ASIC and particularly of the laser diode for the analog signal
5972 transmission. Spare components, still available at CERN, should be prepared for this action.

5973 The installation of a single GaAs sector, as described below, will be considered.

5974 **9.6.3 The 2016 Shutdown**

5975 The BCM1F system very likely will need a replacement after 2016 because of damage and cur-
5976 rent rate capability limits. A possible new system should be able to handle higher rates. The
5977 optical transmission of signals should have a wider dynamic range. Digital transmission will
5978 be the preferred option. The new system should explore existing or standard components be-
5979 cause it is unreasonable to develop specific components for such a low number of detector
5980 modules. Standardization within CERN or CMS/ATLAS should be considered.

5981 The baseline design should be for a replacement of the BCM1F system with a very similar de-
5982 tector design. There is an upgrade option under investigation, described below, for a significant
5983 enhancement of its capabilities.

5984 **9.6.4 Pad Detectors using GaAs Sensors**

5985 The possibility of the replacement or supplement of the inner BSC rings using GaAs sensors
5986 will be investigated. These GaAs sensors will be subdivided in pads of $5 \times 6 \text{ mm}^2$, as shown in
5987 Figure 9.2, allowing particle flux measurements with finer granularity.

5988 GaAs sensors are investigated within the BCM-DESY group. The signal to noise ratio is excel-
5989 lent and the leakage current per pad is at room temperature below 500 nA at an appropriate
5990 operating voltage.

5991 The radiation tolerance has been tested so far only in an high intensity electron beam up to
5992 depositions of 1 MGy. The result is shown in Figure 9.3. The signal amplitude dropped to 15%

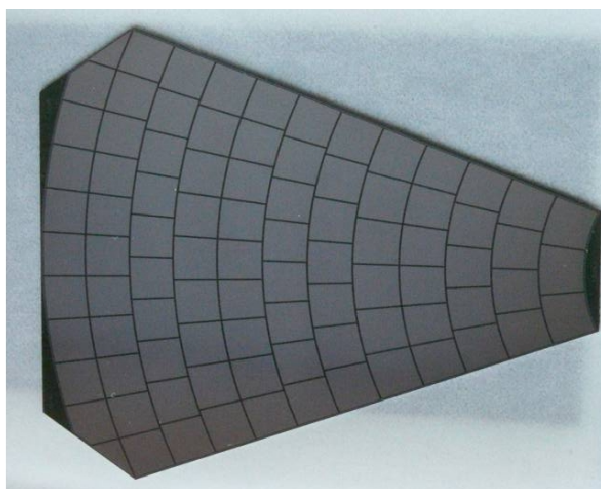


Figure 9.2: A prototype of a GaAs sensor sector with pads of about 30 mm² area.

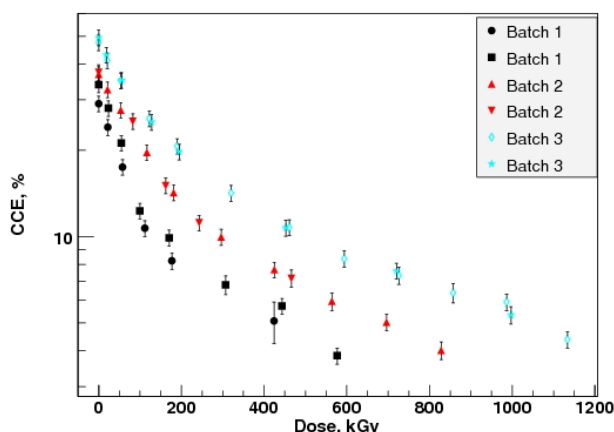


Figure 9.3: The CCE as a function of the absorbed dose for the GaAs sensors with different donor concentrations. The donor is Te for the batches 1 and 2 and Sn for batch 3.

5993 of the original one, but is still sufficient to count Mips. The leakage current at room temperature
 5994 is only slightly increasing up to this dose, and still non-critical for operation of the sensor.

5995 The R&D will be focused first on irradiation tests. Since radiation hard FE ASICs will be needed
 5996 a close collaboration with other groups in or outside BCM will be necessary

5997 9.7 Beam Scintillator Counters Replacement

5998 It is foreseen to replace the beam scintillator counters in the 2012 shutdown, with an option to
 5999 delay this replacement until 2016 depending upon their performance at the end of 2010 with a
 6000 decision being taken during the 2010-2011 extended technical stop. If the replacement is done
 6001 during the 2012 shutdown, there may be further optimisation during the 2016 shutdown to
 6002 ensure that they function for the remainder of nominal LHC running.

6003 For the replacement of the beam scintillator counters a number of proposals have been put for-
 6004 ward; what is presented below is one example of how to construct such a replacement system.
 6005 However there is an array of opinion as to what the functionality and scope of such an upgrade
 6006 should be. A timeline of milestones in the foreseen decision process are outlined to achieve a

6007 engineering design review early in 2011.

6008 9.7.1 Functionality of the Current BSC System

6009 The Beam Scintillation Counter (BSC) [?] is a simple, stand-alone CMS beam monitoring
6010 device. It uses polyvinyl-toluene (PVT) plastic scintillator tiles mounted on the Hadronic For-
6011 ward Calorimeters (HF) facing the IP. The layout and photos of the installed tiles of the the 2
6012 BSC stations is shown in figure 9.4.

6013 The primary purpose for the installation of the BSC system is to monitor various aspects of the
6014 beam background during the early commissioning and low luminosity phases of the LHC in
6015 the region of the CMS experiment. However, the BSC became the most important minimum
6016 bias and beam halo triggering detector in CMS during the commissioning phases and remains
6017 an integral part of CMS data triggering. The BSC has provided the primary trigger for data
6018 analysis for some of the early CMS papers.

6019 The BRM group have several subsystems installed, each focusing on a particular task while
6020 providing some redundancy between two or more sub-detectors[19, 21]. The BCM2[?] system
6021 at $\pm z = 14.36\text{m}$ is a safety system capable of monitoring relative halo and IP product rates
6022 by integrating the leakage current of the diamond sensors. The BCM1F [?] provides beam
6023 monitoring on a bunch by bunch scale but with its position at $\pm z = 1.8\text{m}$ and $5 \times 5\text{mm}$ diamond
6024 area, gives a relatively small field of view of the overall beam dynamics. The purpose of the
6025 current BSC falls somewhere between these two subdetectors with the aim of bunch-by-bunch
6026 beam monitoring in a position where beam background and collision product yields can be
6027 distinguished and compared. Measurements of beam halo timing and rate can be made from
6028 single bunches up to $\mathcal{L} = 10^{32}$ until radiation damage to the scintillator tiles becomes excessive
6029 or saturation of the channels due to large particle flux occurs.

6030 The BSC can effectively be split in to three detector areas: the inner BSC1 tiles, designated D1-
6031 D8 in Fig. 9.4(a), which cover the η range of $3.9 < \eta < 4.4$; the outer BSC1 tiles, designated
6032 P1-P8 also in Fig. 9.4(a), which partially cover the η range of $3.2 < \eta < 3.4$; and the BSC2 tiles,
6033 shown in Fig. 9.4(c) and (d), which cover the η range $4.5 < \eta < 5.7$ with a 30% coverage in ϕ .

6034 9.7.1.1 Present Limitations

6035 The BSC uses large area scintillator tiles which give it a high sensitivity required for the early
6036 phases of the LHC running when luminosity and bunch occupancy are low. When the luminos-
6037 ity increases, the signals will pile-up and result in a loss of some information of the beam halo
6038 and minimum bias events. A system with a dynamic range capable of coping with luminosities
6039 ranging from $10^{27} - 10^{35}$ will produce reliable data beyond the expected luminosities without
6040 losses due to saturation and be operational for the lifetime of CMS. The outer tiles of the BSC1
6041 (see 9.4) are not complete in ϕ and have two different channel areas and radii making individ-
6042 ual channel rates more difficult to equalize and complicating the geometrical acceptance. The
6043 timing of beam halo and collision products provides a method of differentiating particles aris-
6044 ing from collisions at the I.P from those of beam halo and beam gas interactions. At the time
6045 of designing the BSC, the only possible position available for installation was on the HF front
6046 faces at a distance of $\pm 10.86\text{m}$. This is within 2.6ns of a point in Z where the incoming beam
6047 background passes through the outgoing collision products plus the beam background from
6048 the opposite direction (see section 9.7.2.3). With a time resolution of 3ns, it is difficult to differ-
6049 entiate between the two bunch categories and so the BSC2 tiles were installed in an attempt to
6050 reduce the ambiguity of identifying background from collision products. The scintillator tiles,
6051 fibers and PMTs will gradually become damaged by radiation. Indeed, after their use in the

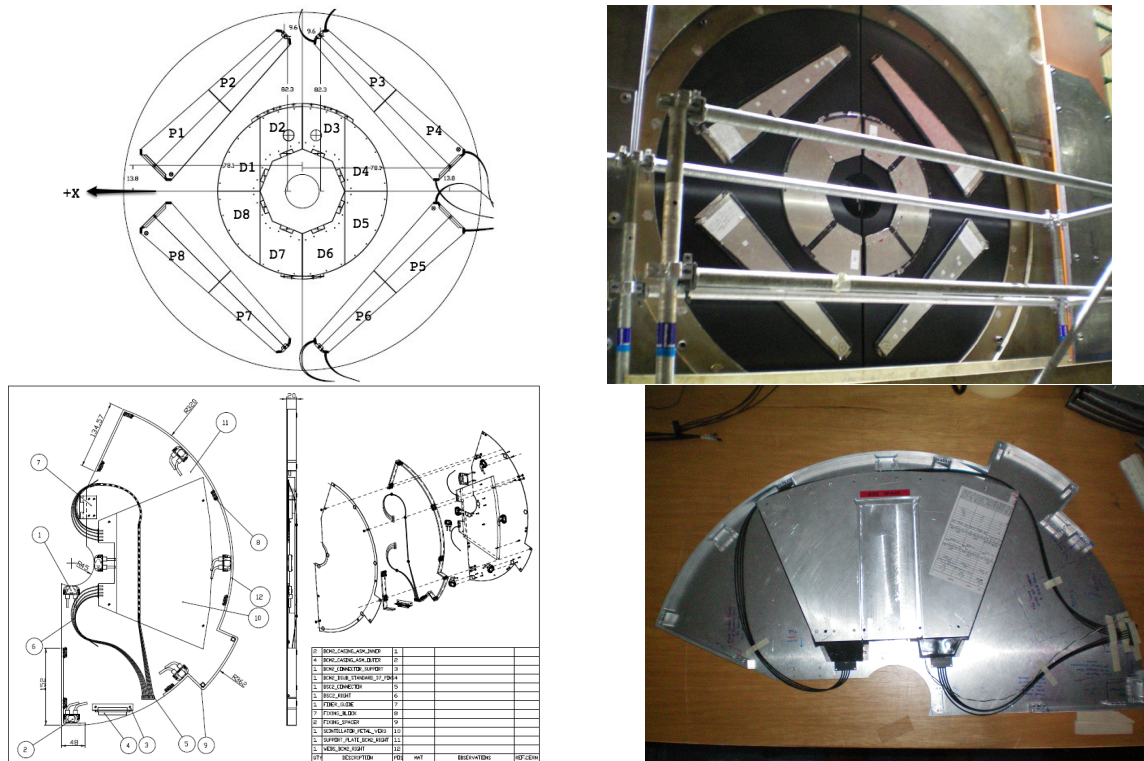


Figure 9.4: The BSC1 tile layout on HF. a) CAD Drawing of BSC geometry and channel names. b) Photo of installed scintillator tiles. c) BSC2 engineering drawing. d) BSC2 tile inside the BCM2 housing before installation.

6052 OPAL endcaps [?] the condition of the hardware is not fully understood. There is no way of
 6053 testing the front end system and calibrating for any loss of light output.

6054 In summary, the present limitations of the BSC are:

- 6055 • Failure of front end components due to radiation damage.
- 6056 • Condition and Radiation hardness of PVT scintillators not fully understood.
- 6057 • Lack of continuous symmetry in ϕ (outer tiles).
- 6058 • Limited time discrimination due to proximity of bunch/beam background crossing
 6059 region.
- 6060 • Timing resolution is only just adequate for the current location (3ns).
- 6061 • Will saturate at luminosities above $\mathcal{L} \approx 10^{32}$ and possibly for Heavy Ion runs.
- 6062 • No *in-situ* calibration method available.

6063 9.7.1.2 Future Functionality

6064 No system yet exists for monitoring and triggering on beam background and minimum-bias
 6065 products in the $\eta = 3 - 5$ region at nominal LHC luminosities. LHC operation during the past
 6066 few months has shown that understanding beam dynamics is vital, as seen from the studies
 6067 on expected beam halo and beam gas [40? ?]. A detector that can trigger and veto on such
 6068 events, as well as monitor them will be a very useful addition to the CMS triggering system
 6069 as a whole. As minimum-bias events scale with luminosity, the upgrade system could be able
 6070 to indirectly measure the luminosity in CMS. Many improvements can be made to the existing

6071 BSC design which are outlined in Table 9.3 along with the implications of these requirements.
6072 A more detailed note on possible future functionality is in preparation and will be released
6073 soon.

6074 The BSC min-bias triggers have been extensively used in event triggering and offline analysis
6075 but, due to the incomplete coverage of the BSC (total $1.2m^2$ per end, not fully symmetric in ϕ),
6076 it is not a long-term solution when high-luminosities and Heavy Ion runs require that min-bias
6077 triggers and beam halo vetoing must be highly reliable and have a large acceptance. There-
6078 fore an upgrade with a larger, symmetrical coverage in ϕ and greater rapidity range will be
6079 beneficial.

Desired Features	Requirement	Details
Symmetrical coverage in ϕ	To increase the acceptance for monitoring and triggering	A complete 360° detector area encircling the beam pipe
Increased dynamic range	To provide proper operation up to maximum luminosity	More channels with smaller area and/or tunable sensitivity
Improved time resolution	To discriminate between collision products/halo with greater certainty	≤ 2 ns front-end signals
Beam background/Collision product discrimination	Use time-of-flight information to monitor relative quantities of background and collision fragments	Determined primarily by installation location and hardware time resolution
Cost effectiveness	Must be financially viable for the lifetime of CMS	Radiation hard detector medium or replaceable cheaper options
Radiation Hardness	Front end materials must be able to survive more than 5 years of continuous running	Quartz or Radiation Hard plastic scintillators as a detector medium. Radiation hard PMTs or other readout devices
Maintenance	Minimal access requirements for repairs and replacements	Any exchangeable parts must be easy to extract and replace for reasons of radiation safety
In-Situ Calibration	Ability to check and set up individual channel response	The channel occupancy for each event needs to be determined. A method of calibrating individual channels remotely is desirable

Table 9.3: Desired functionality of the BSC upgrade. These characteristics will help in deciding the correct channel geometry, material and method of readout. Additional to these aims, mechanical and environmental factors such as radiation hardness and required services must be considered.

6080 In summary, the upgrade of the BSC detector should provide efficient, robust minimum bias
6081 and beam background triggering improving the readout of CMS and importantly, vetoing on
6082 beam gas events. It will also provide an online relative luminosity measurement by monitor-
6083 ing of the minimum bias rates. To provide this functionality up to the LHC design luminosity,
6084 an upgrade of the BSC system needs to be designed, built and installed during the 2012 shut-
6085 down. This should be done during the 2012 shutdown due to the age of the currently installed
6086 hardware.

6087 9.7.2 Environmental Conditions

6088 A major factor of the upgrade design is the environmental conditions that the BSC upgrade
6089 must operate in. The design limits are defined by the radiation flux, magnetic field strength,
6090 available space and the amount of extra infrastructure allowed.

9.7.2.1 Radiation Fluence & Dose

Probably the most important consideration in the design of the BSC upgrade is the radiation environment that the front end detector must be capable of operating in. Simulations of radiation fluence, calculated for 10 years of LHC operation have been made [? ?] for various areas in CMS. The summary of these results that pertain to the BSC region are given in Table 9.4 and Table ???. These numbers will govern the types of materials used and the geometry of the upgrade as detailed in section 9.7.6. Another important consideration is the likelihood of HF neutron induced activation of the polyethylene which will cause random events in the detector tiles if mounted directly on the front face. These *activation events* must be filtered out in some way without introducing a bias in the triggering. One method would be to use two detector layers separated by several radiation lengths of absorber and increasing the distance from the polyethylene face. Coincidences between the layers would allow for discrimination between real events and activation events while increasing the distance will reduce the amount of neutrons incident on the BSC detector elements.

η region	Average Energy	Avg Multiplicity per p-p collision
0 – 3	50 GeV	28
3 – 5.3	380 GeV	20
5.3 – 7.8	2110 GeV	13

Table 9.4: Multiplicity and energy of all particles in various pseudorapidity ranges[?]

The majority of the particle flux stems from collision products rather than beam background [? ?]. Information of beam background and p-p collision products has been taken primarily from [?] and [?].

During LHC operation, the instantaneous luminosity varies by a factor of 10^7 , from $10^{27} \text{ cm}^{-2}\text{s}^{-1}$ for collisions between two nominal pilot bunches to the nominal LHC luminosity $10^{34} \text{ cm}^{-2}\text{s}^{-1}$. These instantaneous luminosities correspond to a rate of primary events of between 10 and 10^8 Hz. The corresponding expected particle flux at the HF front face varies from $1 \text{ cm}^{-2}\text{s}^{-1}$ for luminosities of $10^{27} \text{ cm}^{-2}\text{s}^{-1}$ to $10^7 \text{ cm}^{-2}\text{s}^{-1}$ for nominal luminosity. Nearly 50% of the particles are charged pions. 25% is neutral pions. The rest is made of approximately equal quantities of neutrons, electrons, kaons etc [?]. The flux dictates the details in the design of the BSC upgrade in terms of channel size and materials. Channels which are too large could saturate and would not give useful information on channel occupancy. Choosing channels sizes that are too small would result in an expensive, complicated detector which gives no gains over one with the optimum channel size. The expected photoelectrons reaching the PMT is calculated using a 25cm^2 quartz tile (≈ 100 photons per 1cm traversed material) with a 5% light collection efficiency and a 20% quantum efficiency of the PMT). Proposals of potential detector materials, sizes and front-end readout electronics are given in section 9.7.6.

9.7.2.2 Albedo Events

A phenomenon known as Albedo or “after-glow” has been noted in the BSC Minimum Bias triggers on technical trigger bits 40 and 41. These triggers are important for selecting minimum bias events and accidental triggering could reduce the data taking efficiency of CMS¹. These albedo effects cause the BSC Minimum Bias trigger to continue to fire with a low probability long after the instance of the bunch crossing. Figure 9.5 shows the number of triggers fired per

¹The L1 trigger rule prevents any subsequent triggering for 2BX (50ns) after the first trigger. A false trigger would lose data for up to 3 bunch crossings.

6128 bunch number (BX) summed over run number 123596 (Before) and 123818 (After). Figure 9.6
 6129 shows MC simulation results for 450GeV and 7TeV. It should be noted from the simulation that
 6130 the effects are expected to be essentially independent of \sqrt{s} and to first order only dependent
 6131 upon the collision rate. However, the total sum of these late hits is expected to be 10 - 20% of
 6132 the total and therefore a coincidence is not required for all tiles, as it is not expected to degrade
 6133 the trigger performance of the BSC substantially.

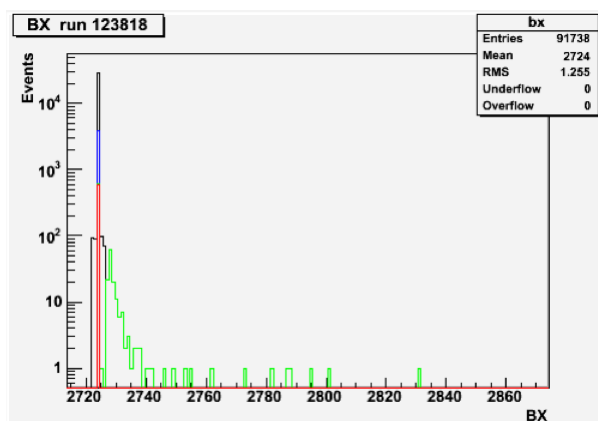


Figure 9.5: Histograms of the BSC Minimum Bias Triggers per bunch crossing (BX) where black is the distribution for all the Express Stream Events, blue for any BSC trigger, green for 40&41 and red for 40&41& (No BeamHalo BSC trigger)& (technical bit 0 (BPTX AND)) [?].

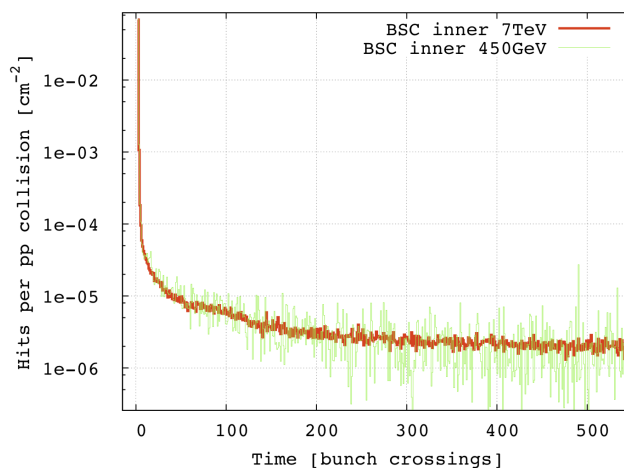


Figure 9.6: Results from MC simulations showing the long tails in arrival time for scattered particles. This may explain the higher incidence of late triggers seen in figure 9.5. [?]

6134 It is suspected that the albedo effects are due to particle scattering and activation from the HF
 6135 polyethylene face. Moving the BSC detector away from the HF face is therefore a worthwhile
 6136 consideration. (See section 9.7.4).

6137 9.7.2.3 Bunch Crossings in Z

6138 With the two LHC beams traveling in opposite directions, there are several points along the
 6139 beam-pipe axis where they overlap, crossing these points at precisely the same instance. By

6140 measuring the arrival time of a bunches (or more precisely, the beam halo² and collision prod-
 6141 ucts that travel with the bunches) with respect to the CMS bunch clock, it is possible to deter-
 6142 mine if the signals originate from outgoing halo and collision products, or incoming beam halo
 6143 only. Therefore, in order to allow discrimination between the incoming and outgoing particle
 6144 bunches, it is vitally important to avoid installing the upgrade detector on or close to any of
 6145 these crossing locations. Figure 9.7 shows the locations of these nodes for 25ns bunch spacing.
 6146 Optimal locations fall halfway between these locations and are given in Table 9.5 and Fig. 9.7.

Z location	Location in CMS
$\pm 1.875\text{m}$	BCM1F locations
$\pm 5.625\text{m}$	Inner barrel
$\pm 9.375\text{m}$	Endcaps. T1 region
$\pm 13.12\text{m}$	Middle of HF
$\pm 16.875\text{m}$	Inside rotating shields
$\pm 20.625\text{m}$	Inside TAS volume

Table 9.5: Optimum positions for the upgrade installation with regard to timing and then Beam1 and Beam 2 crossing locations.

6147 The values in Table 9.5 were calculated by:

$$6148 \quad \Delta t = \text{Min} \left| \frac{2z}{c} - n(Bx) \right|$$

6149 where z is the distance from the I.P, $n = 1,2,3\dots$ and $Bx = 25\text{ns}$.

6150 Some of these locations are unavailable or simply not practical. However, the current BSC2
 6151 location on the Castor table ($Z = \pm 14.36\text{m}$) will be available as is the current BSC1 location on
 6152 the HF front faces ($Z = \pm 10.86\text{m}$). More details are given in section 9.7.4.

6153 9.7.3 Performance of the BSC Minimum Bias Triggers

6154 Using the openHLT ntuple data [?], an approximate calculation of the BSC minimum bias
 6155 trigger performance can be made by looking at how they reacted in the presence or absence of
 6156 true minimum bias events. The offline HLT software is capable of performing quick primary
 6157 vertex reconstruction from the tracker and pixel data and stored the results in branches of a
 6158 ROOT tree in terms of positions in x,y and z and also the number of primary vertices counted
 6159 per event.

6160 Figure 9.8 compares the *L1TechBSC_minBias_threshold1*, *L1Tech_BSC_minBias_threshold2* and
 6161 *L1Tech_BPTX_plus_AND_minus* technical trigger bits with the existence or absence of one or
 6162 more primary vertices, taken from the *recoVrtNtrk* branch. The zero bias trigger was the BPTX
 6163 therefore the BSC numbers are unbiased.

6164 The BSC minimum bias triggers have so far performed well, triggering on 99% of minimum
 6165 bias events, as shown in Table9.6, strongly suggesting that an upgraded detector specifically
 6166 aimed at minimum bias triggering will be important for CMS.

²“Halo” here is used generally to refer to all beam losses which occur before the beam enters the CMS cavern. This is normally broken down in to 2 components; Inelastic beam gas events in the region $20\text{m} < Z < 500\text{m}$; Elastic beam gas events and true beam halo which interact at the tertiary collimators (TCTs) 150m upstream of CMS.

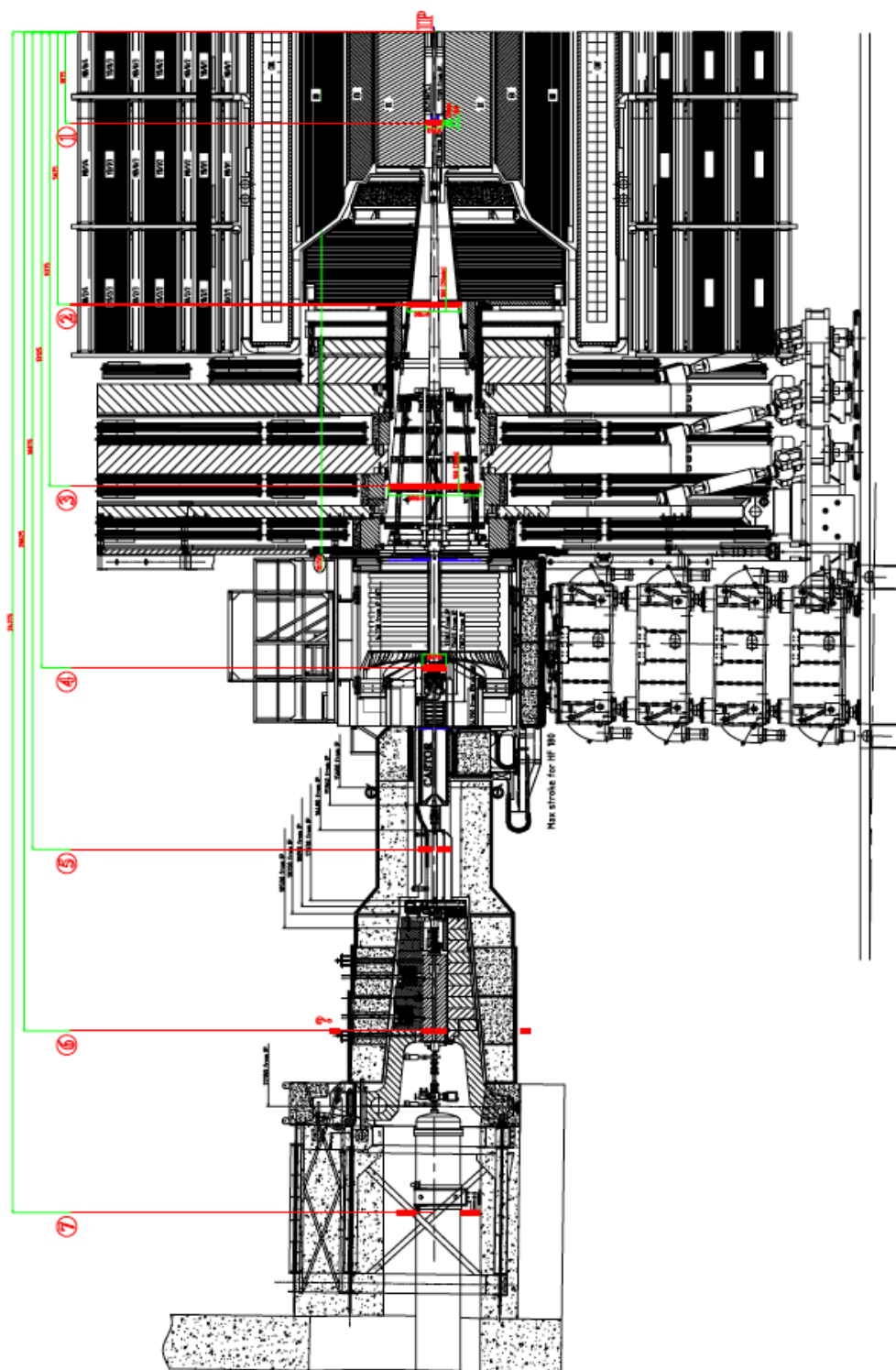


Figure 9.7: Sagittal view of one side of the CMS detector. The red lines indicate the locations where incoming background bunches have the greatest time separation from the outgoing collision products and background from the opposite direction. These locations are optimal to distinguish between the beam background and collision product yield using time-of-flight methods.

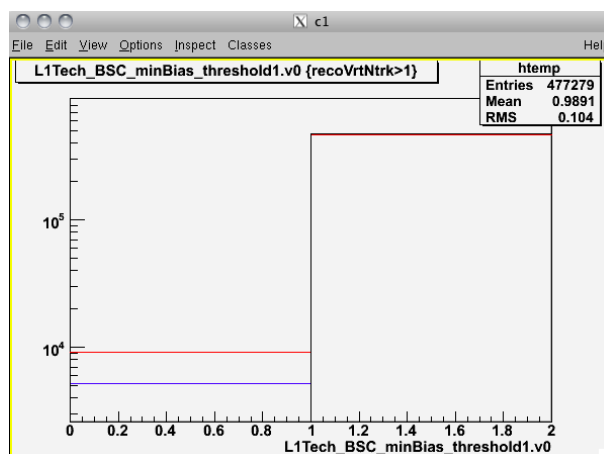


Figure 9.8: Performance of the BSC minimum bias triggers with the BPTX zero bias trigger. Events with one or more vertex are considered to contain a minimum bias event. Blue line: BSC MinBias Threshold1. Red line: BSC MinBias Threshold2. Black line: BPTX Zero Bias.

Trigger	% True Positives	%False Negatives
BSC MinBias Threshold1	99%	1%
BSC MinBias Threshold2	98%	2%
BPTX Zero Bias	100%	0%

Table 9.6: Performance of the BSC minimum bias and BPTX zero bias triggers during 2010.

6167 9.7.4 Available Locations

6168 It was initially foreseen that the upgrade detector would fill the space previously reserved on
 6169 the -Z end of CMS for the Totem T1 sub-detector at $Z \approx \pm 10.7\text{m}$. However, T1 installation is
 6170 now expected to go ahead in the winter shutdown of 2010-2011 so the BSC upgrade will remain
 6171 in the HF region between $Z \approx \pm 10.6\text{m} - 15\text{m}$. This will be beneficial in terms of accessibility
 6172 for additional services, for example, new and existing high voltage cables, signal fibers etc.
 6173 However, as with the current BSC system, the possible installation locations are close to a p-p
 6174 crossing node (9.375m , $\Delta Z = 1.49\text{m}$) where incoming and outgoing beam halo and collision
 6175 products are indistinguishable in time. This will need to be taken in to consideration if certain
 6176 functions are to be carried out by the upgrade detector.

6177 There is a 10 cm deep volume reserved within the Totem T1 detector volume³. This could allow
 6178 the upgrade detector to be moved towards the I.P and away from the HF polyethylene face.
 6179 This has two major advantages. First, it moves to a position where the incoming/outgoing
 6180 bunch crossing Δt is increased from 2.6ns to 3.9ns, making the distinction of the two beams
 6181 easier to achieve. Secondly, it moves the detector elements away from the activated HF calor-
 6182 imeter, thus reducing the back-scatter effects that could propagate in to the L1 trigger. If the
 6183 detector was to be installed here, consideration would have to be given to the extent of the
 6184 effect of the additional BSC material on the performance of the surrounding detectors.

6185 For the BSC2 upgrade, there is some limitation on the minus-side of the CMS detector due to
 6186 the presence of Castor. Here, the upgrade detector must be located within the BCM2 volume,
 6187 as it is now. On the plus-side, there is more available room and the upgrade detector could
 6188 be located at various places along the Castor table, for example, a more ideal location near to
 6189 $Z = 16\text{m}$. This also opens up the opportunity for a more elaborate double layered detector to

³To be installed in the 2010-2011 shutdown on the +Z side of CMS only

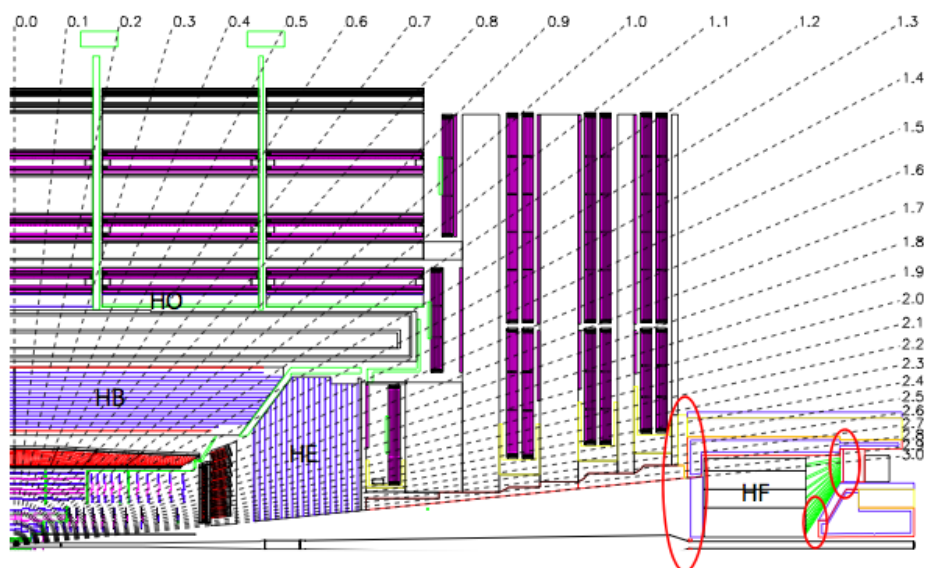


Figure 9.9: Longitudinal view of CMS showing the HF region and possible location(s) for the BSC upgrade.

6190 reduce noise.

6191 9.7.5 Read-Out System

6192 For simplicity and reliability, the readout system will continue to use electrical signal cables
 6193 as opposed to optical fiber. The front-end readout components must be able to withstand the
 6194 harsh radiation and magnetic field environment in the CMS cavern. Silicon Photomultipliers
 6195 (SiPM) are one possible choice provided they can be situated in a location where hadron fluxes
 6196 are low. Radiation hard, multi-channel PMTs are another option. These could be situated in
 6197 the PMT boxes of the current system where they would benefit from shielding due to the HF
 6198 calorimeter.

6199 The back-end readout of the upgrade requires that signals from individual channels are con-
 6200 solidated and their timing evaluated in logic to determine if they are minimum bias, Beam 1
 6201 background or Beam 2 background. The current trigger system uses cumbersome NIM logic
 6202 to achieve this. For the upgrade, there are two possible modern solutions; a CAEN logic board
 6203 [?] or a generic trigger board [?]. Either of these solutions would allow for more elaborate
 6204 coincidence algorithms to be developed in software rather than in NIM hardware. The result-
 6205 ing outputs of the coincidence algorithms will then be sent to the Level 1 Global Trigger. For
 6206 inserting monitoring and luminosity information in to the CMS event stream, there are a num-
 6207 ber of options to be investigated. These include the HCAL QIE [?], the PLT board and the
 6208 SCal method which is under development. The current style of monitoring system, using VME
 6209 based Analog-Digital Convertors (ADC), Time-Digital Convertor (TDC) and scalers could be
 6210 built upon for the upgrade detector, keeping some compatability with the BCM1F detector [?].

6211 9.7.5.1 Possible Detector Materials

6212 The upgrade detector will be in one of the most extreme enviroments in CMS with regards to
 6213 radiation flux and energy. For this reason, the choice of materials is vitally important and sev-
 6214 eral are under inverigation at the present time. The present system uses PVT plastic scintillator
 6215 tiles. These are relatively inexpensive and for the outer regions ($\eta \approx 3$) may be a sufficient

6216 material if changed every 5 years or so. Radiation hard plastic scintillators⁴ also look like a
 6217 promising option. Tests need to be carried out on some materials before they can be put in to
 6218 CMS. Quartz with high OH content is known to be very radiation hard and is a perfect material
 6219 to employ for the inner most channels, both in front and behind HF. The University of Iowa are
 6220 currently developing high-OH quartz plates with P-Terphenyl (PtP) coating to increase light
 6221 yield [?]

6222 **9.7.6 Proposed Prototype System**

6223 The proposed system will fulfill the following:

- 6224 • Provide absolute minimum bias rates and triggers from tiles located on HF at $Z =$
 6225 $\pm 10.86\text{m}$ which are shielded from incoming background but almost in line-of-sight
 6226 with the interaction region.
- 6227 • Beam background monitoring and veto triggering from the tiles located on the Cas-
 6228 tor table at $Z \approx \pm 14\text{m}$ and inner ring of tiles on HF.
- 6229 • Online relative luminosity monitoring from information of the minimum bias rates.
- 6230 • ‘Noise cancellation’ from fake hits (activation events) by the use of two layers of
 6231 detectors and coincidence detection.
- 6232 • Feed data in to the CMS data via the CMS global trigger (L1-Level) and S-link, HCAL
 6233 QIE or PLT readout board

6234 Figures 9.10, 9.11 and 9.12 show the proposed Minimum-Bias/Beam Background detector with
 6235 its geometry and channel layout. Table 9.7 lists the materials of interest to be used in the de-
 6236 tector. The proposal is for 8 inner channels and 16 outer channels per end to replace the BSC1
 6237 system (HF front face) and a further 8 channels per end to replace the BSC2 tiles on the Castor
 6238 tables. This gives a total of 64 channels.

Component	Options to be explore
Detector Material	High-OH quartz, PtP coated Quartz, Radiation Hard Plastic Scintillator(Outer Region), BC-408 plastic scintillator (Outer region)
Light guides	quartz core-quartz clad fibers, air-core fibers
Front End Readout	SiPM, Multichannel PMT
Back End Readout	VME modules, CAEN Logic board Generic Trigger Board (EUDET or Wiener)

Table 9.7: Materials under investigation for the upgrade front-end including detector materials and readout devices.

6239 **9.7.6.1 Triggering System**

6240 The proposed system has active detector elements (quartz plates, radiation hard scintillator)
 6241 mounted on the I.P facing side of the HF calorimeters and on the Castor table, only a few cen-
 6242 timeters from the beam pipe. The HF mounted elements will be in an ideal location to perform
 6243 accurate minimum bias monitoring and triggering as they have an almost direct line-of-site to
 6244 the I.P. The minimum bias trigger would be primarily achieved using these 48 channels and

⁴Available from Amcrys’ European distributors, Detec Europe. All documentation is currently only available in Russian.

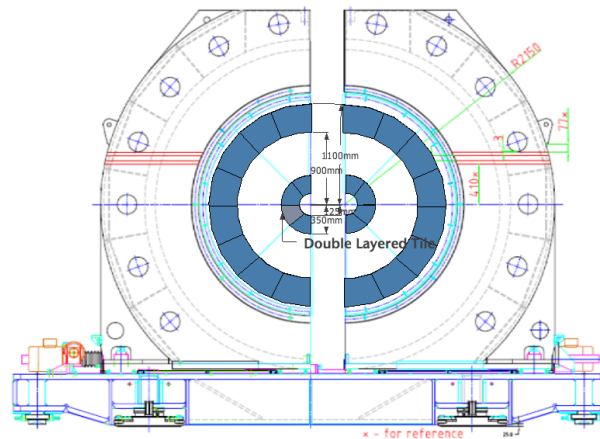


Figure 9.10: Simple concept drawing of the front-end upgrade for the BSC. Quartz or radiation hard plastic scintillator may form the inner annular ring while radiation hard scintillator or BC408 may form the outer annular ring. R & D will determine the number and size of segments as well as the boundary between the radiation hard detector material and scintillator.

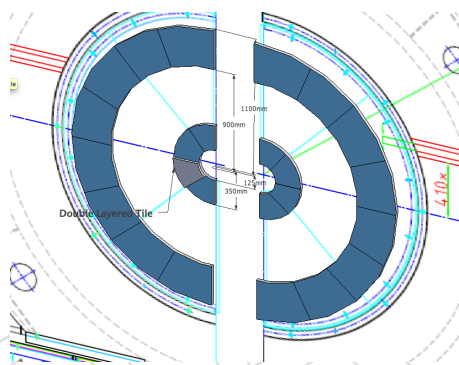


Figure 9.11: 3D view of the proposed upgrade geometry. One or more tiles can be fitted with an extra layer to enable discrimination (by coincidence detection) of true events and noise or activation events from neutrons emitted from the activated HF polyethylene material.

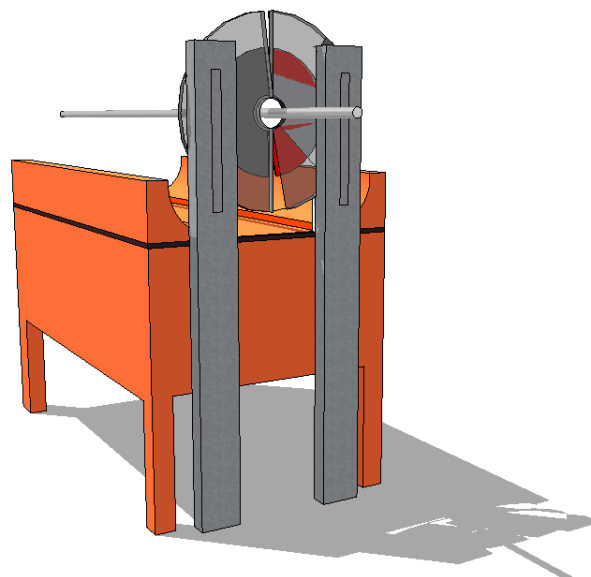


Figure 9.12: Inner BSC halo monitor situated on the Castor table ($Z = \pm 14.4\text{m}$) with full ϕ coverage and appropriate tile segmentation. (concept drawing only; not final design.) As space is very limited on one of the Castor tables, the BSC2 upgrade should ideally fit within the BCM2 envelope. For the opposite Z end, a more elaborate detector could be installed in the available space in a more ideal location.

6245 with the use of dedicated VME triggering boards which are configurable in software, a *major-*
6246 *ity over threshold* logic could be implemented that will make the minimum bias trigger highly
6247 tunable and accurate, even if several channels are not operating optimally.

6248 The innermost of these elements will also be able to detect beam halo passing through the
6249 CMS detector. The elements situated on Castor will form the primary beam halo detector by
6250 using time-of-flight methods to determine the direction of halo. These channels, together with
6251 the inner channels on HF, will form a pair of two, three or four-fold coincidence beam halo
6252 triggers, resulting in a selection of veto triggers of variable sensitivity and accuracy.

6253 **9.7.7 Summary and Milestones for Beam Scintillator Counters Upgrade**

6254 It is clear that there will be an ongoing need from CMS for a BSC-type system for beam mon-
6255 itoring and triggering of minimum bias and beam background events, far beyond the lifetime
6256 of the currently installed system. The BSC has so far outperformed its expectations with a high
6257 triggering efficiency on minimum bias events. However, the detector was not designed to run
6258 beyond a few years or beyond $\mathcal{L} \approx 10^{32} \text{cm}^{-2} \text{s}^{-1}$. This document proposes a prototype design
6259 for the detector to replace the current system which will focus on the aim of triggering on min-
6260 imum bias events and vetoing on beam halo with a high efficiency and purity. It should also be
6261 capable of providing an online relative luminosity measurement by monitoring the minimum
6262 bias rates and normalizing the data with the most recent Van-de-Meer luminosity scans.

6263 A strong need for a replacement has already been indicated for the BSC system for a detector
6264 with powerful beam monitoring and triggering capability. It should be noted that the BSC
6265 has been the primary detector for monitoring beam conditions at CMS for the LHC and, as
6266 such, provides the 2 key figures of merit on background conditions at CMS for the CCC, which
6267 are subsequently reported on LHC page 1. This functionality will also be required from any
6268 upgrade. Informal discussions with members both inside and outside the present BRM project
6269 have indicated several groups who are potentially interested in collaboration on this upgrade.
6270 As the prototype develops, this collaborative effort should be encouraged and developed.

6271 The expected list of milestones and decision points expected in the design and construction of
6272 the Beam Scintillator Counter Upgrade is given below:

- 6273 • Sept 2010: CMS Note detailing functionality of the upgrade. The note will explain
6274 all detector components under consideration and the implications to be considered
6275 for each.
- 6276 • Dec 2010: Report on the outcome of tests carried out of the various detector tech-
6277 nologies for the upgrade. The note will give details regarding their performance,
6278 longevity, mechanical issues and designs of prototype channels.
- 6279 • Feb 2011: Technical Design Report (TDR) for the BSC upgrade outlining the chosen
6280 design, its performance and construction which will lead to an Engineering Design
6281 Report (EDR).
- 6282 • Jan 2012: HF Calorimeters will be in the garages allowing access to the current sys-
6283 tem and installation of the upgrade. Arrangements of work packages, manpower
6284 and necessary special tooling will be made.
- 6285 • August 2012: Installation of the completed Beam Scintillator Counters upgrade

9.8 Pixel Luminosity Telescope

6286

6287 The Pixel Luminosity Telescope (PLT) is a dedicated CMS luminosity monitor that is based on
 6288 single-crystal, diamond, pixel sensors. It is designed to provide a high-precision measurement
 6289 of the bunch-by-bunch relative luminosity on a time scale of a few seconds and a stable high-
 6290 precision measurement of the integrated relative luminosity over the entire lifetime of the CMS
 6291 experiment. The PLT is comprised of two arrays of eight small-angle telescopes situated one
 6292 on each end of CMS. The telescopes are 7.5 cm long and consist of three equally-spaced planes
 6293 of diamond pixel sensors. They are located 5 cm radially from the beam line at a distance of 1.8
 6294 m from the central collision point. Figure 9.13 shows a sketch of a PLT array and indicates its
 6295 location within CMS. The telescope planes consist of single-crystal diamond sensors each with
 6296 an active area of $3.6 \text{ mm} \times 3.8 \text{ mm}$ that are bump bonded to the PSI46v2 CMS pixel readout
 6297 chip[?].

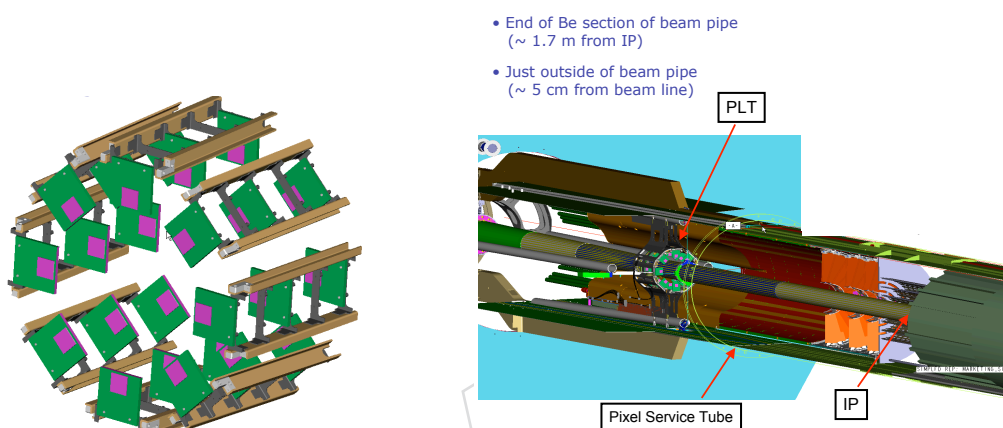


Figure 9.13: Sketch of one of the PLT telescope arrays and its location within CMS. The magenta squares on the telescope planes indicate the locations of the diamond sensors.

6298 In addition to its primary luminosity function, the PLT will also provide important beam con-
 6299 ditions monitoring. It will be sensitive to possible collisions occurring in the orbit gap. It will
 6300 sample the beam halo just outside of the beam pipe and will locate the centroid of the beam
 6301 collision point in real time in intervals of a few seconds.

9.8.1 Diamond Pixel Sensors

6302

6303 Diamond sensors are crucial for the PLT application since they will operate efficiently with only
 6304 a moderate decrease in signal size over the entire lifetime of CMS. Studies have shown that the
 6305 PSI46 pixel readout will also continue to function up to these exposures[?]. Very importantly,
 6306 unlike for silicon sensors, this radiation hardness does not require any cooling of the diamond
 6307 sensors.

6308 Single-crystal diamond is used for the sensor material rather than polycrystalline diamond
 6309 since the distribution of pulse heights of single crystal diamond is large and well separated
 6310 from zero, ensuring that any efficiency changes due to threshold drifts will be small. The
 6311 single-crystal diamond sensors are Chemical Vapor Deposition (CVD) diamond with nomi-
 6312 nal thickness of $500 \mu\text{m}$ supplied by Diamond Detectors Ltd. Their physical area of 4.7 mm
 6313 $\times 4.7 \text{ mm}$ is the largest size currently available for commercial, single-crystal, detector-grade
 6314 diamond. Although a larger diamond size would be preferred for ease of handling during pro-
 6315 cessing, the present area is more than sufficient for the solid angle coverage required for the
 6316 PLT.

6317 Before irradiation, a single crystal diamond yields full charge collection at an applied field of
 6318 less than $0.4 \text{ V}/\mu\text{m}$ with a leakage current less than $1 \text{ pA} / \text{cm}^2$. A minimum ionizing particle
 6319 normally incident to the $500 \mu\text{m}$ diamond produces a mean signal of about 22,000 electrons well
 6320 above the noise level in pixel electronics and well above the pixel threshold values of 2,000 to
 6321 3,000 electrons. At the location of the PLT just outside of the beam pipe, the particle fluence
 6322 over the 500 fb^{-1} integrated luminosity expected during Phase 1 calculated by simulations is
 6323 about $2 \times 10^{15} \text{ particle} / \text{cm}^2 / \text{second}$. [?] Although at this radiation dosage, single-crystal
 6324 diamond show about a 40% loss in charge collection efficiency [?], the signal from a minimum
 6325 ionizing particle is still well above the set threshold values. At this dosage, there is no increase
 6326 in leakage current. Figure 9.14 shows the pulse height distribution from ^{90}Sr β particles incident
 6327 on a $500 \mu\text{m}$ thick single-crystal diamond before irradiation and after an exposure of 1.5×10^{15}
 6328 $/ \text{cm}^2$ 24 GeV protons.

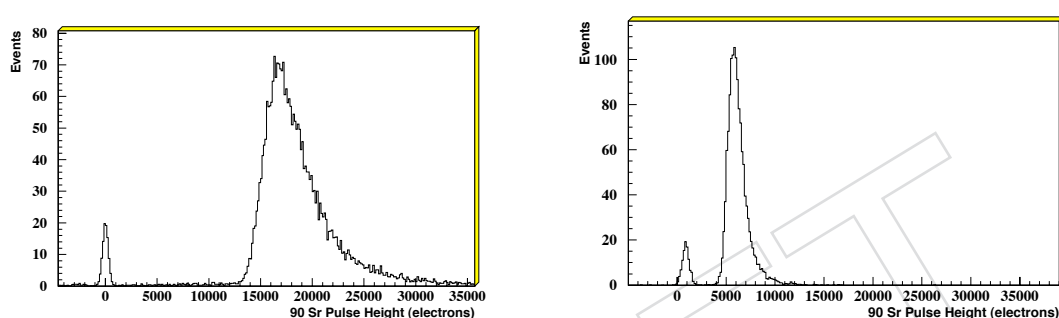


Figure 9.14: Pulse height of ^{90}Sr /beta particles in a $500 \mu\text{m}$ thick single crystal diamond. Before irradiation on the left and after exposure to $1.5 \times 10^{15} / \text{cm}^2$ 24-GeV protons on the right. Pedestal events are also shown to indicate signal separation form zero.

6329 Deposition of the pixel electrode pattern on the diamonds and the bump-bonding of the di-
 6330 amond sensors to the pixel readout chips is carried out “in-house” at the Princeton Institute
 6331 of Science and Technology Materials (PRISM) micro-fabrication laboratory. Following surface
 6332 preparation, electrodes are sputtered onto the diamond surface using a Ti/W alloy target as an
 6333 under bump metalization (UBM). A $4 \text{ mm} \times 4 \text{ mm}$ electrode is deposited on one side of the
 6334 diamond using a shadow mask. On the other side, a pixel pattern is deposited using a standard
 6335 lift-off photolithographic process. The pattern covers an area of $3.9 \text{ mm} \times 4.0 \text{ mm}$ and consists
 6336 of an array of 26×40 pixels with pitch of $150 \mu\text{m} \times 100 \mu\text{m}$ matching that of the PSI46 chip.
 6337 Each UBM pixel electrode is $125 \mu\text{m} \times 75 \mu\text{m}$ with $25 \mu\text{m}$ gaps between electrodes. The pixe-
 6338 lated diamond sensors are then bump-bonded to the readout chip using a flip-chip procedure.
 6339 Approximately cylindrical indium bumps with diameters of $15 \mu\text{m}$ and heights of $7 \mu\text{m}$ to 8
 6340 μm are evaporated onto the pixel pads on both the readout chip and the diamond sensor. This
 6341 step requires a thick layer of photoresist built up from two layers of intermediate thickness.
 6342 Depositing the indium bumps on readout chip wafers using this thick photolithographic pro-
 6343 cess is relatively straightforward since chips at the periphery of the wafer could be sacrificed.
 6344 Depositing the indium bumps on the individual diamond pieces required considerably more
 6345 development. It is necessary to remove a thick meniscus of photoresist that forms at the edge
 6346 of the diamond during the photoresist spinning process without compromising the integrity
 6347 of the pixel pattern close to the edge of the diamond. A procedure was developed for forming
 6348 a custom-fit frame around each diamond so that the photoresist would fully spin off the dia-
 6349 mond onto the sacrificial frame leaving a uniform layer on the diamond. After indium bump
 6350 deposition, the diamond sensors are then bump-bonded to the readout chip using a Research
 6351 Devices MA-8 flip-chip bonder with an optically-controlled alignment precision of better than

6352 2 μm . The electromechanical bond is then formed by applying pressure. The indium bumps
6353 are not reflowed. The readout chip has an array of 52×80 channels larger in area than the
6354 diamond sensors and the diamonds are bonded to columns 13 through 38 and rows 41 through
6355 80 at the top edge readout chip. A completed detector mounted on a hybrid board is shown in
6356 Fig. 9.15.

+



Figure 9.15: Bump bonded detector.

6357

6358 9.8.2 Readout

6359 The readout of the PLT utilizes extensively the chips and VME electronic modules that have
6360 been developed for the CMS pixel detectors. The diamond sensors are bump-bonded to the
6361 PSI46v2 pixel readout chip that is used in CMS pixel detectors. This chip outputs a fast-or
6362 signal at each LHC bunch crossing (40 MHz rate) that indicates the number of double columns
6363 with pixels above threshold. This signal from each of the three planes in a telescope will be
6364 used to form a 3-fold coincidence indicating the number of particles traversing the telescope.
6365 The number of these 3-fold coincidences in the array of PLT telescopes provides the measure
6366 of the instantaneous luminosity. This luminosity will be recorded for each of the beam crossing
6367 in an LHC orbit.

6368 In addition to the fast-coincidence information, the full pixel information will also be read out
6369 from the PSI46 chip at a triggered rate of about 10 KHz. This will provide information on the
6370 row and column address of the hit pixels and the hit pixel pulse height. This information will
6371 be very powerful in achieving low systematic errors on the luminosity. Two of the largest po-
6372 tential sources of systematics in the fast-coincidence luminosity measurement are coincidences
6373 caused by accidental hits leading to an over estimate of the luminosity and two-particle over-
6374 laps in a telescope leading to an under estimate. Both of these effects are proportional to the
6375 number of interactions per bunch crossing. Simulations have shown that each is a few percent
6376 at full LHC design luminosity. By using the pixel information, these effects can be measured
6377 and corrected to a few per cent of themselves. The full pixel information will also be used to
6378 diagnose the corresponding fast-or coincidence signals for those bunch crossing in which the
6379 full pixel readout is triggered.

6380 Several custom circuits have been designed for the PLT. The hybrid board is a rigged-back
6381 flex circuit on which the telescope detector planes are mounted and wire-bonded. The hybrid
6382 boards have flexible pig tails that plug into the HDI circuit that forms the backbone of the
6383 telescopes. The HDI houses the CMS TBM chip that orchestrates the readout of each of the
6384 chips on the telescope planes and distributes control signals and bias voltage to the detectors

6385 on the hybrid boards. The HDI's from four telescopes, connect to a port card, a semicircular
 6386 rigged-backed flex circuit, that is located on the PLT/BRM carriage at the rear of the telescopes.
 6387 For each set of four telescopes there is also an optoboard located at the foot of the PLT/BRM
 6388 carriage that houses the optical components, AOH's and DOH's, for the optical readout and
 6389 control signals. The AOH and DOH optical hybrids are the same as those used in the CMS
 6390 tracker.

6391 The PLT will provide two types of data: full pixel readout at a few kHz, and fast-OR hit-
 6392 counting information at the bunch crossing rate of 40 MHz. In the full readout mode, the data
 6393 acquisition process will be identical to that of the CMS pixel detector. Data fragments consisting
 6394 of addresses and pulse height information from each readout chip framed by header and trailer
 6395 packets supplied by the TBM will be sent to the Front End Driver (FED), where the data will be
 6396 digitized and merged into the CMS data stream. Both full pixel readout and fast readout will
 6397 use the FED VME module developed by Vienna. The full readout chain will be the same as
 6398 the existing CMS pixel system and therefore will not require any specialized development. The
 6399 fast out used to extract luminosity information in realtime will require only modification of the
 6400 firmware on the FED's FPGA. In particular, the system will need to fill a histogram having one
 6401 bin for each of the 3564 bunch crossings. Data accumulated in this array will be shipped to a
 6402 dedicated PC for further accumulation and distribution to the different luminosity consumers.
 6403 See Fig. 9.16.

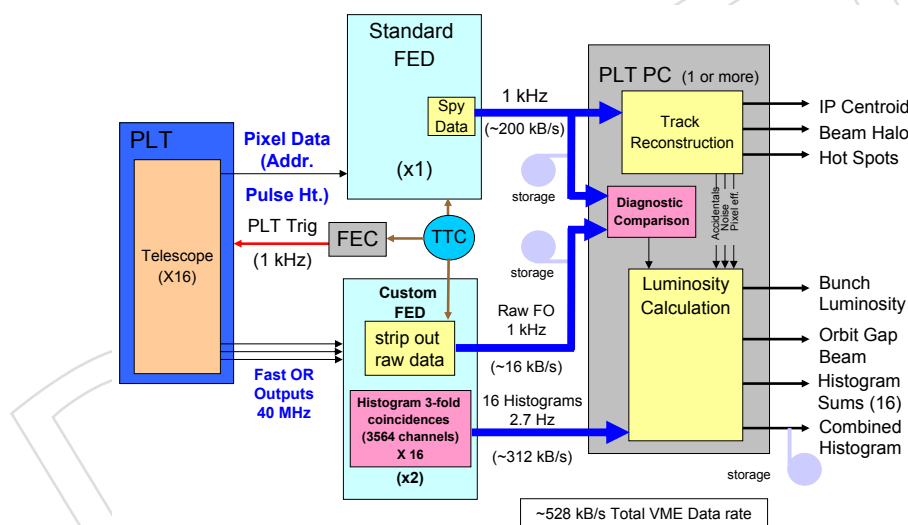


Figure 9.16: Schema diagram of the PLT readout.

6404 The PLT data correspond to the number of telescopes that were hit during a bunch crossing.
 6405 A similar logic design was completed for the HLX FPGA for the HF based luminosity. The
 6406 firmware would take partially processed data from the ROCs and histogram it over a complete
 6407 orbit, thereby providing a per-bunch representation of luminosity, including empty bunches.
 6408 The occupancy histograms are transmitted to a PC via VME once roughly every 0.37 s, which
 6409 is safely within the 5.8 s (worst case) histogram overflow time. The occupancy histograms
 6410 comprise about 7 KB of data which is transmitted to the PC at a rate of approximately 0.16
 6411 Mbps. Many other design elements of the HLX firmware system, for example the handling of
 6412 the LHC clock signals and the interaction with the CMS DAQ will be directly transferable to
 6413 the PLT design.

6414 The readout synchronization with the CMS DAQ system will also be similar to the HLX-based

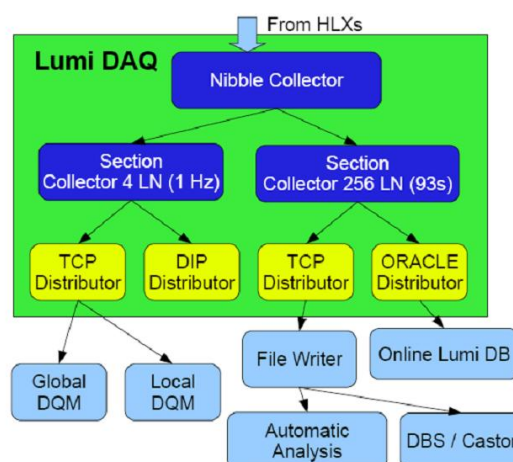


Figure 9.17: Software class hierarchy in HF based online readout framework.

6415 luminosity system. Luminosity histogramming begins on an OC0 command. Data is then
 6416 accumulated for a programmable number of orbits (called a 'lumi nibble') and then shipped to
 6417 the readout PC. Since this readout path is independent of the main DAQ system, the PLT will
 6418 be able to provide realtime luminosity information even when the CMS DAQ is down—e.g.,
 6419 during the injection and ramping phases of LHC.

6420 A large amount of online software for the handling of luminosity data has already been de-
 6421 veloped for the HF-based luminosity monitor. Most of this will be directly transferrable to the
 6422 PLT. Dedicated online software was developed to process the raw data on a dedicated PC and
 6423 to provide an interface with the CMS Database (DB), CMS and LHC. The class architecture
 6424 of the online software can be seen in Fig 9.17. Processing the histogram data is split into sev-
 6425 eral classes. The NibbleCollector class is used for basic processing, such as the data integrity
 6426 checks. Once this has been achieved, the data is forwarded to the SectionCollector class, where
 6427 it is aggregated. Once the desired number of nibbles has been collected, the data is forwarded
 6428 to distributors, which output the data to various monitoring systems and in various formats,
 6429 including CMSSW DQM, Oracle DB, ROOT, gif, and LHC DIP.

6430 An effort has gone into developing software to log luminosity data and to make it available to
 6431 users doing offline analysis. As is the case for the online software, the vast majority of this
 6432 software will be directly applicable to the PLT data.

6433 9.8.3 Performance

6434 9.8.4 Test Beam Results

6435 9.8.5 Status

6436 The PLT project has undergone several CMS reviews and was approved for production at an
 6437 Engineering Design Review held in November of 2009. The construction of the PLT is by now
 6438 well advanced and the project is on schedule for the PLT to be completed and ready for in-
 6439 stallation by the end of the year. Sixty diamond sensors have been ordered and delivered.
 6440 Forty-seven of these have been characterized of which thirty-four have passed selection crite-

6441 ria. The ones that failed are being returned to the vendor for replacement. Twelve detector
6442 planes have been assembled with an additional eight planes ready in the first week of July.
6443 Twelve detector planes have been tested of which ten have passed the criteria for use in the
6444 PLT. The production rate has reached three planes per week and we expect the remaining
6445 planes to be completed and tested by the beginning of October. Prototype custom firmware
6446 for the fast-or FED has been developed by the Vienna HEPHY group and is currently under
6447 test. A full optical readout of a prototype telescope using prototype HDI's, port card and opto-
6448 board has been successfully completed and was used in a beam test at Fermilab in March. All
6449 of the final production hybrid boards have been delivered. All of the production HDIs have
6450 been delivered and will soon be under test. All of the production port cards type Version A
6451 have been delivered and have been successfully tested. Version B of the port card is currently
6452 under design. The optoboard has been designed and will be in production by the end of July.
6453 The design of the mechanical support cartridge for the PLT telescopes has been completed will
6454 be out for production by mid July. We expect a complete system with all of the final prouction
6455 components including firmware and DAQ software to be completed by the end of September.

6456 9.8.6 Installation Plan

6457 9.9 Beam Position Timing for the Experiments

6458 The Beam Position Timing for the Experiments (BPTX) are 2 LHC standard Beam Position mon-
6459 itors installed 175m upstream of the interaction points on the incoming beam pipes. These
6460 devices are absolutely essential for CMS, providing both the absolute reference timing of the
6461 beams, through a scope-based readout device, as well as jitter measurements of both the LHC
6462 beams and all LHC clocks with respect to each other. Additionally, they provide the zero-bias
6463 trigger to the L1 Global Trigger, and through this trigger determine the L1 trigger timing. This
6464 trigger is essential for understanding the absolute efficiency of all CMS triggers and will con-
6465 tribute to the studies determining and reducing systematic effects in the data. All of these
6466 triggers are presently tuned to have variations and jitters $< 500\text{ps}$, insignificant given the phase
6467 measurements at the L1 trigger of 6.125 ns.

6468 The present set of triggers was provided with a simple NIM logic, so that it was flexible to meet
6469 the highly variable needs in the first months of CMS running. This decision for flexibility was
6470 a considerable boon, which has resulted in 16 trigger inputs being provided from the BPTX de-
6471 vice to the L1 trigger, indicating the success and reliability of the devices. These triggers, while
6472 still the main L1 trigger seed to the HLT at a luminosity of $10^{27}\text{cm}^{-2}\text{s}^{-1}$, will have an increased
6473 prescale at high luminosities. However, it is clear that for all periods of heavy ion running, and
6474 for all start-up periods following shutdowns, the zero-bias triggers will be essential for deter-
6475 mining that CMS, in particular the trigger, is recommissioned efficiently, and to remeasure the
6476 absolute experimental timing.

6477 To this end, it is foreseen, before the 2012 shutdown, to complement the NIM-based trigger
6478 system by a simple VME based trigger system. This will consist of VME-based discriminators,
6479 and a FPGA-based generic logic unit (CAEN V1495). This can be commissioned in parallel to
6480 the minimum system, so that no downtime is caused.

9.10 Validating and Updating the CMS Cavern Simulation: LHC RADMON, Medipix, Neutron Detectors, Passives and Activation Measurements

The impact of neutron radiation on the electronic equipment associated with the Large Hadron Collider, both for the experiments and the machine itself, is a worrying aspect of the accelerators operation. Damage caused by neutron radiation includes breaking inter atom bonds within materials and causing Single Event Upsets (SEUs), where the neutron causes a transistor to flip bits within a microprocessor or memory. SEUs are particularly worrying as they can cause data corruption and even destruction of devices. Measurements are currently made in the CMS cavern using LHC RADMON units, passive radiation monitors, the HF RADMON units and the experimental Medipix-based detectors using a USB readout system developed by the Czech Technical University. What is learned from these monitors in the 2010-11 running periods and beyond will be used to design the monitoring for the period beyond that.

9.10.1 Data from currently installed neutron monitors

The Medipix based detectors can give us the information absent from the RADMON system. Medipix chips were developed at CERN and evolved from the silicon pixel detectors used in many high energy physics experiments. The current version of the chip, Medipix2, features 65,536 pixels which each contain the necessary electronics for detecting the creation of a cloud of electron-hole pairs in the sensors semiconductor layer, which is bump bonded to the chip. The chip is able to determine the position of the incident particle as well as determine the particles energy through the use of energy thresholds [2]. Neutron radiation cannot be readily detected by the Medipix chip alone, so layers of neutron converter materials must be applied. For the ATLAS-MPX and CMS-MPX systems two types of neutron converters, Lithium Fluoride (LiF) and Polyethylene (PE), were applied over the chip by the Czech Technical University (CTU). 1 Thermal neutrons impacting the LiF layers cause the emission of α -particles, while the PE layer will emit protons when hit by fast neutrons.

9.10.2 Proposed Improvements to Slow Monitoring

Given the danger of premature demise of equipment due to larger than expected fluxes of neutrons, it should be anticipated that an array of diagnostic tools might be needed to qualify simulated neutron flux maps of the cavern. As such it is currently foreseen, that looking to the upgrades in 2012 and 2016, the following devices will be made available:

- LHC RADMON units (or their successor)
- HF RADMON units.
- Medipix Gigabit-ethernet neutron cameras
- Passive neutron monitors (see section on passive monitoring).

The LHC RADMON units presently in use will continue to be so. The cabling and scope of these devices is such that they are already fairly flexible to be portable to any location in the cavern if a problematic region is suspected. If the LHC upgrades these devices, it is expected that the same will happen in the CMS cavern.

Also anticipated is the development of the Canterbury-CTU Neutron Camera, the next iteration of the Medipix based detection systems. It utilises the same Medipix chips as the current system but replaces the USB readout with the gigabit Ethernet-based MARS Readout board developed at Canterbury. The use of an Ethernet connection will allow for faster data transfer over greater

6524 distances. It is foreseen that up to 10 of these devices will be installed in the CMS cavern during the
 6525 2012 shutdown. The Gigabit Ethernet connection and ability to read data at 100fps will allow
 6526 for real-time radiation monitoring and particle identification. A prototype MARS readout
 6527 has been operational for many months, with a production copy currently in the final stages of
 6528 development.

6529 9.10.3 Passives

6530 The studies ongoing at the moment and also from reading the doses from the passives acces-
 6531 sible during the 2010-2011 extended technical stop will highlight areas which are understood
 6532 and those where there is less understanding or even disagreements, demonstrating gaps in
 6533 the present shielding configuration. In particular, this will be used to qualify the simulations
 6534 presently available for the radiation map in the CMS cavern. While the studies show so far
 6535 that the level agreement between simulations and the measured radiation field in the cavern is
 6536 good, there are several problematic areas. As such there will be a need to review for every long
 6537 shutdown the positions chosen for the passive detectors to get integrated fluxes. Similarly,
 6538 there should be a flexible approach, to allow a quick measurement of vulnerable electronics
 6539 to determine the cause of operational problems. Additionally, as the integrated luminosity in-
 6540 creases, and hence the integrated dose to electronics, vulnerabilities may be exposed. It should
 6541 be possible to quickly rule in or out radiation as the cause of these problems. To enable a flex-
 6542 ible approach to this problem, it should be foreseen to have a range of passives available for
 6543 installation in case of need in both of these shutdowns.

6544 9.11 Required Resources: Manpower Requirements, Schedule, and 6545 Expression of Interest By Institutes

6546 9.11.1 Manpower requirements

6547 Table 9.8 shows the required manpower for each of the proposed upgrades. These manpower
 6548 estimates are given in Full Time Equivalent (FTE) Man-Years. They include only the required
 6549 manpower to design, build, test and install the detectors. In all cases it is assumed that there
 6550 is further manpower available to commission and utilise these detectors from the standard
 6551 Maintenance and Operation.

Sub-detector	Manpower (FTE Man-Years)			
	Physicist	Engineer	Technician	Total
BCM	4	0.5	0.5	5
BCM1F	4	3	2	9
BSC	3-5	1	1.5	5.5-7
FSC	3	1	2	6
Medipix/Neutron	1.5	0	1	2.5
Passives	0.25	-	0.25	0.5
PLT	6	7	6	19
Total	21.75	12.5	12.25	66.5

Table 9.8: Manpower requirements for each of the proposed upgrades to the CMS beam instrumentation. This is broken down into three categories of manpower: physicist, engineer and technician. The allocation in the column is in terms of full-time-equivalent man-years (FTE MY).

6552 **9.11.2 Proposed Schedule**

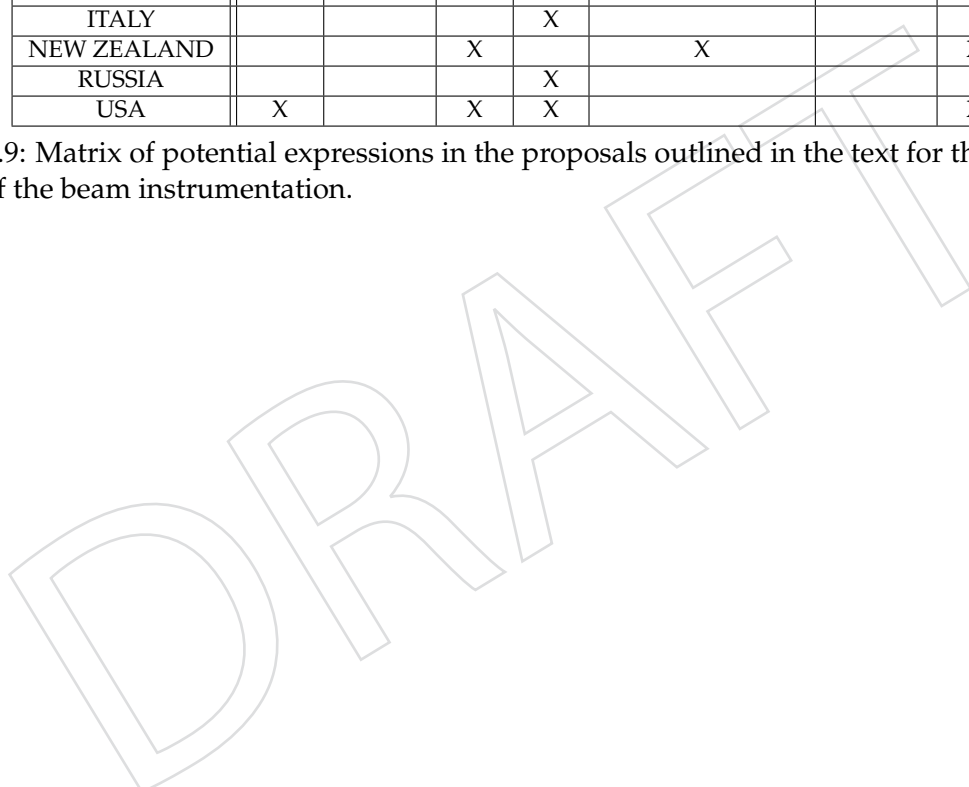
6553 The milestone schedule is shown in the charts below for the 2012 shutdown and the 2017 shut-
 6554 downs.

6555 **9.11.3 Expression of Interest by institutes**

6556 Table 9.9 shows the matrix of the institutes (and a country-basis) against the proposed aspects
 6557 of improvements on the beam instrumentation. All expressions of interest are at this stage
 6558 provisional.

Country	Subdetector						
	BCM	BCM1F	BSC	FSC	Medipix/Neutron	Passives	PLT
AUSTRIA							X
BELGIUM				X			
CERN	X	X	X	X	X	X	X
GERMANY	X	X	X			X	
FINLAND							
ITALY				X			
NEW ZEALAND			X		X		X
RUSSIA				X			
USA	X		X	X			X

Table 9.9: Matrix of potential expressions in the proposals outlined in the text for the improvement of the beam instrumentation.



DRAFT

6559 Chapter 10

6560 CMS Common Systems, Infrastructure and 6561 Facilities

6562 10.1 Introduction

6563 This section describes the consolidation and upgrade programme for the common systems,
6564 infrastructure and facilities of the CMS experiment, which is planned between now and the
6565 end of the long LHC shutdown presently scheduled for 2016.

6566 The individual particle and energy detection sub-systems deployed in the CMS experiment are
6567 the responsibility of sub-collaborations of institutes (in some cases including CERN), which
6568 take responsibility for their construction, maintenance and upgrade. Associated common sys-
6569 tems, infrastructure, facilities and technical projects, which are needed to satisfactorily assem-
6570 ble and maintain the sub-detectors and to allow them to function together as a technically co-
6571 herent scientific apparatus, are provided and maintained either by CERN as the host laboratory
6572 or using common CMS collaboration resources.

6573 10.1.1 Overview of the CMS Common Systems

6574 These systems, which form part of the responsibilities of the CMS central technical team, are
6575 listed below:

6576 1. Safety systems for the protection of personnel and equipment

- 6577 • The Detector Safety System which protects the experimental apparatus.
- 6578 • Remote sensors including cameras, microphones systems and devices to mea-
6579 sure position changes, mechanical strain, and environmental conditions.
- 6580 • The nitrogen, dry air and compressed air systems for inertion, environmental
6581 stabilization and pneumatic control.
- 6582 • Fire and smoke detection and fire extinguishing systems.
- 6583 • Radioprotection precautions, measuring devices and equipment tracability sys-
6584 tems.
- 6585 • Access control.
- 6586 • Safety Training.

6587 2. **Magnet** The 4T superconducting solenoid coil, including the power, cryogenic, monitor-
6588 ing, control and safety systems needed to operate it, along with field measuring devices
6589 and field simulations.

6590 3. **Yoke, Shielding and Moving Systems** The segmented flux return yoke (which also forms
6591 the structural backbone of CMS), the radiation shielding system and the moving systems,

- 6592 with the associated surveying or monitoring equipment needed to open and close these
6593 elements safely and efficiently for maintenance, repair, consolidation or upgrade.
- 6594 **4. The Experimental Beampipe** This covers the beampipe in the range $\pm 18\text{m}$ either side of
6595 the interaction point; its support structures for operation, maintenance and bakeout; and
6596 the tooling necessary to install, remove and maintain it. Included in this category is also
6597 the set of removable radiation shielding necessary to protect maintenance personnel from
6598 regions of the beampipe and nearby detectors which will become progressively activated
6599 by collision products.
- 6600 **5. The Beam Radiation Monitoring System** The beam radiation monitoring system consists
6601 of an array of active and passive devices, designed to monitor beam conditions and the
6602 radiation field at LHC Point 5. The purpose of the system is to protect the CMS detector
6603 from damage (via a beam abort and injection inhibit capability); to optimize collision
6604 conditions for data-taking; and to monitor the accumulated dose and induced activity
6605 throughout the detector.
- 6606 **6. Logistics and Integration** This includes interfaces to subsystem tooling and the capability
6607 for controlling temperature and humidity in specific working areas.
- 6608 **7. Experiment Service Infrastructure** This delivers power, IT network, cooling, operating
6609 gas, inertion gas, instrument air and dry air to the experimental cavern for the operation
6610 of the subsystems and the magnet. It includes the cooled rack systems in the experimental
6611 and service caverns and the piping and cabling network. It also includes the local count-
6612 ing and control rooms, including: the principal CMS control room in surface building
6613 SCX at LHC Point 5, the underground electronics cavern including the commissioning
6614 control room contained within it, and the surface DAQ barrack.
- 6615 **8. Beam, Radiation, Cosmic Ray, or Environmental Test Facilities** These facilities are for
6616 investigating long-term performance or anomalous behaviour of installed detector sys-
6617 tems and for testing detector systems proposed for consolidation or upgrade.
- 6618 **9. Surface Assembly Buildings, Workshops, Laboratories, and Storage space** These are
6619 needed to sustain the construction, testing, maintenance, operation and upgrade of the
6620 subsystems. This includes areas capable of dealing with activated equipment.

6621 10.1.2 Funding

6622 Funding for CMS central systems, common projects and common facilities comes from sev-
6623 eral sources: the host laboratory provisions made by CERN; CMS Maintenance and Operation
6624 budgets; and, where applicable, CMS upgrade project budgets. Responsibility for coordinat-
6625 ing such projects rests with Technical Coordination. The attribution of a given item to one or
6626 other of these funding sources is subject to interpretation. In this document, work is classified
6627 as a host laboratory expense if it is listed as such under the General Conditions for Experi-
6628 ments or, in the case of assembly buildings or experimental caverns, if it is independent of the
6629 specifications of the installed experiment. It should be noted that the provisions in the Gen-
6630 eral Conditions are basic and restricted to providing an overall framework complying with
6631 basic personnel protection requirements and satisfying basic infrastructure and service needs.
6632 In particular, they do not cover equipping laboratory or experimental areas with infrastructure
6633 or services adapted to supplying detectors (specialised power, cooling, compressed air, net-
6634 work etc). Site-specific safety features, including those linked to the efficiency of operating
6635 or maintaining an experiment or assembly area, or protecting the experimental apparatus, are

6636 also generally not included. Nevertheless, CERN departments generally make contributions
6637 beyond the basic minimum and reasonable precedents exist for all such attributions herein.
6638 Work can be charged to Maintenance and Operation budgets if they cover operation, repair or
6639 routine replacement of already installed equipment. This includes replacement of equipment
6640 which fails or becomes inoperable or un-maintainable before the end of its design lifetime. All
6641 other tasks, including consolidation, are attributed to the upgrade.

6642 **10.2 Safety Systems**

6643 Safety in the CMS surface halls and underground caverns at LHC Point 5 is considered the
6644 responsibility of the CMS Technical Coordinator with authority delegated to the GLIMOS, an
6645 Experiment Safety Officer appointed by the PH department head in consultation with CMS
6646 management and the Health, Safety, and Environment Unit.

6647 **10.2.1 General safety**

6648 Basic personnel protection is provided throughout CERN by the Level 3 alarm system, typi-
6649 cally triggering evacuation and fire brigade intervention in response to smoke, flood, or oxy-
6650 gen deficiency sensors. Protection against beam-related hazards at CMS is provided by the
6651 LHC Access Safety System and the RAMSES radiation monitoring equipment. Additional pro-
6652 tection systems, particularly against fire hazards, have been installed by CMS (and in several
6653 other experiments), many with the dual function of personnel and detector protection. Work
6654 is needed on further cavern-specific features including the safe areas and the evacuation route.
6655 Operational experience has shown that the installation of a magnetic-field tolerant public ad-
6656 dress system from surface control room to underground caverns is necessary at Point 5, because
6657 mobile phones are unreliable or inoperative in the fringe field of the CMS solenoid magnet.

6658 **10.2.2 Detector Safety System (DSS)**

6659 The Detector Safety System (DSS) is a hardware protection system, based on redundant PLCs
6660 and triggered by a relatively small number of sensors (smoke, temperature, pressure, humidity,
6661 current, etc). It applies a carefully reviewed and tested action matrix to initiate safety interlock
6662 actions when pathological conditions are detected. Its actions are generally applied at a coarse
6663 level (e.g. switching off racks, groups or racks, or even entire power systems) to protect the
6664 detector, an individual sub-component, or an ancillary system. These protective actions are not
6665 designed with rapid incident recovery in mind and expert intervention is generally required to
6666 release the applied interlocks. DSS is not a personnel safety system, although its actions may
6667 incidentally protect personnel as well as equipment. DSS and its sensor system are designed
6668 to be completely independent from the Detector Control System, which takes care of detailed
6669 monitoring and fine-tuning; the operational cycling between off, standby and on conditions;
6670 and should generally react to, or correct, abnormal conditions in sub-detectors well before DSS
6671 is triggered. The main improvement required is in the user interface, which, while suitable for
6672 specialists and adequate for commissioning, is unsuitable for use by trained, but non-expert,
6673 shift crew. Improvements are also desirable in the arrangement of the DSS system within racks
6674 at Point 5. Satellite systems should also be deployed to protect equipment at the electronics
6675 integration centre and at beam-test facilities.

6676 **10.2.3 Sensor systems**

6677 Although a certain number of magnetic field, position and environment condition sensors were
6678 incorporated in the original CMS design, the operational requirement for a sophisticated sen-

6679 sor, camera and monitor network arose from unforeseen difficulties in CMS opening/closing;
6680 in magnetic field operation; in temperature pressure and humidity control; combined with var-
6681 ious LHC and CMS technical incidents, notably the September 19 2008 LHC incident and the
6682 October 2009 CMS endcap cooling leak. Work is needed to consolidate and properly exploit the
6683 system and to extend it to give new diagnostic information in key areas within the detector and
6684 along the beampipe, using new developments in fibre-optic-based multi-parameter sensors.

6685 **10.2.4 Nitrogen, dry air and compressed air**

6686 A system of air compressors and liquid nitrogen dewars on the surface at Point 5 provides
6687 air and nitrogen for a variety of different purposes. Nitrogen or dry air are used by several
6688 subsystems to eliminate fire risk, maintain low humidity and exclude any possible helium con-
6689 tamination. In many cases this is, or will become, an essential year-round detector protection
6690 requirement. Since humidity is dangerous for Silicon sensors, operation of the Tracker at low
6691 temperatures from 2013 onwards will set much stricter requirements on dew point within the
6692 detector volume and in the volume within the solenoid vacuum tank between the endcap and
6693 barrel detectors. Nitrogen and dry air are also both used for instrument control in regions
6694 of high magnetic field, in particular for opening and closing valves in the subsystem gas and
6695 cooling distributions. This application is also clearly crucial for safe detector operation. Large
6696 amounts of liquid nitrogen are also needed to cool down the magnet cryogenic system from
6697 room temperature, but in future this activity will not factorize from subdetector commission-
6698 ing and consequent high gaseous nitrogen demand. Lastly, a high flow gaseous nitrogen fire
6699 suppression system protects the detectors and cables in the inter-element spaces of the flux
6700 return yoke.

6701 The proposed improvements consolidate the system, partially factorize the different functions
6702 and introduce spare capacity, increased reliability and redundancy. In particular it is proposed
6703 to purchase a nitrogen separation micro-plant (to reduce the cost/m³ of nitrogen gas in view
6704 of the foreseeable increased demand) and to install higher capacity air compressors.

6705 **10.2.5 Fire prevention: detection, and extinguishing**

6706 Examples of CMS-specific systems installed in addition to the basic Level 3 requirements are
6707 non-magnetic fire extinguishers in high field regions; the sniffer system (aspiration and analysis
6708 of air from a network of tubes incorporated into the apparatus, recently re-designated by HSE
6709 as a Level 3 system); the water-mist local fire extinguishing system; the water-foam area fire
6710 extinguishing system; and the in-rack CO₂ fire extinguishers. Following a large investment
6711 during 2009, most of these systems meet the requirements of the initial CMS configuration
6712 and will be maintained and consolidated using M&O A budgets. However, as additions or
6713 expansions of existing CMS apparatus occur, corresponding expansions of these protection
6714 networks will be needed. The first and immediate case is the expansion of the rack fire detection
6715 and extinguishing system for the high level trigger processing farm, which needs expansion to
6716 cope with data rates expected from 2011 onwards.

6717 **10.2.6 Radioprotection precautions, measuring devices and equipment trace- 6718 ability**

6719 CERN as host laboratory takes responsibility for radioprotection, including the provision of
6720 procedures, qualified RP experts; measuring equipment; and the funding for local buffer zones
6721 and storage areas and central workshops, which can handle radioactive materials. These re-
6722 sources, while legally satisfactory, are not, however, sufficient to allow efficient maintenance

6723 and operation of the experiments. Recognizing this problem, CERN has trained selected per-
6724 sonnel (staff and users) from each LHC experiment as radio-protection experts and assistants
6725 (Swiss national qualification) which allows some RP screening procedures to be accelerated. In
6726 addition, CERN is supporting the creation of Class C radioactive workshop areas at Point 5,
6727 although the costs of tailoring this to CMS maintenance needs will have to be met from CMS
6728 M&O funds (see section on 10.9.2).

6729 The logging, tracing, and RP screening of equipment moving in and out of the CMS exper-
6730 imental cavern is mandatory for radioprotection reasons. LHC experiments have developed
6731 equipment management databases with simple user interfaces, linked to required radioprotec-
6732 tion procedures. Since these are generally applicable to equipment management, a fraction of
6733 the running and development costs (mostly in materials) is met by the experiment budgets.
6734 Similar arguments apply to the procedures and software developed to authorize and control
6735 interventions on the experimental apparatus.

6736 Operational experience shows that much maintenance time is lost waiting for RP measure-
6737 ments from an overloaded central CERN RP service. In view of the expanding need for, and
6738 importance of, such measurements as activation levels increase, CMS intends to purchase RP
6739 screening equipment (such as a portable gamma spectroscope), which will allow these proce-
6740 dures to be streamlined or carried out locally.

6741 **10.2.7 Access control**

6742 Basic site and underground access control at Point 5, including the LHC access control system
6743 governing personnel and material access to the experimental cavern, is provided and main-
6744 tained by CERN as host laboratory. Additional features necessary for the efficient mainte-
6745 nance, operation and protection of CMS equipment are the responsibility of the experiment.
6746 Examples are the expansion of the LHC access key delivery system capacity at Point 5 to allow
6747 more workers through each UXC access point and the addition of a modified anti-theft sys-
6748 tem to prevent workers accidentally leaving the site with access keys, which can bring re-start
6749 of the whole LHC complex to a halt. Assuring fast personnel access to the experiment ser-
6750 vice cavern (USC), adjoining the experimental cavern, during beam operation and shutdown
6751 is a fundamental CMS design assumption, although not an LHC-wide requirement, and some
6752 work remains to consolidate what will be a versatile and reliable system. Additionally, CMS
6753 will purchase an electronically operated key cabinet, linked to the personnel database, to give
6754 access to keys to sensitive areas or systems (e.g. RP veto) to authorized persons and will also
6755 wish, for security reasons, to implement access control on the projected new office building at
6756 Point 5 and the integration and production areas in Building 904.

6757 **10.2.8 Safety training**

6758 Training and refresher training of CERN personnel and users in specialized skills such as the
6759 construction of scaffolding or the use of harnesses, nacelles or lasers in the specific Point 5 envi-
6760 ronment is essential to completing complex, multi-activity maintenance or upgrade operations
6761 in the timescales available. Such training of additional personnel is the responsibility of the
6762 experiment. Similarly, specific training suggested by the CMS GLIMOS to reinforce the level
6763 of safety awareness and emergency reaction at Point 5 and in CMS surface assembly sites is
6764 also the responsibility of the experiment. Items include assistance in creation of the Point 5
6765 specific L4C course and other documentation; safety signalisation (multi-lingual); experiment
6766 related safety equipment (harnesses, alarm panels, safety rails); safety-enhancing equipment
6767 (e.g. ladders with working platform), and training of CMS collaboration personnel to enhance
6768 their own safety or that of the working team.

6769 **10.3 Magnet Consolidation and Upgrade**

6770 **10.3.1 Introduction**

6771 The lifetime of the CMS solenoid will be limited by the number of cycles from zero to full field
6772 and back to zero, the cyclic strain from which will eventually lead to increased resistance of
6773 the pure aluminium stabilizer. In order to minimize unnecessary cycles, and in particular to
6774 further reduce the risk of fast discharges, modification to the cold box , the power breakers and
6775 the control system are envisaged.

6776 **10.3.2 Power systems**

6777 The key elements are:

- 6778 1. The Power Converter (PC) which is made of 4 modules, with spare parts in hand to
6779 replace one module (thyristors bridge, transformer).
- 6780 2. The Direct Current to Current Transformer (DCCT) arranged as a redundant pair and
6781 used for magnet current regulation. There is one spare.
- 6782 3. The main transformer 18kV/400V (ERD1/55) for which there is no reserved spare. The
6783 reservation of a spare and the replacement time is being discussed with the EN-EL group.
- 6784 4. The main 20kA DC switch breakers, and resistance contactors for which there are sev-
6785 eral sets of spare parts for the open/closed command circuit, plus spares to replace the
6786 electrical contacts.

6787 **10.3.3 Vacuum pumping systems**

6788 The key elements are:

- 6789 1. The two primary pumping units, which are fully redundant and for which spare parts
6790 are available.
- 6791 2. The two diffusion pumps, directly attached to the helium phase separator and to the
6792 magnet cryostat, located in the experimental cavern, which cannot be easily accessed.
6793 Replacement would require a warm up of the coil and thus an estimated 6 week period
6794 with no magnetic field availability. Spare components are available.
- 6795 3. The Vacuum gauges for which spares are available.

6796 **10.3.4 Safety and control systems (MSS, MCS)**

6797 The system performs adequately, but two consolidations are considered necessary. A spare
6798 MSS chassis unit needs to be built with up-to-date electronics which can be more easily main-
6799 tained and replaced. In addition, the 55V battery system needs to be modified by replacing the
6800 chargers and their supervision. This is the responsibility of PH-DT group and a cost estimate is
6801 pending. These upgrades/consolidations are in synergy with the needs for the M1 test facility
6802 (described in paragraph 10.8.3.1.5).

10.3.5 Cryogenic systems

Despite the solid performance of the system so far, three critical failures have been identified, any of which could cause the magnet to be unavailable for long periods (several months).

- 1. Helium compressor units:** There are two compressors of different kinds, each working within a different pressure range and arranged in series, so that one cannot work without the other. Both compressors are designed for full maintenance every 40,000 hours. Taking an average run time per year of 8000 hours, the availability between major maintenance work is 5 years. At present, the first full maintenance is scheduled for 2012. Nevertheless, if one of the two compressors stopped and had to be repaired, the magnet would be stopped for the duration of the repair. Although, these compressors are still listed in the manufacturers catalogue, for construction to order, they are custom-built and not available off-the-shelf. In case a full replacement became necessary, the magnet would be unavailable for several months (procurement, manufacturing, installation, cool-down). If spare compressors were constructed and reserved for CMS, the magnet stop would be limited to the dismantling and replacement time. Installing these spares in SH5 would allow for compressor repair or revision without stopping the installation (and the magnet as a consequence) for any significant time. The available space in building SH5 and the layout of the compressor system were indeed designed to allow for two redundant compressors and full redundancy is the best solution to minimize the risk of extended magnet down-time. To take full advantage of this redundancy, a control process would be needed to allow the load to be transferred to the redundant compressors without stopping the cryoplant.
- 2. Compressor lubricant separation unit** Periodic pollution problems have been observed in the whole installation, encountered with a frequency of one to 6 months, causing the magnet to be off, so far with no serious effects on data-taking. One possible explanation is that the helium compressor lubricant (BREOX) is found in the coalescers (4 stages) of the High Pressure unit, indicating that the separation is not efficient enough. This risk is likely to increase with time. Modification of the separation unit to cure the problem requires the installation to be stopped for a few months with magnet off. It has therefore to be implemented during the shutdown of 2012 or 2016. Clearly, the 2012 shutdown is more favorable, provided the decision is taken in due time and resources are made available. This is a problem common to the other LHC experiments and the machine. The study for the upgrade is being led by the CERN cryogenics group TE-CRG.
- 3. Cold Box** The cold box contains 3 turbines. There is one spare unit covering turbine 1 and turbine 2, plus critical components to limit the time for major repairs (2 weeks instead of 6). There is no spare for turbine 3, as it is not considered as a critical element for the process. Nevertheless, when a regeneration of the turbine filter is necessary, turbine 3 is used to avoid a full stop of the cryogenics (which causes a magnet ramp down). This situation is considered adequate.

10.3.6 Miscellaneous

Spare parts are needed for small components and for the command and control systems (filters, seals, switches, transducers, etc.).

10.3.7 Field measurement and mapping

The magnet team is charged with developing and maintaining accurate maps of the magnetic field within the tracking volume, within the return yoke and in other regions where magnetic forces or field sensitivity might be significant. The mapping and simulation of the field within the tracking volume rapidly reached an accuracy of 1 part in 10^4 . However, significantly more sophisticated simulations were needed to accurately reproduce the field in the return yoke. Unexpected field sensitivity of detector components led to the installation of a large additional network of Hall probes to provide additional detailed bench-marking data. Similarly, initial simulations underestimated the fields in some parts of the forward region by as much as a factor five, leading once again to unexpected field sensitivity. Although the current field models are extremely good, substantial work remains to fully implement the flux-loop measuring system in the return yoke and to both calculate and measure the substantial effect on the end-cap field of introducing the extra shielding disk YE4 (part of the forward muon upgrade and described in section 10.4).

10.4 Yoke, Shielding, and Moving Systems

One of the unique features of the CMS design is the capability to quickly open and close the detector for repair and maintenance by separating the 13 major elements along the beam line, without removing the beampipe. Though proven to work, (for instance during the emergency cooling bushing repair of winter 2009-10), moving several thousand tons with clearances as small as 4 cm currently requires very many experts to be present and poses unnecessary risks to the beam pipe and detector components. In addition, several simple maintenance operations could be done dramatically faster if partial opening of the detector were possible with the beampipe still under vacuum.

Studies and tests are underway to make the movements safer and more reproducible, by improving the guiding, monitoring and hydraulic traction systems, concentrating on parts of the movements when elements are in close proximity. An example is the system proposed for making small relative movement between endcap disks, illustrated in Figure 10.1.

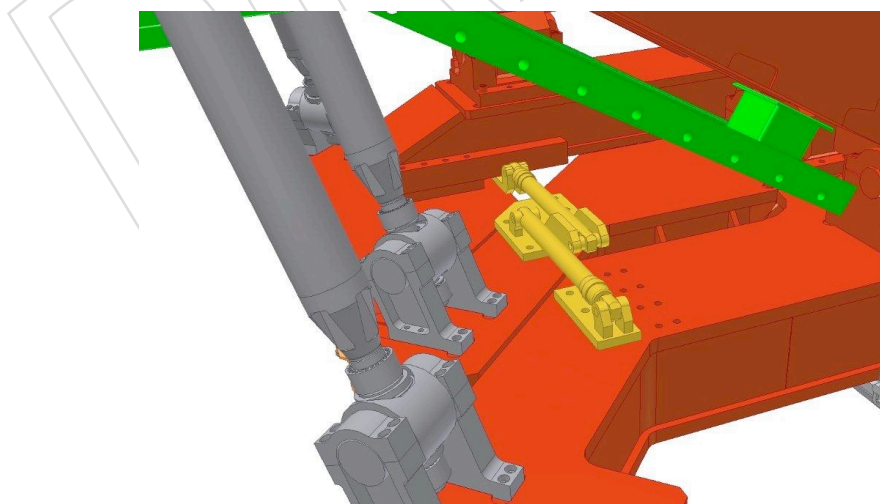


Figure 10.1: Inter-disk hydraulic jacks between YE1 and YE2 (act with symmetric pair on opposite side).

6872 In the course of this upgrade the compressed air source should be changed for safety and
6873 economy reasons from bottles to a system of redundant compressors. The system must be
6874 redundant because a failure of pressurized air in the course of an opening or closing can result
6875 in uncontrollable movements of heavy detector elements.

6876 10.4.1 YE4 Disks

6877 At present, each endcap of the CMS magnet return yoke consists of three 12-sided, regular
6878 polygonal disks (YE1, YE2 and YE3), 14m in diameter with respective steel thicknesses of 600
6879 mm, 600 mm and 235 mm, each supported on its own endcap cart and standing on either
6880 greasepads or, during opening and closing of the detector, on airpads. These disks also act
6881 as the support structure for the endcap detectors. The YE4 disks to be added at each end of
6882 the CMS yoke are supported from the YE3 cart as highlighted in Figure 10.2. They carry no
6883 detectors, but are part of the overall shielding design of the high luminosity CMS detector, de-
6884 scribed in the TDR and required for luminosities $> 2 \times 10^{33} \text{ cm}^{-2}\text{s}^{-1}$ to reduce beam-related
6885 background in the forward muon system and, in particular, in the presently incomplete 4th
6886 stations of CSCs and RPCs, which are targeted for installation starting in 2012. The main back-
6887 grounds causing random hits in this station originate from leakage through gaps in the forward
6888 shielding structures (HF shielding, collar shielding and rotating shielding) needed to allow for
6889 closure tolerances. These leaking particles, which cannot hit the detector directly, cause back-
6890 ground mainly due to albedo from the blockhouse shielding and the cavern endwalls. The
6891 thickness and composition of YE4 is optimized accordingly.

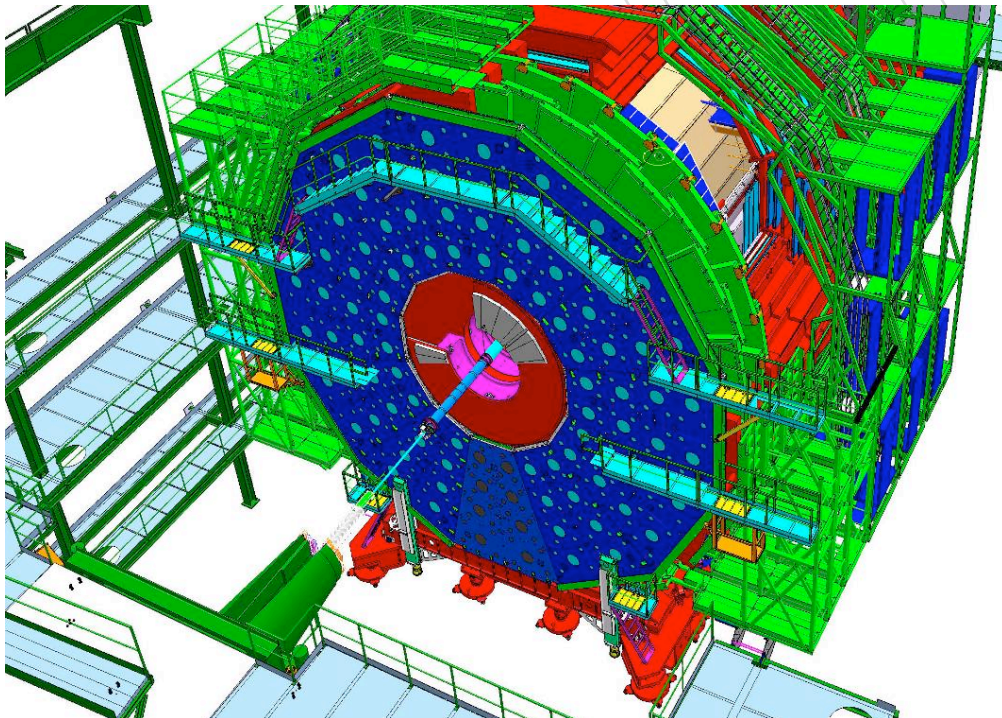


Figure 10.2: The YE4 disk.

6892 To allow for assembly in the underground experimental cavern, where the crane capacity is
6893 limited to 20 tons, the 14m diameter, 125mm deep YE4 disks are each assembled underground
6894 from 12 hollow, trapezoidal, sector-casings with 25mm thick steel walls. Each casing will be
6895 filled with a specially adapted shielding concrete at CERN for a final weight of 6.8t. The Tech-
6896 nical Specification for the YE4 disks is described in CERN EDMS Document CMS-SY-FS-0021.

6897 Manufacturing drawings of the disks are complete and production has been launched in Pak-
6898 istan. Assembly tooling drawings are nearing completion.

6899 The assembly of the YE4 disks is one of the key activities determining the critical sequence in
6900 the 2012-13 shutdown. Assembly of a disk can only be achieved if the corresponding endcap
6901 is fully closed or with the disks fully together with YE1 in the 3.7m, partially-open position.
6902 This position is incompatible with most activities on the barrel or endcap detectors and com-
6903 pletely at odds with the critical sequence planned for the 2016 shutdown (installation of new
6904 beampipe, pixel tracker, and HCAL front ends).

6905 In the TDR concept, service work on the 4th endcap muon station is achieved by fully open-
6906 ing the corresponding endcap, to enable the YE4 disk support to be transferred from the YE3
6907 cart to the blockhouse shielding of the cavern endwall. Partial re-closure of the endcap then
6908 opens the required working space. This procedure is cumbersome, particularly because it in-
6909 volves lengthy and delicate procedures such as opening and closing the corresponding YE1
6910 disk (linked to YE2 and YE3 via cable chains). To improve flexibility for installation or main-
6911 tenance of the 4th muon station, a “YE4 push-back” jacking system is being designed. This
6912 will allow a YE4 disk to be pushed back from the corresponding YE3 by about 2.5m, without
6913 needing to open endcap disks 1 to 3. The concept is illustrated in Figure 10.3.

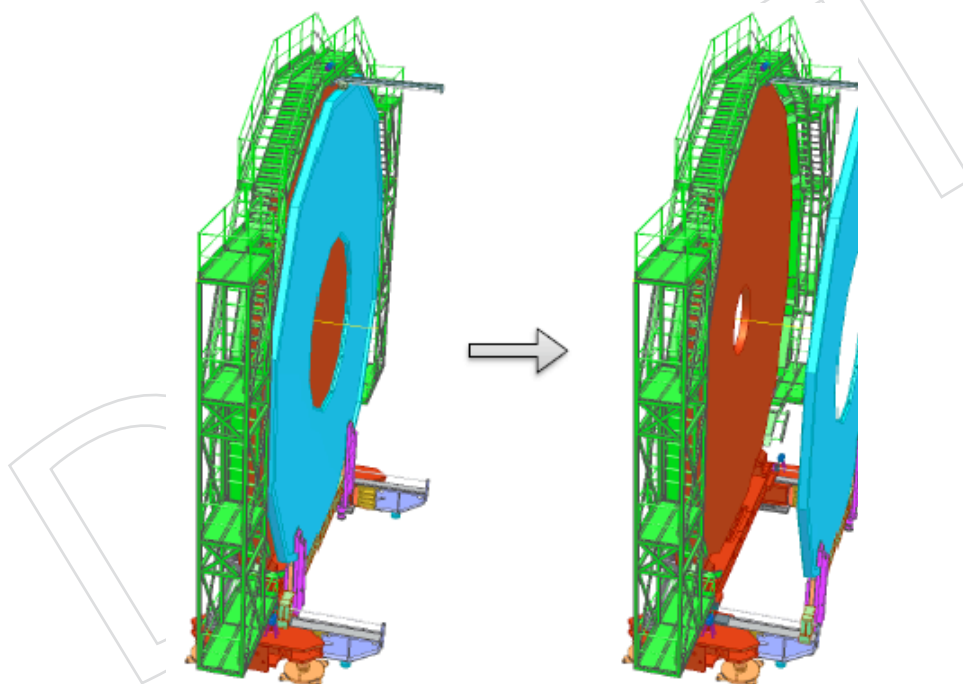


Figure 10.3: The YE4 push-back system.

6914 10.4.2 Radiation shielding

6915 When LHC is operating close to or at design luminosity, the severe radiation environment
6916 caused by collision products will cause substantial activation of the beampipe, the tracker bulk-
6917 head and the pre-shower disk. This means that appropriate shielding has to be available to
6918 protect personnel during maintenance and upgrade activities. Sophisticated shielding precau-
6919 tions already exist for the very forward ZDC detector, installed in the TAN at 150m from the
6920 interaction point, and for the HF, whose front face is equipped with lead shielding doors and is
6921 routinely stored in its shielded garage. After 2010, precautions will also be necessary inside the

6922 main experimental cavern. The beam pipe, flanges and pumps and the CASTOR calorimeter
 6923 will become particularly radioactive and will require shielding first.

6924 An example of shielding for the HF beampipe and 13.5m flange is illustrated in Figure 10.4.

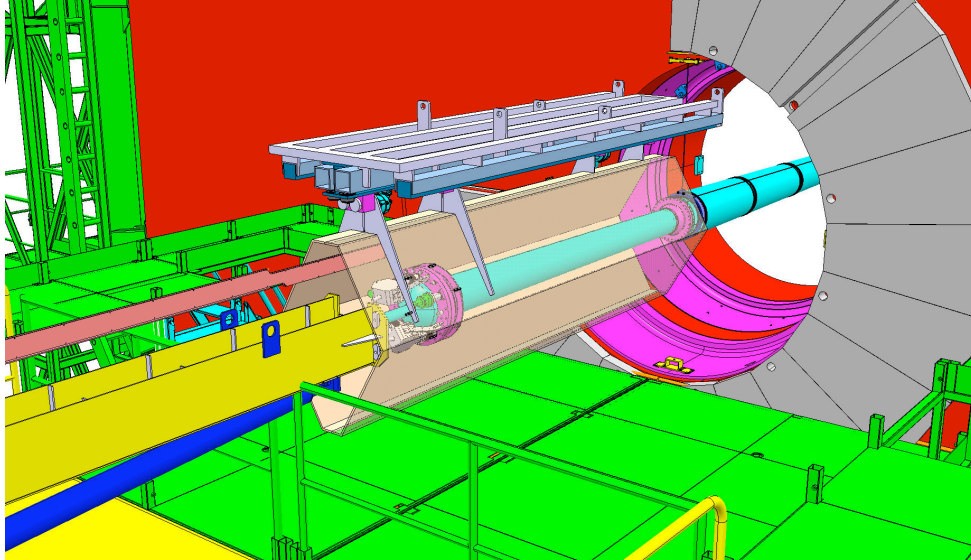


Figure 10.4: A possible design for shielding the beam pipe.

6925 The endcap Electromagnetic Calorimeter crystals will also become activated and will have to be
 6926 masked by shielding, especially during partially open maintenance configurations. The tracker
 6927 bulkhead also contains easily activated materials and is expected to be accessed regularly dur-
 6928 ing maintenance, thus a shielding disk has to be built that allows opening sectors for access.
 6929 A modular shielding design is foreseen making it possible to add shielding plates as required.
 6930 The support structures for these shielding elements and a first thin shielding layer must be
 6931 ready for the 2012 shutdown. Design work is proceeding.

6932 10.4.3 Forward Region

6933 The Forward region containing the rotating shield and the HF tower, which supports the HF
 6934 calorimeter, are far forward detectors and the collar shield requires a substantial revision. Op-
 6935 erational experience revealed a variety of problems:

- 6936 1. The first ramp up of the CMS solenoid after dismantling and rebuilding the HF tower
 6937 leads to movements of the HF, its tower and the iron structures mounted on it, which
 6938 are not fully predictable or reproducible. Since part of the beampipe support relies on
 6939 stability of these structures, the risks are considerable. The mechanical tolerances in the
 6940 set-up are large enough to cause the direction of forces between the HF and the iron yoke
 6941 and those between the collar shield and the rotating shield to change several times during
 6942 the field ramping. However, after the first ramp to operating field, the system settles and
 6943 later ramps of the magnet do not cause problems. There is no easy mechanism in the
 6944 current design to stabilize the tower sufficiently during the first ramp.
- 6945 2. Before every opening of the yoke, a beam pipe support has to be mounted extending
 6946 from 16.5m to 13.7m. The integrated installation time is 7.6 man hours of which the large
 6947 majority has to be spent close to flanges or pumps. As soon as these are significantly acti-
 6948 vated this procedure can no longer be followed. Conceptual designs under study include

6949 a permanent beam pipe support from the FIN, which will make any regular manipulation
6950 close to the flanges obsolete.

6951 3. Maintenance or removal/re-installation of CASTOR, BCM2 or TOTEM T2 requires per-
6952 sonnel to spend extended periods in very close proximity to the beampipe and to objects
6953 which will easily become activated. With the present radiation shielding structure (in-
6954 ner shell removed from the thin part of the rotating shielding to make way for CASTOR),
6955 CASTOR will have to be removed once the luminosity at Point 5 exceeds $2 \times 10^{33} \text{ cm}^{-2} \text{ s}^{-1}$
6956 to maintain acceptable dose rates to systems in the experimental cavern.

6957 4. The CASTOR detector cannot be adequately shielded from magnetic field due to the lo-
6958 cation of breaks between the different radiation shielding structures which also provide
6959 magnetic shielding.

6960 An integrated solution is under study. It is already clear that any solution which could resolve
6961 all the issues listed above would require a radical re-design, with introduction of a second
6962 raiser structure (for whose jacks the provision was made in the initial CMS cavern design). The
6963 concept is illustrated in Figure 10.5.

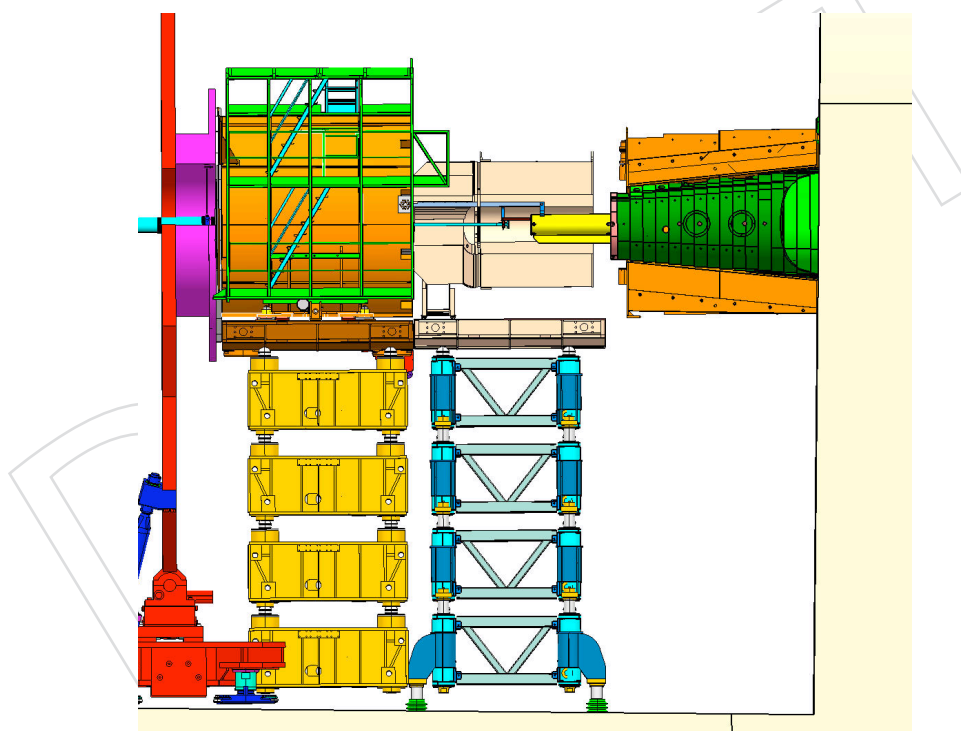


Figure 10.5: Concept for a revised forward region support and shielding structure.

6964 10.5 Experimental Beampipe

6965 The CMS beam pipe is a symmetrical structure extending 18m from the interaction point to ei-
6966 ther end of the experimental cavern as shown in Figure 10.6. It is constructed from a continuous
6967 central section and 4 additional sections at each end. The central pipe, spanning the interaction
6968 point, is 6.2m long and consists of an 0.8mm thick beryllium cylinder of 58mm bore, 3.8m in
6969 length and braised at each end to conical, end-pieces made of 0.8mm stainless steel. Each end

6970 piece is attached, via a dual-bellow flange system, to a conical end-cap pipe, made of 0.8 to
 6971 1.2mm thick stainless steel, following the $\eta = 4.9$ cone and terminating in a thin window before
 6972 a flange at 10.7 m which couples it to the HF pipe.

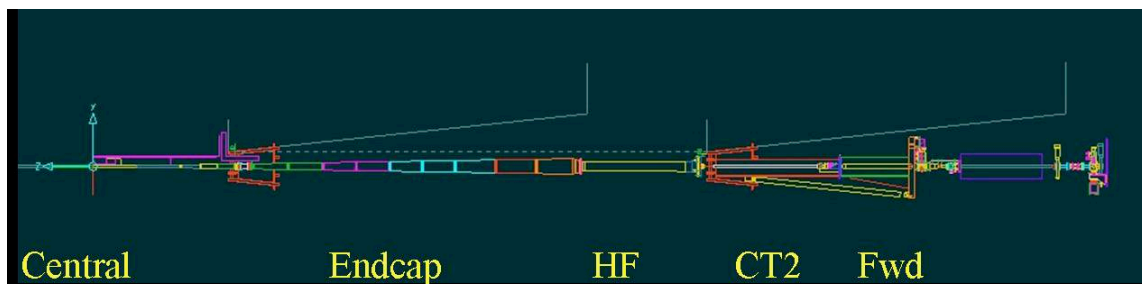


Figure 10.6: CMS beampipe from the interaction point to 18m.

6973 The HF pipe is almost 3m long, also slightly conical, varying in diameter from 170mm to
 6974 208mm and is constructed from 1.2 mm thick stainless steel. It terminates in a thin window
 6975 flange which carries 3 ion pumps and reduces the inner diameter to 58mm, for coupling to the
 6976 CASTOR-T2 (CT2) pipe. This cylindrical pipe again terminates in a flange and bellow system,
 6977 which couples it to the cylindrical, stainless steel forward pipe, 2.4 m long, which terminates at
 6978 the junction to the TAS absorber at 18m.

6979 The main features of the beampipe are:

- 6980 • The Be central section which presents minimal material to particles emerging from
 6981 the interaction point.
- 6982 • The conical outer sections along lines of η (allowing the use of stainless steel while
 6983 still minimising background in the muon system).
- 6984 • The thin reducing window at the end of the endcap pipe.
- 6985 • The HF and CT2 pipes which allow forward calorimetry up to $\eta = 7$, external to the
 6986 return yoke.
- 6987 • The placement of pumps and flanges out of the detector acceptance.

6988 The radius and thickness of the central beryllium section are important parameters affecting the
 6989 physics performance of the CMS tracking system. The impact parameter resolution and vertex
 6990 resolution could be substantially improved by fitting a re-designed pixel tracker, which has an
 6991 additional fourth tracking layer within the limited space between the beampipe and the strip
 6992 tracker, and thus ensuring the first measured point, given by the radius of the first layer, is as
 6993 close to the beam line as possible. The support system proposed for the upgraded pixel tracker,
 6994 which allows independent mechanical closure of the two half cylinders around the beam pipe,
 6995 would already allow such a 4-layer system to be installed, but with installation tolerances so
 6996 small as to pose a substantial risk. Reduced risk and better performance can be obtained if
 6997 the beampipe radius can be reduced. This requirement has to be balanced against assuring a
 6998 margin for safe and efficient operation of the accelerator and minimizing background in the
 6999 experiment.

7000 The required beam aperture determines the theoretically minimum inner diameter for any new
 7001 beam pipe. During injection the beam occupies the largest aperture in the vertical plane and in
 7002 case of an asynchronous beam dump the beam is largest in the horizontal plane. The dimension
 7003 of the beam pipe must be chosen so that, taking into account all possible mechanical tolerances
 7004 of the beam pipe, all installation tolerances and all possible movements of the pipe during
 7005 operation, the wall of the pipe can never approach the beam closer than the limiting distance

7006 required by the beam aperture. As a prudent precaution for the safety of the detector, no
 7007 element of the beam-pipe within it should have a smaller aperture than the closest machine
 7008 element to the interaction region, which in the CMS case is the TAS absorber, situated at 18m,
 7009 which currently has an of inner radius of 18mm.

7010 During the design of the currently installed LHC experiment beampipes, conservative aper-
 7011 ture estimates lead to the request for a stay-clear cylinder of 14mm radius around the nominal
 7012 beam line close to the interaction point. Operational experience with LHC shows that this es-
 7013 timate was indeed very conservative and investigations are ongoing to determine whether the
 7014 diameter of the “stay-clear” zone can be reduced. The following mechanical factors have been
 7015 considered to contribute to limiting the practicably achievable minimum inner pipe radius,
 7016 such that the “stay-clear” cylinder is always contained within the physical pipe:

- 7017 • Construction tolerances causing the pipe radius to be less than nominal.
- 7018 • Mechanical sagging of the pipe between supports.
- 7019 • The precision with which the pipe can be surveyed into place.
- 7020 • Time-dependent movements of the beam pipe supports (attached through the Tracker,
 7021 Tracker support and barrel Hadron Calorimeter to the central yoke wheel). These
 7022 may be caused by displacements of the whole cavern with respect to the plane of the
 7023 LHC machine, settling or flattening of the central yoke wheel, or distortions due to
 7024 the magnetic field.

7025 In Table 10.1 the original estimates of these mechanical contributions are compared with the
 7026 values or upper limits inferred from measurements on the installed system.

Table 10.1: Mechanical contributions to displacements.

Quantity	Original Estimate	Measurement
Construction tolerance	2.6mm	<0.6mm
Installation tolerance	2.6mm	2.7mm
Sagging between supports	2.2mm	<3.0mm (r=25mm pipe)
YB0 yoke distortion	1.4mm	<0.5mm
Field-induced yoke distortion	1.2mm	<1.0mm
Cavern movements	5mm	<1.0mm
Linear sum	15mm	<8.8mm
Assumed “stay-clear” radius	14mm	14mm
Min Beampipe radius	29mm	~ 23mm

7027 These figures indicate that a reduction in central beampipe inner radius by as much as 6mm
 7028 may be achievable based on improvements in the knowledge and control of mechanical factors.

7029 The LHC experimental beam pipes working group coordinates beam pipe aperture studies.
 7030 The current target within this group is to demonstrate that a 50mm diameter central section
 7031 inner diameter is possible for CMS and ATLAS in common. This allows for a comfortable
 7032 safety margin. A preliminary review of aperture calculations has confirmed that the reduction
 7033 from 29mm to 25mm inner radius at the CMS interaction region, is acceptable providing the
 7034 sum of all uncertainties can be controlled to 11mm or better, still assuming a 14mm radius
 7035 “stay-clear” cylinder.

7036 The remaining factor limiting the minimum pipe radius is the vacuum impedance along the
 7037 pipe and the consequent ability of the pumps at 13.5m and 18m to maintain a sufficiently low

7038 residual pressure. Once again, preliminary calculations, combined with observations of the
7039 achieved pressure during 2009-2010, indicate that a 25mm radius would be acceptable.

7040 Therefore the current baseline is to construct a new central beryllium beam pipe with an in-
7041 ner radius of 25mm, and to install it together with the new pixel detector in 2016. This will
7042 also require a revision of the support collars. For background minimization reasons, the $\eta=4.9$
7043 opening angle of the conical part of the beam pipe will be preserved, leading to the cylindrical
7044 part being shorter by about 280mm at each end. Two options for this construction are being
7045 investigated. In the first case, the conical part would again be made out of stainless steel, lead-
7046 ing to a shorter beryllium section. Detailed background studies have to be performed to judge
7047 the possible effects of this. Alternatively the length of the central Beryllium section would be
7048 maintained, and it would consist of a cylindrical part with conical ends connecting to the stain-
7049 less steel conical sections at the same z as now. This is technically possible, but undoubtedly
7050 considerably more complex and expensive. For both solutions detailed calculations using finite
7051 element modeling have to be done to estimate the mechanical strength and the deflection.

7052 Meanwhile, parallel calculations have been started to establish whether a 23mm inner radius
7053 would indeed be possible with acceptable safety margins. In this respect a review of the con-
7054 servatively set 14mm radius "stay-clear" is eagerly awaited. Such a step would improve the
7055 pixel performance still further, as it is just sufficient to allow the close-fitting inner pixel layer
7056 to contract from a 16-sided polygon to a 12-sided polygon. A final decision on the pipe diam-
7057 eter is needed by CMS in late 2011, although if parity with ATLAS is considered an essential
7058 economy, the decision may have to be taken earlier.

7059 **10.6 Logistics and Integration**

7060 **10.6.1 Cranes and rigging equipment**

7061 CERN provides and maintains the overhead beam cranes in the surface buildings such as 186
7062 and 904. However, at the Point 5 site, the 2 x 80t surface cranes with 120m long cables and the
7063 single 20t underground crane are maintained by CERN at the expense of the CMS collaboration.
7064 Similarly, CERN provides a transport manager and a single crane driver, while all additional
7065 transport personnel (crane drivers, riggers, forklift operators) are charged to the collaboration.
7066 Typically one additional rigger is routinely needed to complete a minimum team and this rises
7067 to three during shutdown work, in order to have effective flow of material around the sur-
7068 face and underground areas. The specialized rigging equipment needed to lift, manoeuvre,
7069 install and remove detector and infrastructure elements has generally been designed by CMS
7070 engineers. The EN-HE group provides assistance in keeping track of equipment certification.
7071 Significant changes to the endcap muon tooling will be needed once the YE4 disks are installed.

7072 **10.6.2 Tooling and Working platforms**

7073 The modular design of CMS allows for access to many potential work areas simultaneously.
7074 However, the tooling to allow this is highly specialized. Heavy support structures, such as
7075 those needed for the very large platforms used for installation or maintenance of the beampipe,
7076 or major components within the solenoid vacuum tank, or on the endcaps, could reasonably
7077 be made using concrete blocks during assembly, but for future maintenance this is risky, time-
7078 consuming and incompatible with the low-dust environment needed once activation becomes
7079 a reality. Similarly, the intensive use of scaffolding during construction was cost- and risk-
7080 effective because of the long periods spent in static configurations, the need for access to entire
7081 surfaces simultaneously and the excellent relationship with a specialist scaffolding contractor

7082 using a compression-clamp coupler system. The revised CERN frame contract for scaffolding
7083 provides exclusively for the rapid assembly, ring-lock type, secured by hammered wedges and
7084 unsuitable for use next to sensitive detector elements.

7085 Various specialist maintenance structures, all designed to be installed and removed with the
7086 beampipe in place, were already constructed for use during the final stages of construction.
7087 These include a tubular structure for the support of the 20t installation platform, which gives
7088 a very stable work area at about 2m below the beamline between barrel and fully open end-
7089 caps, a set of telescopic towers which can be installed more rapidly to give access for lighter
7090 work at the same level and a multi-level cylindrical framework which fits inside the end of the
7091 solenoid vacuum tank. Maintenance on the mobile wheels and disks generally requires rapid
7092 access to very specific regions, and for this the ideal working platform for the barrel wheels is a
7093 specialized scissor-lift with a small footprint and 15m height range, while in the endcap vary-
7094 ing designs of nacelle with 2-axis adjustable basket and a similar height reach are best suited.
7095 These scissor lifts and nacelles are, for the most part, unobtainable for rental locally, and have
7096 had to be purchased by CMS .

7097 Purchase and maintenance costs are very high. Although invaluable, they do not cover all
7098 rapid maintenance scenarios. To provide additional access solutions, a range of custom-built,
7099 light weight platforms is being designed by the integration office to fulfill identified needs.
7100 These include light-weight platforms for use inside the solenoid vacuum tank and inside the
7101 endcap inner cones. In the medium term, it will become necessary to maintain the Tracker at
7102 low temperature even during maintenance periods (to arrest the effects of reverse annealing).
7103 This will necessitate the design and construction of an insulated, climate controlled enclosure
7104 incorporating the end of the solenoid vacuum tank, which should be easily mountable on heavy
7105 or light-weight platforms.

7106 The currently available maintenance configurations of CMS are largely determined by the need
7107 to support the beampipe, which has support points at 3.7m, 6m, 10.7m and 13.2m. Maintenance
7108 structures for the endcap in a fully open position have to accommodate suitable support and
7109 many intermediate scenarios involve precise placements of the major elements so that they can
7110 form the basis of beam pipe support. Engineering studies are underway for cantilevered support
7111 structures which may allow more freedom and increase the options for the 2016 shutdown in
7112 particular.

7113 **10.6.3 Logistics support teams**

7114 The estimated M&O A costs currently approved depend on an outdated LHC operating pattern
7115 in which an annual (approx 4 month) shutdown occurs from mid-November until mid-March.
7116 The estimates for mechanical support in particular were based on a model where, on average,
7117 one end of CMS was opened during each such shutdown and a single maintenance cycle is
7118 performed on moving equipment and access devices. It is estimated that extra logistic teams
7119 would be required from the Collaboration, from CERN contract Field Support Units (FSU),
7120 survey and beampipe support, and from other contractors during a 4 month period each year.
7121 In addition, the availability of 4-5 additional CERN staff technicians, who were involved in
7122 subsystem work until early 2010, to assist in heavy logistic activities has been taken for granted
7123 and halves the amount of spending needed on mechanical FSU.

7124 In the current operating model, there is an estimated total of 34 months actual shutdown,
7125 (2+15+2+3+12) in the period 2010-2016. Experience shows that additional expenses actually
7126 start at least one month in advance of each winter stop or shutdown since manpower can
7127 typically be obtained for a minimum of 3 months. Thus there are 39 months of installation

7128 and logistics activity. In a plan assuming no overtime and avoiding working at both ends
 7129 of the detector simultaneously, then approximately 23 months follow the original model of
 7130 M&O A financed shutdown and are roughly covered by the existing M&O A provision. This
 7131 leaves a remaining 16 months of activity which is identifiably upgrade-related. For this period,
 7132 workshop, survey and beampipe support requirements are assumed to be comparable to those
 7133 needed during installation. Under these frugal assumptions, an additional 3M CHF would be
 7134 needed to support the logistics of upgrade installation during the period 2010-2016. A more
 7135 detailed breakdown of this estimate is given in Table 10.2.

Table 10.2: Logistic Support: 2010 - 2016.

Item	Upgrade	CERN/host	M&O A	M&O B	Totals
Crane drivers/riggers	184	351	266		801
Add. equipment/tooling maintenance	480		480		960
Collab. cabling/detector teams	800		900		1700
Contractors	200		180		380
Workshops	240	400	280		920
Survey & Beampipe	150		125		275
Field coordination	160		250		410
Technical staff/FSU	464	2925	565		3954
Stores & misc.	160		230		390
Totals .	2838	3676	3276	0	9790

7136 10.6.4 Engineering Integration

7137 10.6.4.1 Organisation

7138 The Engineering Integration Centre (ENIC) in Building 904 is staffed by collaboration and
 7139 CERN personnel and reports directly to Technical Coordination. It is organized as a joint
 7140 project between the CERN electronics, engineering, infrastructure and experimental area man-
 7141 agement teams and has links to every detector subsystem through dedicated link persons. The
 7142 centre is entrusted with defining and maintaining CMS standards of engineering coherence,
 7143 quality, change control and documentation. It ensures that these standards are followed by all
 7144 contributors, including CERN as host lab and CERN as institute and it supports all CMS sys-
 7145 tems in finding solutions to engineering problems. It also maintains the as-built model of the
 7146 experiment, provides a CAD translation service and develops and maintains the Equipment
 7147 Management Database.

7148 10.6.4.2 Resources

7149 The dedicated manpower, equipment and operating costs for the integration centre in the con-
 7150 struction phase amounted to about 2M CHF/year and came from two main sponsor institutes
 7151 (CERN and ETHZ), with the facilities dimensioned to allow project engineers, draughtsmen or
 7152 subsystem link-persons from other institutes to integrate effectively for short or long periods.
 7153 Entire integration responsibilities within particular geographical areas were delegated to part-
 7154 ner institutes (e.g. Torino for the barrel wheels, Wisconsin-PSL for endcap disks) and several
 7155 institutes provided engineering staff to the centre for considerable periods of time. The du-
 7156 ties of the Integration Office are to optimise tooling and technical procedures, with an eye to
 7157 schedule efficiency and ALARA constraints, as a component of the EAM and TC sequencing

7158 and scheduling responsibilities. It must also maintain the as-built model drawings library, a
 7159 CAD translation service and the Equipment Management Database essential for traceability.
 7160 As far as upgrades are concerned, the ENIC will be responsible for ensuring the integration of
 7161 infrastructure improvements and of new or modified subdetectors, considering them as black
 7162 boxes with an envelope (possibly complex) and defined interfaces, including those with exist-
 7163 ing services. Much of the focus is likely to be on the integration of new and modified services,
 7164 shielding and tooling, and on balancing subsystem physics optimisation with all the physical,
 7165 electrical and thermal constraints imposed by the existing CMS detector. Of the current 1.2
 7166 MCHF foreseen budget for 2010-2016, (see Table 10.3), approximately 25% is funded by CERN
 7167 to cover host lab responsibilities, 25% from M&O A to cover minimum collaboration require-
 7168 ments for consolidating, maintaining and operating the experiment, 25% from special institute
 7169 contributions and the remaining 25% from existing upgrade projects. The equivalent resources
 7170 for upgrade should be maintained at the current level of around 350-400 kCHF/year during
 7171 2011-12, allowing for the provision of the equivalent of two full-time engineers and one project
 7172 associate (potentially through institute contributions). This level should be maintained until at
 7173 least the end of 2016.

Table 10.3: Engineering Integration Center: Annual Operating Costs 2010-2016 (kCHF).

Person	Category	FTE	Totals	CMS	CERN	M&O A	Upgrade
EIC	Eng/App Phys.	100%	180	180	0	0	0
Librarian/sys support	CAD Draftsman	100%	96	0	0	96	0
Integration Eng. M&O	Eng./Draftsman	100%	120	60	0	60	0
Mu as-built consolid.	Engineer	20%	20	0	0	20	0
Upgrade Engineer	Engineer	50%	75	0	0	0	75
EMD manager	Developer/Eng	100%	150	0	150	0	0
EIC assistant	Sr. draftsman	100%	150	0	150	0	0
Beampipe supports	Engineer	50%	50	0	0	50	0
YE4 engineer	Engineer	100%	150	0	0	0	150
EMD assistant	Student Tech.	50%	40	0	20	20	0
CSC Upgrade Engineer	Engineer	75%	0	0	0		75
Short term visitors	Engs.& Assts.	50%	30	0	0	15	15
materials							
Computers/peripherals			35	0	10	15	10
Software licenses			15	0	0	15	0
Consumables			12	0	0	6	6
Physical Models			20	0	0	20	0
Totals .			1218	240	330	317	331

7174 10.6.5 Electronic and Electrical Integration

7175 The Electronic and Electrical systems Integration Centre (ELIC) in building 904 is described
 7176 in Section 10.9.3.2. Consolidation and subsequent operation using M&O funds has been ap-
 7177 proved and is described in Section 9.

7178 The Electronic and Electrical Systems Integration effort is combined with general electronics
 7179 support and is led by an Electronic Systems Coordinator who reports to Technical Coordina-
 7180 tion. Additional host lab personnel consists of 0.5 FTE staff engineer (currently assigned mostly

7181 to beam radiation monitoring), and two engineers supported by M&O A specialising in read-
7182 out electronics and detector power systems respectively. Half of the costs of these last two
7183 should be transferred to upgrade from 2011,

7184 **10.7 Experiment Service Infrastructure**

7185 The infrastructure and common systems supporting operation of the CMS experiment at Point
7186 5 were brought progressively into operation from 2006 onwards. Following partial commis-
7187 sioning in surface assembly building SX5, underground operation of detector elements began
7188 in late 2007, with progressively larger fractions of the detector and its associated systems be-
7189 coming active. There were substantial periods with the full detector operational during 2008
7190 and 2009, for both cosmic ray and beam tests. Since November 2009, the experiment has been
7191 in routine operation.

7192 **10.7.1 Responsibilities**

7193 Apart from primary power, raw cooling water, and the civil engineering structures (surface
7194 buildings, shafts and caverns), which are considered part of the infrastructure provided by
7195 CERN as host laboratory, the provision, maintenance and operation of the specific infrastruc-
7196 ture and common systems needed for operation of the CMS detector and its surface facilities
7197 (which include control room, maintenance laboratories, etc.) is the responsibility of the CMS
7198 Collaboration. Contracts and service agreements with CERN departments cover key features of
7199 the industrial-scale infrastructure. The total CMS investment in the infrastructure and common
7200 installations needed for the low luminosity detector was about 40 MCHF, with an additional 6
7201 MCHF spent on the power, cryogenic and control systems of the magnet.

7202 **10.7.2 Consolidation and Upgrade**

7203 The currently installed services infrastructure has proven to be adequate for operation of the
7204 current detector at reasonable efficiency at low luminosity. However, several systems have
7205 little or no margin and some weaknesses in design or implementation have become apparent
7206 with operational experience. Consolidation and upgrade will be needed to allow continued
7207 reliable operation and to cope with the significantly increased load expected from an upgraded
7208 detector, and from improving accelerator performance. Radiation damage and activation will
7209 make other changes necessary. Silicon-based detectors will require more power and additional
7210 cooling, including continued effective cooling during periods when the detector is being main-
7211 tained. More processors will be needed to cope with increasing data-rates and this will require
7212 a substantial expansion in the number of cooled racks required to house them. By 2016, parts of
7213 the infrastructure will already have been operating for 10 years and obsolescence will become
7214 an increasing threat to reliability. As availability of spares and expertise (particularly for con-
7215 trol systems) decreases and the MTBF becomes shorter, replacement of certain elements with
7216 up-to-date equivalents will become necessary to maintain reliable and cost-effective operation.

7217 The following sections describe the actions currently being considered.

7218 **10.7.3 Cooling Systems**

7219 **10.7.3.1 Chilled water for fluorocarbon plants**

7220 At higher radiation loads, silicon-based detectors are vulnerable to damage from reverse an-
7221 nealing, which can be halted by reducing the operating temperature and maintaining the de-
7222 tector cold even when not operational. For instance, it is believed that the Tracker will have to

7223 be run with coolant temperature as low as -25°C to halt reverse annealing. Reliability of the
7224 cooling will become more critical to minimize radiation damage and ensure smooth operation.
7225 The fluorocarbon cooling systems of the silicon-based detectors (Pixel tracker, Strip Tracker
7226 and Preshower) are connected (for historical and budgetary reasons) to the same branch of
7227 the primary chilled water feed as the Heating, Ventilation and Cooling (HVAC) system serv-
7228 ing the caverns and surface buildings. All other subsystems are fed by separate chilled water
7229 branches. This shared supply presents a reliability risk due to the radically different require-
7230 ments and criticality of the Tracker and HVAC cooling functions. The detector circuit must
7231 be separated from HVAC, or alternatively a backup system must be provided, so that condi-
7232 tions in the Tracker are maintained even if the HVAC system is shut-down. This work should
7233 be done concurrently with revision of the primary coolant loop to allow operation at lower
7234 temperatures.

7235 **10.7.3.2 Computer farm**

7236 The cooling capacity for the event filter farm in the SCX building determines the maximum
7237 processing power available and hence the rate capability. The existing system, sized for a lu-
7238 minosity of a few $\times 10^{32}$, was already observed to be vulnerable in high summer, since its max-
7239 imum observed power consumption was 550kW, compared with the installed cooling capacity
7240 of 600kW. From 2011 onwards, with 50ns bunch-spacing and high bunch currents, pileup will
7241 already reach the design value. In order to maintain a steady build-up of processing capac-
7242 ity so that HLT performance can be maintained as luminosity increases, the cooling capacity
7243 must be increased to 1MW as soon as possible. This implies a complex intervention involving
7244 3 CERN departments (GS,EN and PH). The concrete slab in the SUX building must be up-
7245 graded to house the bigger pumps (GS/SEM), which are sized to allow $150\text{ m}^3/\text{h}$ of water flow
7246 (EN/CV). The electrical distribution must be upgraded to power this new equipment (EN/CV)
7247 and it must be incorporated in the control system (EN/CV). Finally, monitoring instrumenta-
7248 tion must be added (PH/CMX).

7249 **10.7.3.3 RPC Cooling**

7250 The operating temperature of the endcap RPC system, is observed to increase from layer to
7251 layer with distance from the barrel, reaching 22°C at the $-z$ end, layer 3 and 21°C at the $+z$
7252 end layer 3. This is very close to the 24°C critical value at which the detectors are known to
7253 become unstable. The coupling of the endcap cooling circuit to the temperature sensitive areas
7254 of the RPC is quite poor. Attempts to improve the cooling system performance over the last
7255 year have typically gained only $3/4$ degree and any further reduction of the cooling water
7256 input temperature from its current value of 16.5°C would entail insulation work on largely
7257 inaccessible pipework between USC and UXC, to prevent condensation. Several strategies are
7258 under investigation to improve this situation. Since the RPC temperature roughly tracks the
7259 cavern temperature, a reduction of the cavern temperature HVAC set-point to 19° or even 18°C
7260 should be attempted. (This corresponds to the original design value!). Forced circulation of
7261 cool, dry air between the second and third endcap disks is an interim measure for which a
7262 design study is ongoing, but the small, irregular gap will impede homogeneous cooling. The
7263 probable definitive solution is to re-design the RPC chamber cooling plate so that it couples to
7264 the whole outer surface of the RPC, not just to the electronics. Initial tests of this scheme have
7265 proven quite successful and it is likely to be implemented for the new layer 4 RPCs which are
7266 part of the forward muon upgrade (see Section 3.4)..

7267 10.7.3.4 RE4 cooling

7268 The common peripheral supply and return water cooling manifolds on YE3 are pre-equipped
7269 with connections for the CSC ME4 chambers, but not for the RPC RE4s. These manifolds will
7270 have to be either removed or modified in situ. The work involves drilling holes and welding
7271 half couplings to service the new distribution lines. A study of the temperature and pressure
7272 drops expected in the new circuits will determine whether an upgrade of the pump and heat
7273 exchanger is needed.

7274 10.7.3.5 Leak tolerance/ detection/ suppression

7275 The 9 October 2009 leak of a bushing in one distribution circuit fed from the YE1 peripheral
7276 cooling water manifold exposed the vulnerability of CMS to such leaks and emphasized the
7277 importance of detecting and shutting the leaking circuit rapidly to prevent serious damage to
7278 the detector as a whole. Since then, a very large investment has been made in replacing all the
7279 endcap bushings and installing leak detection cables and associated collector trays. 10 months
7280 of operation have since passed with no further leaks from the endcap disk manifolds.

7281 However, a major vulnerability still remains. Of the 136 feed or return shutoff valves on YE1,
7282 87 are inaccessible, meaning that a leak on one of these circuits would necessarily entail a
7283 shutdown of the whole YE1 manifold, which provides cooling for all CSCs and RPCs along
7284 with the cable trays of the endcap ECAL and the readout boxes of HCAL. Action to improve
7285 the disposition of isolating valves, at least on YE1, seems to be an essential mitigating action
7286 against this risk. This will involve an integration effort to find places for the new valves and
7287 careful planning of how to dismount the existing system and insert new components.

7288 One further incident, a leak in the cooling of a peripheral rack mounted high on the outermost
7289 endcap disk on the z end, caused no damage, but highlighted the risk to the detector from leaks
7290 originating in any of the uppermost peripheral racks. A further extension of the leak detection
7291 system is needed to allow for early detection and prompt fixes.

7292 10.7.3.6 USC rack system extension

7293 Many subsystems and central systems plan major Trigger and DAQ upgrades in 2016. To allow
7294 for parallel commissioning of new systems alongside the old, and to accommodate expansion
7295 of the existing system, an extension of the rack service network (power/cooling/ control/fire
7296 detection) into the zone currently occupied by the commissioning control room will be needed.
7297 It is intended to install this infrastructure between 2012 and 2014.

7298 10.7.3.7 SCX Control room

7299 The cooling system of this Control room, the nerve centre of CMS, should be separated from
7300 that of the filter farm in the floor above.

7301 10.7.4 Electrical Distribution

7302 Power cuts and transients on the electrical network can damage power supplies, trigger and
7303 readout components and processors. The LHC power distribution system which feeds the un-
7304 derground areas is subject to both external and internal disturbances and transients. If such
7305 incidents are localized to the CMS experiment, or the experiment recovery time is longer than
7306 that of the LHC machine, then substantial amounts of collision data can be lost. In case of a loss
7307 of power, essential systems for the safety of the detector and personnel, as well as for shutdown

7308 of the detector, are already backed up by UPS and a local diesel generator. However, opera-
7309 tional experience has shown that maintaining full control of the detector is essential during any
7310 power incidents to allow a quick and safe recovery. As a consequence, it is proposed to extend
7311 UPS and diesel coverage to the entire surface control room in the SCX building.

7312 Substantial work has also already been done to make the CMS system immune to common
7313 short-lived power transients, such as re-connection of the static var compensators (active filters)
7314 at LHC Point 6. Additional filters for rapid transients on the 400kV network are proposed to
7315 improve the immunity to very fast transients. To enable the detector system to ride through
7316 power glitches or very short outages safely, the on-board sub-detector low voltage systems
7317 are fed through a battery-stabilized UPS acting as a filter. Those systems not yet connected to
7318 this filter exhibit significantly higher down-time and damage rate. It is therefore proposed to
7319 extend the filter coverage to all low voltage, plus some high voltage, systems underground.

7320 **10.7.5 Heating, Ventilation and Air Conditioning (HVAC)**

7321 **10.7.5.1 Ventilation**

7322 After the LHC incident on Sept 19 2008, authorisation for access to underground facilities at
7323 Point 5 was made contingent on achieving adequate shaft-USC, USC-UXC and UXC-LHC over-
7324 pressures. The establishment and monitoring of these overpressures required sealing work
7325 and the installation of differential pressure sensors. Overpressure depends partly on optimis-
7326 ing ventilation systems, but largely on making effective air-seals around cableways, doors and
7327 shielding. These seals must also be fire-proof. After consigning sealing work to a Swiss special-
7328 ist company, CMS now has the best pressure differentials at LHC during beam operation. CMS
7329 is awaiting CERN-HSE advice about what pressure differentials need to be maintained during
7330 shutdowns for smoke protection. Depending on the result, substantial further work to revise
7331 the PM 54 and PM56 shafts and their safe areas may become compulsory, in which case these
7332 activities would be better classified under Safety and Safety Systems. CMS Technical Coordi-
7333 nation already considers some modifications to be highly desirable, thus the main uncertainty
7334 is the budget to which this work can be attributed.

7335 **10.7.5.2 Cavern Humidity**

7336 In high summer, the underground cavern humidity has been observed to fall as low as 10%.
7337 This is not ideal for people, electronic systems and many adhesives. The HVAC system needs
7338 to be modified, if necessary using temporary portable humidifiers, so as to be capable of main-
7339 taining a minimum humidity of 30%.

7340 **10.8 Beam, radiation, cosmic ray or environmental test facilities**

7341 **10.8.1 Introduction**

7342 Over the next decade, CMS will require the use of test beams and other test facilities for two
7343 main tasks. The first is to better understand the existing detector and may involve activities
7344 such as precise calibration, diagnosis of anomalous signals seen in the CMS detector, measure-
7345 ments of radiation damage, etc. The second is to research, develop and qualify replacement
7346 or upgraded detectors and to establish baseline calibration data. In the near future, these two
7347 activities will overlap, with the emphasis then gradually moving from understanding of the
7348 existing detector to preparations for the future.

10.8.2 Better understanding of the existing detector

The experience of previous collider experiments (e.g. ZEUS, CDF) has shown that once the initial debugging period is over, fine details start to emerge that require exercising realistic production elements of the installed system under controlled conditions. CMS has planned for this possibility and all CMS subsystems have either preproduction prototypes or spare modules that can be used, if and when a detailed study of a particular behaviour is needed.

Such studies typically take place in either cosmic ray or particle beam facilities, possibly combined with irradiation facilities to simulate background conditions or integrated radiation dose. As LHC approaches its design energy and luminosity, these measurements will be complemented and often surpassed in significance by real-life data coming from the experiment. By that time, R&D for new detectors will be approaching maturity and the irradiation and test facilities will continue to be used for the qualification and eventual calibration of the new devices.

10.8.3 R&D for Consolidation and Upgrade

Existing CMS subsystems have been designed and, as far as possible, qualified to operate for at least 10 years at LHC design luminosity of $10^{34} \text{ cm}^{-2}\text{s}^{-1}$. An exception is the forward muon system, where an additional station and a high η component were always foreseen for luminosities exceeding $2 \times 10^{33} \text{ cm}^{-2}\text{s}^{-1}$. Parts of other subsystems may be replaced or revised because of poorer than expected performance, obsolescence, radiation damage or because technology and experience provide an opportunity to consolidate and improve the detector, so as to maximize the physics output from LHC Phase 1 (where luminosities $\sim 2 \times 10^{34} \text{ cm}^{-2}\text{s}^{-1}$ are eventually expected). For LHC Phase 2 (with target luminosities $\sim 5 \times 10^{34} \text{ cm}^{-2}\text{s}^{-1}$ and 300fb^{-1} per year) CMS (notably the tracking systems) will have to be re-equipped with new detector technologies. Based upon experience from construction of the existing detector, the research, prototyping, development and production phases will likely require a full decade and thus must be started now.

The lively detector testing programmes of the last 2 years indicate that R&D for new detection techniques is already actively underway for the most vulnerable areas. CMS is currently studying silicon photomultipliers (SiPM), for HCAL readout, forward RPCs constructed with different materials (due to an enforced supplier change), new silicon strip and pixel technologies, thick GEMs (Gas Electron Multiplier) for high η triggering and tracking, heavy fibers, new scintillating crystals, use of quartz plates in calorimetry and longitudinal segmentation of HCAL readout. Details are to be found in the chapters of this document concerned with individual subsystems. As in previous experiments, the important instrumentation used for beam monitoring and luminosity measurement (such as the recently tested diamond-tracking telescopes devices for luminosity monitoring) is likely to undergo R&D throughout the lifetime of CMS, in a continuous quest for better precision and robustness.

The facilities required for these test and calibration activities are summarized below.

10.8.3.1 Existing facilities, with examples of current use and investments proposed

10.8.3.1.1 SPS North area: H2 beamline: This is the location of a permanent combined calorimetry test apparatus consisting of a spare ECAL barrel supermodule, two HCAL barrel preproduction prototypes, sectors of HO, and a 20° sector of HE.

- **Description, status and recent applications** Following successful combined calorimetry tests which took place in 2006 for the barrel and in 2007 for the endcap, this

apparatus was used in 2010 with the explicit goal of finding and studying causes of single-crystal noise events in the ECAL barrel, which are observed in data from CMS. The installation uses an existing two-axis rotating platform that can precisely adjust the pion beam incidence on ~ 100 t of equipment, allowing fine η - ϕ scans. A key feature of the H2 beam line is the available pion energy range from 2 to 300 GeV, achieved by using a very low energy tertiary beam that complements the secondary beam. Given the importance of a wide energy range for both energy resolution and detector linearity, CMS has equipped the H2 beam line with additional instrumentation (moving platforms, veto and TOF counters, and a Cerenkov counter for particle identification) which allows the available beam to be fully exploited. The calorimetry system is a likely candidate for further long-term study. The combination of a crystal ECAL and scintillator-brass sampling HCAL is highly non-compensating. In addition, ECAL readout electronics, cooling pipes and support rails appear as dead material between the two calorimeters, with a negative effect upon the precision of jet energy measurements.

- Future requirements** In order to keep the setup fully operational, CMS will require preservation of this test area with a large energy spread of as many particle types as possible. This includes conservation of the very low energy tertiary beam line that is indispensable for good quality calorimetry measurements. Given the fragility of the optical fibres for readout and laser light injection, as well as the need to keep the same trigger and readout settings, CMS must retain exclusive use of control room HNA 370. In addition, an enclosure is needed to control the temperature of the ECAL detectors.

10.8.3.1.2 SPS North area H4 beamline: This area has an η - ϕ moving platform in an enclosure with controlled temperature and humidity, equipped with an interlocked hut housing a high power calibration laser, similar to that in use in the installed CMS experiment.

- Description, status and recent applications** Studies of irradiated ECAL crystals are usually done in this facility. Environmental control is needed for high precision measurements because of the rather strong influence of environmental parameters on PbWO_4 crystal and avalanche photo-diode (APD) response, making such a controlled environment necessary for high precision measurements.
- Future requirements** The major requirement in this area is continued maintenance of the already installed equipment: air-conditioning, moving platform, laser enclosure. CMS intends to continue using this facility at least for several weeks per year. At the moment the fixtures on the η - ϕ table in H2 allow data to be taken either with an ECAL barrel supermodule or an ECAL endcap setup of four supercrystals. A feasibility study is underway to see if modification of the existing structure could allow both modules to be mounted at the same time. The expected price for this custom modification is of the order of 100 kCHF.

10.8.3.1.3 Large area cosmic ray tracking telescope: This device is part of the RPC Muon effort and is located in an area at the ISR.

- Description, status and recent applications** This telescope has been used predominantly for detailed performance optimization and production-testing of Resistive Plate Chambers (RPCs) and is currently been used to evaluate the efficiency of prototype RPCs with gaps made from bakelite panels sourced from a new manufacturer.

- **Future requirements** The existing hardware (scintillation counters and electronics) is over 30 years old and close to being unmaintainable. As CMS activities in the ISR have to be transferred to building 904 (Preveessin) to make way for a waste treatment facility, it is not cost-effective to move the existing telescope. A new large area telescope, with options for precision tracking, will be constructed in building 904, in time for production testing of RPCs assembled for the forward muon upgrade.

10.8.3.1.4 Irradiation Facilities

- **Description, status and recent applications** The CMS subsystems near the beamline close to the interaction point will be exposed to high levels of radiation from collision products. Similarly, the outer subsystems and all services in the underground cavern have to operate in a mixed radiation field of charged particles, photons and neutrons. During the R&D phase for the existing CMS detectors, they have all been qualified for long-term operation in such an environment by being exposed, in short periods at various irradiation facilities at CERN and elsewhere, to corresponding 10-year integrated doses of radiation. The key facilities presently available are:

1. Gamma Irradiation Facility (GIF), presently standalone, but previously in a muon beam at the CERN SPS.
2. IRRAD facility at the CERN PS.
3. Intense low energy pion beams at PSI (Villingen, Switzerland).
4. Low energy neutron irradiation facilities at various reactors worldwide.

At least three ongoing projects are using these facilities: The first two are studying CMS subsystem behaviour in closer to realistic conditions, working with lower field intensities and mimicking the time between fills and during technical stops, when annealing processes can occur. One is performed with pixel detectors irradiated at PSI, the other with endcap ECAL crystals irradiated at the IRRAD facility. CMS is also participating in a common CERN-wide project to study filtering of any radiation-induced contaminants in RPC working gases. In view of the high cost of these gases, it is very important to recover as much as possible of the gas without compromising the detector performance. These tests are carried out in the GIF, which uses an intense Cesium source to simulate the background rate conditions under which muon detectors, in particular, are required to operate. It is to be expected that testing and qualification of any new gas-based detector, such as a micro-pattern gas detector (MPGD), will require the same facility.

- **Future requirements** Radiation dose rates and integrated doses for SLHC are going to be higher than for LHC, so all new detectors will have to be tested for radiation hardness. In addition to facilities outside CERN, the already existing CERN facilities such as GIF and the PS irradiation facility, for which various upgrades are planned, will continue to be needed. For continued usefulness, the GIF should be re-installed in an SPS extracted beam-line and the source should be replaced. In practice, the radiation shielding and shutter mechanism will also have to be replaced. A contribution from experiments is expected to be solicited. Data obtained during first few months of CMS running indicate that, as long suspected, the actual deterioration in detector performance may depend not only on the integrated dose, but also on the mixture of gamma, neutron and charged hadron fluences. From that aspect, a possibility to expose detectors and front end electronics to a realistic mixture of particles becomes very important. CMS thus expects more use for the mixed field

7484 irradiation facility already existing at the PS and expects to be asked to contribute to
7485 construction of a more extensive facility.

7486 **10.8.3.1.5 High Magnetic Field Facility: M1 magnet** This facility is in the SPS North
7487 Area beamline H2

7488 • **Description, status and recent applications** The only test facility at CERN where a
7489 detector can be exposed to high energy particles in the presence of a strong magnetic
7490 field is in the H2 beam-line, where the M1 superconducting magnet recovered from
7491 NA22 experiment, which has a 1.40m bore, can reach fields of up to 3 T. This highly
7492 versatile facility was instrumental in confirming correct performance for numerous
7493 CMS components. Experience at CMS and elsewhere confirms that magnetic field
7494 tolerance should not be taken for granted, even when accounted for at the design
7495 stage. Recent tests at M1 investigated the behaviour of irradiated silicon pixel de-
7496 tectors, which are influenced by strong magnetic fields because of the effect on the
7497 drift paths of charge carriers in the silicon. Unfortunately, the last time the magnet
7498 was refurbished was in 1994 and the current state of both hardware and software is
7499 precarious. As the test programme of 2010 highlighted, almost the entire vacuum
7500 system and a large part of the control and monitoring system consists of equipment
7501 that is obsolete and is now becoming unreliable, risky to operate, very difficult to
7502 maintain and a drain on skilled personnel. Modern communication devices and
7503 analysis tools are strongly needed for safety and to limit the time spent by techni-
7504 cians for operation. The existing control software (written in Labview 2) should be
7505 replaced by the contemporary CERN standard-issue magnet control system built on
7506 top of a new hardware that will replace the existing CAMAC interfaces. Further
7507 operation is not possible until these revisions have been carried out.

7508 • **Future requirements** Many new detectors and their front end electronics and power
7509 distributions will have to be tested in a strong magnetic field. The estimate for the
7510 hardware refurbishment of M1 is of the order of 400 kCHF, without taking into ac-
7511 count manpower costs. As several non-CMS groups expressed an interest in using
7512 M1, a proposal is being made to CERN PH and TE departments and the EN-MEF
7513 group to share costs with CMS in order to create a general high-field test facility.
7514 Unfortunately, the magnet refurbishment is an extremely urgent matter for CMS,
7515 whereas an agreement on the modalities of cost sharing will probably take some
7516 time to arrange. For reasons of manpower availability, the ideal time to conduct
7517 such a refurbishment is during an extended period of LHC operation. In the near-
7518 term, this implies 2011 or the second half of 2013. In order to reduce the pressure on
7519 M1 refurbishment, with its consequent demands on skilled CMS manpower and to
7520 provide a simpler, cheaper solution to short term, high field validation tests of small
7521 objects such as pixel detector prototypes and electronic components, CMS proposes
7522 to purchase a small 4T magnet from a commercial vendor at an estimated cost of 70
7523 kCHF (not including installation costs).

7524 **10.9 Surface assembly buildings, workshops, laboratories, and** 7525 **storage space**

7526 **10.9.1 Introduction**

7527 The construction and assembly of new detector components and the maintenance and repair of
7528 existing ones requires substantial surface facilities at CERN. The large facilities at the ISR and

7529 building 867 used for reception, assembly and testing of the muon detector and electromagnetic
7530 calorimeter of the low luminosity CMS have been re-assigned by CERN to other uses. The plan
7531 for future CMS surface facilities at CERN envisages a concentration of effort at a small number
7532 of sites in order to gain economies of scale in the provision of infrastructure, in communica-
7533 tions, and in the use of host laboratory, or common CMS, facilities and personnel. For example,
7534 such concentration ensures that a CERN staff TSO and support technicians can be assigned to
7535 each of the sites, so that there is the best synergy with the priority activity of operating CMS
7536 efficiently and that the infrastructure of these few large sites can be accepted into the general
7537 site access control and monitoring. The provision of office and meeting space for CMS staff
7538 working permanently or intermittently at these sites is a key ingredient of the plan.

7539 For maintenance of equipment exposed to beam in UXC (including activated material), activity
7540 will be concentrated at Point 5 (building SX5, 2000m², plus an external control barrack), which
7541 will be equipped with a Class C work area for lightly activated materials. Specialist electronic
7542 maintenance and mechanical work on activated objects, requiring workshop facilities rated
7543 better than Class C, will need access to the common specialist electronic and mechanical ra-
7544 dioactive workshops being provided by CERN at Meyrin and Preveessin.

7545 For upgrade activities (i.e. newly built equipment) and for maintenance and testing of non-
7546 activated equipment that do not originate from a defined zone around the beampipe, activ-
7547 ity will be concentrated in buildings on the Meyrin and Preveessin sites (Meyrin building 186,
7548 2000m², and Preveessin building 904, 2000 m²). The Preveessin site offers transport access to
7549 SX5 without a border crossing and is therefore suitable for storing tooling, ready-use electronic
7550 spares, etc. It is also the site of the existing CMS centres for Electronics Integration and Engi-
7551 neering Integration.

7552 **10.9.2 Operation Support Centre (OSC) at Point 5**

7553 **10.9.2.1 SX5 building**

7554 The SX5 hall is now being developed as the CMS Operation Support Centre. In the past this
7555 building was used for the surface assembly of CMS and, since the lowering of the CMS detector,
7556 has been used to store assembly tooling. The size of SX5 is 100 x 20 m² at 20m height. It contains
7557 2 80-tonne cranes and a DAQ/control barrack. Work on the reconfiguration of SX5 was delayed
7558 by a protracted local planning process, which was needed because of previous environmental
7559 impact commitments. This centre is considered as an operational requirement for the existing
7560 detector, whether or not upgrades are carried out, and therefore it is funded by host laboratory
7561 and M&O A budgets only.

7562 The proposed layout of the OSC is shown in Figure 10.7. The areas assigned to subsystems
7563 correspond to the minimum requirements requested by their field coordinators.

7564 The SX5 hall will be divided longitudinally into sections. Starting from the left, the first is the
7565 PX56 shaft, normally closed by the 2m thick pit-head cover. Next to this, a section 20m x 10m
7566 with access doors on both sides, is devoted to logistics, transport arrivals and departures and
7567 staging, particularly of items to be raised and lowered from/to UXC. The next section, of area
7568 65 x 18m, is access controlled and contains five subsidiary areas.

- 7569 1. A logistics and infrastructure area.
- 7570 2. A storage place for activated material, notably sections of the beampipe and shielding.
- 7571 3. A walled radiation laboratory (following broadly the Swiss Class C regulations: permit-

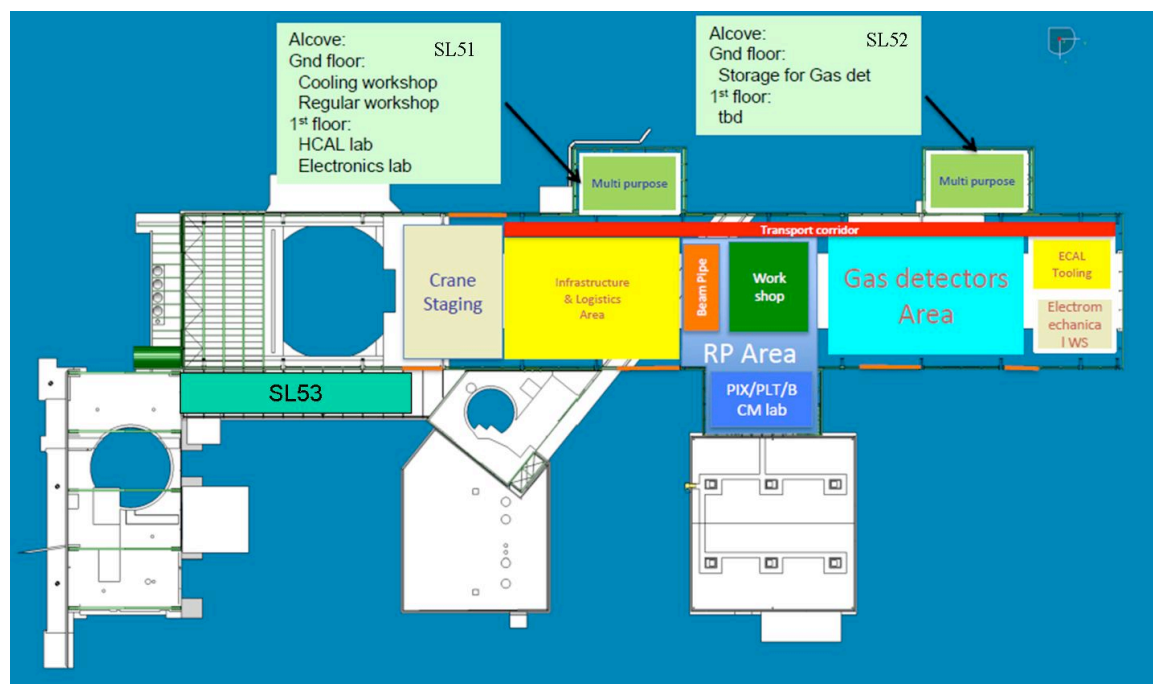


Figure 10.7: Proposed layout of the SX5 building showing the maintenance and operations areas.

- 7572 ted total activity 1-100 x the limiting activity per isotope [LA] below which no special
 7573 work area is required.). This work area covers the requirements of ECAL, HCAL and
 7574 CASTOR calorimeters, TOTEM and the beampipe system. This area also acts as a buffer
 7575 zone for the temporary storage and measurement of equipment removed from the UXC.
- 7576 4. A area attached to the radiation laboratory in the SHL building consisting of a temperature-
 7577 controlled semi-clean (\sim class 100000), class C radioactive laboratory area (ground floor),
 7578 with a room above for pixel trackers and beam monitors, equipped with a load platform
 7579 to allow delivery and removal of objects by crane.
- 7580 5. An area that accommodates 3 types of gas-ionization muon chambers (Drift tubes, Cath-
 7581 ode Strip Chambers, Resistive Plate Chambers) and the alignment system. Facilities
 7582 within this area will allow faulty units from the corresponding subsystems to be opened,
 7583 diagnosed, repaired and re-qualified for installation. It is expected that spare drift tube
 7584 chambers, spare cathode strip chambers and spare resistive plate chambers will also be
 7585 kept under continuous active test in these areas.

7586 The final 12m section is devoted to infrastructure support, especially electro-mechanics (e.g.
 7587 rack system) and it concludes with a multi-level storage system, installed against the south end
 7588 of the building. The alcoves on the north side, originally designed for Barrel HCAL assembly,
 7589 will be modified. The upper floor of the SL51 (nearest PX 56) will be extended, equipped
 7590 with a projecting loading platform and dedicated to electronics work; the lower floor will be
 7591 a workshop (non-radioactive) for cooling and moving/hydraulic systems. The second alcove,
 7592 SL52, is already occupied by the Point 5 general mechanical workshop and this will stay in
 7593 place. A small, independently accessible user workshop will be added.

7594 10.9.2.2 Green barrack

7595 The “green barrack” (ex-OPAL experiment control barrack, recuperated as a control room for
7596 surface magnet tests) provides an on-site operation support room for the Tracker and Muon
7597 systems. It also features a rack room with sufficient racks to support the subsystem laborato-
7598 ries, which will be used to control data-taking in the test areas. An additional room has been
7599 loaned to the TOTEM experiment as a control room. The remaining room is used as a DAQ de-
7600 velopment facility and remains equipped as such, so that test data from the adjacent subsystem
7601 laboratories can be centrally recorded.

7602 10.9.2.3 SL53 Offices

7603 There is currently no permanent office space at Point 5. Two small laboratories and the small
7604 meeting room adjacent to the control room, along with the “green barrack” are used to support
7605 control room operations. The CMS collaboration obtained a surplus temporary barrack which
7606 has acted as the office quarters for the last 8 years, but which is now nearing the end of its useful
7607 life. During shutdowns, typically 50 technical team staff and collaborators are present daily at
7608 Point 5, along with several long-term contractor teams numbering up to 30 people. During
7609 operation, the technical team is reduced to a core of about 15-20, to which up to 20 support
7610 personnel from subsystems may be added, depending on the work programme. Office space is
7611 therefore needed for about 20 personnel plus a similar number of visitors. A conference room,
7612 with a capacity for about 60 people, is needed to allow the existing small conference room to
7613 be given over entirely to control room support/overflow.

7614 CERN is committed to constructing a suitable office block on the existing foundation slab of
7615 the never-constructed SL53 building (see Figure 10.7), which was originally conceived for cov-
7616 ered transfer of heavy material between SX5 and the PM54 shaft, a function now rendered
7617 superfluous by UPS installation blocking the pathway in SDX.

7618 10.9.2.4 Visitor facilities

7619 Outreach, in the form of welcoming VIP, funding agency, collaboration and public visitors
7620 to Point 5, is an additional consideration in designing the SX5 facility. The particular design
7621 features of CMS and the cavern system make underground visits feasible year round and visits
7622 to the experimental cavern frequently possible. Visitor facilities will be incorporated in the new
7623 office building SL53, which connects with a potential display area in the SDX building near the
7624 PM54 shaft and thence to the control room. Initiatives in partnership with the commune of
7625 Cessy, the Pays de Gex and the Department de l’Ain may result in a substantial science-tourism
7626 facility next to the Point 5 site, with the potential for shared facilities.

7627 10.9.2.5 Funding for Point 5 reconfiguration

7628 The OSC project is foreseen in four stages, which will maximum use of the availability of the
7629 resident technical staff, who will eventually run the facility.

- 7630 • **Stage 1** This encompasses urgent items which could be needed as soon as the next
7631 extended technical stop or shutdown, plus preparation of the site for construction of
7632 the permanent office facilities. The total cost of this phase is estimated at 900 kCHF,
7633 approximately equally split between CERN host lab costs and CMS collaboration
7634 M&O A expenses.
- 7635 • **Stage 2** This covers setting up the subsystem laboratories, for a cost of just over 500k
7636 CHF, approximately equally split between collaboration M&O A and M&O B.

- 7637 • **Stage 3** This covers completion of the permanent offices and meetings rooms, plus
7638 basic visitor facilities, for a total estimated cost of 1.2 M CHF, of which the vast
7639 majority (1.0 MCHF) has been foreseen by CERN as host laboratory.
- 7640 • **Stage 4** This is dedicated to providing handling facilities and working areas for sub-
7641 system materials which have been activated. The estimated cost of this final phase
7642 is 85 kCHF.

7643 A breakdown of the estimated costs to complete the re-configuration is shown in Table 10.4.
7644 The host lab and M&O A contributions have been approved.

Table 10.4: Total Cost for the complete reconfiguration (all numbers in kCHF).

	Total	CERN	M&O A	M&O B
Stage 1	974	425	499	50
Stage 2	530	0	270	260
Stage 3	1205	1000	205	0
Stage 4	85	0	85	0
Grand Total – all Stages	2794	1425	1059	310

7645 10.9.3 Building 904, Preveessin

7646 The principal laboratory area allocated by CERN to CMS in compensation for the loss of the
7647 laboratory areas centered on Building 184 (ISR) and in building 867, is Building 904 on the
7648 Preveessin site, which offers about 2000m² of contiguous laboratory space. Two large adjacent
7649 areas of about 1000m², each accessible with modern cranes of 12t and 20t lift capacity, are very
7650 well suited to house detector construction and assembly lines and diagnostic facilities for large
7651 detector components. An adjacent 800m² area is already in use as an Electrical systems, Elec-
7652 tronics and Trigger test and integration centre. This is being upgraded using M&O A funds
7653 to provide a 5% DAQ slice, giving the opportunity to pre-test hardware or firmware modifi-
7654 cations to Trigger and DAQ before deploying them in CMS at Point 5. A further, separated,
7655 300m² laboratory with a light beam crane will become available in the medium term. The CMS
7656 Engineering Integration Centre has been established on the upper floor of 904 for almost 15
7657 years and various offices and labs around it are scheduled to become available for CMS use.

7658 10.9.3.1 Detector Assembly and Test Centre

7659 Building 904 is foreseen to be the primary laboratory for all future calorimetry and muon up-
7660 grade projects requiring large amounts of space. The first production projects in this build-
7661 ing will involve assembly and testing of Cathode strip Chambers (CSCs) and Resistive Plate
7662 Chambers (RPCs) for the CMS Forward Muon upgrade. All 72 CSCs of the ME4/2 layer will
7663 be assembled in building 904. Assembly of these trapezoidal chambers (~3.3m x 1.3m) requires
7664 large, precision machines which will be sent to CERN from a previous production site at Fer-
7665 milab. A large fraction of the 200 RPC chambers planned for the CMS upgrade will also be
7666 produced in building 904. Acceptance tests, fault diagnostics and necessary repairs of RPCs
7667 built at other worldwide sites will also be done in 904. The projected layout during this phase
7668 is shown in Figure 10.8.

7669 The basic building, as delivered, required substantial renovation and modification, which is
7670 being done by CERN (GS dept) as host laboratory overseen by the CMS Technical Coordination
7671 and Experimental Area Management teams.

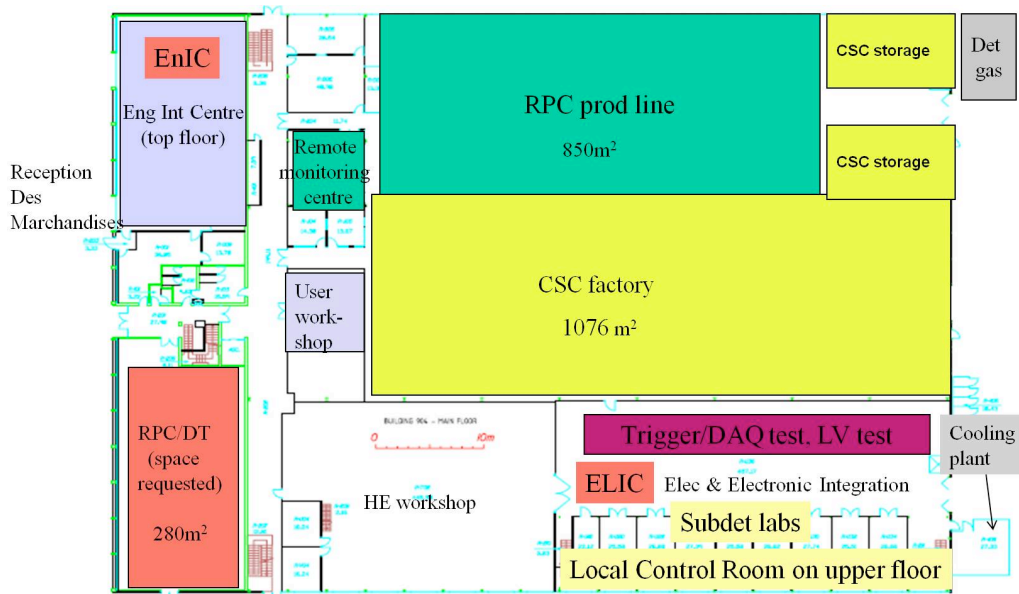


Figure 10.8: Proposed layout of Building 904 for the next 5 years showing the assembly areas for CSCs and RPCs, the CMS Integration Centre and the Trigger/DAQ test area.

7672 This first stage of the 904 programme involves repairing the roof, filling-in inspection pits in
 7673 the floor, installing fire protection systems, re-surfacing the floor, installing a storage platform
 7674 and providing network hubs, This will be completed approximately on-time during Autumn
 7675 2010. Simultaneously a rigid storage tent will be installed an adjacent site to allow tooling and
 7676 other installation equipment to be transferred from SX5 and building 904.

7677 The assembly of Resistive Plate Chambers (RPCs), in particular, requires very strict environ-
 7678 mental control. The required conditions, which are maintained naturally in the ISR, namely
 7679 temperature of 21 ± 2 °C and relative humidity 40 ± 10 %, will be hard to reproduce in a building
 7680 the size of 904 without a very large investment, which is probably not feasible on the timescale
 7681 needed for the forward muon upgrade. CMS has made a proposal to CERN-GS department
 7682 that would involve installing four laboratory rooms [~ 10 -15m x 6m x 3m] within Building 904
 7683 and controlling the temperature and humidity inside them using upgraded capacity from the
 7684 existing cooling plant, which is already in use for the racks of the electronics, trigger and DAQ
 7685 integration centre. The second stage of the Assembly and Test centre project will start with the
 7686 installation of these huts and the construction of a framework for the specialized infrastruc-
 7687 ture for gas, detector-related cooling, detector electrical power and network connections for
 7688 the assembly areas. These will be a shared responsibility of CERN (GS and PH departments).
 7689 The next stage of moving facilities and equipment from ISR and SX5, installing the detector
 7690 production lines and connecting the specialized services they require will get underway before
 7691 the end of 2010. Any further insulation of the building shell (roof and walls) will continue as
 7692 a fourth stage of the refurbishment, in parallel with, and factorized from, detector work inside
 7693 the building.

7694 10.9.3.2 Building 904 Electronics Integration Centre

7695 The building 904 electronics integration centre consists of a central platform with installed elec-
 7696 tronics racks surrounded by a collection of several small laboratories equipped with the trigger
 7697 and DAQ electronics for each of the main components of the CMS detector. The centre provides
 7698 a unique environment for subdetector and trigger/DAQ experts to commission and integrate

7699 new developments and upgrades into the central Trigger/DAQ system of CMS without affect-
7700 ing the operation of the experiment at SX5. With the upgrade of the building 904 services, as
7701 described above, corresponding improvements are needed in the electronics integration centre
7702 for central air, access control and other routine services.

7703 Currently, a complete slice of the global calorimeter trigger (GCT) is permanently installed
7704 in building 904. This system receives input from the regional calorimeter trigger (RCT) and
7705 provides output to the global trigger (GT). The next components to be installed are a complete
7706 GT and the cabling up of the RCT. This work is foreseen to be completed well in advance of the
7707 2012 shutdown. In particular, the building 904 setup will be used to pre-commission the Optical
7708 GT Interface (OGTI) from the GCT to the GT for 2011 operation. Similar developments on the
7709 central DAQ slice in building 904 will provide for a complete test bench for pre-commissioning
7710 of all hardware, firmware and critical software components before deployment in SX5.

7711 For the Phase 1 upgrades, the common working area of the electronics integration centre will
7712 be extensively used to burn-in upgrade electronics. For the HCAL Phase 1 upgrades, approx-
7713 imately 1/3 of the entire front-end services and low-voltage power will be operated continu-
7714 ously to ensure data integrity and front-end stability. Known potential problems, such as slow
7715 control and monitoring induced noise sources, will be investigated and eliminated, if found,
7716 through the appropriate hardware, firmware and software modifications. The HCAL back-end
7717 readout based on the μ TCA technology will begin its integration phase for the 2012 shutdown
7718 where optical splitters will allow the upgrade electronics to parasitically readout and gener-
7719 ate trigger primitive information for data coming from the current front-end readout system.
7720 Effective integration and reliability of the HCAL upgrade depends on an extensive burn-in
7721 program for the front-end electronics based in 904 in advance of the 2016 Phase 1 upgrade and
7722 an upgraded back-end readout test slice for pre-commissioning in building 904 for subsequent
7723 parasitic operation in SX5 following the 2012 shutdown.

7724 For the trigger Phase 1 upgrades, the integration of the serial link board (SLB) communication
7725 from the ECAL and HCAL back-ends to the RCT must be achieved in building 904 in advance
7726 of any modifications to the SX5 system. The hardware-level calorimeter trigger system is a
7727 critical online system whose data integrity must be maintained with high reliability. The DAQ
7728 integration for the trigger system also requires burn-in and testing in building 904 in advance
7729 of installing the system in SX5. The current 904 infrastructure has been extensively used for SLB
7730 testing between ECAL, HCAL and the RCT and a similar intense program of checks and burn-
7731 in is planned for the Phase 1 upgrades and 2012 shutdown maintenance and modifications.

7732 **10.9.3.3 Building 904: Offices and small laboratory/workshop areas**

7733 Some additional offices and labs are foreseen within or near building 904. Adjacent to the ex-
7734 isting CMS mechanical integration centre, the current electrical workshop will be adapted as a
7735 pipework laboratory, and the electrical storage areas will be converted into storage for electron-
7736 ical components. The present "Kicker lab", 280 m², will be adapted as a detector development
7737 laboratory, which will contain activities such as the current prototyping test of Micro Pattern
7738 Gas Detectors.

7739 Adjacent to building 904 and the tooling storage tent, barrack 933 will provide approximately
7740 20 offices. Minor refurbishment costs (approx 10 kCHF) should be foreseen.

7741 10.9.4 Other facilities

7742 10.9.4.1 Building 892, Preveessin

7743 The catacombs associated with ISR point 4 were converted into substantial locked storage en-
7744 closures for muon system spares. Material still required is destined to be transferred to the
7745 basement of building 892. Similarly one of the ECAL test benches currently in building 867,
7746 along with the mechanical workshop adjacent to it, will be transferred to the ground floor of
7747 building 892. Substantial refurbishment work to the shell of the building, a host lab responsi-
7748 bility, is estimated to cost 300k CHF and may be required during 2011. Detailed requirements
7749 are still to be negotiated.

7750 10.9.4.2 Buildings 186 and 28, Meyrin

7751 The size of building 186 is roughly 2000m² on 2 floors. This building contains the 600m² CMS-
7752 funded TIF clean facility used to commission the Tracker, preshower and beam monitors. It
7753 includes a scaled down readout system and infrastructure including rack water cooling and
7754 detector fluorocarbon cooling. It is adjacent to the PH department silicon facility. The upper
7755 floor contains smaller clean areas used for Tracker and Preshower component assembly and
7756 testing, pixel tracker final integration and testing, and beam scintillation counter and diamond
7757 beam monitor labs. All these facilities will be needed for upgrades. In extreme circumstances
7758 it is conceivable to transfer the Tracker back to the TIF if a major fault should occur before it is
7759 strongly activated.

7760 However, as is the case for Building 904, the cooling plants are unreliable and the mini-DAQ
7761 now obsolete. The rough estimated cost of a basic refurbishment is 82 kCHF, which is to
7762 be split equally between CERN as host, CMS M&O A and CMS upgrade funds. Subsystems
7763 involved would take care of specific facilities from upgrade or M&O B funds as appropriate.

7764 It is important to retain the use of offices, workshops and labs in the adjacent building 28.

7765 10.9.4.3 Alignment test benches

7766 The surveyed test benches used for calibration of alignment components on barrel muon drift
7767 chambers and of the MAB structures, which provide a link between barrel chamber layers,
7768 are needed during major shutdowns. They require an environment which is stable from the
7769 mechanical, temperature and humidity point of view. The environment should be lockable and
7770 relatively clean, with adequate lighting. The area adjacent to the ISR I4 collision hall met these
7771 criteria automatically. CMS is working with CERN departments to identify possible alternative
7772 areas. Costs of the transfer should be born by CERN as host lab.

7773 10.10 Planning and Coordination

7774 10.10.1 Organization

7775 The coordination of technical operation and of maintenance, consolidation and upgrade activ-
7776 ities during accesses, technical stops and shutdowns is the responsibility of the CMS central
7777 technical team. The present organization of this team is illustrated in Fig 10.9.

7778 For those subsystems where major upgrade or revision work is anticipated, the currently dor-
7779 mant branch of subdetector coordination populated by the subdetector technical coordinators
7780 is expected to be restored. As in the construction phase, each will be responsible for planning
7781 and coordinating all technical aspects of the approved upgrade or revision project, according to

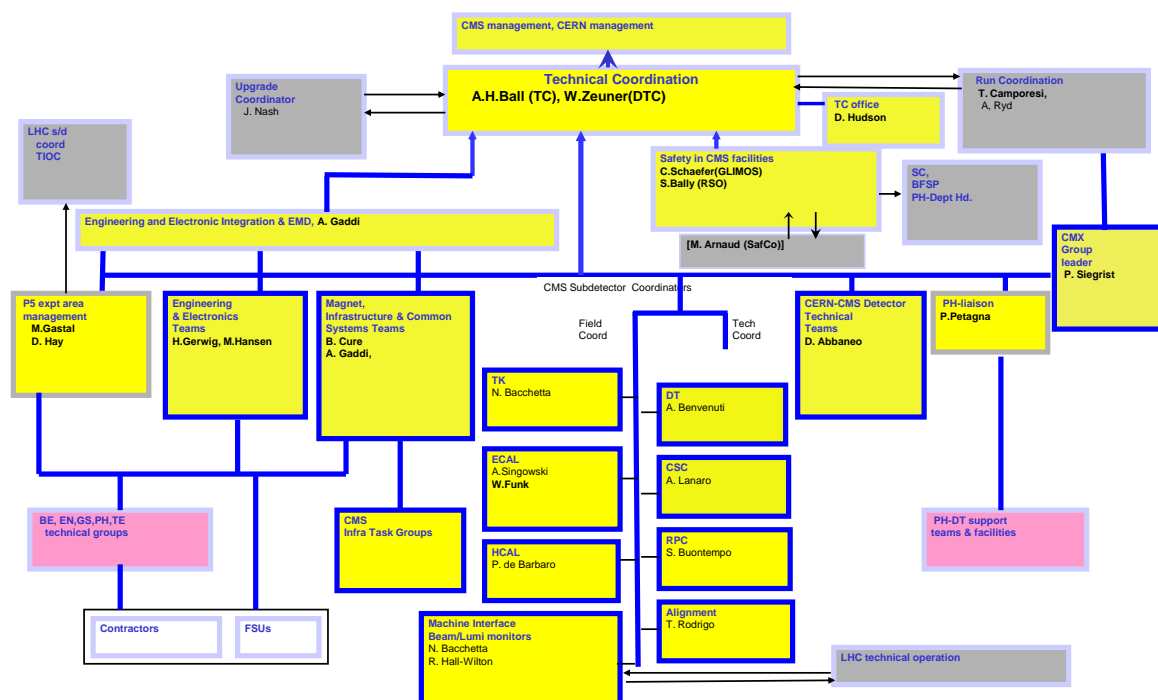


Figure 10.9: Organization of the CMS central technical team.

7782 guidelines agreed with CMS technical coordination and scrutinized by the Engineering Design
 7783 Review process. This responsibility includes QA/QC, delivery of finished items to point 5, pre-
 7784 installation testing and any repairs or rework needed. The existing field coordination structure
 7785 will deal with installation, post-installation testing, commissioning, integration into CMS, and
 7786 subsequent maintenance and operation. Both arms of subdetector coordination, which depend
 7787 on continuity of experienced personnel with project responsibility, were crucial to the success
 7788 of the low luminosity CMS detector and must be maintained and supported. A small number
 7789 (2-3) of additional central team task coordinators, drawn from the collaboration, will be put in
 7790 place as soon as specific manpower plans for the central field teams are addressed.

7791 10.10.2 LHC planning 2010-2016

7792 The duration of the 2012 LHC shutdown is estimated at 15 months, a duration chiefly de-
 7793 termined by the time required for splice consolidation to allow the LHC to operate at higher
 7794 energy. The duration of the 2016 shutdown is currently considered to be around 1 year and de-
 7795 termined by the needs of experiments, with the CMS request of 12 months currently the longest.
 7796 Incorporation of LINAC4 into the injector chain, the main accelerator activity, is estimated to
 7797 take only 6 months in 2016.

7798 Extended technical stops are expected to occur at year-end 2013-14, with duration similar to the
 7799 9-11 weeks foreseen for 2010, and at year-end 2014-15, with duration estimated at 12 weeks.
 7800 As has been demonstrated in 2009-10, rapid opening of CMS, giving a few days access for

7801 light repair work in any location, followed by closing and a return to beam-ready condition, is
7802 possible in a 10-11 week shutdown. At least 3 weeks of this time is dedicated to the cycle of
7803 re-pressurizing the beampipe to 1 atmosphere with Neon and eventually restoring operating
7804 vacuum.

7805 **10.10.3 General constraints on planning**

7806 The possible timeframes for installation at Point 5 of the various consolidation and upgrade
7807 features is in most cases determined by their potential for readiness relative to the two major
7808 LHC shutdowns planned in 2012 and 2016. The pixel tracker and beampipe replacements are
7809 still being designed; clearly they will require a long shutdown and cannot be ready for 2012-13.
7810 In contrast, for many items in the forward muon upgrade, the design is mature, procurements
7811 are proceeding, assembly lines are being setup and construction is imminent. All modifica-
7812 tions which involve significant individual or collective radiation dose to personnel must be
7813 completed as soon as possible (ALARA principle). The same argument applies to modifica-
7814 tions or additions related to minimizing these doses. Where consolidation or upgrades are
7815 aimed at reducing or eliminating a large risk to the availability of the detector or the efficiency
7816 of data-taking, it is clearly prudent to execute them at the earliest opportunity after they are
7817 ready.

7818 In order to repeat, in 2013 and 2017, the “unprecedented state of readiness” for first beam,
7819 achieved in 2009, the same integration of commissioning activities into the planning must
7820 be foreseen. The independently serviced wheels and disks of CMS allow for significant re-
7821 qualification tests and pre-commissioning work to be carried out concurrently with mainte-
7822 nance and installation activities, as was routinely the case from early 2006 onwards. In addi-
7823 tion the detector must be closed, the magnet commissioned to full-field and extensive cosmic
7824 ray tests undertaken, early enough to leave sufficient margin before accessibility is lost to re-
7825 open and remedy any faults detected. The value of this was conclusively demonstrated by the
7826 MTCC in 2006 and the CRAFT exercises of 2008 and 2009. The planning being developed is
7827 therefore based on having partial or full infrastructure and services (HVAC, gas, cooling, elec-
7828 tricity, DAQ) available continuously as soon as possible during each shutdown, so as to allow
7829 post-installation testing and commissioning of new detector parts to proceed smoothly and in-
7830 tensively. In addition, CMS will be closed and the magnetic field raised to 3.8T a minimum of
7831 10 weeks before first beams are expected to circulate. It should be noted that this important
7832 safety margin may be hard to maintain in 2016, should all other shutdown activities indeed
7833 prove to require substantially less time than those at CMS.

7834 The possible logistic configurations of opening CMS are severely limited by beampipe support
7835 requirements, the size of the experimental hall and the procedures for beampipe bake-out. The
7836 basic set of configurations available at either end of the detector are illustrated in Fig 10.10,
7837 Fig 10.11, and Fig 10.12. The possibilities for configuring the two ends differently vary from
7838 unrestricted to highly constrained, depending on what tasks are being done.

7839 The attribution of activities to the two major shutdowns is determined by the constraints out-
7840 lined above and particularly the logistic configurations needed for installation of the new
7841 beampipe and pixel tracker during the 2016 shutdown. Most of this shutdown must forcibly
7842 be spent with both endcaps fully open in configurations G through J. A further period is spent
7843 partially open (configuration E at both ends) for beampipe bake-out, during which, however,
7844 no other work on the detector is admissible due to safety constraints. Since installation of the
7845 forward muon upgrade requires very substantial periods of work in logistic positions C and E
7846 with closed, or partially closed, endcaps, this automatically leads to a requirement to complete

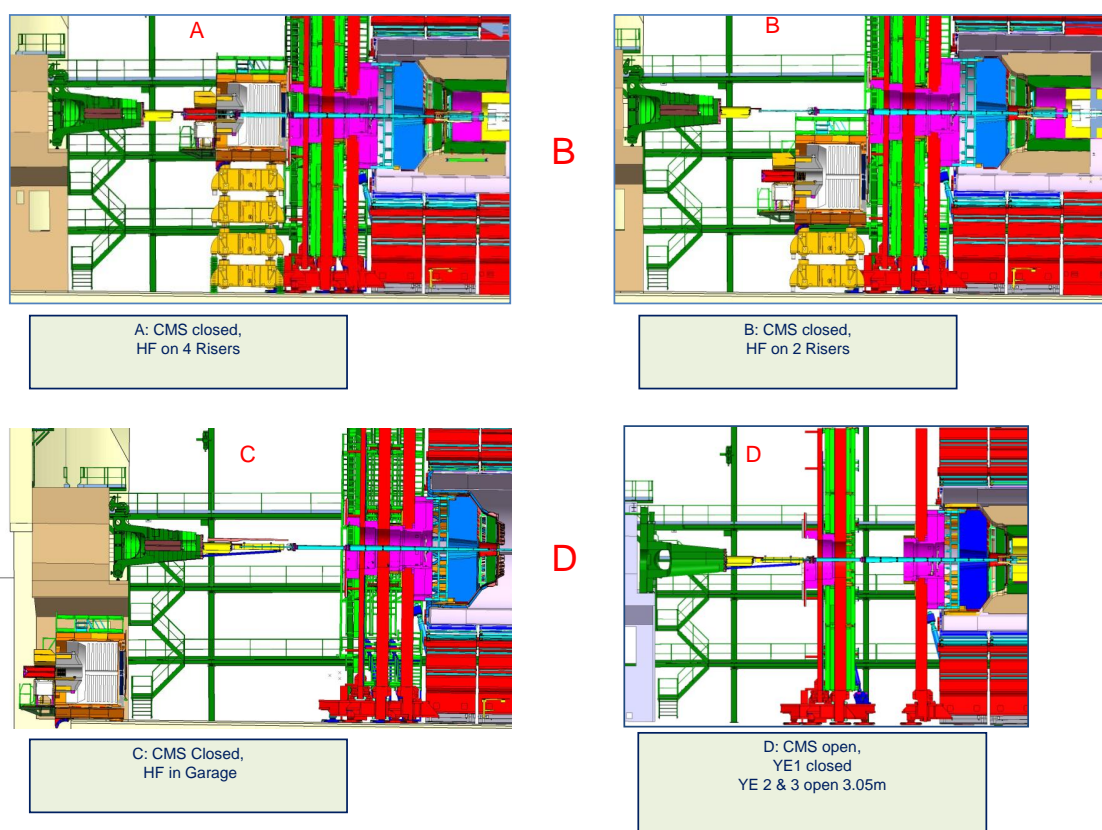


Figure 10.10: Possible opening configurations A - D of the CMS Detector.

7847 this upgrade during the 2012-13 shutdown or in the technical stop(s) of 2013-14 and 2014-15.
 7848 The work (particularly construction of the YE4 shielding walls) factorizes between the plus
 7849 and minus z ends, so that the likely 2012-13 planning features sequential periods with the +z
 7850 endcaps closed, then the -z endcaps closed.

7851 It is essential to complete installation of the YE4 shielding disks at both ends before magnet
 7852 re-commissioning starts in order to keep the magnetic field and forces symmetric. To accom-
 7853 modate the likely installation of these disks before the detector elements (CSC, RPC) of the
 7854 forward muon upgrade are ready, the potential of the newly conceived YE4 pushback system
 7855 (see Section 10.4.1) must be exploited to give rapid access for CSC and RPC installation without
 7856 opening the yoke. Opportunities for completing the installation are envisaged in the 2013-14
 7857 or 2014-15 extended year-end technical stops,

7858 Following the pattern established during construction, the detailed CMS planning being ap-
 7859 plied in the field must be flexible, ready to exploit opportunities presented by LHC schedule
 7860 changes (even if not yet officially recognized) and factorized enough to be easily adapted to
 7861 changed circumstances. Examples are the possible delayed start of the first long shutdown and
 7862 the need to carry out currently unforeseeable maintenance work. Contingencies must also be
 7863 kept in hand for effectively using any unforeseen machine repair stops of substantial duration,
 7864 for reacting to late delivery of items to be installed and for accommodating maintenance work
 7865 additional to what is now planned.

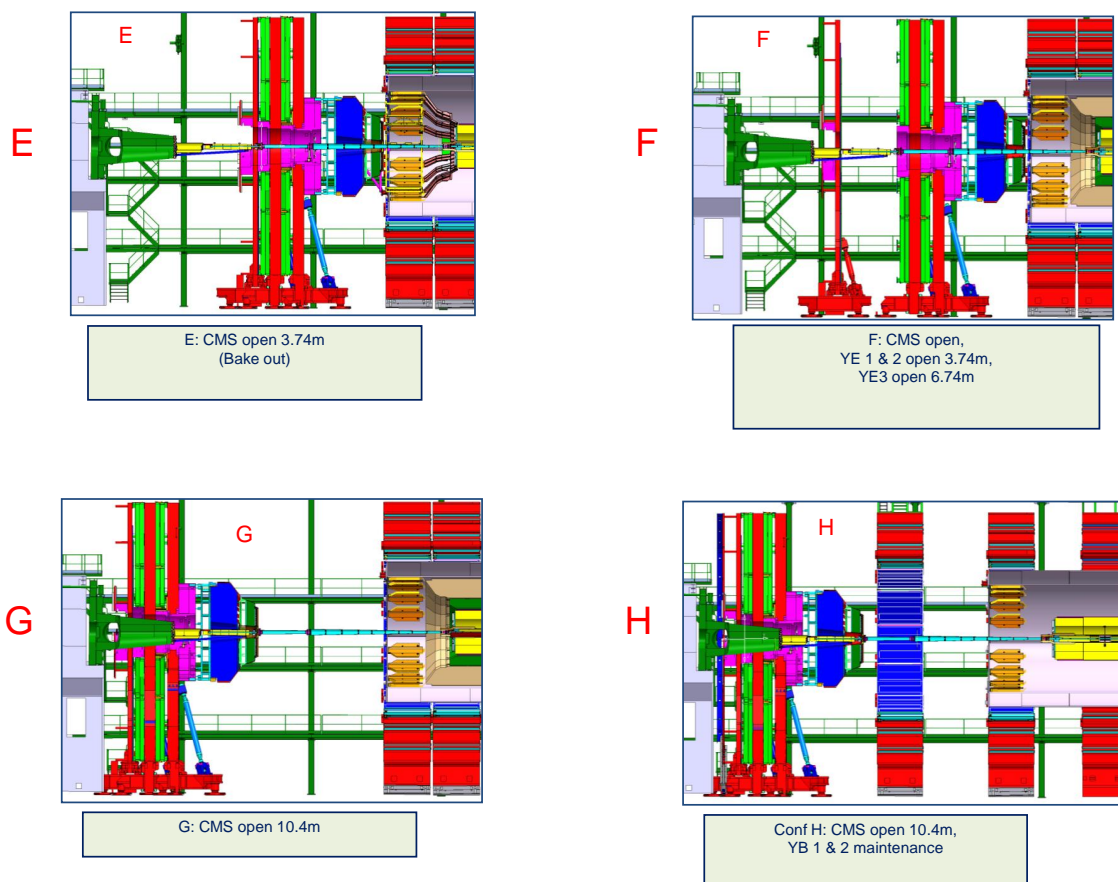


Figure 10.11: Possible opening configurations E - H of the CMS Detector.

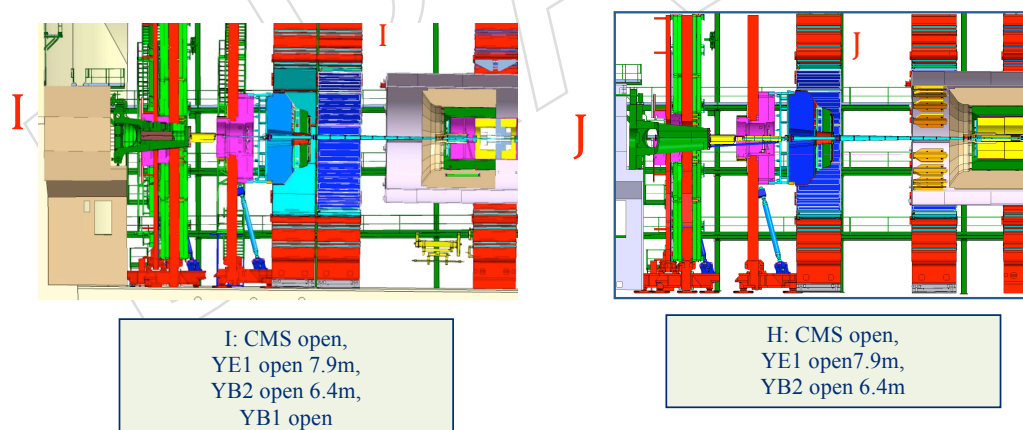


Figure 10.12: Possible opening configurations I - J of the CMS Detector.

7866 **10.10.4 Shutdown 2012-13**

7867 Assuming no force majeure constraints, such as an unexpected requirement for beam-pipe
7868 bake-out, the current list of detector activities in UXC during 2012-13 is:

- 7869
- Improve barrel-endcap seal for cold Tracker.
 - 7870 • Test beampipe region RP shielding + opening under vacuum.

- 7871 • Replace HO & CASTOR phototransducers.
- 7872 • Build YE4+z shielding wall and install pushback system.
- 7873 • Build YE4-z shielding wall and install pushback system.
- 7874 • Install 4th muon endcap station +z (ME+4/2, RE+4/2, RE+4/3) and possibly RE-4/2,
7875 RE-4/3 for -z)
- 7876 • Replace HF phototubes +z and -z (while HF is in garage).
- 7877 • Modify Forward Structures (for ALARA and so that CASTOR, TOTEM and ZDC are
7878 removable for pp running and re-installable for ion-ion or $\beta^* = 1500\text{m}$). The most
7879 extensive modifications are needed at the -z end where CASTOR is installed.
- 7880 • Remove and maintain one or both ends of the forward pixel system (with BCM
7881 removed).
- 7882 • Install Pixel Luminosity Telescope (PLT).
- 7883 • Install BSC extension, with possible installation of FSC stations.
- 7884 • Install ZDC crane.

7885 Very many infrastructure and common systems consolidations will be also be carried out. Per-
7886 haps the most critical are in the magnet cryogenic system where it is essential to reduce risks
7887 to the magnet availability and lifetime by improving contaminant filtering in the cold box and
7888 installing redundant compressors in the surface cryogenic plant.

7889 After this shutdown CMS should be ready for beams at 6.5 TeV, instantaneous luminosity 2-5
7890 $\times 10^{33} \text{ cm}^{-2}\text{s}^{-1}$, bunch-spacing of 25, 50 or 75 ns and integrated luminosity $\sim 50 \text{ fb}^{-1}$.

7891 Fig 10.13 illustrates a likely critical sequence for activities on the +z end of the detector during
7892 the 2012-13 shutdown, assuming the shutdown starts on 5 Dec 2011. (note that the detailed
7893 planning developed from this summary already reaches 250 discrete tasks). The sequence
7894 shown is for the +z end. For the -z end, the periods in configurations E and H are interchanged
7895 and the period in configuration C is used in priority to install new forward support structures.

7896 10.10.5 Technical stops 2013-14 (if applicable) and 2014-15

7897 Exploiting the flexibility offered by the YE4 push-back system, and assuming no force majeure
7898 constraints forcing more extensive opening for maintenance, the current plan assumes the fol-
7899 lowing critical detector activities during these technical stops.

- 7900 • Install 4th muon endcap station -z (ME4/2, RE4/2, RE4/3) (RE4 removal/re-installation
7901 if applicable).

7902 10.10.6 Shutdown 2016

7903 The current plan for detector activities in UXC during 2016 is:

- 7904 • Remove pixel tracker, BCM and PLT.
- 7905 • Remove part or all of the beampipe in the region $(-18\text{m} < z < +18\text{m})$.
- 7906 • Re-install beampipe with new central Be section, radius 23-25mm (to be determined).
- 7907 • Bakeout beampipe $(-18\text{m} < z < +18\text{m})$.
- 7908 • Install 4 layer, low-mass pixel tracker, re-install BCM and PLT.
- 7909 • Rebuild HB/HE front end +z and -z.
- 7910 • Replace ME1/1 endcap muon station readout electronics (both +z and -z) for im-

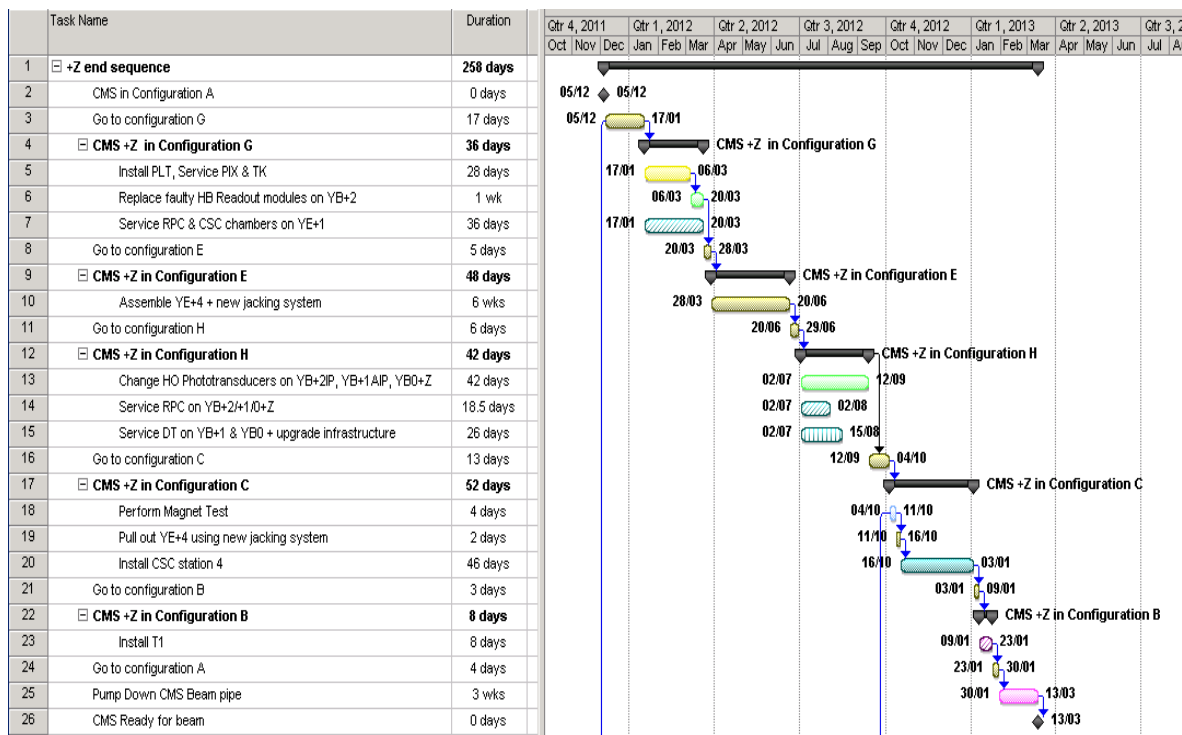


Figure 10.13: Provisional planning for the sequence of major tasks on the +z end of the CMS Detector during the 2012-2013 shutdown.

7911
7912
7913
7914
7915
7916
7917
7918

proved granularity.

- Revise muon barrel front-end electronics.
- Replace BSC with rad hard solution in maintainable location.
- Replace BCM1 and BCM2.

In addition, very substantial modifications to the trigger and readout electronics in the USC are foreseen to prepare for higher luminosity and to address obsolescence issues.

After this shutdown, CMS should be ready for beam energies of 7 TeV, instantaneous luminosity 2×10^{34} and integrated luminosity 300 fb^{-1} .

DRAFT

7919 Chapter 11

7920 Cost, Schedule, and Management

7921 11.1 Cost

7922 This section gives a high level cost estimate for the program of upgrades and improvements
7923 described in the chapters 3-10 of this Technical Proposal. This cost estimate has been rolled up
7924 from detailed cost estimates that have been collected from all of the sub-detectors.

7925 Since different methodologies are used for developing cost estimates among the national fund-
7926 ing agencies that support the CMS collaborating institutions, the following ground rules have
7927 been established to produce a consistent cost:

- 7928 1. Cost estimates are for M&S only.
- 7929 2. All costs are given in calendar year 2010 Swiss Francs.
- 7930 3. All items reported by the sub-systems are without contingency. It is expected that differ-
7931 ent funding agencies will handle the issue of contingency according to thier own prac-
7932 tices.
- 7933 4. There will be a CMS common fund to provide a global project contingency. This is cur-
7934 rently proposed to be 10% of the project base cost and would be paid as part of the com-
7935 mon "taxed" items for the upgrade. This global project contingency is included in the cost
7936 estimate.

7937 The resulting cost estimate is given in Table 11.1.

7938 11.2 Schedule

7939 There are two long shutdowns of more than a year each. Most installation of the upgraded
7940 detectors will be done in these two shutdowns. The installation activities in each shutdown are
7941 determined by

- 7942 • when a given upgraded subsystem will be ready to install; and
- 7943 • what is the next available shutdown that offers adequate time to install the detector.

7944 The readiness of a sub-detector or sub-system for installation depends on the completion of a
7945 sequence of steps that include: completion of R&D; design, development, and testing of proto-
7946 types of the detector, its electronics and all supporting systems; preproduction runs leading to a
7947 successful Production Readiness Review; procurement of production parts; establishment and

Table 11.1: Summary of Costs of CMS Phase 1 Upgrades and Improvements

Detector	cost (M&S Only)
	KChF
CSC	5,570
DT	2,200
RPC endcap	4,220
HCAL	5,817
HF - Phototubes	1,990
Pixel Tracker	17,350
Trigger	4,600
DAQ	6,700
Beam Instrumentation	1,540
Magnet, Power, and Cryo	1,330
Infrastructure	6,315
Test Beam facilities	610
Safety Systems	964
Electronics Integration	1,575
engineering Integration	3,666
Total	64,447
10% of which, Common Fund	6,445

7948 debugging of production facilities; production and assembly of components according to rigorous
7949 quality control; integration and commissioning outside the experiment; and transportation
7950 to Point 5 and installation into CMS.

7951 It might be necessary, and is certainly desirable, to assemble and operate each upgrade de-
7952 tector or component at CERN, often in a specially prepared "integration center" or "burn-in
7953 facility". The best results have been achieved in CMS when detectors have been installed in
7954 such a facility and exercised thoroughly for as long as a year before installation in the exper-
7955 iment. The construction and outfitting of these integration areas are an essential part of the
7956 upgrade project. In many cases, it will be possible to reuse areas built and equipped for the
7957 original construction of CMS.

7958 Once the detector is installed in CMS, it is necessary to connect it to services, check it out locally,
7959 and integrate it with the rest of CMS.

7960 The objective of all these steps is to have a detector that is ready to operate when beam first
7961 appears after the startup. Deliverables, in addition to the detector itself, include all calibration,
7962 alignment, and controls hardware, software and techniques; local reconstruction programs that
7963 are fully implemented within CMSSW; a full simulation package with starting values for all
7964 geometrical parameters; a very accurate description of the material in the detector and its dis-
7965 tribution; and a complete set of drawings and documentation.

7966 Since there are only two long shutdowns planned, one in 2012 and one in 2016, the scheduling
7967 problem comes down to trying to get as many of the subsystems ready to install in 2012, with
7968 the remainder installed in 2016. It is also an option to use the short "technical stops" planned
7969 each year to install parts of the detector. Table 11.2 shows our current understanding of the
7970 installation schedule.

Table 11.2: Installation Activities in 2012 and 2016 Shutdowns

device	install in 2012	install in technical stops	install in 2016	comment
CSC and RPC endcap 1	X			if not completed earlier Must be ready before shutdown
CSC and RPC endcap 2		X		
CSC and RPC endcap 2			X	
ME1/1 Electronics			X	
DT electronics relocation			X	
Outer Hadron Calorimeter (HO)	X			
Forward Hadron Calorimeter (HF)	X			
CASTOR	X			
Pixel Luminosity Telescope	X			
Barrel Hadron Calorimeter (HB)			X	
Endcap Hadron Calorimeter (HE)			X	
Pixel replacement			X	
Trigger replacement			X	
DAQ upgrade			X	

7971 Human and budgetary resources are required at each step of this process. The timely avail-
7972 ability of these resources will be critical to having the upgrades for each shutdown ready on
7973 schedule.

7974 This installation schedule assumes that the work on outfitting Building 904, SX5, and any other
7975 integration centres proceeds quickly enough so that it is never in the critical path for construc-
7976 tion or installation activities.

7977 The ideal plan for the muon system upgrade would be to have both endcaps of the RPCs and
7978 the CSCs ready to install in 2012. The CSCs are mounted first on the fourth disk and the RPCs
7979 are mounted over them. The RPCs are scheduled be completed in 2012 and would be available
7980 for installation. However, the funding for the CSCs is not yet in place. By the time funds are
7981 available, there will not be enough time to fabricate planes for both CSC endcaps by 2012. It
7982 does seem feasible to have one endcap of CSCs ready for installation in 2012. This would allow
7983 us to install one set of endcap muon chambers, CSCs and RPCS, in 2012. Since CSC construction
7984 would continue, it might be possible to use the short “technical stops” of a few months in 2014
7985 and 2015 to install additional CSCs and RPCs on the second endcap. This is possible because
7986 the fourth disk is at the end of CMS and is accessible for installation without requiring any
7987 opening of CMS. The remaining endcap RPCs and CSCs that could not be installed in these
7988 short shutdowns, would be installed in 2016. Moreover to save funds, the electronics for the
7989 second CSC endcap will be the CFEBS that are recovered when they are replaced by DCFEBs on
7990 one of the ME1/1 chambers. This will also have to happen in 2016 since the new DCFEB cards
7991 and supporting electronics are still being developed and cannot be ready by 2012. In 2016, the
7992 access to the ME11 detectors is compatible with the other work going on in Point 5.

7993 The HO SiPM is a commercial device that can be purchased as a stock item. The HO upgrade
7994 will be ready to install in 2012 and will provide several years of operational experience with a
7995 large system of SiPMs before the HB/HE HPDs are replaced with SiPMs.

7996 The SiPMs for the HB and HE must have more pixels per unit area, faster reset times and be
7997 more radiation tolerant than the HO SiPMs. These SiPMs must be developed in the next two
7998 years and be thoroughly checked out in beam tests and radiation exposures before one can
7999 commit to procuring the parts for the whole system. Substantial engineering is required for the
8000 additional front end electronics. Since these detectors are critical for the CMS physics program,
8001 the R&D for the new SiPMs must be given the highest priority to establish that there is in fact
8002 an upgrade path. At present, the only fallback position is to continue to use the HPDs with all
8003 their limitations and problems.

8004 The backend electronics for the Hadron Calorimeter needs to be available to debug the up-
8005 graded calorimeter front end sensors (SiPMs) and electronics. It is highly desirable to accelerate
8006 the R&D on the back end so that it can be used in parallel to the current electronics during the
8007 early part of the run that starts in 2013 so that any operational problems can be found before
8008 committing to full production.

8009 The R&D on the pixel detector upgrade is well along and the basic ideas have been proven.
8010 However, it will be a great challenge to complete the final design, carry out the detailed and
8011 rigorous testing of the new readout chip and to construct this detector, which is much larger
8012 than the one that it will replace, in the allotted time of five years. This is another crucial detector
8013 for the CMS physics program and it must be ready to do physics when the beam returns after
8014 the 2016 shutdown.

8015 Trigger changes must be prepared in time to accommodate the upgraded calorimeter and muon
8016 detectors. The wholesale replacement of the trigger system with a new basic infrastructure
8017 poses real risks to CMS. When the new system begins to operate after the 2016 shutdown,
8018 CMS will be able to double its data in about a year. There may well be a physics discovery in
8019 progress. A functioning trigger must be available on day one of the resumption of the collider
8020 run. The trigger group will implement a scheme for detailed emulation and parallel operation
8021 to achieve this goal.

8022 The DAQ similarly must be ready to function reliably before the run resumes in 2017 to support
8023 commissioning activities. Large scale testing of the replacement switching capacity is planned.

8024 Beam monitoring systems will be upgraded and maintained in 2012 and 2016 as required. Ma-
8025 jor changes to the BSC will occur in 2016.

8026 The LHC program is driven by physics. The early operation of the machine has been very suc-
8027 cessful. It now appears that the machine will be capable of sustained running at higher lumi-
8028 nosity than had been considered possible without the upgrades of 2012. This brings certain
8029 physics goals into range if the machine keeps running beyond 2011 and through most of 2012.
8030 If it is decided to do this, the whole upgrade will simply be delayed by a year. The basic plan
8031 will not change. However, the extra year to prepare for the shutdowns, which would now be in
8032 2013 and 2017, would probably increase the chances of having all the equipment ready to install.

8033 **11.3 Management Structure**

8034 This section provides an initial attempt to describe a management structure for the program
8035 of improvements and upgrades. This section outlines ideas for the management of the project.
8036 These ideas are still being discussed within the collaboration, with the expectation that a new
8037 structure will be agreed during 2011, and fully in place early in 2012.

8038 It took more than a decade to construct the CMS detector and to develop the software and

8039 computing systems for analyzing the data. During this period, the experiment had a very
8040 stable leadership team. This played an important role in the success of the effort.

8041 Recently, CMS has changed its governance to one that it concluded was more appropriate to
8042 operations and maintenance of the detector, efficient data collection, correct and prompt data
8043 reduction, and physics analysis. These changes, detailed in a new constitution that went into
8044 effect in 2008, features more turnover in the leadership. In particular, the spokesperson is
8045 elected by the Collaboration Board for a term of two years and cannot serve additional terms.

8046 The Phase 1 Upgrade Construction Project will last for at least 6 years and is also responsible
8047 for making sure that the R&D for Phase 2 is completed in this period. This requires the stability
8048 that existed in the original construction project. Since the upgrade project will span the terms
8049 of three or four different spokespersons, the Upgrade Construction Project Management plan
8050 must ensure that the continuity of the project.

8051 **11.3.1 Organizational Principle**

8052 The Upgrade will not have a parallel and separate organization from the existing subsystem
8053 structure of CMS. Instead it will share the existing CMS structure with detector operations.
8054 Responsibility, however, will be clear because there will be individuals appointed at each level
8055 within the existing organization whose assignment it is to accomplish the upgrade. It is ex-
8056 pected that some personnel in each subsystem will work exclusively on the upgrade; some
8057 only on detector operations; and some will split their time between those two activities. We
8058 rely on the leaders of the subsystems and those responsible for the upgrade to resolve the com-
8059 petition for resources so that all CMS' goals are achieved. The Upgrade leadership will include
8060 a person at an appropriate level in the collaboration management who will be in a position to
8061 represent the upgrade and argue effectively for adequate resources to carry it out.

8062 **11.3.2 Phase 1 Upgrade Construction Project Manager**

8063 The Upgrade will always compete for resources with ongoing operations and data analysis.
8064 The interests of the Upgrade must be represented in all the discussions of resources and must
8065 be able to compete effectively with the other projects for resources. To achieve this, CMS will
8066 appoint a Phase 1 Upgrade Construction Project Manager (Upgrade PM).

8067 The Upgrade PM is initially nominated by the Spokesperson after broad consultation in CMS,
8068 and endorsed by the Management Board (MB) and the Collaboration Board (CB). The proposal
8069 is for the Upgrade PM to be appointed to a two year term that is renewable indefinitely until
8070 the project ends.

8071 The Upgrade PM sits on all relevant committees and boards that the Deputy Spokespersons sit
8072 on.

8073 **11.3.2.1 Role and Responsibilities of the Phase 1 Upgrade Construction Manager**

8074 The task for the Upgrade PM is

- 8075 • to work with the leadership and members of CMS to define the scope of the upgrades
8076 and complete the Technical Design;
- 8077 • to deliver the full scope of the upgrade meeting all technical requirements, on sched-
8078 ular and within budget; and
- 8079 • to ensure that all necessary R&D for the Phase 2 Upgrade that is needed in this
8080 period is successfully completed.

8081 **11.3.3 Phase 1 Upgrade Construction Project Deputy Program Managers**

8082 The Upgrade PM, in close consultation with the Spokesperson may propose candidates for
8083 deputies. They are nominated by the spokesperson and their appointment must be approved
8084 by the MB and the CB.

8085 Deputies would be appointed for an initial term of two years and their terms may be renewed
8086 by the Upgrade PM with the concurrence of the spokesperson.

8087 **11.3.3.1 Role and Responsibilities of the Deputy Upgrade PMs**

8088 The Deputies Upgrade PMs report to the Upgrade PM. Their job is to help the Upgrade PM
8089 carry out his/her responsibilities. One of the deputies represents the Upgrade PM in all func-
8090 tions when the Upgrade PM is not available. It is expected that the Upgrade PM will assign
8091 each deputy specific responsibilities within the overall project. It would be natural for one of
8092 them to have a particular responsibility for the Phase 2 R&D.

8093 **11.3.4 Phase 1 Upgrade Construction Technical Coordinator**

8094 The Upgrade PM also works with the Spokesperson and the CMS Technical Coordinator to
8095 appoint a Phase 1 Upgrade Construction Project Technical Coordinator. We refer to this person
8096 as the "Upgrade Technical Coordinator"

8097 According to Annex 10 of the CMS Constitution, "The mission of the Technical Coordinator is
8098 to assure the integration, installation, and safe, effective technical operation of the sub-detectors
8099 and the magnet including any upgrades which may be undertaken." The Technical Coordina-
8100 tor must be involved deeply in the design of the upgrades to make sure that new devices can
8101 be successfully installed and integrated in the detector and is directly involved when devices
8102 begin to appear at CERN. The CMS Technical Coordinator carries out his/her mission through
8103 the Technical Coordination Team.

8104 Because the Technical Coordinator's responsibilities extend to the support of the existing de-
8105 tector, surface facilities, utilities and services, there will be a Phase 1 Upgrade Technical Coor-
8106 dinator who reports to the CMS Technical Coordinator and the Upgrade PM and specializes in
8107 technical coordination of the upgrade.

8108 The Upgrade Technical Coordinator should be at the same level as a Deputy to the CMS Tech-
8109 nical Coordinator.

8110 **11.3.4.1 Manner of Appointment and Term of Service**

8111 The Phase 1 Upgrade Technical Coordinator will be appointed by the CMS Spokesperson in
8112 close consultation with the Upgrade PM and the CMS Technical Coordinator. The appointment
8113 must be endorsed by the CMS MB and CB.

8114 **11.3.4.2 Role and Responsibilities of the Phase 1 Upgrade Technical Coordinator**

8115 The mission of the Upgrade Technical Coordinator is to act on behalf of the CMS Technical
8116 Coordinator to assure the integration, installation, and safe, effective technical operation of the
8117 upgraded sub-detectors and electronics with the rest of CMS.

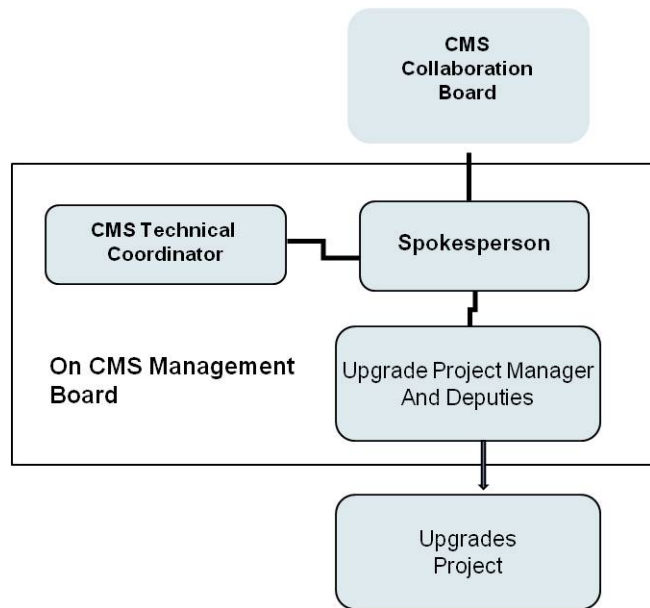


Figure 11.1: High level interactions between Upgrade Project leaders and CMS collaboration and technical leadership

11.3.5 Interaction among the CMS Spokesperson, CMS Technical Coordinator, and Upgrade PM

8118
8119

8120 The Upgrade PM and Upgrade Technical Coordinator will be members of the CMS Management Board, which is chaired by the CMS spokesperson. The Technical Coordinator is also a member of the MB.

8123 In addition to their interactions through the Management Board, the Spokesperson, Technical Coordinator, Upgrade PM, and Upgrade Technical Coordinator will work together to optimize the use of CMS resources to achieve all of its objectives, including the achievement of the detector upgrades. These interactions are shown graphically in Fig. 11.1

11.3.6 Upgrade Subsystem Project managers

8127

8128 Upgrade subsystem managers are appointed for all subsystems having a significant Phase 1 R&D Upgrade project and/or a significant Phase 2 R&D Upgrade program. A possible organization chart down to the subsystem level is shown in Fig. 11.2.

8131 The subsystems currently involved in the Upgrade are:

- 8132 • RPC Muon detector;
- 8133 • CSC Muon detector;
- 8134 • DT Muon detector;
- 8135 • Hadron Calorimeter systems;
- 8136 • Electromagnetic calorimetry;
- 8137 • Pixel tracker;
- 8138 • Silicon Strip tracker;
- 8139 • Trigger systems;
- 8140 • Data Acquisition systems;

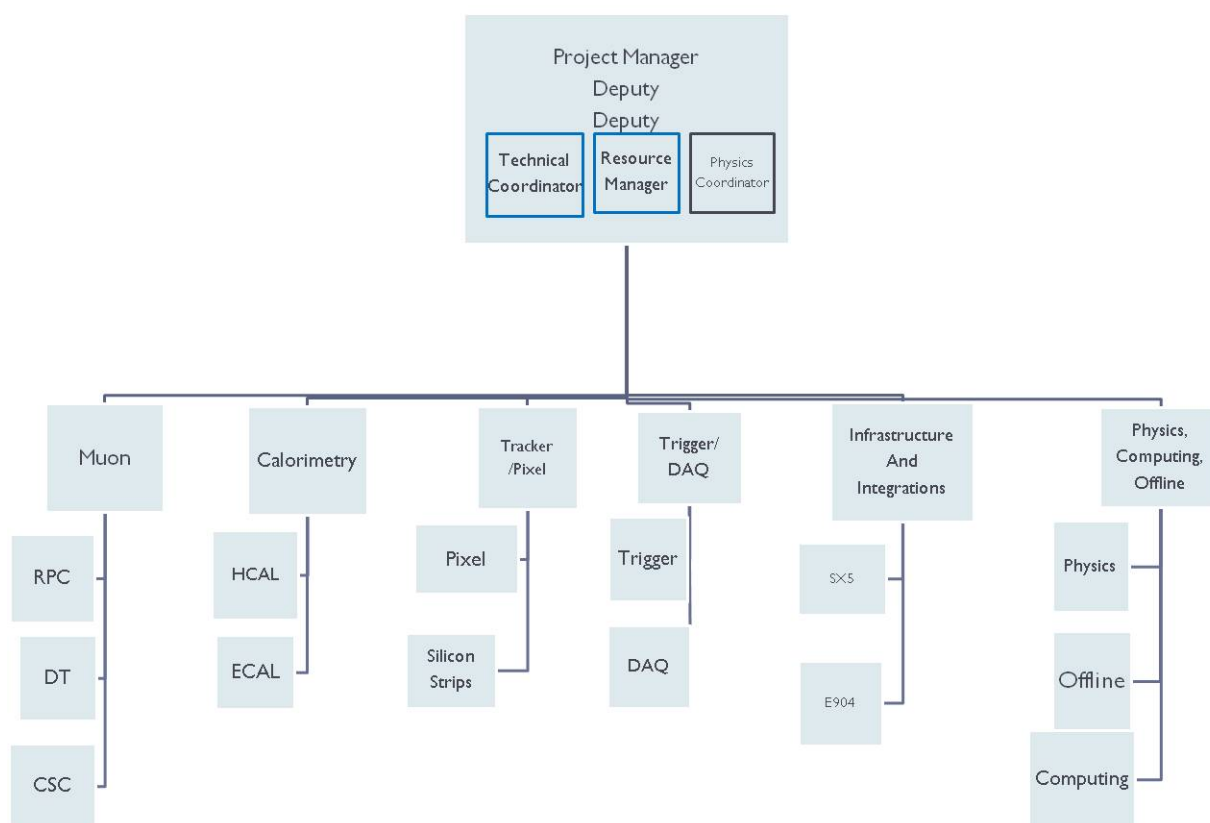


Figure 11.2: Possible organization of the CMS Phase 1 Upgrade Construction Project showing subsystems

- 8141 • Surface buildings;
- 8142 • Point 5 facilities;
- 8143 • Physics;
- 8144 • Offline; and
- 8145 • Computing.

8146 Upgrade Subsystem Managers are responsible for delivering the full scope of their respective
 8147 upgrade projects on schedule and within their budgets. They will draw effort from their re-
 8148 spective subsystems and, where appropriate, from CMS common resources.

8149 Appointments are made by the spokesperson with the agreement of the Upgrade PM and the
 8150 relevant subsystem PM. In making these appointments, the spokesperson will follow the sub-
 8151 system's practices for making appointments at the level of deputy subsystem managers.

8152 They are appointed for a two year renewable term. Reappointment is made by the spokesper-
 8153 son with and agreement of the Upgrade PM and the relevant subsystem PM.

8154 **11.3.7 Cross Subsystem Coordinators**

8155 The Upgrade PM may decide to appoint coordinators for groups of subsystems. One such
8156 organization of the subsystems into groups is shown in Fig. 11.2. If coordinators are needed,
8157 they are appointed by the Upgrade PM with a specific charge. They serve as long as he/she
8158 feels they are serving a useful purpose. Coordinators carry out their tasks by working with the
8159 relevant subsystem Upgrade Project Managers.

8160 Coordinators may, for example, be responsible for facilitating communications and sharing of
8161 ideas and work among the groups in their charge. They may organize joint reviews.

8162 **11.3.8 CMS Phase 1 Upgrade Construction Project Office**

8163 The purpose of the Project Office is to assist the Upgrade PM in managing all aspects of the
8164 upgrade project.

8165 Key functions include

- 8166 • Maintaining the cost estimate, preparing annual budgets and tracking actual project
8167 costs
- 8168 • Maintaining the schedule and milestones and tracking the completion dates
- 8169 • Developing and maintaining a “change control” process for cost, scope, and schedule
8170 so that all deviations from the original plan and the current plan are well understood
8171 and documented
- 8172 • Developing and enforcing standards, developing requirements and specifications,
8173 and preparing interface documents
- 8174 • Providing oversight and technical advice to the subprojects
- 8175 • Conducting regular reviews of technical progress, cost and schedule
- 8176 • Allocating contingency to keep the project on schedule
- 8177 • Providing regular reports and accounting to CMS management

8178 One possible staffing plan for the Upgrade Project Office is shown in Fig. 11.3.

8179 **11.3.8.1 CMS Phase 1 Upgrade Construction Project Resources Manager**

8180 The task of the Phase 1 Upgrade Construction Project Resources Manager is to assist the CMS
8181 Resources Manager in carrying out his/her responsibilities with respect to the Upgrade.

8182 According to the CMS Constitution, “The CMS Resources Manager is in charge of all mat-
8183 ters related to the resources for the CMS project, except those which naturally fall under the
8184 direct jurisdiction of the Institutes. He/she is concerned, together with the Link-persons to
8185 CMS funding agencies, with establishing and maintaining relations with the funding agencies,
8186 with drawing up relevant agreements and with obtaining endorsement for these and any other
8187 agreements to which the Institutes of CMS are party. He/she also presents the annual budget
8188 and expenditures report to the CMS Resources Review Board.”

8189 The Upgrade Resources Manager is at the same level as a CMS Deputy Resources Manager
8190 and is appointed by the CMS Resources Manager in consultation with the Upgrade Project
8191 Manager and the CMS Spokesperson. The Deputy Upgrade RM is (or temporarily becomes if
8192 exceptionally seconded from elsewhere) a CERN staff member.

8193 The Upgrade Resources Manager will work with the CMS Resources Manager and the sub-
8194 systems to establish the cost book for the upgrade project and to track the costs and prepare

8195 reports for the upgrade project.

8196 The Upgrade Project Manager, the Upgrade Resources Manager, and the PM and Upgrade
8197 PM for each subsystem will work out whether the normal subsystem Resources Manager can
8198 handle the added work associated with the upgrade or that a subsystem Upgrade Resources
8199 Manager should be appointed.

8200 **11.3.8.2 CMS Phase 1 Upgrade Construction Project Electronics Coordinator**

8201 According to the CMS Constitution, “Under the overall oversight of Technical Coordination,
8202 the Electronics Coordinator coordinates, monitors and supports the development, procurement
8203 and installation of electronics systems for the CMS experiment.”

8204 The task of the Phase 1 Upgrade Construction Project Electronics Coordinator is to assist the
8205 CMS Electronics Coordinator in carrying out his/her responsibilities with respect to the Up-
8206 grade.

8207 **11.3.8.3 CMS Phase 1 Upgrade Construction Project Physics Coordinator**

8208 The task of the Phase 1 Upgrade Construction Project Physics Coordinator (Upgrade Physics
8209 Coordinator) is to ensure that the physics case for the upgrade is completely and effectively
8210 developed and that physics calculations and simulations as well as existing data are used to
8211 optimize the upgrades. He/she is also responsible for communicating upgrade physics issues
8212 and concerns to the Physics Analysis groups and the Physics Coordinator, soliciting input and
8213 assistance concerning the upgrade from the CMS Physics organization, and responding to any
8214 concerns or questions about the physics reach of the upgrades.

8215 The Upgrade Physics Coordinator will be proposed by the Upgrade PM in consultation with
8216 the CMS Physics Coordinator, nominated by the Spokesperson, and approved by the Collabo-
8217 ration Board.

8218 **11.3.8.4 CMS Phase 1 Upgrade Construction Project Software Coordinator**

8219 The mission of the Phase 1 Upgrade Construction Project Software Coordinator (Upgrade Soft-
8220 ware Coordinator) is to supervise the development and deployment of the upgrade design
8221 software, including programs to simulate the performance of all interesting detector configu-
8222 rations and the programs needed to analyze them; and in conjunction with the subdetectors
8223 and their DPGs to develop the simulation, local reconstruction, calibration, alignment, and
8224 monitoring software.

8225 The Upgrade Software Coordinator will ensure that all software for the upgrade conforms to
8226 CMS standards and is integrated into the CMSSW software release framework..

8227 **11.3.8.5 Administrative and Clerical Support**

8228 The Administrative and Clerical support group will assist the Upgrade Project Management
8229 team in various items including the preparation of reports, scheduling and conducting of meet-
8230 ings and workshops, arranging travel, organization of reviews, tracking of action items and
8231 milestones, and preparation of documentation.

8232 It is the responsibility of the Upgrade Project Manager (or designee) to recruit the staff and
8233 monitor their performance.

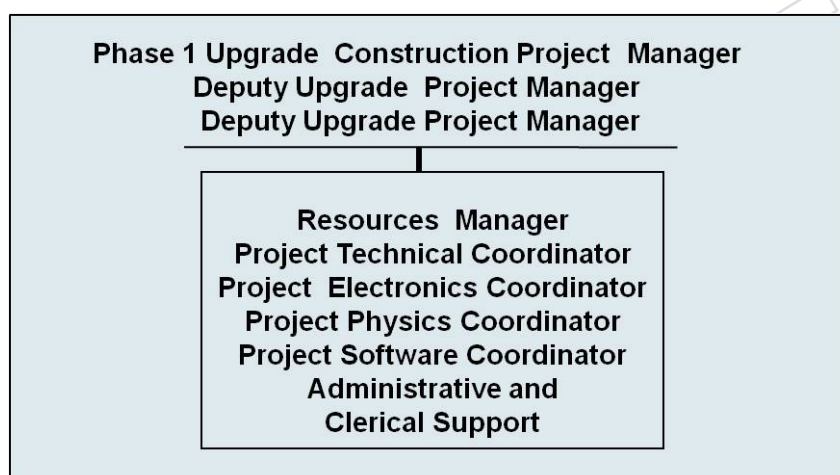


Figure 11.3: A possible CMS Phase 1 Construction Project Office staffing plan

DRAFT

References

8234

8235

-
- 8236 [1] C. Collaboration, "The CMS experiment at the CERN LHC", *JINST* **3** (2008) 1–334,
8237 arXiv:hep-ph/XXXXXX. doi:10.1088/1748-0221/3/08/S08004.
- 8238 [2] C. Collaboration, "Upgrade Projects under Development".
8239 <https://cms-docdb.cern.ch/cgi-bin/DocDB/ShowDocument?docid=3096>,
8240 November, 2010.
- 8241 [3] Z. inc, "Web site". <http://www.zecotek.com>.
- 8242 [4] H. inc, "Web site". <http://www.hamamatsu.com>.
- 8243 [5] C. collaboration, "this is a place holder". <http://www-cdf.fnal.gov>.
- 8244 [6] D. Kotlinksi, "Status of the CMS pixel detector", *JINST* **4** (2009) P03019.
- 8245 [7] A. Dominguez, "The CMS pixel detector", *NIM A* **581** (2007) 343.
- 8246 [8] K. Arndt et al., "Silicon sensors development for the CMS pixel system", *NIM A* **511**
8247 (2003) 106.
- 8248 [9] T. Rohe et al., "Radiation hardness of CMS pixel barrel modules", *NIM A* **612** (2010) 493.
- 8249 [10] G. Cerati et al., "Radiation tolerance of the CMS forward pixel detector", *NIM A* **600**
8250 (2009) 408.
- 8251 [11] Y. Allkofer et al., "Design and performance of the silicon sensors for the CMS barrel pixel
8252 detector", *Nucl. Instrum. Meth.* **A584** (2008) 25–41, arXiv:physics/0702092.
8253 doi:10.1016/j.nima.2007.08.151.
- 8254 [12] CMS Collaboration, *CMS Physics Analysis Summary TRK-10-005* **TRK-10-005** (2010).
- 8255 [13] P. Merkel, "Experience with mass production bump bonding with outside vendors in the
8256 CMS FPIX project", *NIM A* **582** (2007) 771.
- 8257 [14] "Pac Tech Packaging Technologies, Nauen, Germany". <http://pactech.de>.
- 8258 [15] W. Erdmann, "Upgrade plans for the CMS pixel barrel detector", *to be published in NIM*
8259 **A** (2010).
- 8260 [16] A. Affolder, P. Allport, and G. Casse, "Studies of charge collection efficiencies of planar
8261 silicon detectors after doses up to $10^{15}n_{eq}cm^{-2}$ and the effect of varying diode
8262 configurations and substrate types", *NIM A* **604** (2009) 250–253.
8263 doi:10.1016/j.nima.2009.01.072.

- 8264 [17] "PICMG μ TCA website". <http://www.picmg.org/v2internal/microTCA.htm>.
- 8265 [18] CMS Collaboration, "CMS: The TriDAS project. Technical design report, Vol. 2: Data
8266 acquisition and high-level trigger",. CERN-LHCC-2002-026.
- 8267 [19] CMS Collaboration, "The CMS Experiment at the CERN LHC", *JINST* **3** (2008) S08004.
- 8268 [20] CMS Collaboration, "Trigger Study Group: HLT performance",. CMS DP-2010/029.
- 8269 [21] A. Bell, "Beam & Radiation Monitoring for CMS", in *IEEE Nucl. Sci. Symp. Conf. Rec.*,
8270 p. 2322. 2008.
- 8271 [22] A. MacPherson, "Beam Condition Monitoring and radiation damage concerns of the
8272 experiment", in *Proceedings of the XV LHC Project Chamonix Workshop*, p. 198. 2006.
- 8273 [23] R. J. Tapper, "Diamond Detectors", *Rep. on Prog. in Phys.* **63** (2000) 8.
- 8274 [24] D. C. et al., "Validation of synthetic diamond for a Beam Condition Monitor for the
8275 Compact Muon Solenoid Experiment", *IEEE Trans. Nucl. Sci* **54** (2007) 182.
- 8276 [25] R. E. et al., "A diamond-based Beam Condition Monitor for the CDF experiment", *IEEE*
8277 *TRans. Nucl. Sci* **2** (2006) 709.
- 8278 [26] M. B. et al., "CVD diamonds in the BaBar radiation monitoring system", *Nucl. Phys. B*
8279 **150** (2006) 164.
- 8280 [27] W. de Boer et al., "Radiation Hardness of Diamond and Silicon sensors compared.",
8281 *Phys. stat. Sol.* **204** (2007) 3004.
- 8282 [28] L. F.-H. et al., "Development of a CVD diamond Beam Condition Monitor for CMS at the
8283 Large Hadron Collider", *NIM A* **552** (2005) 183.
- 8284 [29] B. D. et al., "The Beam Loss Monitor System", in *Proceedings of the XIII LHC Project*
8285 *Chamonix Workshop*. 2004.
- 8286 [30] C. Zamantas, "The real-time data analysis and decision system for particle flux detection
8287 in the LHC accelerator at CERN". PhD thesis, Brunel University, 2006.
8288 CERN-THESIS-2006-037.
- 8289 [31] R. S. et al., "Beam interlocks for LHC and SPS", in *Proceedings of International Conference*
8290 *on Accelerator and Large Experimental Physics Control Systems, ICALEPCS, Gyeongju*.
- 8291 [32] B. Todd, "A Beam Interlock System for CERN high energy accelerators". PhD thesis,
8292 Brunel University, 2007. CERN-THESIS-2007-019.
- 8293 [33] J. Kaplon and W. Dabrowski, "Fast CMOS Binary Front End for Silicon Strip Detectors at
8294 LHC Experiments", *IEEE Trans. Nucl. Sci* **52** (2005) 2713.
- 8295 [34] J. T. et al., "Optical readout and control systems for the CMS Tracker", *IEEE Trans. Nucl.*
8296 *Sci* **50** (2003) 1067.
- 8297 [35] J. Furltova, "Search for exotic processes in events with large missing transverse
8298 momentum in ZEUS at HERA". PhD thesis, Hamburg University, 2004.
8299 DESY-THESIS-2004-046.
- 8300 [36] G. A. et al., "Thin scintillating tiles with high light yield for the OPAL endcaps", *NIM A*
8301 **417** (1998) 266.

- 8302 [37] C. Ohm, "Phase and intensity monitoring of the particle beams at the ATLAS
8303 experiment". PhD thesis, Linköping University, 2007. urn:nbn:se:liu:diva-9614.
- 8304 [38] C. Pignard and T. Wijnands, "Radiation tolerant commercial of the shelf components for
8305 the remote readout of PIN diodes and Radfets", in *Proceedings of the RADECS Conference,*
8306 *Cap d'Agde*. 2005.
- 8307 [39] T. Wijnands, "Radiation monitoring for equipment in the LHC tunnel", in *EDMS*
8308 *Document 565013*, <https://edms.cern.ch/>. 2005.
- 8309 [40] S. Mueller, "Design, Commissioning and Performance of the CMS Beam Condition
8310 Monitor 2 and Simulation Studies of the Radiation Environment near CMS at LHC". PhD
8311 thesis, CERN/Karlsruhe University, 2010.
- 8312 [41] M. Raymond and G. Hall, "CMS microstrip tracker readout at the SLHC", in *Topical*
8313 *Workshop on Electronics for Particle Physicists*, p. 345. Naxos, 2008.
- 8314 [42] P. Moreira et al., "The GBT, a proposed architecture for multi-Gbps data transmission in
8315 high energy physics", in *Topical Workshop on Electronics for Particle Physicists*, p. 71.
8316 Prague, 2007.
- 8317 [43] L. Amaral et al., "The versatile link, a common project for super-LHC", *JINST* **4** (2009)
8318 P12003.
- 8319 [44] B. Allongue et al., "Custom DC-DC converters for distributing power in SLHC trackers",
8320 in *Topical Workshop on Electronics for Particle Physicists*, p. 289. Naxos, 2008.
- 8321 [45] CMS Tracker Collaboration, K. Klein et al., "System tests with DC-DC converters for the
8322 CMS silicon strip tracker at SLHC", in *Topical Workshop on Electronics for Particle*
8323 *Physicists*, p. 294. Naxos, 2008.
- 8324 [46] M. Huhtinen, P. Lecomte, D. Luckey et al., "High-energy proton induced damage in
8325 PbWO₄ calorimeter crystals", *Nucl. Instr. and Meth.* **A 545** (2005) 63–87.
- 8326 [47] P. Lecomte, D. Luckey, F. Nessi-Tedaldi et al., "High-energy proton damage study of
8327 scintillation light output from PbWO₄ calorimeter crystals", *Nucl. Instr. and Meth.* **A 564**
8328 (2006) 164 – 168.
- 8329 [48] D. Renker, P. Lecomte, D. Luckey et al., "Comparison between high-energy proton and
8330 charged pion induced damage in PbWO₄ calorimeter crystals", *Nucl. Instr. and Meth.* **A**
8331 **587** (2008) 266 – 271.
- 8332 [49] CMS Collaboration, "The CMS Electromagnetic Calorimeter Project - Technical Design
8333 Report", *CMS TDR 4*, CERN/LHCC **97-33** (1997).
- 8334 [50] F. Nessi-Tedaldi, "A parameterization of the anticipated evolution with delivered
8335 luminosity of the contribution to the CMS ECAL energy resolution from hadron damage
8336 to crystals", *ETHZ-IPP-2010-05* (2010).
- 8337 [51] G. Dissertori, P. Lecomte, D. Luckey et al., "A study of high-energy proton induced
8338 damage in Cerium Fluoride in comparison with measurements in Lead Tungstate
8339 calorimeter crystals", *Nucl. Instr. and Meth.* **A 622** (2010) 41 – 48.

DRAFT

8340 Appendix A

8341 Phase 2 R&D

8342 While this document concentrates on upgrades before the major shutdown in 2020, significant
8343 R&D is required to handle the instantaneous and integrated luminosity that will follow. The
8344 Phase 2 R&D will build on the design of the Phase 1 upgrades. In some cases, the Phase 1 up-
8345 grades produce detectors that can operate successfully throughout Phase 2; in other cases, they
8346 provide an infrastructure that can facilitate the additional modifications necessary for Phase 2;
8347 and finally, the demands of Phase 2 may require the complete replacement of some detectors or
8348 electronic systems. Another coupling between the Phase 1 upgrade and the R&D for the Phase
8349 2 upgrade is that they take place over the same 5 to 6 year period from 2011-2016. During this
8350 period, they will compete for human and financial resources. It will be a challenge for CMS to
8351 manage these two activities together so that CMS will retain the formidable physics capability
8352 that it possesses today not only throughout the next decade but for the one following it.

8353 To provide a complete picture of the upgrade activities that CMS will be carrying out in the
8354 first half of this decade, we outline the requirements for Phase 2 R&D in this appendix.

8355 A.1 The Phase 2 Tracker Upgrade

8356 A.1.1 Introduction

8357 An increase of the LHC luminosity well above its original design figure of $10^{34} \text{ cm}^{-2}\text{s}^{-1}$ re-
8358 quires a substantial upgrade of the CMS Tracking system to cope with the much more demand-
8359 ing requirements and implement additional functionalities. A scenario with instantaneous lu-
8360 minosities of $5 \times 10^{34} \text{ cm}^{-2}\text{s}^{-1}$ at a rate of 40 MHz, corresponding to approximately 100 pileup
8361 events per bunch crossing, results in an integrated luminosity of up to 3000 fb^{-1} after several
8362 years of high-luminosity operation. The tracking system has to be enhanced in three main as-
8363 pects: (i) higher radiation resistance, with respect to both instantaneous and integrated levels;
8364 (ii) higher readout granularity, to keep the channel occupancy at an adequate level; (iii) ability
8365 to contribute information for the Level 1 trigger. This will allow CMS to achieve the enhanced
8366 discrimination required by the increased pileup.

8367 In addition, the new tracker concept has to comply with constraints coming from the existing
8368 CMS detector, services, infrastructures and available space in the underground caverns. It is
8369 currently foreseen to re-use the services (cables, fibers and pipes) running from the patch panel
8370 "PP1" to the back end. Since they are interleaved with those of other subdetectors, replacing
8371 them would add considerable complication and risks, and would substantially increase the
8372 length of the required shutdown. This constraint translates to a limit in the total available cross
8373 section of conductors, cooling pipes, and number of optical channels.

8374 Such requirements and constraints drive a series of challenging developments:

- 8375 • Silicon sensors have to maintain adequate performance after accumulated radiation
8376 levels ~ 10 times higher than the requirements of the present Tracker. Thus higher
8377 granularity and thinner sensors are required everywhere, and radically different op-
8378 tions may be useful for the innermost pixel layers.
- 8379 • More advanced ASIC technologies have to be used. The main challenges are to cope
8380 with the high instantaneous rates in the inner pixel layers, to limit the power con-
8381 sumption with the higher granularity, and to implement the new trigger function-
8382 ality.
- 8383 • Novel powering schemes have to be employed to reduce the cross section of con-
8384 ductors inside the tracking volume and take full advantage of the lower operating
8385 voltage of the front-end ASICs, while remaining within the constraint of the existing
8386 supply cables.
- 8387 • More efficient cooling methods have to be used to reduce the mass of cooling pipes
8388 and heat exchangers, as well as the mass flow of the coolant, and to cope with the
8389 constraints from the existing pipes.
- 8390 • High-speed data links are required to handle the increased data volume generated
8391 by the increased granularity and by the trigger output, and still maintain compati-
8392 bility with the installed optical fibers.
- 8393 • Novel module concepts and electronics architectures need to be developed to imple-
8394 ment on-detector data reduction, which allows the trigger functionality to be imple-
8395 mented while maintaining the bandwidth at an acceptable level.

8396 Some details about these developments are given in the following sections, along with some
8397 preliminary ideas of possible detector concepts.

8398 **A.1.2 Sensor development**

8399 The sensor R&D for a SLHC Tracker Upgrade is obviously a key issue. Three main phases can
8400 be identified:

- 8401 1. Evaluate different sensor technologies.
 - 8402 (a) A large campaign to evaluate planar technology with different substrates has started
8403 and will go on for about 1.5 years.
 - 8404 (b) Two submissions are ongoing to evaluate the 3D technology for the innermost pixels.
- 8405 2. Wafer submission with all relevant geometries and connection schemes to evaluate close-
8406 to-final designs (planar and 3D if needed).
- 8407 3. Pre-series of the final design.

8408 The first phase concentrates mainly on the issue of radiation hardness, but addresses already
8409 several geometry, design, connectivity and final testing strategy issues. Fig. A.1 presents the
8410 wafer design used in the evaluation campaign on planar technology (item 1.a above), while the
8411 different types and thicknesses are shown in Table A.1.

8412 All structures of the wafer will be subjected to neutron and proton irradiation to evaluate the
8413 materials with their final mixed fluences which mimic the conditions at different radii. This
8414 procedure emphasizes the real operational conditions of the chips and has been developed
8415 together with RD50 representatives. Basically, all structures will be evaluated for Signal/Noise
8416 after the different irradiation and annealing steps. This evaluation should be finished by the
8417 beginning of 2012. It is designed to be exhaustive, and the most relevant parts are briefly
8418 described below.

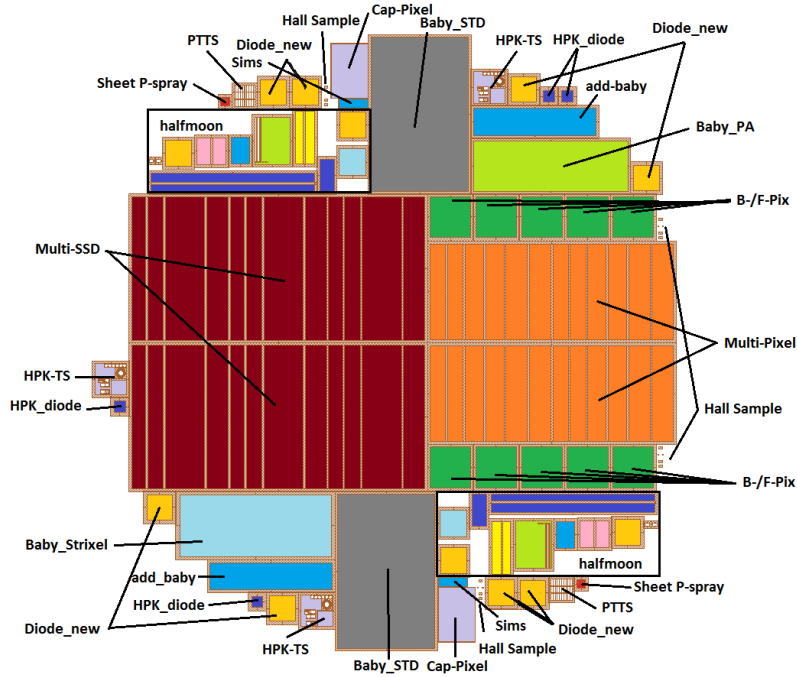


Figure A.1: HPK wafer design

Table A.1: Summary table showing the number of wafers ordered for the different combination of materials, thicknesses and production technologies. FZ stands for FloatZone, MCz for magnetic-Czochralski and EPI for epitaxial.

Substrate Type Active thickness (μm)	FZ			MCz	EPI		Total
	100	200	300	200	150	100	
p-in-n	6	6	6	6	6	6	36
n-in-p (p-stop)	6	6	6	6	6	6	36
n-in-p (p-spray)	6	6	6	6	6	6	36
p-in-n (double metal)		6					6
n-in-p (p-stop; double metal)		6					6
n-in-p (p-spray; double metal)		6					6
Total	18	36	18	18	18	18	126

8419 The multi-geometry strip structures represent the future outer strip detectors; they have differ-
8420 ent pitches and strip widths to evaluate and optimize inter-strip capacitances and inter-strip
8421 resistances as well as breakdown behavior. The multi-geometry long pixel structure has 1.25
8422 and 2.5 mm long pixels to evaluate a possible use in the intermediate layers. We are testing
8423 different pitches, widths and different bias schemes. The halfmoon, also known as standard
8424 test structure, is an improved version of the former CMS one. It is designed to evaluate the
8425 process quality of the future vendor, and to investigate if it can also be used to evaluate the
8426 process parameters before and after irradiation. The minisensor has been introduced mainly
8427 to evaluate the radiation and annealing behavior. The Lorentz sensor is a standard sensor to
8428 evaluate the Lorentz angle with respect to different technologies, irradiation levels, tempera-
8429 ture and voltages. The diodes will give us information about depletion voltage, trapping field
8430 configuration and Signal/Noise. The double metal pieces will allow us to evaluate different
8431 routing schemes, as well as the Baby_PA and Long Pixel structures, where we try to insert the
8432 PA into the sensor. Pixel detectors have been submitted to evaluate the n-in-p types. These

8433 sensors are also valuable to test potential new bump bonding companies. At the end, one or
8434 two of these technologies will be chosen.

8435 We are evaluating in a parallel workflow (item 1.b) the 3D technology, where we are working
8436 with two different producers. We are testing the double-sided double type column technique
8437 (DDTC). One submission has been received already and is partially bump bonded. The sec-
8438 ond submission is in the design stage, and larger sensors will be produced to enable full pixel
8439 module qualification.

8440 In the second phase of the testing we will submit real size structures in the chosen technology
8441 (e.g. 2.5 cm and 5 cm long strips) as well as another larger field of long pixels, but with a
8442 geometry that should be similar to the final one where the pitches and widths will be defined.
8443 At that point we should have a conclusion on whether the planar technology (e.g. EPI) can give
8444 sufficient signal, or if trapping requires 3D sensors.

8445 As a last phase we intend to order final design sensors in a pre-series to allow, if needed, a
8446 last opportunity for minor changes before we order the full series production. This scheme has
8447 proved to be very useful during the sensor production of the current CMS Tracker.

8448 **A.1.3 ASIC development**

8449 The ultra-high luminosity at the SLHC, with proportional increases in occupancy and radi-
8450 ation levels, presents severe challenges. For occupancy reasons the granularity will have to
8451 increase in all regions of the tracker. However, the present average trigger rate of 100 kHz
8452 must be maintained at SLHC to avoid major modifications to other sub-detectors and trigger-
8453 ing systems, which implies that tracking information will have to be included in the L1 trigger
8454 decision.

8455 **A.1.3.1 SLHC FE chip-specific challenges**

8456 The biggest challenge for the on-detector readout is power, both consumption and provision.
8457 Advanced CMOS technologies will help, but power savings per chip will depend on function-
8458 ality, which may increase. At present, it is assumed that 130 nm CMOS technology will be used
8459 for SLHC. MPW (multi-project wafer) access to the technology has recently been negotiated,
8460 and it has already been characterised for HEP applications. Mass production of readout chips
8461 has to start several years before installation, so the proposed development is timely, and the
8462 technology appears to be adequate and affordable, although more expensive than the present
8463 0.25 μm CMOS.

8464 Power provision is a major challenge. Since 130 nm chips operate at half the supply voltage
8465 of 0.25 μm , the supply current doubles even if the total SLHC tracker power remains the same
8466 as at the LHC. The result is increased power dissipation and voltage drops in cables. Hence
8467 the need for a more advanced power distribution, and the choice to develop on-detector DC-
8468 DC conversion, which has implications for FE chip design. Front end specifications have been
8469 developed. A number of relevant issues are still open and are the subject of wider tracker R&D.
8470 Some examples are:

- 8471 • Sensor signal polarity (n-side readout of p-substrate or vice-versa).
- 8472 • Solutions for each signal polarity seem essential to optimise power consumption and
8473 limited dynamic range available for the reduced supply voltages.
- 8474 • Sensor-FE chip coupling: DC coupling simplifies sensor design and reduces cost,
8475 but requires the FE chip to sink or source leakage currents.

- 8476 • Sensor strip lengths and pitches: capacitance and leakage current, hence noise, de-
8477 pend on length and pitch, requiring optimization of the amplifiers.
- 8478 • Local DC-DC conversion implies stringent requirements on power supply rejection
8479 performance, which still need to be fully explored.
- 8480 • Control and readout interfaces must be defined using standard electrical and sig-
8481 nalling protocols.
- 8482 • Module assembly and interconnect technology have to be optimized for large scale
8483 manufacture. Bump-bonding may be preferred, although it reduces flexibility dur-
8484 ing prototyping.
- 8485 • The provision of suitable data for the L1 trigger logic, and the study of system issues
8486 permitting this to be achieved with adequately low power and impact on material.

8487 The exact architecture of the final chips will depend on the studies of the performance of de-
8488 signs matched to different sensor choices, and also on system level constraints. The overall
8489 readout system must be well integrated, so the whole system must be considered early in its
8490 definition, specification and evaluation.

8491 A.1.3.2 CMS Binary Chip (CBC) development

8492 The current strip tracker readout system uses non-sparsified analog readout and analog data
8493 optical transmission, with digitization and zero-suppression performed off-detector. The non-
8494 sparsified approach allows a robust and simple synchronous system, where simple checks can
8495 be incorporated to identify front end chips which may go out of synchronisation. The biggest
8496 challenge for the SLHC on-detector readout is power consumption. Higher granularity means
8497 more front end chips. Un-sparsified binary readout has been taken as baseline readout archi-
8498 tecture for the strip tracker at SLHC. Although this means giving up pulse height information,
8499 we can retain the simplicity and robustness of the present system with known, occupancy in-
8500 dependent, data volumes. The relative simplicity of the front end chip should also lead to the
8501 lowest power solution. The CMS Binary Chip (CBC) prototype has recently been submitted for
8502 fabrication in 130 nm CMOS [41]. The CMS tracker has adopted on-detector DC-DC conver-
8503 sion as a baseline option, which has implications for the FE chip design. In particular, the front
8504 end amplifier can be sensitive to supply noise likely to be present in DC-DC power systems,
8505 and the CBC incorporates on-chip regulation to provide robustness against this.

8506 The main CBC specifications are: (i) both signal polarities can be accommodated; (ii) sensor
8507 coupling can be DC or AC, tolerating up to $1 \mu\text{A}$ DC leakage; (iii) noise must be less than
8508 $1000 e^-$ for a sensor capacitance of 5 pF; (iv) power consumption must be less than 0.5 mW /
8509 channel for 5 pF sensor capacitance; (v) pipeline is 256 deep (latency up to 6.4 μsec), plus 32
8510 deep buffer for triggered events.

8511 The CBC prototype chip occupies an area of $7 \times 4 \text{ mm}^2$ and has been designed for wire-bonding
8512 at $50 \mu\text{m}$ input pad pitch. We expect to learn a lot from this prototype including functionality
8513 and performance issues such as noise, power, radiation hardness (ionizing and single-event
8514 effects). This will provide valuable input to further chip and system developments. These may
8515 include adapting the chip for different input pitch and/or bump-bonding to simplify mod-
8516 ule construction and remove the need for separate pitch adapters. System aspects have also
8517 been considered and while the first prototype will not contain all the features required for in-
8518 terfacing with the envisaged GBT-based off-detector link, a clear route is identified to future
8519 compatibility. Fig. A.2 shows a model of a module with two hybrids carrying CBC chips.

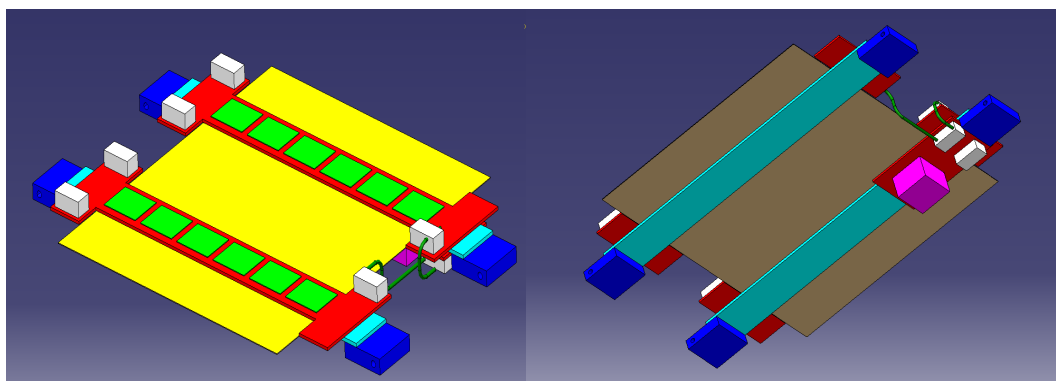


Figure A.2: Model of a possible readout module based on the CBC chips. Two readout hybrids are mounted on a sensor with ~ 2.5 cm long strips. In this version the DC-DC power converter is integrated on the opposite side.

8520 **A.1.3.3 Summary and outlook for ASIC developments**

8521 The evaluation of the CBC prototypes will provide valuable input for further development of
 8522 the chip, but also for issues of general interest like noise rejection and the integration of on-
 8523 chip DC-DC conversion. In parallel with the CBC design, progress is being made to define the
 8524 required functionalities for modules that should provide information for the L1 trigger, which
 8525 will require the development of more complex ASICs.

8526 For the innermost pixel detector, the most important requirement is to be able to cope with the
 8527 high instantaneous rates without data losses. Benefits in the tracking performance could be
 8528 obtained by utilizing smaller pixels, if the chip were able to operate with substantially lower
 8529 thresholds. Such goals should be achievable using more advanced ASIC technologies. The final
 8530 chip will have to be optimized depending on the sensor choice (i.e. planar vs 3D technology).

8531 **A.1.4 Data links**

8532 **A.1.4.1 The GigaBit Transceiver**

8533 The need for increased bandwidth to transfer the data from the front-end chips to the back-end
 8534 electronics is addressed by the development of the GBT chipset [42]. In addition to the larger
 8535 data rates, the SLHC environment imposes more severe requirements in terms of radiation
 8536 tolerance.

8537 The operation of the Tracker requires the transmission of data from three systems: the Data Ac-
 8538 quisition (DAQ), the Timing Trigger and Control (TTC), and the Slow Control (SC). The GigaBit
 8539 Transceiver architecture allows us to transmit data simultaneously from the three systems in
 8540 the same link, aiming at a total bandwidth of ~ 5 Gb/s in the version currently under develop-
 8541 ment. Such requirements can be met using deep submicron CMOS commercial technologies;
 8542 the GBT chipset is being designed and fabricated in 130 nm.

8543 The GBT architecture offers clear advantages in terms of development, production, installation
 8544 and maintenance, since all functionalities are combined in a single system. It offers the possi-
 8545 bility of a drastic reduction in the number of optical fibers, thanks to the large bandwidth. In
 8546 addition, early modelling studies clearly show beneficial simplifications by using a single sys-
 8547 tem, as compared to the current ring-architecture for the controls, which required a non-trivial
 8548 matching of the granularity of control and readout as well as a rather complicated integration
 8549 of the services.

8550 The link consists of bidirectional point-to-point optical fiber links between the counting room
8551 and the detector electronics. In the counting room, which offers a radiation-free environment,
8552 transmitter and receiver are implemented in commercial off-the-shelf components and FPGAs.
8553 At the front-end, the GBT chipset is composed of the GigaBit Transceiver ASIC (GBT13), the
8554 GigaBit Laser Driver (GBLD) and the GigaBit TransImpedance Amplifier (GBTIA), which are
8555 all developed in 130 nm CMS technology.

8556 The GBT frame is composed of 120 bits transmitted over a single bunch crossing interval (25 ns),
8557 resulting in a line data rate of 4.8 Gb/s. Of the 120 bits, 4 bits are used for the frame header,
8558 and 32 bits for the for the Forward Error Correction. This leaves 84 bits for data transmission,
8559 corresponding to a bandwidth of 3.36 Gb/s available for the user. Of the 84 bits, 4 are reserved
8560 for the Slow Control, 16 for the TTC and 64 for the DAQ, corresponding to bandwidths of
8561 160 Mb/s, 640 Mb/s and 2.56 Gb/s, respectively.

8562 The error correction capability is necessary for robust operation in the SLHC environment. The
8563 high radiation levels result in relatively high rates of Single Event Upsets (SEU). In addition
8564 to errors in the internal ASIC logic, particles can generate spurious events in the photodiodes,
8565 faking the arrival of a data bit. Errors tend to occur as bursts, rather than isolated events, which
8566 makes error correction more difficult. The option chosen in the GBT allows correction of up to
8567 16 consecutive wrong bits, and the decoding of the error code is done well within one bunch
8568 crossing interval, hence with minimal impact on the latency.

8569 It is conceived that communication between the GBT and the front-end ASICs may be imple-
8570 mented through serial bidirectional links, (“e-links”), allowing the GBT to serve several front-
8571 ends with bandwidths multiple of 80 MB/s. Such flexibility will allow the GBT to be used
8572 efficiently in different regions of the detector producing different data rates.

8573 **A.1.4.2 The Versatile Link**

8574 The GBT is complemented by the Versatile Optical Link, which allows developing and qualify-
8575 ing the optical part of the link [43]. The project is composed of a Versatile Transceiver (VTRx)
8576 in the front-end, plus back-end components and passive optical components (fibers and con-
8577 nectors). Some details about the Versatile Transceiver are given below.

8578 The VTRx is the only component of the Versatile Link which requires custom development due
8579 to the stringent and exotic requirements deriving from operation inside the detector volume
8580 (minimal size and mass, high radiation environment, operation in strong magnetic field). It
8581 is developed starting from a commercially standard transceiver of the SFP+ family, which is
8582 well-suited for the required customization. The VTRx includes (i) a Transmitter Optical Sub-
8583 Assembly (TOSA), which features a laser diode qualified for use in the HEP environment and
8584 the laser driver developed in the context of the GBT project (GBLD); (ii) a Receiver Optical
8585 Sub-Assembly (ROSA), which contains a p-i-n photodiode qualified for use in the HEP envi-
8586 ronment, and (iii) the Trans-Impedance Amplifier developed in the context of the GBT project
8587 (GBTIA).

8588 The design of a customized VTRx involves the following main aspects: (i) minimize mass and
8589 volume by avoiding metals wherever possible; (ii) avoid any magnetic material; (iii) qualify
8590 commercial photodiodes in terms of bit error rate from SEU; (iv) optimize choice of photodiode
8591 and design of GBTIA and ROSA; (v) derive requirements for the Forward Error Correction.

8592 **A.1.4.3 Outlook**

8593 The ongoing developments are expected to be concluded in 2012. The links will be used for
8594 the upgrade of other CMS subdetectors and will support the system developments for the
8595 upgraded Tracker. Given the timescale for the full Tracker upgrade, a further iteration in the
8596 link development is possible; the phase space for upgrades involves higher bandwidth and/or
8597 reduced power and mass. A possible target for bandwidth would be 10 Gb/s per link, which
8598 is the current performance limit of commercially available SFP+ Transceivers. This increase in
8599 bandwidth would require the design of a new chipset in a more advanced CMOS technology,
8600 as well as redesign of PCBs. Reduction of power can be pursued through careful revision of
8601 the chips design, as well as link components and architecture.

8602 **A.1.5 Power distribution**

8603 The 130 nm CMOS technology currently envisaged for the front-end electronics of the Up-
8604 graded Tracker requires 1.2 V for the analog circuitry, while the digital part can operate at
8605 significantly lower voltage (e.g. 0.9 V). The total load current is likely to be significantly higher
8606 than for the present system due to the higher granularity and increased functionality required,
8607 although the power requirements for the digital and the analog parts are expected to be of the
8608 same order. In addition, the optoelectronics components will require a voltage of 2.5 V at least,
8609 with substantially lower current. These basic facts, combined with the constraint from installed
8610 power cables and the need for minimizing the cross section of conductors inside the tracking
8611 volume define the basic requirement for the power distribution: (i) support the distribution of
8612 different voltage domains; (ii) decrease the current in the conductors from the power supplies
8613 to the load.

8614 **A.1.5.1 DC-DC converters**

8615 A power distribution based on DC-DC converters has been chosen as baseline for the Tracker
8616 Upgrade [44]. The main conversion stage is provided by a buck converter, bringing the voltage
8617 down from 10-12 V to the operating voltage, or else to an intermediate voltage (e.g. 2.5 V).
8618 Since ferromagnetic materials cannot be used in the magnetic field, the converter has to rely
8619 on air-core inductors. The chip implementing the power switches and the control circuitry
8620 must be developed in a technology capable of sustaining 12V with some safety headroom.
8621 Two technologies have been identified which provide the required high voltage transistors
8622 and are compatible with the radiation levels, and prototype ASICs have been fabricated in
8623 both technologies, thus demonstrating that the required conversion ratio and efficiency can be
8624 achieved. A close-to-final ASIC prototype with an efficiency target of $\sim 90\%$ is expected during
8625 2011.

8626 In parallel, a switched capacitor converter has been designed in 130 nm technology, which
8627 could serve as an on-chip stage to further divide by two the voltage, in a scheme with two
8628 conversion steps.

8629 **A.1.5.2 System aspects**

8630 Besides the ASIC development, the implementation of a power distribution based on DC-DC
8631 converters requires the study of substantial system issues, as well as the optimization of the
8632 distribution scheme [45].

8633 Both the buck converter and the switched capacitor converter have the potential of injecting
8634 significant noise into the system, thus compromising the functionality of the readout electron-
8635 ics. A lot of progress has been made in investigating system issues related to the integration

8636 of a buck converter, as well as the optimization of the PCB design and the possible need of
8637 shielding. Studies have been made using spare sub-assemblies of the present tracker as a test
8638 case. For the on-chip switched capacitor, a significant series of tests are planned with the CBC
8639 prototypes.

8640 The overall optimization of the conversion scheme is a very complex topic, involving several
8641 different aspects that can have substantial impact on the detector quality, such as overall com-
8642 plexity of the system, susceptibility to noise, robustness wrt to failure of individual compo-
8643 nents, power consumption, and mass of the conductors. Since we are close to a definitive proof
8644 of the feasibility of this option, the focus in the future will move from ASIC development to
8645 system design, which will have to be optimized for the chosen detector concept.

8646 **A.1.6 CO₂ cooling**

8647 The upgraded CMS Silicon Tracker will most likely dissipate at least as much power as the
8648 present one (if not more), while silicon sensor operation will require more stringent tempera-
8649 ture control to limit the leakage current in the high radiation environment of the SLHC. CO₂
8650 two-phase cooling appears to be a promising option to improve upon the present mono-phase
8651 fluorocarbon system, since it will achieve enhanced cooling performance with a lightweight
8652 system. Some of the main advantages of CO₂ cooling are: (i) the high latent heat allows the use
8653 of small pipes, as well as large heat load per single channel, possibly reducing needs for man-
8654 ifolding; (ii) the high heat transfer coefficient allows smaller heat-exchanger contacts; (iii) CO₂
8655 is a natural substance, which is more environmentally friendly and less expensive than fluoro-
8656 carbons. The use of CO₂ cooling will contribute to an improved detector quality, while auto-
8657 matically ensuring compliance with the constraint of the cross section of the installed pipes.

8658 The R&D for the Tracker Upgrade will move from the design and construction of the cooling
8659 plant to the pixel "Phase I" upgrade.

8660 The first phase of the R&D consists of (i) characterizing through laboratory measurements the
8661 heat transfer and mass flow of two-phase CO₂ in small channels using the parameter range
8662 relevant for operation in CMS, (ii) deriving guidelines for detector cooling optimization (di-
8663 mensions of the pipes and heat exchangers, and operating pressure), (iii) developing numerical
8664 models that correctly describe the flows and heat transfers relevant for the CMS tracker. This
8665 part, which is now well underway, will provide all the information needed for the pixel and
8666 for the whole tracker cooling design.

8667 Some aspects of the engineering design, such as compliance with the installed pipes and with
8668 safety aspects related to the installation in the CMS cavern, will also be studied and solved
8669 for the pixel plant, which will then be applicable in a straightforward way to the full tracker
8670 system. Most of the effort will go into the design and engineering of the system, and analysis of
8671 system aspects such as manifolding, which will pose novel challenges due to the much larger
8672 scale of the system.

8673 **A.1.7 Modules with trigger functionality**

8674 Besides maintaining the current tracking performance in the more congested SLHC environ-
8675 ment, a novel and most challenging requirement has been identified for the Phase 2 Tracker
8676 upgrade, namely the contribution to the Level-1 trigger. The trigger system needs to maintain
8677 an output rate of 100 kHz despite the 10-fold increase in luminosity, and that appears to be
8678 impossible to achieve using only information from the calorimeters and muon detectors. At
8679 present, tracking information is used in the High Level Trigger where it achieves a rate reduc-
8680 tion of a factor of ~ 100 in the muon rate. Unfortunately, a flattening of the Level-1 rate as a

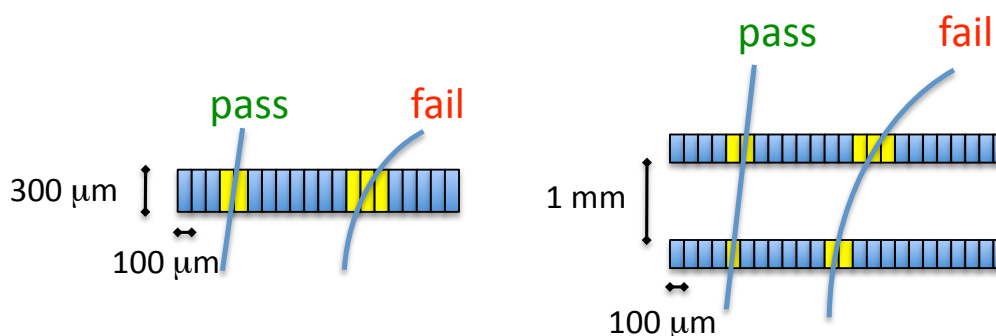


Figure A.3: Sketch showing the principle of p_T discrimination in a single sensor (left) and in stacked sensor pairs (right).

8681 function of p_T is observed, which suggests that increasing the threshold will not help unless
 8682 tracking information is included. Similar evidence is found for electron, tau, and jet triggers.

8683 Delivering information for the Level-1 trigger involves sending out signals at 40 MHz, which
 8684 requires data reduction to keep the overall bandwidth at an acceptable level. The strategy
 8685 that is being pursued in CMS exploits the strong bending power of the 3.8 T magnetic field to
 8686 design modules that are able to reject, in real time, signals from low- p_T particles. The discrim-
 8687 ination can be done within a single sensor, based on cluster width, or by correlating signals
 8688 from stacked sensor pairs, as shown in the sketches of Fig. A.3. A correlated pair of hits in a
 8689 sensor stack is called a “stub”. Rejecting hits from tracks below a p_T threshold of 1 GeV (or
 8690 larger) yields a reduction of the data volume by one order of magnitude, and this makes data
 8691 transmission at 40 MHz feasible.

8692 Different implementations of p_T modules are under study, and briefly discussed below.

8693 A.1.7.1 Strip p_T modules

8694 Two variants of strip p_T modules based on stacked sensors have been studied. In both options,
 8695 the two sensors are wire-bonded to a single hybrid. This implies that the segmentation along
 8696 the strips cannot be more than two, since the hybrid needs to be placed at the edge of the
 8697 module (and not on top of it), in order to access both sensors. A sketch of a possible module
 8698 is shown in Fig. A.4. These types of sensors could be suitable for the outer part of the Tracker
 8699 (e.g. $R > 40\ \text{cm}$) due to the relatively long strips, which would cause too large an occupancy at
 8700 the inner radius.

8701 In the first variant, corresponding strips on the two sensors are bonded to neighboring channels
 8702 on the readout ASIC. In the second variant, top and bottom strips are bonded to the same
 8703 readout channels (see sketches in Fig. A.5). Both versions have been developed using spare
 8704 sensors and hybrids from the current Tracker and tested in a cosmic telescope setup, where
 8705 the discrimination logic has been implemented offline. The performance of the discrimination
 8706 logic has also been measured on LHC data from Tracker Outer Barrel stereo modules by using
 8707 the tracking information to account for the stereo angle of those those modules. All results
 8708 indicate that the required data reduction can be achieved for both module variants. These
 8709 studies represent the first validation of the p_T module concept on real data. The second variant
 8710 has half of the readout channels, which is obviously an advantage. However, the first variant
 8711 allows for more flexibility in the implementation of the discrimination logic, and it also allows
 8712 reading out both sensors for tracking, hence providing more redundancy. Also, in the first
 8713 variant, the readout pitch required is half of the sensor pitch, which leads to a straightforward

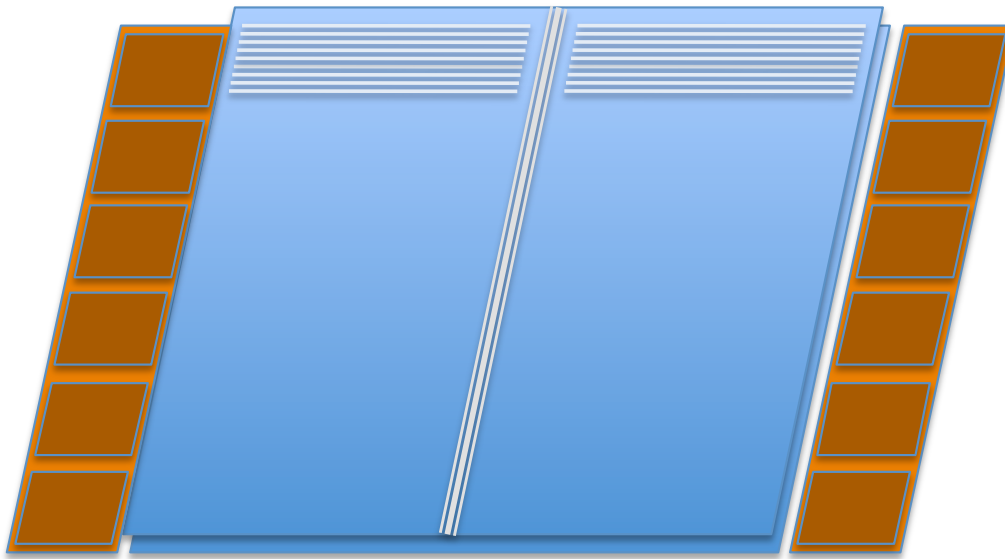


Figure A.4: Sketch of a possible strip p_T module based on two stacked sensors. The two sensors are read out at the edges by the same hybrid. Assuming that the sensor is made out of a 6'' wafer, the strip length is ~ 5 cm.

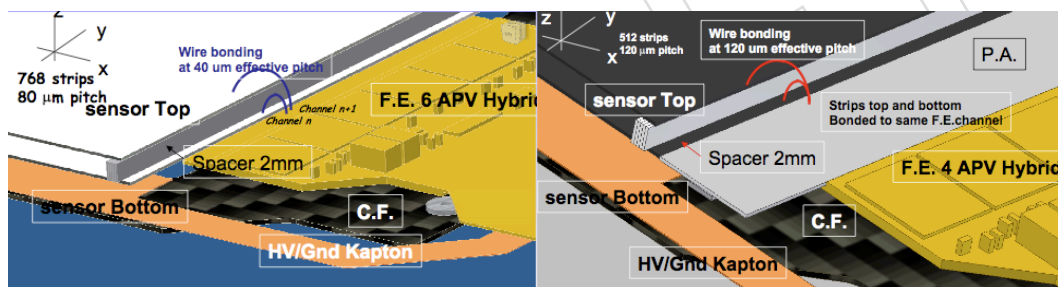


Figure A.5: Left: strip p_T module first variant; the two sensors are directly bonded onto a readout hybrid, top and bottom strips are bonded to neighboring readout channels. Right: strip p_T module second variant; the two sensors are bonded to a pitch adapter, top and bottom strips are bonded to the same readout channel.

8714 module assembly without a pitch adapter (Fig. A.5).

8715 An even simpler p_T module could be designed by selecting clusters on the basis of their width
 8716 in a single sensor. In this case, the hybrid could be placed on top of the sensor and therefore
 8717 the strip length could be shorter than 5 cm. This type of module would only be suitable for use
 8718 at large radii, since the track curvature is measured only over the sensor thickness (Fig.A.3),
 8719 and hence the achievable data reduction is lower, which is not suitable for the most congested
 8720 regions. In addition, the p_T rejection efficiency in such an option is, in principle, affected by
 8721 radiation damage, as it depends on the depletion depth and the Lorentz angle.

8722 In conclusion, strip p_T modules based on stacked sensors appear to be a solid option to build
 8723 modules with trigger capability, since basic technologies are in hand, and the interconnection
 8724 between the two sensors uses wirebonds, the lightest and most power-economic way. The de-
 8725 sign of a front-end chip with the required functionalities and the development of an optimized

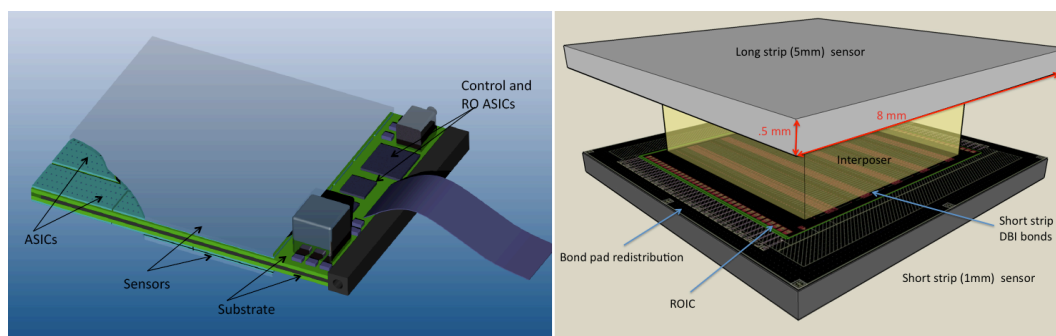


Figure A.6: Two possible implementations of pixellated p_T modules (see text).

8726 electronics architecture is nevertheless a challenging project requiring substantial investments.

8727 A.1.7.2 Pixellated p_T modules

8728 The possibility of developing pixellated p_T modules is also being pursued with substantial ef-
 8729 forts. Compared to strip p_T modules, pixellated modules would also be suitable for use in the
 8730 intermediate radial region ($20 < R < 40$ cm) and would provide tracking information in the z
 8731 view, possibly allowing for some primary vertex discrimination at Level-1. However, the de-
 8732 velopment of pixellated p_T modules is substantially more difficult, and requires the use of more
 8733 advanced technologies. The challenge is the connectivity between the two sensors of the stack,
 8734 which needs to be implemented through an “interposer” or “substrate”. The high granularity
 8735 and the complex connectivity naturally lead to higher mass and power consumption.

8736 Two possible implementations of pixellated p_T modules are shown in Fig. A.6. In the first ver-
 8737 sion (left), each sensor is connected to the ASiCs which are in turn connected to a substrate
 8738 carrying power and signals. A foil of conductive material (e.g. TPG) in the center of the as-
 8739 sembly removes the heat. The substrates are connected together at one edge, while at the other
 8740 edge they extend out of the sensor surface, and carry the auxiliary electronics. ASiCs in one
 8741 layer are programmed as “transmitters”, in the other layers they operate the correlation logic
 8742 and send trigger data out. A pixel size of $\sim 0.1 \times 2$ mm² is envisaged, leading to an overall
 8743 module size of $\sim 48 \times 48$ mm² (or larger, if the interconnection technology is proven to be reli-
 8744 able on large surfaces). The connections sensor-to-ASIC and ASIC-to-substrate could be done
 8745 with direct oxide bonding and bump bonding, respectively; or both with bump bonding, with
 8746 through silicon vias on the ASIC. Alternatively, low-height wirebonds could be used between
 8747 ASIC and substrate, which would not require through silicon vias on the ASIC.

8748 In the second version (Fig. A.6 right), there is only one layer of ASiCs bonded onto a “master
 8749 sensor” with finer granularity (e.g. $\sim 0.1 \times 1$ mm²) with analog connections through an “in-
 8750 terposer” to a “slave sensor” with longer channels (e.g. $\sim 0.1 \times 5$ mm²). Since the electronics
 8751 are only on one side, the module could be cooled from the side of the master sensor. Options
 8752 and issues for the interconnection sensor to ASIC and ASIC to interposer are similar to the first
 8753 version.

8754 In addition to the design of an ASIC with a much higher level of complication, the develop-
 8755 ment of these types of modules requires validating the chosen interconnection technologies on
 8756 large surfaces, and addressing delicate system issues related to the high densities of interleaved
 8757 analogue and digital lines. Such developments require both substantial efforts and financial re-
 8758 sources.

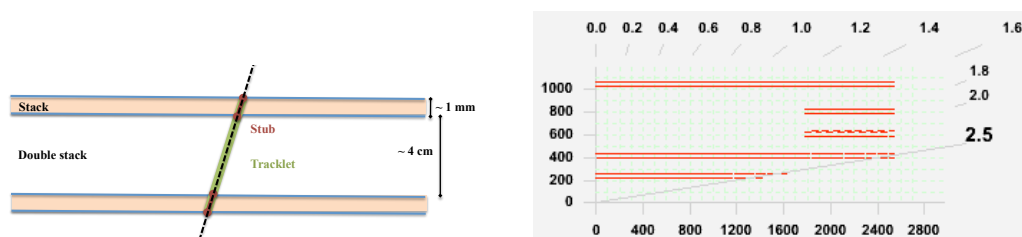


Figure A.7: Left: sketch showing the principle of the double-stack geometry; stubs are reconstructed from two hits in a stack; the two layers in the double-stack are sufficiently close in space that stubs can be correlated to form tracklets, which are then extrapolated out to the next double-stacks. Right: example of Tracker layout based on double-stack barrel-only geometry.

A.1.8 Detector concepts

The module designs presented in the previous section are suitable to send out for every bunch crossing the coordinates of “track stubs” generated by particles above a certain p_T threshold, where the thresholds can be typically between 1 to 2 GeV, or more. This is still an enormous amount of information to be processed at Level-1. Two main approaches can be envisaged:

1. Use the information of Tracker stubs to refine trigger primitives from calorimeters and muon system (improve the momentum estimate of muons and confirm electron candidates).
2. First combine Tracker stubs to form Level-1 tracks, and then combine the tracker primitives with information from calorimeters and muon detectors.

For the second approach (i.e. aiming at reconstructing all the tracks of the bunch crossing at Level-1) the combinatorics are likely to be too prohibitive to be solved in a few clock cycles, unless the detector geometry is optimized for the purpose. For this reason, the “double-stack geometry” has been proposed.

Double-stack geometry. A double stack consists of two layers of p_T modules (built out of stacked sensors), placed at a distance of few cm; the two layers of the stack have the same ϕ segmentation (i.e. the inner layer is a shrunken version of the outer one). With such geometry, it appears possible to correlate stubs reconstructed in the two stacks and to form “tracklets”. A tracklet should have sufficient precision in the determination of the direction and the momentum (measured over a few cm distance) to extrapolate to a sufficiently small region onto the next double-stack, and correlate with tracklets reconstructed there (see Fig. A.7). The extrapolation is obviously affected by the multiple scattering in the detector material.

An example of a tracker layout entirely based on pixellated p_T modules with double-stack geometry is shown in the right sketch of Fig. A.7. Such a detector concept is optimized to reconstruct all tracks at Level-1. Its feasibility and performance as a tracking device critically depend on the possibility of building lightweight pixellated p_T modules in a reliable technology with moderate power consumption and an affordable price.

The left sketch of Fig. A.8 shows an option where pixellated p_T modules populate the inner part, in a single-stack barrel geometry, while the outer part is populated with “standard” read-out modules. This option would aim at improving the Level-1 trigger with the “stubs” from the p_T modules, while limiting overall power consumption and cost, and possibly improving tracking performance with a lightweight region dedicated to tracking only.

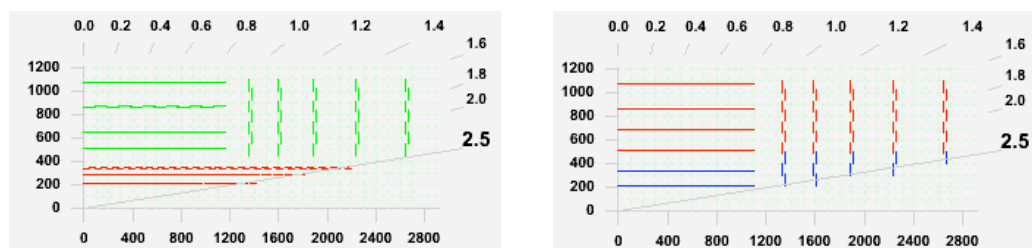


Figure A.8: Left: Tracker layout with single-stack pixellated p_T modules in the inner part (in barrel geometry), and “standard” readout modules in the outer part. Right: Information for the Level-1 trigger comes from strip p_T modules in the outer part (in barrel or endcap geometry), while the inner part is populated with stereo strip modules, or with long pixels, to provide some precise coordinates in the z view.

8791 The right sketch of Fig. A.8 shows an option where the information for the Level-1 trigger
 8792 comes from strip p_T modules in the outer part (in barrel or endcap geometry). The inner part
 8793 could be populated with stereo strip modules, or with long pixels to provide some precise
 8794 coordinates in the z view. This option should provide good tracking performance due to the
 8795 use of the lightweight strip p_T modules, and offers substantial advantages in terms of feasibility
 8796 and cost. Its viability as a solution for the Level-1 trigger has to be investigated. It should be
 8797 noted that the double-stack geometry is not applicable exclusively to pixellated p_T modules
 8798 since it could be employed also for strip p_T modules, if required.

8799 All these sketches assume an inner pixel detector with approximately the same boundaries as
 8800 the present one. Moving the boundaries to large radii and adding one more layer in the inner
 8801 pixel detector may or may not be beneficial, depending on whether the first layers of the outer
 8802 tracker will be pixellated or not. It has been recently proposed to investigate the possibility that
 8803 the inner pixel detector contribute to the Level-1 trigger, reading out only “regions of interest”
 8804 determined by the calorimeter triggers.

8805 Dedicated software tools are being developed to facilitate the modelling of these detector con-
 8806 cepts, and to characterize them in terms of basic properties (such as power consumption, mate-
 8807 rial, expected occupancy and tracking performance) prior to the full detector simulation. Effort
 8808 has started also to model the full chain of data processing for the Level-1 trigger, at least for
 8809 some of the proposed options. Design, modelling and simulation studies are the key for choos-
 8810 ing the optimal option for the CMS Tracker Upgrade, together with the R&D on the hardware
 8811 components.

8812 A.1.9 Outlook

8813 The upgrade of the CMS Tracker for the high-luminosity operation of the LHC is a formidable
 8814 challenge. A substantial amount of R&D is already ongoing, and all major aspects are receiving
 8815 attention. Some of the developments, in particular those addressing the most advanced tech-
 8816 nologies, may soon be confronted with the lack of financial resources. Together with the R&D
 8817 on the components, design, modelling and simulation studies (for tracking and trigger) are the
 8818 key for an optimal choice of detector concept. The progress in the next two years will be crucial
 8819 for the project, as it will lead to the choice of the detector concept to be designed and built.

A.2 Calorimetry in the High Luminosity LHC Era

A.2.1 Introduction

By the end of the current decade, the CMS calorimeters will have recorded an integrated luminosity of over 300 fb^{-1} , will have operated for more than ten years, and will be operating at an instantaneous luminosity of $2 \times 10^{34} \text{ cm}^{-2} \text{ s}^{-1}$ leading to pileup of ~ 40 overlapping interactions per bunch crossing. Around the year 2020 a long shutdown will allow modifications to the LHC that will increase its instantaneous luminosity by around a factor of 5. This Phase 2 upgrade (also called HL-LHC), will provide an integrated luminosity, using luminosity leveling techniques, of around 300 fb^{-1} per year, leading to a total integrated luminosity of about 3000 fb^{-1} over the following decade. The radiation damage to the calorimeters during this era will be far beyond the initial design specifications. It is thus highly likely that significant changes to the calorimeters will have to be made.

The currently implemented CMS electromagnetic calorimeter (ECAL) consists of a barrel section covering $0.0 < |\eta| < 1.45$ and two endcaps covering the region $1.45 < |\eta| < 3.0$. Lead tungstate scintillating crystals are used in both regions, with silicon avalanche photodiode light detectors (APDs) glued to the barrel crystals and vacuum phototriodes (VPTs) glued to the endcap crystals. Each endcap also includes a $3X_0$ thick lead-silicon sampling preshower detector placed in front, covering a slightly smaller fiducial area of $1.653 < |\eta| < 2.6$. The total radiation expected after 3000 fb^{-1} in the barrel region is 5 MRad with a hadron fluence of $6 \times 10^{13} \text{ cm}^{-2}$ at $\eta \approx 0$ and 10 MRad with a hadron fluence of $1.2 \times 10^{14} \text{ cm}^{-2}$ at $|\eta| \approx 1.45$. In the endcap calorimeters the expected total doses and fluencies are considerably higher ranging from 10 MRad at the barrel-endcap interface to 30 MRad with a hadron fluence of $3 \times 10^{15} \text{ cm}^{-2}$ at $|\eta| = 3$. The hadron fluences are mainly low energy ($E > 100 \text{ keV}$) neutrons.

The currently implemented CMS Hadronic calorimeter (HCAL) consists of barrel (HB) and outer barrel (HO) sections covering $0 < |\eta| < 1.3$, two end caps (HE) covering $1.3 < |\eta| < 3.0$ and two forward detectors (HF) covering $3 < |\eta| < 5$. These subsystems are described in Chapters 4 and 5 of this document. The HB and HE are sampling calorimeters with a layered structure of brass absorber plates interleaved with plastic scintillator megatiles. The photosensors, currently Hybrid Photodiodes (HPDs), are located within the CMS solenoidal magnet, but far from the interaction point and deep in the calorimeter in regions of low radiation dose. The HPDs are optically connected to the megatiles through wavelength shifting and optical waveguide fibers. The HO system samples hadronic showers that penetrate through the CMS magnet, and consists of one or two layers of scintillator read out by SiPMs and/or HPDs. In Phase 1, the HPDs used in these subsystems will be fully replaced with SiPMs. The HF resides in the area of greatest integrated radiation dose. To meet the demands of this environment, the HF detectors are composed of steel absorber instrumented with polymer-clad Quartz fibers and readout with photomultiplier tubes.

Our basic working assumption is that we will want to maintain robust calorimetry coverage to $|\eta| < 5$ during HL-LHC operation. Meeting this requirement poses challenges in the barrel region for electromagnetic calorimetry and in the forward region for electromagnetic and hadron calorimetry.

For calorimetry in the barrel and endcap regions, the anticipated operating conditions will have hardware consequences – due to radiation damage, material activation, detector lifetime and software consequences for the trigger and for event and pattern recognition in the face of very significant pileup. There may also be operational concerns, similar to the present observation of anomalous signals in the ECAL, that will manifest themselves over the next few years of

8866 initial running as CMS reaches higher and higher levels of integrated and instantaneous lumi-
8867 nosity. The Phase 1 upgrade will address the needs of Barrel Hadron Calorimetry (HB and HO
8868 subsystems) and allow these to operate effectively into the HL-LHC era. These upgrades are
8869 described in the main body of this Technical Proposal. The Phase 2 upgrade will address the
8870 needs of the Barrel Electromagnetic Calorimetry (EB) and Forward Calorimetry (EE, HE and
8871 HF subsystems) and these are described here.

8872 This appendix is divided into two sections, the first describing the modifications that we are
8873 considering to the barrel ECAL, and the second describing changes to, or replacements of,
8874 the calorimeters in the forward region. These sections summarize some of the questions and
8875 concerns that need to be addressed and outline some of the R&D programs that CMS is (or is
8876 considering) following to ensure effective calorimetry for HL-LHC operations. This list is not
8877 exhaustive but rather is meant to give a flavor of what work lies ahead in the coming decade.

8878 Based upon experience from our development and construction work and operations of the
8879 current CMS Detector, we anticipate 5 years of intensive preparation including all necessary
8880 R&D and decision-making about the configuration of the various ECAL and HCAL detector
8881 components. This will be followed by a construction project that will also last about 5 years,
8882 in order to have the full calorimetry upgrades ready for installation during the shutdown
8883 around 2020 and subsequent HL-LHC operations. The length of this shutdown is expected
8884 to be between 18 and 24 months, which is actually relatively short and could limit some po-
8885 tential upgrade options. The preparation phase includes identification of the physics drivers
8886 that are expected to be important in the HL-LHC era, and development and use of simula-
8887 tion tools to study radiation damage, pile-up effects, and material activation. This effort is
8888 already underway. Such activities will inform the development of one or a few select detec-
8889 tor designs/modifications to meet the physics goals. In parallel with these efforts, extensive
8890 R&D on detector elements and systems must be performed, as well as the development of the
8891 engineering strategies for handling the removal and replacement of highly activated detector
8892 subsystems, particularly in EE and HF. These activities will result in a technical design report
8893 that will form the basis of a HL-LHC Calorimetry Construction Project, expected to start circa
8894 2015.

8895 **A.2.2 Barrel Electromagnetic Calorimeter in the HL-LHC Era**

8896 Although the PbWO_4 crystals are relatively radiation tolerant, there are some effects that, over
8897 time, will reduce their performance. In addition, the APDs will suffer from radiation damage.
8898 The effects we anticipate include:

- 8899 • Hadronic interactions in the crystals that will reduce the transparency of the crystals
8900 [46–48] affecting the ECAL performance in two ways:
 - 8901 - through an overall increase in the stochastic term, due to the lower amount
8902 of light detected, and
 - 8903 - through an increase in the constant term due to induced absorption in the
8904 crystal which modifies the light collection uniformity
- 8905 • In the barrel, an increase in the noise term due to bulk damage in the silicon of the
8906 APDs increasing their dark current.
- 8907 • An increase in the noise term due to a decrease of the signal-to-noise ratio.

8908 Although the barrel performance will degrade over time we expect that its degradation will be
8909 insignificant when compared to other effects, such as the equivalent noise introduced into the
8910 energy measurements due to the pileup of a very large number of overlapping minimum bias

8911 events per bunch crossing at HL-LHC.

8912 **A.2.2.1 Anomalous Calorimeter Signals**

8913 Since the beginning of LHC operation in late 2009, large energy deposits have been observed
8914 in isolated single crystals in the barrel ECAL. The most likely source of these “anomalous cal-
8915 orimeter signals” (ACSs or “spikes”) is hadronic interactions in the APDs. For LHC operation
8916 during the coming years, the particular topology and timing of these events allows a major-
8917 ity to be removed at the trigger stage (at either Level-1 or in the HLT) without affecting the
8918 performance of the ECAL for real physics objects. It is currently unclear how these signals
8919 will evolve with increasing LHC intensity and energy, but it is highly likely that, unless cer-
8920 tain physics triggers (e.g. single EM deposits above 40 GeV or higher) are removed from the
8921 Level-1, some hardware intervention on the barrel ECAL will be necessary.

8922 As mentioned previously, the hardware changes possible are limited by the amount of time
8923 available. In addition, the time available to work on the detectors will be restricted by the very
8924 significant levels of activation of the ECAL. The dose rate expected for the endcap calorimeters
8925 will be around 500 mSv/hr at 30 cm from the detector, even after a cool down period of two
8926 months. This level of activity precludes any option to perform work on the calorimeter without
8927 a complex, and expensive, remote handling system.

8928 In discussing any modifications to the barrel calorimeter it is important to understand that the
8929 detector is divided into two sections separated by an aluminum grid that acts as a thermal
8930 screen. On the inner side, or inner radius, of the grid are the crystals and the APDs. Polyimide
8931 cables connected to the APDs pass through the grid and connect to the front-end electronics.
8932 Accessing anything on the crystal side of the grid requires a complete dismantling of the de-
8933 tector, while reaching the electronics is comparatively easy. Current estimates are that once a
8934 supermodule (SM) is removed from the detector, any intervention on the APDs will require
8935 about 8-9 weeks for dismantling and re-assembly, while interventions on the electronics would
8936 take about 2 weeks. In both cases the time of the intervention itself is not included.

8937 As discussed above, the main concern is to limit the effect of the Anomalous Calorimeter Sig-
8938 nals. Various potential remedies requiring hardware interventions on the barrel ECAL are
8939 under consideration; in order of decreasing complexity they are:

- 8940 1) To read out each APD separately. Although each crystal is equipped with two APDs,
8941 their signals are combined upstream of the front-end electronics making it impossi-
8942 ble to distinguish signals in a single APD. By reading out each one individually we
8943 believe we could almost completely eliminate the ACS problem. However, to do this
8944 would require a complete dismantling and re-assembly of the whole calorimeter.
- 8945 2) To modify the very-front-end analogue electronics to exploit the difference between
8946 the risetime of the signals from the ACS and from crystal scintillations. Because
8947 of their different origins, the ACSs have a faster rise-time than signals from energy
8948 depositions in the crystals. This difference could be used to identify the ACS at the
8949 individual crystal level. This would require a complete redesign of the electronics
8950 and most likely the off-detector electronics.
- 8951 3) Leave the very-front-end electronics intact and change the Front-End boards. This
8952 board currently generates the trigger primitives and stores the data until a Level-1
8953 Trigger Accept is received. It could be replaced with one that uses higher bandwidth
8954 data links (e.g. 10 Gbs) to send crystal-level information to the off-detector elec-
8955 tronics with every bunch crossing. With this the Level-1 decision could include the

8956 off-line ACS suppression techniques but will require a re-design of the off-detector
8957 electronics.

8958 As a prelude to this work we will evaluate the activation level of the barrel at each stage of
8959 LHC operations and prepare plans for handling the supermodules. We will conduct an engi-
8960 neering study on how to extract supermodules from CMS in order to understand the different
8961 operational steps and to define the required tooling. We will also estimate the precise time re-
8962 quired and the risks of each of the options listed above, as well as evaluating the possibilities
8963 of parallelism of the various tasks.

8964 If and when we have decided which of the above options to pursue, we will begin the develop-
8965 ment program of the new version of the readout. This will entail design and prototyping steps,
8966 followed by testing and qualification with our spare supermodule in beam tests. We anticipate
8967 that this last phase will begin no earlier than 2015.

8968 In addition there are other changes to the on-detector read-out electronics that might be nec-
8969 essary. One of these is to reduce the risk of failure of the control system. Currently, groups
8970 of up to 200 crystals are controlled by a single “ring” and, although there is some redundancy
8971 built-in, it is possible that they can fail. New chips are currently being designed at CERN (the
8972 GBT project), and ECAL will participate in the system design. The new architecture is point-
8973 to-point with redundancy, so the chance of losing large fractions of the detector due to failure
8974 of the control system is greatly reduced.

8975 There are other possibilities that are being discussed, that would require modifications to other
8976 sub-detectors. For example, one or two fine-grained outer tracker layers equipped with lead
8977 absorbers – to act as a barrel Preshower – could possibly aid in distinguishing ACS from normal
8978 signals. This possibility, along with others, will be examined through simulation in the coming
8979 months.

8980 In summary, an upgrade to the barrel detector is motivated by the presence of the Anomalous
8981 Calorimeter Signals and the danger that, at the highest luminosities, they will use up much
8982 of the available trigger bandwidth. Possible upgrades to the read-out electronics to improve
8983 redundancy and to introduce high speed data links need to be investigated. We will prepare
8984 plans for intervention on the supermodules for the different options. Substantial effort will
8985 be needed to evaluate in detail the feasibility of carrying out any of these options.

8986 **A.2.2.2 Minimum R&D for the ECAL Barrel Upgrade**

- 8987 a. Detailed engineering studies of the mechanics of removing the supermodules and
8988 performing any intervention on them.
- 8989 b. Electronics R&D to prepare possible changes to the readout to address the anoma-
8990 lous signals and improve redundancy, and to develop high speed links.
- 8991 c. The development of radiation tolerant low voltage regulators for the endcap elec-
8992 tronics and a more robust control system architecture.

8993 **A.2.3 Forward Calorimetry in the HL-LHC Era**

8994 The calorimetry elements, both ECAL and HCAL, forward of $|\eta|$ greater than 1.5 represents
8995 a very challenging situation in terms of radiation damage and pileup relative to the barrel
8996 regions of ECAL and HCAL. To identify and deal with the challenges to Forward Calorimetry
8997 in the HL-LHC era and to develop a common strategy for a new ECAL-HCAL endcap, a joint
8998 ECAL/HCAL taskforce has been established to address:

- 8999 (1) the physics objectives that will be relevant for Phase 2 of LHC operations;
9000 (2) the identification and execution of the relevant R&D for the new technologies re-
9001 quired to properly inform credible subdetector designs; and
9002 (3) the production of a technical design report in which designs for calorimetry in the
9003 endcap/forward region are presented that can meet the challenges of the physics
9004 objectives in the 2020 era;

9005 The Taskforce activities have led to a consensus that most of the elements of forward calorime-
9006 try will require upgrade or replacement by 2020.

9007 Figure A.9 shows the radiation map expected for the forward calorimetry. Shower maximum
9008 is located within the EE and hence the highest integrated doses for $|\eta| < 3.0$ are expected in
9009 the PbWO_4 crystals. The HE benefits from lying in the shadow of the EE so the region most
9010 affected by radiation exposure is the inner most layers at smallest (r, z) -values corresponding
9011 to $2.2 < |\eta| < 3.0$ as shown in Figure A.10. The proximity of HF to the beam and its forward
9012 location $3 < |\eta| < 5$, mean intense doses, shown in Figure A.11, are expected there.

9013 As the integrated luminosity of the LHC increases and as the EE is increasingly exposed to
9014 radiation – from both electromagnetic and hadronic sources [49] – attendant reduction in sub-
9015 detector performance is expected in the PbWO_4 crystals and VPT photosensors of the ECAL
9016 endcap and Preshower endcap detectors. As already mentioned in Section A.2.2 in the discus-
9017 sion of radiation damage of the PbWO_4 in the ECAL barrel, there will be loss of transmission
9018 of light in the crystals. The VPTs will suffer from a darkening of the front window and a re-
9019 duction of the quantum efficiency of the photocathode and dynode surfaces. These effects are
9020 anticipated and are being quantified. The noise term in the resolution function σ/E dominates
9021 the resolution up to ~ 300 GeV for 500 fb^{-1} and still dominates above 1000 GeV for 3000 fb^{-1} .
9022 In the Preshower, bulk damage to the silicon will increase the leakage current and lower the
9023 charge collection efficiency, resulting in a decrease of the signal-to-noise ratio.

9024 Moreover, the activation of the materials of the EE will make repairs very difficult. While
9025 CMS is investigating robotic repair possibilities should the crystal calorimetry configuration
9026 be maintained, it is likely that the present EE will need to be replaced with an appropriate
9027 calorimeter whose technology is to be decided by physics objectives.

9028 The radiation effects to the HE and HF subdetectors were anticipated during the design and
9029 construction of CMS. We expect at minimum considerable repair and refurbishing of these
9030 devices beyond that accomplished in Phase 1 upgrades with radiation hard components and
9031 photodetectors able to withstand the instantaneous and integrated luminosity of the HL-LHC.

9032 Tools using MARS and Fluka codes exist and are able to estimate the radiation load and activa-
9033 tion of materials at any point in the calorimeters if the materials, location, and beam luminosity
9034 are provided. These tools are appropriate for the work of designing new EE, HE, and HF
9035 detectors and will be utilized by the Taskforce. This issue is particularly important for any re-
9036 placement strategies for the EE. An example of the power of this tool is shown in Figure A.12
9037 and demonstrated for PbWO_4 in [46].

9038 A.2.3.1 Physics Simulations for the Forward Calorimetry

9039 The simulation effort is directed toward deciding on the important physics objectives for which
9040 the forward calorimeter is needed and finding solutions for each of the many challenges that
9041 the forward calorimeters will face. The design possibilities that deal with the challenges listed
9042 above range from a forward calorimetry configuration that preserves the excellent EM resolu-

9043 tion of the present PbWO_4 crystal calorimeter to a configuration that emphasizes jet or MET
9044 resolution by optimizing compensation in a combined ECAL-HCAL endcap. The choices are
9045 to be based on physics objectives.

9046 To assess the effect of forward calorimetry on HL-LHC physics, several physics processes have
9047 been identified that are regarded as likely to be important for study in that era. These include

- 9048 • Standard Model benchmarks
 - 9049 • rare top decays,
 - 9050 • triple gauge boson production,
 - 9051 • triple differential cross section for jets, and
 - 9052 • observation of Higgs boson decays to $Z \gamma$.
- 9053 • new physics processes
 - 9054 • SUSY b-jets or photons plus missing E_T ,
 - 9055 • compositeness and vector-vector scattering.

9056 These event topologies must be simulated with both radiation damage effects and event pileup
9057 included. Toward the Higgs to $Z \gamma$ final state, work is progressing on an initial study of
9058 $Z \rightarrow e^+e^-$ with event pileup, to assess where the performance of the current CMS detector
9059 begins to deteriorate – with and without radiation damage. Studies of the other processes will
9060 follow. The nature of the needed instrumentation to address the physics relies on the simula-
9061 tions to answer whether powerful EM calorimetry is required, whether high quality jet energy
9062 measurement (and missing energy measurement) are preferable, or both are needed. If either
9063 of the latter is essential, then it is likely that compensating calorimetry will be the concept of
9064 choice.

9065 One complication, as mentioned earlier, in the study of the effect of radiation damage, is that
9066 during the accretion of radiation damage the detector performance will be degraded by in-
9067 creasing pileup. At an instantaneous luminosity of $5 \times 10^{34} \text{ cm}^{-2} \text{ s}^{-1}$, pileup of 100-200 inter-
9068 actions per bunch crossing is to be expected, a truly daunting challenge. Pileup and radiation
9069 damage studies will be done in concert to ascertain which is the dominant source of detector
9070 performance degradation at any point of operation at a given integrated and instantaneous
9071 luminosity.

9072 Work is in progress on developing a version of the CMS fast simulation MC that has incorpo-
9073 rated in it detailed radiation damage test beam results [50] as a function of fluences at different
9074 luminosities as a function of η . This version of fast simulation already is capable of any level
9075 of pileup that CMS will experience. This tool will be used to generate the effects of the radi-
9076 ation damage and pileup at different instantaneous and integrated luminosities on different
9077 critical aspects of CMS calorimetry function such as mass and energy resolution and missing
9078 transverse energy in different types of physics signals.

9079 **A.2.3.2 Strategies for Implementing the Forward Calorimetry**

9080 Very different strategies for implementing the forward calorimetry and a different detector
9081 R&D will be necessary depending on the physics objectives. These will be determined by a
9082 combination of Monte Carlo studies and analysis of the data that CMS is presently accumulat-
9083 ing and will depend upon whether we want to achieve excellent EM resolution or emphasize
9084 jet or MET resolution by optimizing compensation in the combined ECAL-HCAL endcap. The
9085 correct configuration of the forward calorimetry is probably somewhere in between these two
9086 poles.

9087 If the objective is to obtain the best EM resolution, one approach would be to rebuild the EE in
9088 more or less the same configuration as the present CMS endcap but with new radiation hard
9089 crystals and photodetectors. The HCAL detectors in the forward region would remain essen-
9090 tially the same with perhaps improvements based on radiation hardening in certain limited
9091 areas of the HE and HF.

9092 Another strategy would be to enhance the particle-flow capabilities of the endcap region cov-
9093 ered by the central tracking system ($1.3 < |\eta| < 2.4$). This could be done using a fine granular-
9094 ity EE, introducing an HE with finer transverse and longitudinal segmentation and reducing
9095 the dead material between the EE and HE components.

9096 At the other pole of design options, solutions that produce an endcap compensating calori-
9097 meter would require development of techniques to equalize electron and hadronic response
9098 by using detectors combining scintillation light emission and detection and Cerenkov light
9099 and detection, such as could be achieved by addition of Cerenkov (EM) sensitive layers to the
9100 hadron calorimeters. A second approach would be to use wavelength filtered photosensors to
9101 read out crystals. GaAs and GaInP Geiger mode APDs are possible photosensors that can be
9102 used to image light of different wavelengths with good efficiency.

9103 A.2.3.3 Forward Calorimetry Technology R&D

9104 Development of appropriate technical designs for accomplishing the various configurations for
9105 forward calorimetry for HL-LHC operation will require significant R&D on new radiation hard
9106 detector technologies, radiation hard front end electronics, fast triggering and readout. This
9107 effort must start early in the current decade. In order to inform any decision on calorimetry for
9108 2020, several areas of investigation are underway or planned. We divide the various initiatives
9109 into three categories: detector R&D specialized to the best possible electromagnetic resolution;
9110 R&D specialized to producing a compensating forward calorimeter; and R&D which would be
9111 required no matter which of these two directions the physics objectives indicate. As might be
9112 expected, since a major amount of R&D must go into developing radiation hard components,
9113 most of the R&D will fall into the third category. Some of the listed R&D are useful for the
9114 barrel ECAL also.

9115 I. Detector R&D aimed at optimum electromagnetic resolution:

9116 a. R&D to select a replacement radiation hard crystal to replace the present
9117 PbWO_4 crystals. Two candidates are currently under investigation, $\text{LYSO}(\text{Ce})$
9118 and PbWMO . While $\text{LYSO}(\text{Ce})$ is attractive because of its brightness, speed
9119 and radiation hardness, its relatively high cost would restrict its use to a
9120 limited volume of the EE. The less costly PbWMO option requires further
9121 study of its radiation hardness. A further crystal type, CeF_3 , is under con-
9122 sideration. This material has been demonstrated to be extremely radiation
9123 hard, but no industrial production is currently available [51].

9124 II. Detector R&D specialized to developing a compensating calorimeter:

9125 a. Techniques to equalize e/h by using detector layers combining scintil-
9126 lation light emission and detection and Cerenkov light and detection.
9127 Possible options for Cerenkov (EM) and scintillation sensitive layers in-
9128 clude Quartz plates, crystal plates, crystal fibers, and liquid scintillator in
9129 Quartz tubes.

9130 b. Techniques to equalize e/h using wavelength filtered photosensors to
9131 read out crystals. GaAs and GaInP Geiger mode APDs are possible pho-
9132 toensors that can be used to image light of different wavelengths with

9133 good efficiency.

9134 III. Detector R&D to develop radiation hard components common to Approaches I and
9135 II:

- 9136 a. Studies of use of SiPM and GaAs photodetectors in the existing HE and
9137 HF. With the use of more extensive longitudinal sampling, the radiation
9138 damage to the innermost layers of the HE – where waveshifted scintilla-
9139 tion light levels would be reduced – could be reweighted appropriately.
9140 Photosensor noise issues can be improved by using smaller pixel sizes in
9141 the devices or through cooling.
- 9142 b. R&D on new materials to replace the plastic scintillation tiles in regions
9143 where these are vulnerable. Options include LYSO(Ce) crystal plates,
9144 quartz tiles coated with waveshifter, aluminum or quartz cells containing
9145 liquid scintillator that can be filled and flushed, and quartz tubes contain-
9146 ing liquid scintillator.
- 9147 c. R&D on new readout fibers, necessary to transmit the light from tiles to
9148 the SiPMs. The current approach employs a photosensor readout that is
9149 located remotely and connected via waveshifting fiber. Existing waveshift-
9150 ing fibers are vulnerable to radiation damage and must be replaced with
9151 an alternative. Possibilities include use of liquid-in-capillaries, novel wave-
9152 guide structures, and crystal fibers.
- 9153 d. Development of gas calorimetry options. Several approaches might be
9154 used to replace existing vulnerable layers in the HE. These include GEM
9155 detectors or planar structures.
- 9156 e. R&D on secondary emission ionization calorimetry for its speed and ra-
9157 diation hardness.
- 9158 f. Use of quartz core-quartz clad (QQ) fiber to replace the existing quartz
9159 core-polymer clad (QP) fiber in HF.
- 9160 g. The development of more robust light sources for calibration and tracking
9161 of the calorimetry gains.
- 9162 h. The development of radiation tolerant low voltage regulators for the end-
9163 cap electronics and a more robust control ring architecture.

9164 A.3 Muon System Phase 2 Upgrades

9165 A.3.1 R&D Issues for the Muon Drift Tubes in Phase 2

9166 For the Phase 2, the DT detector itself should be able to cope with the higher luminosity, but
9167 the DT electronics will need to be revised. First, the luminosity increase will cause a wors-
9168 ening of the radiation environment. The radiation tests carried out on the current front end
9169 DT electronics indicate that some regions will experience an unacceptably high a rate of single
9170 event upsets and some regions eventually will not survive the total irradiation dose. Second,
9171 the Level-1 trigger system will have to cope with high rates. The only effective way to increase
9172 the trigger rejection power will be an improvement of its p_T resolution, in order to limit the
9173 feedthrough of mismeasured low momentum muons to high momentum, as is now done at
9174 normal LHC luminosities in the High Level Trigger. Since the p_T measurement is intrinsically
9175 limited by the multiple scattering in the material in front of the DT system, a big improvement
9176 in trigger rate control will come from the use of the Tracker data. Different possibilities to get
9177 Tracker hits and improve transverse muon momentum resolution by matching them to the DT

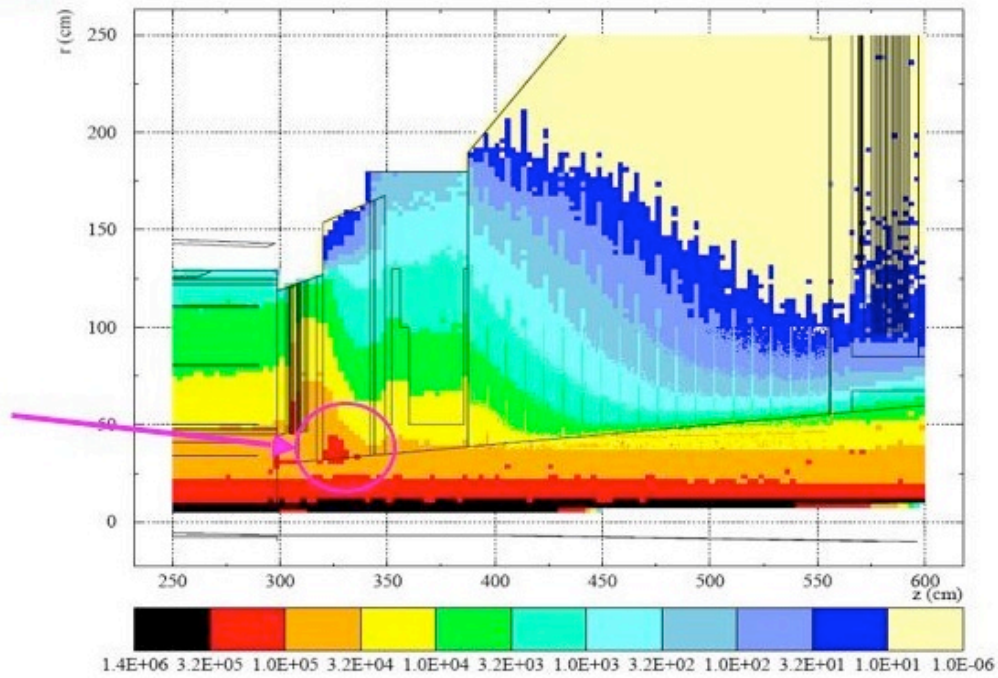


Figure A.9: A map from Fluka of the radiation field in the endcap region including EE and HE detectors. Dose units are Gy. The dose is clearly greatest at smallest values of (r, z) -coordinates.

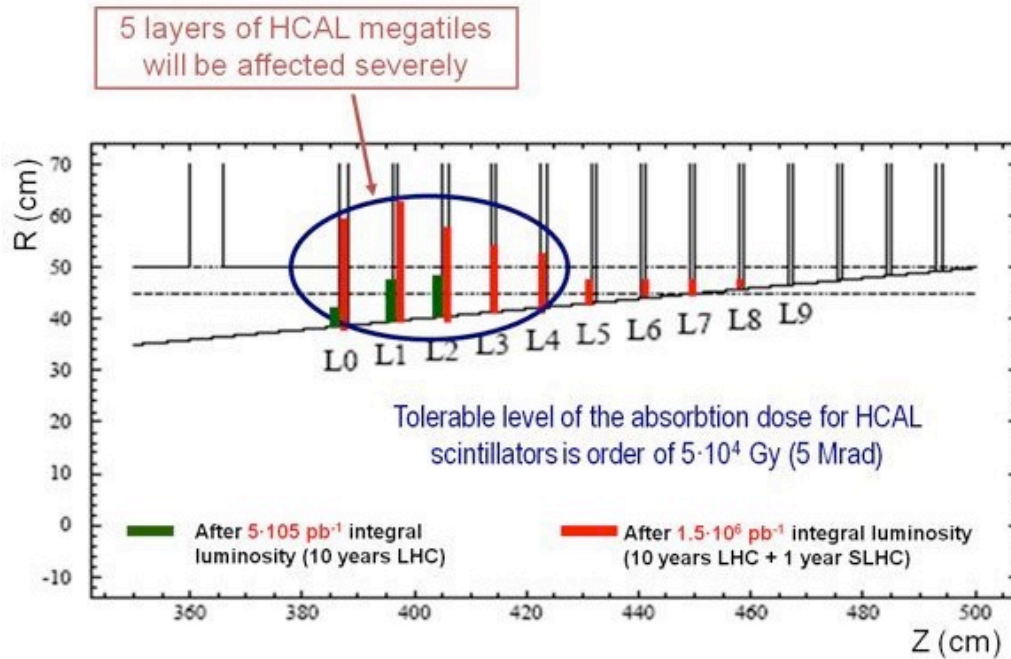


Figure A.10: A schematic of the HE detector showing layers suffering significant radiation damage. The regions of HE most vulnerable to damage are at the smallest (r, z) -values. The angled boundary corresponds to $\eta = 3$.

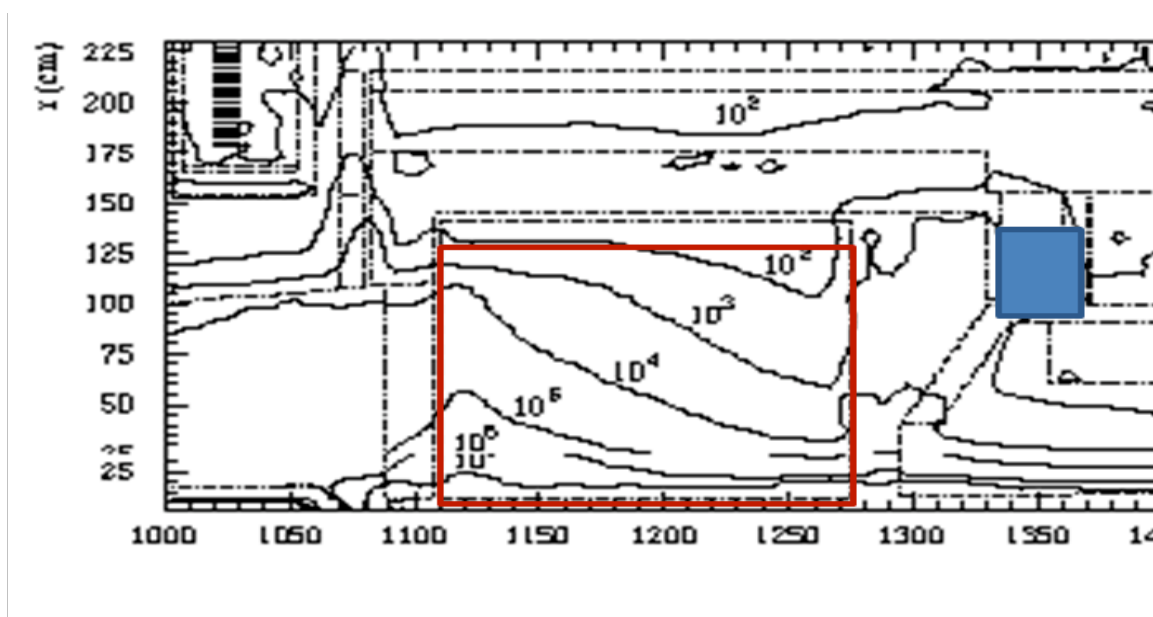


Figure A.11: Radiation fields in the HF detector. Doses are in Gy. The horizontal axis (z) is in centimeter units and the collision point is to the left. The blue highlighted region represents the location of the PMT readout.

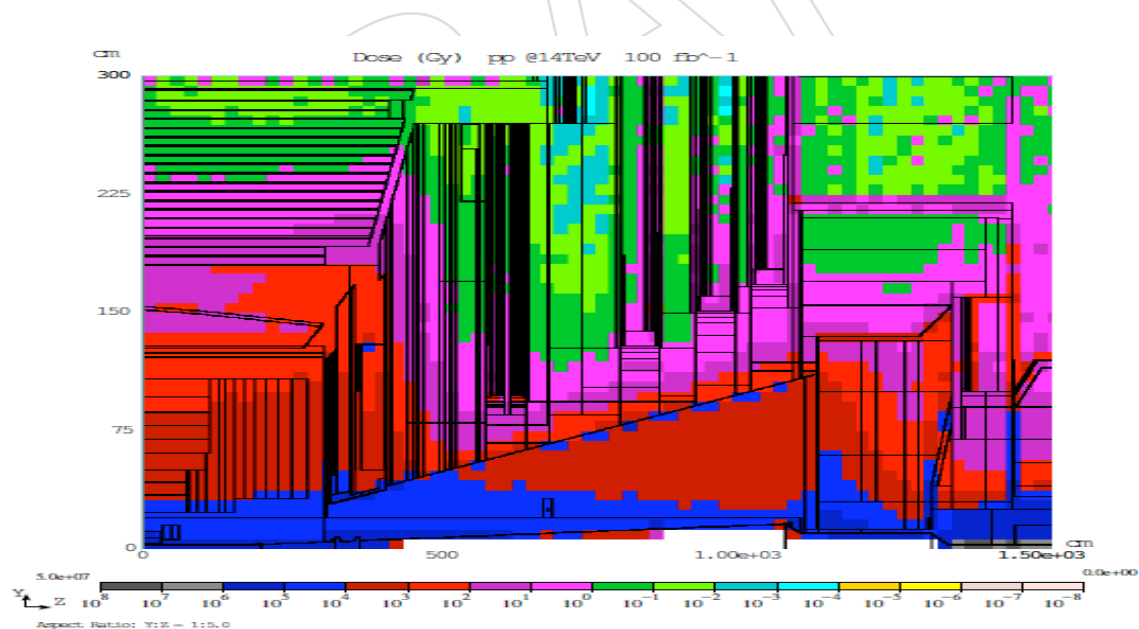


Figure A.12: A MARS code representation of the radiation field for the CMS endcap and forward regions. The calculation assumes pp collisions at 14 TeV with an integrated luminosity of 100 fb^{-1} .

9178 trigger primitives are under study. Several technical solutions can be worked out, but these are
9179 strongly dependent on ultimate choices of the new Tracker design.

9180 A.3.2 RPC Phase 2 Upgrades

9181 The CMS Forward Muon system comprises four stations, namely RE1 to RE4. At this time only
9182 the first three are instrumented with Resistive Plate Chambers, since the fourth station RE4 was
9183 initially descoped. The phase 1 upgrade will add the RE4 station which provides coverage up
9184 to $|\eta| = 1.6$.

9185 The RPC muon system provides both a level 1 high p_T trigger and an offline muon identi-
9186 fication. The trigger consists of the coincidence of at least three RE stations which provides
9187 the bunch crossing identification. The RE system as presently configured covers the region
9188 $0.9 < |\eta| < 1.6$. For this η region extensive tests were performed over several years in order to
9189 validate the RPC technology, the gas mixture and operational characteristics, namely particle
9190 rates of the order of few 10 Hz/cm^2 . These were successful in concluding that this η region
9191 could be successfully instrumented with the current design of RPC chambers. However, in the
9192 high particle rate environment and radiation conditions at a higher $|\eta| > 1.6$ region additional
9193 studies would be required. Thus the high η region of CMS is presently vacant and presents an
9194 opportunity to instrument it with a detector which would be suitable for operation at the Phase
9195 2 luminosity of the LHC.

9196 The high η environment of the phase 2 LHC presents hostile conditions of particle fluence rates
9197 of several 100 Hz/cm^2 up to several kHz/cm^2 at a luminosity of $10^{35} \text{ cm}^2 \text{ s}^{-1}$. In addition, the
9198 rates of thermal neutrons, low energy protons and γ s must be taken into consideration.

9199 Careful studies will be undertaken to simulate the expected background for $|\eta| > 1.6$. As part
9200 of this simulation, the increase of the CMS physics capability in this region must be quanti-
9201 fied. This preliminary study must also clearly define the ideal detector requirements for safe
9202 operation.

9203 At this time, Micropattern detectors (MPGDs) seem to be a promising candidate technology to
9204 instrument the currently vacant zone in the forward part of CMS ($1.6 > |\eta| > 2.1$), although
9205 other options could be possible in case the background would be consistently lower than fore-
9206 seen now. Using MPGDs with enhanced readout granularity in $\eta - \phi$, and an improved rate
9207 capability by two orders of magnitude, one could complete the forward RPC system with good
9208 trigger and tracking efficiency. While there are several types of MPGDs, two types look promis-
9209 ing for this application, namely the micromegas (MM) and the gas electron multiplier (GEM).
9210 Both these detectors have the potential for producing large area ($1\text{m} \times 2\text{m}$) detectors with cost
9211 effective industrial processes. They have demonstrated stable, long term operation and have
9212 negligible discharge probability. Both types of MPGDs have already been installed success-
9213 fully in other experiments. In the LHCb first muon station, where expected rates are ~ 500
9214 kHz/cm^2 , triple GEMs have been installed, and ATLAS is considering the micromegas for its
9215 muon upgrade.

9216 The full understanding of the operation of GEM detectors in high neutron and γ fluxes, as ex-
9217 pected in the high η region, require additional studies in CMS. The main topics of investigation
9218 are:

- 9219 • Large size detector prototyping and performance studies.
- 9220 • Ageing studies.
- 9221 • A detailed mechanical design.

- 9222 • Integration studies for mechanical envelope services and routing in CMS.

9223 **A.3.3 CSC Phase 2 Upgrades**

9224 For LHC Phase 2, a new track trigger in conjunction with the existing CSC muon information
9225 should be sufficient to allow Level-1 muon triggering at an acceptable rate and momentum
9226 threshold. Therefore, the potential Phase 2 upgrades for the CSC system are more oriented to-
9227 wards handling high particle and background rates. Depending on experience with these rates
9228 at various luminosities, deployment of the upgraded cathode (DCFEB) boards could be ex-
9229 panded from the ME1/1 chambers to other types of chambers as well, in order to dramatically
9230 improve their high-rate capability. Likewise, expansion of the use of replacement TMB mezza-
9231 nine cards to other types of chambers would result in better trigger-level spatial resolution in
9232 addition to higher rate capability. The anode (ALCT) on-chamber boards could have their mez-
9233 zanine cards swapped with new ones containing high-performance logic (FPGAs). This could
9234 allow for dramatically better position resolution, as well as improved time resolution that could
9235 enable a slow-particle trigger if desired. The CCB boards would need replacement only in the
9236 case that the clocking of the experiments via the TTC system needs to be changed. Finally,
9237 the CSC system data flow is most concentrated in several crates of DDU and DCC readout
9238 modules, and replacement is only contemplated if there are surprises with background particle
9239 rates. The numbers of the boards mentioned are: 2268 DCFEB, 468 TMB mezzanine, 540 ALCT
9240 mezzanine, 60 CCB, 36 DDU, and 4 DCC.

9241 **A.4 Trigger R&D for Phase 2**

9242 **A.4.1 Introduction**

9243 In order to meet the challenges of Upgrade Phase 2 operation the suggested approach is to
9244 hold the overall Level-1 trigger rate at the LHC value of 100 kHz by increasing the readout
9245 bandwidth. This approach avoids rebuilding front-end and readout electronics as much as
9246 possible since these were designed for an average readout time of less than 10 μ s. It also permits
9247 use of front-end buffers for an extension of the Level-1 Accept (L1A) latency rather than for
9248 more post-L1A storage before readout.

9249 Operating the LHC with 50 ns bunch crossing spacing at 5×10^{34} implies a pileup 200 min-
9250 bias events/crossing. This is a factor of more than 10 greater than the LHC design luminosity
9251 (10^{34}) figure of 20 min-bias events per 25 ns bunch crossing and will degrade all occupancy-
9252 dependent trigger algorithms that rely on forms of isolation to identify electrons, muons, taus
9253 and missing energy signals. Since running the SLHC at 40 MHz will be retained as an option to
9254 mitigate these difficulties, we require that all CMS detector and electronics designs for SLHC
9255 upgrades work with a 25 ns bunch spacing and handle an occupancy consistent with 5×10^{34}
9256 at 50 ns bunch spacing. This requires a more performant trigger with additional information,
9257 such as tracking data, used to reduce the trigger rates against the much higher backgrounds.
9258 The size of regions sampled for trigger decisions will need to shrink to handle the increased
9259 backgrounds.

9260 **A.4.2 Upgrade Phase 2 Trigger Strategy**

9261 The strategy for the upgrade follows the present strategy of TriDAS evolution during LHC
9262 running of first operating any hardware Level-1 (L1) trigger virtually in the Filter Farm Higher
9263 Level Trigger (HLT) code using emulation compared with the data read from the L1. During
9264 the first phase of CMS LHC operation, the L1 algorithms involve data from the calorimeter and

9265 muon systems. Once the trigger rate reduction power of these subsystems is fully exploited,
9266 the next step is to use tracking information.

9267 The CMS Upgrade Phase 2 Trigger R&D centers on integration with a L1 tracking trigger for
9268 identification of tracks associated with calorimeter and muon trigger objects. The track infor-
9269 mation provides a sharp momentum threshold and also is used for isolation. This information
9270 would be used to combine with the calorimeter at L1 to reject π^0 s and reject jets from pileup.
9271 The tracks would be used to sharpen p_T thresholds and reduce accidentals and wrong crossing
9272 determinations in the muon system. Implementation would not only require rebuilding the
9273 tracker, but also rebuilding the calorimeter and muon trigger systems in order to provide out-
9274 puts with suitable granularity and other information to combine with the L1 tracking trigger.

9275 For the Upgrade Phase 2 the L1 trigger data would need combination between tracking and cal-
9276 orimeter and muon triggers at a regional level with finer granularity than presently employed.
9277 After this regional correlation stage, the physics objects made from tracking, calorimeter and
9278 muon regional trigger data would be transmitted to the Global Trigger. The important new
9279 feature is that some of the tracking, isolation, and other regional trigger functions would be
9280 performed in combinations between regional triggers in a new hardware layer composed of
9281 regional cross-detector trigger crates.

9282 The additional layer of processing for combination of tracking information, increased algo-
9283 rithm complexity and larger trigger data volume due to finer trigger granularity motivates an
9284 extension of the present CMS 3.2 μ s L1 latency. A longer latency would also be needed for use
9285 of FPGA embedded serializers and deserializers, addition of more serialization and deserial-
9286 ization steps to use high speed serial links or use of buffers to incorporate commercial serial
9287 links running asynchronously with respect to the LHC clock. The CMS L1 latency is limited
9288 by the front-end analog storage capacity of the tracker and preshower electronics. Since it is
9289 expected that these detectors will be replaced for the SLHC, it is reasonable to assume that their
9290 electronics will be replaced also and that this limitation can be removed. The next limitation is
9291 the ECAL digital memory depth of 256 40 MHz samples corresponding to time of 6.4 μ s. This
9292 is proposed as the CMS SLHC L1 latency baseline.

9293 A.4.3 Upgrade Phase 2 Track Trigger R&D

9294 A source of trigger primitives not used in the current CMS L1 trigger system is the strip and
9295 pixel tracker. Presently this information is added only in the HLT, where it effectively reduces
9296 rates and backgrounds. For the proposed Phase 2 upgrade the complete tracking systems will
9297 need to be replaced due both to radiation exposure and to be able to handle the higher oc-
9298 cupancy in collisions with 200 to 400 interactions. This complete rework of the tracker opens
9299 up the possibility to read out trigger primitive information from the tracker for use in the L1
9300 trigger.

9301 The tracker can provide information of four types: (1) the simple presence of a track match
9302 validates a calorimeter or muon trigger object, e.g. discriminating electrons from hadronic (π^0)
9303 backgrounds in jets; (2) adding precise track hits improves precision on the p_T measurement,
9304 sharpening thresholds in the muon trigger; (3) the degree of isolation of an e , μ or τ candidate;
9305 and (4) the primary z -vertex location within the 30 cm luminous region derived from project-
9306 ing tracks found in trigger layers, providing discrimination against pileup events in multiple
9307 object triggers (e.g. in lepton plus jet triggers, jets inconsistent with the lepton z vertex could
9308 be rejected). In the HLT, track matching to electron L1 objects reduces the rate by a factor of 10.
9309 A similar rejection factor is achieved for muons by adding tracker measurements for isolation
9310 and p_T . We would like to retain the ability at SLHC luminosities of 10^{35} $\text{cm}^{-2}\text{s}^{-1}$ to have an

9311 open L1 trigger for single electron and muons with thresholds in the range from 20 to 30 GeV.
9312 Different concepts for tracking trigger primitive generation are currently explored by the tracker
9313 community. Most effort is currently put into studying modules that will provide p_T discrimi-
9314 nation in the front ends by correlating hits in two closely stacked sensors. Current indications
9315 are that two or more layers of these modules will be required in order to provide useful in-
9316 formation to enhance the current L1 electron, μ , and τ triggers. To maintain the eta coverage
9317 of the current trigger and control the rate, the track trigger has to cover the full eta range -2.5
9318 $< |\eta| < 2.5$. The most straightforward way to accomplish this is to have long barrel modules
9319 at radii less than ~ 50 cm. The trigger primitives considered are the stubs that are formed by
9320 pairs of hits in the closely stacked sensors, or tracklets that are obtained by linking up stubs.
9321 The stubs provide only minimal p_T information as the lever arm for two hits separated by 1
9322 to 2 mm only allows the possibility to apply a threshold to remove hits from low momentum
9323 tracks. However, the tracklets that link up two stubs allow a much more precise momentum
9324 determination. At these small radii the sensors naturally have to be (long) pixels of no more
9325 than a few millimeters in z in order to keep the occupancies low. This fine segmentation in z
9326 allows determination of the track vertex along the z-axis with a precision of about 1 mm.

9327 Another area of active research is development of algorithms to use of tracking trigger primi-
9328 tives to accomplish track matching, isolation, p_T measurement and z vertex determination. We
9329 are pursuing conceptual designs for the interfaces to the calorimeter and muon triggers that al-
9330 low their Phase 1 upgrades to add tracking trigger primitives when they become available. The
9331 improvements in the calorimeter and muon trigger to report more precise $\eta - \phi$ coordinates are
9332 important for the performance of the track trigger in order to reduce road sizes and reduce the
9333 combinatorial problem when linking the coarse information from the outer detectors with the
9334 very precise information from the tracker.

9335 **A.4.3.1 Upgrade Phase 2 Calorimeter Trigger R&D**

9336 The primary idea to reduce the Phase 2 SLHC rate by an order of magnitude is to use tracking
9337 in the Level-1 trigger system to identify the lepton tracks, isolate them from other tracks in
9338 the event, and perhaps also to ascertain that all the lepton tracks and jets triggering the event
9339 originate from the same interesting primary vertex. To reduce the volume of data examined by
9340 the trigger system, the calorimeter trigger can provide seed information for the objects found
9341 by it. The better position resolution calorimeter trigger provides, the better it is for the tracker
9342 trigger processing.

9343 We would like to design and implement the upgraded calorimeter trigger with the best possible
9344 position resolution already at Phase 1. The reason for such an early implementation of position
9345 resolution is primarily for Phase 2 matching with tracker. Our early studies indicate that we
9346 are able to specify the electron and τ object position to half-a-tower resolution (0.04 in $\eta - \phi$).

9347 The Phase 2 SLHC related R&D that we propose to conduct is:

- 9348 • Simulation studies to determine the best position resolutions for electron, τ , jet and
9349 MET objects that can be achieved.
- 9350 • Identify data flow and bandwidth required to carry the position information for all
9351 objects between the various cards.
- 9352 • Prototype cards with sufficient number of links with appropriate bandwidth be-
9353 tween cards to carry the position information

9354 **A.4.3.2 Upgrade Phase 2 CSC Muon Trigger R&D**

9355 The high luminosity of Upgrade Phase 2 CSC Trigger will require a Level-1 muon trigger for
9356 the endcap that can handle increased occupancy by at least a factor 10 (for 50ns bunch spacing
9357 and $L=5 \times 10^{34}$), and possibly higher due to larger than linear growth effects in the number of
9358 chamber-level trigger patterns fired due to neutron backgrounds. In addition, to take advantage
9359 of the increased luminosity for physics, generally one needs to maintain similar p_T thresholds
9360 as used for LHC running, and this will require improving the momentum resolution of the
9361 trigger because the rate predominantly comes from mis-measured real muons. Therefore, data
9362 points from an inner silicon tracking device are also required to be matched to Level-1 muon
9363 candidates, and a refit of the momentum to improve the momentum resolution. To seed the
9364 tracker regions to include into the trigger, refined η , ϕ , and p_T information is required from the
9365 CSC trigger.

9366 The R&D required to prepare a Phase 2 Muon Trigger includes high bandwidth serial links (optical
9367 from the Muon Port Cards on the detector, and copper between the Sector Processor and
9368 Muon sorter track-finding cards in the underground counting room), and very large FPGAs
9369 to accommodate the increased functionality and much higher number of logic tests required in
9370 the track-finding (scales approximately as the square of the number of segments used). Naively
9371 scaling the existing track-finding algorithms to 20 times higher input occupancy does not seem
9372 feasible, thus accurate simulations and projections are required to ascertain the expected background
9373 levels, and new methods of track-finding should be investigated. Thus, a third R&D
9374 area on alternative CSC track-finding algorithms is proposed, such as using a pattern-based
9375 approach rather than a cut-based one. This could be implemented into high density FPGAs,
9376 or possible dedicated ASICs such as the AM++ associative memory design, into the Sector
9377 Processor design.

9378 For the serial link technology, 10 Gbps would solve the need for the optical link connections
9379 from the detector. Thus investigation and prototyping of serializer-deserializer (serdes) chips
9380 (possibly using those embedded into FPGAs) and opto-transceivers approaching that bandwidth
9381 are planned. Additionally, R&D on backplane communication using serial links is foreseen.
9382 For implementation of logic into large state-of-the-art FPGAs, the Xilinx Virtex-5 and
9383 Virtex-6 chips will be taken as starting points for the research.

9384 This hardware R&D will complement the simulation studies we are conducting to evaluate
9385 the performance of the upgraded CSC trigger with estimated Upgrade Phase 2 background
9386 levels. Moreover, the improved precision of the muon candidates will be used in studies with
9387 tracker stubs to contribute to the conceptual design for a second stage regional muon track-
9388 finder linking and fitting tracker stubs.